

UNIVERSITA' DEGLI STUDI DI PADOVA

Dipartimento di Ingegneria Industriale DII

Corso di Laurea Magistrale in Ingegneria Meccanica

Anno accademico 2014/2015



**Comparison of knee biomechanics during isokinetic flexion-extension
or fitness exercises by means of experimental
and musculoskeletal simulations**

Relatore: Prof. Nicola Petrone

Correlatore: Dott. Giuseppe Marcolin

Laureando: Mattia Nardon

N° matricola: 1057329

Table of contents

1.Introduction	1
2.Skeletal muscle and Electromyography	3
2.1.Muscle architecture	3
2.2.Muscle contraction and force exerted	4
2.3.Electromyography	7
3.The knee: anatomy, physiology and in-vivo studies	9
3.1.Anatomical features and movements	9
3.2.Muscles involved during the flexion-extension movement	11
3.3.Passive structure of the knee	12
3.4.Line of action and moment-arm of the major muscles and ligaments acting at the knee joint	15
3.5.Maximum load at tibia and femur	21
3.6.Knee contact forces and ACL strain: in-vivo measurement and analytical models	22
3.7.In vivo-study of the knee flexors and extensors balance	26
4.Musculoskeletal modeling: the software OpenSim	27
4.1.Choice of the model and Scaling	27
4.2.Inverse Kinematics (IK)	30
4.3.Inverse Dynamics (ID)	31
4.4.Static Optimization (SO)	32
4.5.Joint Reaction Analysis	33
4.6.Knee modeling in gait_2392 model	33
5.Aim of the study	35
PART 1: KNEE ISOKINETIC FLEXION-EXTENSION	
6.Material and Methods of Part 1	39

7.Data analysis of Part 1	45
7.1.Evaluation of flexors and extensors balance	45
7.2.Kinematic analysis	45
7.3.Kinetic analysis	46
7.4.OpenSim simulations	48
7.5.EMG analysis	49
7.6.Analytical simulations	50
7.6.1.Model 1	50
7.6.1.1 Model definition and Reference systems position	50
7.6.1.2.COMs position	53
7.6.1.3.Muscular forces and Reaction loads at tibia	54
7.6.1.4.Forces acting on tibia	61
7.6.1.5.Force acting at ACL and PCL	61
7.6.1.6.Forces acting on femur	63
7.6.2.Model 2	66
7.6.2.1. Model definition and COMs position	66
7.6.2.2. Muscular forces and Reaction loads at tibia	68
7.6.2.3.Forces acting on tibia	74
7.6.2.4.Force acting at ACL and PCL	74
7.6.2.5.Forces acting on femur	75
7.6.3.Comparison with OpenSim results	77
8.Comparative evaluation and discussion of results of Part 1	79
8.1.Comparison and evaluation of Torque and Flexors and extensors balance	79
8.2.Comparison and evaluation of electromyography and OpenSim muscle activation	85
8.3.Comparison and evaluation of analytical models and OpenSim model	95

PART 2: LEG EXTENSION EXERCISE (preliminary study)	
9.Material and Methods of Part 2	123
10.Data analysis of Part 2	127
10.1.Kinematic analysis	127
10.2.Kinetic analysis	127
10.3.OpenSim simulations and EMG analysis	130
10.4.Comparison of analytical models and OpenSim simulations	131
11.Results and Discussion of Part 2	133
11.1.Results of exercises performed at M1	135
11.2.Results of exercises performed at M2	147
11.3.Discussion of results of Part 2	159
12.Conclusion	165
APPENDIX	169
A.1.Results of Subject 1 (S1)	171
A.2.Results of Subject 2 (S2)	191
A.3.Results of Subject 3 (S3)	211
A.4.Results of Subject 4 (S4)	231
A.5.Results of Subject 5 (S5)	251
A.6.Results of Subject 6 (S6)	271
References and notes	291
RINGRAZIAMENTI	295

1.Introduction

The knee is one of the most complex joints of the human body and most often affected by injuries. In this study the knee biomechanics during isokinetic flexion-extension and during fitness exercises was investigated in order to predict, with a not-invasive approach, articular loads and tensions at ligaments or tendons of the major structures involved during the movement and in order to predict possible injuries caused by a wrong execution of the movement and to suggest possible solutions to avoid this problem.

In literature there are many studies about the knee flexion-extension. Van Eijden et al. (1986), Yamaguchi et al. (1989), Herzog et al. (1993) investigated in particular the line of action and the moment arm of the most important muscles and ligaments acting during the movement and they suggested an analytical schematization of the femur-patella articulation; D'Lima et al. (2005, 2006, 2007, 2013) focused on implantable devices which allow to measure contact forces on tibia and femur during daily life activities; Beynon et al. (1992, 1997, 1998) examined the tension at the anterior cruciate ligament by means of differential transducer embedded directly to the central part of the ligament; Noyes et al. (1984) and Amis et al. (2003) tested ligaments and tendons in order to obtain important mechanical properties, in particular the ultimate tension at breakage.

The results of these previous studies, were used in this thesis in order to define some analytical models useful to obtain the forces at the major muscles acting at the knee joint, the articular loads acting at tibia and femur and the tension at the anterior and posterior cruciate ligaments. Moreover, the results were compared with those deriving from another analytical model defined in a previous thesis work and also with the results of numerical simulations obtained by the software OpenSim. This software allowed to predict articular loads and muscular forces too, but not the tension at anterior and posterior cruciate ligaments; moreover, in order to validate the results obtained by the numerical simulations, the muscular forces were compared with electromyographic signal recorded in vivo during the exercises.

To investigate widely the knee biomechanics during flexion-extension, first isokinetic exercises at different velocities, by using an isokinetic machine, were performed in order to evaluate the influence of the velocity on biomechanical parameters; after that, the knee flexion-extension was investigated during a typical fitness exercise, the leg-extension exercise, performed with two different type of machines at different loads in order to evaluate the influence of the machine and the influence of the load.

2.Skeletal muscle and Electromyography

2.1.Muscle architecture

The skeletal muscle has the following hierarchical organization (fig.2.1):

- fascicles (about 150 muscle fibers): which are comprised of a number of muscle fibers;
- muscle fibers (dia. $\approx 100 \mu\text{m}$): which are comprised of myofibrils;
- myofibrils (dia. $\approx 1\text{-}3 \mu\text{m}$): which are comprised of sarcomeres arranged in series;
- sarcomeres: the sarcomere is the functional unit of the muscle contraction and it is defined by two types of myofilaments, actin and myosin; each sarcomere can be delimited by two lines, the z-lines (fig.2.2).

These previous elements are surrounded by connective tissue, which sustains the muscle and reduces the friction between the fibers during the contraction mechanism; it is possible to identify the epimysium, which surrounds the fascicles, the perimysium, which surrounds the muscle fibers, the endomysium, which surrounds the muscle fibers (fig.2.1).

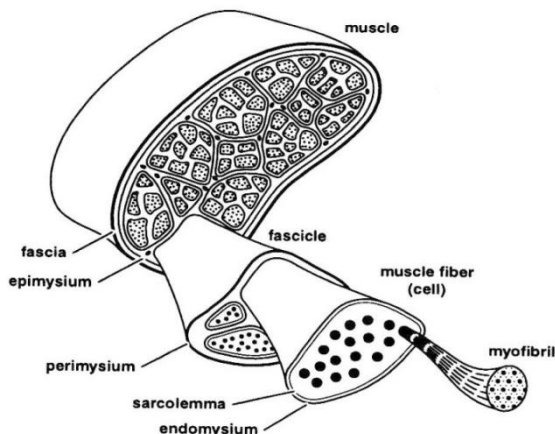


Fig. 2.1: Muscle architecture: fascicles, muscle fibers, myofibrils and connective tissue. (Nigg et al., [23])

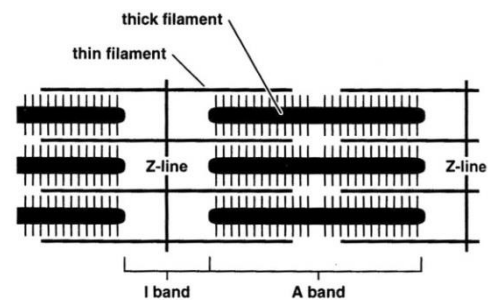


Fig.2.2: Sarcomere: thick filament (myosin), thin filament (actin) and z-line. (Nigg et al., [23])

According to the orientation of the fibers, it is possible to identify two main classes of muscles: fusiform and pennated muscles. In fusiform muscles, the fibers are oriented in the same direction of the line of action of the muscle; in pennated muscles, instead, the fibers have a different orientation which is defined by using the pennation angle α , which is the angle between the line of action and the direction of the fibers (fig.2.4).

Pennated muscles can be divided into unipennated, bipennated or multipennated muscles according to the different orientation of the fibers.

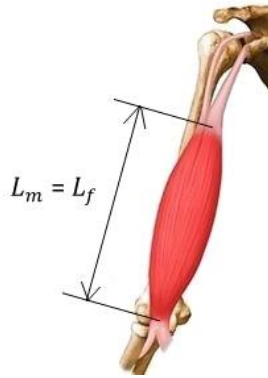


Fig.2.3: Example of fusiform muscle (biceps brachialis)
 L_f : length of fibers; L_m : length of muscle.
 (Muscle Atlas, [36])

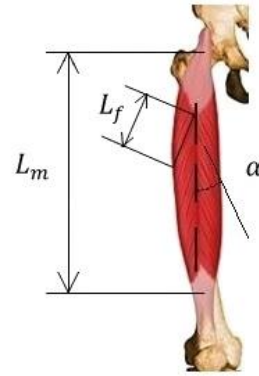


Fig.2.4: Example of bipennated muscle (rectus femoris).
 L_f : length of fibers; L_m : length of muscle
 α : pennation angle. (Muscle Atlas, [36])

An important parameter related to the orientation of the fibers is the physiological cross section area, PCSA, which is defined as:

$$PCSA = \frac{Vol}{L_f}$$

in which Vol is the volume of the muscle and L_f is the length of the fibers. The length of the fibers is equal to the length of muscle L_m only for fusiform muscles (fig.2.3 and fig.2.4).

2.2. Muscle contraction and force exerted

The muscle contraction starts with an electrical impulse, the action potential, which is transmitted by the nervous system. This impulse originates at the spinal cord from a motor neuron, and, by an axon, reaches the muscle fibers with the motor-endplates (fig.2.5). The muscle fibers innervated by the same motor neuron are called motor unit.

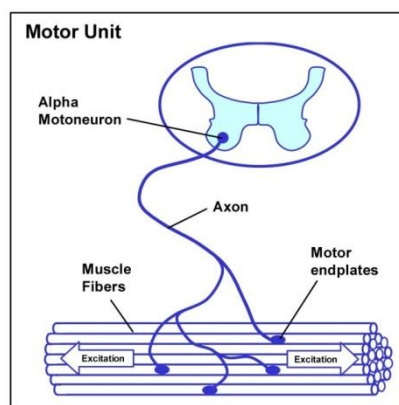


Fig.2.5: Motor unit. (Konrad P, [19])

When the impulse reaches the muscle, it determines a relative movement between actin and myosin, and this movement changes the length of the sarcomeres in terms of distance between the z-lines. By considering the distance between the z-lines, it is possible to identify three types of contraction:

- concentric contraction: during the muscle contraction the distance between the z-lines decreases; this could be defined as the normal behavior of the muscle, because the muscle exerts a force and decreases its own length;
- eccentric contraction: during the muscle contraction the distance between the z-lines increases; in this phase, typically the muscle works as a brake, because it exerts a force but its length increases;
- isometric contraction: during the muscle contraction the distance between the z-lines doesn't change; in this phase, which is a stance phase, the muscle exerts a force in a fixed position without stroke.

The force exerted by the muscle in these three situations is different. This different behaviour should be emphasized if we consider the contraction velocity of the fibers as it is shown in fig.2.6, in which it is possible to identify the concentric phase ($v > 0$), the eccentric phase ($v < 0$), the isometric phase (point at $v = 0$).

In this schematization, the force is normalized to the isometric force P_0 and the contraction velocity is normalized to the velocity at which the force is null, v_{max} .

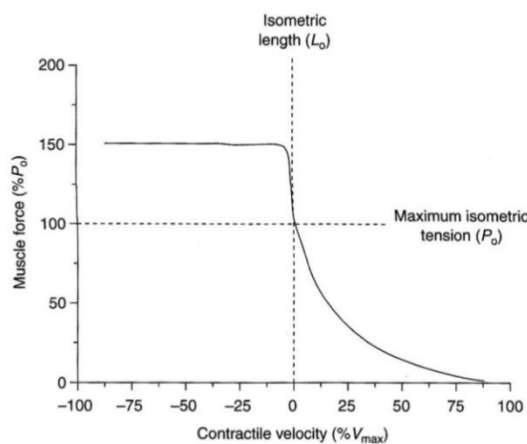


Fig.2.6: Force-velocity relation. (Peterson et al., [25])

Other two important parameters which can modify the force are the length of the sarcomeres and the percentage of activation of the muscle. About the percentage of activation, this is associated with the number of muscle fibers which are excited during the muscle contraction. About the length of the sarcomeres, it is possible to identify an optimal length at which the force reaches its maximum; this length, L_0 , is the length at the isometric condition. The relation muscle force-length of the sarcomere is shown in

fig.2.7: the active curve is generated by the sarcomeres, the passive curve by the connective tissue. The total force is the sum of the two curves. However, typically the passive contribution is ignored.

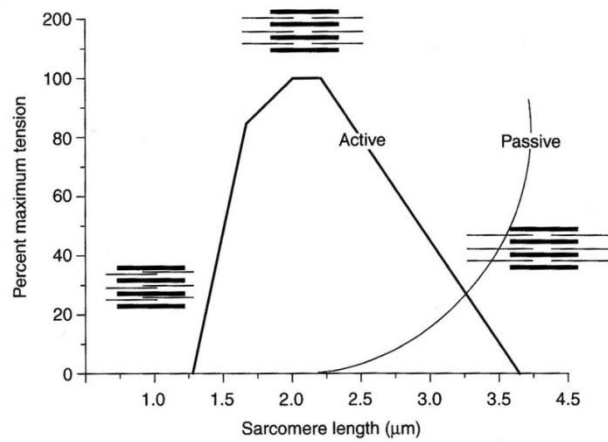


Fig.2.7: Muscle force-length of the sarcomere relation: active and passive contribution. (Peterson et al., [25])

By combining the contraction velocity and the length of the sarcomeres it is possible to obtain a 3-axis representation of the muscular force (fig.2.8):

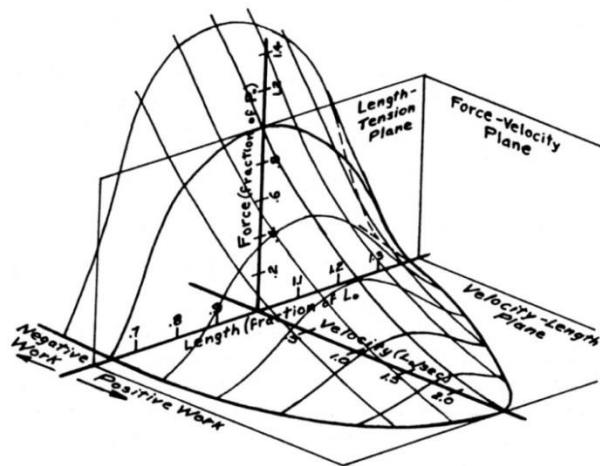


Fig.2.8: Representation of the force-length-velocity relation (only for Att%=100%). (Force-length-velocity relation, [37])

By combining also the percentage of activation, it is possible to obtain the force-length-velocity relation (without considering the connective tissue) for the concentric phase:

$$F(v, L) = F_0 \cdot F_L' \cdot \frac{1-v'}{1+\frac{v'}{K}} \cdot \text{Att}\%$$

in which

$$F_0 = \sigma_0 \cdot PCSA \cdot \cos(\alpha)$$

$$F_L' = -6,25 \cdot \left(\frac{L}{L_0}\right)^2 + 12,5 \left(\frac{L}{L_0}\right) - 5,25$$

σ_0 : strength during isometric contraction

L_0 : optimal length of the sarcomeres (at isometric contraction)

$$v' = v/v_{\max}$$

$$K = 0,15 - 0,25$$

Att% : percentage of activation

In the eccentric phase, the relation can be written as:

$$\frac{F}{F_0} = 1,8 - 0,8 \frac{v_{\max} + v}{v_{\max} - 7,6 \cdot v}$$

2.3. Electromyography

When the action potential reaches the muscle fibers with the motor-endplates, it travels along the surface of the fibers like an electrical dipole. To detect the signal, bipolar electrodes and a differential amplification are used (fig.2.9).

Thus, it is possible to define what Electromyography is: ‘Electromyography (EMG) is an experimental technique concerned with the development, recording and analysis of myoelectric signals. Myoelectric signals are formed by physiological variations in the state of muscle fibers membrane’ (cit. from Konrad P, [19]).

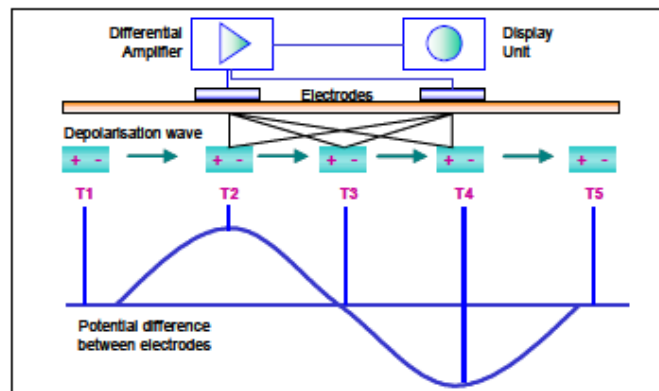


Fig.2.9: Model of electric dipole travelling along the muscle fiber. Surface electrodes are shown. (Konrad P, [19])

There are two different types of electrodes: surface electrodes (not-invasive technique), which are applied on the skin, and wire electrodes (invasive technique), which are applied deeper inside the muscle. In this study, only the surface electrodes were used.

Because of the quality of the EMG signal by using electrodes depends strongly on skin conditions and electrodes positioning, here below there are some general guidelines from the Konrad P, [19]:

- have a good skin impedance condition by cleaning the skin, for example with alcohol, until the skin receives light red color;
- use small electrodes;
- put the electrodes at the minimum distance allowed (the minimum distance recommended is 2 cm);
- apply electrodes in parallel to the muscle fiber direction and in the middle portion of the muscle.

Although the respect of these guidelines, the EMG signal acquired is a raw signal and must be analyzed.

The techniques which were used in this thesis to analyze the signal will be explained in par.7.5.

3.The knee: anatomy, physiology and in-vivo studies

3.1.Anatomical features and movements

The knee is one of the most complex joints of the human body. It has two articulations: the tibiofemoral articulation, between distal epiphysis of femur and proximal epiphysis of tibia, and the femur-patella articulation, between distal epiphysis of femur and the patella base(fig.3.1). Because of the anatomical features of the contact surfaces between femur and tibia and between femur and patella, the most important movement of the knee is the flexion-extension movement, which is the rotation around the X-X' axis in fig.3.2. The flexion angle φ_k is defined as the angle between the longitudinal axis of the femur and the longitudinal axis of the tibia (fig.3.1); in particular, during the flexion movement the flexion angle increases its value, during the extension movement it decreases. Other movements of the knee are the internal and external rotation, which is the rotation around the tibia longitudinal axis Y-Y' in fig.3.2, and the rotation around the Z-Z' axis in fig.3.2; however these movements are quite small and they are possible only when the knee is in flexion.

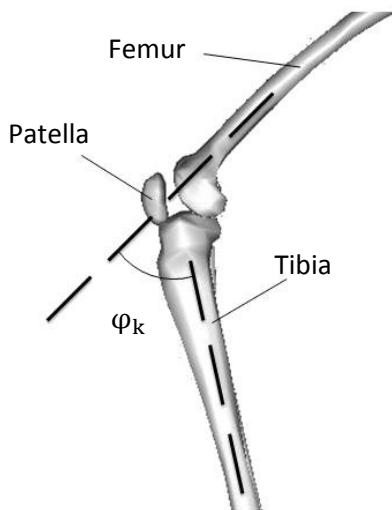


Fig.3.1: Representation of the knee joint.
(from Lower Limb London model, OpenSim)

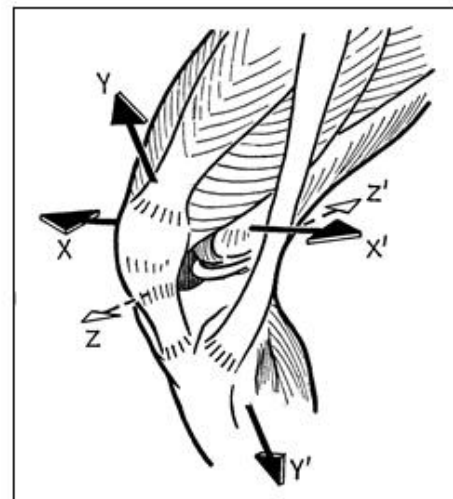


Fig.3.2: Rotational axis of the knee.
(Kapandji AI, [14])

During the flexion-extension movement, the two condyles of the femur describe a rotational-translational movement on the tibia plateau (fig.3.3). In the first phase of the flexion there is only the rotational movement and in the last phase there is only the translational one; in the middle phase there is both rotation and translation. The phase in which there is only rotation is different for the medial and for the lateral condyle: for the medial condyle there is pure rotation until 10° - 15° of flexion; for the lateral condyle there is pure rotation until 20° of flexion. During the flexion-extension movement, the patella moves too: it

moves with respect to the femur for a distance which is twice its own length (fig.3.3,1) and simultaneously it moves around a point on the tibial tuberosity (fig.3.4,2).

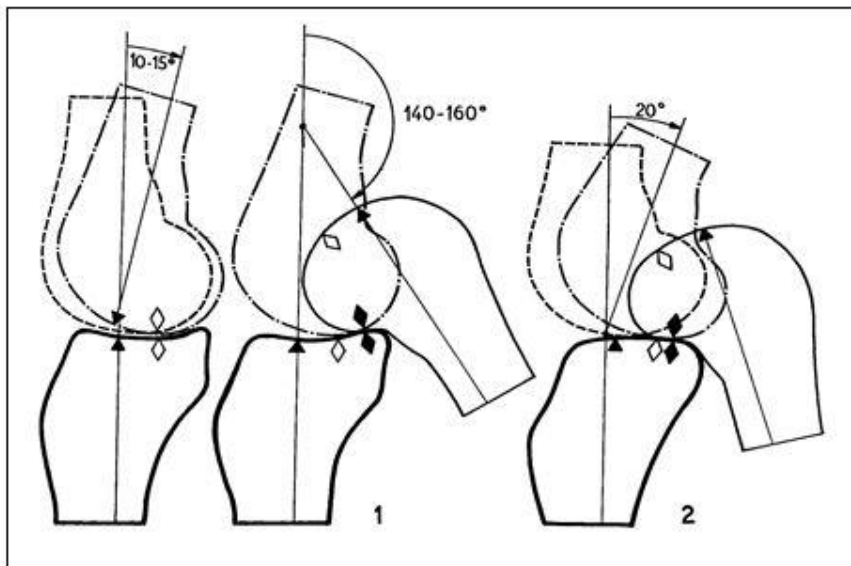


Fig.3.3: Rotation and translation of the femoral condyles during the knee flexion-extension movement: 1,medial condyle; 2, lateral condyle. (Kapandji AI, [14])

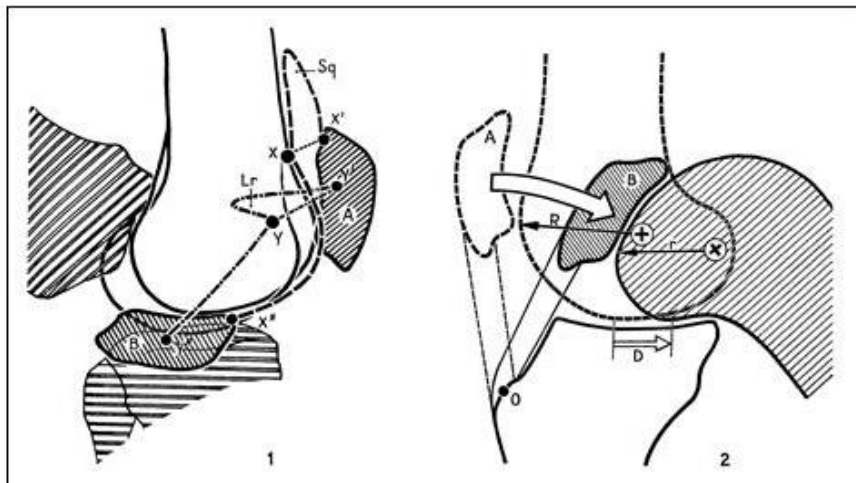


Fig.3.4: Patella movement during the knee flexion-extension movement with respect to tibia: 1, relative movement with respect to femur; 2, rotational movement. (Kapandji AI, [14])

3.2. Muscles involved during the flexion-extension movement

The most important muscles which act at the knee joint during the flexion-extension movement are:

Flexor muscles (fig.3.5):

- Biceps femoris long-head and short-head (BFL, BFB);
- Semimembranosus (SM);
- Semitendinosus (ST).

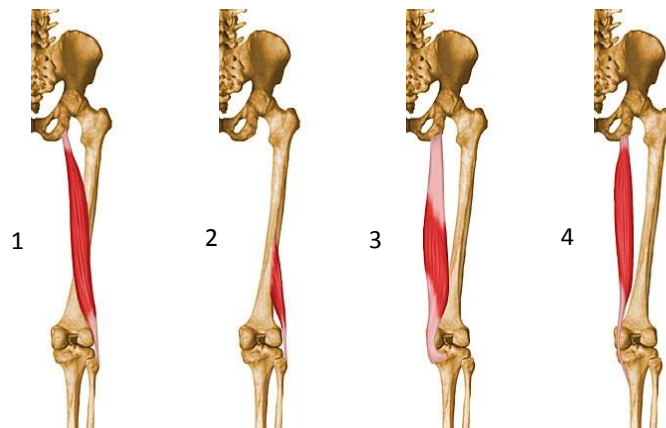


Fig.3.5: Flexor muscles: 1:Biceps femoris-long head; 2:Biceps femoris-short head; 3:Semimembranosus; 4:Semitendinosus. Right leg, rear view. (Muscle Atlas, [36])

Extensor muscles (fig.3.6):

- Rectus Femoris (RF);
- Vastus Medialis (VM);
- Vastus Intermedius (VI);
- Vastus Lateralis (VL);

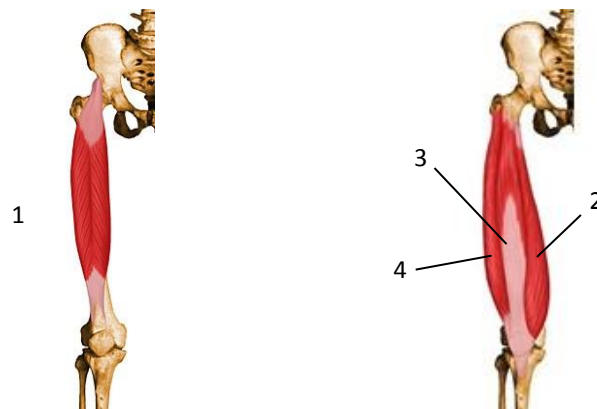


Fig.3.6: Extensor muscles: 1: Rectus femoris; 2: vastus medialis; 3:vastus intermedius; 4:vastus lateralis. Right leg, front view. (Muscle Atlas, [36])

3.3. Passive structure of the knee

The right execution of the flexion-extension movement and the right execution of the internal-external rotation are allowed by some cartilaginous structure and ligaments (fig.3.7 and fig.3.8):

- between tibia and femur there are two menisci, which reduce the friction between the two surfaces;
- lateral collateral ligament (LCL) and medial collateral ligament (MCL), which control the lateral stability during the flexion-extension movement;
- anterior cruciate ligament (ACL) and posterior cruciate ligament (PCL): the ACL restricts the anterior displacement of the tibia, the PCL restricts the posterior displacement of the tibia (anterior and posterior referred to an axis perpendicular to the longitudinal axis of the tibia); ACL and PCL are also involved into the translational mechanism of the condyles;
- the patellar tendon and the tendon of the quadriceps, which constrain the patella to the tibia and let it move around the tibial tuberosity (fig.3.8);
- articular capsule, which is a synovial and fibrous membrane which enclose the joint with synovial fluid.

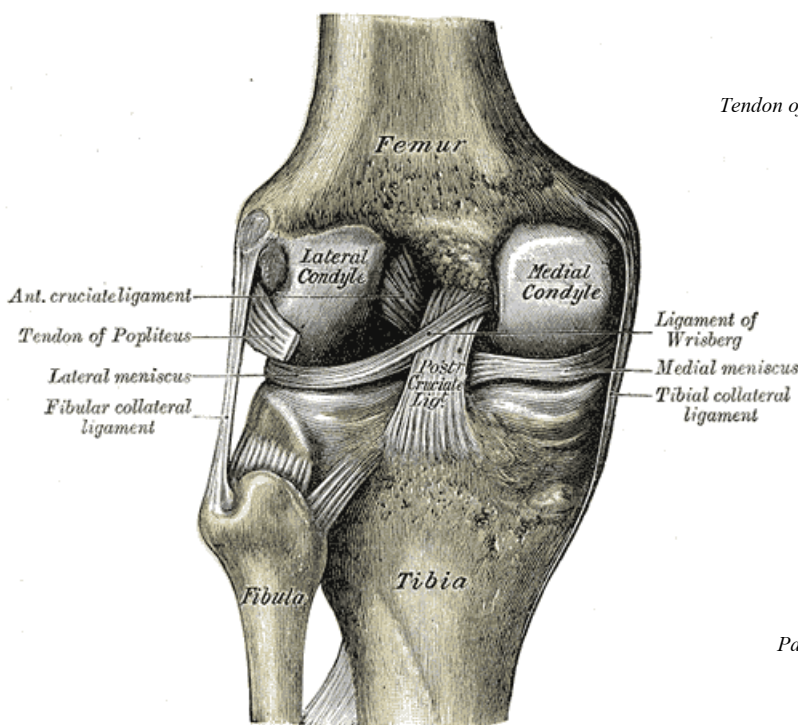


Fig.3.7: Left knee, posterior view. (Gray et al., [11])

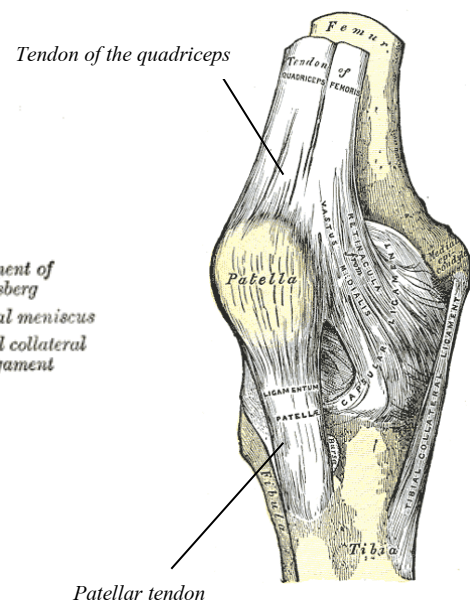


Fig.3.8: Patellar tendon and tendon of the quadriceps. (Gray et al., [11])

Ligaments and tendons have a structure which has a hierarchical organization similar to the muscular one (fig.3.9): tendon (or ligament) is composed primarily of collagen fibers, which are organized in microfibrils; microfibrils group into subfibrils; subfibrils aggregate further to form fibrils and then, at the next level of tendon organization, fibrils are aggregated in fascicles; at the end, the fascicle bundles are aggregated to form the tendon (or ligament). The difference between tendon and ligament is in that tendon connects muscle to bone, ligament attaches one articulating bone to another one across a joint and guides the joint movement.

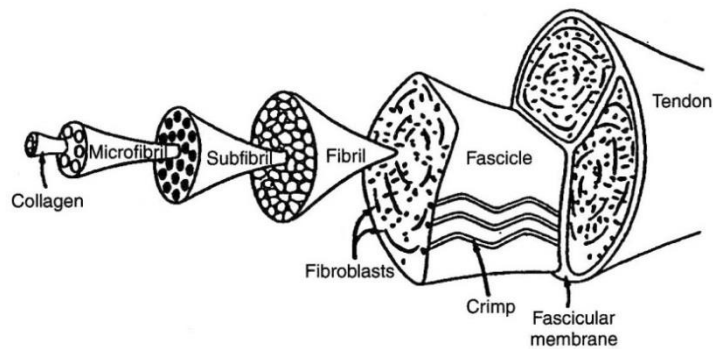


Fig.3.9: Tendon (or ligament) hierarchical organization. (Peterson et al., [25])

Tendons and ligaments can be tested in a tensile test in order to obtain some useful mechanical properties, in particular their maximum load at breakage. Fig.3.10 shows a typical force-deformation curve, which can be divided into four parts. In the first part the curve is not linear, because of the heterogeneous distribution of the fibers; in the second part there is a certain linearity, when fibers align in the direction of the force acting; there follows the third region in which the curve flattens out for the microfailure of some fibers; in the last part the curve drops down rapidly when the complete rupture of the tendon occurs.

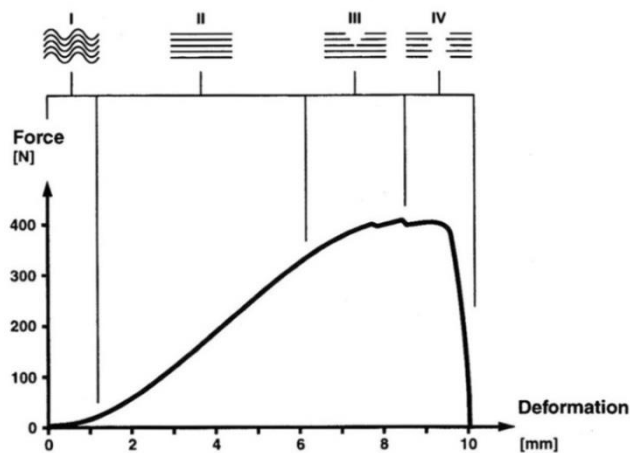


Fig.3.10: General force-deformation relation for ligament or tendon. (Nigg et al. [23])

In literature there are some values of the maximum sustainable load for the most important knee ligaments and tendons of the muscles which act at the knee joint:

- ACL: 1725 ± 269 N (Noyes et al. 1984, [24])
- PCL: $739 \div 1627$ N (Amis et al. 2003, [1])
- patellar tendon: central third: 2900 ± 260 N (Noyes et al. 1984, [24])
medial third: 2734 ± 298 N (Noyes et al. 1984, [24])
- tendon of the quadriceps: medial: 371 ± 46 N (Noyes et al. 1984, [24])
central: 266 ± 74 N (Noyes et al. 1984, [24])
lateral: 249 ± 54 N (Noyes et al. 1984, [24])
- semitendinosus: 1216 ± 50 N (Noyes et al. 1984, [24])

The variability of the results is related to the gripping effects of the tensile test and, in particular, to the age of donors.

About patellar tendon and tendon of the quadriceps, the results suggested by Noyes et al. 1984, [24] refer to different fascicles. To obtain a mean value, it is necessary to consider another study done by Kawaguchi et al. 2014, [16], in which the influence of different fascicles of the ACL was tested: the results reveals that central portion of the tendon provided from 66% to 84% of the total force of the ligament. Thus it is reasonable to consider as maximum force of the ligament the force exerted by the central part. Moreover, it is reasonable to extend the results obtained for the ACL to the other ligaments or tendons.

About the tendon of the quadriceps, the maximum force exerted by the central fascicle differs very much from the maximum force exerted by the central fascicle of the patellar tendon; because the patellar tendon can be considered an extension of the tendon of the quadriceps, it is reasonable to assume the same maximum force in both tendons and to consider the force of the patellar tendon as reference value also for the tendon of the quadriceps.

About the maximum force at biceps femoris (short and long head) and semimembranosus, the tendons of these muscles were not studied widely because they are not used to reconstruct ACL or PCL ruptures as it happens instead for the other ones. However by considering the maximum isometric force of the muscles in gait2392_model used in OpenSim simulations (chap.4), it is possible to evaluate the maximum load for biceps femoris and semitendinosus: maximum force at biceps femoris-short head: 2000 ± 70 N, maximum force at biceps femoris-long head: 2000 ± 70 N, maximum force at semimembranosus: 3000 ± 86 N (because the maximum isometric force of biceps femoris-short head and biceps femoris-long head are more or less twice the maximum isometric force of the semitendinosus, and the maximum isometric force of semimembranosus is more or less three times the maximum isometric force of semitendinosus).

Here below, the reference values for the maximum force at the major knee ligaments or tendons which are used in this thesis are summarized:

- ACL: 1725 ± 269 N
- PCL: 1180 ± 447 N
- patellar tendon: 2900 ± 260 N
- tendon of the quadriceps: 2900 ± 260 N
- semitendinosus: 1216 ± 50 N
- biceps femoris-short head: 2000 ± 70 N
- biceps femoris-long head: 2000 ± 70 N
- semimembranosus: 3000 ± 86 N

3.4.Line of action and moment-arm of the major muscles and ligaments acting at the knee joint

In the literature there many studies about the orientation and the moment arm of the major muscles and ligaments acting at knee during the flexion-extension movement. The studies which were used to define the analytical models of this thesis (par.7.6) are described in what follows:

Van Eijden et al. (Van Eijden et al. 1986, [32]), by analyzing 10 cadaver specimens with MRI techniques, obtained the angles shown in fig.3.11: the angle α , which is the inclination of the patellar tendon with respect to the longitudinal axis of the tibia (TA); the angle δ , which is the inclination of the tendon of the quadriceps with respect to the longitudinal axis of the femur (FA); the angles γ , β and ε which can be used to obtain the orientation of the patella.

Fig.3.12 and fig.3.13 show the results for the angle α and δ at different values of the knee flexion angle. α and δ are positive as shown in fig.3.11.

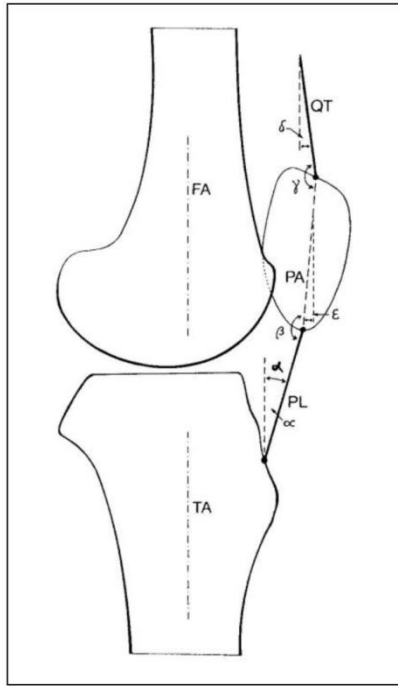


Fig.3.11: Representation of the angles evaluated in Van Eijden's study. (Van Eijden et al. 1986, [32])

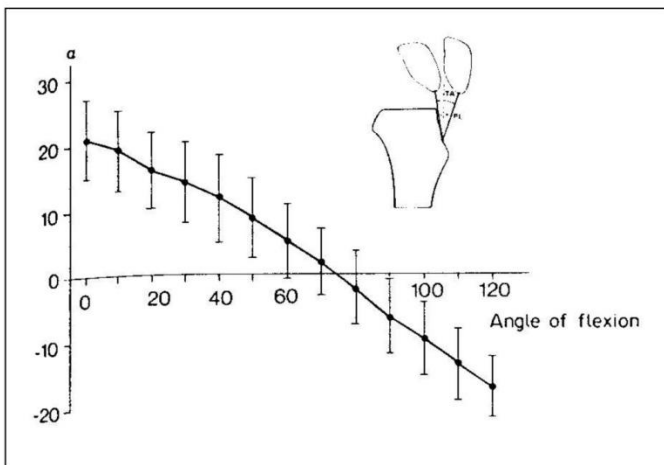


Fig.3.12: α angle [°] at different knee flexion angles [°] in Van Eijden's study. (Van Eijden et al. 1986, [32])

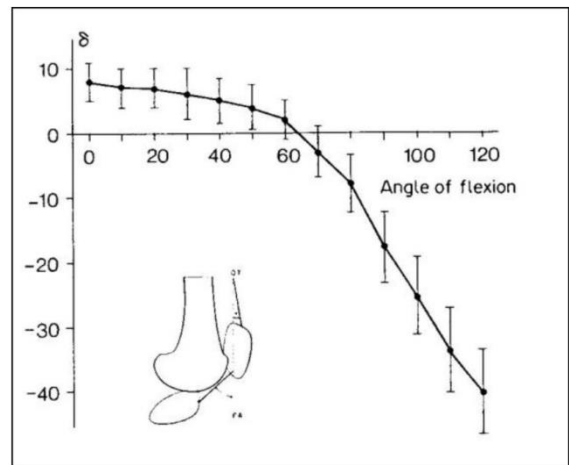


Fig.3.13: δ angle [°] at different knee flexion angles [°] in Van Eijden's study. (Van Eijden et al. 1986, [32])

In the study done by Van Eijden et al., an explicit relation between the angles and the knee flexion angle wasn't suggested. However, by considering the mean values in the representation and by interpolating the results with the software Excel it is possible to obtain the following equations for α and δ :

$$\alpha [^\circ] = -8,4734 \cdot \varphi_k^6 + 50,457 \cdot \varphi_k^5 - 110,75 \cdot \varphi_k^4 + 109,99 \cdot \varphi_k^3 - 52,907 \cdot \varphi_k^2 - 2,0575 \cdot \varphi_k + 21,091$$

$$\delta [^\circ] = 4,4936 \cdot \varphi_k^5 - 13,01 \cdot \varphi_k^4 - 3,1278 \cdot \varphi_k^3 + 15,807 \cdot \varphi_k^2 - 8,9712 \cdot \varphi_k + 7,6405$$

in which φ_k [rad].

Van Eijden et al., described also the patellofemoral articulation with an analytical model which is shown in fig.3.14. By using this model and the results above, it was possible to obtain the relation between the force at the patellar tendon, F_{pL} , and the force at the tendon of the quadriceps, F_q , and the relation between the force at the tendon of the quadriceps and the force exerted by the patella to the femur F_p (fig.3.15). In this model, the force exerted by the patella F_p acts in a direction which is perpendicular to the contact surface as shown in fig.3.14.

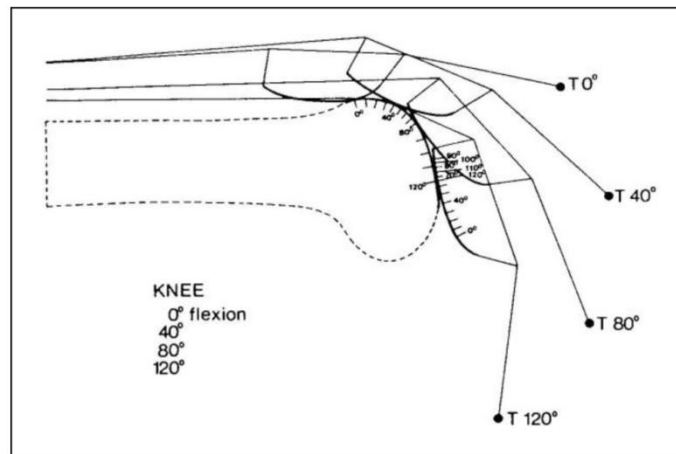


Fig.3.14: Analytical model of the tibiofemoral contact in Van Eijden's study.
(Van Eijden et al. 1986, [32])

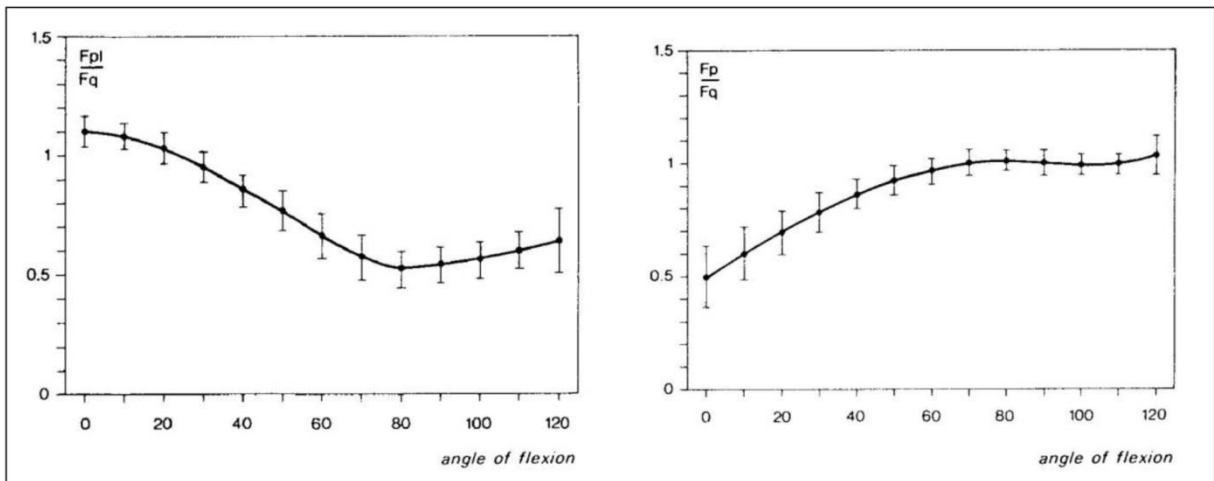


Fig.3.15: Ratio F_{pL}/F_q and ratio F_p/F_q as a function of the knee flexion angle in Van Eijden's study.
(Van Eijden et al. 1986, [32])

By interpolating the results ad done above, the ratio F_{pl}/F_q and ratio F_p/F_q can be evaluated by using these equations:

$$F_{pl}/F_q = -0,1676 \cdot \varphi_k^5 + 0,743 \cdot \varphi_k^4 - 0,7943 \cdot \varphi_k^3 - 0,1234 \cdot \varphi_k^2 - 0,0742 \cdot \varphi_k + 1,1026$$

$$F_p/F_q = 0,0332 \cdot \varphi_k^5 - 0,0485 \cdot \varphi_k^4 - 0,1657 \cdot \varphi_k^3 + 0,1399 \cdot \varphi_k^2 + 0,505 \cdot \varphi_k + 0,4974$$

in which φ_k [rad].

The inclination of the patella which is shown in fig.3.14, can be evaluated by considering the angle ε between the axis of the femur and the axis of the patella (fig.3.16). This angle is positive as shown in fig.3.11.

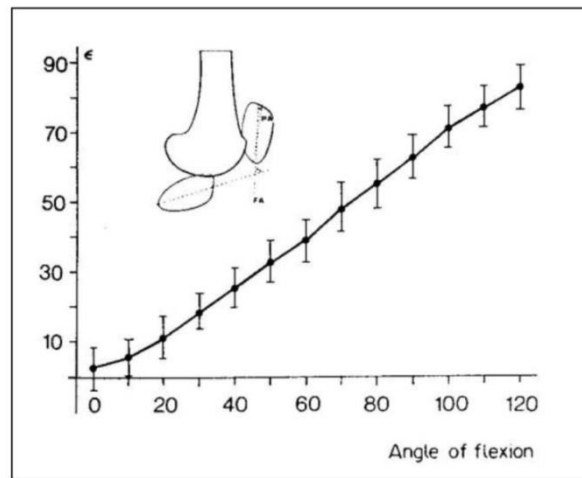


Fig.3.16: Angle ε between the axis of the femur and the axis of the patella in Van Eijden's study. (Van Eijden et al. 1986, [32])

By interpolating the results as done above, it is possible to obtain the following equation for ε :

$$\varepsilon [^\circ] = -5,1281 \cdot \varphi_k^5 + 26,76 \cdot \varphi_k^4 - 55,185 \cdot \varphi_k^3 + 58,369 \cdot \varphi_k^2 + 10,868 \cdot \varphi_k + 2,1715$$

in which φ_k [rad].

The study of Van Eijden et al. has the following limitations:

- no relation of moment arms was suggested;
- no ligaments were considered;
- no flexors muscles were considered.

Another analytical model was suggested by Yamaguchi et al. (Yamaguchi et al. 1989, [34]). The femoral condyles are represented as ellipses, the tibia plateau as a line segment and the patella as a rectangle (fig.3.17). By considering the equilibrium of the patella and by solving the equations with the Newton-Raphson method, Yamaguchi et al. obtained, for different values of the knee flexion angle, the inclination of the forces F_{pl} and F_q , the ratio F_{pl}/F_q and the ratio F_p/F_q .

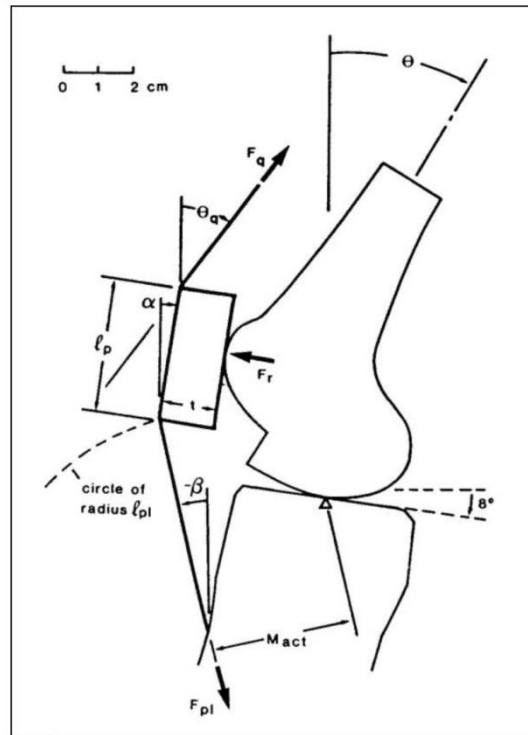


Fig.3.17: Analytical model of the knee in Yamaguchi's study. (Yamaguchi et al. 1989, [34])

Although the results were in good agreement with the results of the study done by van Eijden et al., this model has the following limitations:

- to solve the equations, the inclination of the quadriceps was obtained by the results of the study done by Van Eijden et al.;
- the model was scaled by using only one human skeleton lab;
- the Newton-Raphson method is inherently imprecise;
- no relation of moment arms was suggested;
- no ligaments and no flexors muscles were considered.

Another study was done by Herzog et al. (Herzog et al. 1993, [13]). From 5 cadaver specimens, it was possible to obtain, with MRI techniques, the line of action and the moment arm of the following muscles and ligaments: patellar tendon, biceps femoris-long head, semimembranosus, semitendinosus, ACL, PCL, MCL and LCL. To obtain the results, a best fitting polynomial regression equation was used. About the line of action, the results were expressed with respect to the y-axis of the axis system embedded to tibia which is shown in fig.3.18.

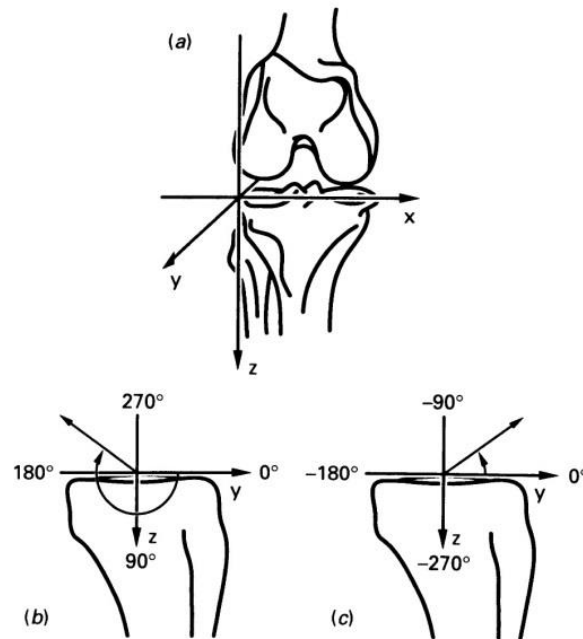


Fig.3.18: Reference system adopted in Herzog's formulation; a) anterior view, b) and c) lateral view. (Herzog et al. 1993, [13])

To predict the line of action, the following equation was suggested:

$$\text{line of action } [^\circ] = A_0 + A_1 \cdot \varphi_k + A_2 \cdot \varphi_k^2 + A_3 \cdot \varphi_k^3$$

in which φ_k is the flexion angle in $[^\circ]$ and $A_0 - A_3$ regression coefficients in tab.3.1:

	r^2	A0	A1	A2	A3
Patellar tendon	0.98	-0.744D+02	-0.575D-01	-0.475D-02	0.309D-04
Biceps femoris	0.99	0.275D+03	-0.872D+00	-0.712D-03	0.000D+00
Semimembranosus	0.99	0.260D+03	-0.888D+00	-0.852D-03	0.000D+00
Semitendinosus	0.99	0.255D+03	-0.816D+00	0.263D-03	-0.619D-05
ACL	0.99	0.227D+03	-0.448D+00	0.000D+00	0.000D+00
PCL	0.82	-0.660D+02	0.737D+00	-0.496D-02	0.000D+00
MCL	0.85	0.259D+03	-0.699D-01	0.000D+00	0.000D+00
LCL	0.89	-0.718D+02	-0.159D+00	0.000D+00	0.000D+00

Tab.3.1: Regression coefficients $A_0 - A_3$ for the line of action in Herzog's study; the numbers are given in double precision. (Herzog et al. 1993, [13])

The moment arm can be evaluated in a similar way with the following equation:

$$\text{moment arm [cm]} = B_0 + B_1 \cdot \varphi_k + B_2 \cdot \varphi_k^2 + B_3 \cdot \varphi_k^3 + B_4 \cdot \varphi_k^4$$

in which φ_k is the flexion angle in [°] and $B_0 - B_4$ regression coefficients in tab.3.2:

	r^2	B0	B1	B2	B3	B4
PT	0.92	0.471D+01	0.420D-01	-0.896D-03	0.447D-05	0.000D+00
Bf	0.99	0.146D+01	-0.926D-02	0.855D-03	-0.878D-05	0.238D-07
Sm	0.99	0.284D+01	-0.161D-01	0.681D-03	-0.880D-05	0.277D-07
St	0.99	-0.411D+00	-0.586D-01	0.690D-03	-0.531D-05	0.000D+00
ACL	0.99	-0.642D+00	-0.431D-01	0.130D-02	-0.131D-04	0.475D-07
PCL	0.98	0.184D+01	-0.739D-01	0.963D-03	-0.396D-05	0.000D+00
MCL	0.51	0.586D-01	-0.167D-01	0.130D-03	-0.000D+00	0.000D+00
LCL	0.59	0.558D+00	-0.198D-01	0.171D-03	-0.000D+00	0.000D+00

Tab.3.2: Regression coefficients $B_0 - B_4$ for the moment arm; the numbers are given in double precision. (Herzog et al. 1993, [13])

The limits of this study are:

- line of action and moment arm of the tendon of the quadriceps weren't considered;
- only biceps femoris-long head is considered and not biceps femoris-short head.

3.5. Maximum load at tibia and femur

The maximum force needed to break a bone is related to the direction in which the force is applied and it is also related to the portion of bone at which the force acts as well to the speed of load application. At the knee-joint, forces act between tibia and femur and also between patella and femur. These forces are a consequence of the contact between the bones.

The tension acting between tibia and femur depend on the tibiofemoral contact area, which changes in relation to the flexion angle because of the translational-rotational movement of the condyles (par.3.1). In fig.3.19, the mean contact area and the contact point of the condyles are shown. However a mean value of the contact area is about 800 mm² (Nigg et al., [23]). By considering this value and by testing tibia and femur in a tensile test and in a compression test, it was possible to identify the maximum force needed to break the two bones in tension and in compression. Because of the distal epiphysis of the femur and the distal epiphysis of the tibia have a similar structure, it is reasonable to assume a maximum force of about 4000 N in tension and a maximum force of about 5600 N in compression for both bones (Nigg et al., [23]). By other experimental tests, it was possible to relate the maximum tensile force to the maximum shear

force (perpendicular to the axis of the bone): the maximum tensile force is about twice the shear force (Nigg et al., [23]), thus the maximum shear force is about 2000 N.

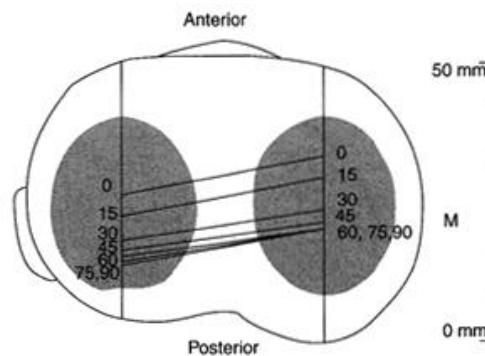


Fig.3.19: Tibiofemoral contact area (mean value) and contact point of the condyles from 0° to 90°. (Peterson et al., [25])

The forces acting between patella and femur depend on the contact area too. This area changes with the flexion angle like the tibiofemoral contact area, and it has a mean value of about 400 mm² (Nigg et al., [23]). In the literature, the forces acting between patella and femur are evaluated only in terms of perpendicular force, perpendicular with respect to the axis of the patella (Van Eijden et al. 1986, [32]; Yamaguchi et al. 1989, [33]). In this thesis, the forces acting at the patellofemoral surface are evaluated in terms of shear and compression load with respect to the femur as described above and they are sum to the shear and compression load deriving from the contact between femur and tibia, although the point of application is different (as described in par.7.6.1.6 and par.7.6.2.5). Then, the previous values of 4000N for the maximum tension load, 5600N for the maximum compression load and 2000 N for the maximum shear load are assumed.

3.6.Knee contact forces and ACL strain: in-vivo measurement and analytical models

In the literature there are some studies about the knee contact forces measured in vivo. The first device, implanted in tibia, was used in 2004 and measured only uniaxial forces; however it was possible to calculate the center of pressure and the mediolateral distribution of forces (D’Lima et al. 2005, [8]; D’Lima et al. 2006 [9]; D’Lima et al. 2005 [10]). In 2005 by using new devices it was possible to measure all components of forces and moments (D’Lima et al. 2007, [6]; D’Lima et al. 2008, [7]; Heinlein B et al. 2009, [12]; Kircking B et al. 2006, [18]; [12]; Kutzner I et al. 2011, [20]). These studies focused on the recovery period after knee arthroplasty in order to evaluate in particular the peak tibial force during daily life

activities. The most important activities which were investigated are walking and stair ascent and descent; however in a recent study (D’Lima et al. 2013, [5]) a peak tibial value of 1,5x BW (BW: body weight) is suggested for the knee extension movement with a resistance to the movement of 0,2x BW. Because of the value of resistance of the knee extension movement analyzed in this thesis is higher than 0,2x BW, the peak tibial force of 1,5x BW can’t be assumed as a reference value for a comparison.

About the anterior cruciate ligament, in vivo studies were done in order to obtain the strain of the ligament as function of the knee flexion angle. In particular, in the study done by Beynnon et al. (Beynnon et al. 1997, [4]; Beynnon et al. 1998, [2]) the strain of the ACL were measured by using a DVRT (Differential Variable Reluctance Transducer, Microstrain Inc., Burlington, VT, USA) embedded to the central part of the ACL of eight healthy subjects (fig.3.20). The subjects were asked to perform some exercises, in particular four cycles of flexion-extension movement without any resistance in a sitting position (fig.3.21). Because there is not resistance during the movement, the flexion phase should be considered the eccentric phase of the extension movement.

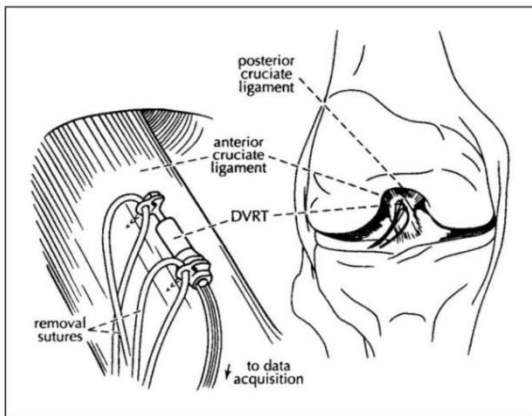


Fig.3.20: DVRT implantation in Beynnon’s study. (Beynnon et al. 1998, [2])

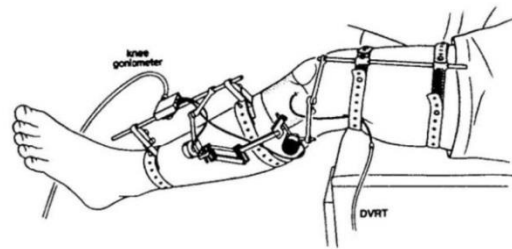


Fig.3.21: Execution of the flexion-extension movement in Beynnon’s study. (Beynnon et al. 1998, [2])

The results are shown in fig.3.22: in the eccentric phase, the ACL is strained between 10° and 38° with a maximum strain of 3,8%, in the concentric phase it is strained between 10° and 27° with a maximum strain of 3,2%.

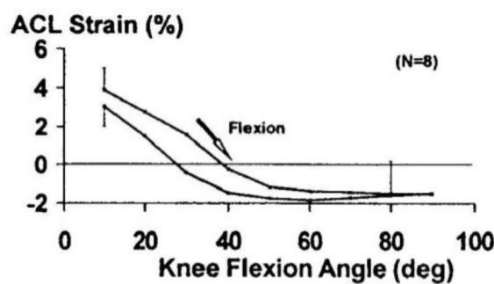


Fig.3.22: ACL strain during the flexion-extension movement in Beynnon’s study. (Beynnon et al. 1998, [2])

The force acting at the ACL is indirectly investigated also in another study done by Kaufman et al. (Kaufman et al. 1991, [15]). In this study the isokinetic flexion-extension movement was investigated: the subjects were asked to perform the exercise at 60°/s and at 180°/s at their maximum effort. By using an analytical model it was possible to obtain the muscular forces and the reaction forces between tibia and femur and between patella and femur. To validate the muscular forces calculated with the model, electromyography was used in order to compare the muscular activation. The results of the contact forces at the tibiofemoral articulation are shown in fig.3.23 and fig.3.24, in which the results are normalized to the body weight (BW). Fig.3.23 shows the results for the extension phase. The maximum compression force at tibia is at 55° knee angle and it has a value of $(4,0 \pm 0,7) \times BW$ at 60°/s and $(3,8 \pm 0,9) \times BW$ at 180°/s. The shear load is positive between 40°-100° with a maximum value of $(0,5 \pm 0,1) \times BW$ at 60°/s and $(0,6 \pm 0,1) \times BW$ at 180°/s at 70°-80°; the shear load is negative from 40° to the full extension with a maximum value of $(0,3 \pm 0,005) \times BW$ at 60°/s and $(0,2 \pm 0,005) \times BW$ at 180°/s at 25°. For the convention used in the model, if the shear load is positive, the force points backward with respect to the longitudinal axis of the tibia; if the shear load is negative, the force points forward with respect to the longitudinal axis of the tibia. Thus, in the range full extension-40° the ACL is strained and the PCL unstrained, in the range 40°-100° the ACL is unstrained and the PCL is strained. These results confirmed the in vivo results obtained by Beynnon et al. (fig.3.22). Fig.3.24 shows the results for the flexion phase. The maximum compression force at tibia is $(2,1 \pm 1,2) \times BW$ at 30° at 60°/s and $(1,6 \pm 1,1) \times BW$ at 40° at 180°/s. The shear load is always positive with a maximum value of $(1,7 \pm 0,8) \times BW$ at 60°/s and $(1,4 \pm 0,5) \times BW$ at 180°/s at 75°. Because of the shear load is always positive, in the flexion phase only the PCL is strained.

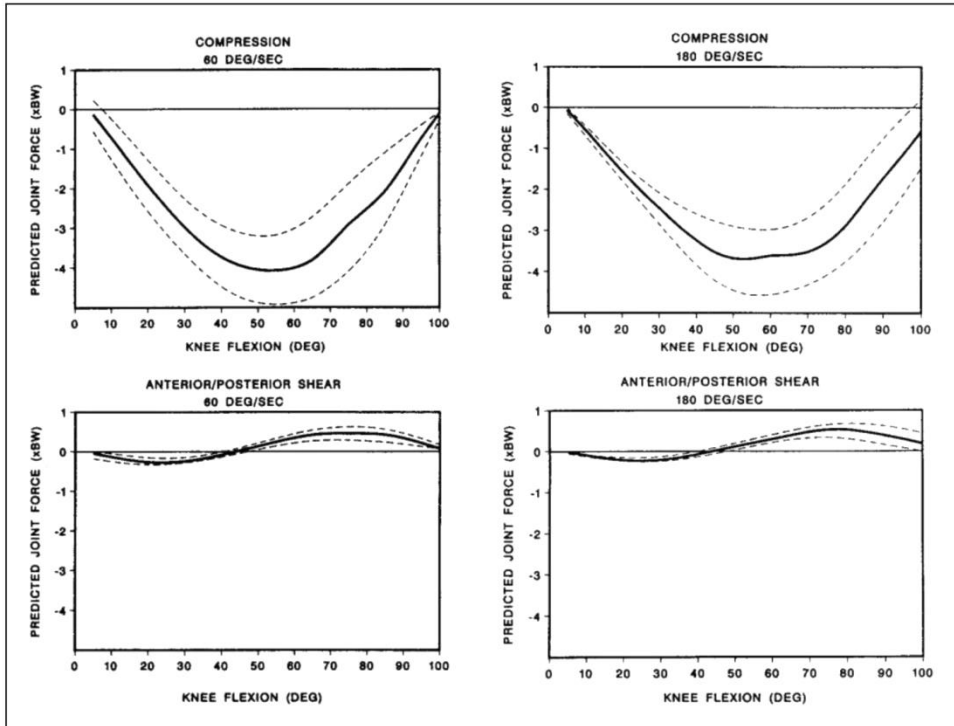


Fig.3.23: Compression load and shear load acting at tibia during isokinetic EXTENSION at 60°/s and 180°/s in Kaufman’s study. Results normalized to BW. Shear force positive: the force points backward. (Kaufman et al. 1991, [15])

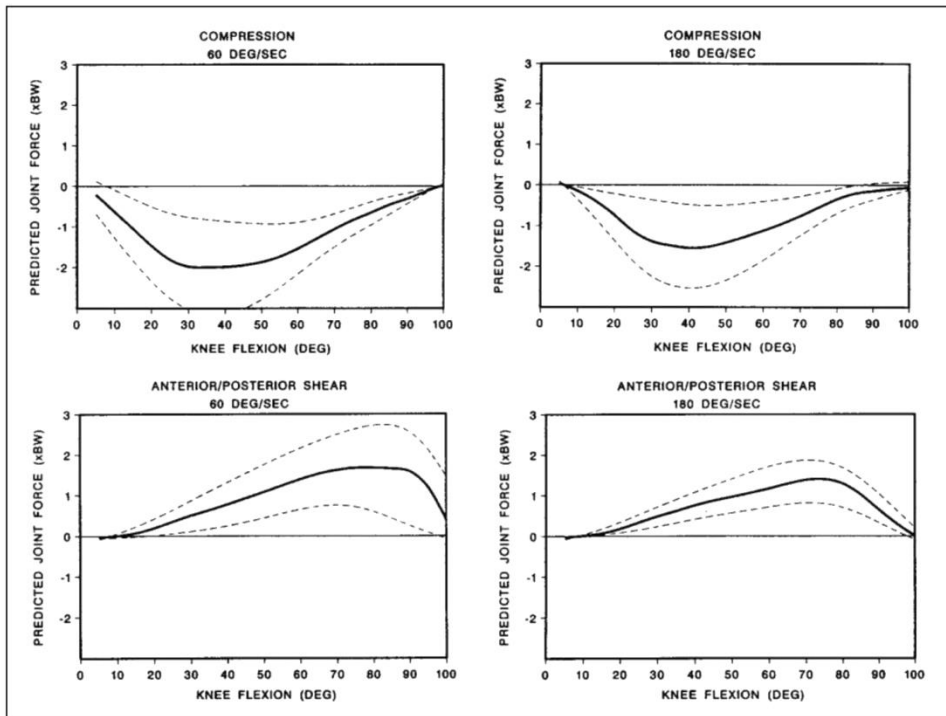


Fig.3.24: Compression load and shear load acting at tibia during isokinetic FLEXION at 60°/s and 180°/s in Kaufman’s study. Results normalized to BW. Shear force positive: the force points backward. (Kaufman et al. 1991, [15])

3.7. In-vivo study of the knee flexors and extensors balance

In literature there are many studies about the knee flexors and extensor balance during the knee flexion-extension. To compare the results of this thesis, the study done by Pontaga I 2004, [26], was chosen. In that study, 11 male subjects with average age $24,3 \pm 4,5$ years were asked to perform the flexion extension movement by using an isokinetic machine, REV9000 by Technogym, at $100^\circ/s$ and $200^\circ/s$. To evaluate the knee flexors and extensor balance, the ratio between the torque in flexion and the torque in extension is used. The importance of this parameter is that it is related to the risk of injuries: if its value is closer to 1, the risk is modest (Worrel 1994, [33]). The results of the study are shown in fig.3.25:

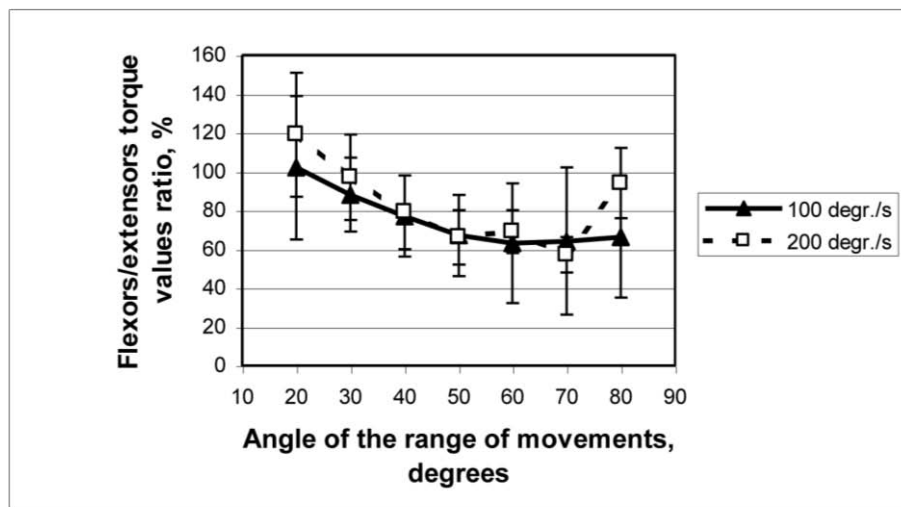


Fig.3.25: Knee flexors-extensors ratio in [%] in Pontaga's study. (Pontaga I 2004, [26])

The minimum knee flexors/ extensors peak torques ratios are $61\% \pm 7\%$ at $100^\circ/s$ and $70\% \pm 9\%$ at $200^\circ/s$. Moreover, the angular positions of the peak torques are the same in the knee extension at the medium and high velocity movements. In the ROM $10^\circ-30^\circ$, the knee flexors/extensors torques ratio has higher value; moreover, in the same ROM, the ratio has higher value at $200^\circ/s$ than at $100^\circ/s$.

4.Musculoskeletal modeling: the software OpenSim

“OpenSim is a freely available, user extensible software system that lets users develop models of musculoskeletal structures and create dynamic simulations of movement.” (cit. from OpenSim support online, [38]).

One of the most important fields in which this software is used is rehabilitation, in order to study people with physical diseases or limited mobility, due to physical or psychological disorders (for example cerebral palsy and osteoarthritis), and to suggest useful treatments, like strengthening exercises. Another important application is in orthopedics, in which OpenSim is used for instance to predict the effect of a tendon transfer in terms of muscle length and in terms of reaction loads acting at the articular joints.

In this study, OpenSim was used to obtain the muscle activation and to evaluate the articular loads acting at the knee joint.

In the paragraphs here below, the aim is to describe how OpenSim works. The steps can be synthetized in:

- 1) choice of the model and Scaling
- 2) Inverse Kinematics
- 3) Inverse Dynamics
- 4) Static Optimization
- 5) Joint Reaction Analysis

Furthermore, at the end of the chapter, the schematization used by the software to analyze the knee will be described.

4.1.Choice of the model and Scaling

First, an appropriate model must be chosen from the models available. In the literature there are different type of models, which differs for: the portion of human body modelled (upper part, lower part or total body models), the number of degrees of freedom (different number of joints and different number of coordinates for each joint), the number and the type of muscles. In this study, the gait2392 model (fig.4.1) was chosen. This model represents the trunk, the pelvis, the legs and the foots; it has twenty-three degrees of freedom and ninety-two muscles. The choice of this model is justified because the exercises considering in this study regard only the lower part of the body.



Fig.4.1: OpenSim model (gait2392_model): bones and muscles are shown.

After that, the model must be scaled: the bones and the muscles of the model must be adapted to the real subject. To do this, it is necessary to know the total weight of the subject and to define an appropriate markerset, which is a virtual reproduction of the experimental markers applied on the skin of the subject (about the markerset used in this thesis see chap.6). Furthermore, the input file for the experimental markers must be a static trial. The scaling tool adapts the model in order to reduce the gap between virtual markers and experimental markers. Fig. 4.2 is an example of scaling in which it is possible to see virtual and experimental markers.



Fig.4.2: Example of scaling (the blue markers are the experimental markers; the pink markers are the virtual markers).

To check the accuracy of the analysis the maximum error between experimental and virtual markers should be less than 2 cm and the maximum RMS (root mean squared) error less than 1 cm (OpenSim

support online, [38]). These values of error and RMS could be obtained with an iterative process by changing the position of the virtual markers and by modifying their weight. Each marker has a proper weight, which defines its importance during the scaling process: a higher value is assigned when the experimental marker is placed in a position which is simple to identify in OpenSim too, and so the position of the virtual marker is quite near to the experimental one.

However, by using the weight of the subject and the markerset it is possible to scale only the bones of the model (in terms of length and inertial properties), but not the muscles. To adapt the muscles, in terms of maximum isometric force, the relations suggested by Lee et al. 2000, [21] should be used:

$$F_{\text{iso MAX adj}} = \frac{SM_{\text{real sub}}}{SM_{\text{model}}} \cdot F_{\text{iso MAX model}}$$

in which $F_{\text{iso MAX model}}$ is the maximum isometric force for the j^{th} muscle in the reference model (gait2392_simbody.osim), $F_{\text{iso MAX adj}}$ is maximum isometric force for the j^{th} muscle adapted to the real subject, SM_{model} and $SM_{\text{real sub}}$ are the “skeletal muscle” of the model and the skeletal muscle of the real subject evaluated by the following expression:

$$SM = 0,244 \cdot \text{weight} + 7,8 \cdot \text{height} + 6,6 \cdot \text{sex} - 0,098 \cdot \text{age} + \text{race} - 3,3$$

in which: weight = [kg]; height = [m]; sex = 0 for female and 1 for male; race = -1,6 for Asians, 1,9 for African-American, 0 for white or Hispanic.

The gait2392_model represents a subject that is about 1,8 m tall and has a mass of 75,16 kg, but no information about sex, age and race are specified. However the maximum isometric force of the gait2392_model is the same of another model available, the FullBodyModel_SimpleArms_Hamner2010 model, which represents a 99-year-old white male subject that is 1,67 m tall and has a mass of 75,16 kg. By considering these information, it has been possible to calculate the SM of the gait2392_model:

$$SM_{\text{model}} = 0,244 \cdot 75,16 + 7,8 \cdot 1,67 + 6,6 \cdot 1 - 0,098 \cdot 99 + 0 - 3,3$$

Moreover if the model adjusted in terms of muscles is still “too weak” at the static optimization analysis (as described in par.4.4), external generalized forces, called actuators, must be used at the coordinates which are weak in order to have a muscular activation less than 1, which is the maximum value allowed.

Fig. 4.3 summarizes the files used in scaling: the model (gait2392_simbody.osim), the markerset (MarkerSet.xml), the setup file with the weight of the markers (Scale_Setup.xml), the experimental position of the markers in a static trial (staticpose.trc). The result is the model scaled in terms of bones

(Scaled_Model.osim); by considering the relation suggested by Lee et al. for the muscles, the model is scaled also in terms of muscles (Scaled_Model_adj.osim).

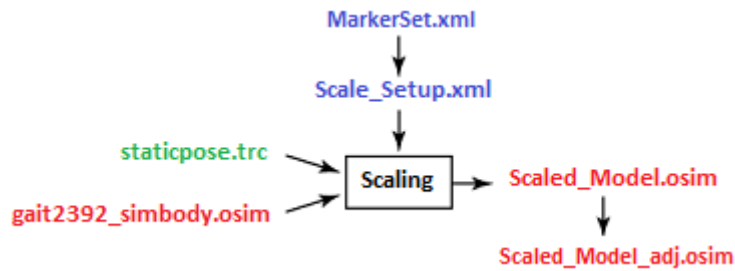


Fig.4.3: Input and output files in Scaling.

4.2. Inverse Kinematics (IK)

With the Inverse Kinematics it is possible to reconstruct the movement in terms of spatial coordinates ; the algorithm used by the software is the following (OpenSim support online, [38]):

$$\min_{\mathbf{q}} \left[\sum_{i \in \text{markers}} w_i \| \mathbf{x}_i^{\text{exp}} - \mathbf{x}_i(\mathbf{q}) \| + \sum_{j \in \text{unprescribed coords}} \omega_j (q_j^{\text{exp}} - q_j) \right]$$

in which: \mathbf{q} is the vector of the generalized coordinates being solved for; $\mathbf{x}_i^{\text{exp}}$ is the experimental position of the marker i , $\mathbf{x}_i(\mathbf{q})$ is the position of the corresponding marker on the model, q_j^{exp} is the experimental values of the coordinate j . Prescribed coordinates (for example fixed joints) are set to their experimental values ($q_j^{\text{exp}} = q_j$).

In the inverse kinematics, the scaled model, deriving from scaling, must be used, so the position of the markers in the IK derives from that obtained by scaling and mustn't be changed. The only thing that is possible to modify to improve the IK results is to modify the weight of the markers. The weight of the coordinates instead should be omitted. As in scaling, to check the accuracy of the IK, the maximum error between experimental and virtual markers should be less than 4 cm and the maximum RMS error less than 2 cm (OpenSim support online, [38]).

Fig.4.4 summarizes the files used in IK: the scaled model (Scaled_Model_adj.osim), the setup file with the weight of each marker (Setup_IK.xml), the experimental dynamic trial (dynamic_trial.trc). The resultant file (IK_results.mot) is a file with the values of the generalized coordinates during the movement.

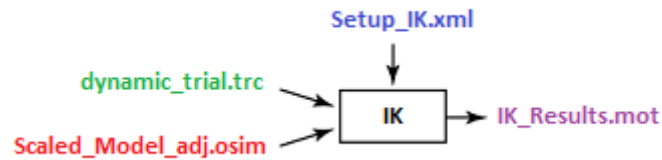


Fig.4.4: Input and output files in IK.

4.3. Inverse Dynamics (ID)

The Inverse Dynamics determines the moments which act at the articular joints. These moments are evaluated by considering the inertial effects deriving from the kinematics (and so are evaluated by considering the generalized coordinates solved at the IK) and the external forces and moments acting during the movement; the muscle single contribution instead is not resolved.

The equation solved by the software is the here below (OpenSim support online, [38]):

$$\boldsymbol{\tau} = \mathbf{M}(\mathbf{q}) \ddot{\mathbf{q}} + \mathbf{C}(\mathbf{q}, \dot{\mathbf{q}}) + \mathbf{G}(\mathbf{q})$$

in which $\boldsymbol{\tau}$ is the vector of the generalized forces being solved for; $\mathbf{M}(\mathbf{q})$ is the system mass matrix; \mathbf{q} , $\dot{\mathbf{q}}$ $\ddot{\mathbf{q}}$ are the vectors of the position, velocity and acceleration respectively; $\mathbf{C}(\mathbf{q}, \dot{\mathbf{q}})$ is the vector of the Coriolis and centrifugal forces; $\mathbf{G}(\mathbf{q})$ is the vector of the gravitational forces.

Fig.4.5 shows the input and the output files for ID, in particular the setup file (Setup_ID.xml), in which the model (Scaled_Model_adj.osim) the external loads (forces.xml) and the results of the IK analysis (IK_results.mot) are specified. The result is a file with the moments acting at the articular joints (ID_forces.sto).

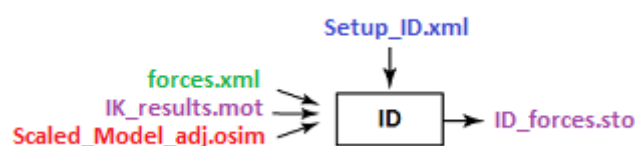


Fig.4.5: Input and output files in ID

4.4.Static Optimization (SO)

With the Static Optimization it is possible to evaluate the muscle forces instant by instant by minimizing the following objective function (OpenSim support online, [38]):

$$J = \sum_{m=1}^n (a_m)^p$$

in which a_m is the activation level of the muscle m and p is an exponent defined by the user. In literature, the most common value for p is 2; thus also in this study the value of p is set to 2. The activation level a_m is defined by the following relation:

$$\sum_{m=1}^n [a_m \cdot f(F_m^0, l_m, v_m)] \cdot r_{m,j} = \tau_j$$

in which $f(F_m^0, l_m, v_m)$ is the force-length-velocity relation, F_m^0 is the maximum isometric force of the muscle m , l_m is the length of the muscle m , v_m is the shortening velocity of the muscle m , $r_{m,j}$ is the moment arm of the muscle m about the j^{th} joint axis, τ_j is the moment acting at the j^{th} joint (the result of the ID).

It is possible to not consider the force-length-velocity relation, so the previous equation becomes a function only of a_m , F_m^0 and $r_{m,j}$:

$$\sum_{m=1}^n [a_m \cdot F_m^0] \cdot r_{m,j} = \tau_j$$

However, in this study the complete equation with the force-length-velocity relation was considered, in order to get more precise results.

The output of the SO are the muscle forces acting during the movement, which can be expressed in terms of [N] or in terms of muscle activation (percentage of the maximum isometric force of each muscle). To validate the results it is useful to compare the muscular activation from that measured with the electromyography. The comparison which was done in this thesis is described in chap.7.

Fig.4.6 shows the input and the output files for the SO. The results are the muscle force (muscle_force.sto) and the muscle activation (muscle_act.sto).

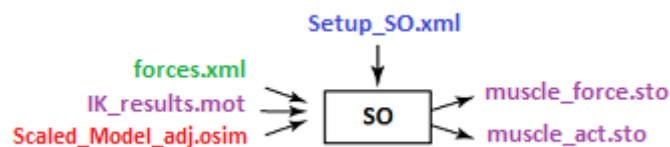


Fig.4.6: Input and output files for SO.

4.5. Joint Reaction Analysis

With the Joint Reaction analysis it is possible to evaluate the reaction forces which act at the articular joints during the movement. Joint Reaction analysis differs from ID because in addition to external loads and inertial effects, also the muscle activation, evaluated by the SO, and the contact forces (deriving from the direct contact bone-bone) are considered.

In fig.4.7 the input and the output files for the Joint Reaction analysis are shown, in particular the setup file (Setup_JR.xml), in which the model (Scaled_Model_adj.osim) the external loads (forces.xml), the muscle forces (muscle_forces.sto) and the results of the IK (IK_results.mot) are specified. The result is a file with the joint reaction loads (ReactionLoads.sto).

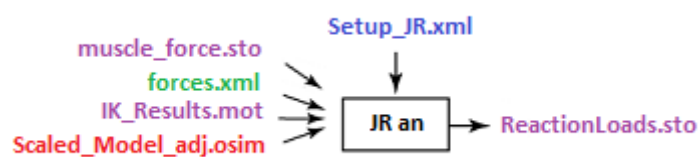


Fig.4.7 Input and output file for Joint Reaction analysis.

4.6. Knee modeling in gait_2392 model

Fig.4.8 and fig.4.9 show how the knee is modelled in gait2392_model: tibia and femur are represented, the patella is omitted. However, this is only a representation, because patella is considered in order to evaluate correctly the contact forces at this joint. As a matter of fact, the contribution given by the patella is evaluated by using the Yamaguchi model (Yamaguchi et al. 1989, [29], as described in par.3.4). Thus the contact forces between tibia and femur but also between patella and femur are considered (as described in OpenSim support online, [36]). Because the patella is not represented, the tendon of the quadriceps isn't shown and the four fascicles of this muscle (rectus femoris, vastus medialis and lateralis, and vastus intermedius) insert indirectly on virtual points which represents the real attachment points on the patella. Another consequence of this modeling, is that the patellar tendon isn't shown. In OpenSim support online, [36], no information about how the force at the quadriceps is calculated. As a matter of fact, as described in par.3.4, by using the Yamaguchi model the moment arm of the tendon of the quadriceps differs from the moment arm of the patellar tendon, and so the force at the quadriceps has different values if it is evaluated by considering one moment arm or the other. Aim of this thesis is to verify how the force at quadriceps was calculated in the software.

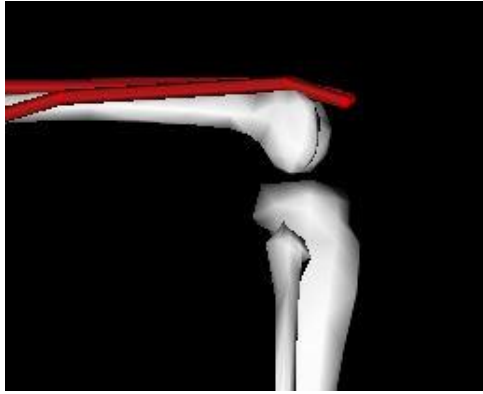


Fig.4.8: Knee modeling in gait2392_model. Tibia, femur and quadriceps are shown (lateral view).



Fig.4.9: Knee modeling in gait2392_model. Tibia, femur and quadriceps are shown (frontal view).

Moreover by using this schematization, no ligaments are considered. Thus, from the simulations it isn't allowed to obtain the forces acting at ACL or PCL.

5.Aim of the study

The study is divided into two parts.

In the first part, the knee flexion-extension was investigated in isokinetic conditions at different velocities by using an isokinetic machine, REV7000 by Technogym (fig.5.1). The aim was to determine the influence of the velocity in terms of performances, in particular by considering muscle activation, and in terms of bio-mechanical parameters. Moreover, in order to validate the results, comparisons between muscle activation obtained by using electromyography and OpenSim and between bio-mechanics parameters obtained by analytical models and numerical model were done. Thus, this first study focused on:

- evaluation of torque performances at different velocities by calculating the flexors and extensors balance;
- evaluation of the muscle experimental electromyographic activation at different velocities and comparison with that obtained numerically by using the software;
- evaluation of the most important bio-mechanical parameters at different velocities and comparison between those obtained by analytical models and those calculated with the software;
- eventually evaluation of safety conditions, in terms of velocity and range of motion, which avoid to overloading articulations, tendons and ligaments.



Fig.5.1: Isokinetic machine, REV7000 by Technogym.

In the second part, the knee flexion-extension was investigated at different intensities of the exercise by using two different types of fitness machines: in the first one, the resistance to the movement is due to a cable connected to a weight stack by a system of pulleys (fig.5.2); in the second one, the resistance is directly due to the weight of some cast iron discs placed on the specific bar (fig.5.3).



Fig.5.2: 'Cables machine'.



Fig.5.3: 'Free-weights machine'.

In this second part, the influence both of the type of bench and the intensity of the exercise on muscle activation and bio-mechanics parameters was examined; in particular, as done for the first part, for each bench the following analysis were done:

- evaluation of the muscle experimental electromyographic activation at different intensities and comparison with that obtained numerically by using the software;
- evaluation of the most important bio-mechanical parameters at different intensities and comparison between those obtained by analytical models and those calculated with the software;
- eventually evaluation of safety conditions, in terms of intensity and range of motion, which avoid to overloading articulations, tendons and ligaments.

Moreover, the results of muscle activation and bio-mechanics parameters of the first bench were compared with those of the second one in order to indicate possible differences and in order to identify eventually the more safety machine.

PART 1: KNEE ISOKINETIC FLEXION-EXTENSION

6. Material and Methods of Part 1

For this first part of the thesis, the knee flexion-extension movement was investigated in isokinetic conditions by using an isokinetic machine, REV 7000 by Technogym, shown in fig.6.1.



Fig.6.1: Isokinetic machine REV 7000 by Technogym.

With this machine, exercises are allowed at shoulder, ankle, wrist and knee and both for the right side and the left side of the body. In this study, only the right knee flexion-extension was investigated. The knee flexion-extension was performed by using the specific bar shown in fig.6.1. The upper extremity of the bar was fixed to the servo-motor of the machine and at the lower extremity there was a device connected to the ankle which lets two degrees of freedom: the translation along the bar and the rotation around the axis perpendicular to the longitudinal axis of the bar.

By using this machine, it was possible to perform isokinetic and also isometric exercises. In isokinetic conditions, the velocity of the movement was fixed and the subject had to perform the exercise against a certain resistance, applied by the servo-motor, which decreased with the increase of the velocity. In isometric exercises, the leg was fixed in a certain position and the subject had to perform his maximum effort both in flexion and in extension in order to evaluate the maximum isometric force.

Both for isokinetic and isometric tests, the output of the machine was the torque applied by the subject evaluated at the servo-motor, which could be considered as a first parameter useful to evaluate the efficiency of the exercise.

In this study six male healthy subjects were tested. The most important parameter in the choice of the subjects was the physical condition, which was good for everyone; after that, weight and height were used to further select them: height: 1,67-1,85 m; weight: 63-88 kg.

Every subject was asked to perform five cycles of flexion-extension at 240°/s, 180°/s, 120°/s and 60°/s in the range 25-95° of the flexion angle measured at the servo-motor with an encoder (as a matter of fact, because the knee and the servo-motor weren't perfectly aligned, the flexion angle measured by the machine and the real knee flexion angle are different (fig.6.2 and fig.7.3)). Between an exercise and the other, there was an enough period for a full recovery. For each velocity the subject was asked to do his maximum both in extension and in flexion and without any stop between the two phases. The choice of these velocities is justified because the aim is to consider a wide range of velocities and to compare the results of this study with those of another previous thesis done by Tregnaghi et al. (Tregnaghi et al. 2010, [30]), in which the same exercises were performed by using the same machine. The results will be compared also with the results obtained by Kaufman et al. (Kaufman et al. 1991, [15]), as described in par.3.6.

After that, isometric tests were done at 95°, 70°, 55°, 40° and 25° of the flexion angle measured by the machine. During the isometric tests, for the first 5 seconds the subject was asked to do his maximum in extension, then there was a period of relax of 10 seconds, and at the end another period of 5 seconds in which the subject was asked to do his maximum in flexion. Between an isometric test and the other, there was an enough period for a full recovery.

Fig.6.2 shows how the exercises were performed. During the tests, the right femur was fixed to the machine by using a specific device; torso, pelvis and left leg could be considered in a fixed position too.



Fig.6.2: Test conditions.

To reconstruct the spatial movement (kinematics), an optoelectronic system (BTS Engineering) was used (fig.6.3). This system is composed by five cameras coaxial with infrared led lamps which illuminate some reflective markers; the markers were placed on the skin of the subject and on the bar of the machine. About the markers on the subject, they were placed in correspondence of sternum, ASIS (right and left), medial and lateral condyle (right and left), medial and lateral malleolus (right and left), first metatarsal bone (right and left). The markers on the left side of the body were used to scale the model in OpenSim. Because during the movement the markers on the medial and lateral malleolus were covered by the bar, a local reference system embedded to right tibia and a static trial, which was done before the tests, were used in order to obtain the trajectory. The static trial was also necessary to scale the OpenSim model. Other three markers were placed on the machine in order to obtain the kinetic conditions during the movement (as described in par.7.3).

The markers on the subject and the reference system embedded to the right tibia are shown in fig.6.4 and fig.6.5. Fig.6.6 shows the static trial.



Fig.6.3: Optoelectronic system (only three cameras are shown).



Fig.6.4: Electrodes and markerset (anterior view).



Fig.6.5: Electrodes and markerset (lateral view).



Fig.6.6: Static trial.



Fig.6.7: Pocket EMG BTS.

To evaluate the exercises in terms of muscular activation, surface electrodes were used. The muscles which were analyzed in this study are Rectus Femoris right, Vastus Lateralis right and Vastus Medialis right for the extension phase, Biceps Femoris caput longus right for the flexion phase (fig.6.4 and fig.6.5). This choice is justified because these muscles are the most involved during the movement and for the easiness in their identification (for the flexion phase other muscles could be chosen, but they were not easy to identify and so the EMG signal wouldn't be precise).

Electromyographic signal was synchronized with the BTS system by using a pocket EMG BTS (fig.6.7), a device which allows to collect the signal and sends the information to the optoelectronic system.

7.Data analysis of Part 1

7.1.Evaluation of flexors and extensors balance

To evaluate the flexors and extensors balance during the exercises, in a similar way to that described in par.3.7, for each subject and each velocity the ratio between the torque at the servo-motor in flexion normalized to the body weight, T_F , and the torque at the servo-motor in extension normalized to the body weight, T_E were used: $R_{F/E} = T_F/T_E$. The normalization to the body weight was done in order to have a better comparison between the subjects and to obtain a ranking of performances.

7.2.Kinematic analysis

To obtain the spatial movement, the trajectory of the markers which were placed on the skin of the subject was used. The trajectory was first reconstructed by using a model with the software Smart Tracker (fig.7.1) and then interpolated by using a protocol created with another software, the Smart Analyzer.

For markers placed on medial and lateral malleolus, a specific protocol was used, because during the movement these markers were covered by the bar and so it wasn't possible to reconstruct the trajectory despite of interpolating the coordinates. To solve the problem, a local reference system embedded to the right tibia and the static trial shown in fig.6.6 were used. During the static trial the markers on the ankle were not covered by the bar and so it was possible to evaluate their position with respect to the local reference system embedded to the right tibia. These coordinates, evaluated during the static trial, were used as offset values to calculate the position of the two markers during the exercises with respect to the local reference system, which was always visible during the movement.

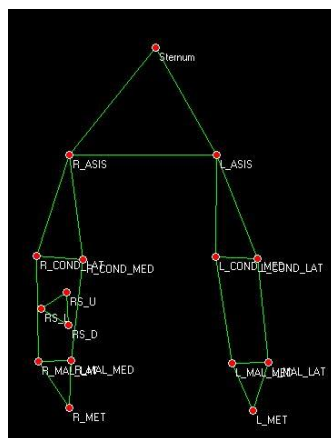


Fig.7.1: Tracker model used in kinematics analysis.

7.3.Kinetic analysis

By considering the torque at the servo-motor and the markers placed on the machine, it was possible to calculate the external forces acting on tibia.

Fig.7.2 shows the markers which were used to obtain the kinetic conditions during the exercises: the marker 1 was put on the center of rotation of the servo-motor, the markers 2 and 3 were put at the lower part of the bar on the mechanism connected to the ankle.

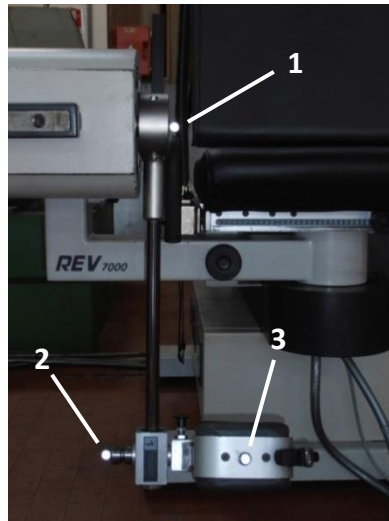


Fig.7.2: Markers on the machine which were used for the kinetic analysis.

Markers 2 and 3 were used to identify the point of application of the force: by using the reference system shown in fig.7.3 the x and the y position of the point of application are defined by the x and y coordinate of the marker 2, the z coordinate by the z coordinate of the marker 3 ($x_{pa} = x_2$, $y_{pa} = y_2$ and $z_{pa} = z_3$ in which x_{pa} , y_{pa} and z_{pa} are the coordinates of the point of application and x_2 , y_2 and z_3 are the x and y coordinates of the marker 2 and the z coordinate of the marker 3 respectively).

In fig.7.3 the force exerted by tibia to bar during the extension phase is shown. The torque at the motor, T , is the result of the force F_M acting perpendicularly to the bar, in the x-y plane and at the point of application calculated above: $T = F_M \cdot r_M$, in which r_M , the lever-arm of the force F_M , is evaluated as distance between marker 1 and 2 in the x-y plane ($r_M = \sqrt{(x_2 - x_1)^2 + (y_2 - y_1)^2}$).

Because of the misalignment of the knee with respect to the axis of rotation of the servo-motor, F_M isn't the real force exerted by tibia (however, the misalignment is modest). The force exerted by tibia, F , has the same point of application calculated above, but it is considered perpendicular to tibia, in the x-y plane and its value is calculated with the following equations:

$$F = F_M \cdot \cos((\theta_F + \varphi_k) - \theta_M)$$

$$F = \frac{T \cdot \cos((\theta_F + \varphi_k) - \theta_M)}{r_M}$$

in which $(\theta_F + \varphi_k)$ is the inclination of force F (see par.7.6) and θ_M is the inclination of the force F_M (and also the flexion angle of the bar).

In the equations above, the force F has been calculated by considering only the x-y plane; it is reasonable to do this because during the exercises the position of the knee was fixed and the only movement allowed was the flexion-extension movement. Thus the components of the force F are only in the x-y plane:

$$F_x = F \cdot \cos(\theta_F + \varphi_k)$$

$$F_y = F \cdot \sin(\theta_F + \varphi_k)$$

$$F_z = 0$$

Moreover, the resultant forces are the net forces acting during the movement; that's because, before every exercise, the machine calculates the moment due to the weight of tibia, foot and bar and subtract it to the global torque measured during the tests.

By changing the sign of the torque T (it is considered positive for the extension phase, negative for the flexion phase), with the same equations written above it is possible to calculate the forces acting during the flexion phase. Moreover, because the force F has been evaluated as force exerted by the tibia to the bar, the force acting on the tibia has components $F_{x \text{ tibia}} = -F_x$; $F_{y \text{ tibia}} = -F_y$; $F_{z \text{ tibia}} = 0$.

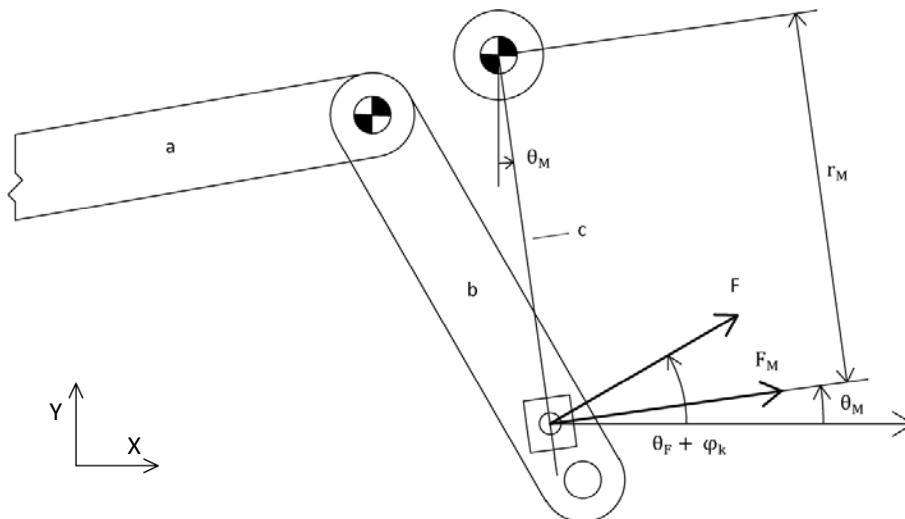


Fig.7.3: Schematic representation of the force F exerted by the tibia to the bar in the extension phase.
a:femur; b:tibia, c:bar of the machine.

7.4. OpenSim simulations

To scale the model, the static trial (fig.6.6) was used. The muscles of the right side of the model were adjusted by using the relation suggested by Lee et al.

The static trial was also used to constrain the model in order to simulate the real conditions during the exercises. Because during the movement pelvis, torso and left leg could be considered in a fixed position, the degrees of freedom related to these bodies were also fixed in the OpenSim model by considering the values of the static trial: it is reasonable to do this because the position of these bodies was more or less the same of that in the static trial. Moreover the degree of freedom related to the flexion movement of the right femur (hip_flexion_r) was fixed because the knee was fixed too; the adduction and the rotation movement of the right femur were instead kept not constrained, in order to let the model follow the trajectory of the markers on the ankle. Thus, the degrees of freedom which were not constrained are: hip_adduction_r, hip_rotation_r, knee_angle_r, ankle_angle_r, subtalar_angle_r, mtp_angle_r.

Both for scaling and inverse kinematics, the conditions related to maximum error and RMS between experimental and virtual markers were satisfied for the right leg: the maximum error was less than 2 cm and the RMS less than 1 cm in scaling and the maximum error was less than 4 cm and 2 cm in inverse kinematics.

The external force was applied as described in the previous paragraph. In fig.7.4. an example of application of the external force during the flexion phase is shown.

Because sometimes the model adjusted in terms of muscles was “too weak” at the static optimization analysis, actuators were put at the following coordinates: knee_angle_r, ankle_angle_r, subtalar_angle_r, mtp_angle_r.

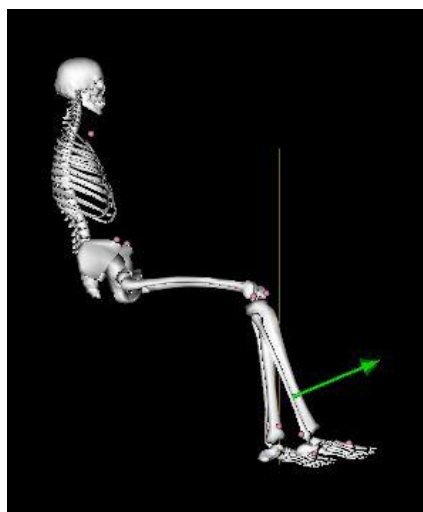


Fig.7.4: Example of application of the external force in flexion in OpenSim simulations.

7.5.EMG analysis

The “raw” EMG signal was rectified and lowpass filtered at 6 Hz. After that, it was normalized to the maximum effort that the subject was able to do during the isometric tests and during the isokinetic tests: as a matter of fact, it happened that the muscular activation was higher during the isokinetic exercises than the isometric ones.

The normalized signal was then compared to the muscular activation obtained by OpenSim simulations by considering the second, the third and the fourth cycle of the isokinetic tests. To compare the results in a quantitative way, the following parameters were used (as done by Tregnaghi et al.):

$$\text{Peak error [\%]} = \frac{\text{Peak}_{\text{EMG}} - \text{Peak}_{\text{OSIM}}}{\text{Peak}_{\text{EMG}}} \cdot 100$$

$$\text{Time error [\%]} = \frac{\text{Peak_Time}_{\text{EMG}} - \text{Peak_Time}_{\text{OSIM}}}{T} \cdot 100$$

$$\text{Area error [\%]} = \frac{\text{Area}_{\text{EMG}} - \text{Area}_{\text{OSIM}}}{\text{Area}_{\text{EMG}}} \cdot 100$$

in which Peak error expresses the difference between the EMG and the OpenSim signal in terms of maximum activation (Peak_{EMG} and $\text{Peak}_{\text{OSIM}}$ are the values of the maximum activation in the EMG signal and in the OpenSim signal respectively), Time error expresses if the two signals are synchronized or not ($\text{Peak_Time}_{\text{EMG}}$ and $\text{Peak_Time}_{\text{OSIM}}$ are the time at which there is the maximum activation in the EMG signal and in the OpenSim signal respectively, T is the time spent for a complete cycle flexion-extension), Area error expresses the difference between the EMG and the OpenSim signal in terms of area during a cycle ($\text{Area}_{\text{EMG}} = \int_T \text{EMG}_{\text{signal}} dt$ and $\text{Area}_{\text{OSIM}} = \int_T \text{OSIM}_{\text{signal}} dt$).

These parameters were evaluated for each subject and expressed as mean and standard deviation by considering the three cycles investigated (second, third and fourth cycle). After that, the parameters calculated for each subject were used to obtain peak error, time error and area error as averaged values by considering all the subjects.

7.6. Analytical simulations

The exercises considered in this study, can be analyzed with an analytical approach.

The first step in the definition of an analytical model, is to divide the human body into “segments” (also called “bodies”), connected together by joints; the length and the inertial properties (mass and moment of inertia) of each segment, are usually defined as function both of the total weight and the total height of the subject. After that, muscles must be considered: they should be represented as forces acting at the segments which they are attached to. Considering muscles as forces, line of action and moment-arm are the most significant parameters used to define them.

About the knee flexion-extension, in the literature there are many analytical 2D-models (as a matter of fact, because of the knee flexion-extension can be considered a planar movement, 2D-models can be used instead of 3D-models) which are different in particular for the schematization of the femur-patella articulation (for example Van Eijden et al. 1986, [31], Yamaguchi et al. 1989, [32], Kaufman et al. 1991, [15] as described in par.3.4 and 3.6). Some schematizations and analytical equations of these previous studies were used in this thesis to define two analytical 2D-models.

The first model has the same schematization and the same inertial properties of the OpenSim model. To get the line of action and the moment-arm of the muscles acting during the exercise, the Herzog’s formulation and the Van Eijden’s formulation were chosen. For the second analytical model, the ‘Dempster protocol’ was used to divide the body into segments and to set the inertial parameters; to define the muscles in terms of line of action and moment arm, anthropometric features taken from another thesis work done by Pontin et al. were used.

7.6.1. Model 1

7.6.1.1 Model definition and Reference systems position

In this model, the schematization and the inertial properties (mass and moment of inertia of each segment) of the gait2392_model are used. Thus not only the mass of each segment is given as a percentage of the total weight, but also the length and the inertial parameters are defined by using only the mass and not the total height yet. (as described in par.4.1).

In this model, the leg is composed by femur, tibia, talus, calcaneus and toes which are connected by the knee-joint (between femur and tibia), the ankle-joint (between tibia and talus), the subtalar-joint (between talus and calcaneus) and the metacarpal joint (between the calcaneus and the toes). Between the bodies there is a hierarchical classification: the femur is the parent of the tibia, the tibia is the parent of the talus, the talus is the parent of the calcaneus and the calcaneus is the parent of the toes. Each segment has its

own reference system; the position of the reference system is expressed with respect to the reference system of the parent body. The inertial parameters, in particular the position of the center mass and the inertia moments, are instead expressed in the reference system of each body.

During the exercise, because the femur is fixed, the knee-joint is represented as a rotational joint fixed to the ground; moreover, the relative movement between talus and calcaneus and also the relative movement between calcaneus and toes are null, talus, calcaneus and toes are considered fixed together and connected to the tibia with a rotational joint. For this reason the reference system of each of these segments has the same orientation. The partition into the three bodies is instead kept for the inertial properties. Fig. 7.5 shows the schematization adopted. The global reference system is centered at the knee-joint center, with the x axis pointed forward. The terminology adopted has the following meaning:

θ_F : angle between femur and y axis

φ_K : relative angle between femur and tibia


φ_a : relative angle between tibia and foot

$x_{tibia}, y_{tibia}, x_{calc}, y_{calc}, x_{talus}, y_{talus}, x_{toes}, y_{toes}$: axis of the reference systems

$\Delta_{y\ tibia}$: coordinate of the center of talus reference system in tibia reference system

$\Delta_{x\ calcn}, \Delta_{y\ calcn}$: coordinates of the center of calcaneus reference system in talus reference system

$\Delta_{x\ toes}, \Delta_{y\ toes}$: coordinates of the center of toes reference system in calcaneus reference system

Sign used for θ_F, φ_K and φ_a : 

The position of knee center is evaluated by using the markers on the lateral condyle. $\Delta_{y\ tibia}, \Delta_{x\ calcn}, \Delta_{y\ calcn}, \Delta_{x\ toes}$ and $\Delta_{y\ toes}$ are considered positives.

The position of the local reference systems with respect to the global reference system is given by the following equations:

Tibia:

$$\begin{aligned} x_{R\ tibia} &= 0 \\ y_{R\ tibia} &= 0 \end{aligned}$$

Talus:

$$\begin{aligned} x_{R\ talus} &= \Delta_{y\ tibia} \cdot \sin(\theta_F + \varphi_K) \\ y_{R\ talus} &= -\Delta_{y\ tibia} \cdot \cos(\theta_F + \varphi_K) \end{aligned}$$

Calcaneus:

$$x_{R \text{ calcn}} = x_{R \text{ talus}} - \Delta_{x \text{ calcn}} \cdot \cos(\theta_F + \varphi_K + \varphi_a) + \Delta_{y \text{ calcn}} \cdot \sin(\theta_F + \varphi_K + \varphi_a)$$

$$y_{R \text{ calcn}} = y_{R \text{ talus}} - \Delta_{x \text{ calcn}} \cdot \sin(\theta_F + \varphi_K + \varphi_a) - \Delta_{y \text{ calcn}} \cdot \cos(\theta_F + \varphi_K + \varphi_a)$$

Toes:

$$x_{R \text{ toes}} = x_{R \text{ calcn}} + \Delta_{x \text{ toes}} \cdot \cos(\theta_F + \varphi_K + \varphi_a) + \Delta_{y \text{ toes}} \cdot \sin(\theta_F + \varphi_K + \varphi_a)$$

$$y_{R \text{ toes}} = y_{R \text{ calcn}} + \Delta_{x \text{ toes}} \cdot \sin(\theta_F + \varphi_K + \varphi_a) - \Delta_{y \text{ toes}} \cdot \cos(\theta_F + \varphi_K + \varphi_a)$$

in which x_{Rj} and y_{Rj} are the coordinates of the center of the j^{th} reference system with respect to the global reference system.

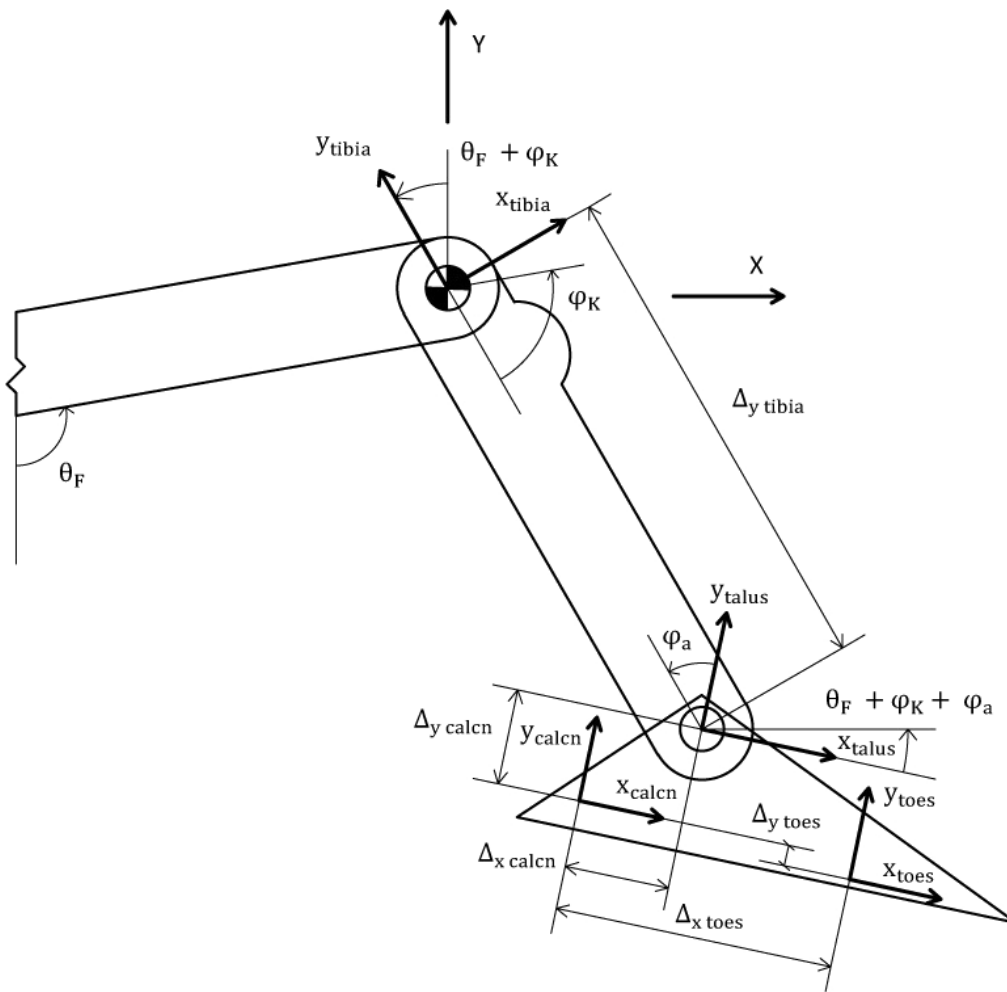


Fig.7.5: Geometry definition and reference systems (global and local). (Model 1)

The sign of the terms in the equations is justified by the convention adopted for the sign of the angles. The value of the angles are obtained as the result of the inverse kinematics calculated with the software OpenSim. Furthermore, $\theta_F = \text{cost}$ (the femur is fixed) and $\varphi_a \cong \text{cost}$. Thus the previous equations are defined as function of the relative angle between femur and tibia: $x_{Rj}, y_{Rj} = f(\varphi_K)$.

7.6.1.2.COMs position

Fig.7.6 shows the position of the center of mass of every segment. The terminology adopted has the following meaning:

COM_j : center of mass of the j^{th} segment

$\Delta_{y G tibia}$: coordinate of COM_{tibia} in tibia reference system

$\Delta_{y G talus}$: coordinate of COM_{talus} in tibia reference system ($COM_{talus} \equiv$ ankle-joint center)

$\Delta_{x G calcn}$, $\Delta_{y G calcn}$: coordinates of COM_{calcn} in calcaneus reference system

$\Delta_{x G toes}$, $\Delta_{y G toes}$: coordinates of COM_{toes} in toes reference system

$\Delta_{y G tibia}$, $\Delta_{y G talus}$, $\Delta_{x G calcn}$, $\Delta_{y G calcn}$, $\Delta_{x G toes}$ and $\Delta_{y G toes}$ are considered positives.

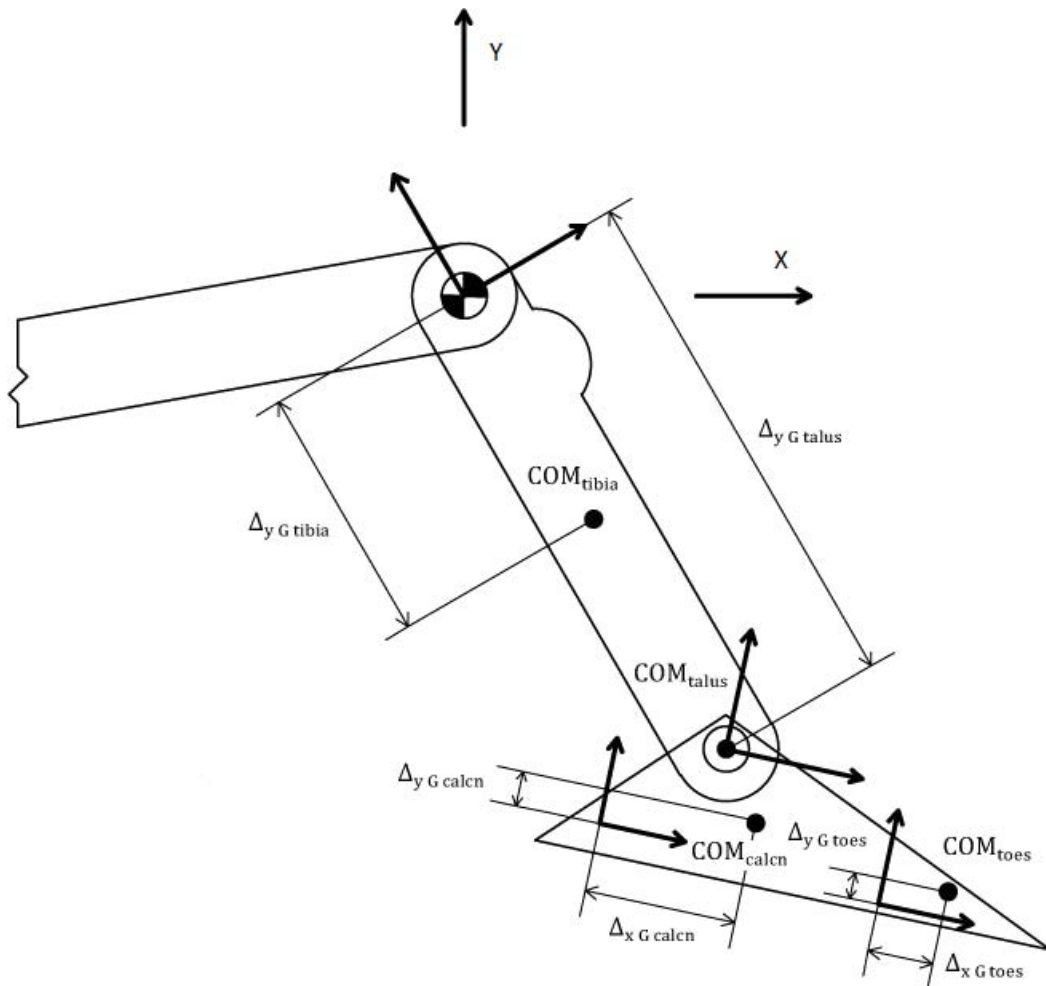


Fig.7.6: COMs position. (Model 1)

The position of the COM in the global reference system is described by these equations:

Tibia:

$$\begin{aligned}x_{G \text{ tibia}} &= \Delta_{y \text{ G tibia}} \cdot \sin (\theta_F + \varphi_K) \\y_{G \text{ tibia}} &= -\Delta_{y \text{ G tibia}} \cdot \cos (\theta_F + \varphi_K)\end{aligned}$$

Talus:

$$\begin{aligned}x_{G \text{ talus}} &= \Delta_{y \text{ G talus}} \cdot \sin (\theta_F + \varphi_K) \\y_{G \text{ talus}} &= -\Delta_{y \text{ G talus}} \cdot \cos (\theta_F + \varphi_K)\end{aligned}$$

Calcaneus:

$$\begin{aligned}x_{G \text{ calcn}} &= x_{R \text{ calcn}} + \Delta_{x \text{ G calcn}} \cdot \cos (\theta_F + \varphi_K + \varphi_a) - \Delta_{y \text{ G calcn}} \cdot \sin (\theta_F + \varphi_K + \varphi_a) \\y_{G \text{ calcn}} &= y_{R \text{ calcn}} + \Delta_{x \text{ G calcn}} \cdot \sin (\theta_F + \varphi_K + \varphi_a) + \Delta_{y \text{ G calcn}} \cdot \cos (\theta_F + \varphi_K + \varphi_a)\end{aligned}$$

Toes:

$$\begin{aligned}x_{G \text{ toes}} &= x_{R \text{ toes}} + \Delta_{x \text{ G toes}} \cdot \cos (\theta_F + \varphi_K + \varphi_a) - \Delta_{y \text{ G toes}} \cdot \sin (\theta_F + \varphi_K + \varphi_a) \\y_{G \text{ toes}} &= y_{R \text{ toes}} + \Delta_{x \text{ G toes}} \cdot \sin (\theta_F + \varphi_K + \varphi_a) + \Delta_{y \text{ G toes}} \cdot \cos (\theta_F + \varphi_K + \varphi_a)\end{aligned}$$

in which x_{G_j} and y_{G_j} are the coordinates of the j^{th} center of mass with respect to the global reference system.

7.6.1.3. Muscular forces and Reaction loads at tibia

At this step of the analysis, it is necessary to consider separately the extension phase and the flexion phase because the forces acting on tibia are different in the two situations.

7.6.1.3.1. Muscular forces and Reaction loads at tibia in Extension

In this analytical approach, the quadriceps is considered the only muscle acting in extension; the other muscles, in particular the antagonist muscles, are ignored. The quadriceps exerts its force on tibia with the patellar tendon. Fig.7.7. shows the forces acting during the movement:

F_{PT} : force at the patellar tendon

R_{tx}, R_{ty} : reaction forces at tibia

W_{total} : total weight of tibia, talus, calcaneus and toes

$F_{\text{ext } x}, F_{\text{ext } y}$: components of the external force

$r_{F_{\text{ext } x}}, r_{F_{\text{ext } y}}, r_{PT}$: moment arm of the x-component of the external force (positive as shown in fig.7.7), moment arm of the y-component of the external force (positive as shown in fig.7.7) and moment arm of the patellar tendon

θ_{PT} : line of action of the patellar tendon with respect to the global reference system

The position of the global center of mass of tibia, talus, calcaneus and toes is defined as:

$$x_{COM} = \frac{m_{tibia} \cdot x_{G\ tibia} + m_{talus} \cdot x_{G\ talus} + m_{calcn} \cdot x_{G\ calcn} + m_{toes} \cdot x_{G\ toes}}{m_{tibia} + m_{talus} + m_{calcn} + m_{toes}}$$

$$y_{COM} = \frac{m_{tibia} \cdot y_{G\ tibia} + m_{talus} \cdot y_{G\ talus} + m_{calcn} \cdot y_{G\ calcn} + m_{toes} \cdot y_{G\ toes}}{m_{tibia} + m_{talus} + m_{calcn} + m_{toes}}$$

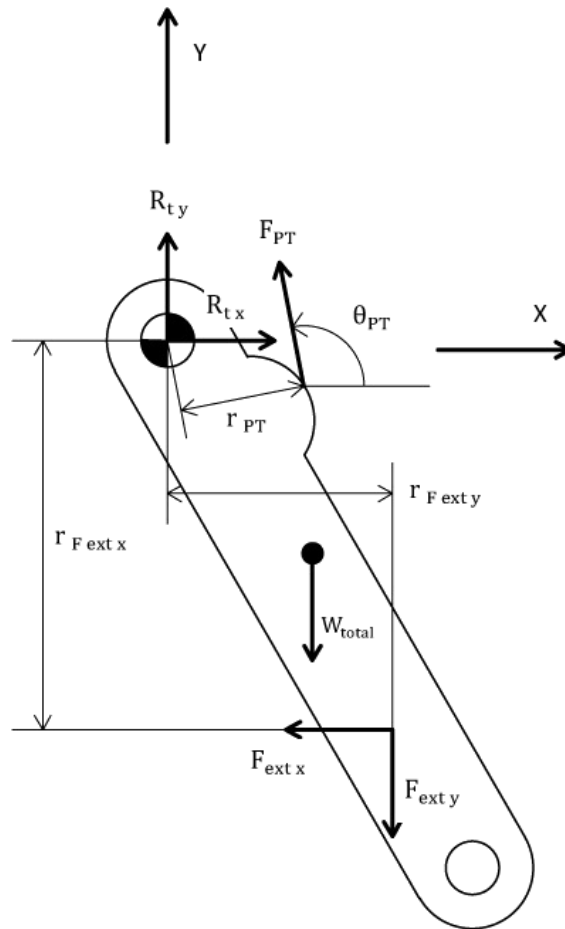


Fig.7.7: Forces acting on tibia in extension. (Model 1)

To get the force which acts at the patellar tendon and the reaction loads at the knee joint, the equilibrium of tibia must be imposed:

$$W_{total} \cdot x_{COM} + F_{ext\ x} \cdot r_{F\ ext\ x} + F_{ext\ y} \cdot r_{F\ ext\ y} + F_{PT} \cdot r_{PT} = I_k \cdot \ddot{\phi}_k$$

$$R_{t\ x} + F_{ext\ x} + F_{PT} \cdot \cos(\theta_{PT}) = (m_{tibia} + m_{talus} + m_{calcn} + m_{toes}) \cdot \ddot{x}_{COM}$$

$$R_{t\ y} + F_{ext\ y} + W_{total} + F_{PT} \cdot \sin(\theta_{PT}) = (m_{tibia} + m_{talus} + m_{calcn} + m_{toes}) \cdot \ddot{y}_{COM}$$

(the right sign of the terms is considered in F_j sign)

in which:

- I_k : moment of inertia around the knee

$$I_k = (I_{G \text{ tibia}} + m_{\text{tibia}} \cdot d_{\text{tibia}}^2) + (I_{G \text{ talus}} + m_{\text{talus}} \cdot d_{\text{talus}}^2) + (I_{G \text{ calcn}} + m_{\text{calcn}} \cdot d_{\text{calcn}}^2) + (I_{G \text{ toes}} + m_{\text{toes}} \cdot d_{\text{toes}}^2)$$

and I_{G_j} and $d_j = \sqrt{x_{G_j}^2 + y_{G_j}^2}$ are respectively the moment of inertia with respect to the COM of the j^{th} segment and the distance of the COM of the j^{th} segment from the knee joint center.

- \ddot{x}_{COM} : acceleration in x direction of the COM

$$\ddot{x}_{\text{COM}} = \frac{m_{\text{tibia}} \cdot \ddot{x}_{G \text{ tibia}} + m_{\text{talus}} \cdot \ddot{x}_{G \text{ talus}} + m_{\text{calcn}} \cdot \ddot{x}_{G \text{ calcn}} + m_{\text{toes}} \cdot \ddot{x}_{G \text{ toes}}}{m_{\text{tibia}} + m_{\text{talus}} + m_{\text{calcn}} + m_{\text{toes}}}$$

$$\ddot{x}_{G \text{ tibia}} = -\Delta_{y G \text{ tibia}} \cdot \text{sen}(\theta_F + \varphi_K) \cdot \dot{\varphi}_K^2 + \Delta_{y G \text{ tibia}} \cdot \text{cos}(\theta_F + \varphi_K) \cdot \ddot{\varphi}_K$$

$$\ddot{x}_{G \text{ talus}} = -\Delta_{y G \text{ talus}} \cdot \text{sen}(\theta_F + \varphi_K) \cdot \dot{\varphi}_K^2 + \Delta_{y G \text{ talus}} \cdot \text{cos}(\theta_F + \varphi_K) \cdot \ddot{\varphi}_K$$

$$\begin{aligned} \ddot{x}_{G \text{ calcn}} = & \Delta_{y \text{ tibia}} \cdot [-\text{sen}(\theta_F + \varphi_K) \cdot \dot{\varphi}_K^2 + \text{cos}(\theta_F + \varphi_K) \cdot \ddot{\varphi}_K] + \\ & -(\Delta_{x G \text{ calcn}} - \Delta_{x \text{ calcn}}) \cdot [\text{cos}(\theta_F + \varphi_K + \varphi_a) \cdot \dot{\varphi}_K^2 + \text{sen}(\theta_F + \varphi_K + \varphi_a) \cdot \ddot{\varphi}_K] + \\ & + (-\Delta_{y G \text{ calcn}} + \Delta_{y \text{ calcn}}) \cdot [-\text{sen}(\theta_F + \varphi_K + \varphi_a) \cdot \dot{\varphi}_K^2 + \text{cos}(\theta_F + \varphi_K + \varphi_a) \cdot \ddot{\varphi}_K] \end{aligned}$$

$$\begin{aligned} \ddot{x}_{G \text{ toes}} = & \Delta_{y \text{ tibia}} \cdot [-\text{sen}(\theta_F + \varphi_K) \cdot \dot{\varphi}_K^2 + \text{cos}(\theta_F + \varphi_K) \cdot \ddot{\varphi}_K] + \\ & -(\Delta_{x G \text{ toes}} + \Delta_{x \text{ toes}} - \Delta_{x \text{ calcn}}) \cdot [\text{cos}(\theta_F + \varphi_K + \varphi_a) \cdot \dot{\varphi}_K^2 + \text{sen}(\theta_F + \varphi_K + \varphi_a) \cdot \ddot{\varphi}_K] + \\ & + (-\Delta_{y G \text{ toes}} + \Delta_{y \text{ toes}} + \Delta_{y \text{ calcn}}) \cdot [-\text{sen}(\theta_F + \varphi_K + \varphi_a) \cdot \dot{\varphi}_K^2 + \text{cos}(\theta_F + \varphi_K + \varphi_a) \cdot \ddot{\varphi}_K] \end{aligned}$$

- \ddot{y}_{COM} : acceleration in the y direction of the COM

$$\ddot{y}_{\text{COM}} = \frac{m_{\text{tibia}} \cdot \ddot{y}_{G \text{ tibia}} + m_{\text{talus}} \cdot \ddot{y}_{G \text{ talus}} + m_{\text{calcn}} \cdot \ddot{y}_{G \text{ calcn}} + m_{\text{toes}} \cdot \ddot{y}_{G \text{ toes}}}{m_{\text{tibia}} + m_{\text{talus}} + m_{\text{calcn}} + m_{\text{toes}}}$$

$$\ddot{y}_{G \text{ tibia}} = \Delta_{y G \text{ tibia}} \cdot \text{cos}(\theta_F + \varphi_K) \cdot \dot{\varphi}_K^2 + \Delta_{y G \text{ tibia}} \cdot \text{sen}(\theta_F + \varphi_K) \cdot \ddot{\varphi}_K$$

$$\ddot{y}_{G \text{ talus}} = \Delta_{y G \text{ talus}} \cdot \text{cos}(\theta_F + \varphi_K) \cdot \dot{\varphi}_K^2 + \Delta_{y G \text{ talus}} \cdot \text{sen}(\theta_F + \varphi_K) \cdot \ddot{\varphi}_K$$

$$\begin{aligned} \ddot{y}_{G \text{ calcn}} = & \Delta_{y \text{ tibia}} \cdot [\text{cos}(\theta_F + \varphi_K) \cdot \dot{\varphi}_K^2 + \text{sen}(\theta_F + \varphi_K) \cdot \ddot{\varphi}_K] + \\ & -(\Delta_{y G \text{ calcn}} - \Delta_{y \text{ calcn}}) \cdot [\text{cos}(\theta_F + \varphi_K + \varphi_a) \cdot \dot{\varphi}_K^2 + \text{sen}(\theta_F + \varphi_K + \varphi_a) \cdot \ddot{\varphi}_K] + \\ & + (\Delta_{x G \text{ calcn}} - \Delta_{x \text{ calcn}}) \cdot [-\text{sen}(\theta_F + \varphi_K + \varphi_a) \cdot \dot{\varphi}_K^2 + \text{cos}(\theta_F + \varphi_K + \varphi_a) \cdot \ddot{\varphi}_K] \end{aligned}$$

$$\begin{aligned} \ddot{y}_{G \text{ toes}} = & \Delta_{y \text{ tibia}} \cdot [\text{cos}(\theta_F + \varphi_K) \cdot \dot{\varphi}_K^2 + \text{sen}(\theta_F + \varphi_K) \cdot \ddot{\varphi}_K] + \\ & -(\Delta_{y G \text{ toes}} - \Delta_{y \text{ toes}} - \Delta_{y \text{ calcn}}) \cdot [\text{cos}(\theta_F + \varphi_K + \varphi_a) \cdot \dot{\varphi}_K^2 + \text{sen}(\theta_F + \varphi_K + \varphi_a) \cdot \ddot{\varphi}_K] + \\ & + (\Delta_{x G \text{ toes}} + \Delta_{x \text{ toes}} - \Delta_{x \text{ calcn}}) \cdot [-\text{sen}(\theta_F + \varphi_K + \varphi_a) \cdot \dot{\varphi}_K^2 + \text{cos}(\theta_F + \varphi_K + \varphi_a) \cdot \ddot{\varphi}_K] \end{aligned}$$

In the previous equations $\dot{\varphi}_k$ and $\ddot{\varphi}_k$ are the angular velocity and the angular acceleration at the knee respectively, which are evaluated by deriving the knee flexion angle.

About the moment arm of the patellar tendon r_{PT} , it is evaluated by using the results of the study done by Herzog et al. (see par.3.4):

$$r_{PT} [\text{cm}] = 4,71 + 0,42 \cdot \varphi_{k+} - 0,000896 \cdot \varphi_{k+}^2 + 0,00000447 \cdot \varphi_{k+}^3$$

in which $\varphi_{k+} = -\varphi_k$ and $\varphi_{k+} [^\circ]$.

About the inclination of the patellar tendon θ_{PT} , two different approaches are used.

In the first approach, the line of action is evaluated by using the relation suggested by Herzog et al. (see par.3.4):

$$\theta_{PTH} [^\circ] = -74,4 - 0,0575 \cdot \varphi_{k+} - 0,00475 \cdot \varphi_{k+}^2 + 0,0000309 \cdot \varphi_{k+}^3$$

By considering the line of action with respect to the global system, and because of the convention adopted in this analytical study:

$$\theta_{PT} [^\circ] = (\theta_F + \varphi_K) + (-\varphi_{PTH})$$

In the second approach, the line of action is evaluated by using the relation suggested by van Eijden et al. (see par.3.4):

$$\alpha [^\circ] = -8,4734 \cdot \varphi_{k+}^6 + 50,457 \cdot \varphi_{k+}^5 - 110,75 \cdot \varphi_{k+}^4 + 109,99 \cdot \varphi_{k+}^3 - 52,907 \cdot \varphi_{k+}^2 + 2,0575 \cdot \varphi_{k+} + 21,091$$

in which $\varphi_{k+} [\text{rad}]$.

By considering the line of action with respect to the global system, and because of the convention adopted in this analytical study:

$$\theta_{PT} [^\circ] = (\theta_F + \varphi_K) + (90^\circ - \alpha)$$

By solving the equations written above, the force acting at the patellar tendon and the reaction loads at tibia are evaluated by the following equations:

$$F_{PT} = \frac{I_k \cdot \ddot{\varphi}_k - W_{\text{total}} \cdot x_{\text{COM}} - F_{\text{ext } x} \cdot r_{F \text{ ext } x} - F_{\text{ext } y} \cdot r_{F \text{ ext } y}}{r_{PT}}$$

$$R_{t_x} = (m_{\text{tibia}} + m_{\text{talus}} + m_{\text{calcn}} + m_{\text{toes}}) \cdot \ddot{x}_{\text{COM}} - F_{\text{ext } x} - F_{PT} \cdot \cos(\theta_{PT})$$

$$R_{t_y} = (m_{\text{tibia}} + m_{\text{talus}} + m_{\text{calcn}} + m_{\text{toes}}) \cdot \ddot{y}_{\text{COM}} - F_{\text{ext } y} - W_{\text{total}} - F_{PT} \cdot \sin(\theta_{PT})$$

7.6.1.3.2. Muscular forces and Reaction loads at tibia in Flexion

In flexion, biceps femoris-long head, biceps femoris short-head, semimembranosus and semitendinosus are considered the muscles acting during the movement. The other muscles, in particular the antagonist muscles, are ignored. Fig.7.8 shows the forces acting during the movement, in particular F_{BFL} , F_{BFB} , F_{SM} and F_{ST} are the forces acting at biceps femoris-long head, at biceps femoris-short head, at semimembranosus and at semitendinosus respectively; the other symbols have the same meaning described in the previous paragraphs.

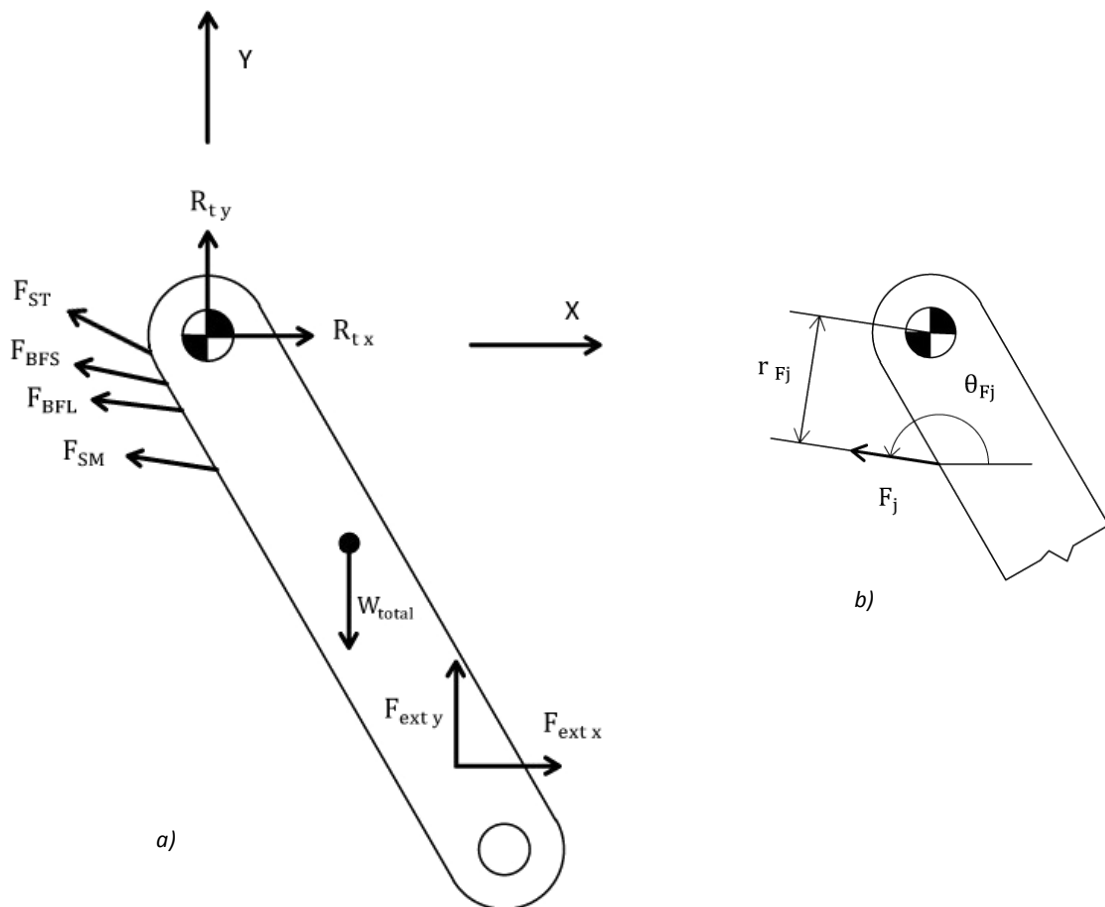


Fig.7.8: Forces acting on tibia in flexion (fig.7.8.a) and schematic representation of moment-arm and line of action of the j-th muscle (fig.7.8.b). (Model 1)

As done for the extension phase, to get the forces acting at the muscles and the reaction loads at the knee joint, the equilibrium of tibia must be imposed:

$$W_{total} \cdot x_{COM} + F_{extx} \cdot r_{F_{extx}} + F_{exty} \cdot r_{F_{exty}} + F_{BFL} \cdot r_{BFL} + F_{BFB} \cdot r_{BFB} + F_{SM} \cdot r_{SM} + F_{ST} \cdot r_{ST} = I_k \cdot \ddot{\varphi}_k$$

$$R_{tx} + F_{extx} + F_{BFL} \cdot \cos(\theta_{BFL}) + F_{BFB} \cdot \cos(\theta_{BFB}) + F_{SM} \cdot \cos(\theta_{SM}) + F_{ST} \cdot \cos(\theta_{ST}) = (m_{tibia} + m_{talus} + m_{calc} + m_{toes}) \cdot \ddot{x}_{COM}$$

$$R_{ty} + F_{exty} + W_{total} + F_{BFL} \cdot \sin(\theta_{BFL}) + F_{BFB} \cdot \sin(\theta_{BFB}) + F_{SM} \cdot \sin(\theta_{SM}) + F_{ST} \cdot \sin(\theta_{ST}) = (m_{tibia} + m_{talus} + m_{calc} + m_{toes}) \cdot \ddot{y}_{COM}$$

(the right sign of the terms is considered in F_j sign)

in which r_{BFL} , r_{BFB} , r_{SM} , r_{ST} and θ_{BFL} , θ_{BFB} , θ_{SM} , θ_{ST} are the moment arm and the line of action of the muscles involved, as shown in fig.7.8.b.

About the biceps femoris long head, the semimembranosus and the semitendinosus, the moment-arm and the line of action are evaluated by considering the Herzog's formulation (as described in par.3.4):

$$r_{BFL} [\text{cm}] = 1,46 - 0,00926 \cdot \varphi_{k+} + 0,000855 \cdot \varphi_{k+}^2 - 0,00000878 \cdot \varphi_{k+}^3 + 0,0000000238 \cdot \varphi_{k+}^4$$

$$r_{SM} [\text{cm}] = 2,84 - 0,0161 \cdot \varphi_{k+} + 0,000681 \cdot \varphi_{k+}^2 - 0,0000088 \cdot \varphi_{k+}^3 + 0,0000000277 \cdot \varphi_{k+}^4$$

$$r_{ST} [\text{cm}] = -0,411 - 0,0586 \cdot \varphi_{k+} + 0,00069 \cdot \varphi_{k+}^2 - 0,00000531 \cdot \varphi_{k+}^3$$

$$\varphi_{BFL} [^\circ] = 275 - 0,872 \cdot \varphi_{k+} - 0,000712 \cdot \varphi_{k+}^2$$

$$\varphi_{SM} [^\circ] = 260 - 0,888 \cdot \varphi_{k+} - 0,000852 \cdot \varphi_{k+}^2$$

$$\varphi_{ST} [^\circ] = 255 - 0,816 \cdot \varphi_{k+} + 0,000263 \cdot \varphi_{k+}^2 - 0,00000619 \cdot \varphi_{k+}^3$$

in which $\varphi_{k+} = -\varphi_k$ and $\varphi_{k+} [^\circ]$. However, the relation suggested for the moment-arm of the semitendinosus doesn't fit correctly the results plotted in the Herzog study (see fig. 5-b, Herzog et al. 1993, [13]). By interpolating the results the following equation was obtain:

$$r_{ST} [\text{cm}] = -1,0748 + 0,8237 \cdot \varphi_{k+} + 4,4485 \cdot \varphi_{k+}^2 - 1,5013 \cdot \varphi_{k+}^3$$

in which $\varphi_{k+} [\text{rad}]$.

About biceps femoris short-head, the moment arm and the line of action are evaluated by using the equations suggested by Pontin (as described in par.7.6.2), because in the study done by Herzog et al. only the long head of biceps femoris was considered.

To solve the equilibrium equations written above, it is necessary to express the force acting at the muscles with respect to the other muscles, in order to get three equations and three variables. To do this, the following equation is used (Nigg et al., [23]):

$$F_i = \left(\frac{r_i}{r_j} \right)^{\frac{1}{p-1}} \left(\frac{N_i}{N_j} \right)^{\frac{p}{p-1}} F_j$$

which expresses the force acting at muscle i , F_i , as a function of the force acting at muscle j , F_j ; in particular this relation is influenced by the ratio of their moment arms r_i/r_j and the ratio N_i/N_j , in which N is the physiological cross-sectional area or the maximum isometric force of the muscle (in this study N is chosen as maximum isometric force). p is a constant which is typically set to 3. In this study N is chosen as maximum isometric force and its value is obtained by the software OpenSim.

By considering this relation, and by setting

$$M_{\text{tot}} = I_k \cdot \ddot{\varphi}_k - W_{\text{total}} \cdot x_{\text{COM}} - F_{\text{ext } x} \cdot b_{F_{\text{ext } x}} - F_{\text{ext } y} \cdot b_{F_{\text{ext } y}}$$

it is possible to obtain the forces acting at the muscles:

$$F_{\text{BFB}} = \frac{M_{\text{tot}}}{\left[b_{\text{BFB}} + b_{\text{BFL}} \left(\frac{b_{\text{BFL}}}{b_{\text{BFB}}} \right)^{0.5} \left(\frac{N_{\text{BFL}}}{N_{\text{BFB}}} \right)^{1.5} + b_{\text{SM}} \left(\frac{b_{\text{SM}}}{b_{\text{BFB}}} \right)^{0.5} \left(\frac{N_{\text{SM}}}{N_{\text{BFB}}} \right)^{1.5} + b_{\text{ST}} \left(\frac{b_{\text{ST}}}{b_{\text{BFB}}} \right)^{0.5} \left(\frac{N_{\text{ST}}}{N_{\text{BFB}}} \right)^{1.5} \right]}$$

$$F_{\text{BFL}} = \frac{M_{\text{tot}}}{\left[b_{\text{BFL}} + b_{\text{BFB}} \left(\frac{b_{\text{BFB}}}{b_{\text{BFL}}} \right)^{0.5} \left(\frac{N_{\text{BFB}}}{N_{\text{BFL}}} \right)^{1.5} + b_{\text{SM}} \left(\frac{b_{\text{SM}}}{b_{\text{BFL}}} \right)^{0.5} \left(\frac{N_{\text{SM}}}{N_{\text{BFL}}} \right)^{1.5} + b_{\text{ST}} \left(\frac{b_{\text{ST}}}{b_{\text{BFL}}} \right)^{0.5} \left(\frac{N_{\text{ST}}}{N_{\text{BFL}}} \right)^{1.5} \right]}$$

$$F_{\text{SM}} = \frac{M_{\text{tot}}}{\left[b_{\text{SM}} + b_{\text{BFB}} \left(\frac{b_{\text{BFB}}}{b_{\text{SM}}} \right)^{0.5} \left(\frac{N_{\text{BFB}}}{N_{\text{SM}}} \right)^{1.5} + b_{\text{BFL}} \left(\frac{b_{\text{BFL}}}{b_{\text{SM}}} \right)^{0.5} \left(\frac{N_{\text{BFL}}}{N_{\text{SM}}} \right)^{1.5} + b_{\text{ST}} \left(\frac{b_{\text{ST}}}{b_{\text{SM}}} \right)^{0.5} \left(\frac{N_{\text{ST}}}{N_{\text{SM}}} \right)^{1.5} \right]}$$

$$F_{\text{ST}} = \frac{M_{\text{tot}}}{\left[b_{\text{ST}} + b_{\text{BFB}} \left(\frac{b_{\text{BFB}}}{b_{\text{ST}}} \right)^{0.5} \left(\frac{N_{\text{BFB}}}{N_{\text{ST}}} \right)^{1.5} + b_{\text{BFL}} \left(\frac{b_{\text{BFL}}}{b_{\text{ST}}} \right)^{0.5} \left(\frac{N_{\text{BFL}}}{N_{\text{ST}}} \right)^{1.5} + b_{\text{SM}} \left(\frac{b_{\text{SM}}}{b_{\text{ST}}} \right)^{0.5} \left(\frac{N_{\text{SM}}}{N_{\text{ST}}} \right)^{1.5} \right]}$$

Thus, it is possible to obtain the reaction loads at tibia:

$$R_{t \ x} = (m_{\text{tibia}} + m_{\text{talus}} + m_{\text{calc}} + m_{\text{toes}}) \cdot \ddot{x}_{\text{COM}} - F_{\text{ext } x} - F_{\text{BFL}} \cdot \cos(\theta_{\text{BFL}}) - F_{\text{BFB}} \cdot \cos(\theta_{\text{BFB}}) + F_{\text{SM}} \cdot \cos(\theta_{\text{SM}}) + F_{\text{ST}} \cdot \cos(\theta_{\text{ST}})$$

$$R_{t \ y} = (m_{\text{tibia}} + m_{\text{talus}} + m_{\text{calc}} + m_{\text{toes}}) \cdot \ddot{y}_{\text{COM}} - F_{\text{ext } y} - W_{\text{total}} - F_{\text{BFL}} \cdot \sin(\theta_{\text{BFL}}) - F_{\text{BFB}} \cdot \sin(\theta_{\text{BFB}}) + F_{\text{SM}} \cdot \sin(\theta_{\text{SM}}) - F_{\text{ST}} \cdot \sin(\theta_{\text{ST}})$$

7.6.1.4. Forces acting on tibia

Once expressed the results in the global reference system, it is useful to express the reaction loads with respect to the tibia reference system in order to obtain the axial force, N , and the shear force, T , which act on tibia (fig.7.9):

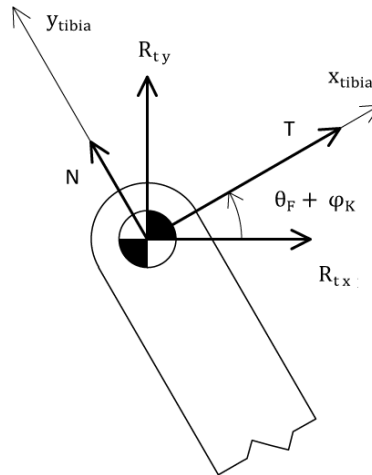


Fig.7.9: Reaction loads expressed in the tibia reference system: N , axial load; T , shear load (positives as shown). (Model 1)

$$T = R_{tx} \cdot \cos(\theta_F + \varphi_K) + R_{ty} \cdot \sin(\theta_F + \varphi_K)$$

$$N = -R_{tx} \cdot \sin(\theta_F + \varphi_K) + R_{ty} \cdot \cos(\theta_F + \varphi_K)$$

7.6.1.5. Force acting at ACL and PCL

Because of the main function of the ACL is to restrain the anterior movement of the tibia and the main function of the PCL is to restrain the posterior movement of the tibia (anterior and posterior referred to the x-axis system of the tibia axis system), it is reasonable to assume that the shear load T acting on tibia is the result of the interaction of the two ligaments. In particular, if the shear load T is positive, the PCL is strained the ACL is unstrained; if the shear load T is negative, the ACL is strained the PCL is unstrained (fig.7.10 and fig.7.11). That's because the shear load T has been evaluated as a reaction force (force acting ON tibia).

About the axial load N acting in the longitudinal direction of the tibia, it is reasonable to assume that it is adsorbed by the bone.

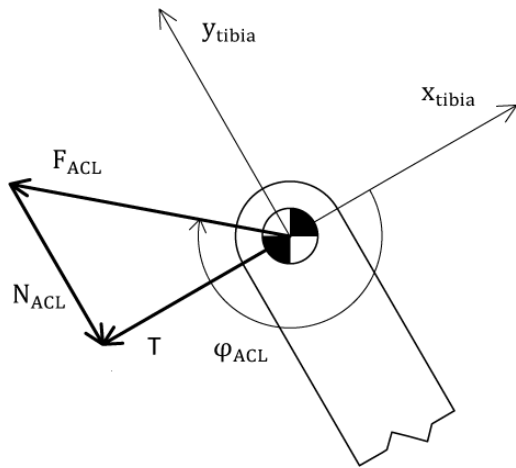


Fig.7.10: Force acting at the ACL. (Model 1)

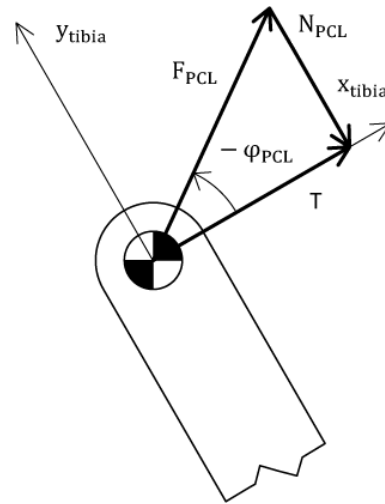


Fig.7.11: Force acting at the PCL. (Model 1)

With these assumptions, it is possible to obtain the force acting at ACL or PCL:

$$F_{ACL} \cdot \cos(\varphi_{ACL}) = T$$

↓

$$F_{ACL} = \frac{T}{\cos(\varphi_{ACL})}$$

$$F_{PCL} \cdot \cos(\varphi_{PCL}) = T$$

↓

$$F_{PCL} = \frac{T}{\cos(\varphi_{PCL})}$$

The angles φ_{ACL} and φ_{PCL} are evaluated by using the results of the study done by Herzog et al. (as described in par.3.4):

$$\varphi_{ACL} [^\circ] = 227^\circ - 0,448 \cdot \varphi_{k+}$$

$$\varphi_{PCL} [^\circ] = -66^\circ + 0,737 \cdot \varphi_{k+} - 0,00496 \cdot \varphi_{k+}^2$$

The force at the ACL (or at the PCL) increases the compression load at the tibia:

$$N_{tibia} = N - |N_{ACL}|$$

in which $N_{ACL} = F_{ACL} \cdot \sin(\varphi_{ACL})$

(or $N_{tibia} = N - |N_{PCL}|$, in which $N_{PCL} = F_{PCL} \cdot \sin(\varphi_{PCL})$).

7.6.1.6. Forces acting on femur

To evaluate the forces acting on femur, it is necessary to consider separately the extension phase and the flexion phase.

7.6.1.6.1. Forces acting on femur in the Extension phase

The forces acting on femur are evaluated by considering the reaction forces at tibia, the force acting at the cruciate ligaments and the forces acting at the patella; as a matter of fact, patella must be considered because it exerts a force on the femur. As described in par.3.4, the force exerted by the patella should be evaluated by considering the contact point between patella and femur, the inclination of the patella with respect to the femoral axis and the ratio F_p/F_q between the force at the quadriceps and the force exerted by the patella. In this study, a simplified approach was used. In this approach, the patella is modeled as a rectangle as in the model used by Yamaguchi et al. (see par.3.4), in order to consider that the force acting at the patellar tendon is different from that acting at the tendon of the quadriceps (fig.7.12); the line of action of the tendon of the quadriceps and the force acting at this tendon are instead evaluated by using the van Eijden's formulation because of the limits of the Yamaguchi approach (as described in par.3.4).

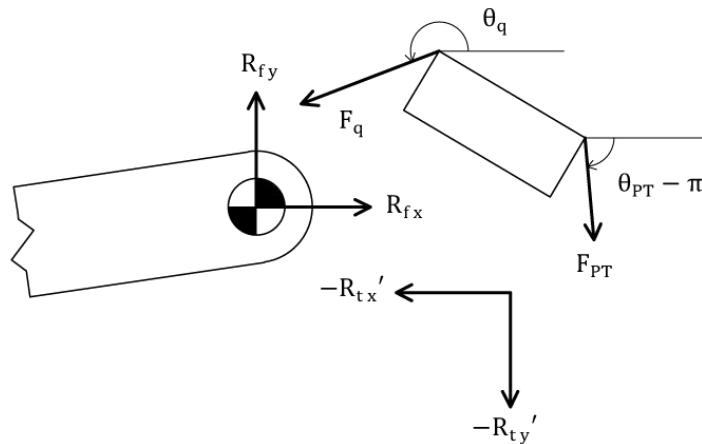


Fig.7.12: Forces acting on femur. (Model 1)

The forces acting on femur can be evaluated by using the following equations:

$$R_{fx} + (-R_{tx}') + F_q \cdot \cos(\theta_q) + F_{PT} \cdot \cos(\theta_{PT} - \pi) = 0$$

$$R_{fy} + (-R_{ty}') + F_q \cdot \sin(\theta_q) + F_{PT} \cdot \sin(\theta_{PT} - \pi) = 0$$

in which R_{fx} and R_{fy} are the reaction forces at femur with respect to the x-axis and the y-axis of the global reference system centered at the knee, and in which the line of action of the tendon of the femur θ_q and

the force at the tendon of the quadriceps F_q are obtained by using the results obtained by Van Eijden et al. (see par.3.4):

$$\theta_q [^\circ] = \theta_F [^\circ] + \delta [^\circ] + 90^\circ$$

in which $\delta [^\circ] = 4,4936 \cdot \varphi_{k+}^5 - 13,01 \cdot \varphi_{k+}^4 - 3,1278 \cdot \varphi_{k+}^3 + 15,807 \cdot \varphi_{k+}^2 - 8,9712 \cdot \varphi_{k+} + 7,6405$

$$F_q = \frac{F_q}{F_{PT}} \cdot F_{PT}$$

in which $F_{PT}/F_Q = -0,1676 \cdot \varphi_{k+}^5 + 0,743 \cdot \varphi_{k+}^4 - 0,7943 \cdot \varphi_{k+}^3 - 0,1234 \cdot \varphi_{k+}^2 - 0,0742 \cdot \varphi_{k+} + 1,1026$

In the previous equations, φ_{k+} [rad].

In the equations above, $R_{t_x'}$ and $R_{t_y'}$ are the reactions forces at tibia by considering the contribution of the cruciate ligaments:

$$R_{t_x'} = T \cdot \cos(\theta_F + \varphi_K) - N_{tibia} \cdot \sin(\theta_F + \varphi_K)$$

$$R_{t_y'} = T \cdot \sin(\theta_F + \varphi_K) + N_{tibia} \cdot \cos(\theta_F + \varphi_K)$$

Thus, the reaction forces acting at femur are:

$$R_{f_x} = R_{t_x'} - F_q \cdot \cos(\theta_q) - F_{PT} \cdot \cos(\theta_{PT} - \pi)$$

$$R_{f_y} = R_{t_y'} - F_q \cdot \sin(\theta_q) - F_{PT} \cdot \sin(\theta_{PT} - \pi)$$

As done for tibia, it is useful to express the forces on femur in the local system of femur:

$$T_f = - (-R_{f_x} \cdot \sin(\theta_F - 90^\circ) + R_{f_y} \cdot \cos(\theta_F - 90^\circ))$$

$$N_f = - ((R_{f_x} \cdot \cos(\theta_F - 90^\circ) + R_{f_y} \cdot \sin(\theta_F - 90^\circ)))$$

in which T_f and N_f are respectively the shear load and the normal load acting on femur. The sign $-$ is justified because R_{f_x} and R_{f_y} are evaluated as reactions.

7.6.1.6.2. Forces acting on femur in the Flexion phase

Because of in the flexion phase the quadriceps doesn't work, and so any force is transmitted between patella and femur, to evaluate the reaction loads at femur, only the reaction forces at tibia and the force acting at the cruciate ligaments are considered.

By using the same symbols of the previous paragraph, the reaction loads at femur with respect to the global reference system and with respect to the femur axis system (shear and axial force) are given by the following equations:

$$R_{fx} = R_{t x'}$$

$$R_{fy} = R_{t y'}$$

$$T_f = - (-R_{fx} \cdot \sin (\theta_F - 90^\circ) + R_{fy} \cdot \cos (\theta_F - 90^\circ))$$

$$N_f = - (R_{fx} \cdot \cos (\theta_F - 90^\circ) + R_{fy} \cdot \sin (\theta_F - 90^\circ))$$

7.6.2. Model 2

In this model, for the schematization and the inertial parameters, the “Dempster protocol” is used; about the muscles, the moment-arm and the line of action are obtained by scaling the model used in a previous thesis done by Pontin et al. (Pontin et al. 2012, [27]). About the tension at ACL or PCL, they are evaluated by using the relations suggested by Herzog et al. as done in the first model.

7.6.2.1. Model definition and COMs position

In the study done by Pontin, the protocol which was used to obtain the inertial properties was the “Clauser Protocol” (Nigg et al. 2003, [23]). In this thesis, instead, the “Dempster protocol” (Nigg et al. 2003, [23]) is used because it is more precise than the other one regarding the definition of the inertial properties of the foot. By using the “Dempster protocol”, the leg is composed by femur, tibia and foot which are connected by the knee-joint (between femur and tibia) and by the ankle-joint (between tibia and foot) (fig.7.13). For each segment:

- its mass is defined as a percentage of the total weight of the subject;
- its length is defined as a percentage of the total height of the subject;
- the position of the COM is defined with respect to a local reference system embedded to the segment and centered at the proximal joint (for tibia, the COM position is evaluated with respect to the knee-joint; for the foot its COM position is evaluated with respect to the ankle-joint);
- its moment of inertia is defined by considering both the total weight and the total height.

Here below, the equations suggested by Dempster to obtain the previous parameters (H_{tot} [m] and m_{tot} [kg] are the total height and the total weight of the subject):

Tibia:

$$m_{tibia} = 4,5\% \cdot M_{tot}$$

$$\Delta_{y \text{ tibia}} = 23,2\% \cdot H_{tot}$$

$$\Delta_{y G \text{ tibia}} = 43,3\% \cdot \Delta_{y \text{ tibia}}$$

$$I_{G \text{ tibia}} = m_{tibia} \cdot (0,302 \cdot \Delta_{y \text{ tibia}})^2$$

Foot:

$$m_{foot} = 1,4\% \cdot M_{tot}$$

$$\Delta_{x G \text{ foot}} = 0,264 \cdot 0,152 \cdot H_{tot}$$

$$\Delta_{y G \text{ foot}} = 0,429 \cdot 0,046 \cdot H_{tot}$$

$$I_{G \text{ foot}} = m_{foot} \cdot \left(0,475 \cdot 2 \cdot \sqrt{\Delta_{x G \text{ foot}}^2 + \Delta_{y G \text{ foot}}^2} \right)^2$$

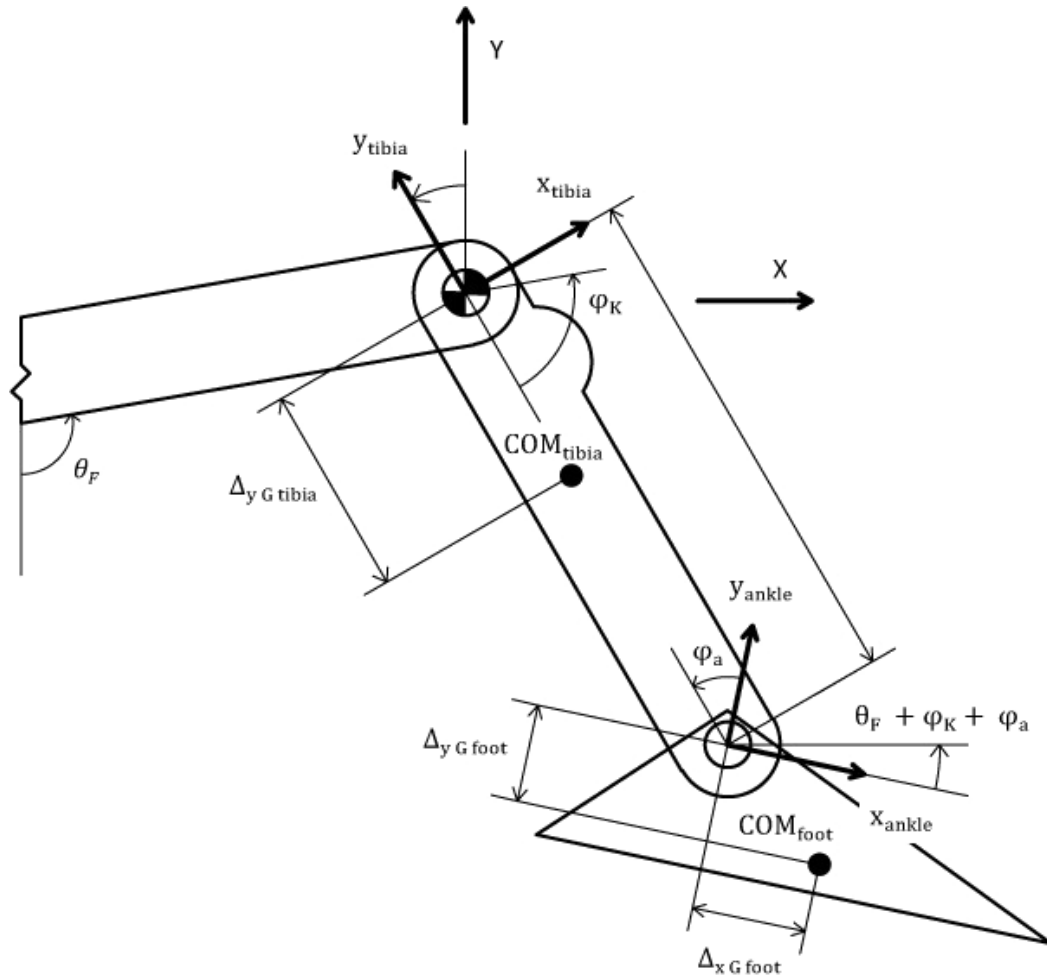


Fig.7.13: Reference systems and COMs position. (Model 2)

The position of the COM of each segment is obtained with the following equations, in a similar way to that used in the previous model by considering the position of COM with respect to the local reference system:

Tibia:

$$x_{G \text{ tibia}} = \Delta_{y \text{ G tibia}} \cdot \sin(\theta_F + \varphi_K)$$

$$y_{G \text{ tibia}} = -\Delta_{y \text{ G tibia}} \cdot \cos(\theta_F + \varphi_K)$$

Foot:

$$x_{G \text{ foot}} = \Delta_{y \text{ tibia}} \cdot \sin(\theta_F + \varphi_K) + \Delta_{x \text{ G foot}} \cdot \cos(\theta_F + \varphi_K + \varphi_a) + \Delta_{y \text{ G foot}} \cdot \sin(\theta_F + \varphi_K + \varphi_a)$$

$$y_{G \text{ foot}} = -\Delta_{y \text{ tibia}} \cdot \cos(\theta_F + \varphi_K) + \Delta_{x \text{ G foot}} \cdot \sin(\theta_F + \varphi_K + \varphi_a) - \Delta_{y \text{ G foot}} \cdot \cos(\theta_F + \varphi_K + \varphi_a)$$

in which $\Delta_{y \text{ tibia}}$ is the length of the tibia, $\Delta_{y \text{ G tibia}}$ is the position of the COM of the tibia in the tibia reference system, $\Delta_{x \text{ G foot}}$ and $\Delta_{y \text{ G foot}}$ the coordinates of the position of the COM of the foot with respect to the foot reference system; θ_F , φ_K and φ_a are the same angles defined in the previous model (their sign is positive as in the previous model: counter clock wise). As in the previous model, $\theta_F = \text{cost}$, $\varphi_a \cong \text{cost}$ and their value is the result of the inverse kinematics calculated with the software OpenSim.

7.6.2.2. Muscular forces and Reaction loads at tibia

As done for the first model, it is necessary to consider separately the extension phase and the flexion phase because the forces acting at the tibia are different in the two situations. In this second model, the line of action and the moment arm of the muscles acting during the exercises are evaluated by scaling the anthropometric features of the model used by Pontin et al., which had been scaled by considering anatomic tables in literature too.

7.6.2.2.1. Muscular forces and Reaction loads at tibia Extension

As in the previous model, in the study done by Pontin et al. the quadriceps is considered the only muscle acting in extension; its force is transmitted to tibia with the patellar tendon. About the patella, it is modeled like a pulley, with radius B_{PT} , and the patellar tendon moves around it with a fixed point on the tibia tuberosity; the position of this point is defined by two coordinates, D_{Q2} and H_{Q2} , which are defined in the tibia reference system (fig.7.14). To scale the anthropometric parameters which are used to define the line of action and the moment arm of each subject, the value of D_{Q2} is used: because of the quite easiness in its identification, its value is obtained with a direct measuring, with respect to the longitudinal axis of tibia, of the distance between the point in which the patellar tendon is fixed to the tibia tuberosity and the center of the knee, which is evaluated approximatively at the midpoint of the distance between the two condyles. By considering the ratio between the new value measured and the value used by Pontin, it is also possible to scale the other parameters. For example, if we consider H_{Q2} , its value can be obtained as:

$$H_{Q2} = \frac{D_{Q2 \text{ measured}}}{D_{Q2 \text{ Pontin}}} \cdot H_{Q2 \text{ Pontin}}$$

in which $D_{Q2 \text{ measured}}$ is the value measured directly and $D_{Q2 \text{ Pontin}}$ and $H_{Q2 \text{ Pontin}}$ are the values used by Pontin et al..

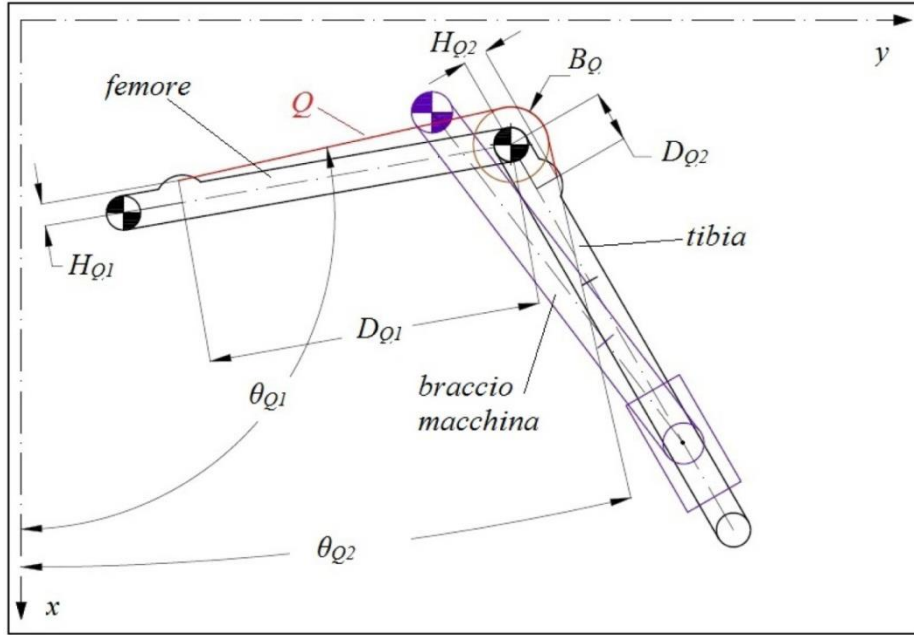


Fig.7.14: Schematization used by Pontin: patella modeled as a pulley. (Model 2)

The inclination of the patellar tendon θ_{PT} in the global reference frame is given by this equation (adapted from that used by Pontin et al.):

$$\theta_{PT} [\text{rad}] = (\theta_F + \varphi_k) [\text{rad}] - \arctan\left(\frac{D_{PT}}{H_{PT}}\right) - \arcsin\left(\frac{B_{PT}}{\sqrt{D_{PT}^2 + H_{PT}^2}}\right) + \pi$$

In the model used by Pontin et al., the moment arm of the patellar tendon B_{PT} is defined as a function of the knee angle; thus the moment arm is obtained by scaling the initial values as described above and then by interpolating the results.

About the forces acting during the exercise, with the same representation in fig.7.7, the force at the patellar tendon and the reaction loads are given by the following equations:

$$F_{PT} = \frac{I_k \cdot \ddot{\varphi}_k - W_{total} \cdot x_{COM} - F_{ext\ x} \cdot b_{F\ ext\ x} - F_{ext\ y} \cdot b_{F\ ext\ y}}{B_{PT}}$$

$$R_{t\ x} = (m_{tibia} + m_{foot}) \cdot \ddot{x}_{COM} - F_{ext\ x} - F_{PT} \cdot \cos(\theta_{PT})$$

$$R_{t\ y} = (m_{tibia} + m_{foot}) \cdot \ddot{y}_{COM} - F_{ext\ y} - W_{total} - F_{PT} \cdot \sin(\theta_{PT})$$

in which:

- x_{COM} and y_{COM} : coordinates of the global center of mass:

$$x_{COM} = \frac{m_{tibia} \cdot x_{G\ tibia} + m_{foot} \cdot x_{G\ foot}}{m_{tibia} + m_{foot}}$$

$$y_{COM} = \frac{m_{tibia} \cdot x_{G\ tibia} + m_{foot} \cdot x_{G\ foot}}{m_{tibia} + m_{foot}}$$

- I_k : moment of inertia around the knee

$$I_k = (I_{G\ tibia} + m_{tibia} \cdot d_{tibia}^2) + (I_{G\ foot} + m_{foot} \cdot d_{foot}^2)$$

and I_{G_j} and $d_j = \sqrt{x_{G_j}^2 + y_{G_j}^2}$ are respectively the moment of inertia with respect to the COM of the j^{th} segment and the distance of COM of the j^{th} segment from the knee joint center.

- \ddot{x}_{COM} : acceleration in x direction of the COM

$$\ddot{x}_{COM} = \frac{m_{tibia} \cdot \ddot{x}_{G\ tibia} + m_{talus} \cdot \ddot{x}_{G\ foot}}{m_{tibia} + m_{foot}}$$

$$\ddot{x}_{G\ tibia} = -\Delta_{y\ G\ tibia} \cdot \text{sen}(\theta_F + \varphi_K) \cdot \dot{\varphi}_K^2 + \Delta_{y\ G\ tibia} \cdot \text{cos}(\theta_F + \varphi_K) \cdot \ddot{\varphi}_K$$

$$\begin{aligned} \ddot{x}_{G\ foot} = & -\Delta_{y\ tibia} \cdot \text{sen}(\theta_F + \varphi_K) \cdot \dot{\varphi}_K^2 + \Delta_{y\ tibia} \cdot \text{cos}(\theta_F + \varphi_K) \cdot \ddot{\varphi}_K + \\ & - [\Delta_{x\ G\ foot} \cdot \text{cos}(\theta_F + \varphi_K + \varphi_a) \cdot \dot{\varphi}_K^2 + \Delta_{x\ G\ foot} \cdot \text{sen}(\theta_F + \varphi_K + \varphi_a) \cdot \ddot{\varphi}_K] + \\ & + [-\Delta_{y\ G\ foot} \cdot \text{sen}(\theta_F + \varphi_K + \varphi_a) \cdot \dot{\varphi}_K^2 + \Delta_{y\ G\ foot} \cdot \text{cos}(\theta_F + \varphi_K + \varphi_a) \cdot \ddot{\varphi}_K] \end{aligned}$$

- \ddot{y}_{COM} : acceleration in the y direction of the COM

$$\ddot{y}_{COM} = \frac{m_{tibia} \cdot \ddot{y}_{G\ tibia} + m_{talus} \cdot \ddot{y}_{G\ foot}}{m_{tibia} + m_{foot}}$$

$$\ddot{y}_{G\ tibia} = \Delta_{y\ G\ tibia} \cdot \text{cos}(\theta_F + \varphi_K) \cdot \dot{\varphi}_K^2 + \Delta_{y\ G\ tibia} \cdot \text{sen}(\theta_F + \varphi_K) \cdot \ddot{\varphi}_K$$

$$\begin{aligned} \ddot{y}_{G\ foot} = & \Delta_{y\ tibia} \cdot \text{cos}(\theta_F + \varphi_K) \cdot \dot{\varphi}_K^2 + \Delta_{y\ tibia} \cdot \text{sen}(\theta_F + \varphi_K) \cdot \ddot{\varphi}_K \\ & + [-\Delta_{x\ G\ foot} \cdot \text{sen}(\theta_F + \varphi_K + \varphi_a) \cdot \dot{\varphi}_K^2 + \Delta_{x\ G\ foot} \cdot \text{cos}(\theta_F + \varphi_K + \varphi_a) \cdot \ddot{\varphi}_K] + \\ & + [\Delta_{y\ G\ foot} \cdot \text{cos}(\theta_F + \varphi_K + \varphi_a) \cdot \dot{\varphi}_K^2 + \Delta_{y\ G\ foot} \cdot \text{sen}(\theta_F + \varphi_K + \varphi_a) \cdot \ddot{\varphi}_K] \end{aligned}$$

7.6.2.2.2. Muscular forces and Reaction loads at tibia in the Flexion phase

In the study by Pontin et al., the muscles which were considered acting in the flexion phase were biceps femoris-long head, biceps femoris-short head, semimembranosus, semitendinosus and gastrocnemius, but the analysis done with the software OpenSim show that the activation of gastrocnemius is null; for this reason in this study this muscle is ignored.

The line of action of the muscles involved during the movement are obtained by using the following equations (Pontin et al., 2012):

$$\theta_{BFL} [\text{rad}] = \arctan2 \left(\frac{D_{BFL1} \sin\theta_1 + D_{BFL2} \sin q + H_{BFL2} \cos q - H_{BFL1} \cos\theta_1}{D_{BFL1} \cos\theta_1 + D_{BFL2} \cos q + H_{BFL2} \sin q - H_{BFL1} \sin\theta_1} \right)$$

$$\theta_{BFB} [\text{rad}] = \arctan2 \left(\frac{D_{BFB1} \sin\theta_1 + D_{BFB2} \sin q + H_{BFB2} \cos q - H_{BFB1} \cos\theta_1}{D_{BFB1} \cos\theta_1 + D_{BFB2} \cos q + H_{BFB2} \sin q - H_{BFB1} \sin\theta_1} \right)$$

$$\theta_{SM} [\text{rad}] = \arctan2 \left(\frac{D_{SM1} \sin\theta_1 + D_{SM2} \sin q + H_{SM2} \cos q - H_{SM1} \cos\theta_1}{D_{SM1} \cos\theta_1 + D_{SM2} \cos q + H_{SM2} \sin q - H_{SM1} \sin\theta_1} \right)$$

$$\theta_{ST1} [\text{rad}] = \theta_1 [\text{rad}] + \frac{\pi}{2} - \arctan \left(\frac{D_{ST1}}{H_{ST1}} \right) - \arcsin \left(\frac{B_{ST}}{\sqrt{D_{ST1}^2 + H_{ST1}^2}} \right)$$

$$\theta_{ST2} [\text{rad}] = q [\text{rad}] + \alpha_{ST} [\text{rad}] + \frac{\pi}{2} \quad \alpha_{ST} = \text{constant}$$

in which θ_{BFL} , θ_{BFB} , θ_{SM} , θ_{ST1} and θ_{ST2} give the line of action of the muscles with respect to the global x-axis system used by Pontin (see fig.7.15.a and fig.7.15.b) and $q = \theta_F + \varphi_K$ (θ_F and φ_K have the meaning described for the first model: θ_F is the inclination of the femur and φ_K is the knee flexion angle). For the other symbols used in the previous equations, see fig.7.15.a and fig.7.15.b. Pontin et al. considered also the fact that the semitendinosus exerts also a force which has a line of action defined by the angle θ_{ST2} in fig.7.15.b.

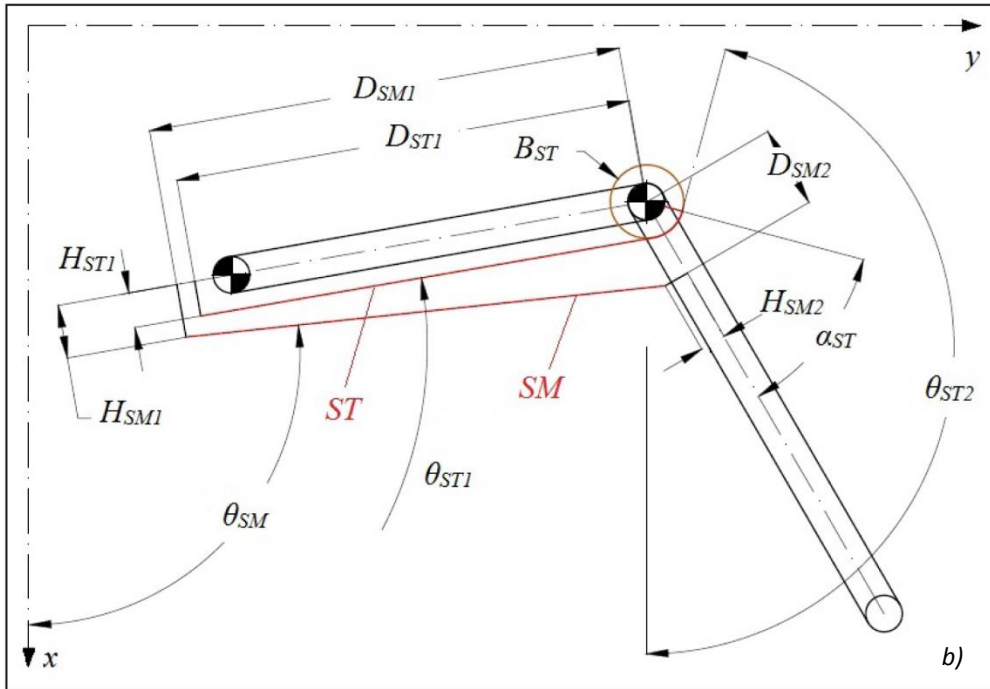
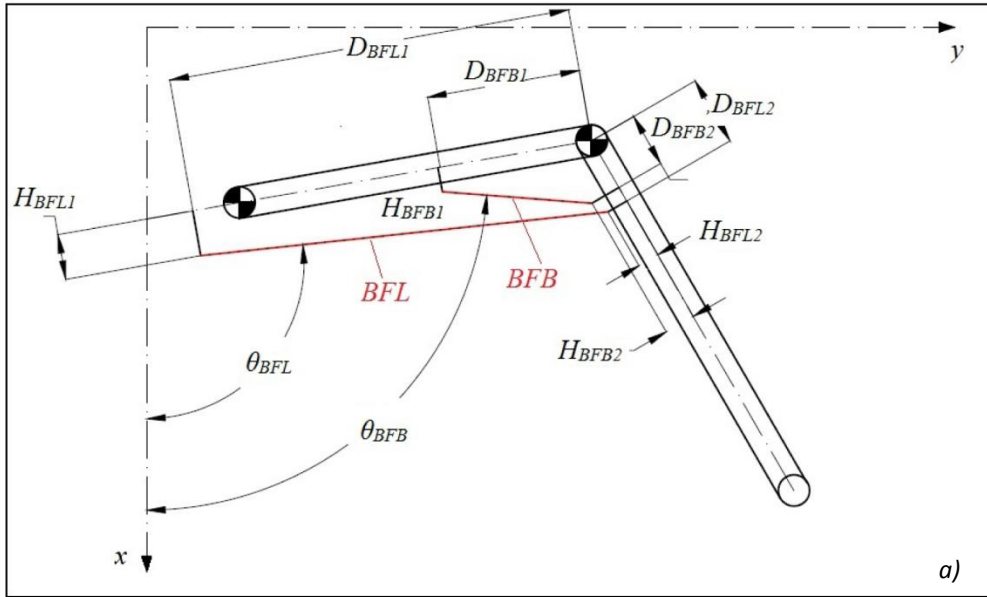


Fig.7.15: Line of action and moment arm of biceps femoris-long head and short head (fig.7.15.a), semimembranosus and semitendinosus (fig.7.15.b) in Pontin's schematization. (Pontin et al. 2012, [27])

About the moment-arm, they are defined as function of the previous angles:

$$B_{BFL} = H_{BFL2} \cos(q - \theta_{BFL}) - D_{BFB2} \sin(q - \theta_{BFL})$$

$$B_{BFB} = H_{BFB2} \cos(q - \theta_{BFB}) - D_{BFB2} \sin(q - \theta_{BFB})$$

$$B_{SM} = H_{SM2} \cos(q - \theta_{SM}) - D_{SM2} \sin(q - \theta_{SM})$$

$$B_{ST} = \text{constant}$$

in which B_{BFL} , B_{BFB} , B_{SM} and B_{ST} are the moment arm of the biceps femoris-long head, biceps femoris-short head, semimembranosus and semitendinosus respectively.

The muscular forces can be evaluated by using the same approach of the first model:

$$F_{BFB} = \frac{M_{tot}}{\left[b_{BFB} + b_{BFL} \left(\frac{b_{BFL}}{b_{BFB}} \right)^{0,5} \left(\frac{N_{BFL}}{N_{BFB}} \right)^{1,5} + b_{SM} \left(\frac{b_{SM}}{b_{BFB}} \right)^{0,5} \left(\frac{N_{SM}}{N_{BFB}} \right)^{1,5} + b_{ST} \left(\frac{b_{ST}}{b_{BFB}} \right)^{0,5} \left(\frac{N_{ST}}{N_{BFB}} \right)^{1,5} \right]}$$

$$F_{BFL} = \frac{M_{tot}}{\left[b_{BFL} + b_{BFB} \left(\frac{b_{BFB}}{b_{BFL}} \right)^{0,5} \left(\frac{N_{BFB}}{N_{BFL}} \right)^{1,5} + b_{SM} \left(\frac{b_{SM}}{b_{BFL}} \right)^{0,5} \left(\frac{N_{SM}}{N_{BFL}} \right)^{1,5} + b_{ST} \left(\frac{b_{ST}}{b_{BFL}} \right)^{0,5} \left(\frac{N_{ST}}{N_{BFL}} \right)^{1,5} \right]}$$

$$F_{SM} = \frac{M_{tot}}{\left[b_{SM} + b_{BFB} \left(\frac{b_{BFB}}{b_{SM}} \right)^{0,5} \left(\frac{N_{BFB}}{N_{SM}} \right)^{1,5} + b_{BFL} \left(\frac{b_{BFL}}{b_{SM}} \right)^{0,5} \left(\frac{N_{BFL}}{N_{SM}} \right)^{1,5} + b_{ST} \left(\frac{b_{ST}}{b_{SM}} \right)^{0,5} \left(\frac{N_{ST}}{N_{SM}} \right)^{1,5} \right]}$$

$$F_{ST} = \frac{M_{tot}}{\left[b_{ST} + b_{BFB} \left(\frac{b_{BFB}}{b_{ST}} \right)^{0,5} \left(\frac{N_{BFB}}{N_{ST}} \right)^{1,5} + b_{BFL} \left(\frac{b_{BFL}}{b_{ST}} \right)^{0,5} \left(\frac{N_{BFL}}{N_{ST}} \right)^{1,5} + b_{SM} \left(\frac{b_{SM}}{b_{ST}} \right)^{0,5} \left(\frac{N_{SM}}{N_{ST}} \right)^{1,5} \right]}$$

As done in the first model, N is chosen as maximum isometric force and its value is obtained by OpenSim.

About the reaction loads, in order to compare the results from those deriving from the first model, it is useful to express the line of action of the muscles with respect to the same global axis system used in the first model (see fig.7.5):

$$\theta_{BFL}' = \theta_{BFL} + \frac{\pi}{2}$$

$$\theta_{BFB}' = \theta_{BFB} + \frac{\pi}{2}$$

$$\theta_{SM}' = \theta_{SM} + \frac{\pi}{2}$$

$$\theta_{ST1}' = \theta_{ST1} + \frac{\pi}{2}$$

$$\theta_{ST2}' = \theta_{ST2} - \frac{\pi}{2}$$

in which θ_{BFL}' , θ_{BFB}' , θ_{SM}' , θ_{ST1}' and θ_{ST2}' are the line of action of the muscles with respect to the global axis system used in the first model. In this way it is possible to evaluate the reaction loads at tibia by using the following equations:

$$R_{tx} = (m_{tibia} + m_{foot}) \cdot \ddot{x}_{COM} - F_{extx} - F_{BFL} \cdot \cos(\theta_{BFL}') - F_{BFB} \cdot \cos(\theta_{BFB}') - F_{SM} \cdot \cos(\theta_{SM}') + F_{ST} \cdot (\cos(\theta_{ST1}') + \cos(\theta_{ST2}'))$$

$$R_{ty} = (m_{tibia} + m_{foot}) \cdot \ddot{y}_{COM} - F_{exty} - F_{BFL} \cdot \sin(\theta_{BFL}') - F_{BFB} \cdot \sin(\theta_{BFB}') - F_{SM} \cdot \sin(\theta_{SM}') + F_{ST} \cdot (\sin(\theta_{ST1}') + \sin(\theta_{ST2}'))$$

7.6.2.3. Forces acting on tibia

As done for the first model, the shear, T, and the axial load, N, acting on tibia are evaluated by the same equations at par.7.6.1.4 :

$$T = R_{tx} \cdot \cos(\theta_F + \varphi_K) + R_{ty} \cdot \sin(\theta_F + \varphi_K)$$

$$N = -R_{tx} \cdot \sin(\theta_F + \varphi_K) + R_{ty} \cdot \cos(\theta_F + \varphi_K)$$

7.6.2.4. Force acting at ACL and PCL

Because of Pontin et al. didn't suggest any relation to evaluate the force at the cruciate ligaments, the relations suggested by Herzog et al. are used as done in par.7.6.1.5 :

$$F_{ACL} = \frac{T}{\cos(\varphi_{ACL})}$$

$$F_{PCL} = \frac{T}{\cos(\varphi_{PCL})}$$

7.6.2.5. Forces acting on femur

To evaluate the forces acting at femur, it is necessary to consider separately the extension phase and the flexion phase.

7.6.2.5.1. Forces acting on femur Extension

As done for the first model, a simplified approach is used.

In this second model, being the patella represented as a pulley, the moment-arm of the quadriceps and the moment-arm of the patellar tendon are the same (fig.7.16); thus the force acting at the quadriceps is the same of that acting at the patellar tendon: $F_q = F_{PT}$.

The inclination of the quadriceps is evaluated with the following equation (adapted from that used by Pontin):

$$\theta_q[\text{rad}] = \theta_F[\text{rad}] + \arctan\left(\frac{D_{Q1}}{H_{Q1}}\right) + \arcsin\left(\frac{B_{PT}}{\sqrt{D_{Q1}^2 + H_{Q1}^2}}\right)$$

in which D_{Q1} and H_{Q1} are the coordinates of the insertion of the quadriceps expressed in the femur axis system (see fig.7.16). The values of D_{Q1} and H_{Q1} are obtained by scaling the initial values as described above.

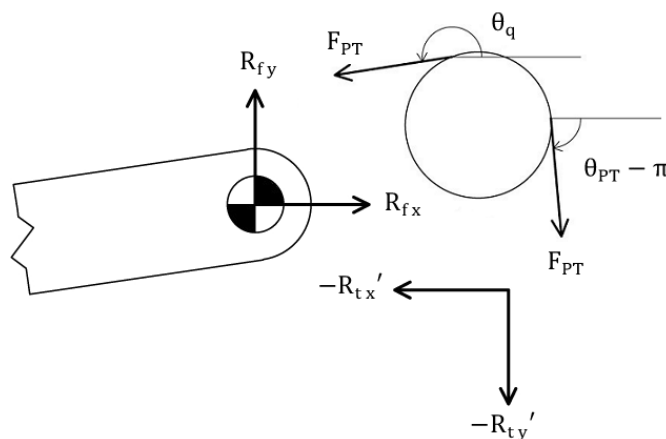


Fig7.16: Forces acting on femur. (Model 2)

The reaction forces at femur are evaluated with the same equations used in the first model:

$$R_{fx} = R_{tx}' - F_q \cdot \cos(\theta_q) - F_{PT} \cdot \cos(\theta_{PT} - \pi)$$

$$R_{fy} = R_{ty}' - F_q \cdot \sin(\theta_q) - F_{PT} \cdot \sin(\theta_{PT} - \pi)$$

As in the previous model, it is also possible to evaluate the shear load and the normal force acting on femur (with respect to the femur axis system):

$$T_f = - (-R_{fx} \cdot \sin(\theta_F - 90^\circ) + R_{fy} \cdot \cos(\theta_F - 90^\circ))$$

$$N_f = - ((R_{fx} \cdot \cos(\theta_F - 90^\circ) + R_{fy} \cdot \sin(\theta_F - 90^\circ)))$$

7.6.2.5.2. Forces acting on femur in Flexion

The reaction loads at femur in the flexion phase are evaluated by using the same relations used in the first model:

$$R_{fx} = R_{t_x}'$$

$$R_{fy} = R_{t_y}'$$

$$T_f = - (-R_{fx} \cdot \sin(\theta_F - 90^\circ) + R_{fy} \cdot \cos(\theta_F - 90^\circ))$$

$$N_f = - ((R_{fx} \cdot \cos(\theta_F - 90^\circ) + R_{fy} \cdot \sin(\theta_F - 90^\circ)))$$

7.6.3. Comparison with OpenSim results

The results of the analytical approach described in the paragraphs above, both for the first and the second model, were compared with those deriving of the OpenSim simulations (when it was possible). In particular, for the flexion phase a direct comparison was possible in terms of force acting at the muscles involved during the movement and in terms of shear and axial load on tibia and femur. For the extension phase, instead, the force at the patellar tendon calculated by the analytical models was compared with the sum of the forces acting at the four fascicles of the quadriceps (rectus femoris, vastus intermedius, vastus medialis and vastus lateralis) calculated with the software OpenSim because of the knee modeling used in gait2392_model (par.4.6). Moreover, because of the great difference in the results of the shear and axial loads acting on tibia obtained by analytical models and OpenSim simulations, for the extension phase other two parameters were calculated; by using the terminology adopted in the previous paragraphs:

$$\text{Tibia Shear (with patella)} = R_{f_x} \cdot \cos(\theta_F + \varphi_K) + R_{f_y} \cdot \sin(\theta_F + \varphi_K)$$

$$\text{Tibia Axial Force (with patella)} = -R_{f_x} \cdot \sin(\theta_F + \varphi_K) + R_{f_y} \cdot \cos(\theta_F + \varphi_K)$$

in which Tibia Shear (with patella) and Tibia Axial Force (with patella) are respectively the shear and the axial load acting on tibia by considering the reaction forces at femur (and so by considering the contribution of the patella). The meaning of these parameters will be explained at the end of this study.

About the force acting at ACL or PCL, only the results obtained by the analytical models are available, because of the knee schematization adopted by the software (par.4.6).

The results of the comparison of analytical models and OpenSim model were obtained in the following way:

- evaluation of biomechanical parameters in extension and in flexion for each subject and for each velocity by considering the second, the third and the fourth cycle;
- for each subject, normalization to the maximum (minimum if flexion) knee moment obtained by considering all velocities;
- evaluation of a mean cycle for each biomechanical parameter by considering the results of all subjects.

8.Comparative evaluation and discussion of results of Part 1

Here below, the results of the comparisons are shown:

- comparison and evaluation of Torque and Flexors and extensors balance;
- comparison and evaluation of electromyography and OpenSim muscle activation;
- comparison and evaluation of analytical models and OpenSim model.

8.1.Comparison and evaluation of Torque and Flexors and extensors balance

The torque at the servo-motor and the flexors and extensors balance at different velocities are shown. For each subject, the torque at the servo motor normalized to the body weight and the ratio $R_{F/E}$ are expressed as a function of the angle of the bar measured at the servo-motor (which is very close to the knee angle). About the ratio $R_{F/E}$, only the range 35°-80° is plotted because of the dispersion of results in the entire range of motion.

The results refer to a mean cycle evaluated by means of the three cycles investigated (second, third and fourth cycle). The results are not expressed as mean and standard deviation by considering all subjects in order to obtain a ranking of performances.

When the torque is positive, there is extension, when it is negative there is flexion.

Torque and flexors and extensors balance of each subject are in Appendix.

Flexors and Extensors balance: Normalized Torque

— S1 — S2 — S3 — S4 — S5 — S6

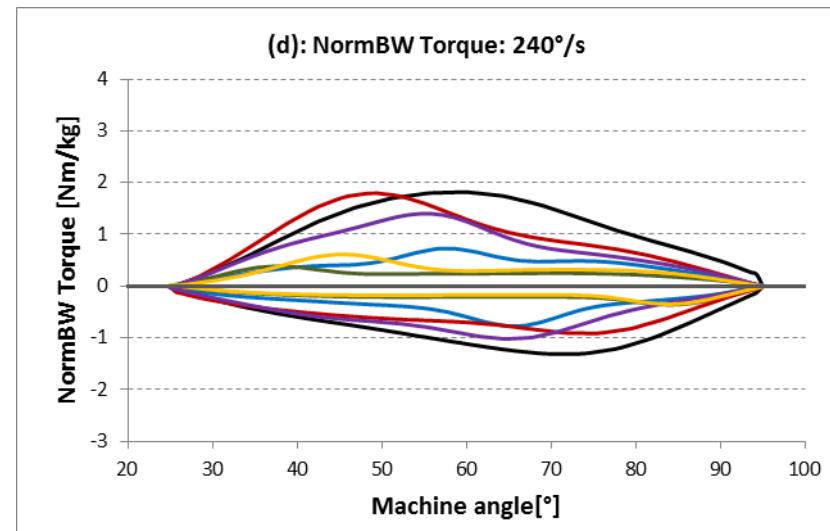
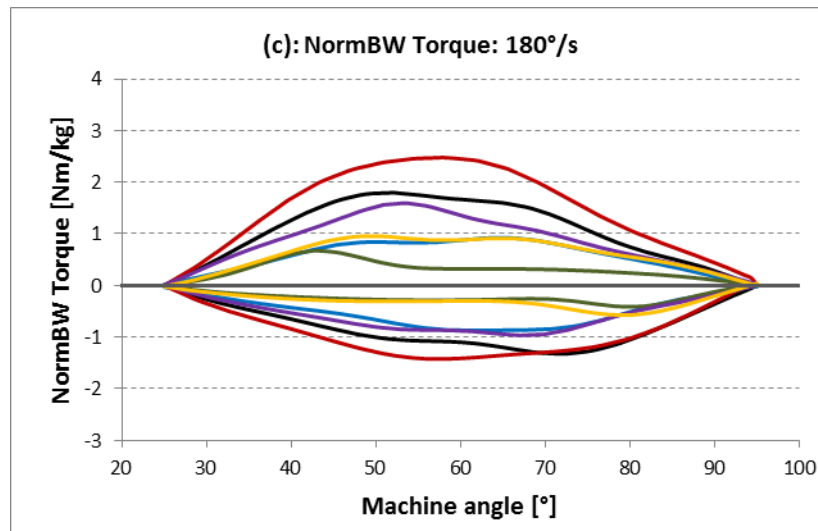
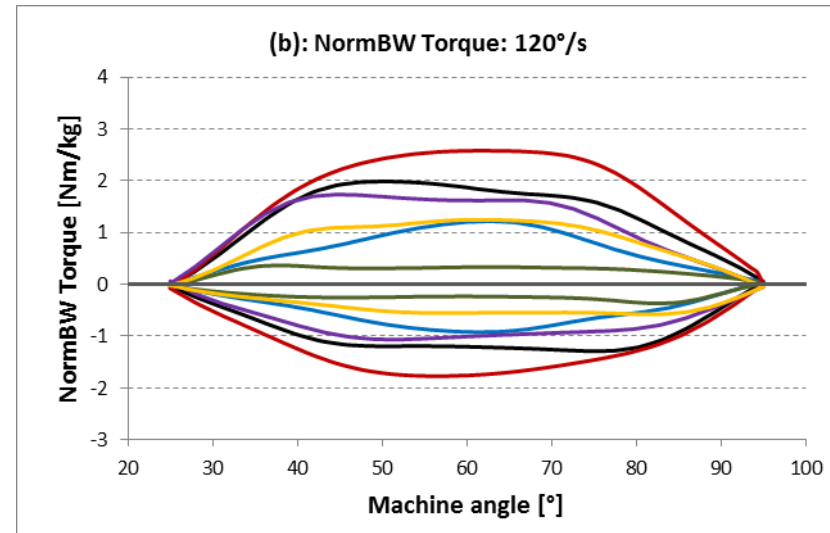
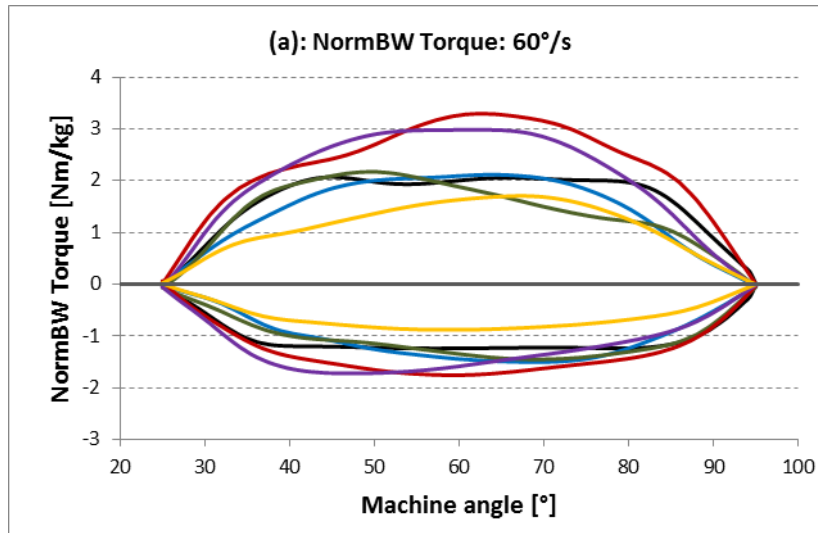


Fig.8.1: Torque (normalized to BW) as a function of the angle at the servo-motor at 60°/s (a), 120°/s (b), 180°/s (c) and 240°/s (d).

Flexors and Extensors balance: $R_{F/E}$

— S1 — S2 — S3 — S4 — S5 — S6

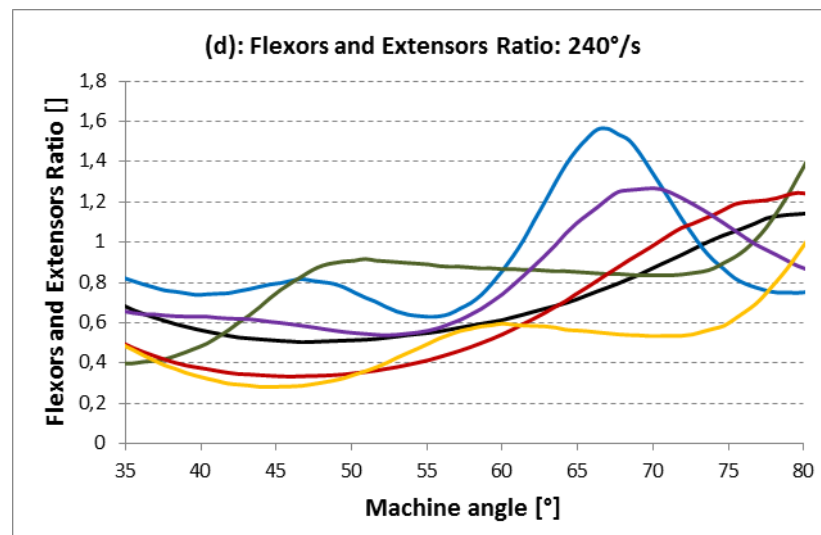
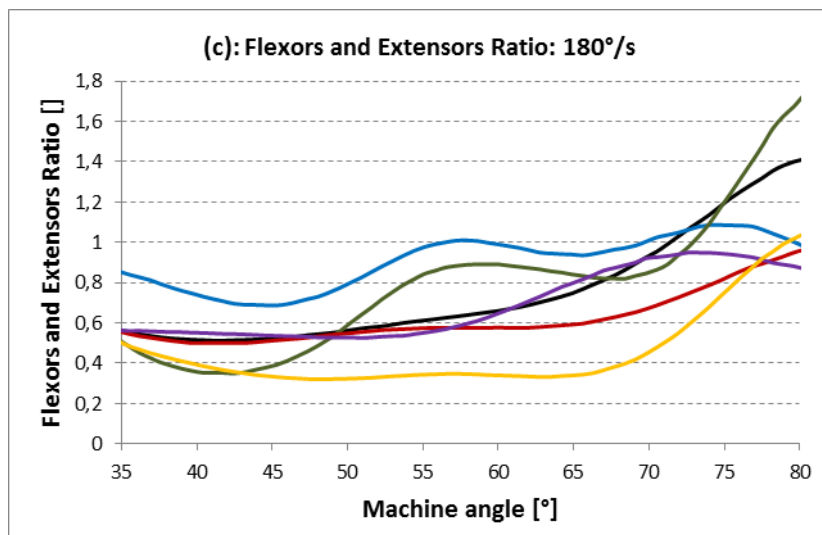
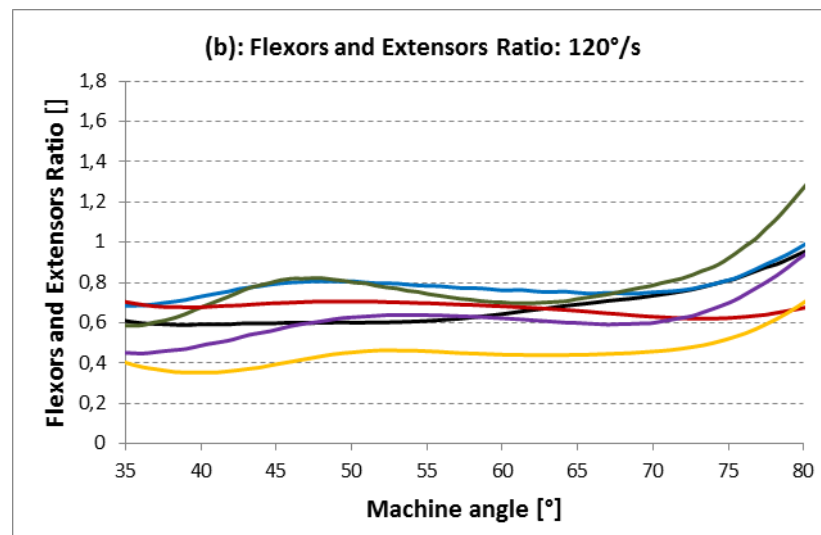
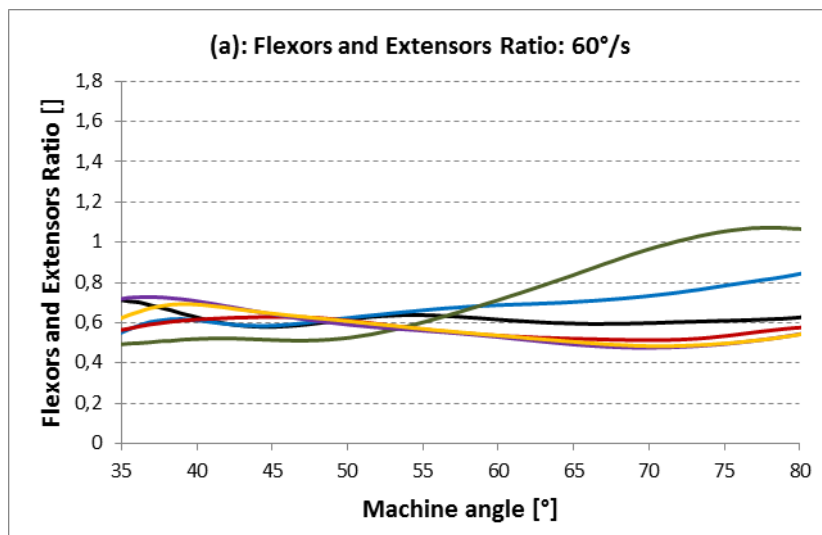


Fig.8.2: Ratio $R_{F/E}$ as a function of the angle at the servo-motor at 60°/s (a), 120°/s (b), 180°/s (c) and 240°/s (d).

Discussion of results

Considering the torque applied at the servo-motor, fig.8.1 allows to rank, by considering the peak values in extension and in extension, the performances of the subjects at different velocities. In particular it is possible to identify that subject 1, 4 and 5 performed the exercises at a higher level of intensity with respect to the other subjects at each velocity and both in extension and in flexion: for subject 1, 4 and 5 the peak value (average values) are in the range 2,1-3,3 Nm/kg in extension and 1,2-1,8 Nm/kg in flexion at 60°/s, 1,8-2,6 Nm/kg in extension and 1,1-1,8 Nm/kg in flexion at 120°/s, 1,6-2,5 Nm/kg in extension and 1-1,4 Nm/kg in flexion at 180°/s and 1,4-1,8 Nm/kg in extension and 0,9-1,3 Nm/kg in flexion at 240°/s; for subject 2, 3 and 6 the peak value (average values) are in the range 1,7-2,1 Nm/kg in extension and 0,9-1,3 Nm/kg in flexion at 60°/s, 0,4-1,2 Nm/kg in extension and 0,4-1 Nm/kg in flexion at 120°/s, 0,8-0,9 Nm/kg in extension and 0,6-0,9 Nm/kg in flexion at 180°/s and 0,4-0,7 Nm/kg in extension and 0,3-0,8 Nm/kg in flexion at 240°/s. Fig.8.1 emphasizes moreover the fact that the profile of the curve is regular both in flexion and extension at each velocity for subject 1; for the other subjects, instead, the profile of the curve is regular only at 60°/s (for subject 4 also at 120°/s) and then it tends, with the growth of the velocity, to decrease rapidly and have peaks both in flexion and extension.

Regarding the ratio between the torque in flexion and in extension, its shape is a consequence of the different torque profile of the subjects at different velocities. Because at 60°/s the torque profile is regular both in extension and in flexion for all subjects, the ratio has a regular shape with a good reliability of results and its value increases gradually from $0,62 \pm 0,12$ at 35° to $0,8 \pm 0,26$ at 80° (average values); at 120°/s because the torque profile has peaks both in extension and in flexion and, moreover, these peaks occur at different angles (in particular the peak values in extension occurs at the end the extension phase (35°-50°) and the peak values in flexion at the end of the flexion phase (50°-80°)), the ratio has a shape which is quite regular but the dispersion of results is higher than at 60°/s and its value increases higher from $0,55 \pm 0,15$ at 35° to $1 \pm 0,32$ at 80° (average values) than that at the previous velocity; irregular torque profile and peaks become more significant at 180°/s and 240°/s at which the ratio ranges from $0,67 \pm 0,18$ at 35° to $1,3 \pm 0,4$ at 80° at 180°/s and from $0,6 \pm 0,2$ at 35° to $1,1 \pm 0,33$ at 80° with a peak of 1,6 at 63° for subject 2 at 240°/s (average values) with a high dispersion of results. Furthermore, by comparing the results of all subjects at different velocities, it appears that the mean value is about 0,6 in the range 35°-60° for all velocities and then it tends to increase, gradually at 60°/s and 120°/s, rapidly at 180°/s and 240°/s. Moreover, the increase appears also for subjects 1, 4 and 5 who performed the exercises at a higher intensity of torque than the others (however, the ratio profile of subject 1 is more regular than those of the others because of his regular torque profile). These findings are not in agree with the results obtained by Pontaga et al. (Pontaga I 2004, [26]; par.3.7): in that study, the ratio has similar values in the range 55-80° at different velocities and then it increases in the range 10°-30°; moreover the increase was higher at high velocities than at slow ones. The different results between the

two studies may be associated with the different type of subjects who were tested: in the previous investigation the subjects had a good training condition which allowed them to use the hamstrings to produce torque with the aim to decelerate the knee extension (and this is the cause of the increase of the ratio in the range 10°-30°); the subjects tested in this study, instead, had a good physical condition but not as good as that of the subjects of the previous study and so they couldn't control as well the movement both in extension and in flexion and in all range of motion.

8.2. Comparison and evaluation of electromyography and OpenSim muscle activation

The comparison in terms of muscular activation at different velocities is shown in what follows. For each velocity the results are expressed as mean of the three cycles investigated of all subjects (standard deviation is omitted in the visualization). The results are expressed both in a qualitative way, by plotting the mean profile of muscular activation as a function of a mean cycle extension-flexion (thus in the first part of the graphs there is extension, in the second part flexion) and in a quantitative way, by calculating Peak error, Time error and Area error as mean and standard deviation, as described in par.7.5. The quantitative parameters are evaluated by considering the mean cycle.

In order to emphasize that this is a comparison with experimental results, the results are shown with a grey background.

The results of the comparison of each subject are in Appendix.

60 °/s

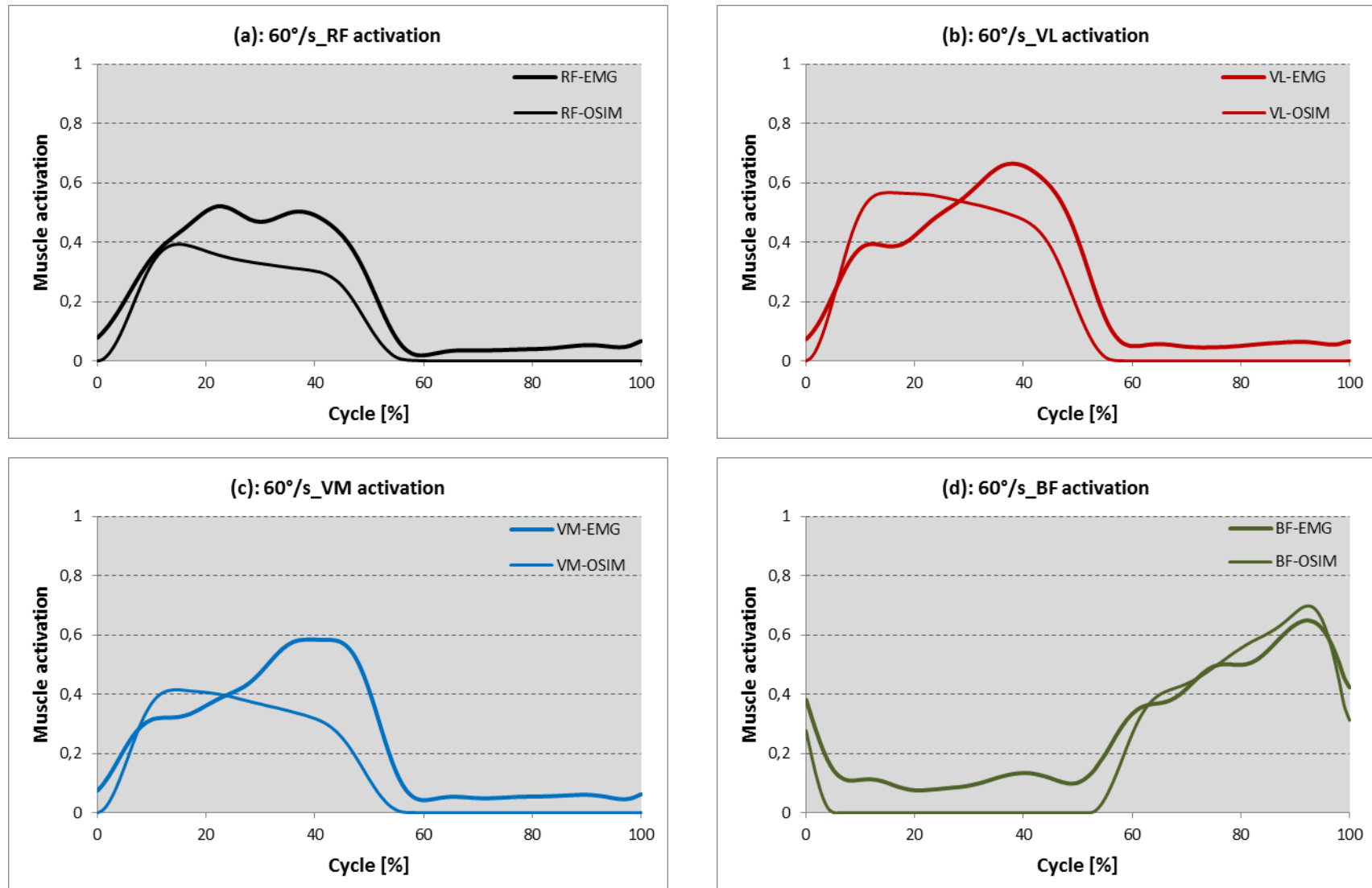


Fig.8.3: EMG and OpenSim muscle activation at 60°/s of RF (a), VL (b), VM (c) and BF (d).

120 °/s

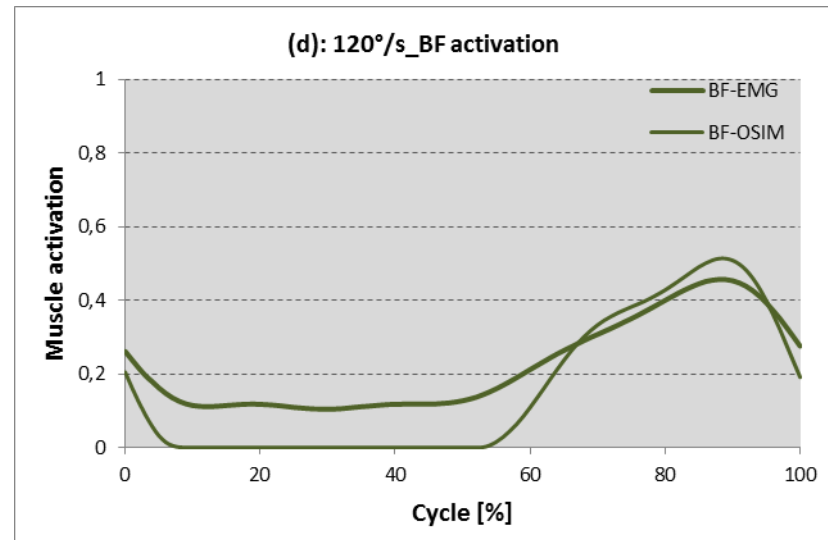
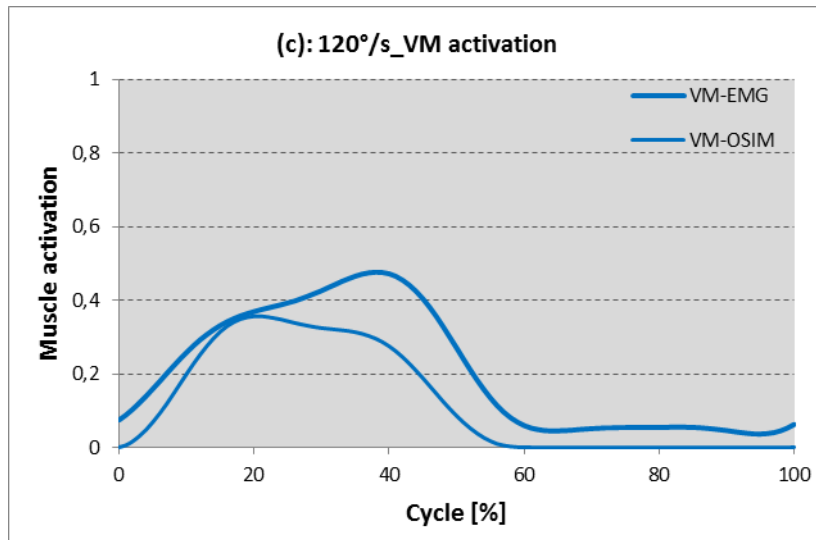
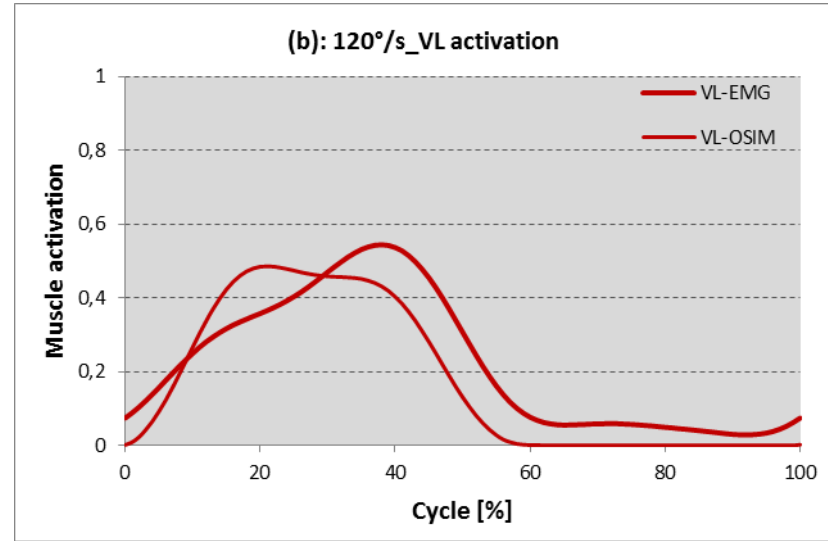
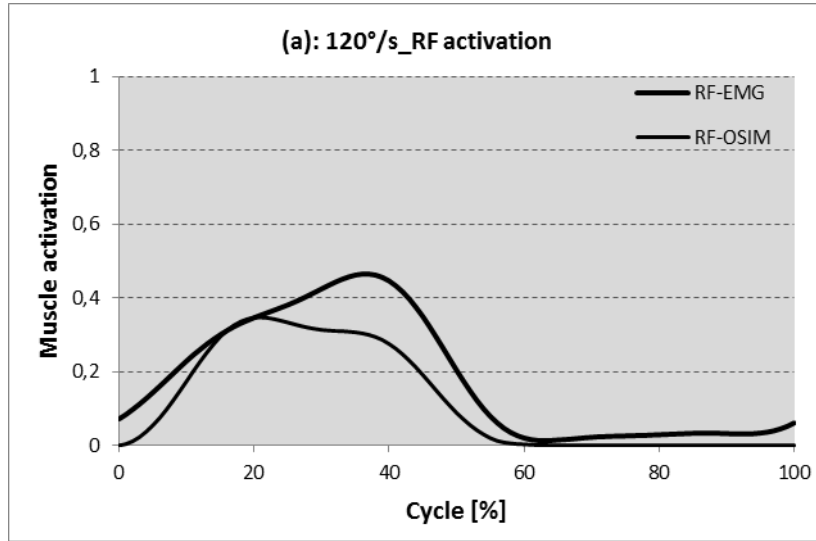


Fig.8.4: EMG and OpenSim muscle activation at 120°/s of RF (a), VL (b), VM (c) and BF (d).

180 °/s

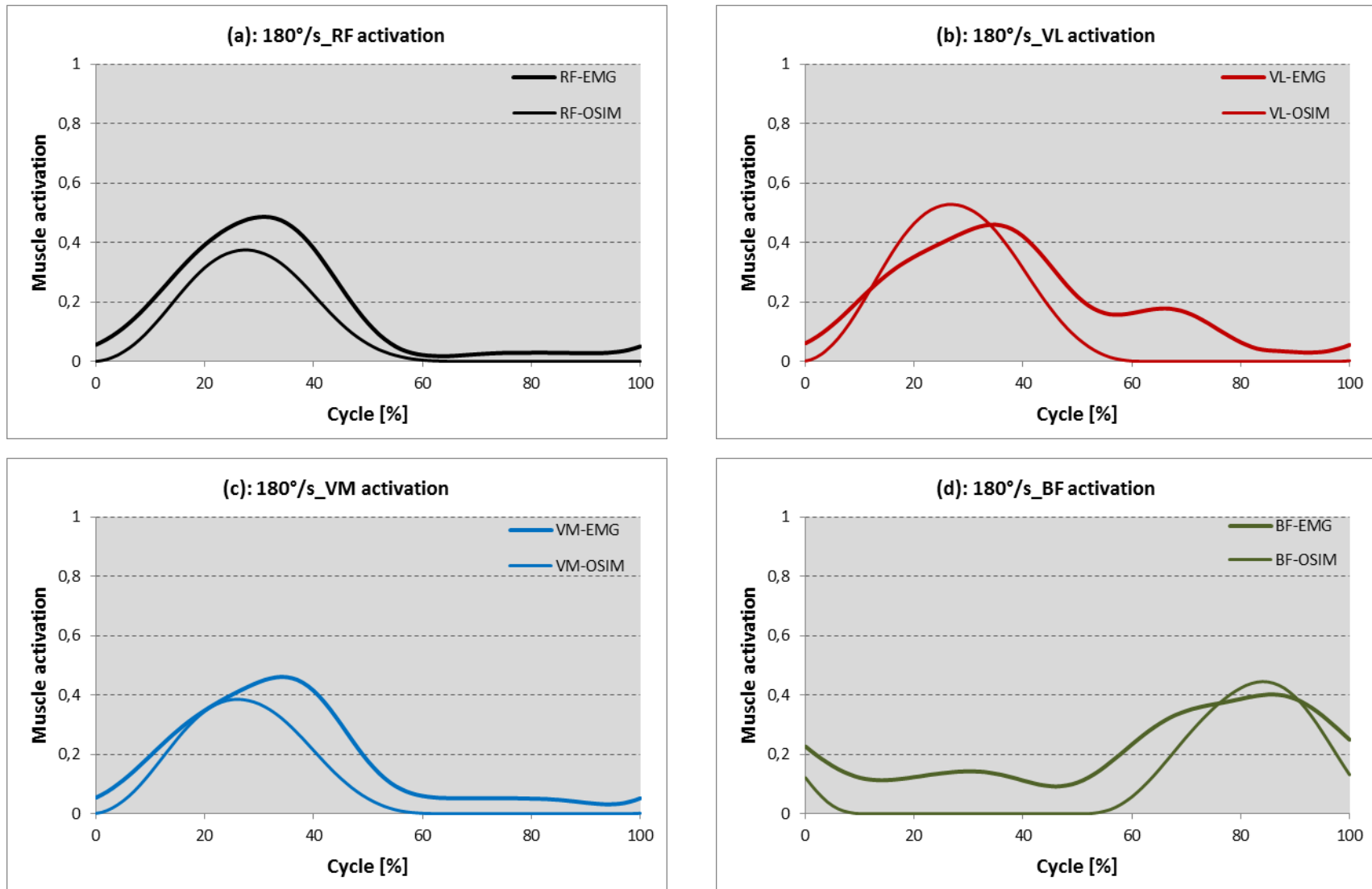


Fig.8.5: EMG and OpenSim muscle activation at 180°/s of RF (a), VL (b), VM (c) and BF (d).

240 °/s

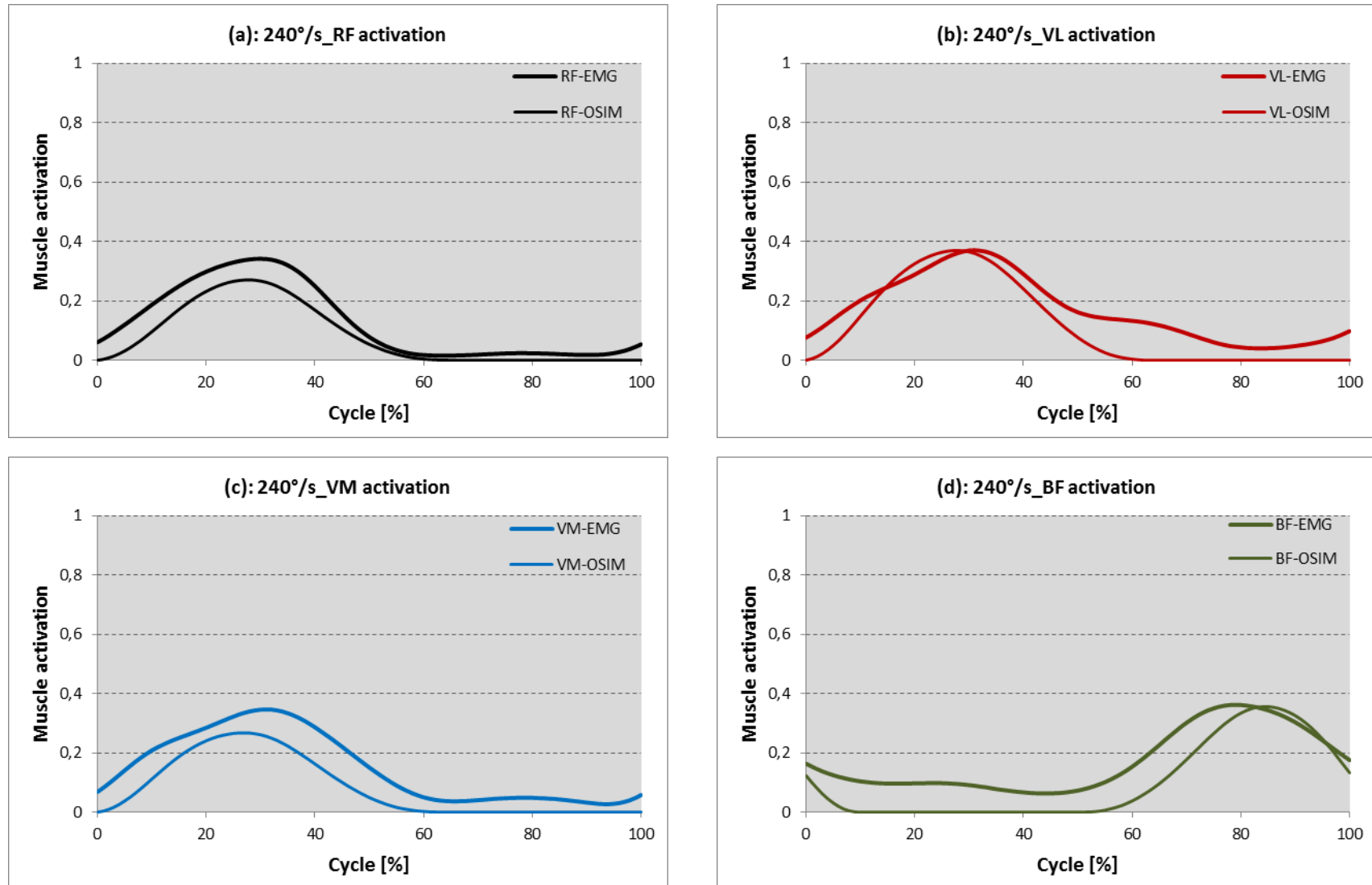


Fig.8.6: EMG and OpenSim muscle activation at 240°/s of RF (a), VL (b), VM (c) and BF (d).

Comparison of EMG signal and OpenSim muscle activation: quantitative results

	60 °/s	120 °/s	180 °/s	240 °/s
RF	23,9±5,8	26,1±7,1	24,5±8,2	20,6±7,3
VL	14,2±8,2	11,1±3,32	-15,2±7,4	2,7±4,3
VM	29,1±7,3	27,1±7,9	17,4±4,8	22,8±1,6
BF	-6,2±2,1	-13,2±9,3	-12,5±7,1	1,3±0,4

Tab.8.1: Peak error in [%] of RF, VL, VM and BF at 60°/s, 120°/s, 180°/s and 240°/s.

	60 °/s	120 °/s	180 °/s	240 °/s
RF	11±4,4	16,6±1,9	4,4±5,2	5,2±6,5
VL	24,3±14,1	19,3±8,6	9,7±3,2	6,3±3,1
VM	27±10	17,8±10,2	8,7±4,5	7,2±4,2
BF	1,3±3,2	1,1±4,2	4,2±3	-6,1±1,1

Tab.8.2: Time error in [%] of RF, VL, VM and BF at 60°/s, 120°/s, 180°/s and 240°/s.

	60 °/s	120 °/s	180 °/s	240 °/s
RF	37,4±7,8	34,1±6,4	38±5,9	35,6±6,7
VL	17,6±11	21,4±5,4	26,4±8,8	32,6±8,7
VM	35,4±8,1	40±6,5	40±4,7	45,4±4,3
BF	21±7,3	29,4±7,2	42,5±9,5	42,2±5,1

Tab.8.3: Area error in [%] of RF, VL, VM and BF at 60°/s, 120°/s, 180°/s and 240°/s.

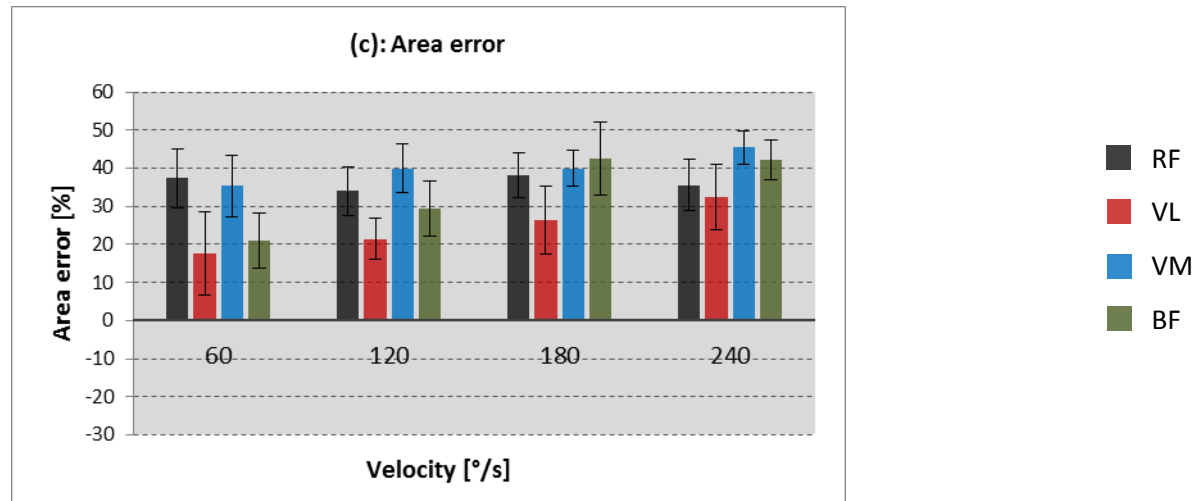
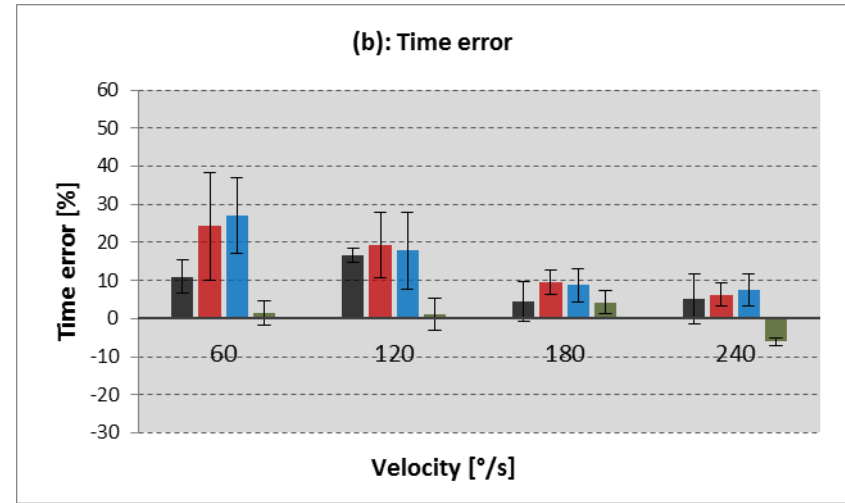
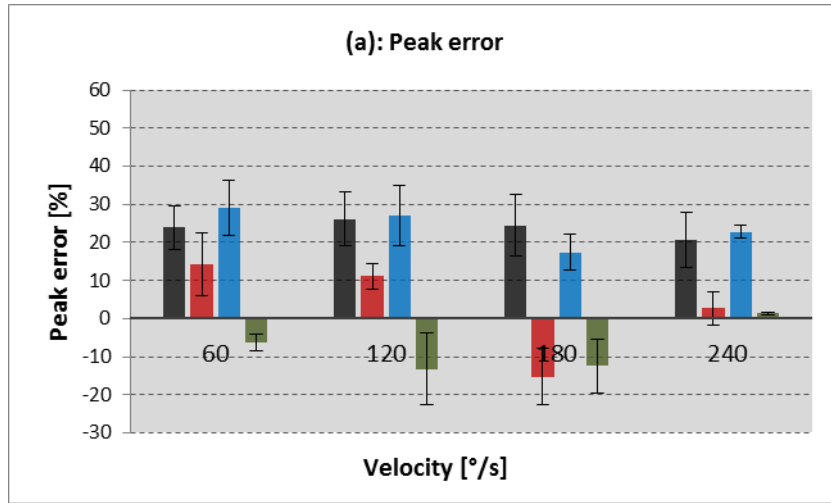


Fig.8.7: Quantitative results of muscle activation analysis: (a): Peak error at different velocities; (b): Time error at different velocities; (c): Area error at different velocities.

Discussion of results

Fig.8.3, fig.8.4, fig.8.5 and fig.8.6 show the average muscle activation profiles obtained by experimental and numerical analysis. By plotting the results as a function of the percentage of the extension-flexion cycle and by considering the average profile, differences between EMG and OpenSim results are emphasized. With a first comparison at different velocities, it is possible to see that the muscular activation profile is more smooth and with less peaks at 180°/s and 240°/s than at 60°/s and 120°/s for each muscle and both for experimental and OpenSim results; at 180°/s and 240°/s there is a second peak value only in the EMG signal of vastus lateralis, but the shape is however regular and smooth. These different findings, should be explained by considering the OpenSim signal at 60°/s and 120°/s shown in fig.8.3 and 8.4: at these velocities the intensity of the exercise increases rapidly, reaches the maximum value and then it tends not to decrease as rapidly as at faster velocity but it tends to have a plateau. This happens for every muscle investigated, extensors and flexors. At the plateau, the probability of peak values in the EMG signal is higher than in the condition at which there is only a peak and not plateau (as at faster velocities). These peaks also leads to a relevant difference between EMG and OpenSim muscle activation, because of peak values in EMG are not associated to an increase of torque and so they can't be simulated by the software. Moreover, at high intensities, the force exerted to the mechanism used to fix the knee during the exercises (fig.6.2) becomes relevant; because this force hadn't be measured by any device, also this force can't be simulated in OpenSim and so this increases the difference between the results too.

By considering for simplicity the peak values of the OpenSim results, the peak values of rectus femoris are $0,4\pm0,04$ at 60°/s, $0,34\pm0,04$ at 120°/s, $0,37\pm0,035$ at 180°/s and $0,27\pm0,038$ at 240°/s; the peak values of vastus lateralis are $0,57\pm0,06$ at 60°/s, $0,48\pm0,06$ at 120°/s, $0,53\pm0,048$ at 180°/s and $0,37\pm0,05$ at 240°/s; the peak values of vastus medialis are $0,42\pm0,04$ at 60°/s, $0,36\pm0,05$ at 120°/s, $0,38\pm0,036$ at 180°/s and $0,27\pm0,037$ at 240°/s; the peak values of biceps femoris are $0,7\pm0,06$ at 60°/s, $0,513\pm0,026$ at 120°/s, $0,45\pm0,03$ at 180°/s and $0,35\pm0,03$ at 240°/s. From these results, it appears that the maximum activation of rectus femoris decreases with the growth of the velocity, despite of at 120°/s and 180°/s is quite similar, and so for the other extensors muscles; the same trend can be identified for biceps femoris. Moreover, the results above show that the activation of rectus femoris is similar to that of vastus medialis for every velocity; the activation of vastus lateralis is instead higher than the other extensors muscles. By comparing also the activation of flexors and extensors muscles, it appears that the activation of biceps femoris is higher than the activation of extensors muscles. Moreover the co-activation of biceps femoris is more or less twice the co-activation of extensors muscles. From the results above, it is possible to see that the reliability of results is good, although the dispersion of results is higher for experimental results.

In fig.8.7 the results of the quantitative comparison of EMG signal and OpenSim muscle activation are expressed. By comparing the results in fig.8.7.a, fig.8.7.b and fig.8.7.c it is possible to see that the error related to the time error is lower than the other errors at every velocity.

Regarding the peak error (fig.8.7.a), the error related to rectus femoris and vastus medialis is positive and higher than the error associated with the other muscles and it is similar at every velocity (from tab.8.1, the peak error of rectus femoris ranges from $20,6 \pm 7,3\%$ at $240^\circ/s$ to $26,1 \pm 7,1\%$ at $120^\circ/s$; the peak error of vastus medialis from $17,4 \pm 4,8\%$ at $180^\circ/s$ to $29,1 \pm 7,3\%$ at $60^\circ/s$); the error related to vastus lateralis is instead positive at $60^\circ/s$, $120^\circ/s$ and $240^\circ/s$ with a high range of values (from tab.8.1, $14,2 \pm 8,2\%$ at $60^\circ/s$, $11,1 \pm 3,32\%$ at $120^\circ/s$ and $2,7 \pm 4,3\%$ at $240^\circ/s$), but it is negative at $180^\circ/s$ (from tab.8.1, $-15,2 \pm 7,4\%$); the peak error associated to biceps femoris is instead negative at $60^\circ/s$, $120^\circ/s$ and $180^\circ/s$ and positive at $240^\circ/s$ (from tab.8.1, $-6,2 \pm 2,1\%$ at $60^\circ/s$, $-13,2 \pm 9,3\%$ at $120^\circ/s$, $-12,5 \pm 7,1\%$ at $180^\circ/s$ and $1,3 \pm 0,4\%$ at $240^\circ/s$).

Concerning the time error (fig.8.7.b), it is possible to identify a common trend: the time error of extensors muscles is positive and it tends to decrease with the growth of the velocity, although the error of rectus femoris increases from $60^\circ/s$ to $120^\circ/s$ and from $180^\circ/s$ to $240^\circ/s$ (from tab.8.2, the error of vastus lateralis ranges between $24,3 \pm 14,1\%$ at $60^\circ/s$ and $6,3 \pm 3,1\%$ at $240^\circ/s$, the error of vastus medialis between $27 \pm 10\%$ at $60^\circ/s$ to $7,2 \pm 4,2\%$ at $240^\circ/s$; the error of rectus femoris at different velocities are $11 \pm 4,4\%$ at $60^\circ/s$, $16,6 \pm 1,9\%$ at $120^\circ/s$, $4,4 \pm 5,2\%$ at $180^\circ/s$ and $5,2 \pm 6,5\%$ at $240^\circ/s$). Biceps femoris tends to have instead an opposite trend: the error is higher (in absolute terms) at fast velocities than at slow ones. Moreover, the error is quite null at $60^\circ/s$ and $120^\circ/s$ (from tab.8.2, the error is $1,3 \pm 3,2\%$ at $60^\circ/s$ and $1,1 \pm 4,2\%$ at $120^\circ/s$), it increases at $180^\circ/s$ (from tab.8.2, $4,2 \pm 3\%$) and in the end it becomes negative (from tab.8.2, $-6,1 \pm 1,1\%$).

In the end, the error related to the area of the signal (fig.8.7.c) is positive at each velocity; for the extensors muscles this is due both for higher peak values of EMG signal than OpenSim muscle activation and for co-activation in EMG signal; for biceps femoris, instead, although the peak values of EMG signal tend to be smaller than those of OpenSim results, co-activation is very high and so this leads to an area error positive at each velocity too. Furthermore, fig.8.7.c illustrates that the error of rectus femoris and vastus medialis is higher than the error of the other muscles at $60^\circ/s$ and $120^\circ/s$ (from tab.8.3, the area errors are $37,4 \pm 7,8\%$ at $60^\circ/s$ and $34,1 \pm 6,4\%$ at $120^\circ/s$ for rectus femoris; $35,4 \pm 8,1\%$ at $60^\circ/s$ and $40 \pm 6,5\%$ at $120^\circ/s$ for vastus medialis; $17,6 \pm 11\%$ at $60^\circ/s$ and $21,4 \pm 5,4\%$ at $120^\circ/s$ for vastus lateralis; $21 \pm 7,3\%$ at $60^\circ/s$ and $29,4 \pm 7,2\%$ at $120^\circ/s$ for biceps femoris); at $180^\circ/s$ and $240^\circ/s$ also the error of biceps femoris increases (from tab.8.3, the area errors are $38 \pm 5,9\%$ at $180^\circ/s$ and $35,6 \pm 6,7\%$ at $240^\circ/s$ for rectus femoris; $40 \pm 4,7\%$ at $180^\circ/s$ and $45,4 \pm 4,3\%$ at $240^\circ/s$ for vastus medialis; $42,5 \pm 9,5\%$ at $180^\circ/s$ and $42,2 \pm 5,1\%$ at $240^\circ/s$ for biceps femoris; $26,4 \pm 8,8\%$ at $180^\circ/s$ and $32,6 \pm 8,7\%$ at $240^\circ/s$ for vastus lateralis). Moreover, the previous results express that there is an increase of the area error with the growth of the velocity.

By the previous results, it appears that OpenSim is a satisfactory tool in biomechanical investigation, because the maximum error is about 40% by considering the area under the signal.

Regarding the reliability of results, it is high for the time error, except for vastus lateralis and medialis at 60°/s and 120°/s, (from tab.8.2 it ranges between 1,1% and 6,5%); for peak error and area error the dispersion of results is instead higher than in the previous one but it is however reasonable (from tab.8.1 and tab.8.3 it ranges from 0,4% to 8,2% for peak error and from 4,3% to 11% for area error).

The results obtained can be compared with those obtained in the previous investigation done by Tregnaghi et al. (Tregnaghi et al., 2010). From that study, time error is higher than peak error and area error at every velocity for all muscles investigated, but the same trend described above can't be found because of the variability of results. About the peak error, it tends to be negative at every velocity both for rectus femoris and vastus lateralis (with a maximum error of about 200% for rectus femoris at 120°/s and about 20% for vastus lateralis at 120°/s), quite null for vastus medialis and positive with an increase of its value with the growth of the velocity for biceps femoris. About the area error, a comparison is more difficult than in previous cases because the results obtained by Tregnaghi show that the error is negative for the first subject and positive for the second one. These differences are related in particular to the physical condition of subjects who performed the exercises; as a matter of fact, the results obtained in this study shown in appendix reveal that the variability of results between subjects is however high.

8.3. Comparison and evaluation of analytical models and OpenSim model

The comparison of analytical models and OpenSim model at different velocities is shown. The results were obtained as averaged values by considering the three cycles investigated of all subject. The results of the comparison of each subject are in Appendix.

For each subject, for the extension phase knee moment, force at the patellar tendon, shear and axial load on tibia and femur, force at the cruciate ligaments and shear and axial load on tibia by considering the reaction forces at femur “Tibia_Shear (with patella)” and “Tibia_Axial Force (with patella)” (par.7.6.3) are shown; for the flexion phase knee moment, force at biceps femoris-long head, biceps femoris-short head, semimembranosus and semitendinosus, shear and axial load on tibia and femur and force at the cruciate ligaments are shown. The results were obtained as mean of the three cycles investigated (standard deviation is omitted in the visualization) and they were normalized to the maximum (or minimum if flexion) knee moment as described in par.7.6.3. Furthermore, the results are compared with the limit values of tension of tendons and ligaments and the limit values of shear and axial load of bones expressed in par.3.5; the limit values were normalized to the maximum/minimum knee moment too. When the limit value is too much higher than the results obtained, it is omitted in the visualization.

In addition to the mean profile of the parameters investigated, the maximum values and the angles at which the maximum is reached are shown. Moreover, for the extension phase the angle at which the ACL becomes unstrained and the PCL strained is shown.

About the normalization to the maximum (minimum if flexion) knee moment, this was done in order to reduce the dispersion of results obtained by using the normalization to the body weight as done for the evaluation of the flexors and extensors balance (as shown in par.8.1). In fig.8.1.1 the torque normalized to maximum at 60°/s is shown. As it is possible to see the results are similar.

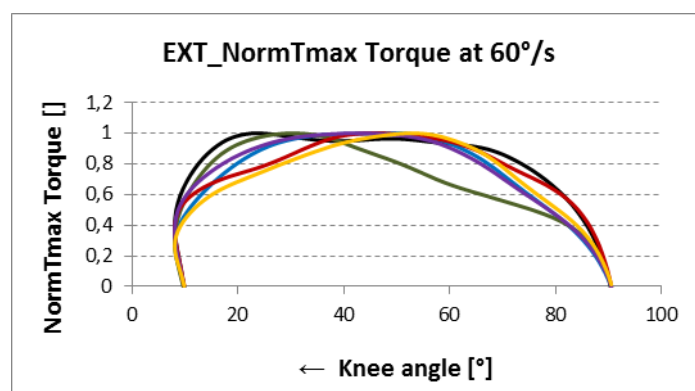


Fig.8.1.1: Torque in extension normalized to maximum at 60°/s for all subjects.

— S1 — S2 — S3 — S4 — S5 — S6

Because of the great difference in the results obtained by the first and the second analytical model, here below (fig.8.1.2) there is a graphical interpretation of the results of subject 1, S1, at 60°/s at 20° and 70° knee flexion angle in order to help to understand in particular the different profile of the shear acting on tibia in the extension phase. The continuous line refers to the first model, the Herzog's formulation; the broken line refers to the second model. The results of the Van Eijden's formulation are omitted because are similar to those obtained by the Herzog's one. Both in extension and flexion, the external force is omitted because it is negligible with respect to the others ($F_{EXT} \approx (1/12) \cdot F_{PT}$; $F_{EXT} \approx (1/8) \cdot F_{BFL}$).

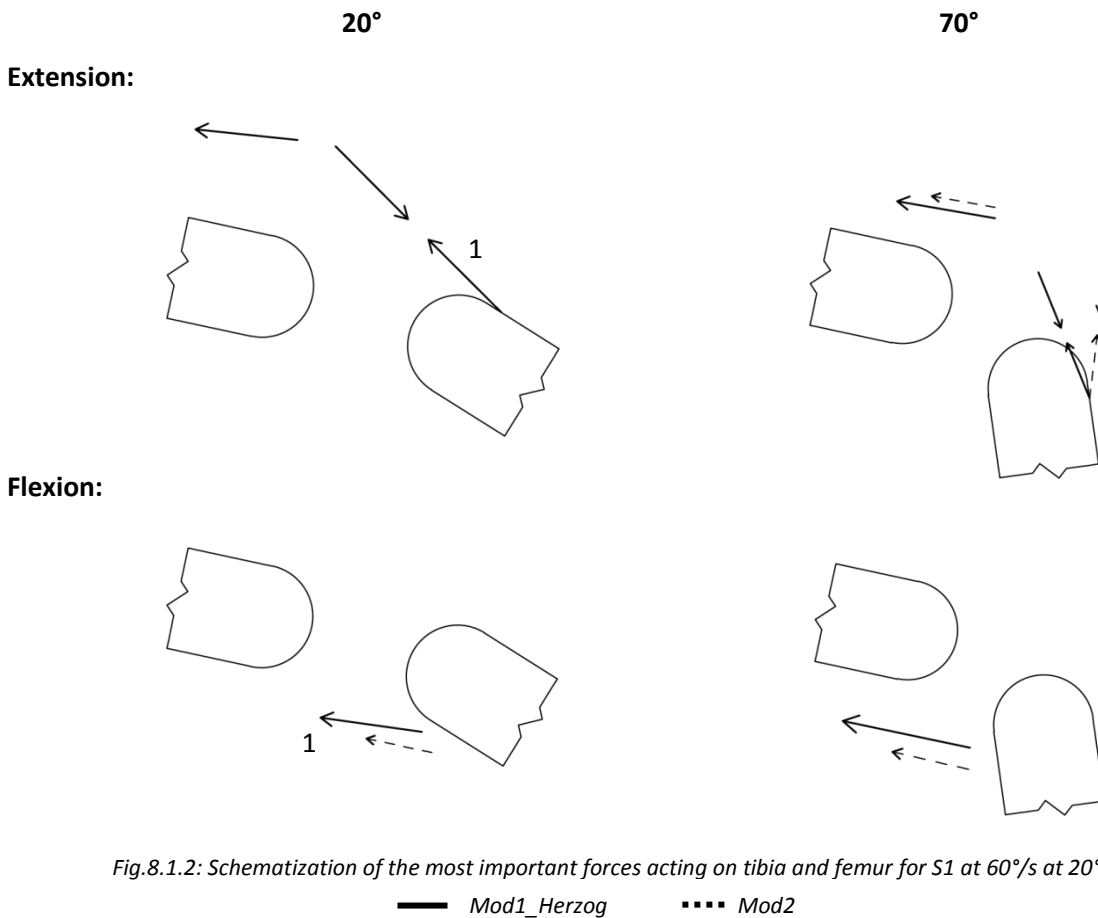


Fig.8.1.2: Schematization of the most important forces acting on tibia and femur for S1 at 60°/s at 20° and 70°.

— Mod1_Herzog ---- Mod2

For the extension phase, patellar tendon and forces acting on patella are shown; the values of the forces are normalized to the force at the patellar tendon at 20°. Both for 20° and 70° the moment arm of the patellar tendon and the tendon of the quadriceps are similar in the two models; moreover at 20° the forces calculated with the second model are omitted because they have more or less the same values and the same inclinations of those of the first model. As it is possible to see, at 70° instead the line of action of the patellar tendon is completely different. For the flexion phase, a mean value of the force acting at biceps femoris-long head, biceps femoris-short head, semimembranosus and semitendinosus is shown; the inclination of this force was evaluated as mean of the inclination of each force. The results are normalized to the force calculated with the first model at 20°. The position of the forces, and so the lever-arm, is

instead arbitrary. As it is possible to see, the mean force calculated with the first model is more or less twice the mean force of the second model; the line of action is instead similar.

For the other subjects and velocities the results are similar.

To make easy the comprehension of the results, fig.8.1.3 synthetizes the convention adopted for the signs of the forces and the relation between the shear acting on tibia and the force at the cruciate ligaments: when the shear is positive, the PCL is strained and the ACL is unstrained; when the shear is negative, the ACL is strained and the PCL is unstrained.

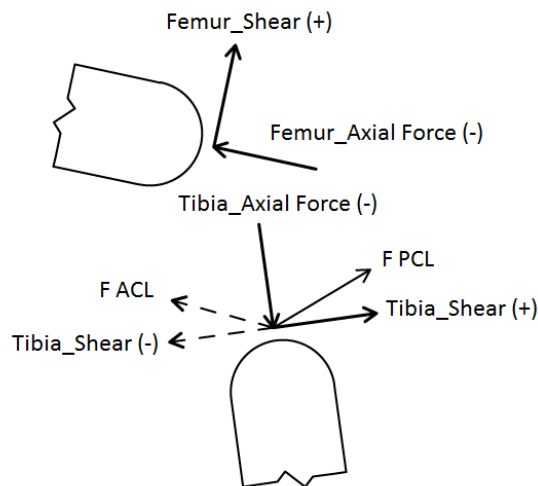


Fig.8.1.3: Convention adopted for the sign of forces.

The terminology adopted here below has the following meaning: “OSIM”: OpenSim; “Mod1_Herzog”: first model, Herzog’s formulation; “Mod1_Van Eijden”: first model, Van Eijden’s formulation; “Mod2”: second model; “F PT”: force at the patellar tendon; “F BFB”: force at the biceps femoris-short head; “F BFL”: force at the biceps femoris-long head; “F SM”: force at the semimembranosus; “F ST”: force at the semitendinosus; “Tibia_Shear”: shear on tibia; “Tibia_Ax Force”: axial load on tibia; “Femur_Shear”: shear on femur; “Femur_Ax Force”: axial load on femur; “Tibia_Shear (with patella)”: shear on tibia by considering the patella (par.7.6.3); “Tibia_Ax F (with patella)”: axial force on tibia by considering the patella (par.7.6.3).

About the ACL/PCL profile, only one curve is used. When it is positive, the PCL is strained and the ACL unstrained; when it is negative the ACL is strained and the PCL unstrained. This is only a representation which was used in this study, in order to compare immediately the results with the shear acting on tibia (when the shear is positive the PCL is strained; when the shear is negative the ACL is strained).

Fig.8.8: 60°/s_Extension

— OSIM — Mod1_Herzog — Mod1_Van Eijden — Mod2 - - - - - limit value

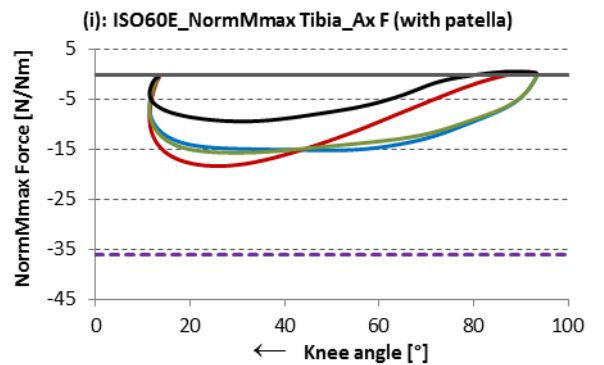
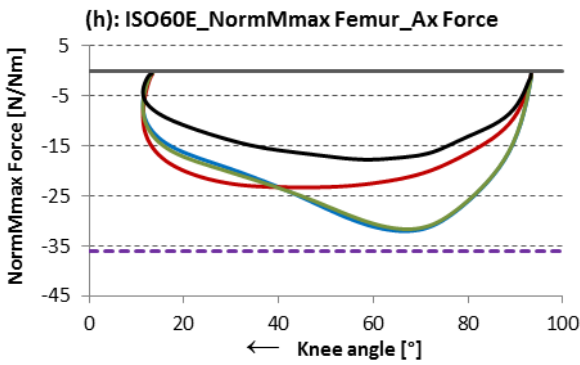
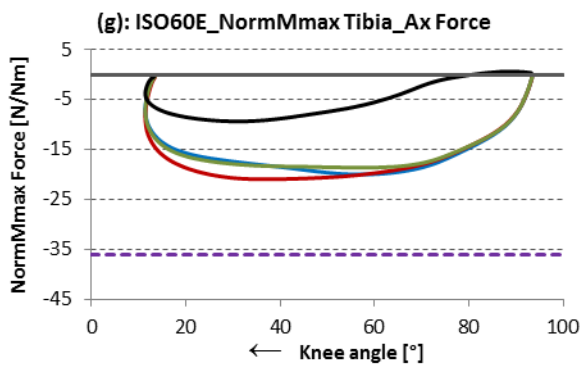
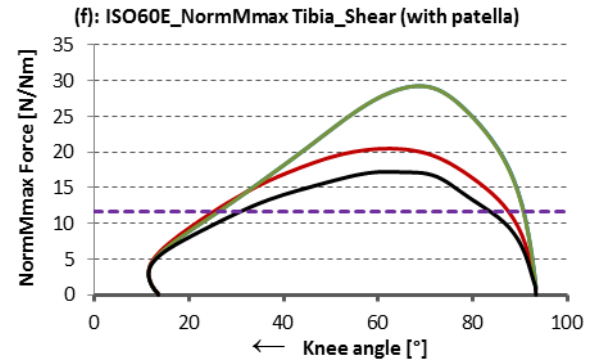
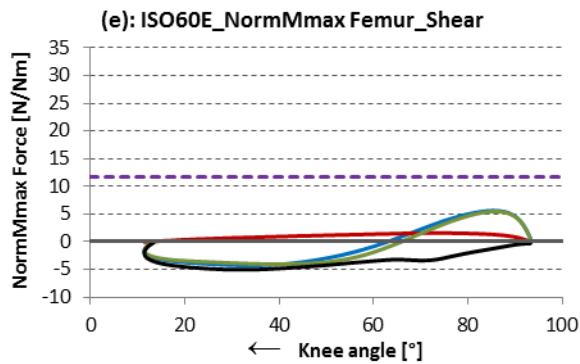
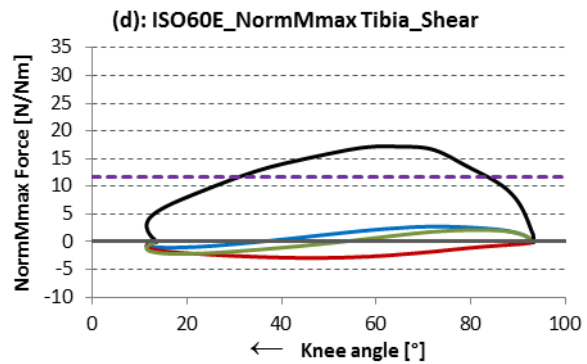
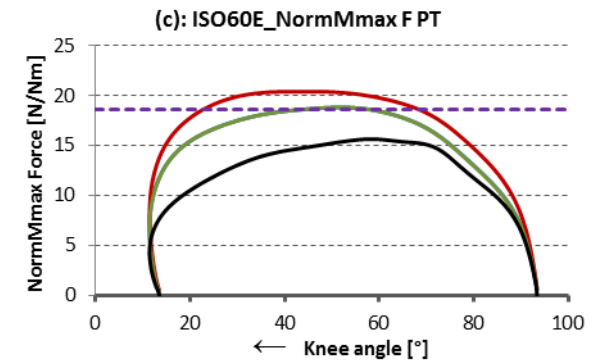
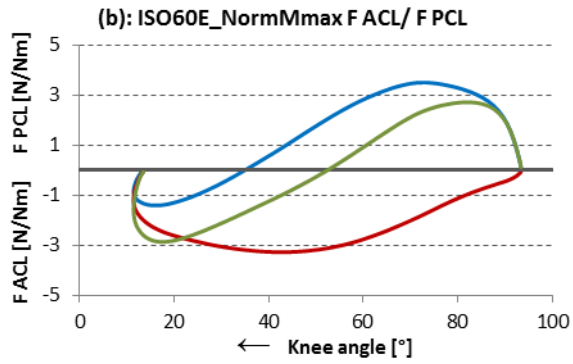
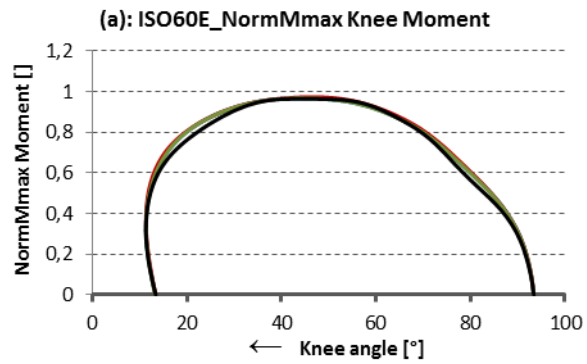


Fig.8.9: 60°/s_Flexion

— OSIM — Mod1 — Mod2 - - - limit value (· · · · OSIM BFL · · · · Mod1 BFL · · · · Mod2 BFL

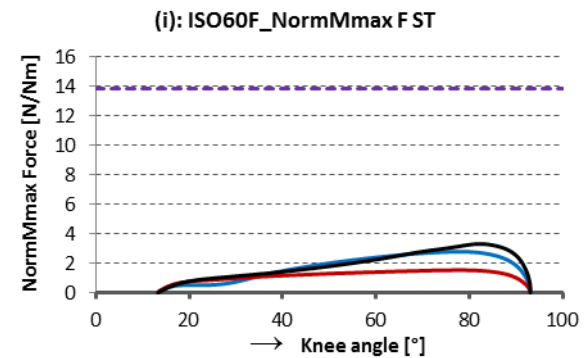
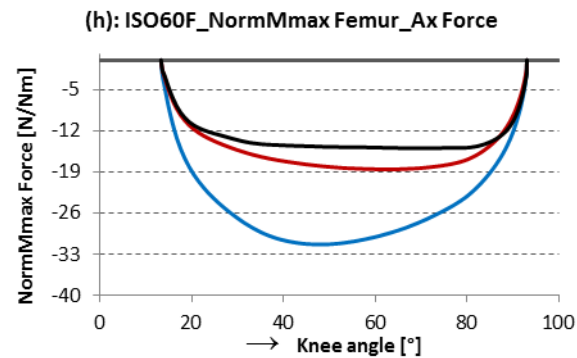
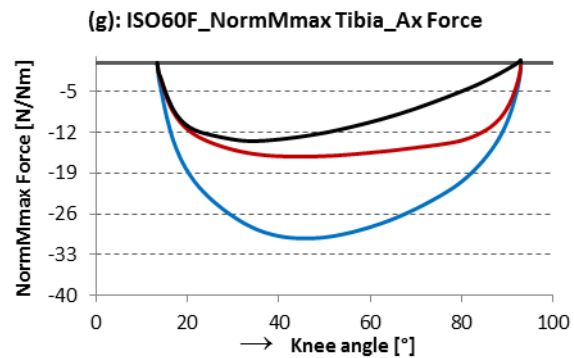
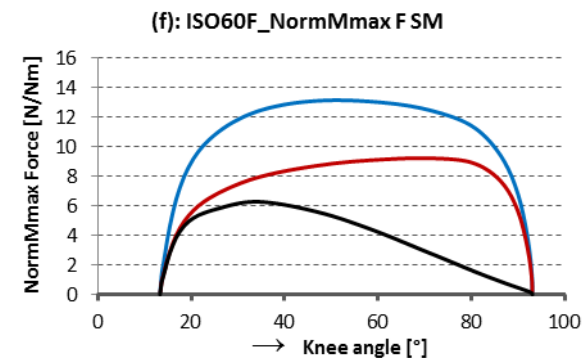
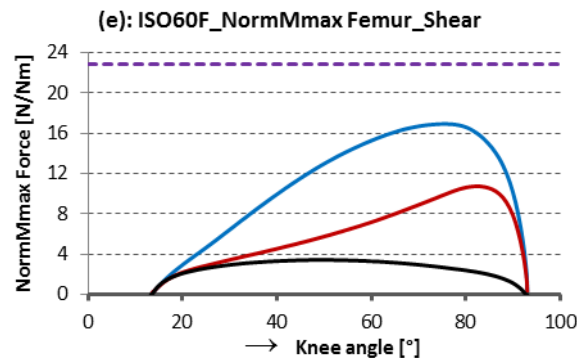
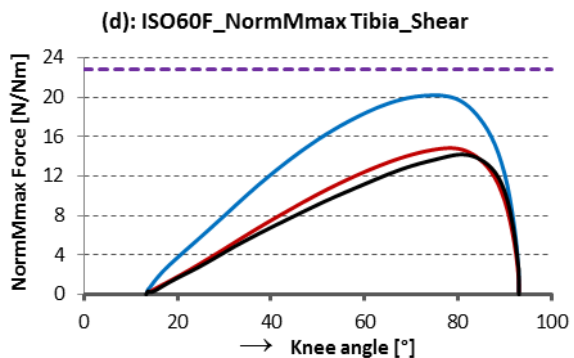
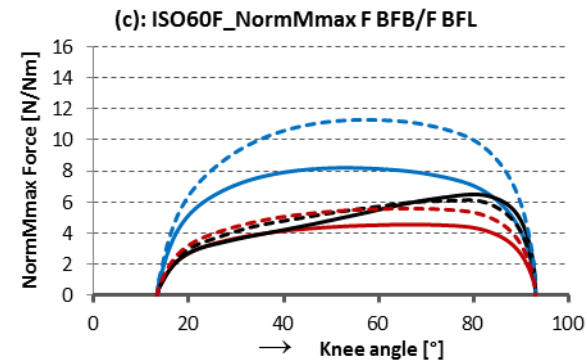
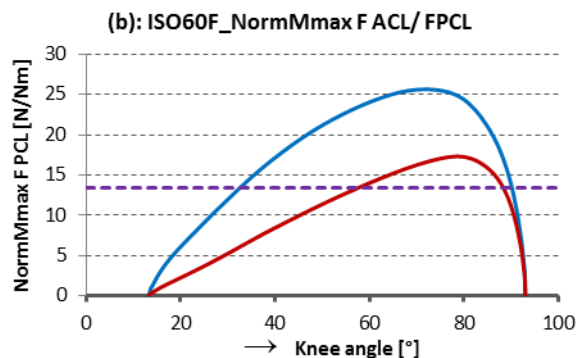
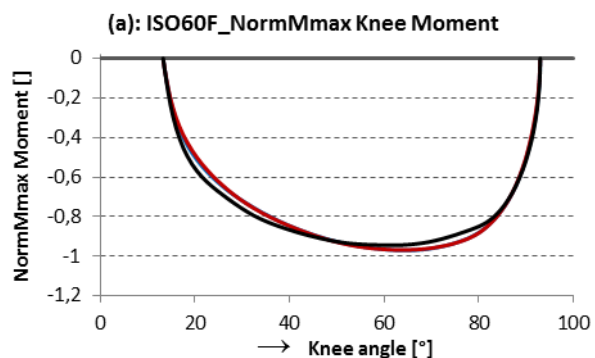


Fig.8.10: 120°/s_Extension

— OSIM — Mod1_Herzog — Mod1_Van Eijden — Mod2 - - - limit value

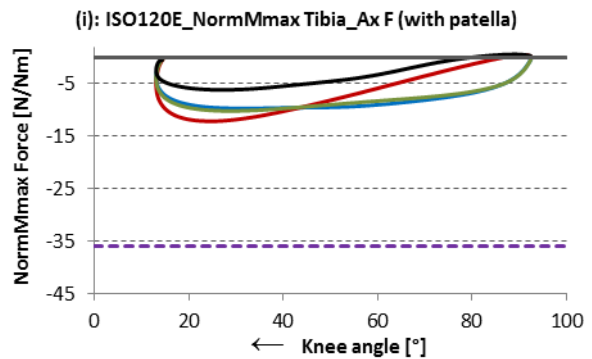
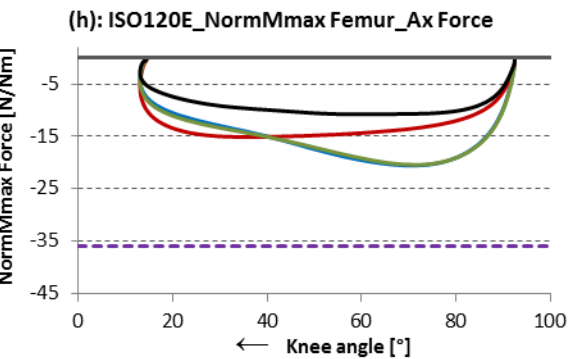
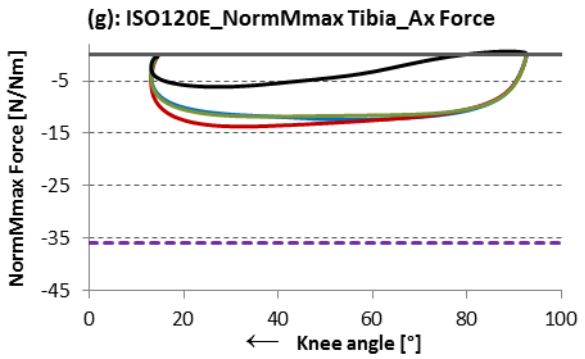
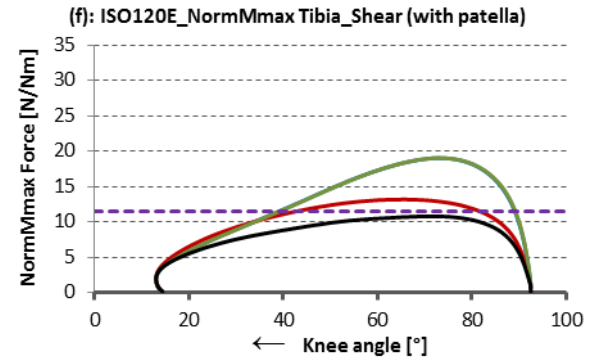
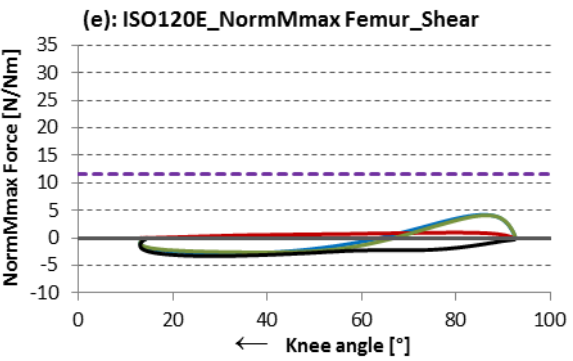
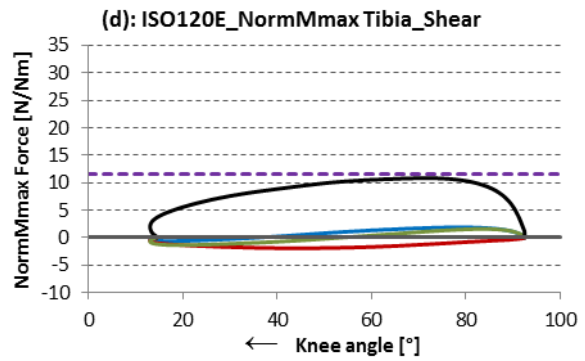
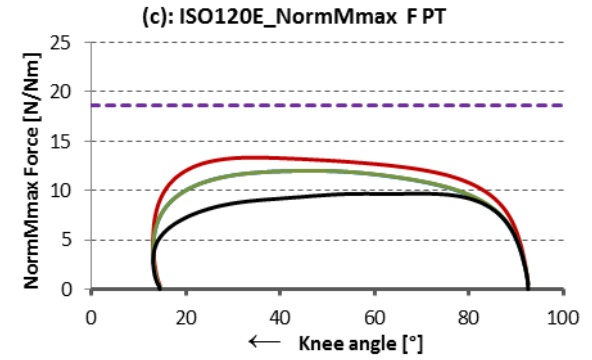
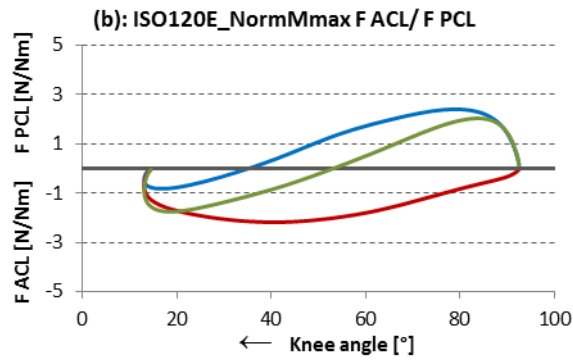
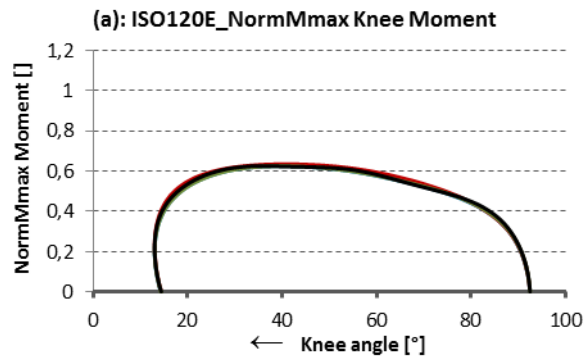


Fig.8.11: 120°/s_Flexion

— OSIM — Mod1 — Mod2 - - - limit value (- - - OSIM BFL - - - Mod1 BFL - - - Mod2 BFL)

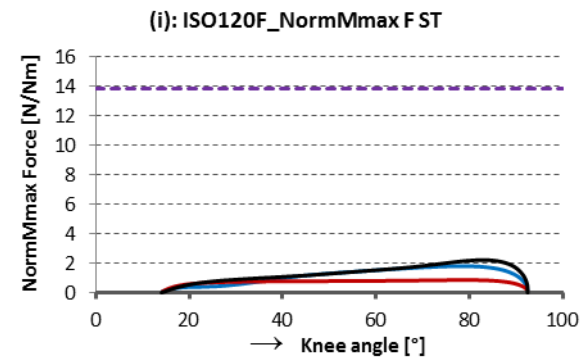
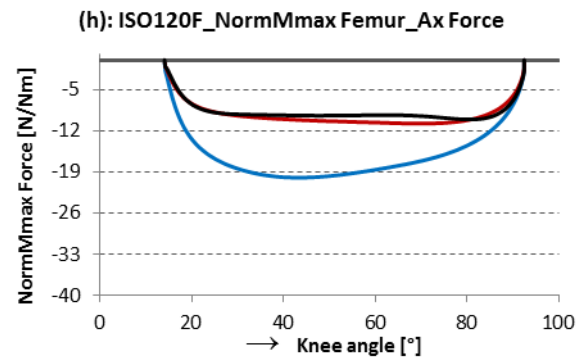
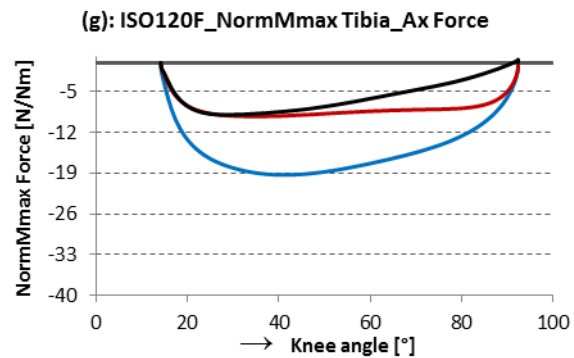
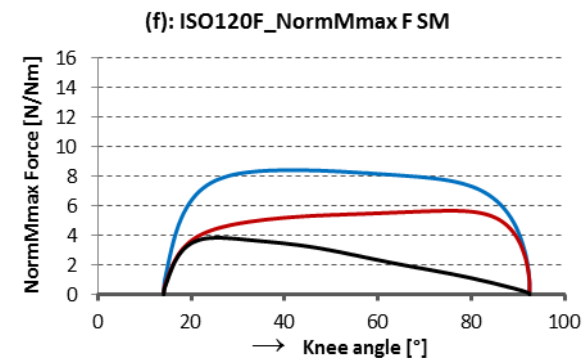
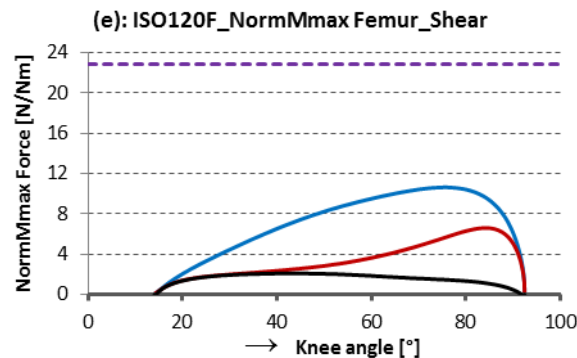
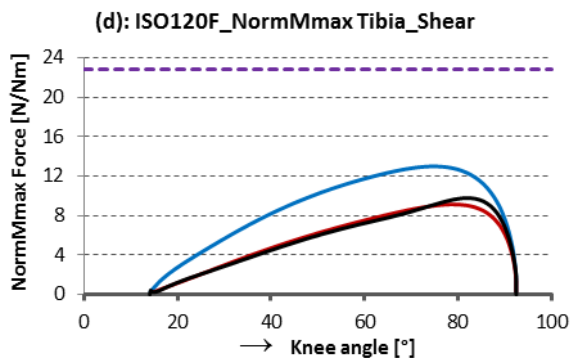
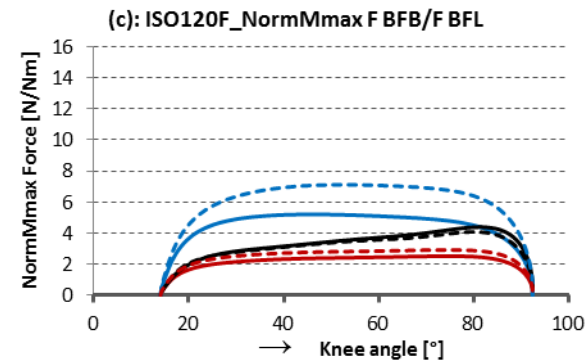
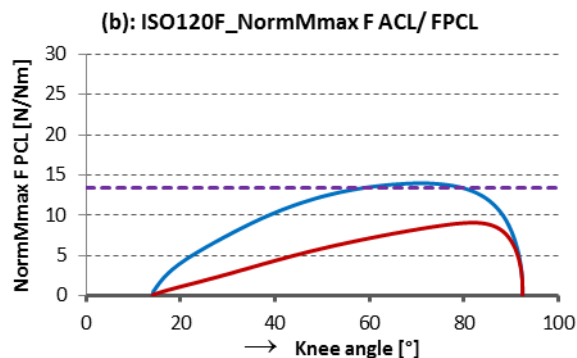
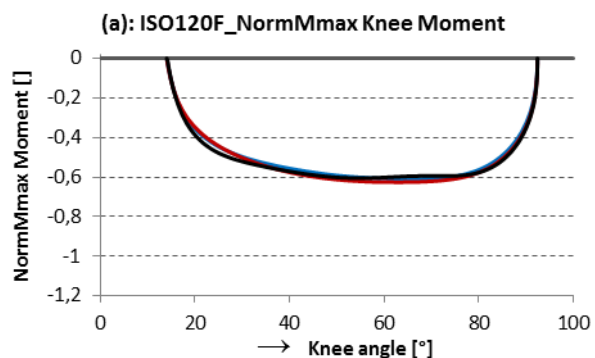


Fig.8.12: 180°/s_Extension

— OSIM — Mod1_Herzog — Mod1_Van Eijden — Mod2 - - - - - limit value

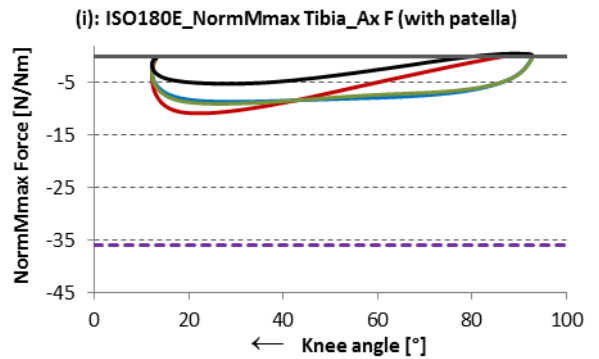
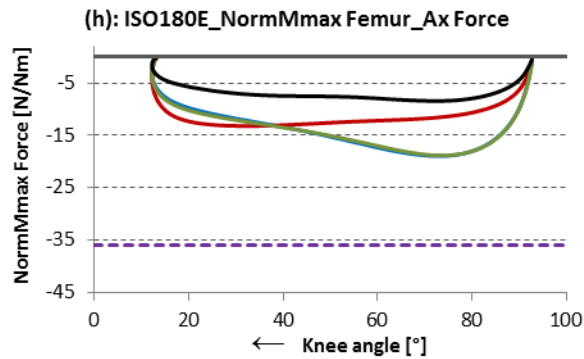
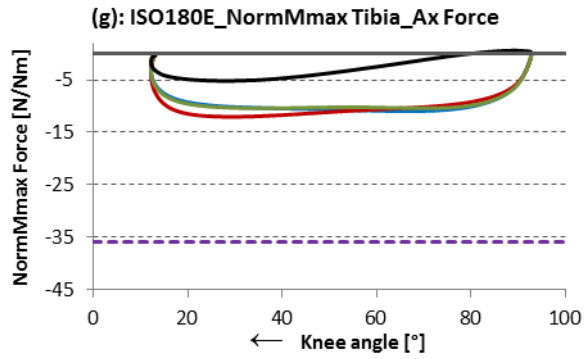
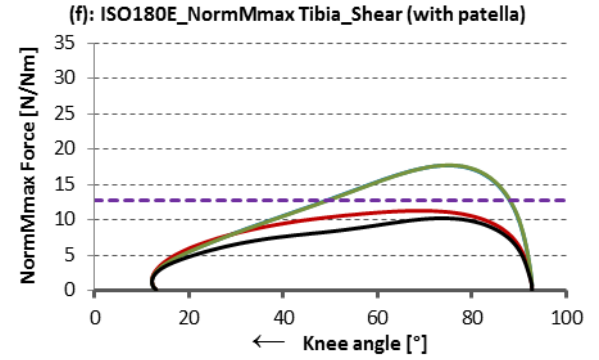
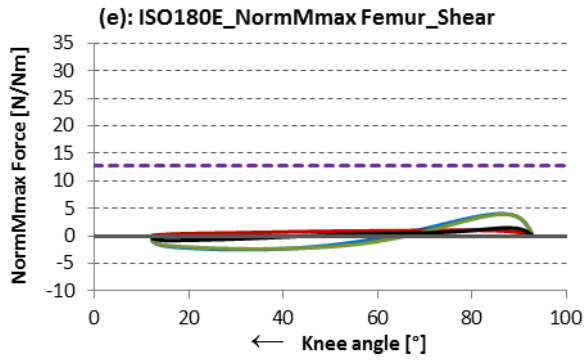
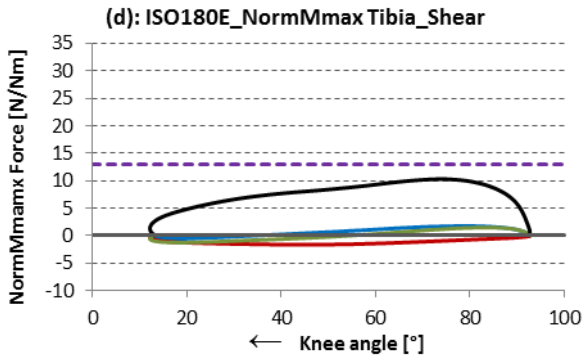
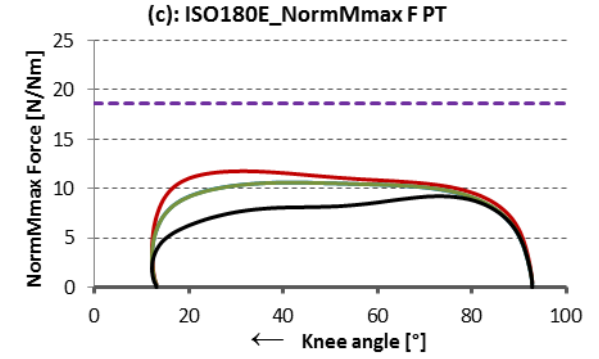
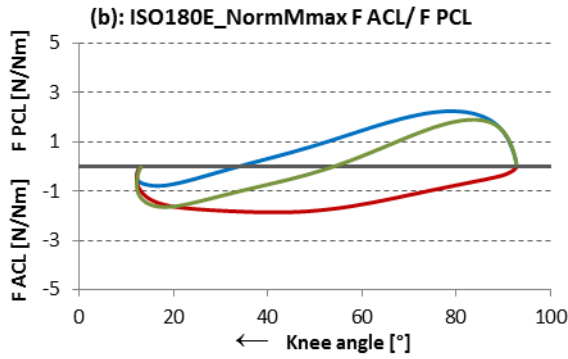
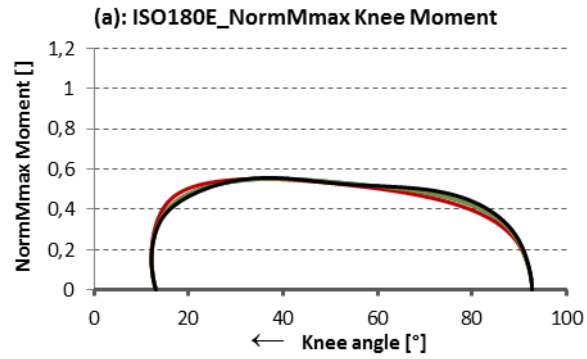


Fig.8.13: 180°/s_Flexion

— OSIM — Mod1 — Mod2 - - - limit value (- - - OSIM BFL - - - Mod1 BFL - - - Mod2 BFL)

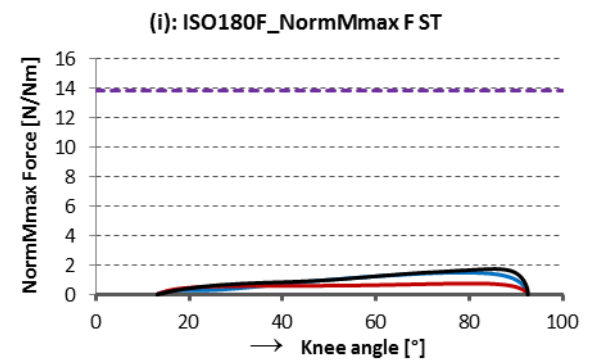
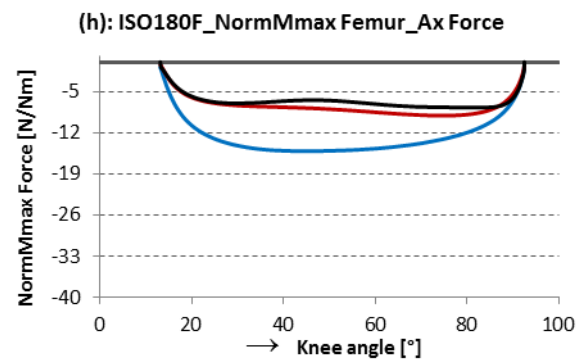
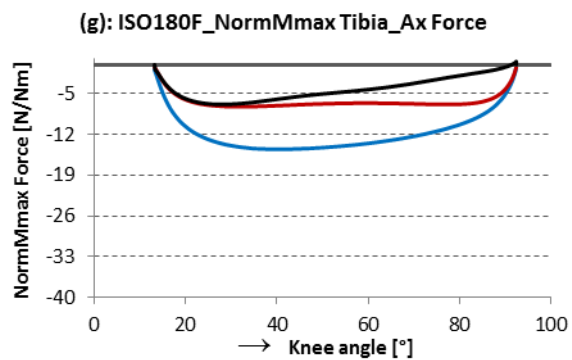
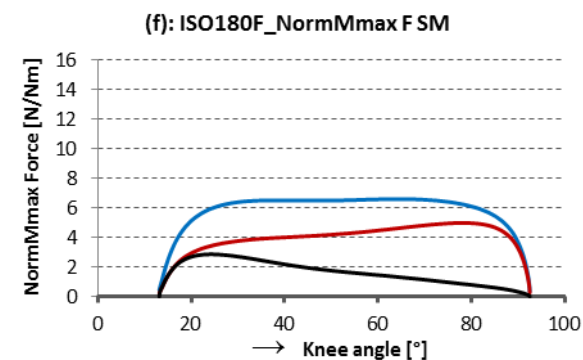
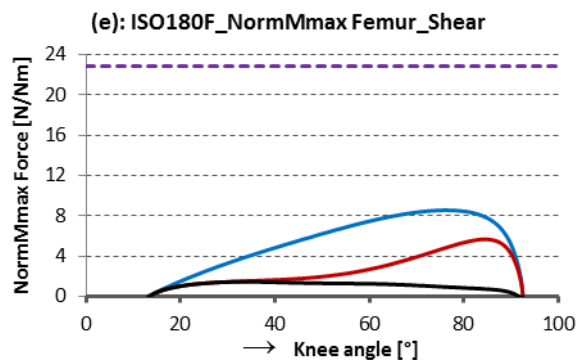
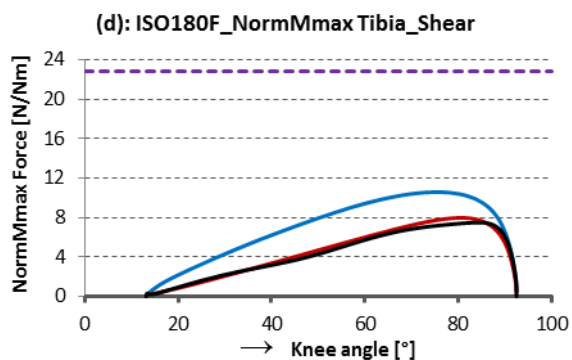
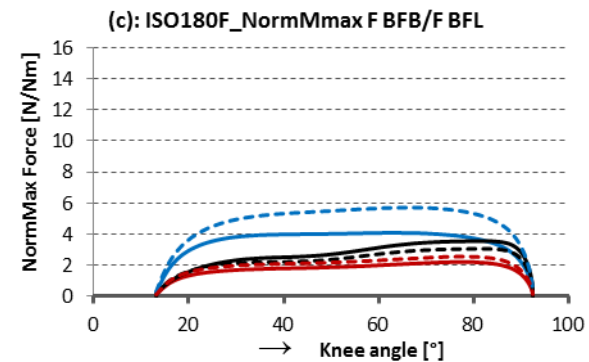
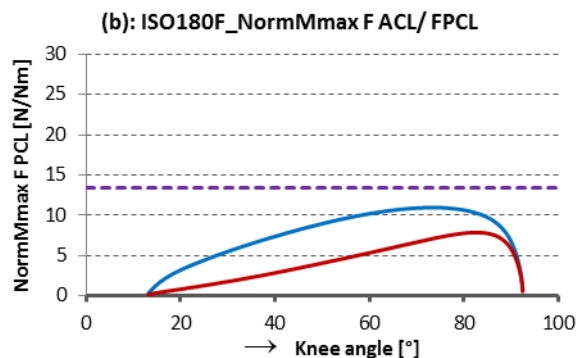
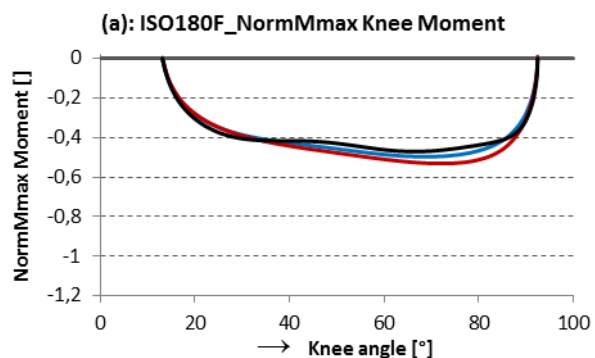


Fig.8.14: 240°/s_Extension

— OSIM — Mod1_Herzog — Mod1_Van Eijden — Mod2 - - - limit value

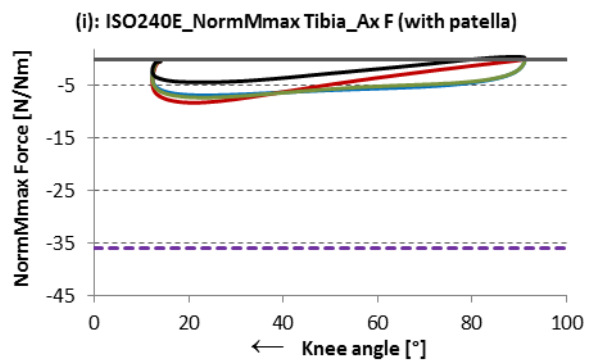
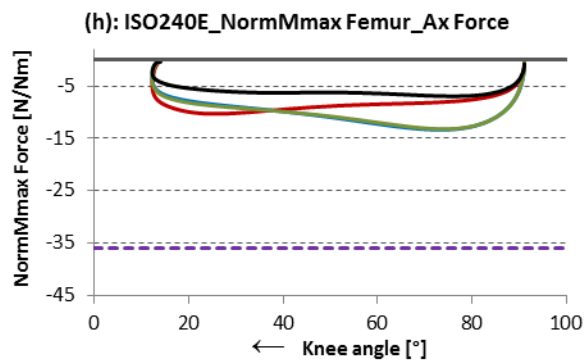
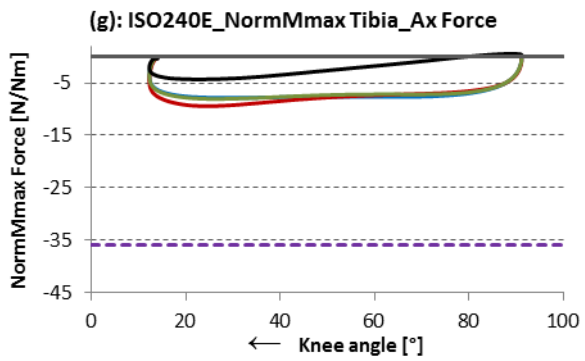
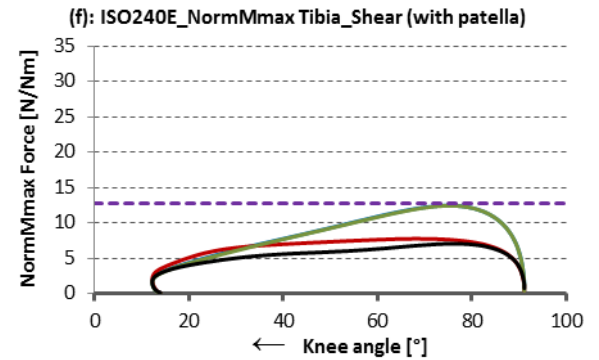
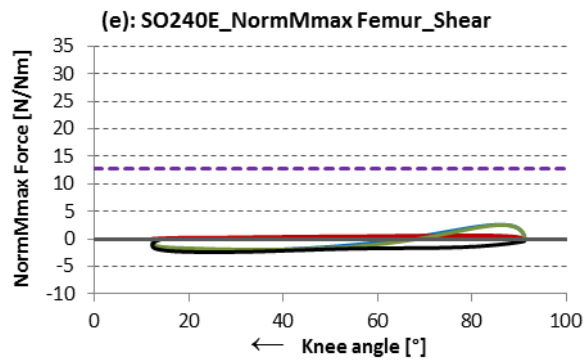
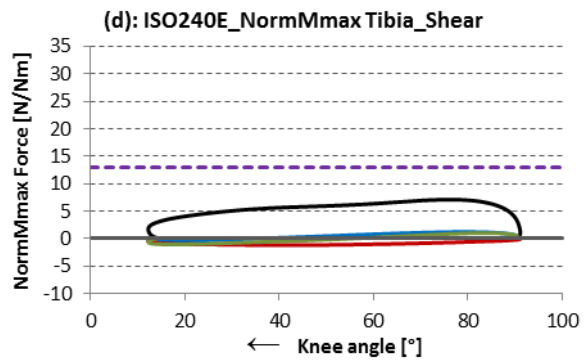
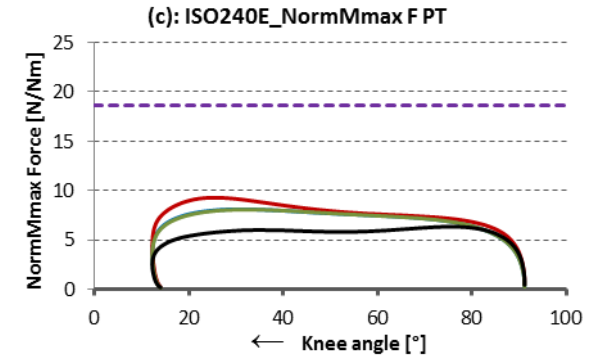
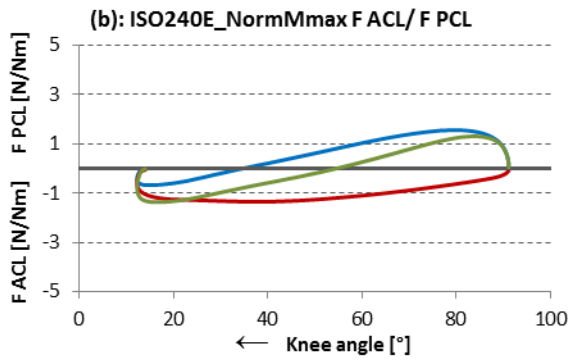
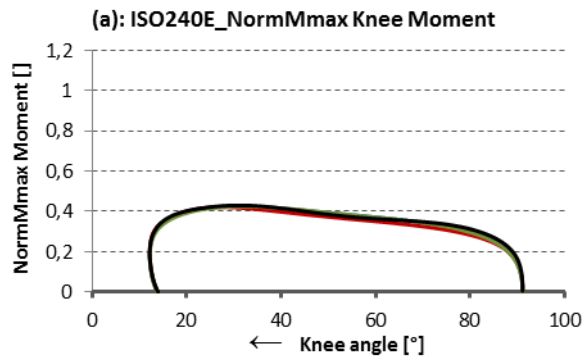


Fig.8.15: 240°/s_Flexion

— OSIM — Mod1 — Mod2 - - - limit value (- - - OSIM BFL - - - Mod1 BFL - - - Mod2 BFL)

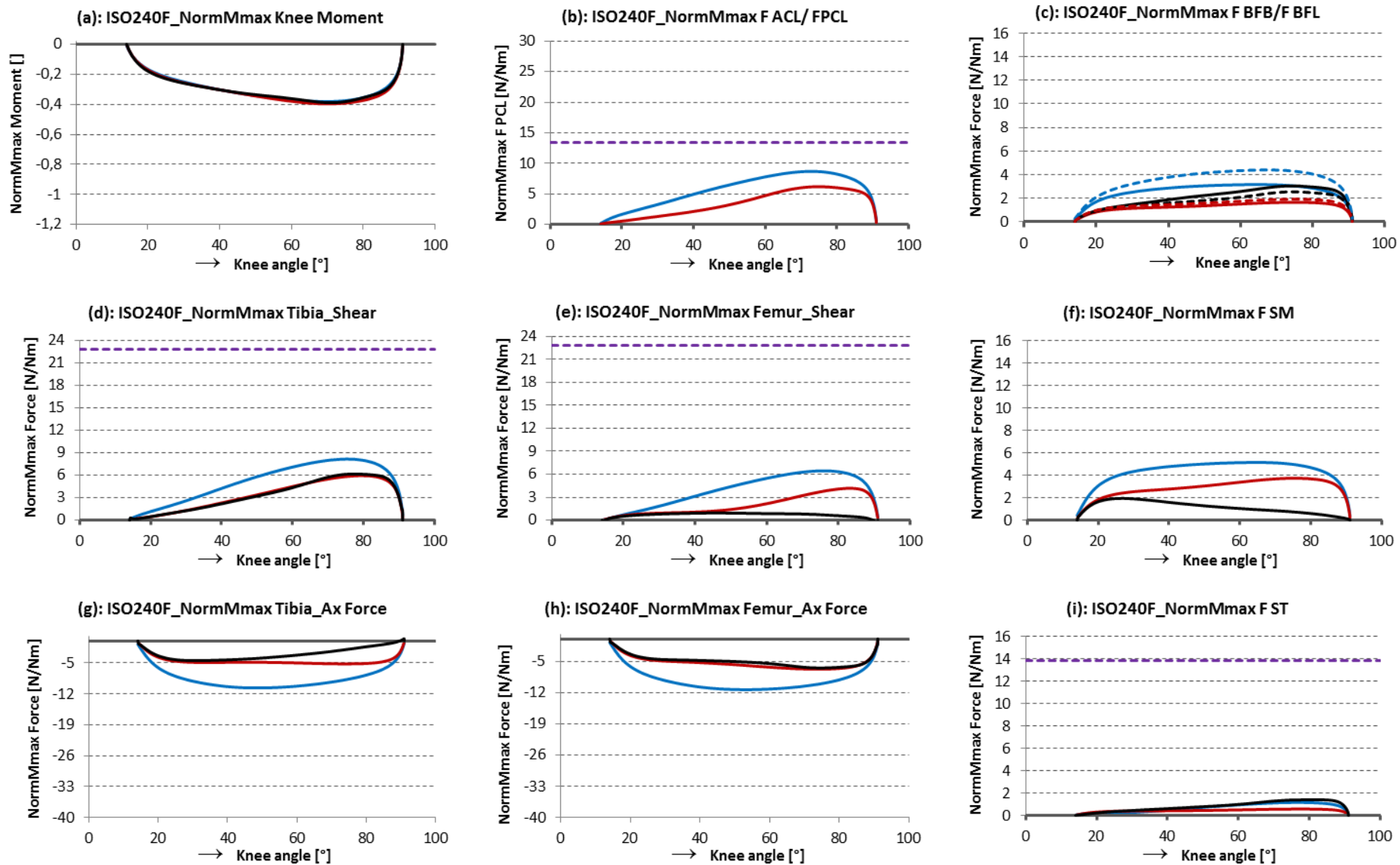
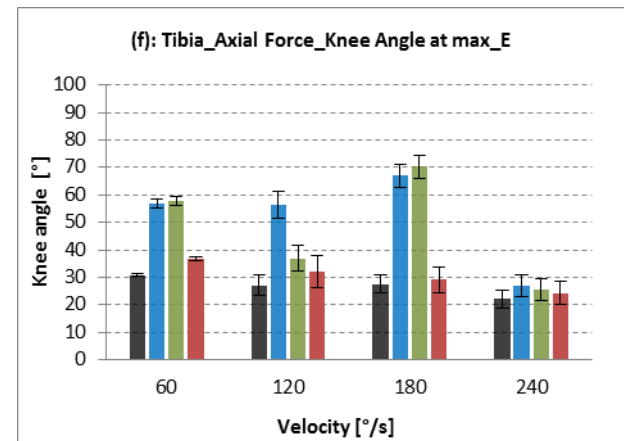
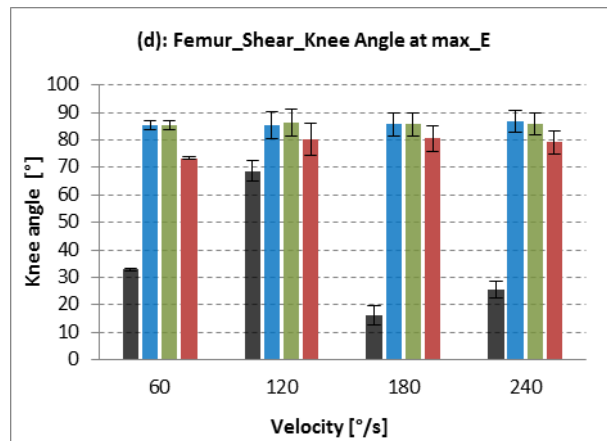
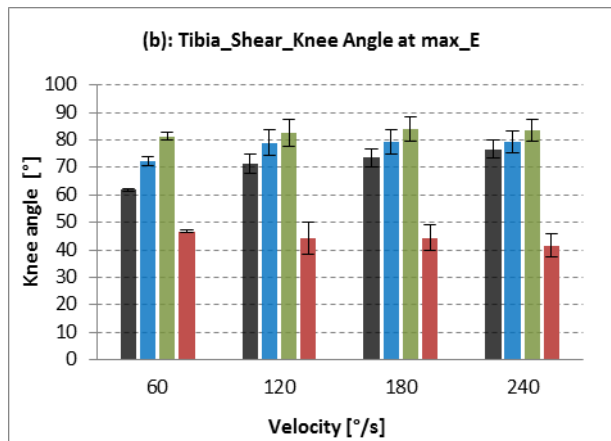
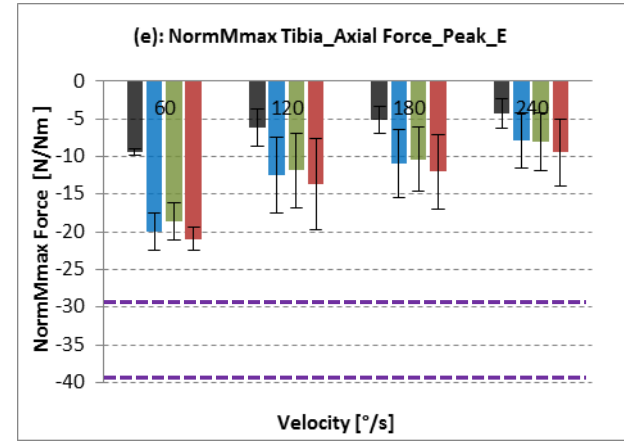
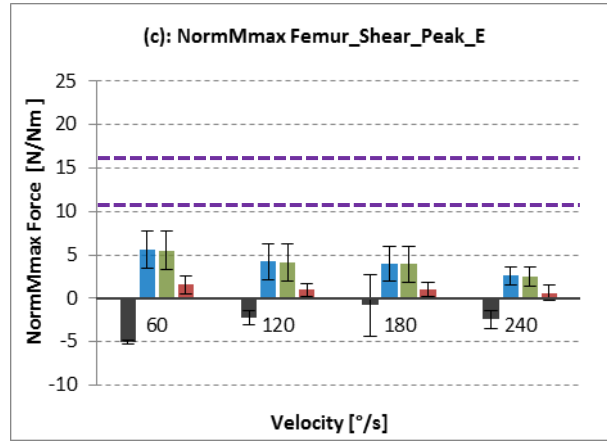
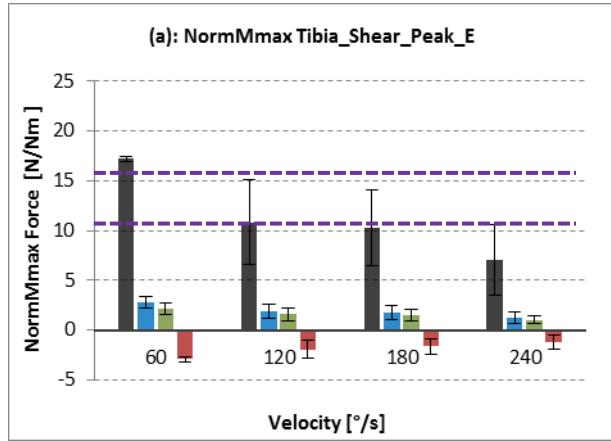
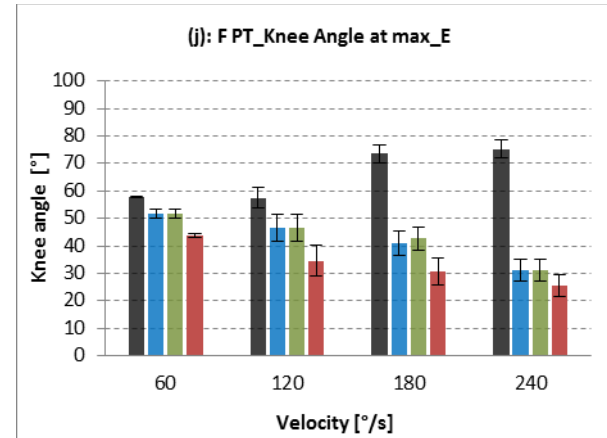
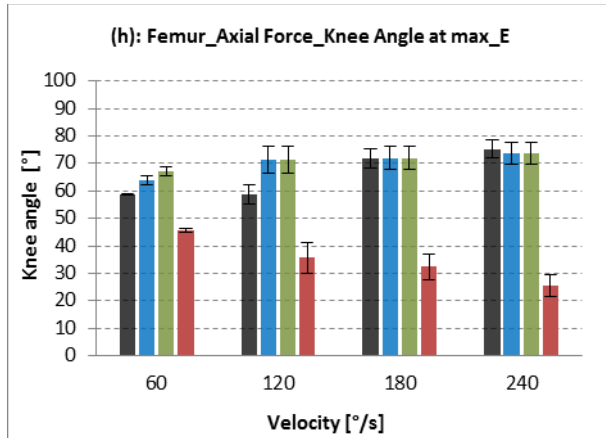
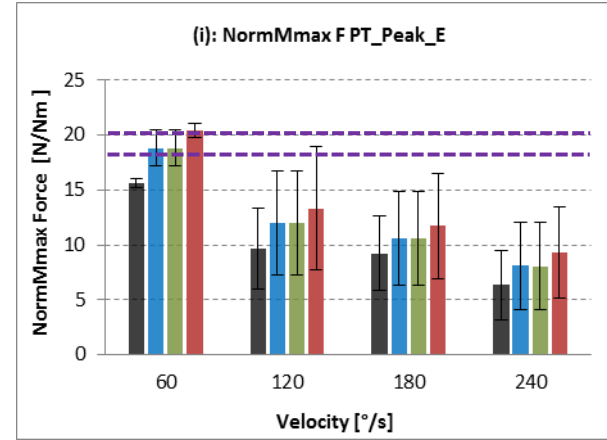
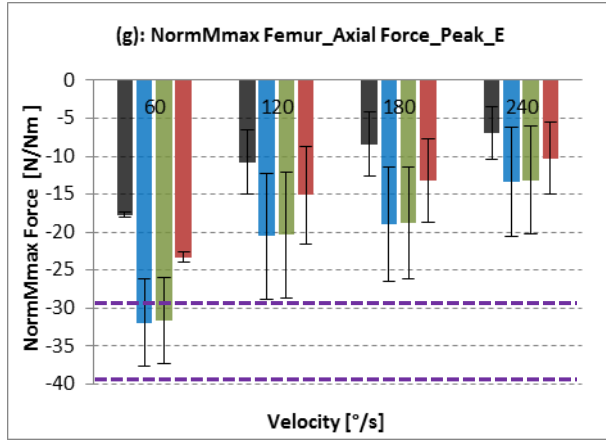


Fig.8.16: Peak values and knee angles at max in Extension

OSIM Mod1_Herzog Mod1_Van Eijden Mod2



OSIM
 Mod1_Herzog
 Mod1_Van Eijden
 Mod2



OSIM
 Mod1_Herzog
 Mod1_Van Eijden
 Mod2

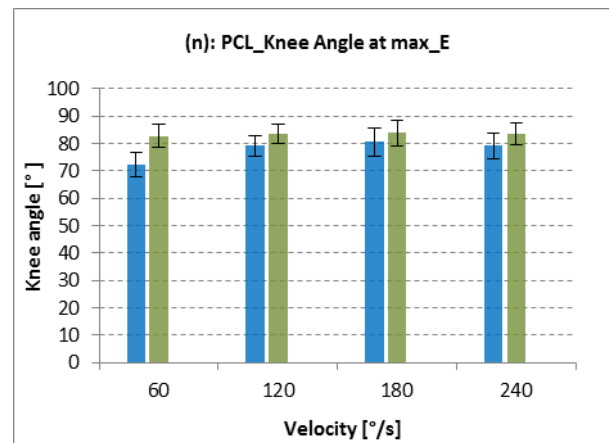
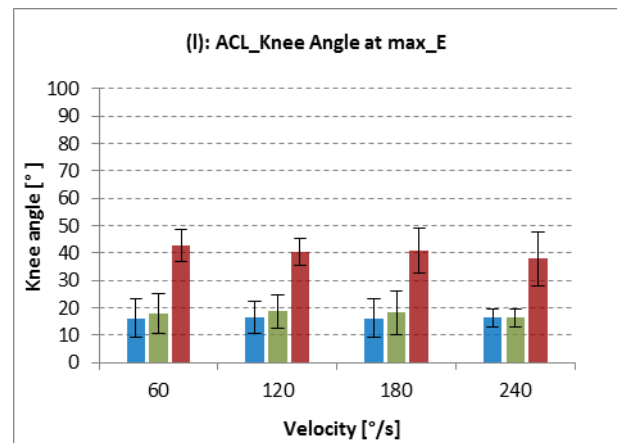
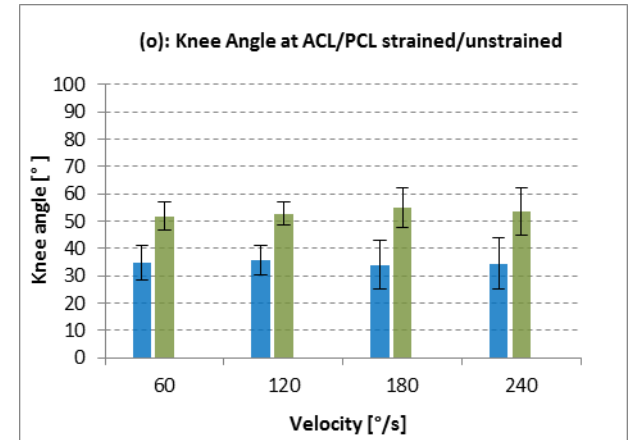
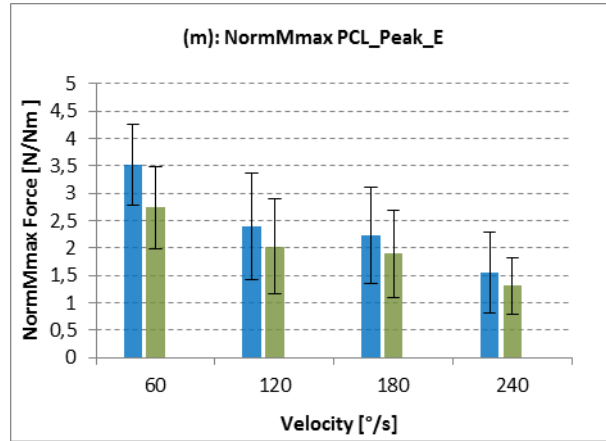
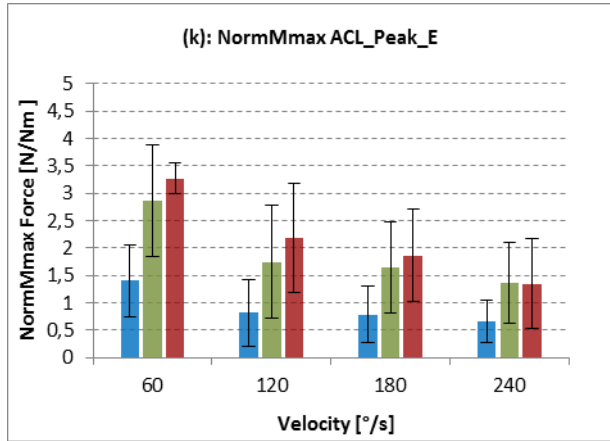
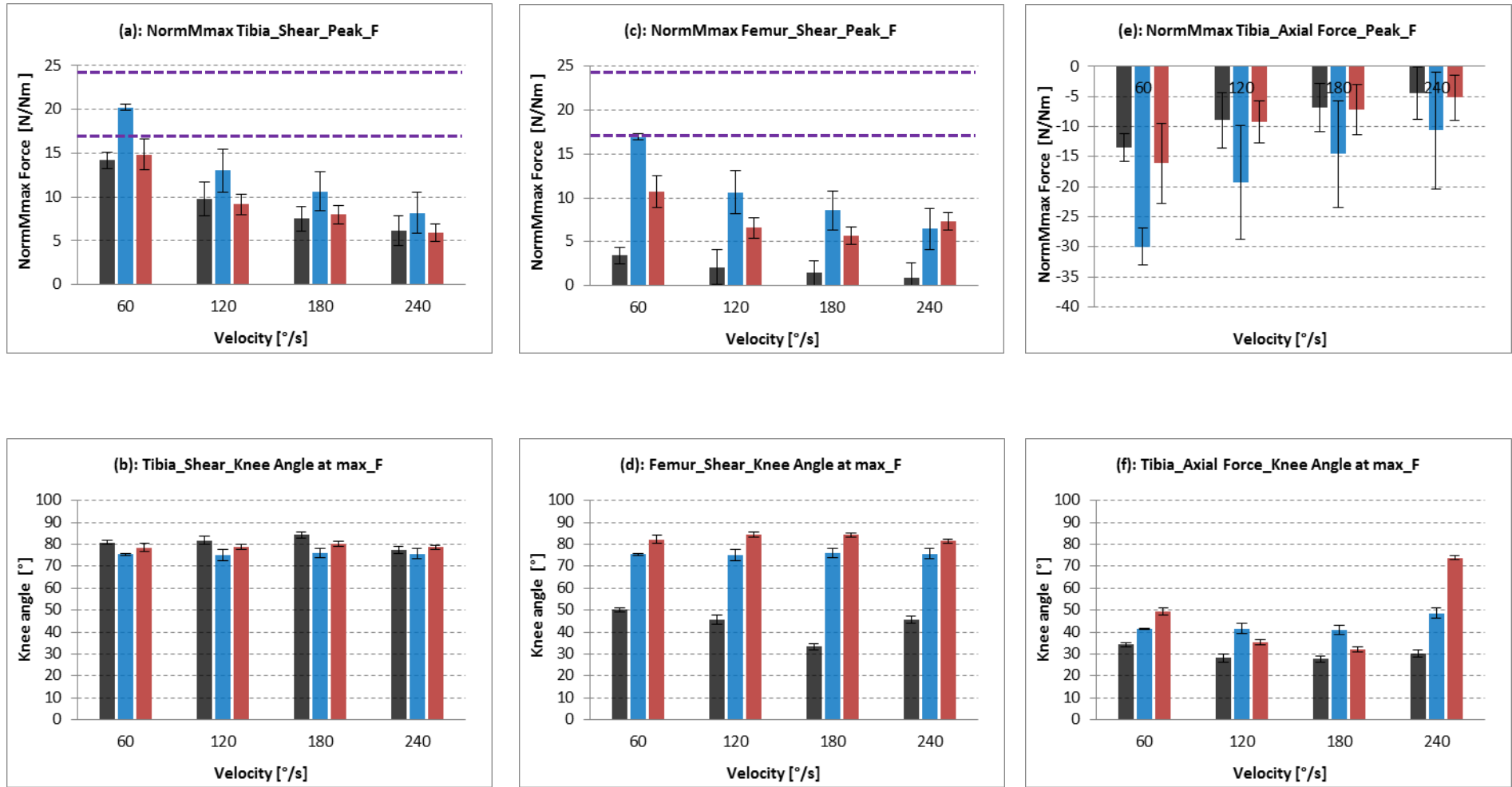
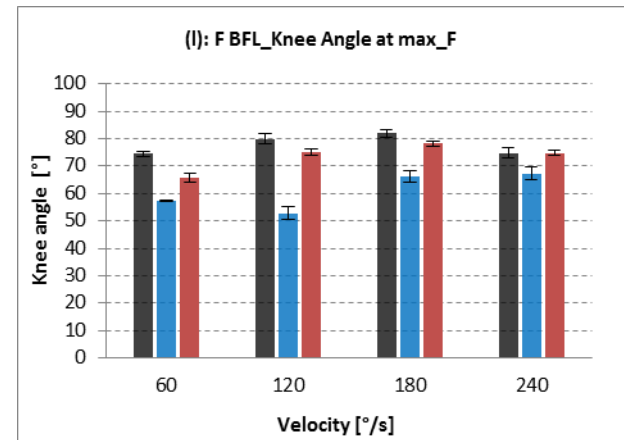
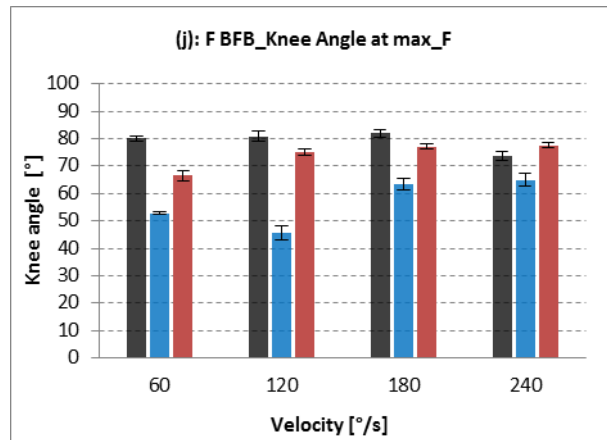
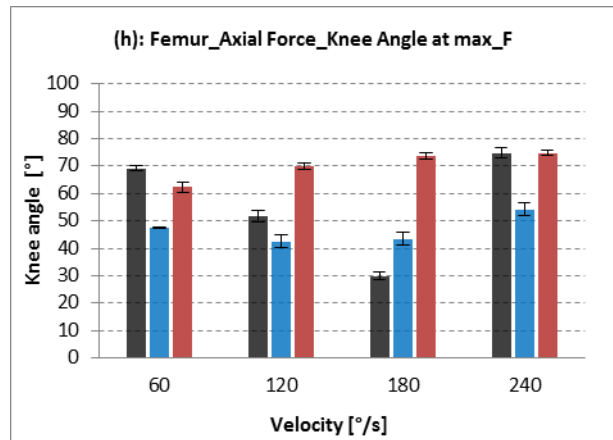
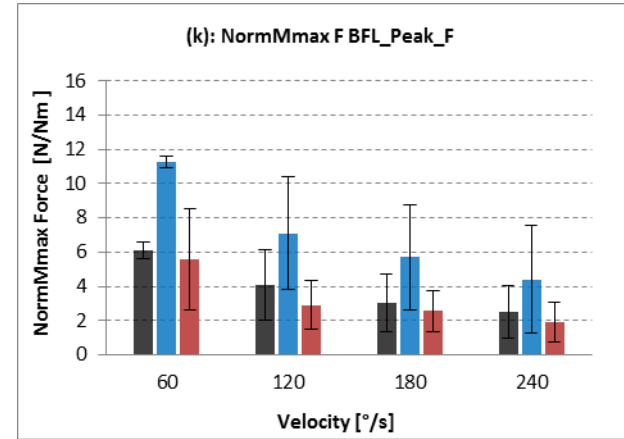
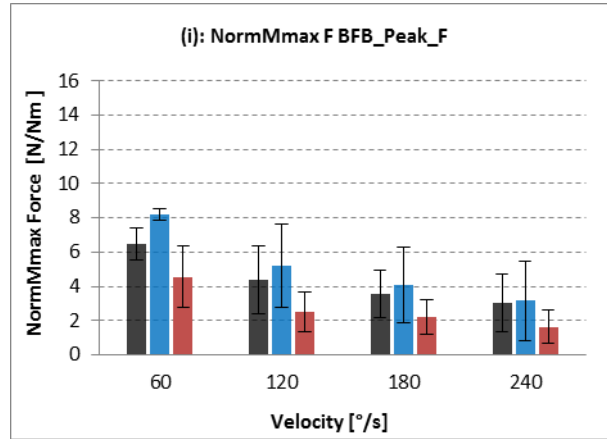
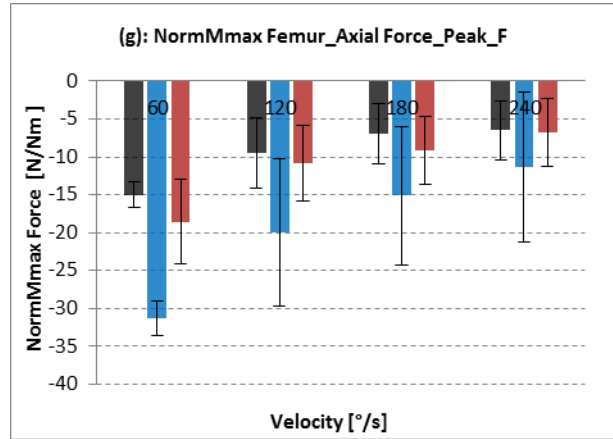


Fig.8.17: Peak values and knee angles at max in Flexion

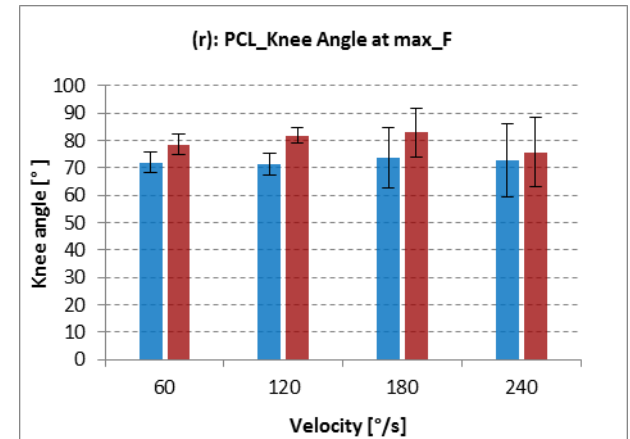
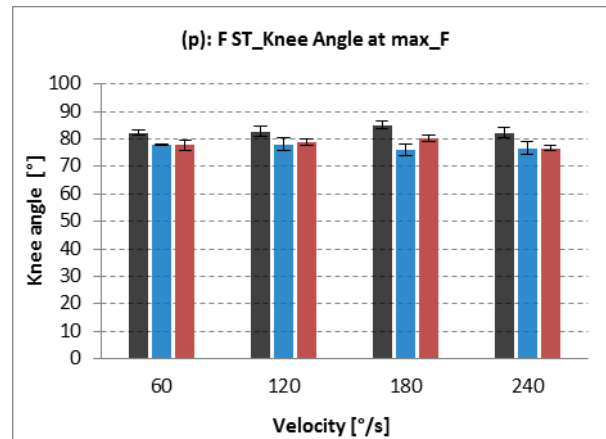
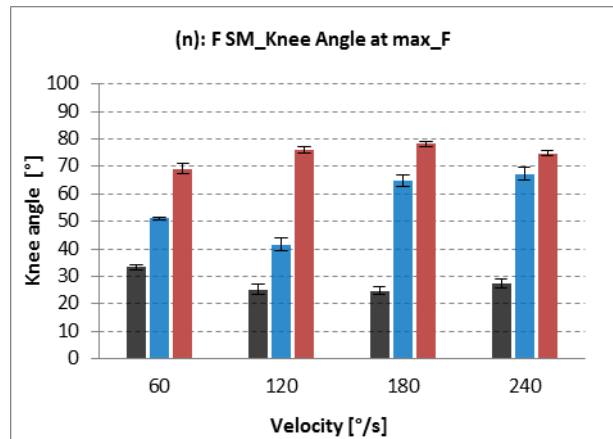
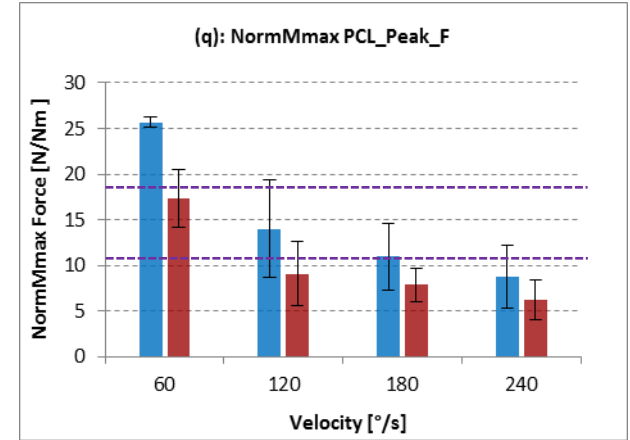
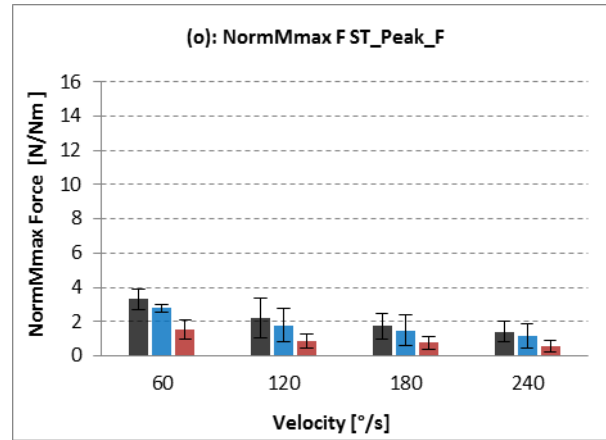
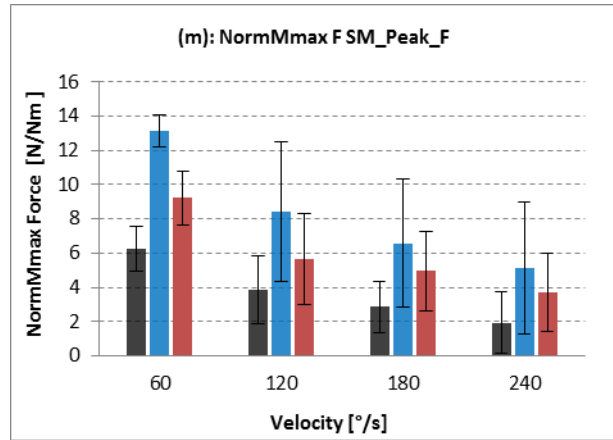
OSIM Mod1_Herzog Mod2



OSIM
 Mod1_Herzog
 Mod2



OSIM
 Mod1_Herzog
 Mod2



Discussion of results

Extension

Fig.8.8, fig.8.10, fig.8.12 and fig.8.14, show the results of the comparison of analytical models and OpenSim simulations in extension in terms of average results.

By comparing the results of the knee moment (fig.8.8.a, fig.8.10.a, fig.8.12.a and fig.8.14.a), it is possible to see that the results obtained by different models are quite coincidence at each velocity; because of the most important parameters which are involved in the determination of the knee moment are the inertial properties and the external forces, by considering that the external forces are the same in all models, the coincidence of the results reveals that the different antropometric schematizations adopted in the first, in the second and in the OpenSim model are equivalent.

The difference between analytical and numerical models increases instead for the force at the patellar tendon (fig.8.8.c, fig.8.10.c, fig.8.12.c and fig.8.14.c), because the results of the first model are close to those of the second but higher than those obtained by OpenSim (moreover, at this step of the analysis, the moment-arm of the first model is that suggested by Herzog et al. also in Van Eijden's approach, so the results of the two sub-models are coincidence): from fig.8.16.i, the maximum value of the force in the first model is $\approx 20\%$ higher than the force in OpenSim model and the force in the second model is $\approx 11\%$ higher than that obtained in the first one at every velocity. Moreover, by considering the angle at which the maximum is reached, from fig.8.16.j it appears that the angle evaluated in analytical models tends to decrease with the growth of the velocity, the angle related to the numerical model tends instead to increase. The difference between analytical and OpenSim models may be due to the fact that the force at the patellar tendon in OpenSim model was evaluated as sum of the forces acting at rectus femoris, vastus medialis, vastus lateralis and vastus intermedius without considering the real line of action of the four fascicles; the difference between the first and the second model is instead associated to the different evaluation of the moment-arm.

Relevant differences occur at the shear acting on tibia: fig.8.8.d, fig.8.10.d, fig.8.12.d and fig.8.14.d illustrate that the force evaluated in the second model is negative in all range of motion and for every velocity, the force calculated in the first model by using the Herzog's formulation is negative from $\approx 38^\circ$ to full extension and positive in the other part of the range (by using the Van Eijden's formulation is negative from $\approx 50^\circ$ to full extension and positive in the other part of the range), the force calculated by the software is instead positive and very high with respect to the others in all range of motion. The difference between the first and second model is related to the different line of action of the patellar tendon, which is the most important force acting during the movement: from fig.8.1.2 it appears that the patellar tendon points forward with respect to the longitudinal axis of tibia at the end of the extension movement (the condition shown at 20° is representative of the last part of extension, from $\approx 38^\circ$ - 50° to full extension) for both

models but is instead negative for the first model and positive for the second in the first part of the movement (the condition shown at 70° is representative of the first part of extension, over ≈38°-50°). The different inclination leads also to differences between the results obtained by using the Herzog's and the Van Eijden's approach; however the error between the two formulations is less than the error with the second model and with OpenSim model. The different shear between analytical models leads to a different activation of the cruciate ligaments: in the second model, the ACL is strained in all range of motion because the shear is always negative; in the first model, with the Herzog's approach the ACL is strained from ≈38° to full extension and the PCL is unstrained, but it is unstrained over ≈38° and the PCL is strained (with the Van Eijden's approach the angle at which the ACL becomes unstrained and the maximum values are higher than those obtained with the Herzog formulation). By comparing however these findings with the results obtained by in-vivo studies done by Beynon et al. (Beynon et al. 1997, [4]; Beynon et al. 1998, [2]; par.3.6) and those obtained with other analytical models by Kaufman et al. (Kaufman et al. 1991, [15]; par.3.6) it is possible to see that the results obtained by the first model are in good agreement with those in the literature; in particular, the shear profile obtained by Kaufman et al. reveals that the ACL is strained at the end of the extension phase and it is unstrained at the beginning when instead the PCL is strained. Because of this good agreement between the results calculated by the first model and those in the literature, the results obtained by the first model are perhaps more reliable than the others, not only for shear on tibia and tension at the cruciate ligaments, but also for shear on femur and axial load on tibia and femur.

To analyze deeper instead the different shear on tibia obtained by using analytical and numerical models, it is necessary to analyze the so called "Tibia_Shear (with patella)": fig.8.8.f, fig.8.10.f, fig.8.12.f and fig.8.14.f illustrate that the shear acting on tibia evaluated by the software is close to the shear evaluated by analytical models by considering the reactions at femur (par.7.6.3). This is due to the fact that the reaction forces evaluated by the software at the knee joint are the same both at the proximal epiphysis of tibia and the distal epiphysis of femur (equilibrium conditions must be respected); in this way however the shear on tibia is not correct because it is the result not only of forces acting on tibia but also of forces transmitted by patella to femur. As a matter of fact, the most important difference on forces acting during the movement at tibia and femur is related to patella. Furthermore, the shear obtained in the second model (by considering the patella) is more close to the OpenSim one than those obtained in the first model. This finding is related in particular to the fact that in the first model the lever-arm of the tendon of quadriceps is different from that of the patellar tendon and consequently the force at the two tendons is different, in the second model instead the lever-arm is the same and so the force is the same (par.7.6.1.6 and par.7.6.2.5). Because the results of the second model are similar to those obtained by the software, this suggests that in the OpenSim model which was used the different lever-arm isn't taken into account.

The difference between analytical and numerical results tends to decrease by considering the reaction forces at femur also for the axial load on tibia as shown in fig.8.8.g, fig.8.10.g, fig.8.12.g and fig.8.14.g and fig.8.8.i, fig.8.10.i, fig.8.12.i and fig.8.14.i; however, the error without considering the patella is less than that related to the shear, because the axial load is negative both for analytical and numerical models in all range of motion at every velocity. Moreover, fig.8.8.g, fig.8.10.g, fig.8.12.g and fig.8.14.g show first that the results obtained by using the Herzog's and the Van Eijden's approach are quite coincidence and secondly that the results of the first model are similar to those of the second model; this is related to the fact that the different line of action leads to relevant differences in terms of shear but not significant differences in terms of axial force (fig.8.1.2). The difference between the first and the second analytical model increases instead by considering the patella (fig.8.8.i, fig.8.10.i, fig.8.12.i and fig.8.14.i): this is due in particular to the different orientation of the tendon of the quadriceps (par.7.6.1.6 and par.7.6.2.5). However, the results obtained for the axial load on tibia are in good agreement with the results obtained by Kaufman et al. (Kaufman et al. 1991, [15]; par.3.6): from that study it appears that tibia is in compression in all range of motion.

The different way in which the reaction forces at the knee-joint are evaluated also leads to differences in terms of shear and axial load on femur. Concerning the shear, fig.8.8.e, fig.8.10.e, fig.8.12.e and fig.8.14.e express that the shear calculated with the second model tends to be positive but very low, the shear calculated by the software tends to be negative in all range of motion, the shear obtained by the first model (the results of Herzog's and Van Eijden's formulation are quite coincidence) is negative and close to that calculated by the software from $\approx 60^\circ$ to full extension and positive in the other part of the range. Although forces on femur are a consequence both of shear and axial load on tibia, it appears, by comparing shear on tibia and shear on femur, that shear on femur is a direct consequence in particular of shear on tibia. The same relation is not instead confirmed for axial load: by comparing axial load on tibia and axial load on femur it is possible to see that the difference between the first (the results of Herzog's and Van Eijden's formulation are quite coincidence) and the second model is higher at femur than that at tibia. The profile of axial load on femur is instead more close to that obtained for axial load on tibia by considering the patella: in both situations, the results are negative for all models, but the profile of the second model is close to the OpenSim one with a peak at the end of the extension phase; the profile of the first model tends to have instead a peak at the beginning of the movement.

By analyzing deeper the maximum values of the forces investigated, from fig.8.16.i it appears that the maximum force at the patellar tendon tends to decrease with the growth of the velocity but it is similar at $120^\circ/\text{s}$ and at $240^\circ/\text{s}$; this is in good agreement with the muscular activation analyzed in par.8.2. Consequently, the same trend can be found for the other forces (fig.8.16.a, fig.8.16.c, fig.8.16.e and fig.8.16.g). By focusing on the force at the patellar tendon, the maximum ranges from $18,82 \pm 1,62 \text{ N/Nm}$ to

8,10±3,97 N/Nm in the Herzog's formulation (the results obtained by using the Van Eijden's approach are quite coincidence), from 20,41±0,62 N/Nm to 9,28±4,16 N/Nm in the second model, from 15,65±0,37 to 6,34±3,18 N/Nm in OpenSim results. From these results it is possible to identify that the maximum value of the force in the first model is ≈20% higher than the force in OpenSim model and the force in the second model is ≈11% higher than that obtained in first one at every velocity. Moreover, at 60°/s the limit condition of maximum tension at the patellar tendon is reached. About the angle at which the maximum occurs, fig.8.16.j shows that the angle evaluated by analytical models tends to decrease with the growth of velocity (in mod1_Herzog from 51,80±5,26° at 60°/s to 31,14±8,83° at 240°/s; the results of mod1_Van Eijden are similar); in the second model from 43,80±5,75° at 60°/s to 25,52±7,43° at 240°/s); on contrary the angle obtained by numerical model tends to increase its value with the growth of the velocity (from 57,83±4,87° to 75,29±5,31° at 240°/s). The results obtained for the analytical models are in good agreement with the fact that the peak of the knee moment tends to occur at lower angles at fast velocities than at slow velocities (fig.8.8.a, fig.8.10.a, fig.8.12.a and fig.8.14.a; on contrary for the results obtained by OpenSim simulations. This may be due to the fact that the force at the patellar tendon was evaluated as sum of the forces acting the four fascicles of the muscle without considering the effective line of of action of each one.

Regarding shear and axial force on tibia and femur, fig.8.16.a, fig.8.16.c, fig.8.16.e and fig.8.16.g show that axial load is higher than shear both for tibia and femur at every velocity. Moreover, by comparing shear on tibia and femur, the last one is higher than the first one; the same thing happens for the axial load. This is reasonable because of the forces trasmitted by patella to femur. By analyzing the shear on tibia (fig.8.16.a) it appears that the maximum force of the first model is reached when the force is positive (although the maximum knee moment is instead reached when the shear is negative) and it ranges between 2,75±0,57 N/Nm and 1,21±0,58 N/Nm in the Herzog's formulation (the results obatined in Van Eijden's approach are quite coincidence), in the second model instead is always negative and in the range -2,92±0,24 N/Nm and -1,186±0,74 N/Nm. The values obtained by OpenSim are not taken into account for the reasons described above. About the shear on femur (fig.8.16.c), the maximum values are positive for the first and the second model, negative for the OpenSim model. The values ranges from 5,63±2,13 N/Nm to 2,57±1,04 N/Nm in Herzog's approach (the results obatined in Van Eijden's approach are quite coincidence), 1,58±1,026 N/Nm to 0,63±0,84 N/Nm in the second model, -5,03±0,19 N/Nm to -2,41±1,025 N/Nm for OpenSim. By comparing fig.8.16.b and fig.8.16.d it is possible to see that the angle at which the maximum shear on tibia and femur is reached is similar at every velocity; moreover for the first model the results related to shear on tibia are similar to those at femur. About the shear on tibia, the maximum is reached at a mean value of 77,53±3,39° in Herzog's formulation, 82,91±4,60° in Van Eijden's approach, 44,353±9,73° in the second model, 70,8±6,23° in OpenSim model; about the shear on femur, 85,82±4,31° in Herzog's formulation, 85,83±4,31° in Van Eijden's approach, 78,42±5,12° in the second model and 35,83±22,32° in OpenSim

model. From these results it appears also that the angle evaluated by the two sub-models of the first model are quite coincidence for the angle associated to the shear on femur. Furthermore, by comparing the previous results with those obtained for the force at the patellar tendon, the angles at which the maximum value of shear both on tibia and femur is reached, is higher than the angle at which there is the maximum force at the patellar tendon. Concerning the axial load on tibia and femur (fig.8.16.e and fig.8.16.g), respectively the maximum values are comprised in the range $-20\pm 2,50$ N/Nm to $-7,84\pm 3,72$ N/Nm in Herzog's formulation (the results obtained in Van Eijden's approach are quite coincidence), $-20,96\pm 1,57$ N/Nm to $-9,42\pm 4,42$ N/Nm in the second model, $-9,35\pm 0,41$ N/Nm to $-4,33\pm 1,96$ N/Nm in OpenSim model and in the range $-31,90\pm 5,69$ N/Nm to $-13,34\pm 7,15$ N/Nm in Herzog's formulation (the results obtained in Van Eijden's approach are quite coincidence), $-23,29\pm 0,65$ N/Nm to $-10,30\pm 4,74$ N/Nm in the second model, $-17,76\pm 0,33$ N/Nm to $-6,95\pm 3,51$ N/Nm in OpenSim model. Fig.8.16.g shows moreover that at $60^\circ/s$ the axial load on femur reaches the critical condition.

About the angles, the angle at which the maximum axial force on femur appears (fig.8.16.h) is similar at every velocity for the first model and it is instead different in the other models: in Herzog's formulation the mean angle is $70,26\pm 6,20^\circ$ (the results obtained in Van Eijden's approach are quite coincidence), in the second model it ranges from $45,78\pm 5,65^\circ$ at $60^\circ/s$ to $25,52\pm 7,43^\circ$ at $240^\circ/s$, from $58,83\pm 4,86^\circ$ to $75,29\pm 5,30^\circ$ in OpenSim model. About the angle related to the maximum axial load on tibia (fig.8.16.f), the values obtained by the first model are similar to those obtained for the axial load on femur at $60^\circ/s$ and $180^\circ/s$ (about 56° at $60^\circ/s$ and 67° at $180^\circ/s$ (results similar for Herzog's and Van Eijden's approach)); the angle evaluated in the second model tends instead to decrease from $36,86\pm 6,14^\circ$ to $24,30\pm 7,02^\circ$; the angle obtained by the numerical simulations tends instead to be similar at each velocity with a mean value of $26,92\pm 9,02^\circ$. By comparing the previous results with those obtained for the angle at which the maximum force at the patellar tendon occurs, it appears that the angle related to the maximum axial load on tibia is more close to the angle at which there is the maximum force at the patellar tendon than the angle associated to the maximum axial load on femur.

In the end, fig.8.16.k and fig.8.16.m show the maximum tension acting at the ACL and PCL respectively. Because of the shear on tibia evaluated with the second model is always negative, only ACL is strained during the exercises and PCL never works; furthermore, the maximum value obtained by this model is higher than those obtained by the others. As described above, these findings are in contrast with experimental and analytical results in the literature; for this reason they are not taken into account. By comparing instead the results obtained by using the Herzog's and the Van Eijden's approach, first it is possible to see that the maximum tension at PCL is higher than that at ACL at every velocity; this is related to the fact that the peak of the shear acting on tibia is positive. For ACL the maximum tension is in the range $1,40\pm 0,64$ N/Nm to $0,66\pm 0,38$ N/Nm in the first approach, $2,86\pm 1,01$ N/Nm to $1,36\pm 0,73$ N/Nm in

the second approach; for PCL $3,52 \pm 0,73$ N/Nm to $1,552 \pm 0,74$ N/Nm in the first approach, $2,74 \pm 0,75$ N/Nm to $1,30 \pm 0,52$ N/Nm in the second one. By comparing the previous results with those described above, they reveals that the difference between the two approaches is significant only in terms of shear acting on tibia and, consequently, in terms of tension at the cruciate ligaments; force at the patellar tendon, shear on femur and axial load on tibia and femur are instead quite coincidence. About the angles at which the maximum of tension at ACL and PCL occur, fig.8.16.l shows that the angle for ACL is similar at every velocity and both for the Herzog's and the Van Eijden's formulation; the mean value is $16,26 \pm 5,93^\circ$ in the first one, $17,75 \pm 6,43^\circ$ in the second one. About the angles related to PCL (fig.8.16.n), it is possible to identify a mean value too but the difference between the results obtained by the first and the second approach is higher than that obtained for ACL: $77,84 \pm 5,12^\circ$ in the first one, $83,43 \pm 4,12^\circ$ in the second one. From these results, it appears that the angle at which the maximum is reached both for ACL and PCL is not related to the velocity of the exercise (and indirectly, it is not related to the intensity). Fig.8.16.o shows that also the angle at which ACL becomes unstrained and the PCL strained isn't related to the velocity of the exercise and that the results obtained by the second approach are higher than those obtained by the first one: the mean angle evaluated with the first approach is $34,75 \pm 8,73^\circ$, $53,25 \pm 7,32^\circ$ with the second one. The fact that the angle at which the maximum values of tension occurs and the angle at which the ACL becomes unstrained and the PCL strained suggests that the most important parameter in the evaluation of the tension at the cruciate ligaments is the inclination of the patellar tendon. As a matter of fact, different line of action leads to different shear acting on tibia and, consequently, different tension at the cruciates; because of the line of action is defined as a function only of the knee angle, it is reasonable that the tension at ACL and PCL isn't influenced, in terms of angles, by external forces. The difference between the results obtained by using the Herzog's formulation and the Van Eijden's formulation is related to the different line of action of the patellar tendon suggested in the two models too. The previous findings on the angles are in good agreement with the results obtained by Kaufman et al. (Kaufman et al. 1991, [15]). From that investigation, it appears that the angle at which the maximum force at ACL and PCL occurs and the angle at which the ACL becomes unstrained are constant at every velocity. In particular, the results suggest a value of 70° - 80° for the angle at which the maximum tension at PCL is reached, 25° for the angle at which the maximum tension at ACL is reached and 40° for the angle at which the ACL becomes unstrained. Also the numerical values are similar to those obtained in this study.

By considering the peak values expressed above and the results of the first model (more reliability) it appears that the limit values are reached only for the axial force on femur and force acting at the patellar tendon at $60^\circ/s$ (fig.8.16.g and fig.8.16.i). Thus, this suggests that the velocity of $120^\circ/s$ should be considered as a safety value in order to not overload the tendon.

About the reliability of results, it is quite good for the angles at which the the maximum occur, but it is instead not as good for the maximum values.

Flexion

Fig.8.9, fig.8.11, fig.8.13 and fig.8.15, show the results of the comparison of analytical models and OpenSim simulations in flexion in terms of average results.

About the knee moment, the similar antropometric schematization leads to quite coincidence results for all models (fig.8.9.a, fig.8.11.a, fig.8.13.a and fig.8.15.a). Moreover, by comparing the results obtained at different velocities, it is possible to see that the profile tends to have a peak at the end of the flexion movement.

Regarding the muscular forces, it appears that the muscular activation of biceps femoris long-head and semimembranosus are similar and higher than the muscular activation of biceps femoris short-head and, in particular, of semitendinosus, which is very low. This happens at every velocity and for every model. About the difference between the results obtained by different models, the results obtained with the first model are higher than those of the second and OpenSim model both for biceps femoris long and short head and semimembranosus, but for semitendinosus they are close to that obtained by the software and however higher than those of the second model. The different profiles between the first and the second analytical model are a consequence of the different moment-arm utilized; as a matter of fact, as described in par.7.6.1.3 and par.7.6.2.2, the forces acting at flexors muscles were evaluated by considering the knee moment, the maximum isometric force and the moment-arm of each muscle, but only the moment-arm is different, because the knee moment is quite coincidence as described above and the maximum isometric force is the same. The difference between analytical and numerical models is related to the different moment-arm too and perhaps to the fact that other muscles which were not considered in this study (for example gracilis) act during the movement and so this might lead to a different sharing of the resultant force which produce movement. However, by analyzing the results obtained for the muscular activation in flexion, it appears that biceps femoris (long and short head), semimembranosus and semitendinosus are the most involved muscles in the movement; thus the different profile obtained is related in particular to the different moment arm.

Concerning the profiles of shear and axial load on tibia and femur obtained by different models, it appears that the results obtained by the second model for shear on tibia and axial load on femur are very close to those of the software and that they are similar at the beginning of the flexion movement, from full extension to about 40-55°, and then they differ for axial load on tibia and shear on femur. The results obtained by the first model are instead always higher than the others because of the high muscular activation of flexors muscles evaluated by this model. However, shear on tibia and femur are positive in all

range of motion for all models; negative for axial load on tibia and femur. Moreover, the profile of shear on tibia and femur are similar; this is reasonable because in flexion the only forces which act on femur are transmitted by tibia. The same thing can be identified for axial load on tibia and femur. Furthermore, these findings suggest the software calculate correctly the forces at the knee joint in flexion.

Because the shear on tibia is positive in all range of motion, only PCL is strained during the movement, as shown in fig.8.9.b, fig.8.11.b, fig.8.13.b and fig.8.15.b. These results, and also those related to the axial load on tibia, are in good agreement with those obtained in the literature by Kaufman et al. (Kaufman et al. 1991, [15]). From that study, it appears that tibia is in compression in all range of motion and that the shear leads to an activation only of PCL.

By analyzing deeper the maximum values of the forces investigated and the angle at which the maximum occur, fig.8.17.i, fig.8.17.k, fig.8.17.m and fig.8.17.o show that the muscular forces tend to decrease with the growth of the velocity, in good agreement with the results obtained for the muscle activation (par.8.2). By considering for simplicity the results of the first model, the maximum force at biceps femoris short-head decreases from $8,19 \pm 0,34$ N/Nm to $3,16 \pm 2,34$ N/Nm, for biceps femoris long-head from $11,28 \pm 0,33$ N/Nm to $4,39 \pm 3,13$ N/Nm, for semimembranosus from $13,14 \pm 0,95$ to $5,14 \pm 3,89$ N/Nm, for semitendinosus from $2,78 \pm 0,19$ N/Nm to $1,16 \pm 0,73$ N/Nm. The maximum values are about 26% higher than those obtained by OpenSim and about 80% higher than those of the second model for biceps femoris short-head, about 86% higher than those of OpenSim and about 120% higher than those of the second model for biceps femoris long-head, about 110% higher than those of OpenSim and about 43% higher than those of the second model for semimembranosus; regarding the force force at semitendinosus, the maximum evaluated by the software is similar to that obtained by the first model and higher than that of the second one: the OpenSim results are about 20% higher those of the first model and about 110% higher than those of the second model. About the angles at which the maximum muscular forces is reached, fig.8.17.j, fig.8.17.l, fig.8.17.n and fig.8.17.p show that for biceps femoris short-head, biceps femoris long-head and semimembranosus the angle evaluated by the first model tends to be similar at $60^\circ/s$ and $120^\circ/s$ and to increase and to be similar again at $180^\circ/s$ and $240^\circ/s$ and that the angle evaluated by the second and OpenSim model tends to have similar values at $60^\circ/s$ and $240^\circ/s$ and to increase and to be similar at $120^\circ/s$ and $180^\circ/s$; moreover, the angle obtained for biceps femoris short-head is similar to that of biceps femoris long-head and semimembranosus at every velocity, except for the results obtained by the software. By considering the results obtained by the first model, the angle at which the maximum occurs is about 45° at $60^\circ/s$ and $120^\circ/s$ and about 65° at $180^\circ/s$ and $240^\circ/s$ for the first model, about 68° at $60^\circ/s$ and $240^\circ/s$ and about 75° at $120^\circ/s$ and $180^\circ/s$. About the angle at which the maximum force at semitendinosus appears, the angle is similar at every velocity and for all models with a mean value of about 79° .

Concerning shear on tibia and femur, fig.8.17.a and fig.8.17.c reveal that the maximum values are similar at every velocity and they decrease with the growth of the velocity. By considering the results of the first

model, they decrease from a mean value of about 18N/Nm to a mean value of about 7 N/Nm; these results are about 43% higher than those of OpenSim and about 45% higher than those of the second model. Moreover the critical limit is reached at 60°/s by the results of the first model. About the angle at which the maximum occurs, it is similar for shear on tibia and femur and also similar at every velocity for all models, except for OpenSim results: from fig.8.17.b and fig.8.17.d, the maximum shear on tibia and femur is reached at a mean value of about 76°. The same trend can be identified for axial load on tibia and femur. By comparing fig.8.17.g and fig.8.17.e, by considering the maximum axial load evaluated by the first model, it decreases (in absolute terms) from a mean value of about 30 N/Nm to 11 N/Nm and it is about 123% and about 83% higher than the results obtained by OpenSim and by the second model respectively. About the angles, fig.8.17.f and fig.8.17.h show that the angle is similar at every velocity except for 240°/s and also similar between tibia and femur. By considering the results of the first model, it has a mean value of about 41° at 60°/s, 120°/s and 240°/s and a mean value of 47° at 240°/s; similar relations can be found for the other models, but not a common trend for tibia and femur.

By comparing the angles at which the maximum of the forces investigated occurs, the previous results express that the maximum tend to be reached at angles which are close to angle at which the maximum knee moment occurs.

In the end, because the shear on tibia is always positive, only PCL works in flexion. From fig.8.17.q it appears that the maximum force evaluated by the first model decreases from 25,66±0,58 N/Nm to 8,69±3,45 N/Nm and that it is higher than that obtained by the second model, which instead ranges from 17,32±3,11N/Nm to 6,17±2,19 N/Nm. About the angle at which the maximum is reached, the fact that it is not influenced by the velocity obtained in extension is confirmed: it has a mean value of about 72,42±8,73° for the first model, 79,78±8,13° for the second one. These results agree well with those obtained by Kaufman et al., because in that study the maximum peak of shear was reached at 75°.

By considering the peak values expressed above and the results of the second model (more reliability) it appears that the limit values are reached only for the force acting at PCL at 60°/s (fig.8.17.q). Thus, as in extension, the velocity of 120°/s should be considered a safety limit.

About the reliability of results, it is quite good for the angles at which the the maximum occur, but it is instead not as good for the maximum values as in extension.

PART 2: LEG EXTENSION EXERCISE
(preliminary study)

9. Material and Methods of Part 2

For this second part of the thesis, the knee flexion-extension movement was investigated during the leg-extension exercise by considering two types of machines which are commonly used in gym (fig.9.1 and fig.9.2). Both machines are multifunctional benches, with a bar for the leg-extension exercise. In the first one, M1, the resistance to the leg-extension movement is due to a cable connected by a system of pulleys to the weight stack located at the back of the machine; in the second one, M2, the resistance to the movement is directly due to the weight of some cast iron discs put on the bar.



Fig.9.1: Bench 1 (M1).



Fig.9.2: Bench 2 (M2).

The exercises at the two machines were performed by subject S5 after the isokinetic ones. Being this a preliminary study, only one subject was tested. The same protocol was used for the two benches. First, the so called 1-repetition maximum (1RM) was found by increasing the load gradually until one complete repetition had been done; after that, other three tests were done at the $\approx 25\%$, $\approx 50\%$ and $\approx 75\%$ of the 1RM by modifying the load. Five repetitions were performed for each of these intensities. To focus only on the influence of the load, the subjects was asked to perform the exercises at the same velocity. The load sequence for the two benches were:

M1: 33 kg (1RM), 10 kg (30%), 15 kg (45%), 25 kg (75%);

M2: 25 kg (1RM), 6 kg (25%), 12 kg (50%), 18 kg (75%).

Between an exercise and the other, there was a sufficient period for a full recovery.

Fig.9.3 and fig.9.4 show how the exercise were performed: although the femur right and left were not fixed as in the isokinetic tests with a specific device, it is reasonable to assume that the knees were fixed during the leg-extension movement too, because of the load conditions and because of the position of the subject. Torso and pelvis could be considered fixed too.

About the ROM, the subject was asked to do the exercise at different loads with the same limits of ROM. However, because of the structural differences between the two machines, the ROM was not equal for M1 and M2: $\approx 25^\circ$ - 90° knee angle for M1 and $\approx 10^\circ$ - 85° knee angle for M2.



Fig.9.3:M1 test conditions



Fig.9.4: M2 test conditions.

As done for the first part of the thesis, the muscular activation was investigated by using surface electrodes; the muscles which were considered in this second part are rectus femoris right, vastus lateralis right and vastus medialis right, in order to compare the results from those deriving from the isokinetic exercises. Only extensor muscles were chosen because during the leg-extension exercise the flexor muscles don't work: there is only extension, concentric and eccentric phase.

The spatial movement was reconstructed by using the same optoelectronic system and the same marker set used for the first part. Other markers were placed on the machines in order to obtain the kinetics conditions during the movement (as described in par.10.2).



Fig.9.5: M1 static trial.



Fig.9.6: M2 static trial.

As done for the first part, a local reference system embedded to the right tibia and a static trial, which was done before the tests, were used to obtain the trajectory of the markers on the right ankle and to scale the OpenSim model. No reference system was placed on the left tibia because only the right side was considered (as described in par.10.1).

10.Data analysis of Part 2

10.1.Kinematic analysis

Although both the right leg and the left leg were involved during the movement, the left leg was considered fixed during the analytical and numerical simulations at the position of the static trial. That is justified because the influence of the left side on the right side is modest. By considering this assumption, we have the same kinematic conditions of the first part of the thesis. Thus, the spatial movement is reconstructed by interpolating the trajectory of the markers and by using the local reference system embedded to the right tibia and the static trial as described in par.7.2. Because of the left tibia is considered fixed, no local reference system was required for the left side.

10.2.Kinetic analysis

The kinematic conditions are different for the two machines.

For M1 the external loads acting during the movement were obtained by considering a load-cell and some markers placed on the machine, as shown in fig. 10.1.

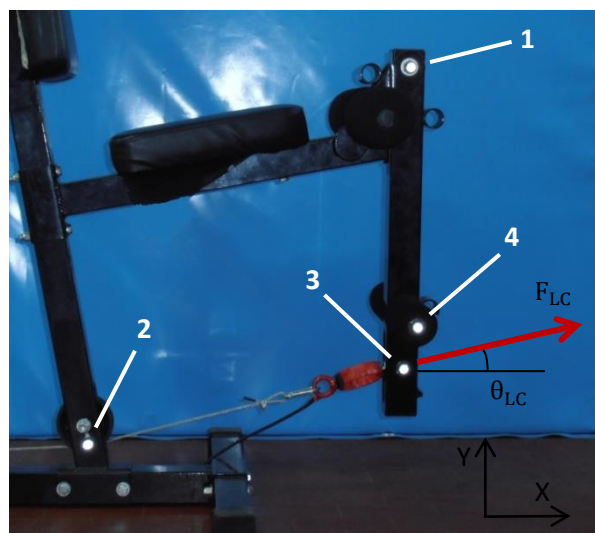


Fig.10.1: Load-cell and markers which were used to obtain the kinetic conditions for M1 (marker 5 not visible).

The value of the force exerted by the tibia to the bar during the movement was measured by using a load-cell put between the cable and the bar; because of the left leg was considered fixed (see par.10.1), the force acting at the right leg was considered a half of the total force measured with the load-cell. This is an assumption because only for subjects with a good physical condition the force exerted by the right leg is equal to that exerted by the left leg. About the direction of the force measured by the load-cell, the coordinates of the markers 2 and 3 were used to calculate the inclination of the force with respect to the x-axis shown in fig.10.1.

By using the reference system shown in fig.10.1, value and inclination of the force were calculated with the following equations:

$$F_{EXT} = F_{LC}/2$$

$$\theta_{LC} = \arctan\left(\frac{y_3 - y_2}{x_3 - x_2}\right)$$

in which F_{EXT} and F_{LC} are the force at the right leg and the force measured by the load-cell respectively; θ_{LC} is the inclination of the force measured by the load cell with respect to the x-axis; x_2, y_2 and x_3, y_3 are the coordinates of the markers 2 and 3 respectively.

The force F_{EXT} isn't the force acting at tibia because its point of application can't be considered the same point of application of the force acting at tibia. As a matter of fact, the point of application of F_{EXT} should be identified with the position of marker 2. About the point of application of the force acting at tibia, it was evaluated by considering the markers 4 and 5 (see fig.10.1), which were placed respectively at the center of the right extremity and at the center of the left extremity of the transversal cylindrical device used to exert the force. The contact point with the right tibia was evaluated at a distance of about 3 cm from the marker 4 and along the direction defined by markers 4 and 5. In this way the thickness of the sponge was ignored, but, considering that during the exercise the real thickness was less than 1,5 cm because of the pressure exerted, it is reasonable to do this. As done for the isokinetic tests, the force exerted by tibia is considered perpendicular to tibia and its value is calculated by the following equations:

$$T_1 = F_{EXT} \cdot \cos(\theta_{LC}) \cdot (y_1 - y_3) + F_{EXT} \cdot \sin(\theta_{LC}) \cdot (x_3 - x_1)$$

$$F_{RT1} = \frac{T_1}{\sqrt{(x_1 - x_{p1})^2 + (y_1 - y_{p1})^2}}$$

in which T_1 is the moment exerted by the force F_{EXT} ; x_1 and y_1 are the coordinates of the markers 1 placed on the center of rotation of the bar; x_{p1} and y_{p1} are the coordinates of contact point calculated above; F_{RT1} is the force acting at tibia.

In this way, the misalignment of the knee with respect to the axis of rotation of the bar is considered too.

As done for the first part, the force acting at tibia was evaluated by considering null the component in the z direction:

$$F_{RT1x} = F_{RT1} \cdot \cos(\theta_F + \varphi_k)$$

$$F_{RT1y} = F_{RT1} \cdot \sin(\theta_F + \varphi_k)$$

$$F_{RT1z} = 0$$

(in the previous equations, the number 1 stands for M1)

For M2, the point of application of the force exerted was evaluated in the same way described for the bench M1 by considering two markers at the extremities of the transversal cylindrical bar and by evaluating the distance of the contact point from the marker on the right extremity. Another marker, marker 6, was placed on the center of rotation of the mechanism and another one, marker 7, on correspondence of the center of mass of the discs. The position of marker 6 changed during the tests because the center of mass was variable.

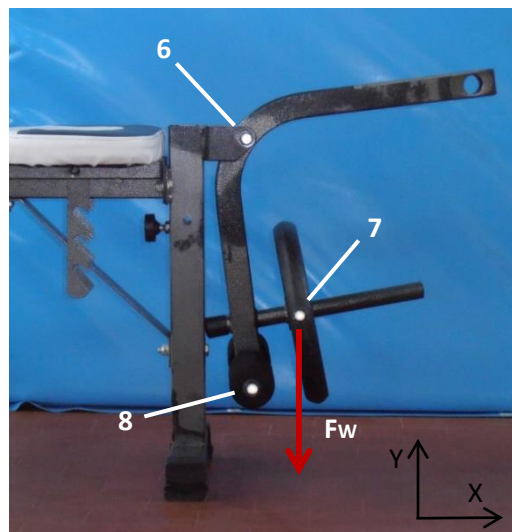


Fig.10.2: Markers used to reconstruct the kinetic conditions for M2 and external force F_w due to the weight of the discs.

By considering the reference system shown in fig.10.2, the force acting at tibia was evaluated with the following equations:

$$T_2 = (m/2) \cdot g \cdot (x_7 - x_6) + I \cdot \ddot{\varphi}_k$$

$$F_{RT2} = \frac{T_2}{\sqrt{(x_6 - x_{p2})^2 + (y_6 - y_{p2})^2}}$$

$$F_{RT2x} = F_{RT2} \cdot \cos(\theta_F + \varphi_k)$$

$$F_{RT2y} = F_{RT2} \cdot \sin(\theta_F + \varphi_k)$$

$$F_{RT2z} = 0$$

(in the previous equations, the number 2 stands for M2)

in which T_2 is the moment exerted by the weight of discs; m is the weight of the discs and the bar (the mass of the bar was evaluated ≈ 1 kg); $I \cdot \ddot{\varphi}_k$ are the inertial effects of the rotation; x_6, x_7, y_7, x_{p2} and y_{p2} are the coordinates of markers 6 and 7 and the coordinates of the point of application of the force; F_{RT2} is the force acting at tibia.

The moment T_2 was calculated by considering the force exerted by the right leg equal to that exerted by the left leg as done for the M1; thus the total mass m was divided by 2.

The inertial effects were evaluated by considering only the discs because of the moment of inertia of the bar was negligible with respect to that of the discs

($I = m_{discs} \cdot (\sqrt{(x_6 - x_7)^2 + (y_6 - y_7)^2})^2$) and by considering the angular acceleration of the knee, $\ddot{\varphi}_k$.

10.3. OpenSim simulations and EMG analysis

The OpenSim simulations and the EMG analysis were done as described in par.7.4 and par.7.5. In particular, for the EMG analysis, the signal was normalized to the maximum effort that the subject was able to do during the isometric tests and during the second, the third and the fourth cycle of the isokinetic tests, as done for the first part of the thesis, without considering the leg-extension exercises. That's in order to compare the muscular activation of the leg-extension tests with that of the isokinetic tests. The comparison with the muscle activation obtained by OpenSim simulations was done by considering the second, the third and the fourth cycle as done for the first part of the thesis.

10.4. Comparison of analytical models and OpenSim simulations

The same approach described in par.7.6 is used, by considering only extension. The comparison is expressed as mean and standard deviation of the second, the third and the fourth cycle. In order to compare the results of the exercises performed at M1 and M2 with those in isokinetic conditions, the results were normalized to the maximum knee moment obtained during isokinetic exercises in extension. As done for the first part of the thesis, maximum values and angles at which the maximum is reached are shown. Because of the different ROM of M1 and M2, in order to compare the results, the maximum was researched in the ROM 25°-80° knee angle both for M1 and M2.

11.Results and Discussion of Part 2

The results of the exercises performed at M1 and M2 are shown. For each bench the comparison in terms of muscle activation, the comparison of analytical models and OpenSim model, the maximum values and the angles at which the maximum is reached are shown. In order to recognize the extension phase and the flexion phase, continuous line is used for the concentric phase, the broken line for the eccentric phase. The same representation is kept in the visualization of the maximum values: the continuous line is used when the peak is reached in concentric phase (or when there is no relevant difference between concentric and eccentric phase), the broken line when the peak is reached in eccentric phase.

About the limit values, they are the same of the isokinetic tests (because the normalization is the same).

11.1.Results of exercises performed at M1

Fig.11.1.1: Muscle activation of RF (a), VL (b) and VM (c) at M1 at 25%.

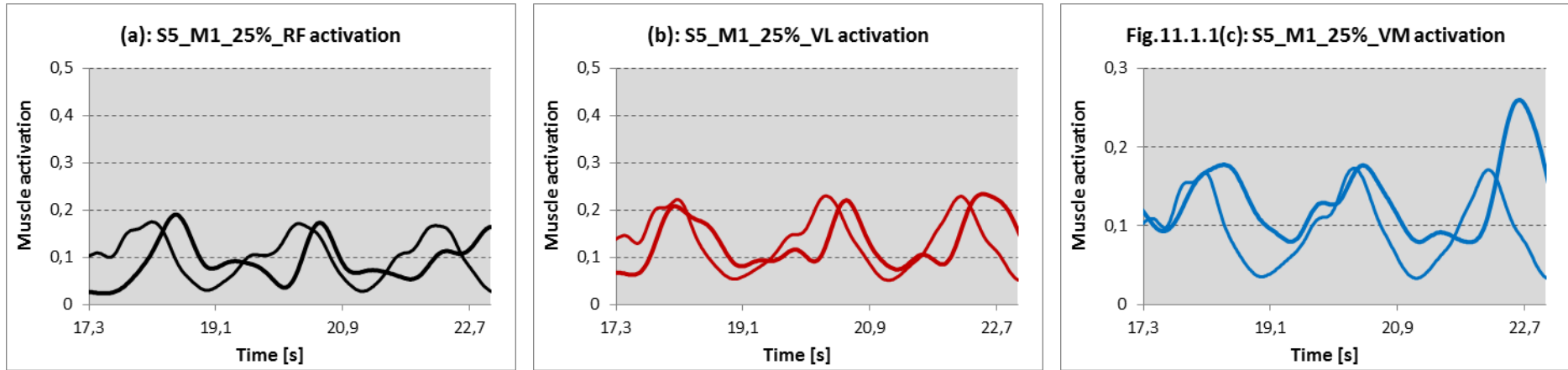
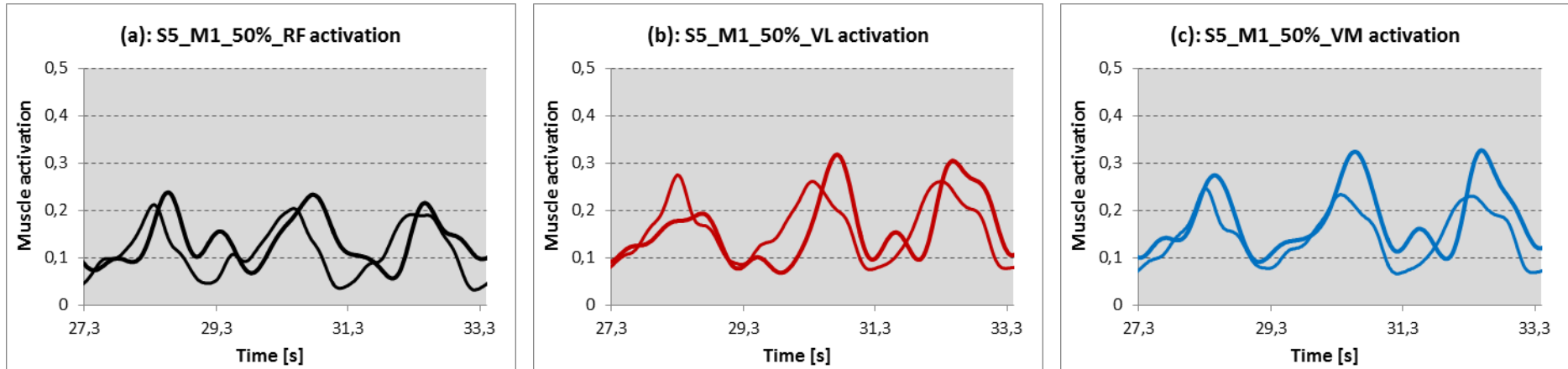


Fig.11.1.2: Muscle activation of RF (a), VL (b) and VM (c) at M1 at 50%.



— RF-EMG — RF-OSIM

— VL-EMG — VL-OSIM

— VM-EMG — VM-OSIM

Fig.11.1.3: Muscle activation of RF (a), VL (b) and VM (c) at M1 at 75%.

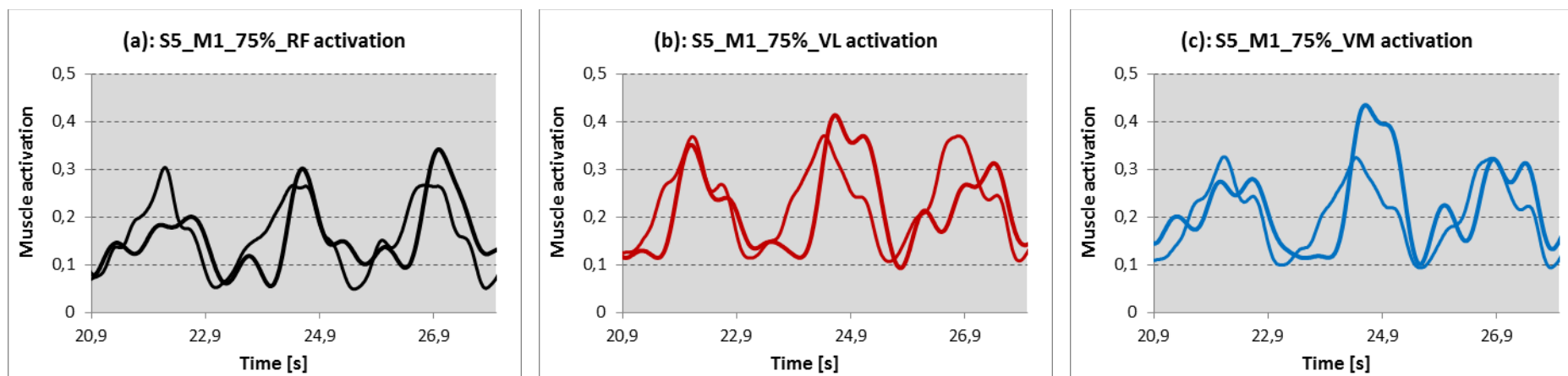
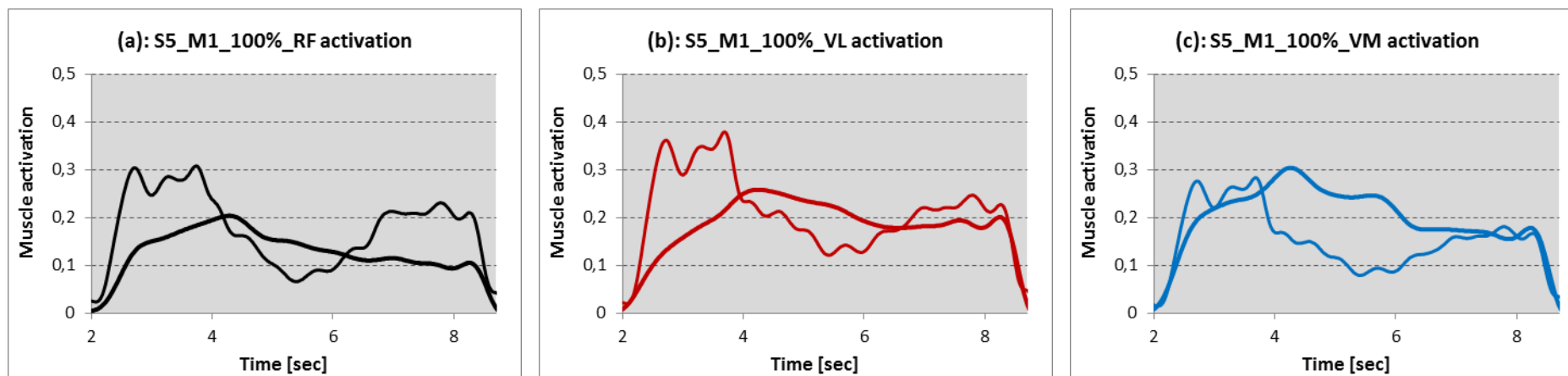


Fig.11.1.4: Muscle activation of RF (a), VL (b) and VM (c) at M1 at 100%.



— RF-EMG — RF-OSIM

— VL-EMG — VL-OSIM

— VM-EMG — VM-OSIM

Comparison of EMG signal and OpenSim muscle activation: quantitative results

	25%	50%	75%	100%
RF	3,40±4,83	9,77±1,2	14±5,19	-50,98±0,00
VL	-1,43±4,7	2,57±32,5	-10,67±14,47	-46,90±0,00
VM	14,83±17,6	22,57±10,86	2,70±21,13	6,58±0,00

Tab.11.1.1: Peak error in [%] of RF, VL and VM at 25%, 50%, 75% and 100% at M1.

	25%	50%	75%	100%
RF	21,63±12,64	6,24±9,89	5,62±13,32	8,99±0,00
VL	8,97±9,93	14,43±7,51	9,61±13,64	10,35±0,00
VM	14,38±9,64	8,18±2,52	9,97±11,22	10,08±0,00

Tab.11.1.2: Time error in [%] of RF, VL and VM at 25%, 50%, 75% and 100% at M1.

	25%	50%	75%	100%
RF	-4,83±9,70	12±4,42	5,26±12,83	-35,37±0,00
VL	6,39±12,81	4,76±13,68	-1,78±5,64	-14,63±0,00
VM	25,4±10,26	12,99±7,70	2,17±6,53	23,87±0,00

Tab.11.1.3: Area error in [%] of RF, VL and VM at 25%, 50%, 75% and 100% at M1.

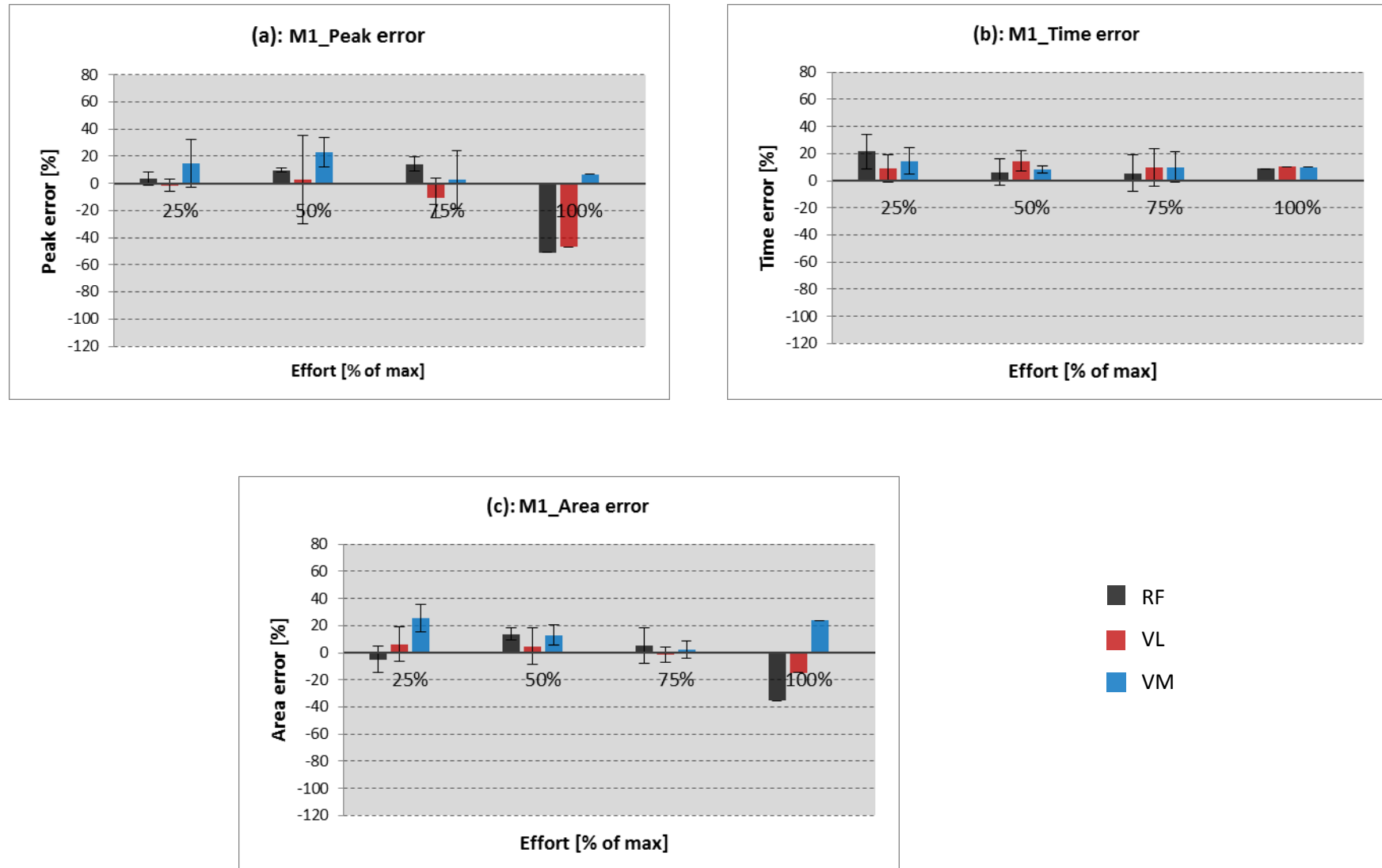


Fig.11.1.5: Quantitative results of muscle activation analysis for M1: (a): Peak error at different velocities; (b): Time error at different velocities; (c): Area error at different velocities.

Fig.11.1.6: M1_25%

— OSIM — Mod1_Herzog — Mod1_Van Eijden — Mod2 - - - - - limit value

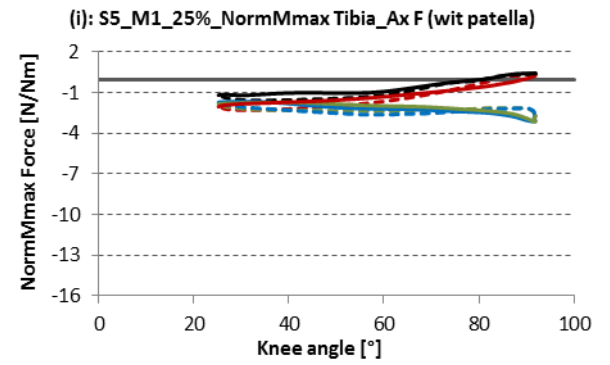
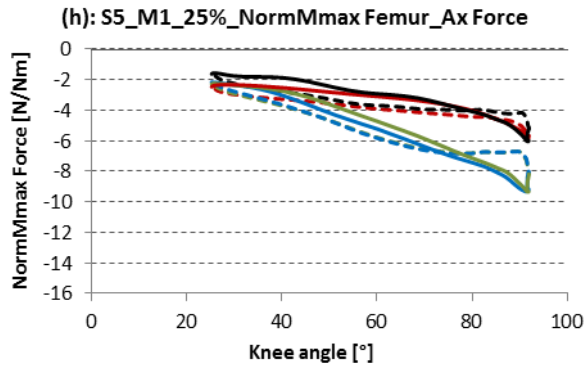
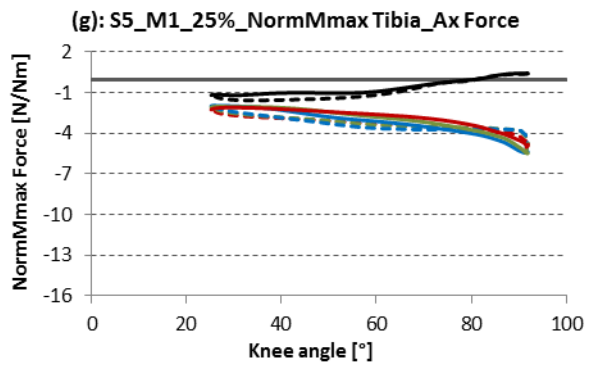
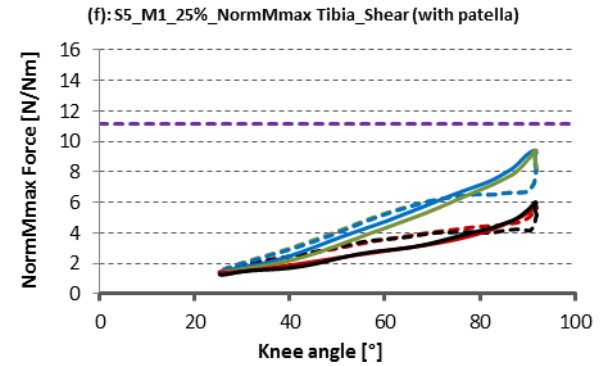
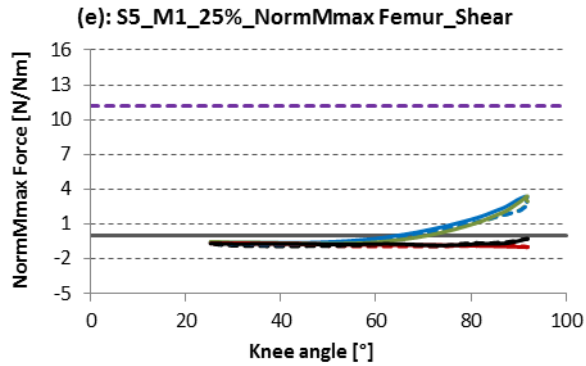
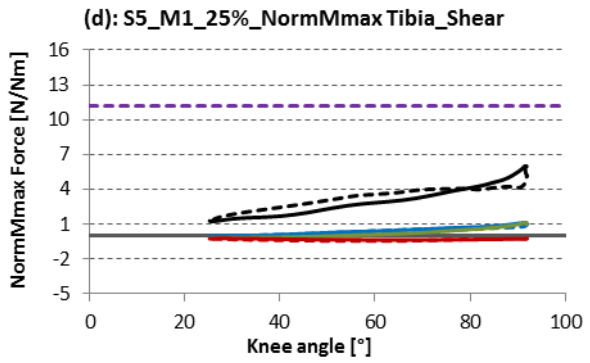
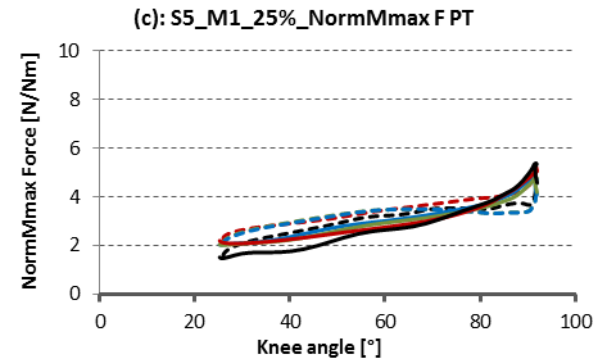
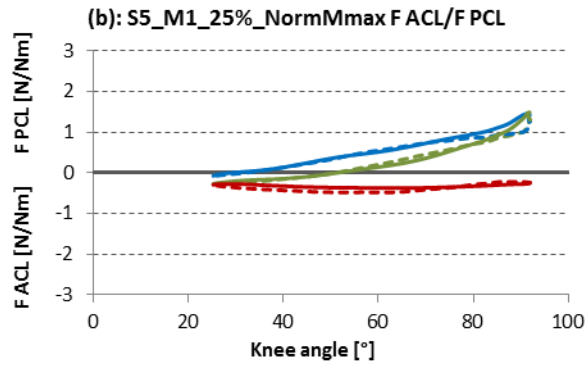
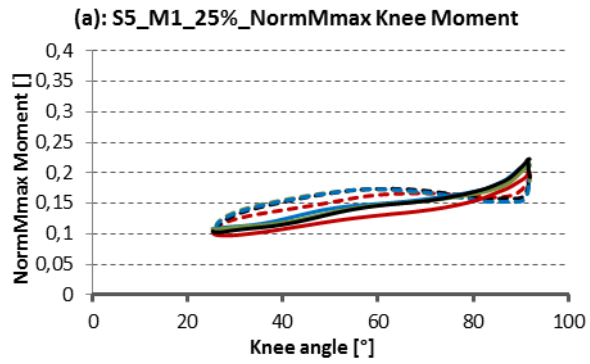


Fig.11.1.7: M1_50%

— OSIM — Mod1_Herzog — Mod1_Van Eijden — Mod2 - - - - - limit value

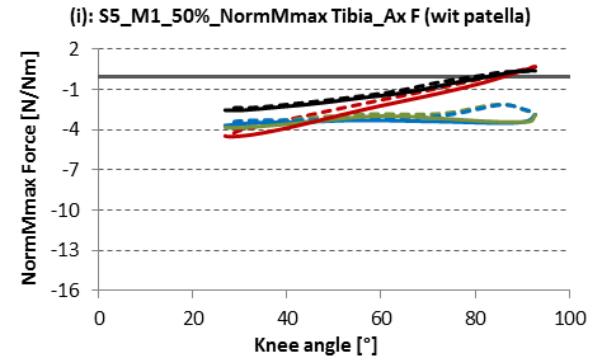
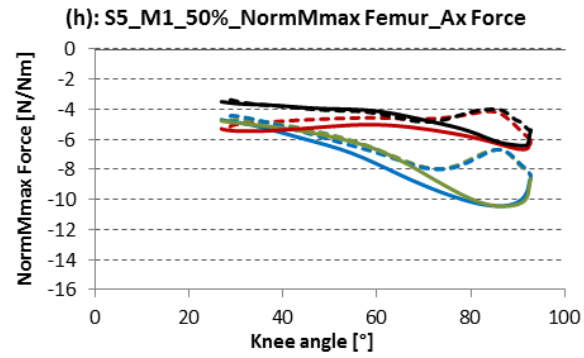
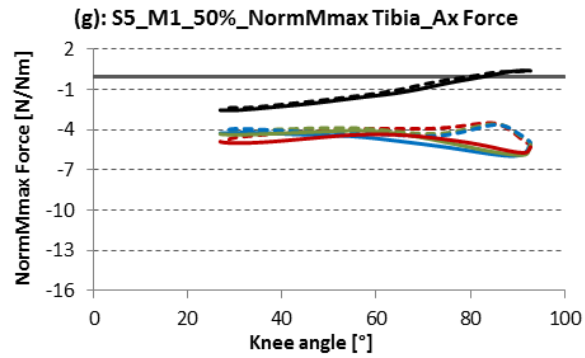
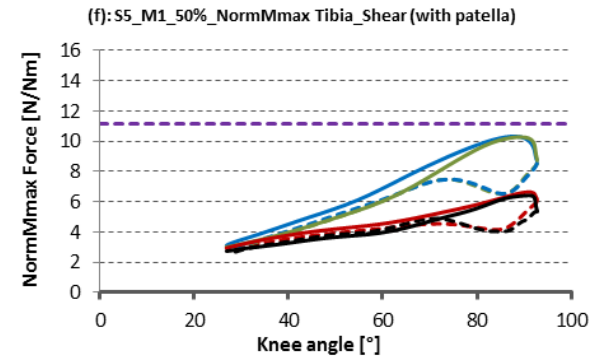
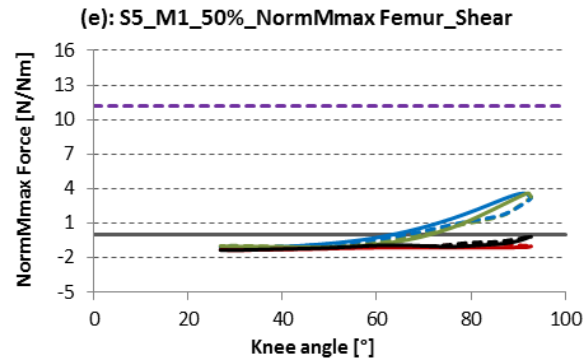
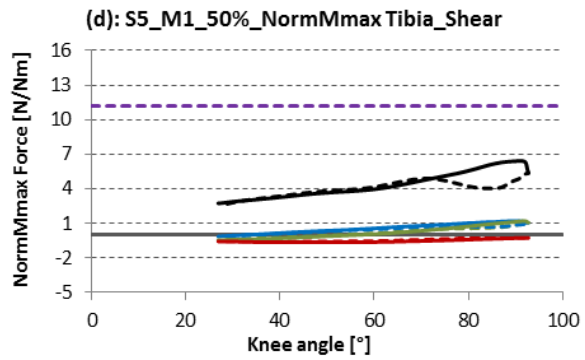
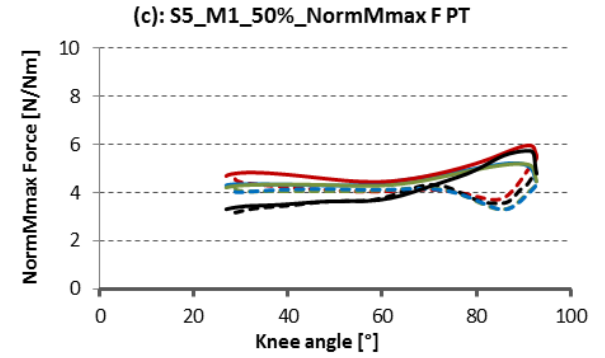
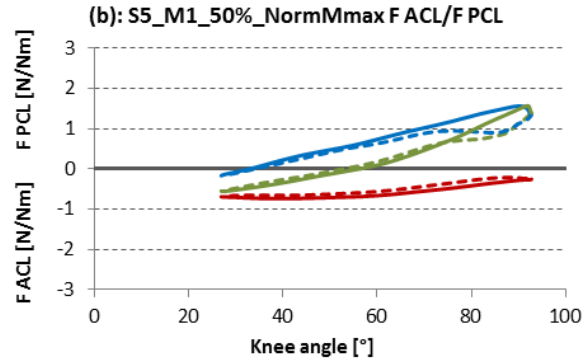
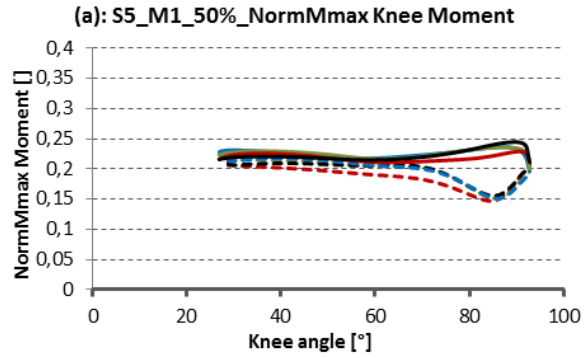


Fig.11.1.8: M1_75%

— OSIM — Mod1_Herzog — Mod1_Van Eijden — Mod2 - - - limit value

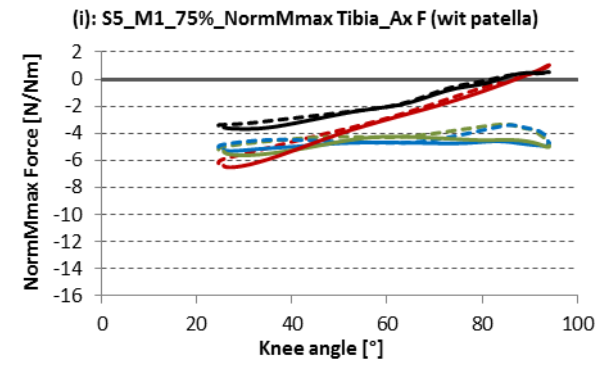
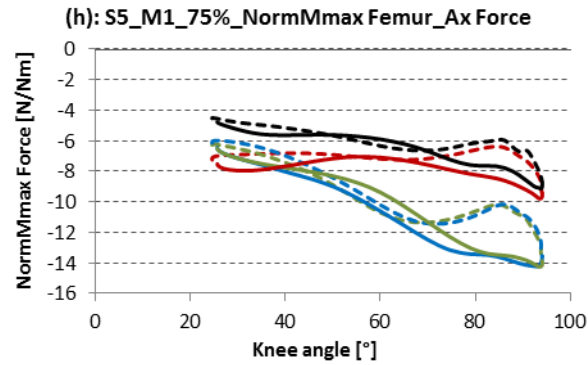
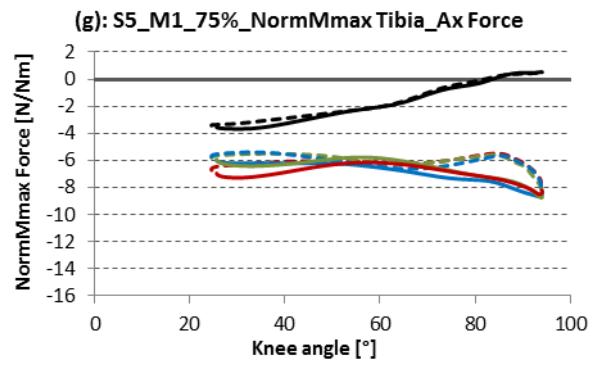
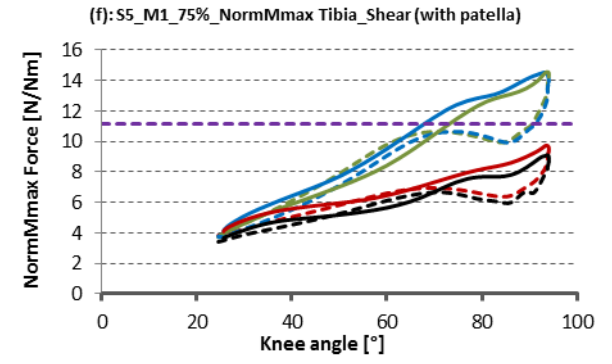
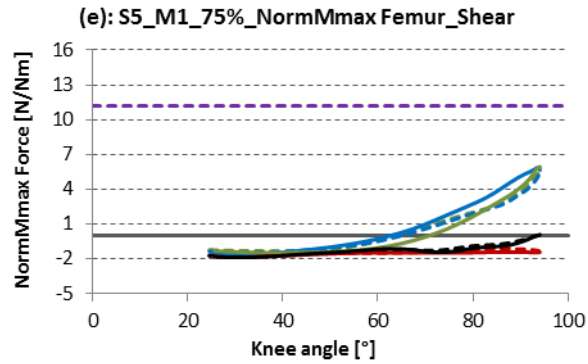
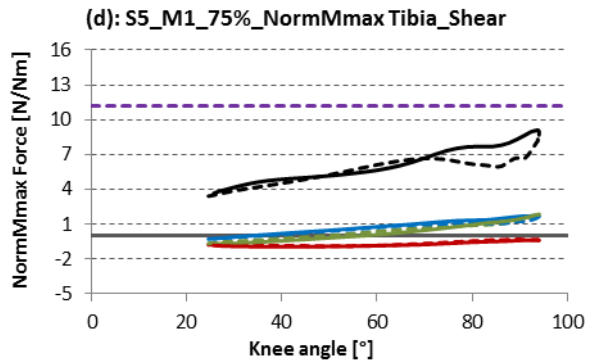
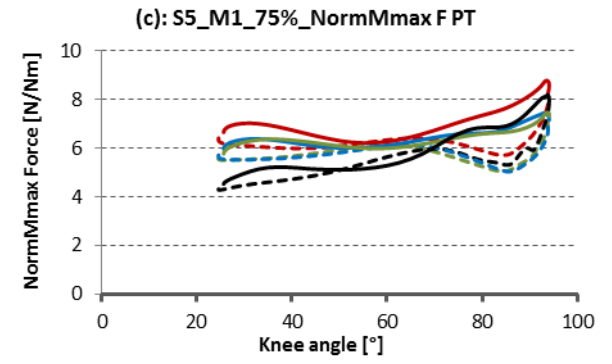
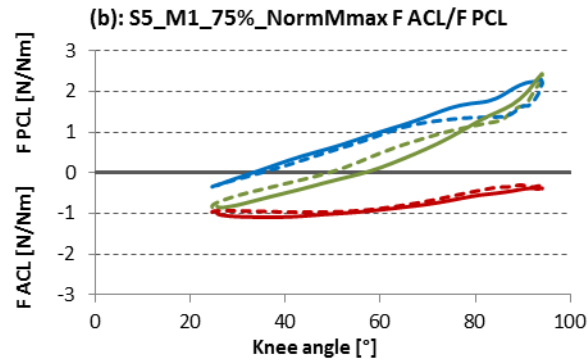
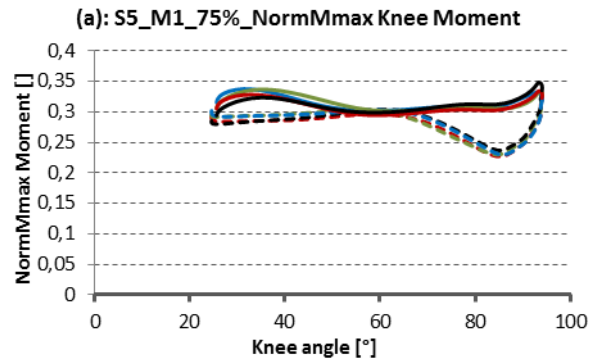


Fig.11.1.9: M1_100%

— OSIM — Mod1_Herzog — Mod1_Van Eijden — Mod2 - - - - - limit value

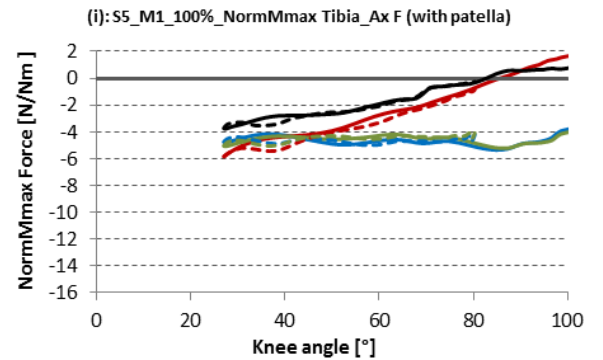
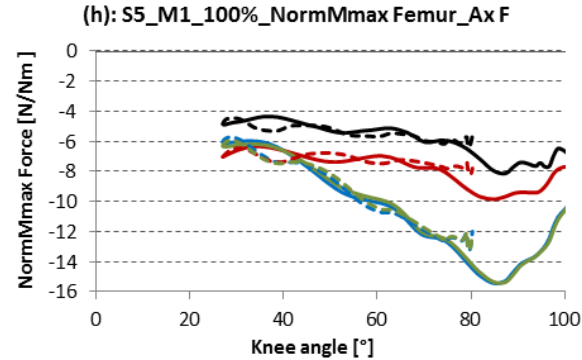
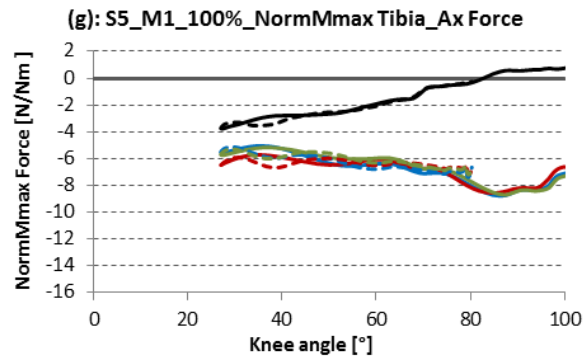
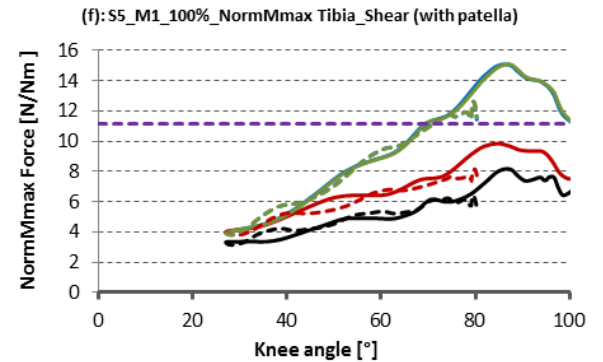
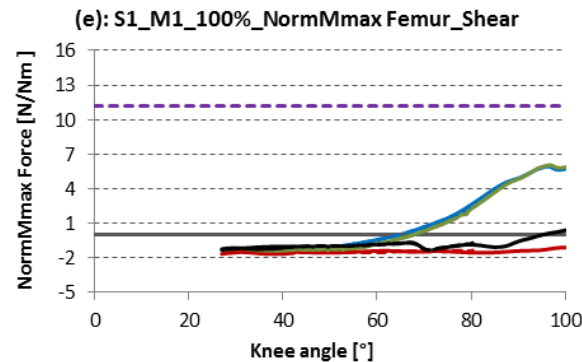
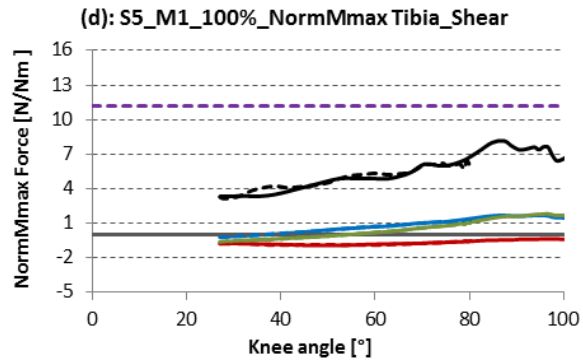
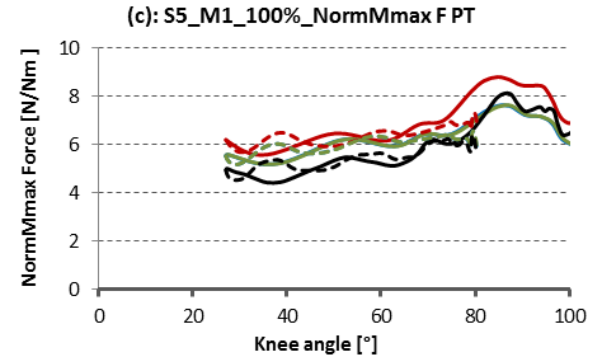
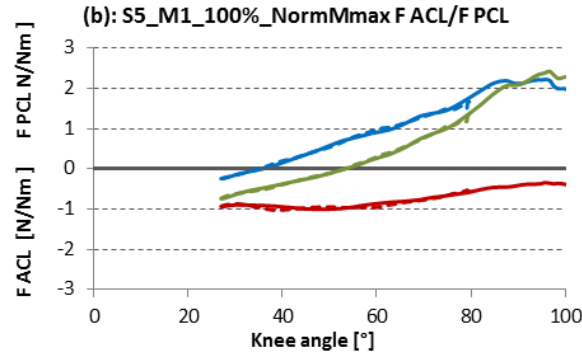
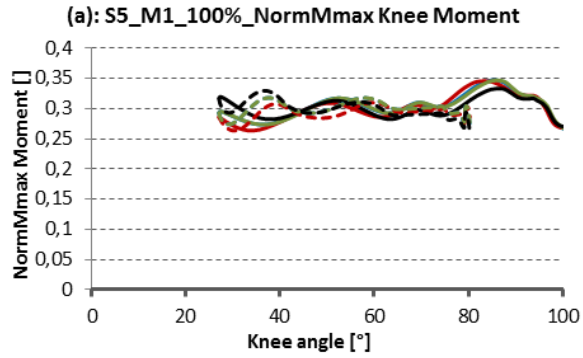
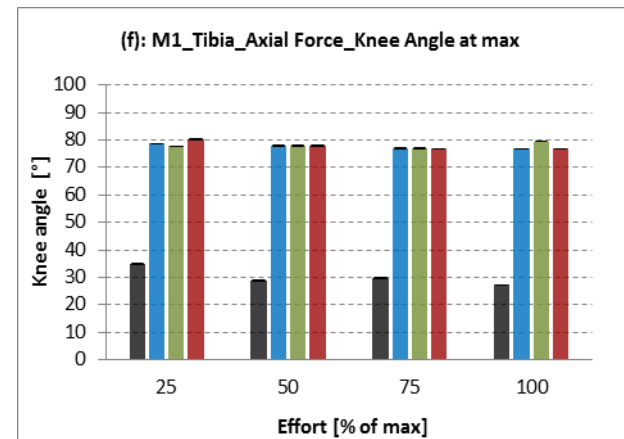
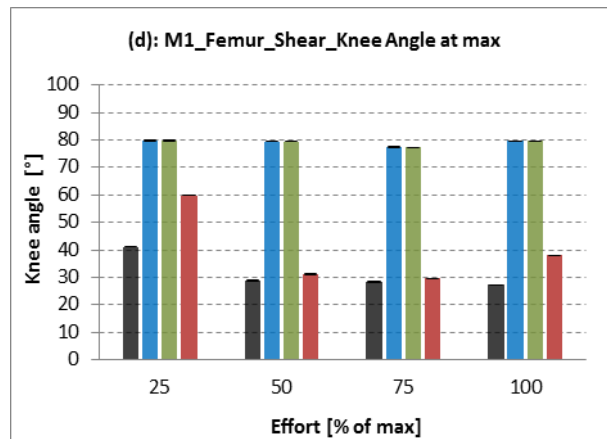
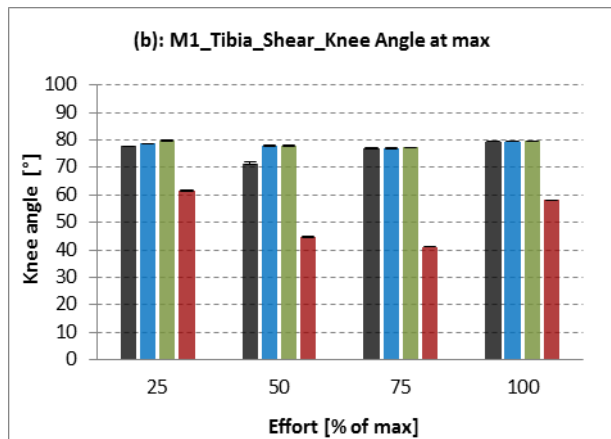
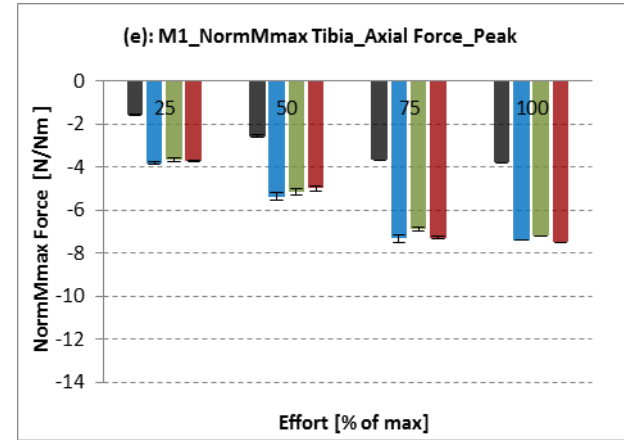
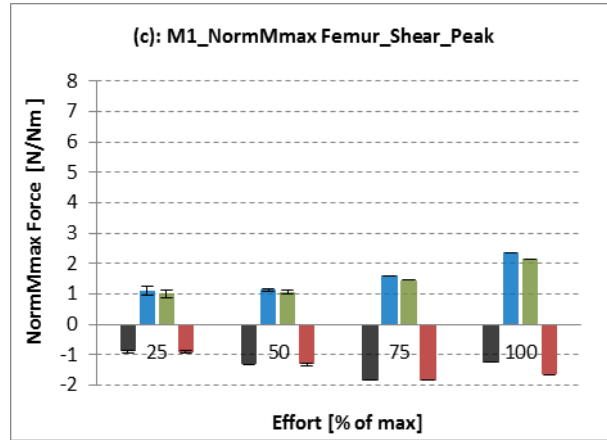
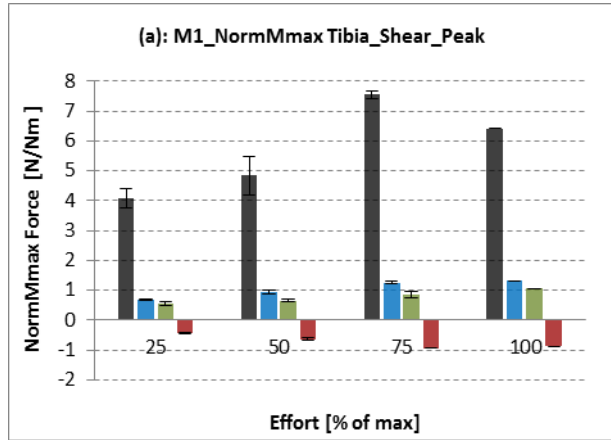
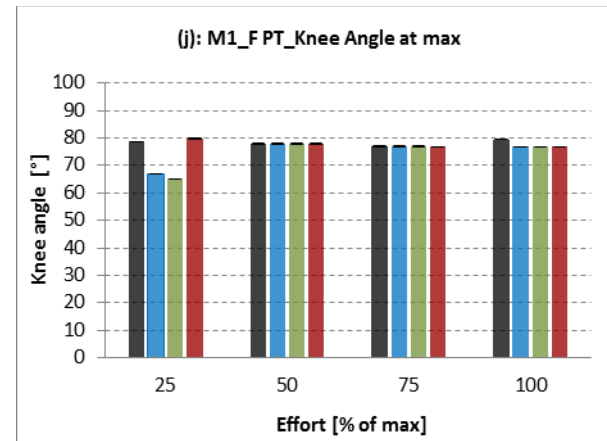
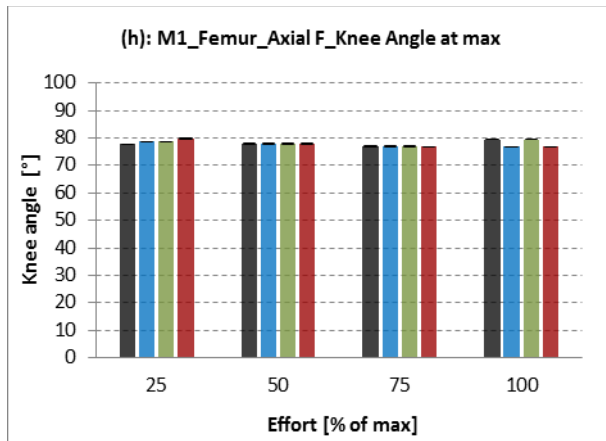
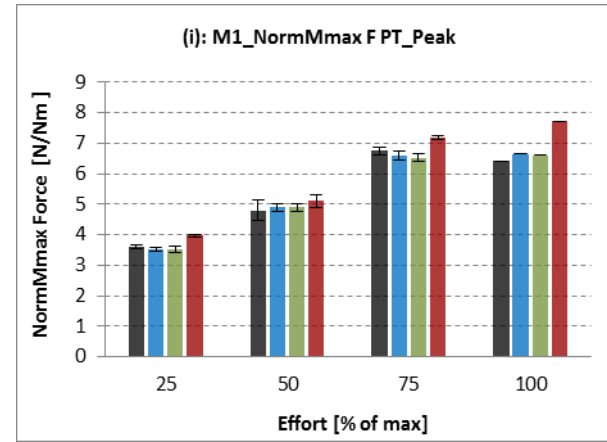
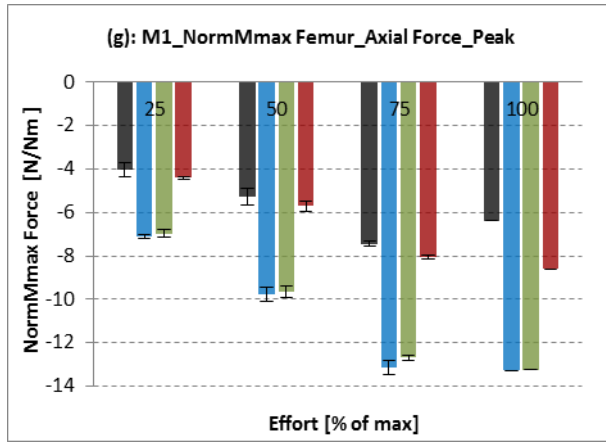


Fig.11.1.10: Peak values and knee angles at max of M1

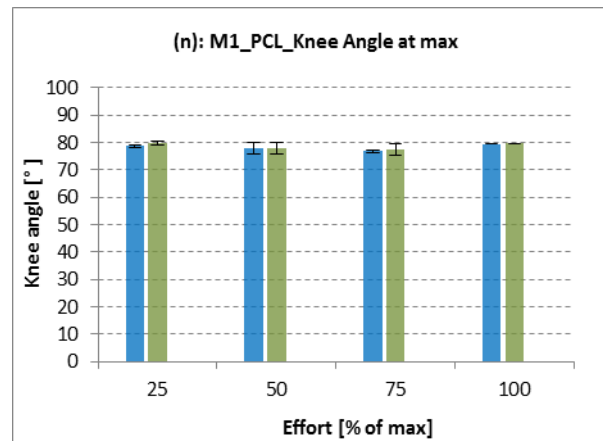
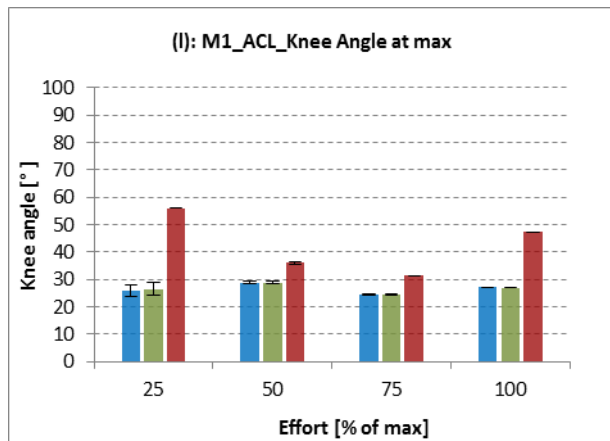
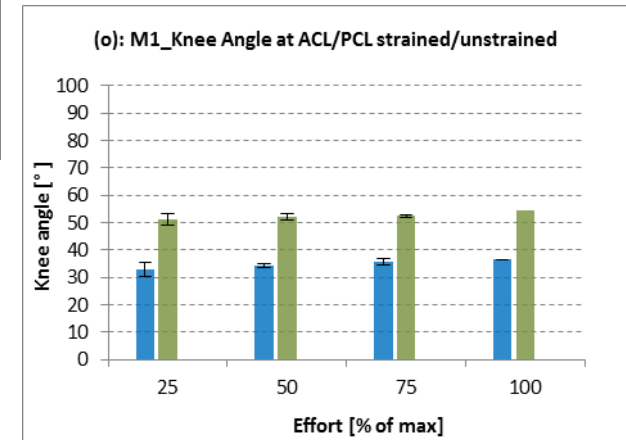
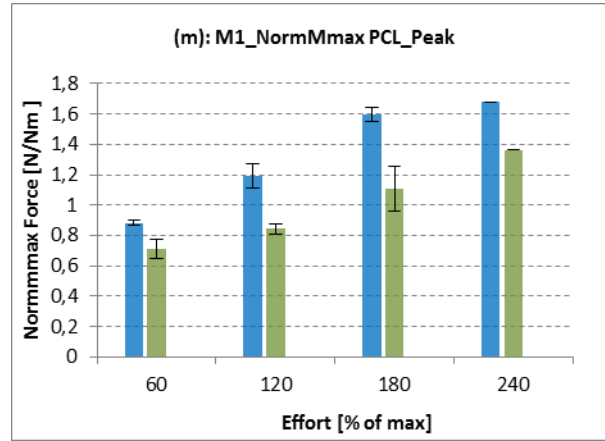
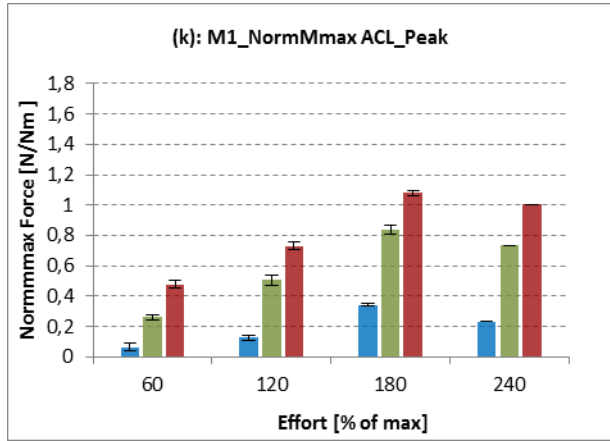
OSIM Mod1_Herzog Mod1_Van Eijden Mod2



OSIM
 Mod1_Herzog
 Mod1_Van Eijden
 Mod2



OSIM
 Mod1_Herzog
 Mod1_Van Eijden
 Mod2



11.2.Results of exercises performed at M2

Fig.11.2.1: Muscle activation of RF (a), VL (b) and VM (c) at M2 at 25%.

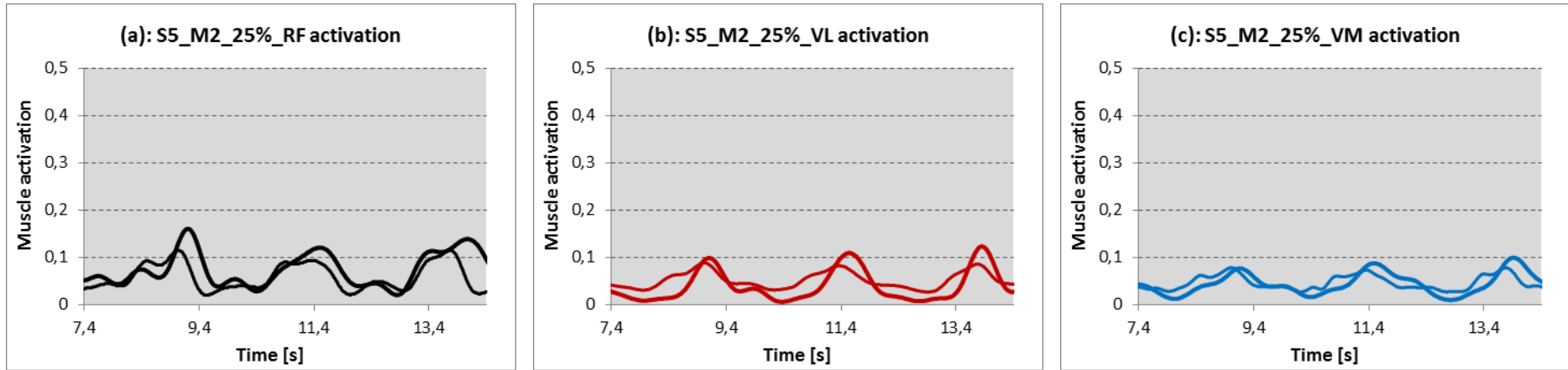
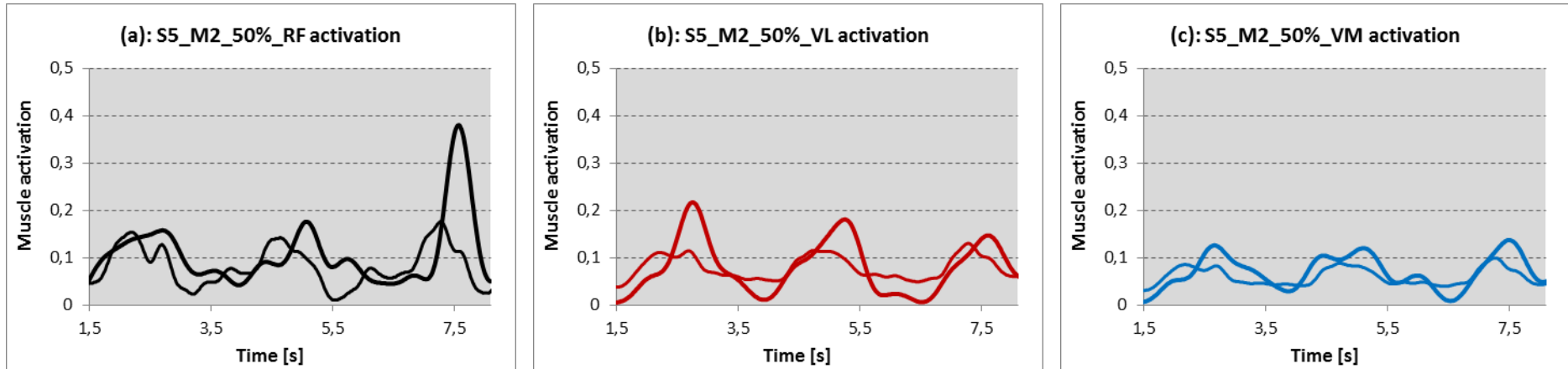


Fig.11.2.2: Muscle activation of RF (a), VL (b) and VM (c) at M2 at 50%.



— RF-EMG - - - RF-OSIM

— VL-EMG - - - VL-OSIM

— VM-EMG - - - VM-OSIM

Fig.11.2.3: Muscle activation of RF (a), VL (b) and VM (c) at M2 at 75%.

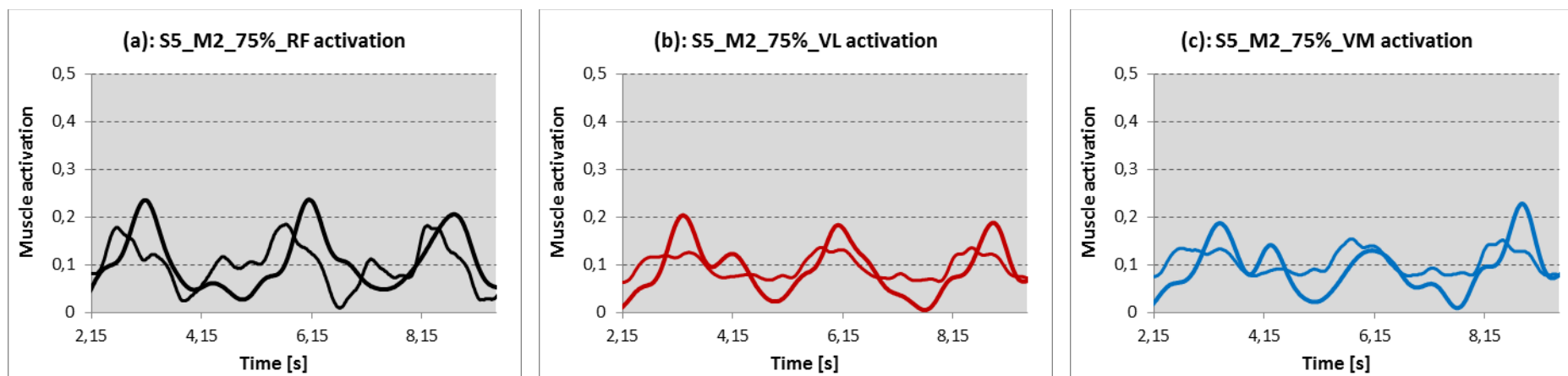
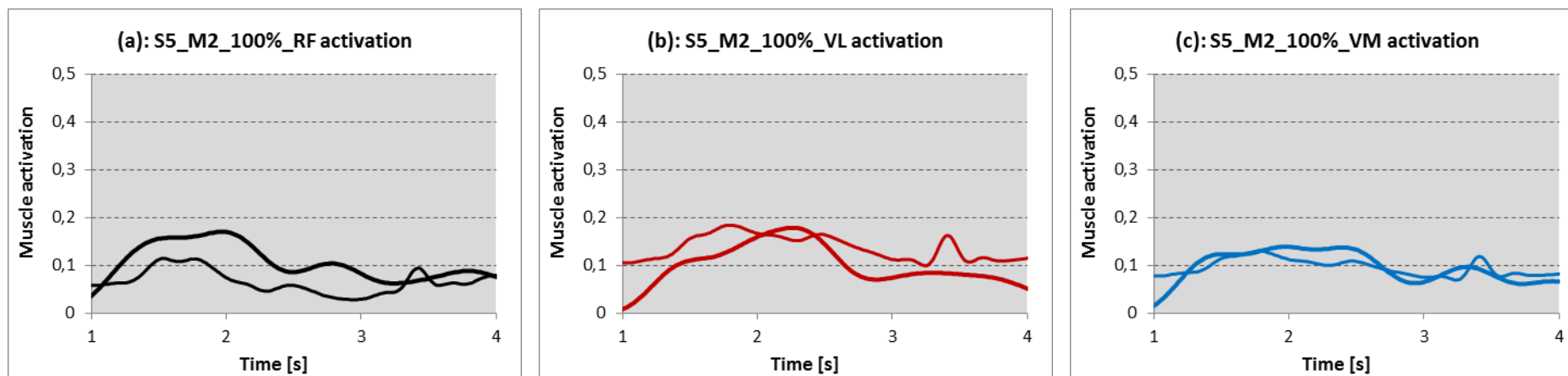


Fig.11.2.4: Muscle activation of RF (a), VL (b) and VM (c) at M2 at 100%.



— RF-EMG — RF-OSIM

— VL-EMG — VL-OSIM

— VM-EMG — VM-OSIM

Comparison of EMG signal and OpenSim muscle activation: quantitative results

	25%	50%	75%	100%
RF	23,07±5,40	25,14±25,88	19,18±6,86	32,94±0,00
VL	22,26±10,13	31,83±18,39	30,53±6,75	-3,37±0,00
VM	11,63±12,59	28,77±2,77	17,51±23,05	6,47±0,00

Tab.11.2.1: Peak error in [%] of RF, VL and VM at 25%, 50%, 75% and 100% at M2.

	25%	50%	75%	100%
RF	7,47±3,20	19,76±8,51	21,52±8,61	15,00±0,00
VL	3,84±2,74	12,34±8,99	6,59±12,10	16,10±0,00
VM	6,68±1,57	17,93±10,14	12,63±8,56	7,23±0,00

Tab.11.2.2: Time error in [%] of RF, VL and VM at 25%, 50%, 75% and 100% at M2.

	25%	50%	75%	100%
RF	18,01±10,36	22,97±12,14	2,26±21,45	38,43±0,00
VL	-41,66±16,72	-3,66±15,69	-16,55±16,30	-36,24±0,00
VM	-15,52±18,49	3,30±12,05	-23,96±21,71	2,18±0,00

Tab.11.2.3: Area error in [%] of RF, VL and VM at 25%, 50%, 75% and 100% at M2.

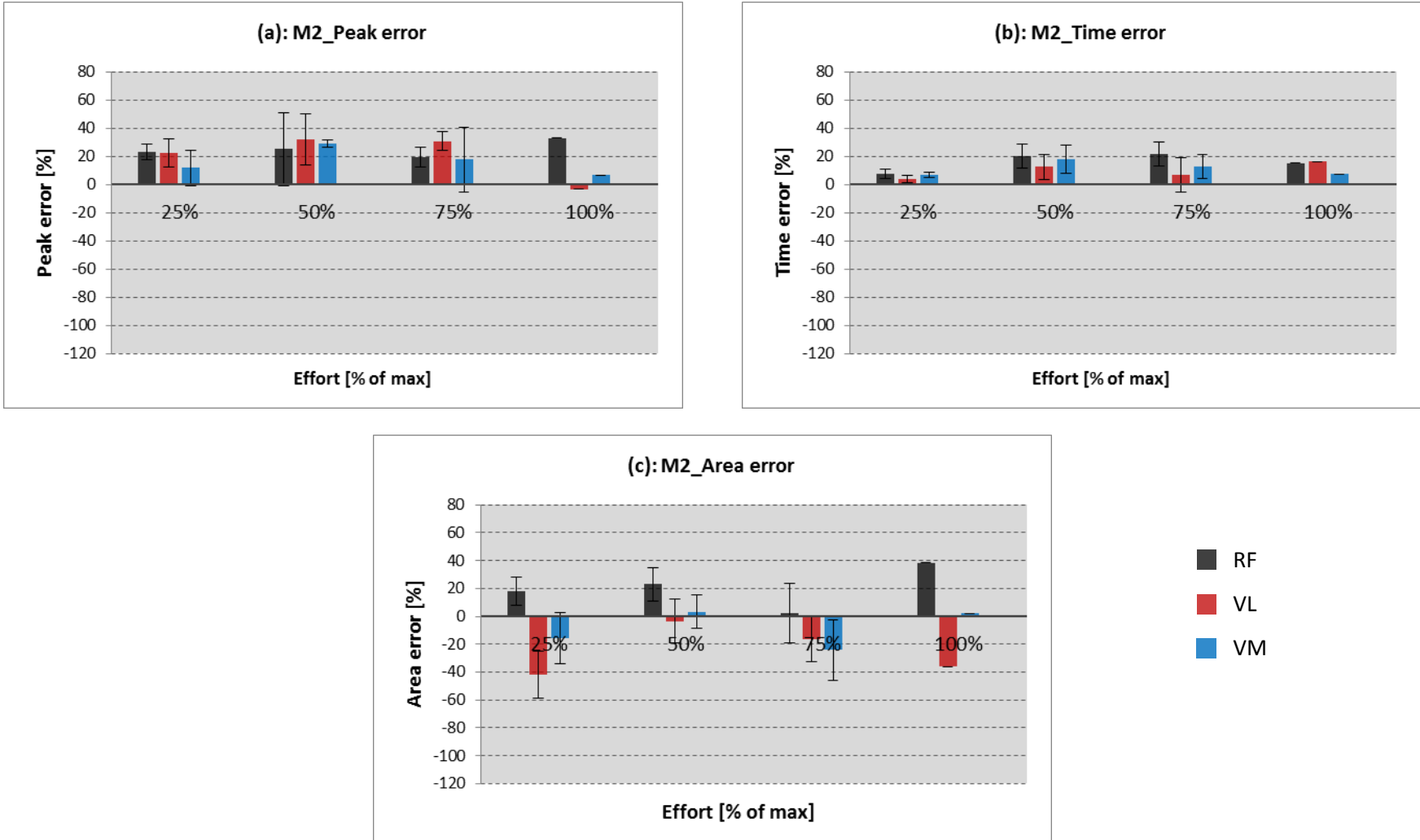


Fig.11.2.5: Quantitative results of muscle activation analysis for M2: (a): Peak error at different velocities; (b): Time error at different velocities; (c): Area error at different velocities.

Fig.11.2.6: M2_25%

— OSIM — Mod1_Herzog — Mod1_Van Eijden — Mod2 - - - - - limit value

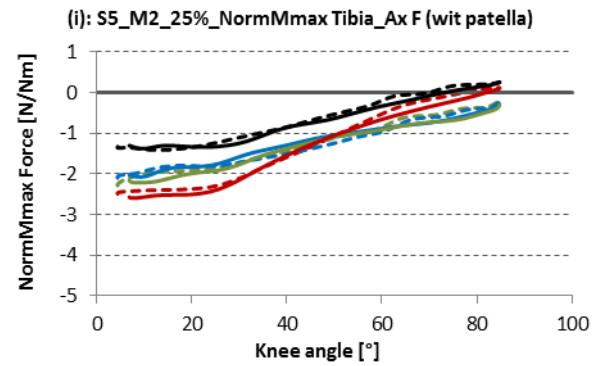
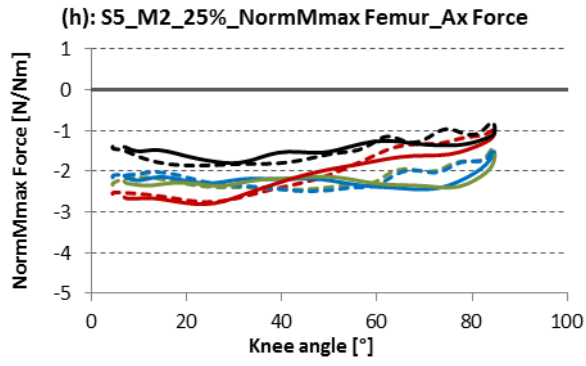
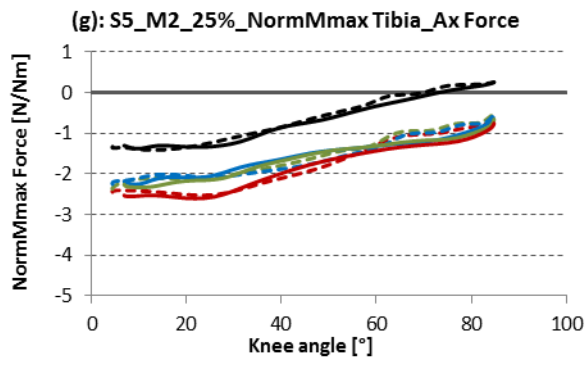
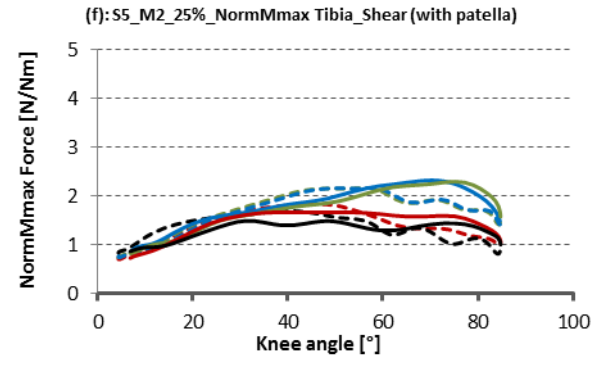
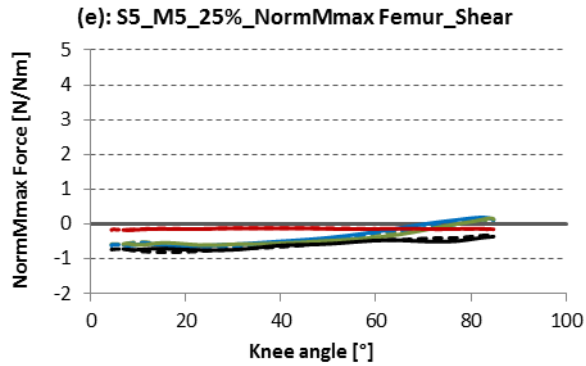
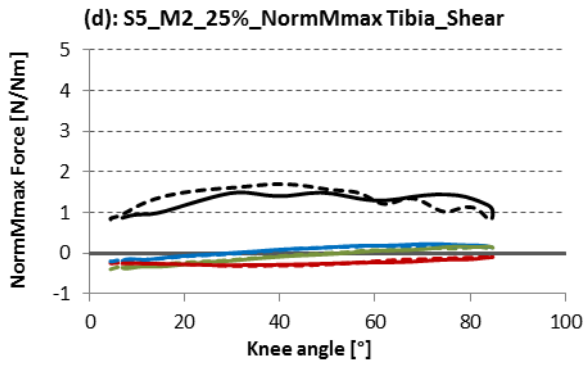
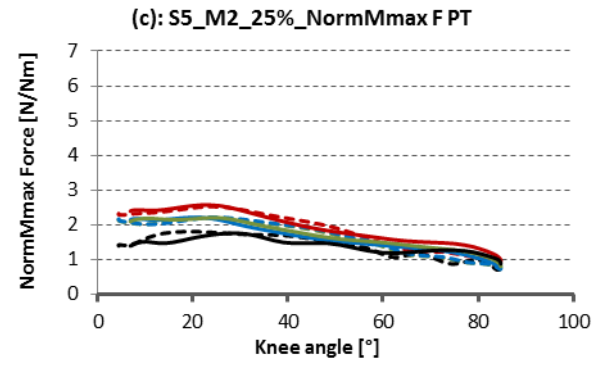
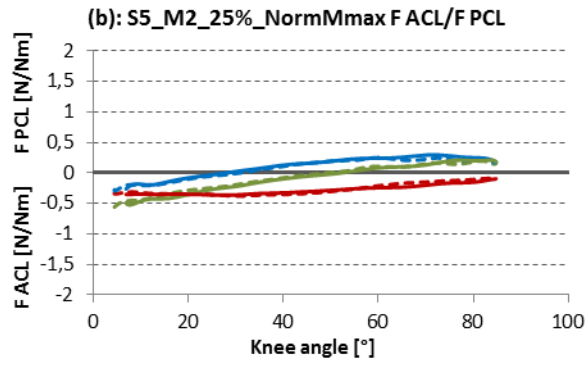
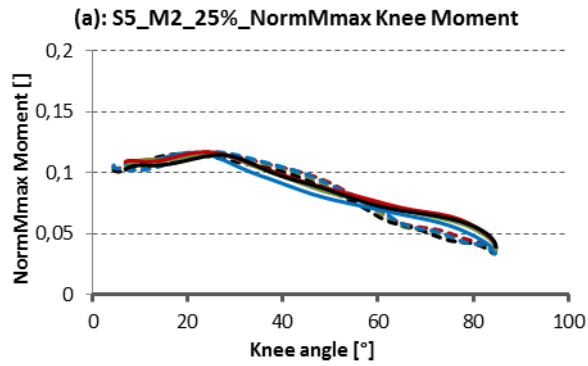


Fig.11.2.7: M2_50%

— OSIM — Mod1_Herzog — Mod1_Van Eijden — Mod2 - - - - - limit value

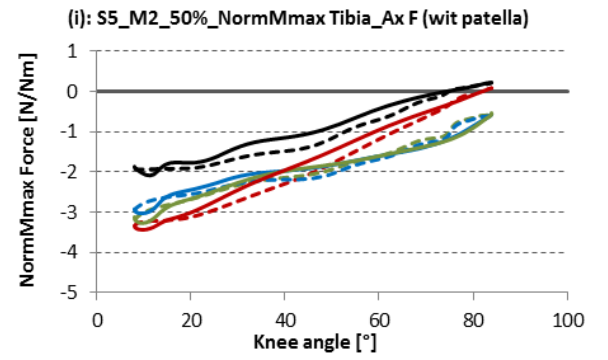
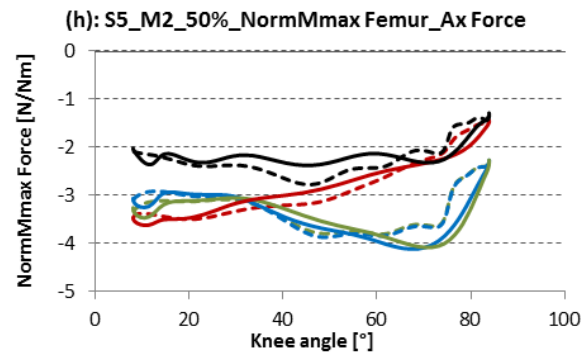
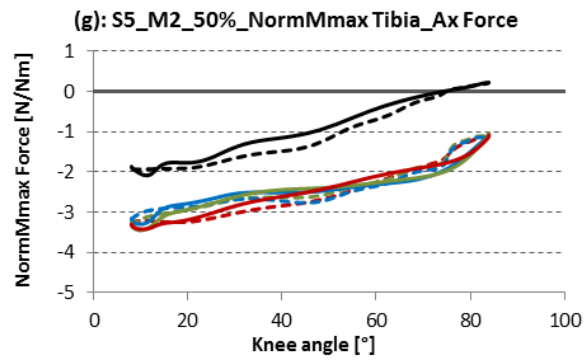
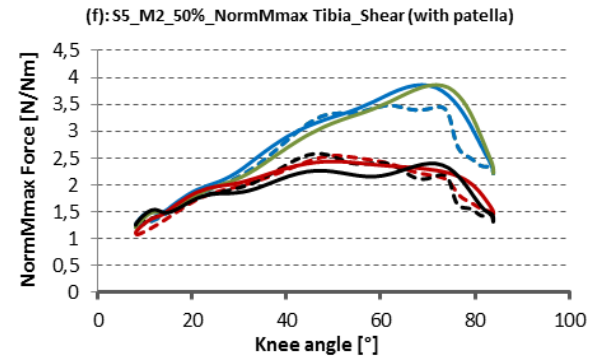
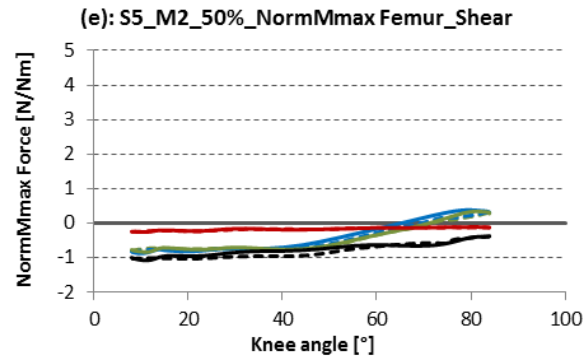
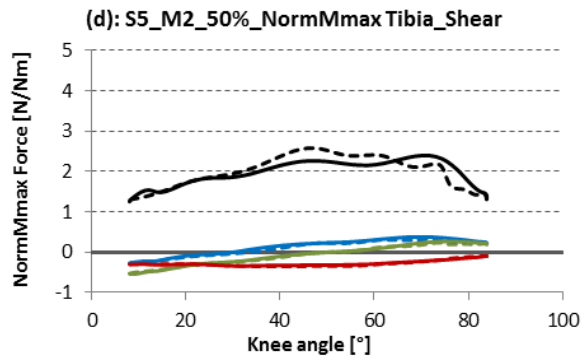
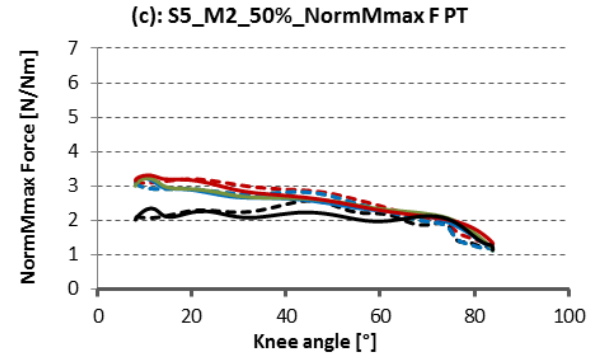
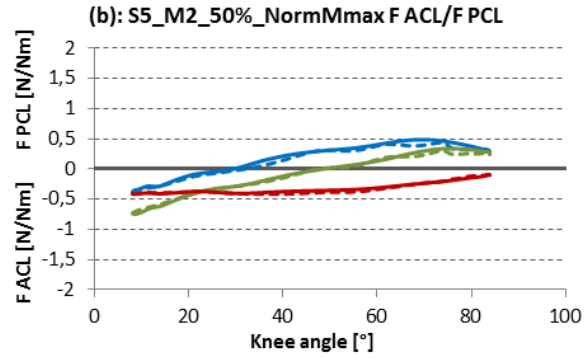
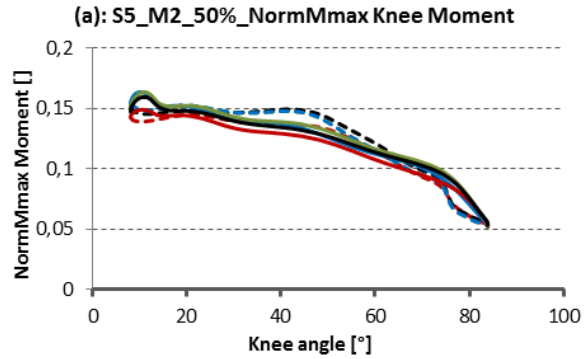


Fig.11.2.8: M2_75%

— OSIM — Mod1_Herzog — Mod1_Van Eijden — Mod2 ••• limit value

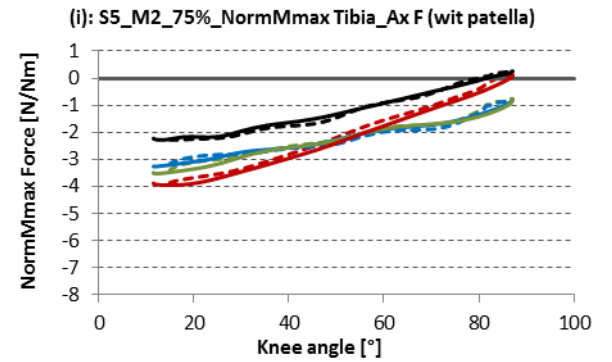
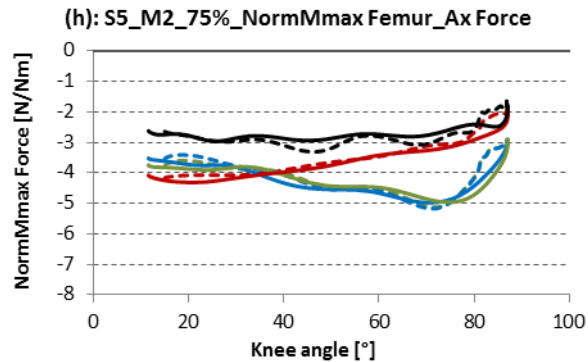
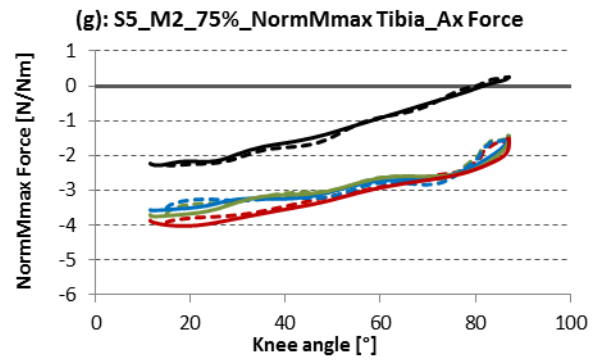
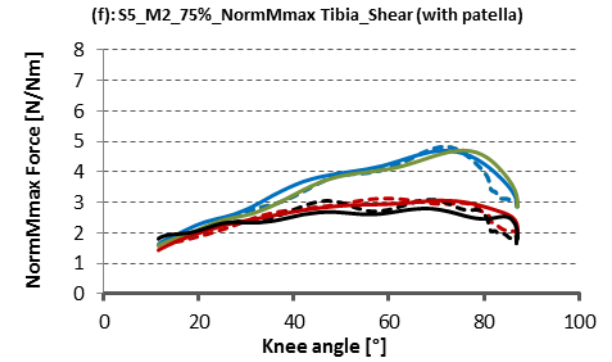
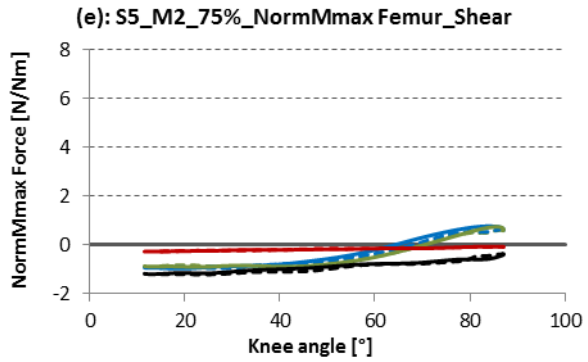
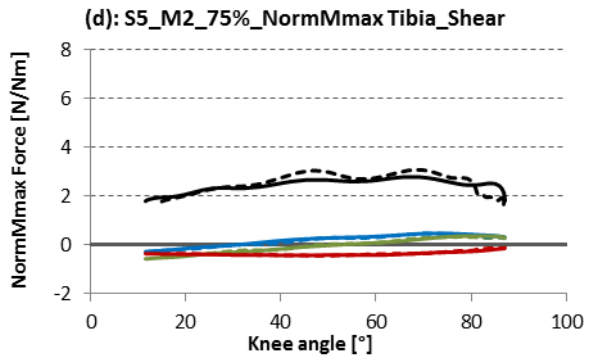
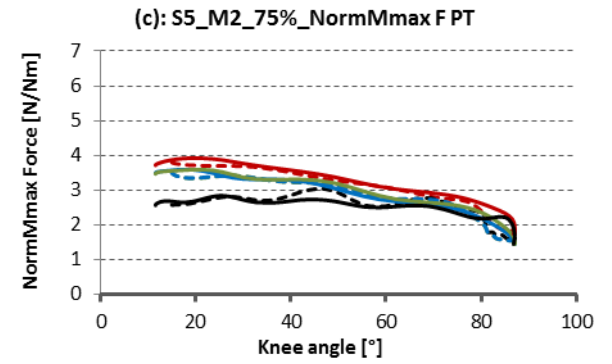
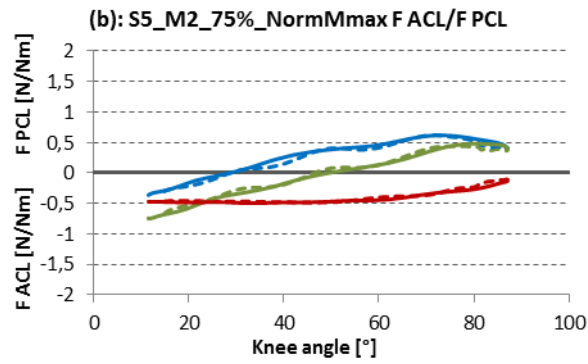
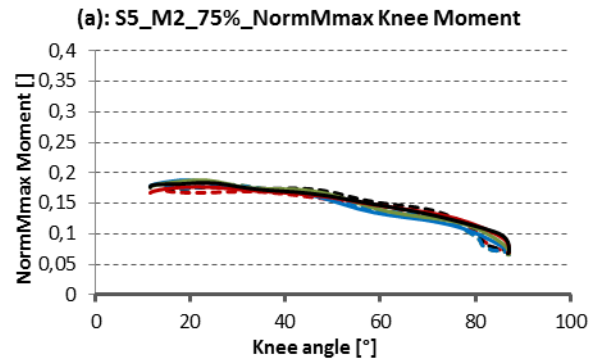


Fig.11.2.9: M2_100%

— OSIM — Mod1_Herzog — Mod1_Van Eijden — Mod2 ···· limit value

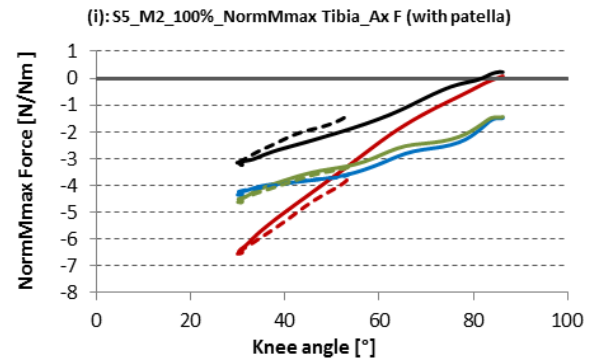
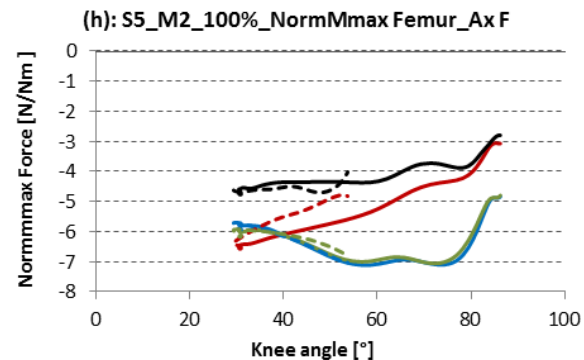
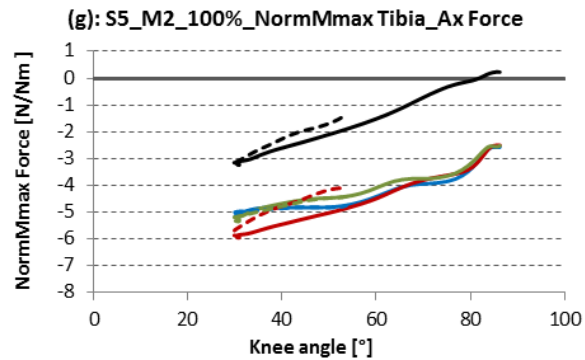
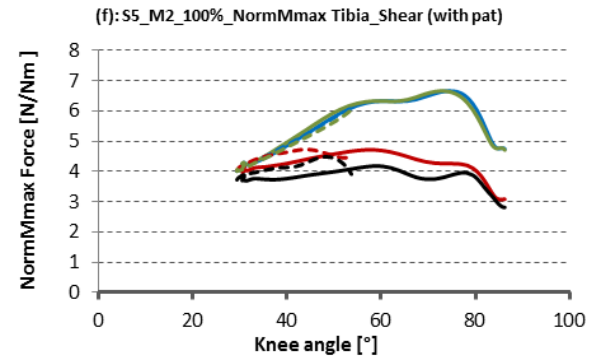
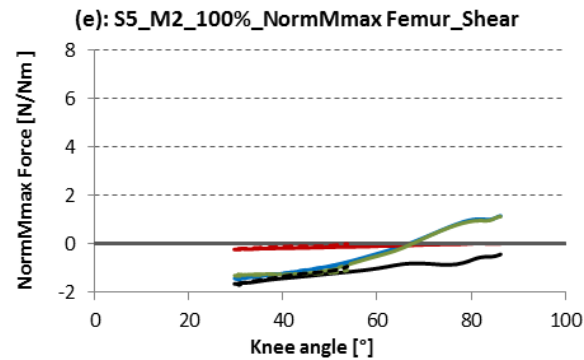
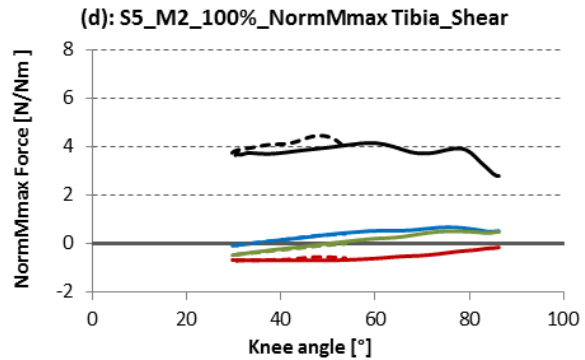
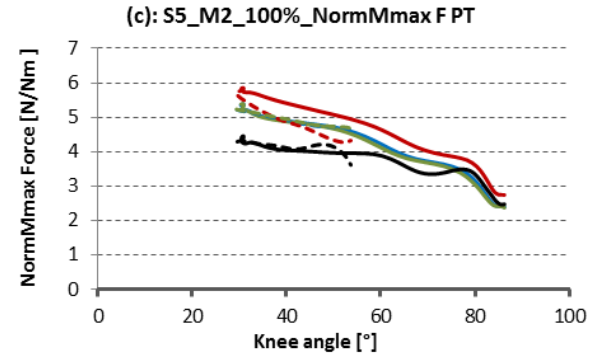
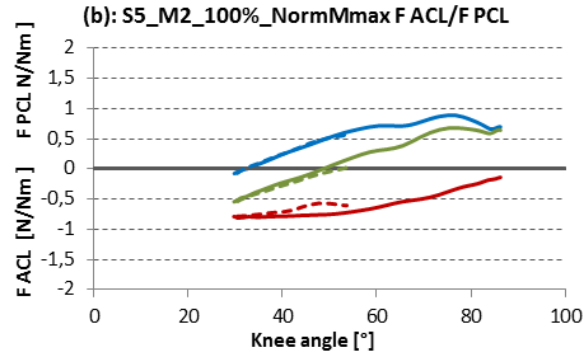
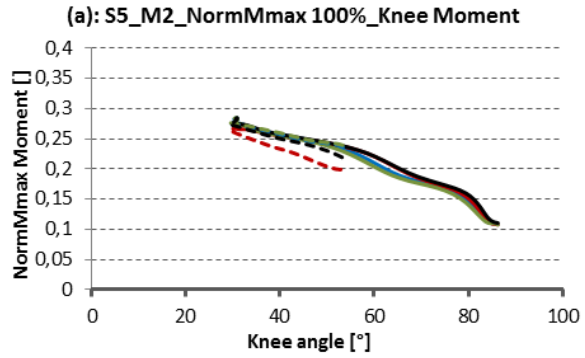
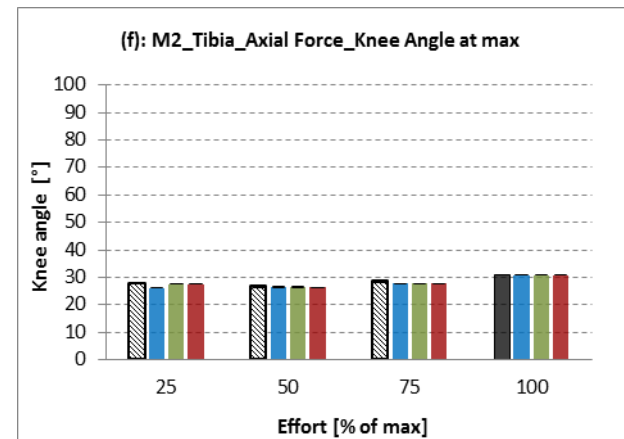
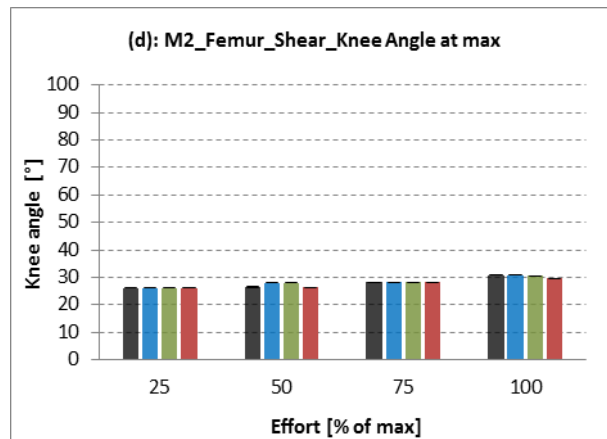
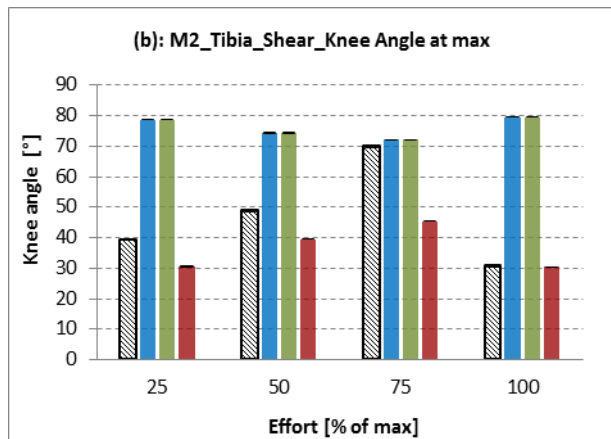
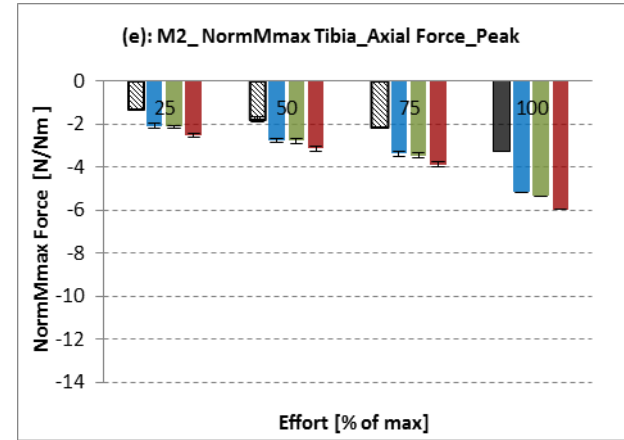
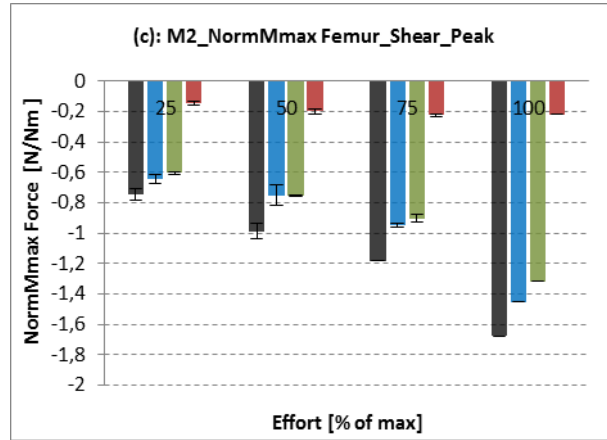
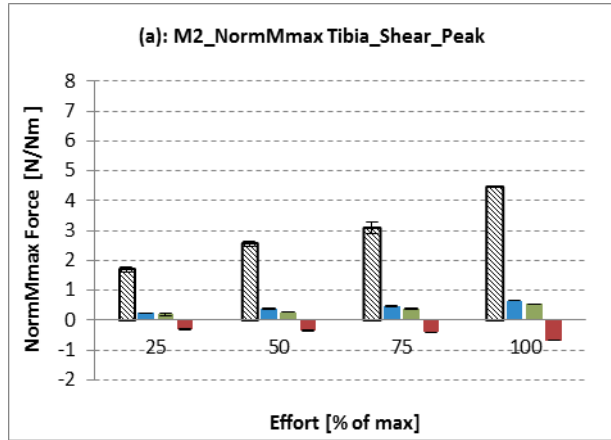
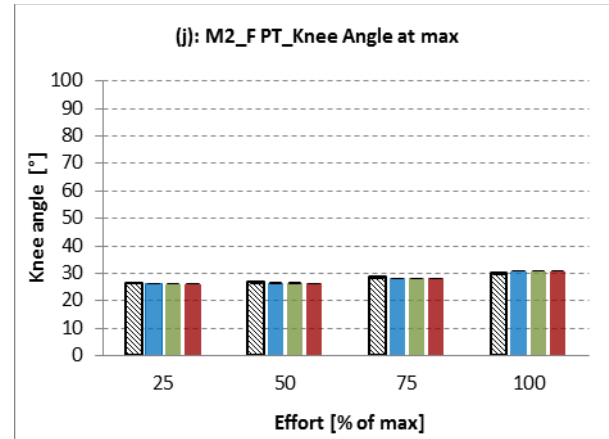
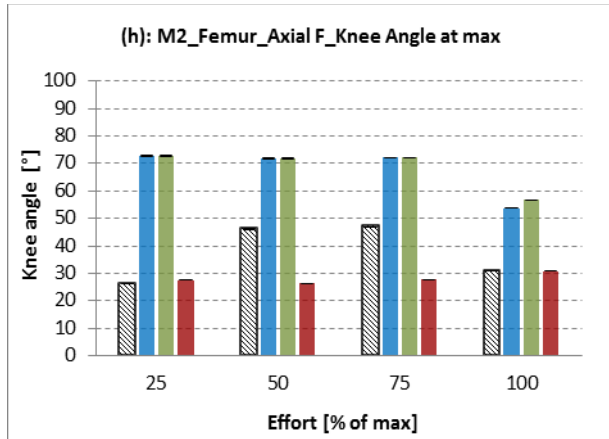
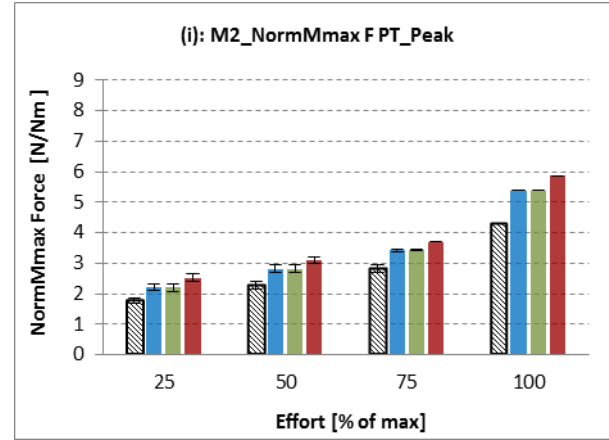
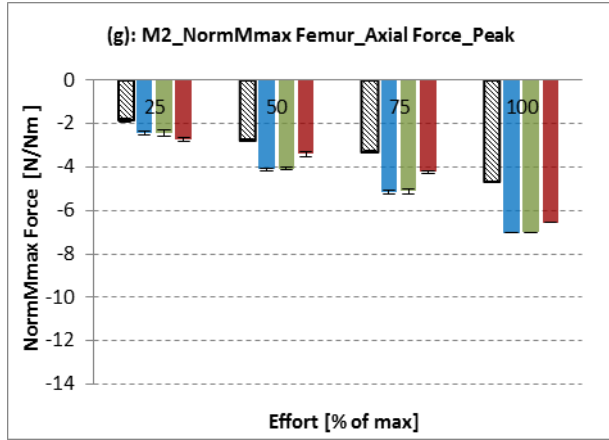


Fig.11.2.10: Peak values and knee angles at max of M2

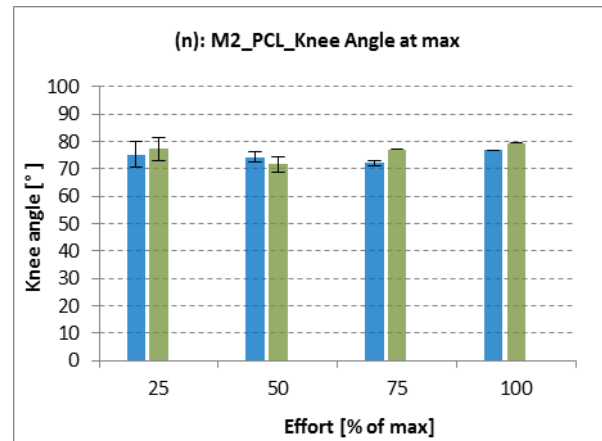
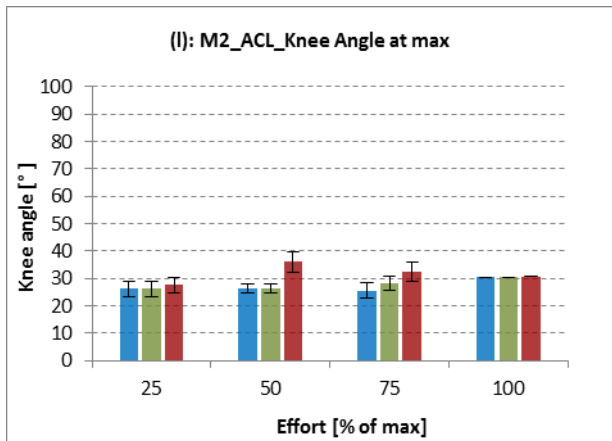
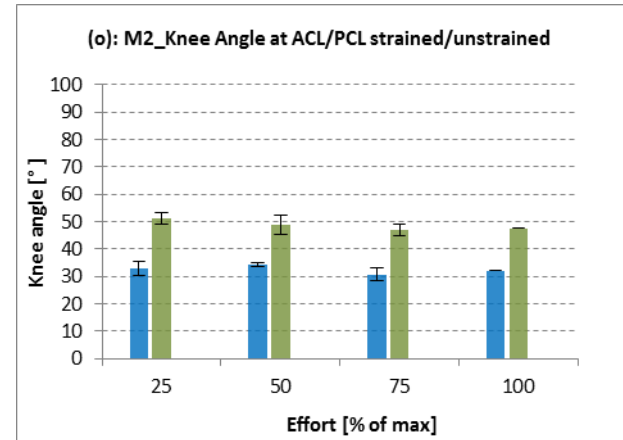
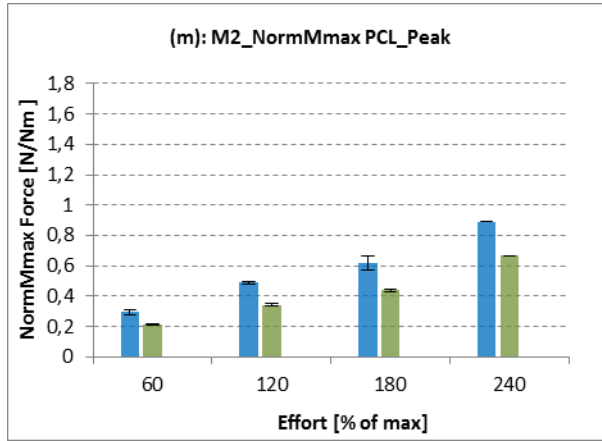
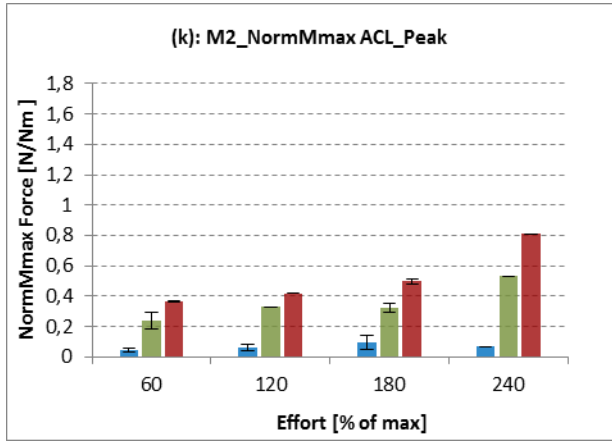
OSIM Mod1_Herzog Mod1_Van Eijden Mod2 OSIM-eccentric



OSIM
 Mod1_Herzog
 Mod1_Van Eijden
 Mod2
 OSIM-eccentric



OSIM
 Mod1_Herzog
 Mod1_Van Eijden
 Mod2



11.3. Discussion of results of Part 2

Comparison of EMG signal and OpenSim muscle activation

By comparing fig.11.1.1., fig.11.1.2, fig.11.1.3, fig.11.1.4 and fig.11.2.1, fig.11.2.2, fig.11.2.3, fig.11.2.4 with fig.A.5.3, fig.A.5.4, fig.A.5.5 and fig.A.5.6 in Appendix it is possible to see that the maximum intensity of muscle activation of part 2, both for M1 and M2, is similar to the muscle activation of exercises performed at 240°/s (by comparing for simplicity the OpnSim results, the maximum activation of rectus femoris is $\approx 0,3$, for vastus lateralis $\approx 0,4$, for vastus medialis $\approx 0,3$ for M1; $\approx 0,15$, for vastus lateralis $\approx 0,2$, for vastus medialis $\approx 0,15$ for M2; $\approx 0,25$, for vastus lateralis $\approx 0,4$, for vastus medialis $\approx 0,25$ for isokinetic exercises at 240°/s). As in isokinetic conditions, the muscular activation of rectus femoris and vastus medialis are similar and the activation of vastus lateralis is instead higher than the previous ones, both for M1 and M2 and at every intensity. By comparing the muscle activation of exercises performed at M1 with those at M2, it appears that the activation is higher in the first condition than in the second one at each intensity (by considering the maximum values and the OpenSim signal for simplicity, the activation of rectus femoris and vastus medialis ranges between $\approx 0,15$ to $\approx 0,3$ and between $\approx 0,2$ to $\approx 0,4$ for vastus lateralis for M1, between $\approx 0,1$ to $\approx 0,15$ for rectus femoris and vastus medialis and between $\approx 0,15$ to $\approx 0,2$ for vastus lateralis for M2). This may be caused by the different type of conditions of application of the external load: in M1, the resistance to the movement is due to the cable, in M2 the external force is due to the weight of the discs. These findings will be explained better below in the comparison of analytical models and OpenSim simulations. However it is possible to identify a common trend both for M1 and M2: for each bench, the activation at 25% and 50% are similar, and so for the activation at 75% and 100%. This might be due to a different perception of the effort of the subject at different intensities: probably, the effort which was perceived beyond 50% was similar, and so from 50% to the maximum. About the shape of the muscle activation profiles, both experimental and numerical, it is more irregular and with more peaks at each intensity, for each muscle and both for M1 and M2 than the signal of exercises performed in isokinetic conditions. This is may be due to the different type of exercises performed in the two parts of the study: in this second part, extensors muscles work also during the flexion phase of the movement in an eccentric way, and this might lead to more peaks and irregularities than in the signal of first part. Although these peaks and irregularities, peak error and area error of results of part 2, both for M1 and M2, for each muscle and for each intensity except for maximum, are similar in terms of maximum values of peak errors and area errors in isokinetic exercises (fig.11.1.5, fig.11.2.5 and fig.A.5.7). About the exercises performed at maximum instead, the difference between EMG and OpenSim results is relevant and higher than in isokinetic exercises, in particular for exercises performed at M1: from fig.11.1.4 it appears that the activation obtained by OpenSim simulations has a peak, decreases in the middle of the range of motion and then it increases again, but the the EMG signal instead has only a peak in the middle of the range of

motion. This is probably related to the limit conditions at which the exercise was performed and perhaps in this conditions the load-cell revealed higher forces than the real ones exerted.

By analyzing deeper the peak error of exercises at M1, from fig.11.1.5.a it is possible to identify that the error tends to be positive, except for 100%; in particular the maximum error is associated to vastus medialis at 25% and 50% and it is positive (from tab.11.1.1, $14,83\pm 17,6\%$ and $22,57\pm 10,86\%$ respectively), to rectus femoris at 75% and 100% (from tab.11.1.1, $14\pm 5,19\%$ and $-50,98\%$ respectively). Moreover, the error related to vastus lateralis tends to be negative at each intensity. By considering the peak error of exercises performed at M2, first it is instead possible to see that the error is positive at every intensity and for every muscle, except for vastus lateralis at 100%. Furthermore, from fig.11.2.5.a the error related to rectus femoris and vastus lateralis tend to be higher than the other errors at every intensity (from tab.11.2.1, $23,07\pm 5,40\%$ and $32,94$ at 100% for rectus femoris at 25%; $31,83\pm 18,39\%$ and $30,53\pm 6,75\%$ for vastus lateralis at 50% and 75%). In the end, by comparing fig.11.1.5.a and fig.11.2.5.a, the peak error of exercises performed at M2 is higher at every intensity and for every muscle of those performed at M1.

Regarding the area error, by comparing 11.1.5.c, 11.2.5.c and fig.A.5.7.c it is possible to see that the errors in isokinetic conditions are always positive and higher than the errors of M1 and M2; moreover, the area errors of this second part are sometimes positive and sometimes negative. In particular, for M1 at 25% and 50% the maximum error is positive and associated to vastus medialis (from tab.11.1.3, $25,4\pm 10,26\%$ and $12,99\pm 7,70\%$ respectively); at 75% the maximum error is positive and related to rectus femoris (from tab.11.1.3, $5,26\pm 12,83\%$), at 100% is negative and associated to rectus femoris (from tab.11.1.3, $-35,37\%$); for M2 the maximum error is negative at 25% and 75% and related to vastus lateralis and medialis respectively (from tab.11.2.3, $-41,66\pm 16,72\%$ and $-23,96\pm 21,71\%$ respectively), positive at 50% and 100% and due to rectus femoris (from tab.11.2.3, $22,97\pm 12,14\%$ and $38,43\%$ respectively). Furthermore, as done for the peak error, by comparing fig.11.1.5.c and fig.11.2.5.c the area error of exercises performed at M2 is higher at every intensity and for every muscle of those performed at M1.

In the end, by considering the results expressed in fig.11.1.5.b it is possible to identify a trend similar to that obtained in isokinetic exercises: the time error at M1 is high at 25% and then it tends to decrease with the growth of the intensity (from tab.11.1.2, the maximum error is related to rectus femoris at 25%, $21,63\pm 12,64\%$). The same trend is not revealed in fig.11.2.5.b: the time error at M2 is higher at 50% and at 75% than at the other intensities (from tab.11.2.2, the maximum error is related to rectus femoris at 75%, $21,52\pm 8,61\%$). Furthermore, by comparing the time errors of this second part with the time errors of the first one, the errors are similar in terms of values.

Although the irregularities and peaks described above, the reliability of results is quite good and higher for peak error and area error than time error as in isokinetic exercises, both for M1 and M2.

Comparison of analytical and OpenSim models

By comparing the exercises performed at M1 with those at M2, the most important difference is that in the first ones the knee moment tends to increase with the growth of the knee angle, in the second ones it tends instead to decrease. This is due to the different way in which the external force is applied. The different trend of the moment, leads to peak values of the other biomechanical parameters investigated in different parts of the range of motion. For this reason only the most important differences are analyzed in this paragraph.

The profile of the biomechanical parameter obtained in this second part, both for M1 and M2, confirms the results obtained in the first one. The results of analytical models and OpenSim model are quite coincident for the knee moment but the difference tends to increase for the force at the patellar tendon. About the shear on tibia, it is always negative in the second model, negative at end of the extension phase and positive at the beginning in the first model (with a different profile for the two sub-models), positive and higher than the others for the OpenSim model. This difference decreases by considering the reaction forces at femur. The same thing happens for the axial load on tibia. Also the profile of shear and axial load on femur are similar to those obtained in isokinetic conditions. The shear calculated with the second model tends to be very low, the shear calculated by the software tends to be negative in all range of motion, the shear obtained by the first model is negative and close to that calculated by the software at the beginning of the movement and positive in the other part of the range. The axial load on femur is instead negative for all models, but the profile of the second model is close to the OpenSim one with a peak at the end of the extension phase; the profile of the first model tends to have instead a peak at the beginning of the movement. Relevant differences between the two sub-models of the first model appear only for the shear on tibia, which lead to the same different profiles of the tension at the cruciate ligaments obtained in isokinetic exercises.

By analyzing widely the results of exercises performed at M2, fig.11.2.6, fig.11.2.7, fig.11.2.8, fig.11.2.9 and fig.11.2.10 show that although the maximum of the knee moment is reached in the concentric phase, the maximum of the force at the patellar tendon, shear and axial load on tibia and axial load on femur evaluated by OpenSim, occur in the eccentric phase; for the shear on femur instead the maximum is reached in the concentric phase. Being only one subject tested, a deeper study will might be done in order to find an answer to this particular behaviour.

By considering fig.11.1.10, fig.11.2.10 and fig.A.7.16 similar trends can be found. In fact, for the isokinetic results for a better comparison the results of the maximum values and the angles at which the maximum is reached should be calculated by considering only subject 5; however, because of the normalization to the maximum, the results are similar by considering all subjects. The maximum force at the patellar tendon evaluated by the first model is lower than that obtained by the second one, but it is higher than that calculated by the software at every intensity. About the angle at which the maximum is reached, it has a similar values at every intensity for all models: for exercises performed at M1 it is about 80°, for exercises performed at M2 it is about 30°. This suggests that the exercises were performed with a good repeatability at every intensity. About the shear on tibia, as in isokinetic conditions, the maximum evaluated by the first model is reached when the shear is positive. About the angle at which the maximum is reached, as in the first part of the study the results obtained by the first model are higher than those obtained by the second one (the results obtained by OpenSim are not taken into account for the reasons described in par.8.3) and similar at every intensity. Moreover, the values obtained for exercises performed at M1 and M2 are similar (fig.11.1.10.b and fig.11.2.10.b) although the peak of the force at the patellar tendon occurs at different angles as described above. However, these findings agree with the results obtained in the first part of the study, because also in isokinetic conditions the angles were different. Regarding the shear on femur, by comparing the results in fig.11.1.10.c, fig.11.2.10.c and A.7.16.c it appears that the results obtained for M1 are similar to those obtained in isokinetic conditions; the shear of femur of the second model are instead negative for all models and very high (in absolute terms). Furthermore, these differences are emphasized by considering the angle at which the maximum shear on femur is reached (fig.11.1.10.d, fig.11.2.10.d and 8.7.16.d: the angle evaluated for M1 has the same trend identify in isokinetic conditions, with similar results of the first model at every intensity and higher than other results (moreover, by considering the results of the first model, the angle is about 80° for M1, about 85° in isokinetic conditions); for M2 instead, the angle is about 28° at every intensity and for all models. Concerning the maximum axial load on tibia and femur, the same trend which was identify in the first part of the study can be identified. Differences occur instead by considering the angles. The angle at which the maximum axial load on tibia is reached is quite constant, with a mean value of about 27°, for M2 at every intensity for all models (fig.11.2.10.f), it is quite constant also for M1 (except for OpenSim) with a mean value of about 79° (fig.11.1.10.f), it depends on velocity and models for isokinetic exercises (fig.A.7.16.f). A similar trend can be identified for the angle related to the axial load on femur: for M2 it is quite constant with a mean value of about 68° for the first model (fig.11.2.10.h), for M1 it is quite constant for all models with a mean value of about 78° (fig.11.1.10.h), in isokinetic exercises it is quite constant for the first model with a mean value of 65° (fig.8.7.16.h).

From these results it appears that the exercises performed in isokinetic and conditions and those performed at M1 are similar; this is related to the fact that the external force applied by the cable in the fitness machine leads to similar effects than those in isokinetic exercises, in particular the different line of action of the cable allows to have a force on tibia which acts in a similar way to that in isokinetic machine. In the end, the evaluation of the tension at the cruciate ligaments. Because of the results obtained by the second model are not in agreement with those in the literature as described in par.8.3, they are not taken into account in this analysis. Fig.11.1.10.k and fig.11.2.10.k confirm that the maximum tension at ACL calculated by the Van Eijden's approach is higher than that obtained by the Herzog's one. The trend obtained for PCL in isokinetic conditions is confirmed too: fig.11.1.10.m and fig.11.2.10.m show that the maximum tension at PCL calculated by the Herzog's approach is higher than that obtained by the Van Eijden's one. Also the fact that the angle at which the maximum is reached and the angle at which the ACL becomes unstrained are not influenced by external forces is confirmed. About the angle related to the maximum tension at ACL, it occurs at $26,64 \pm 2,14^\circ$ in Herzog's approach and at $26,6 \pm 2,27^\circ$ in Van Eijden's approach for M1, at $27,13 \pm 2,83^\circ$ in the first formulation and at $27,78 \pm 2,83^\circ$ in the second one for M2; regarding the angle related to the maximum tension at PCL, it occurs at $78,26 \pm 2,26^\circ$ in the first approach and at $78,71 \pm 2,26^\circ$ in the second one for M1, at $74,63 \pm 4,63^\circ$ in the first one and at $76,39 \pm 4,09^\circ$ in the second one; concerning the angle at which the ACL becomes unstrained, it is reached at $34,84 \pm 2,57^\circ$ in the first approach and at $52,59 \pm 2,16^\circ$ in the second one for M1, at $32,47 \pm 2,51^\circ$ in the first one and at $48,61 \pm 3,53^\circ$ in the second one for M2.

The previous results were obtained by comparing the concentric and eccentric phase of the movement. The maximum values were obtained in concentric phase for all biomechanics parameters investigated, except for the results obtained by the OpenSim simulations for M2, and so for the angles. (However the difference between maximum values in concentric and eccentric was most often very small). About the angle at which the ACL becomes unstrained, no relevant differences between eccentric and concentric phase were found. That's because the force exerted in two phases is similar. This finding is different from those obtained in the literature by Beynon et al. (Beynon et al. 1997, [4]; Beynon et al. 1998, [2]; par.3.6). From that study, it appears that the angle is different in two phases, but this is related to the fact the exercise which was investigated was a flexion-extension movement without any external resistance, and so the only external force was related to the weight of tibia. Without considering external forces, also inertial effects becomes relevant.

12. Conclusion

Aim of the study was to investigate some biomechanical parameters during exercises of knee flexion-extension performed with isokinetic and fitness machines in order to predict possible injuries caused by a wrong execution of the movement and to suggest possible solutions to avoid this problem.

In isokinetic conditions, a first evaluation of the right execution of the movement was done by using the ratio between the torque in flexion and the torque in extension, a parameter which is related to the risk of injuries. Results show that the ratio is quite constant with a value of about 0,6 from full extension to about 60° knee angle and then it tends to increase at every velocity investigated. Optimal condition should be a ratio with a constant value in all range of motion and close to 1; for this reason subjects who were tested should be trained more in flexion.

A more detailed analysis of muscular and articular loads was done by using analytical and numerical models. The numerical results, which were obtained by simulations with the software OpenSim, were first compared with electromyographic signal recorded in-vivo during the exercises. The average results obtained express that the error between electromyographic and numerical muscle activation is higher by considering the peak values and the area below the signal than the error related to the time at which the peaks occur for every velocity and muscle investigated. Moreover, the experimental activation tends to be higher in terms of peak values than that calculated by the software and the difference between the two results constant at every velocity for rectus femoris and vastus medialis, but more variability has been shown by vastus lateralis and biceps femoris; also the area of the electromyographic signal tends to be higher than that obtained by the software, with an increase of the difference with the growth of the velocity for every muscle; the error associated to the instant at which the maximum occurs tends to decrease with the growth of velocity, except for biceps femoris. These findings suggest that the reliability of numerical results is high in terms of instant at which the peak values are reached, but it is not enough good in terms of peak values and area below the signal and this emphasized with the growth of the velocity. A possible solution in order to improve the results should be to collect also the forces at the device which was used to fix the knee, for example by using strain gauges, in order to have a better evaluation of the forces acting during the movement.

After that, the results obtained by OpenSim, were compared with those deriving from analytical models. It has been possible to identify a common trend for every velocity. The coincidence of the knee moment, both in extension and in flexion, calculated by the models, suggests that the anthropometric schematization utilized is equivalent. The different moment-arm of muscles leads instead to relevant differences between analytical and numerical results; in particular the activation evaluated by the first

model tends to be higher than that obtained by the other ones both in extension and in flexion. Furthermore, the different line of action of muscles leads to relevant differences in terms of shear and axial load on tibia and femur. This difference is higher in extension than in flexion. In extension, the results obtained were compared with those in the literature and it appears that the force evaluated by the software and by the second model are not correct in terms of shear acting on tibia, and consequently the tension at the cruciate ligaments is not correct either. As it happens for the shear on tibia, also the axial load on tibia evaluated by the software is not correct, although the error is less than that related to the shear. The difference instead increases again by considering shear and axial load on femur, because of the different lever-arm of the tendon of the quadriceps. Moreover, the results obtained reveals that the software doesn't consider the different moment-arm of tendon of quadriceps and patellar tendon. From these findings, it appears that the results obtained by the first model are more reliable than the others, in particular in the evaluation of the tension at the cruciate ligaments. The results obtained reveals that in extension the ACL is strained from full extension to about 35°-50° knee angle, and then it becomes unstrained at every velocity; furthermore the angle at which the peak of ACL and PCL are reached are not influenced by the velocity of the movement too. About the maximum load at the ligaments, the results show that PCL is more strained than ACL. These findings can have a clinical relevance. As a matter of fact, exercises in the range from full extension to 35°-50° should be avoid in order to not overload the ACL ligament, in particular for subjects after ACL reconstruction during rehabilitation; exercises at low intensity and in the other part of the range of motion should be preferred.

In flexion the results obtained for shear and axial load on tibia and femur obtained by the second model are close to those obtained by OpenSim; the results of the first model are instead higher than the others, as a consequence of the fact the muscular activation of this model is higher than the others. This fact suggests that it is reasonable to assume that the results obtained by the second model and by the software are more reliable than those of the first model. As in extension, the results obtained were compared with those in the literature in order to identify common trends in particular for shear and, consequently, for the tension at cruciate ligaments. The results are in good agreement and reveal that in flexion only PCL is strained and its maximum occur at an angle which is not influenced by the velocity and which is similar to that obtained in extension.

Furthermore, by comparing the results with the limit values in the literature, the velocity of 120°/s has been identified as a safety limit both in extension and flexion in order to not overload the major structures at the knee.

About the fitness exercises, the comparison of experimental and numerical simulations shows more variability in the results with respect to those obtained in isokinetic conditions; however the error related to the instant at which the maximum occur is less than the others. About the comparison of analytical and numerical models, the same trend of the first part of the study is confirmed, in particular the different way in which the software evaluates the reaction forces at the knee joint in extension, the more reliability of results of the first model with respect to the others and the fact that the angles at which the maximum tension at ACL and PCL occur and the angle at which the ACL becomes unstrained are not influenced by external conditions. Furthermore, the most significant aspect of the comparison of the two types of machines investigated, is that with the “cables machine” the knee moment is higher in the first part of the movement than at the end; on contrary with the “free-weight machine” the knee moment is low in the first part but it increases at the end of the movement. This could have a clinical relevance: because of the previous results suggest that the ACL is strained at the end of the range of motion, at the end of the movement, the exercise at the “cables machine” should be preferred than those at the other machine in order to not overload the ACL in healthy subjects and, in particular, subjects after ACL reconstruction during rehabilitation. By comparing instead the results with the limit values in the literature, it appears instead that the critical conditions are never reached.

However, this is only a preliminary study with only one subjected tested. A better analysis should be done by considering more subjects and by evaluating in a more precise way the kinetic conditions.

APPENDIX

A.1.Results of Subject 1 (S1)

Torque at the servo-motor

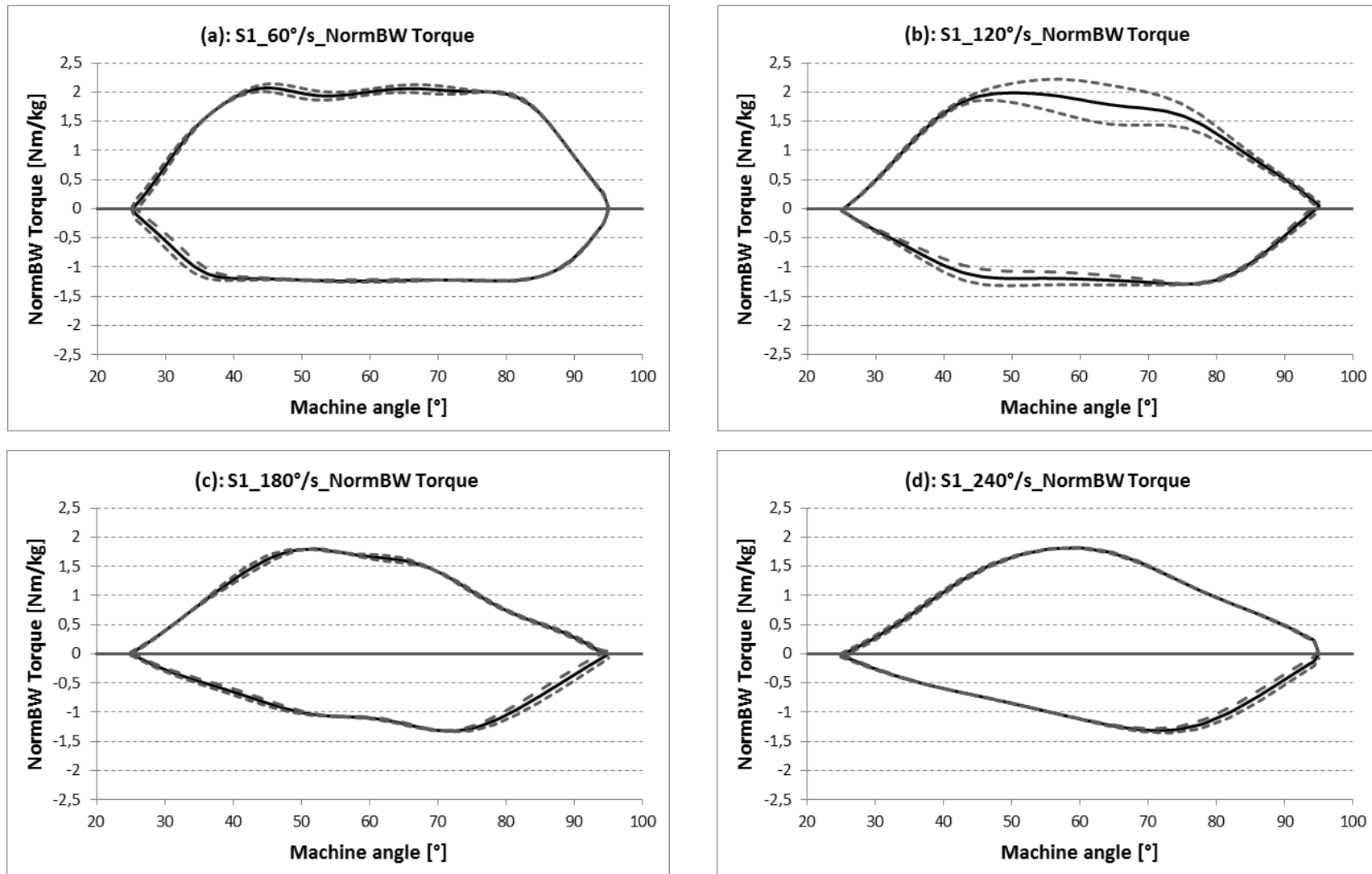


Fig.A.1.1: Normalized Torque of S1 at 60°/s (a), 120°/s (b), 180°/s (c) and 240°/s (d).

Flexors and Extensors Balance

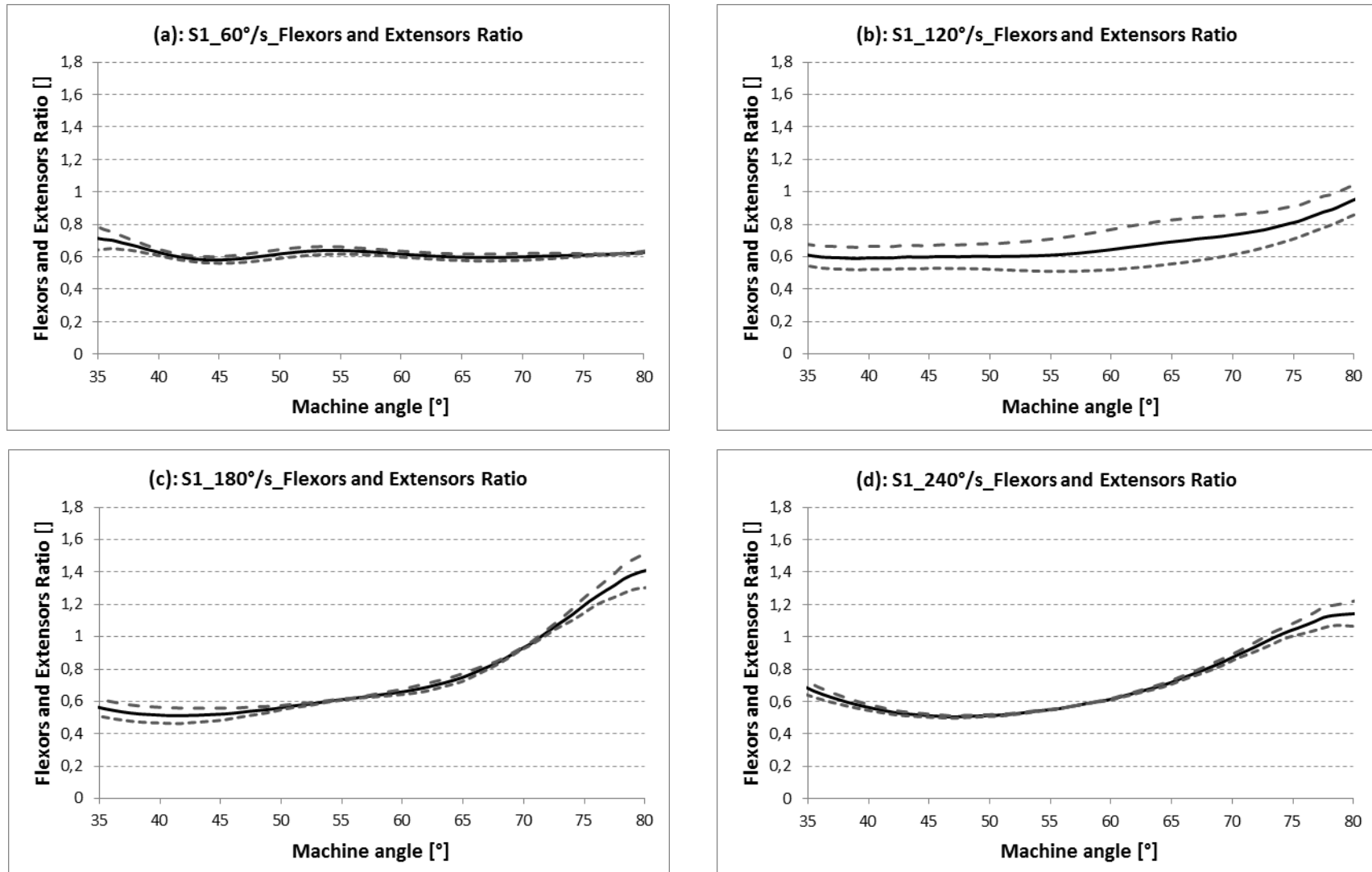


Fig.A.1.2: Flexors and extensors balance of S1 at 60°/s (a), 120°/s (b), 180°/s (c) and 240°/s (d).

Comparison of EMG signal and OpenSim muscle activation

M = 88 kg H = 1,85 m age = 25

adjust ratio for OpenSim: $\frac{SM_{S1}}{SM_{model}} = 1,473$

Maximum effort exerted in isokinetic and isometric exercises [mV]:

	Isokinetic exercise				Isometric exercise				
	60 °/s	120 °/s	180 °/s	240 °/s	ISO_25°	ISO_40°	ISO_55°	ISO_70°	ISO_95°
RF	0,212	0,257	0,152	0,274	0,184	0,193	0,164	0,243	0,317
VL	0,333	0,456	0,399	0,463	0,283	0,366	0,384	0,342	0,414
VM	0,277	0,219	0,197	0,202	0,192	0,171	0,205	0,213	0,268
BF	0,486	0,453	0,39	0,325	0,23	0,152	0,224	0,279	0,306

Tab.A.1.1: Mamimum effort of S1 in [mV] during isokinetic and isometric exercises.

60 °/s

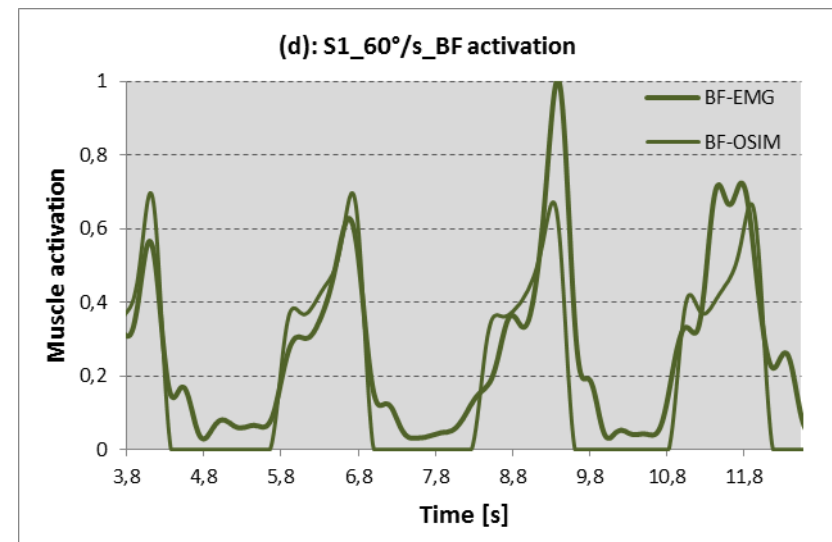
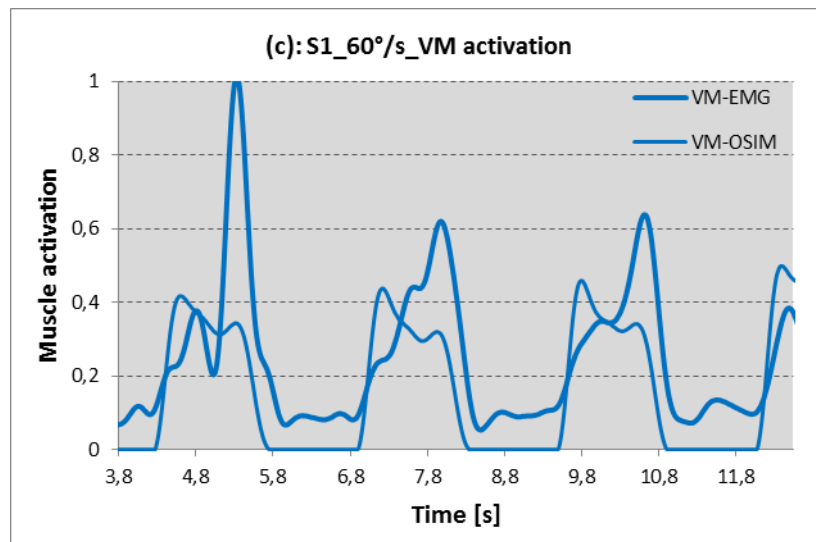
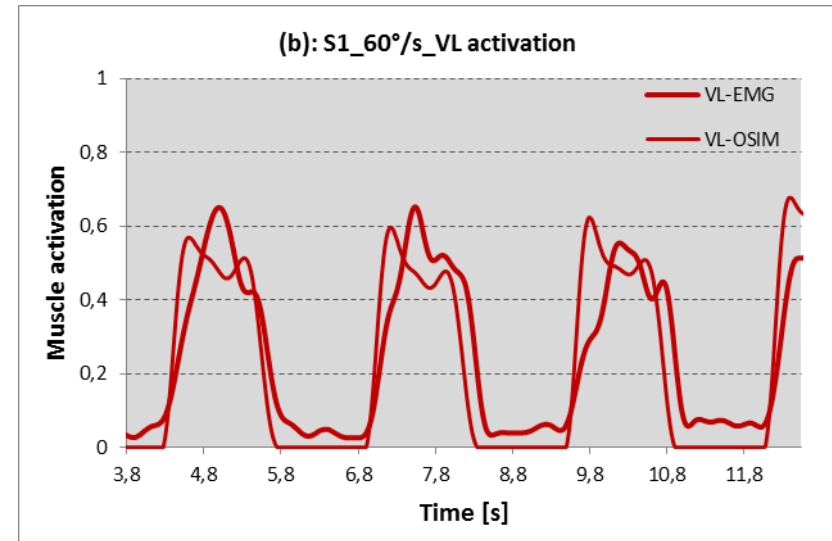
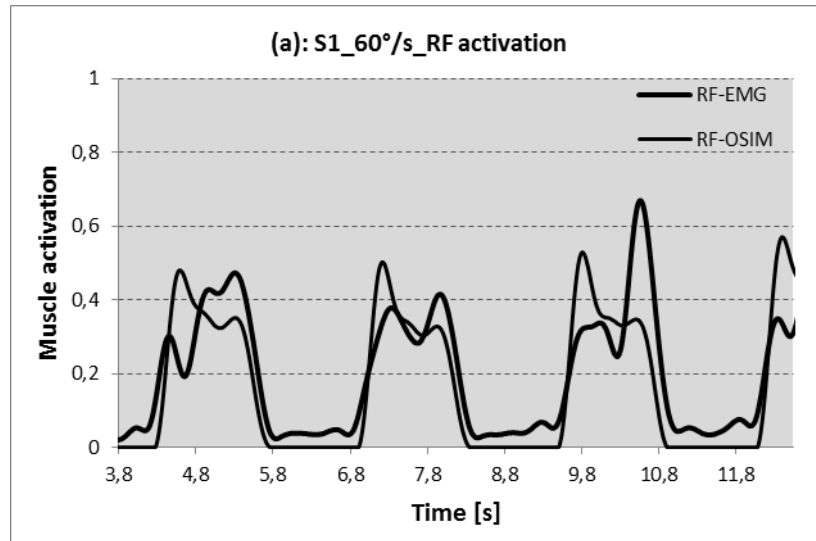


Fig.A.1.3: EMG and OpenSim muscle activation of S1 at 60°/s of RF (a), VL (b), VM (c) and BF (d).

120 °/s

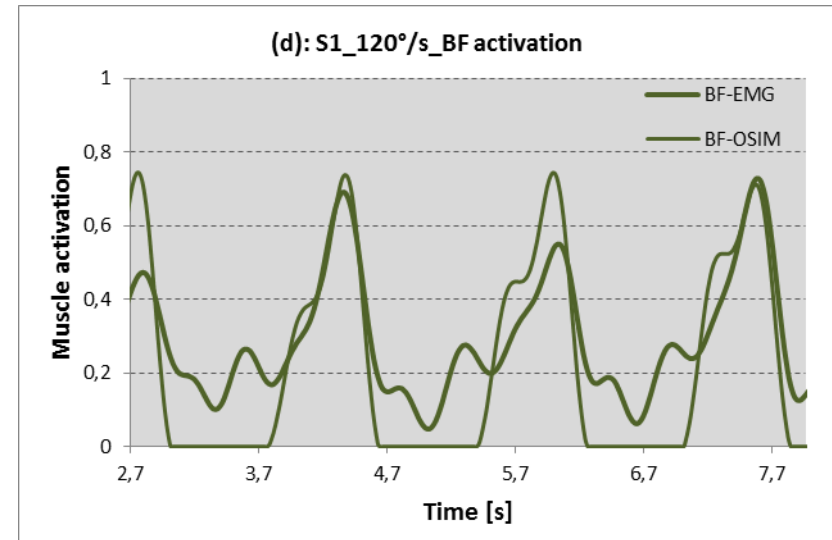
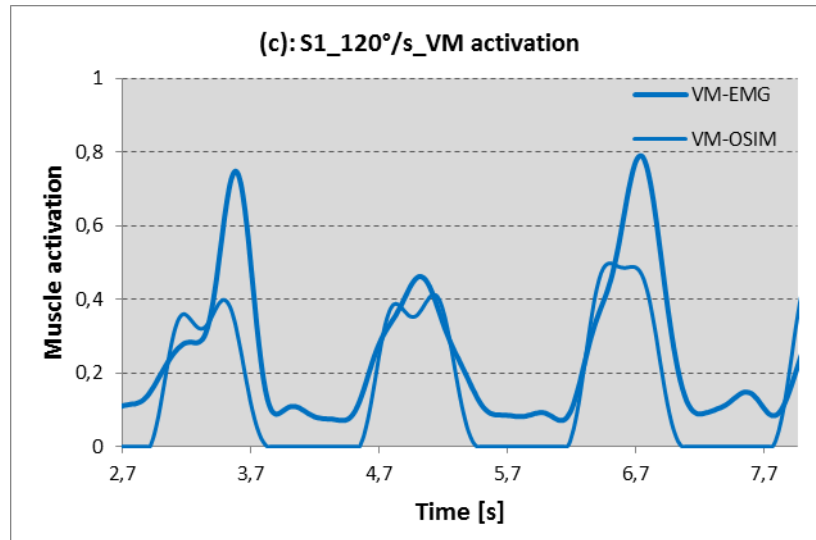
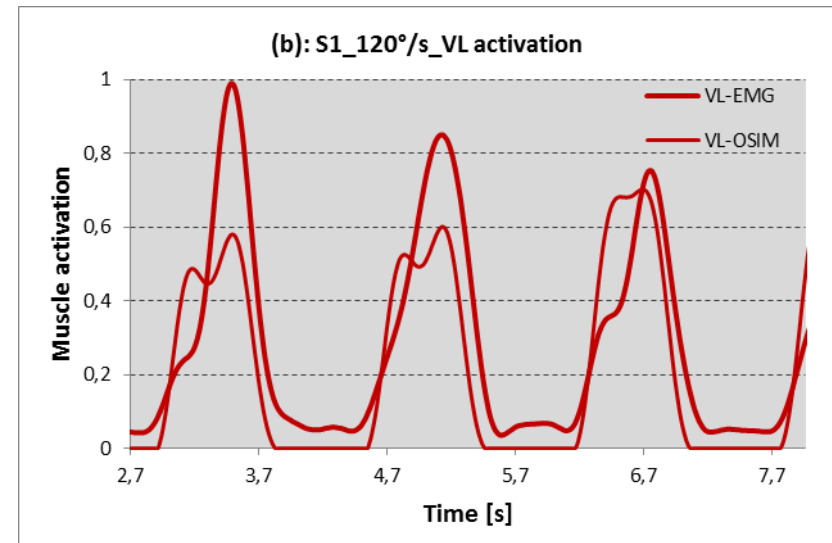
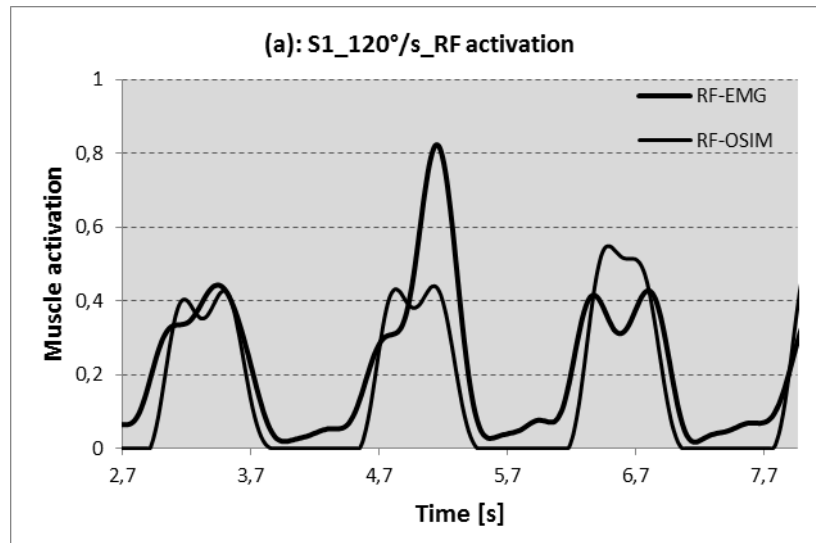


Fig.A.1.4: EMG and OpenSim muscle activation of S1 at 120°/s of RF (a), VL (b), VM (c) and BF(d).

180 °/s

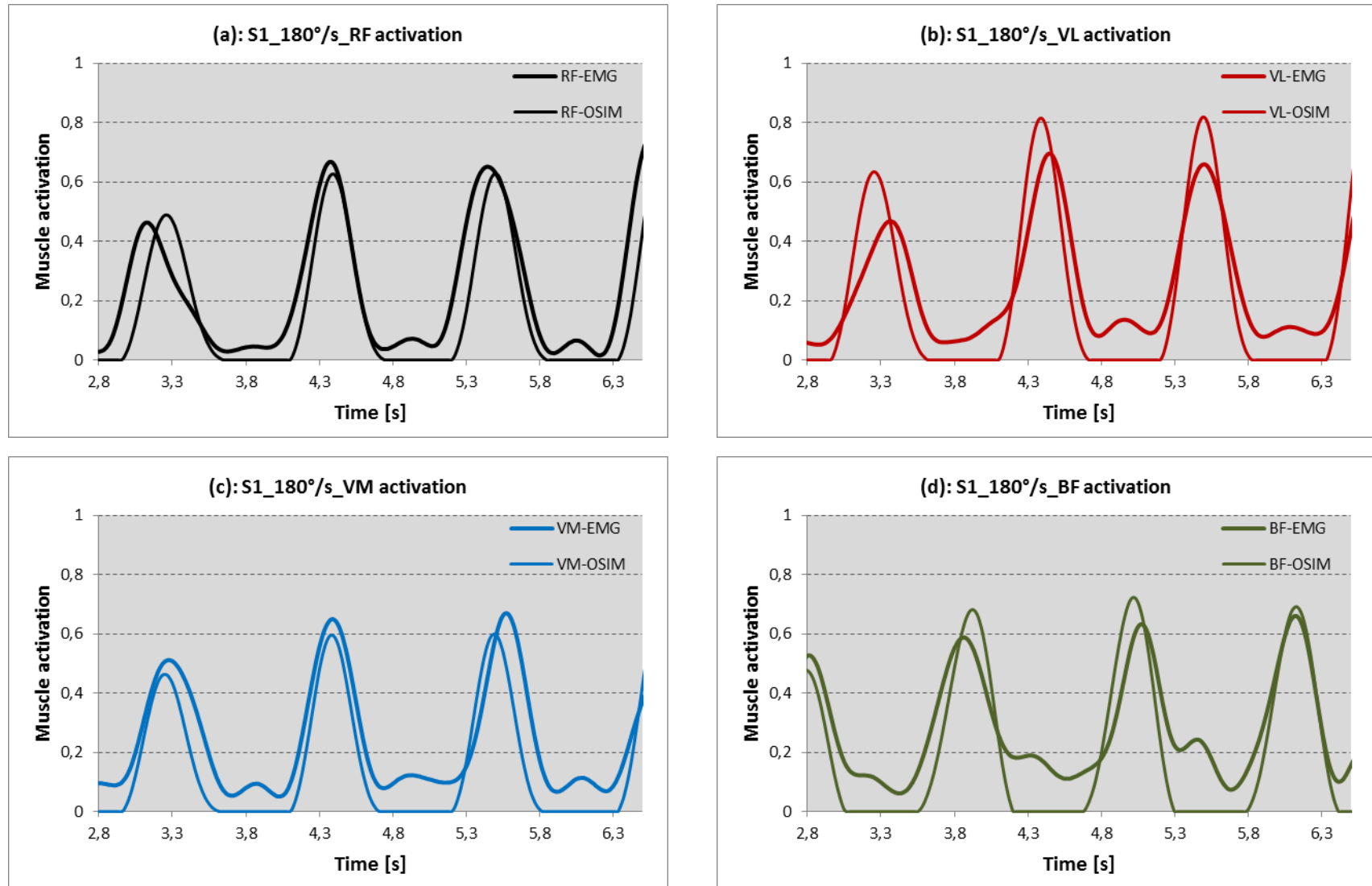


Fig.A.1.5: EMG and OpenSim muscle activation of S1 at 180°/s of RF (a), VL (b), VM (c) and BF (d).

240 °/s

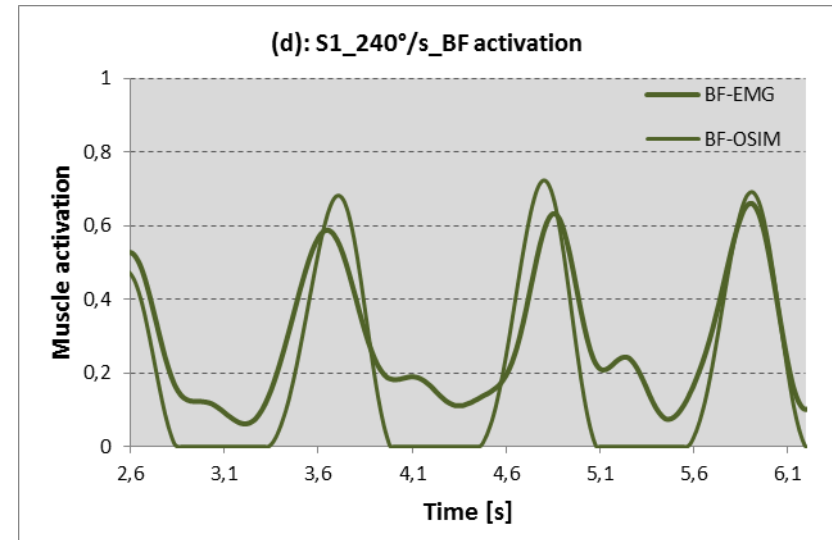
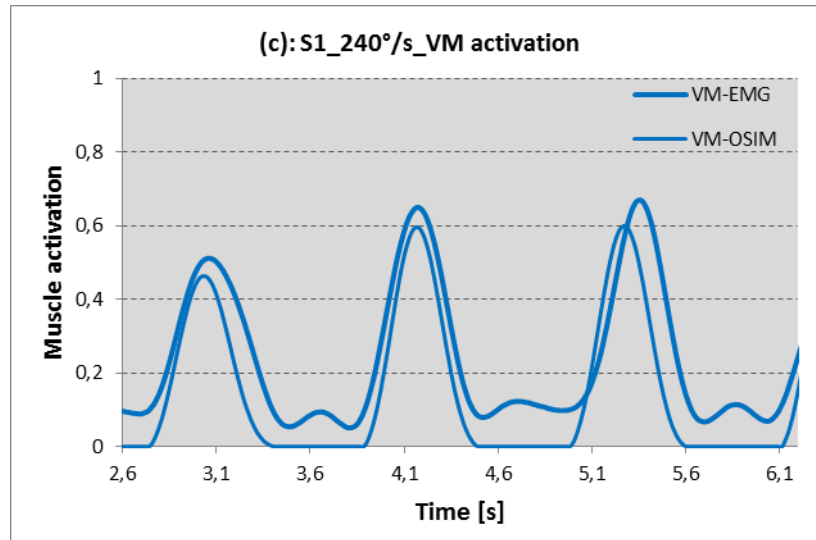
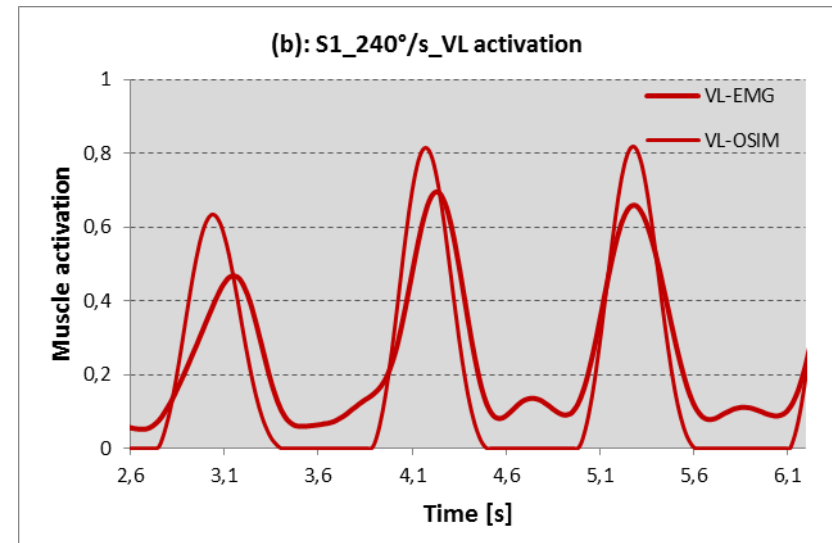
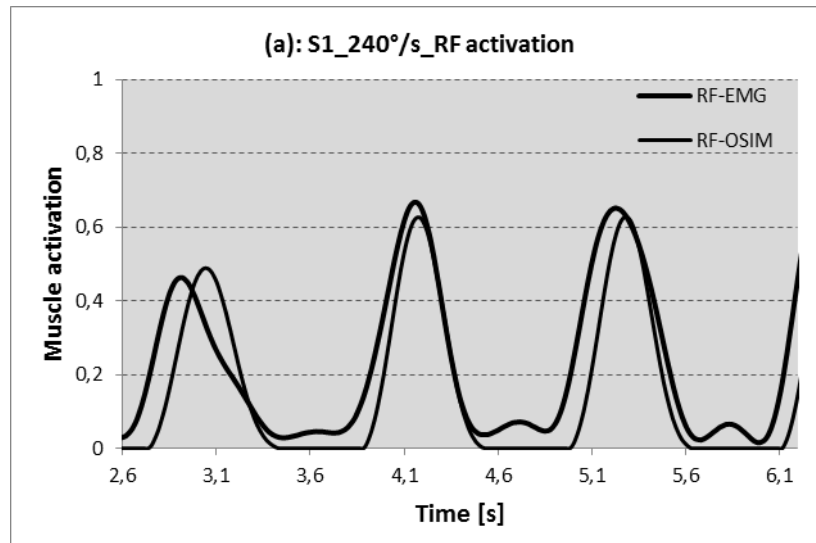


Fig.A.1.6: EMG and OpenSim muscle activation of S1 at 240°/s of RF (a), VL (b), VM (c) and BF (d).

Comparison of EMG signal and OpenSim muscle activation: quantitative results

	60 °/s	120 °/s	180 °/s	240 °/s
RF	-0,51±20,96	7,37±37,43	1,43±6,05	13,78±14,85
VL	2,87±13,41	25,79±17,53	-25,57±9,26	-4,24±11,22
VM	38,74±17,38	31,50±18,58	9,39±1,22	28,75±7,40
BF	9,98±22,10	-13,20±19,64	-11,64±6,05	11,97±1,79

Tab.A.1.2: Peak error of S1 in [%] of RF, VL, VM and BF at 60°/s, 120°/s, 180°/s and 240°/s.

	60 °/s	120 °/s	180 °/s	240 °/s
RF	26,47±1,33	5,63±10,94	-5,87±3,56	-5,55±4,48
VL	10,23±5,56	1,33±2,31	6,73±1,21	7,00±1,95
VM	28,30±2,25	4,37±10,92	3,50±2,76	3,93±2,81
BF	-2,23±3,74	-0,18±2,19	-0,73±6,82	-0,40±5,14

Tab.A.1.3: Time error of S1 in [%] of RF, VL, VM and BF at 60°/s, 120°/s, 180°/s and 240°/s.

	240 °/s	180 °/s	120 °/s	60 °/s
RF	11,39±3,17	8,38±9,94	8,79±14,32	13,78±14,85
VL	0,99±7,18	13,77±15,56	-7,19±10,80	-4,24±11,22
VM	30,30±8,86	35,64±4,78	25,94±7,58	28,75±7,40
BF	1,82±13,87	3,44±3,59	11,36±0,65	11,97±1,79

Tab.A.1.4: Area error of S1 in [%] of RF, VL, VM and BF at 60°/s, 120°/s, 180°/s and 240°/s.

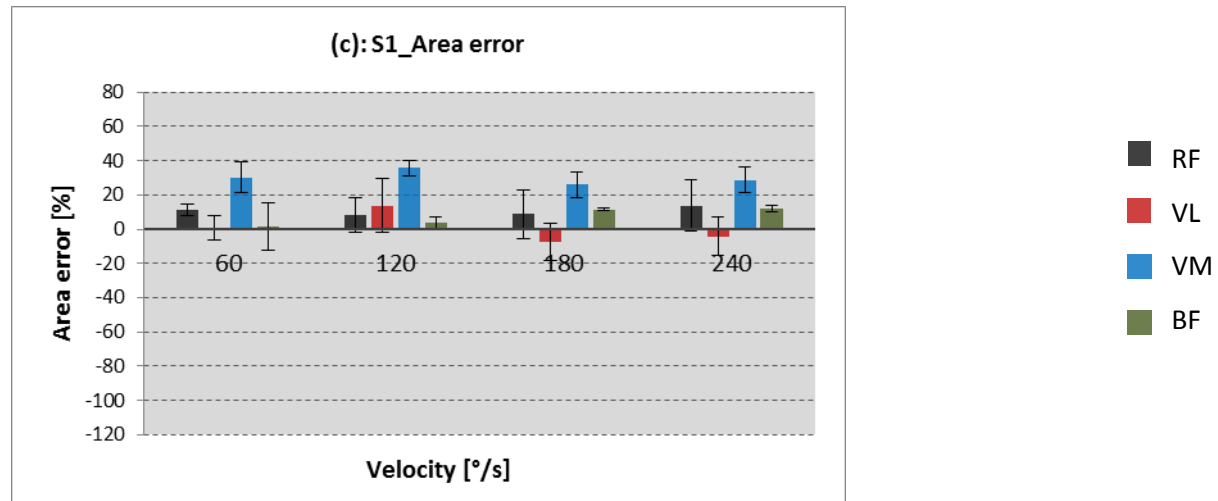
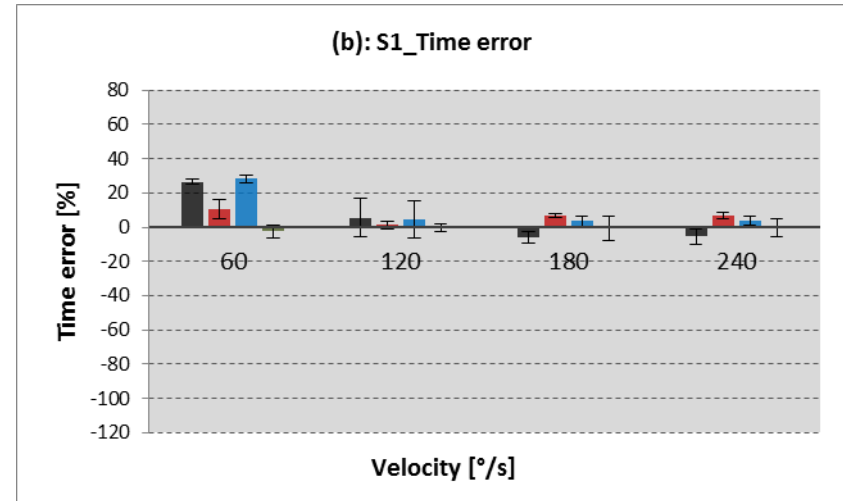
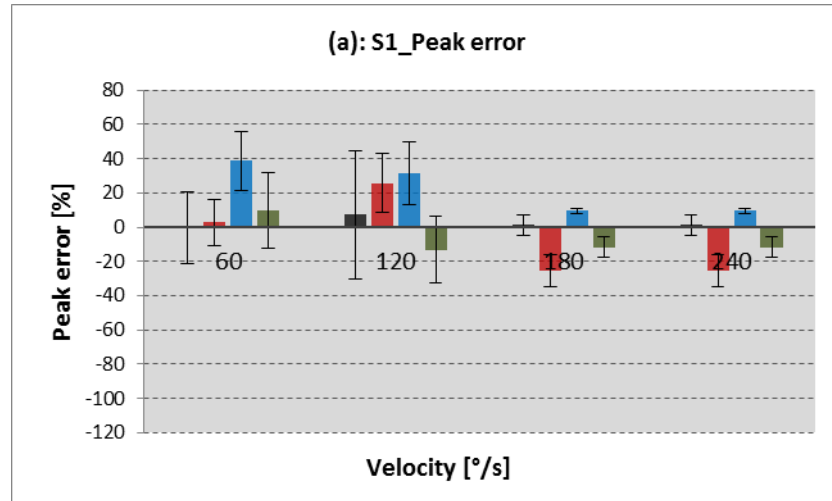


Fig.A.1.7: Quantitative results of muscle activation analysis of S1: (a): Peak error at different velocities; (b): Time error at different velocities; (c): Area error at different velocities.

Comparison of analytical models and OpenSim model

Model 1: parameters

$$\text{Tibia: } m_{\text{tibia}} = 4,34 \text{ kg} \quad I_{G \text{ tibia}} = 0,087 \text{ kg} \cdot \text{m}^2 \quad \Delta_{y \text{ tibia}} = 0,52 \text{ m} \quad \Delta_{y \text{ G tibia}} = 0,224 \text{ m}$$

$$\text{Talus: } m_{\text{talus}} = 0,117 \text{ kg} \quad I_{G \text{ talus}} = 8,8 \cdot 10^{-4} \text{ kg} \cdot \text{m}^2 \quad \Delta_{y \text{ talus}} = 0,52 \text{ m} \quad \Delta_{y \text{ G talus}} = 0,52 \text{ m}$$

$$\text{Calc: } m_{\text{calc}} = 1,463 \text{ kg} \quad I_{G \text{ calc}} = 0,0036 \text{ kg} \cdot \text{m}^2 \quad \Delta_{x \text{ calc}} = 0,042 \text{ m} \quad \Delta_{y \text{ calc}} = 0,036 \text{ m}$$

$$\Delta_{x \text{ G calc}} = 0,087 \text{ m} \quad \Delta_{y \text{ G calc}} = 0,026 \text{ m}$$

$$\text{Toes: } m_{\text{toes}} = 0,254 \text{ kg} \quad I_{G \text{ toes}} = 8,8 \cdot 10^{-5} \text{ kg} \cdot \text{m}^2 \quad \Delta_{x \text{ toes}} = 0,155 \text{ m} \quad \Delta_{y \text{ toes}} = 0,0017 \text{ m}$$

$$\Delta_{x \text{ G toes}} = 0,03 \text{ m} \quad \Delta_{y \text{ G toes}} = 0,005 \text{ m}$$

Model 2: parameters

$$\text{Tibia: } m_{\text{tibia}} = 3,96 \text{ kg} \quad I_{G \text{ tibia}} = 0,067 \text{ kg} \cdot \text{m}^2 \quad \Delta_{y \text{ tibia}} = 0,43 \text{ m} \quad \Delta_{y \text{ G tibia}} = 0,186 \text{ m}$$

$$\text{Foot: } m_{\text{foot}} = 1,232 \text{ kg} \quad I_{G \text{ foot}} = 0,0076 \text{ kg} \cdot \text{m}^2 \quad \Delta_{x \text{ G foot}} = 0,074 \text{ m} \quad \Delta_{y \text{ G foot}} = 0,037 \text{ m}$$

$$D_{Q2} = 0,08 \text{ m} \quad H_{Q2} = 0,026 \text{ m} \quad D_{Q1} = 0,3 \text{ m} \quad H_{Q1} = 0,03 \text{ m}$$

$$B_{PT} [\text{m}] = 0,0097 \cdot \varphi_{k+}^5 - 0,0215 \cdot \varphi_{k+}^4 - 0,0098 \cdot \varphi_{k+}^3 + 0,0366 \cdot \varphi_{k+}^2 - 0,0141 \cdot \varphi_{k+} + 0,0464 \quad \varphi_{k+} [\text{rad}]$$

$$\text{BFB: } D_{\text{BFB1}} = 0,2 \text{ m} \quad D_{\text{BFB2}} = 0,04 \text{ m} \quad H_{\text{BFB1}} = 0,04 \text{ m} \quad H_{\text{BFB2}} = 0,03 \text{ m}$$

$$\text{BFL: } D_{\text{BFL1}} = 0,49 \text{ m} \quad D_{\text{BFL2}} = 0,04 \text{ m} \quad H_{\text{BFL1}} = 0,04 \text{ m} \quad H_{\text{BFL2}} = 0,03 \text{ m}$$

$$\text{SM: } D_{\text{SM1}} = 0,49 \text{ m} \quad D_{\text{SM2}} = 0,5 \text{ m} \quad H_{\text{SM1}} = 0,4 \text{ m} \quad H_{\text{SM2}} = 0,035 \text{ m}$$

$$\text{ST: } D_{\text{ST1}} = 0,49 \text{ m} \quad H_{\text{ST1}} = 0,5 \text{ m} \quad B_{\text{ST}} = 0,4 \text{ m} \quad \alpha_{\text{ST}} = 0,52 \text{ rad}$$

Fig.A.1.8: S1_60°/s_Extension

— OSIM — Mod1_Herzog — Mod1_Van Eijden — Mod2 - - - limit value

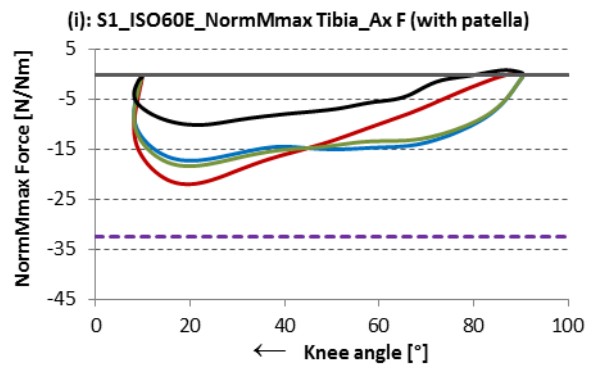
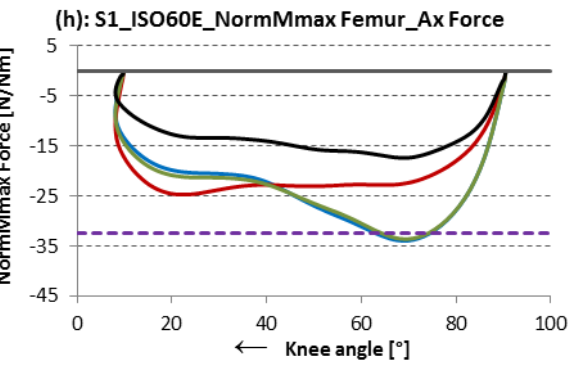
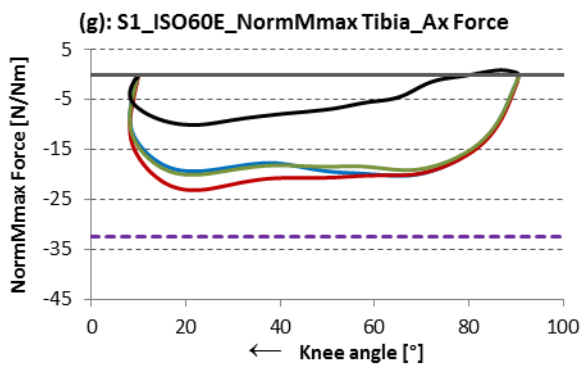
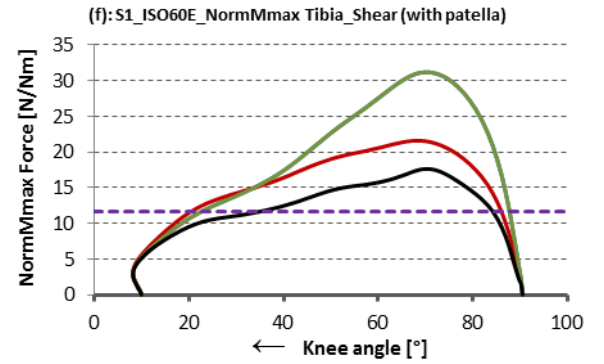
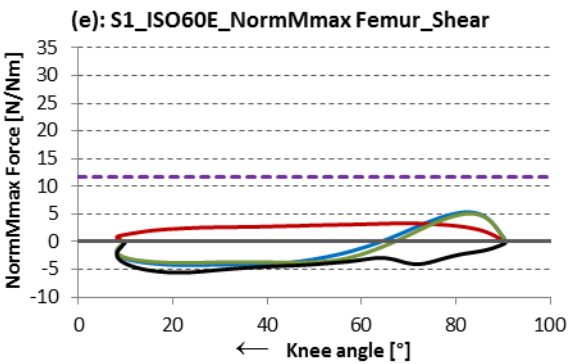
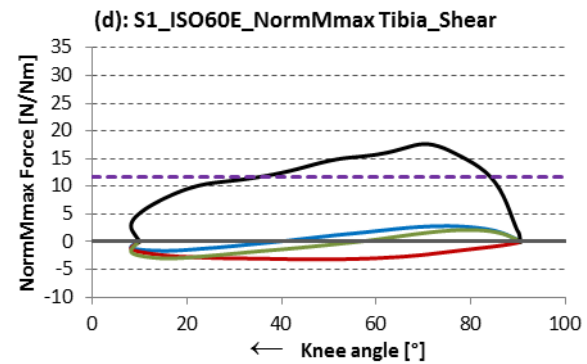
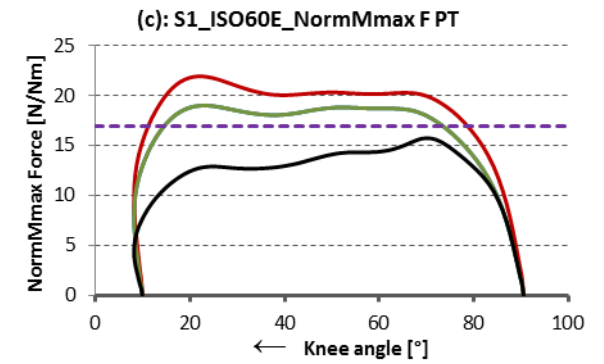
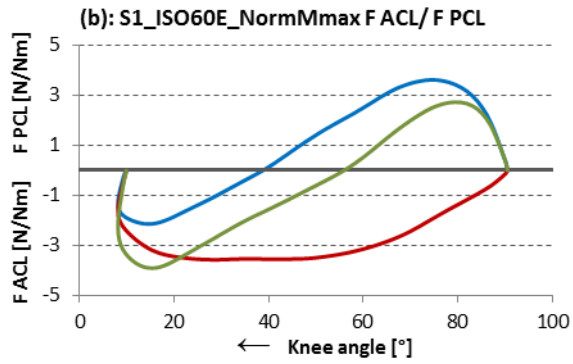
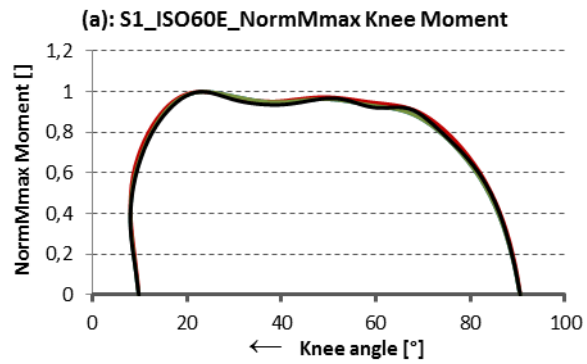


Fig.A.1.9: S1_60°/s_Flexion

— OSIM — Mod1 — Mod2 - - - limit value (•••• OSIM BFL •••• Mod1 BFL •••• Mod2 BFL)

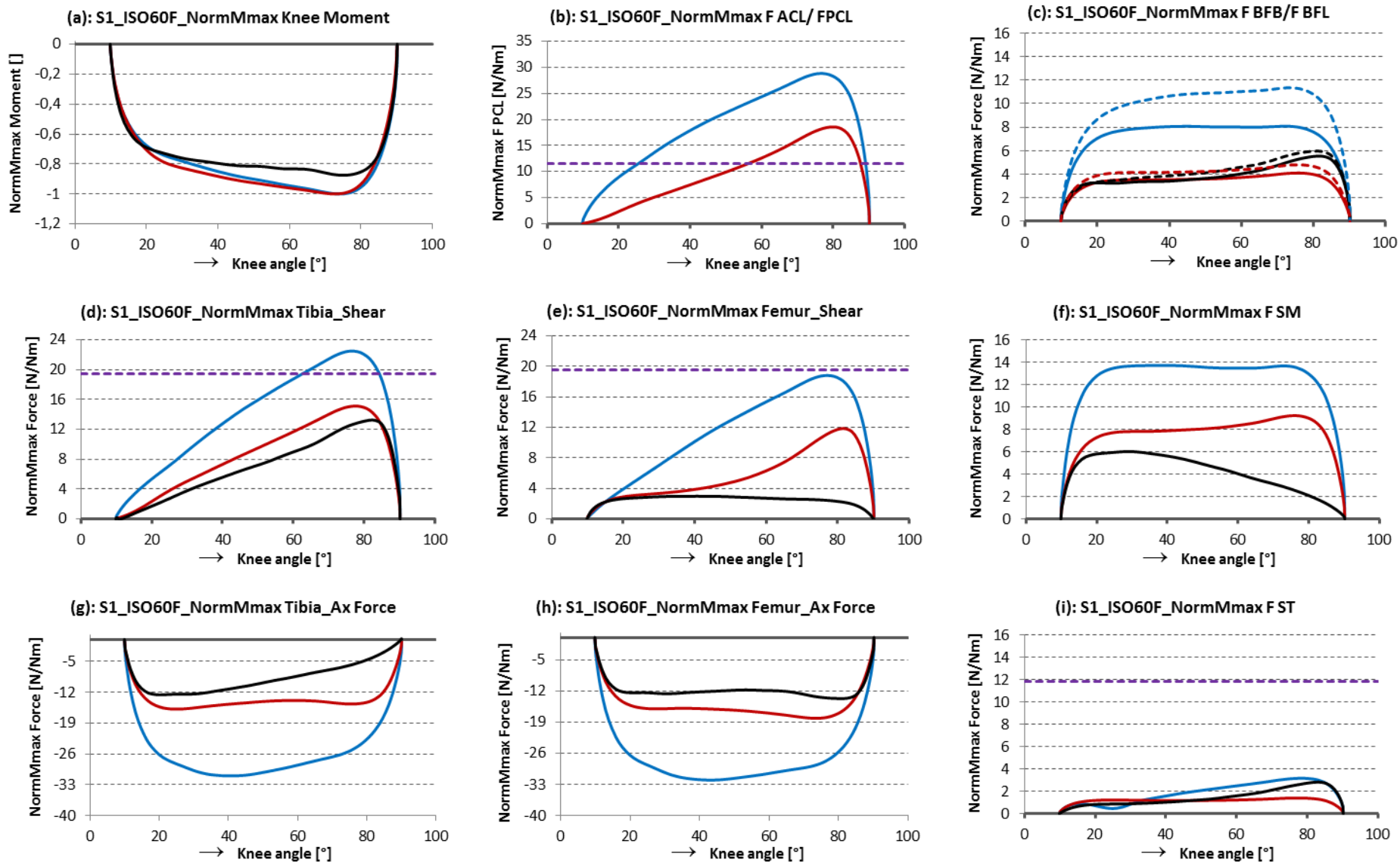


Fig.A.1.10: S1_120°/s_Extension

— OSIM — Mod1_Herzog — Mod1_Van Eijden — Mod2 - - - - limit value

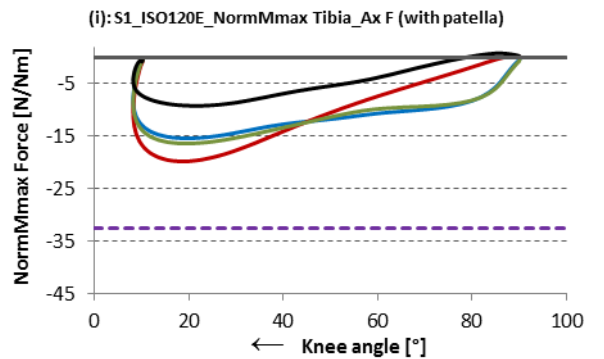
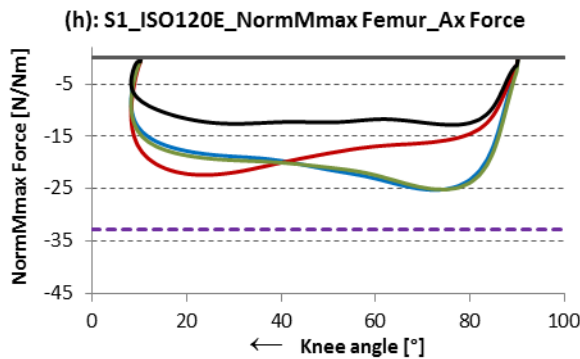
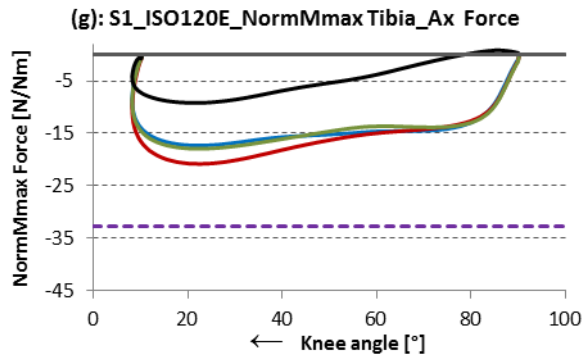
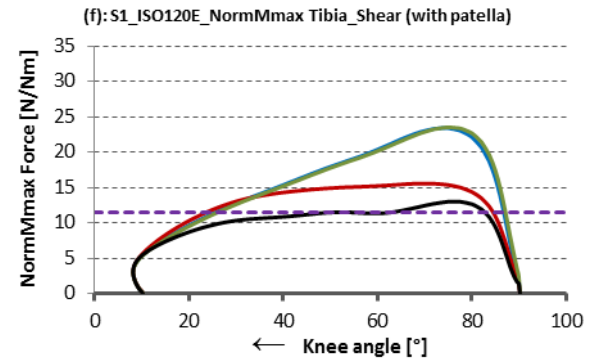
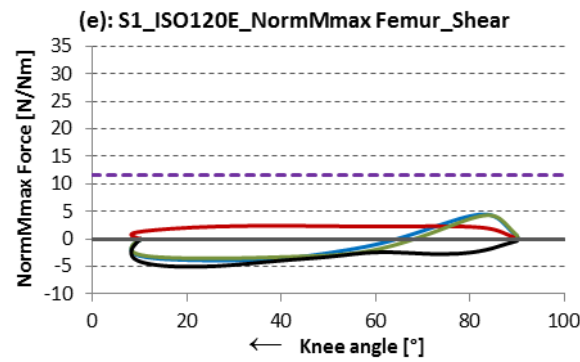
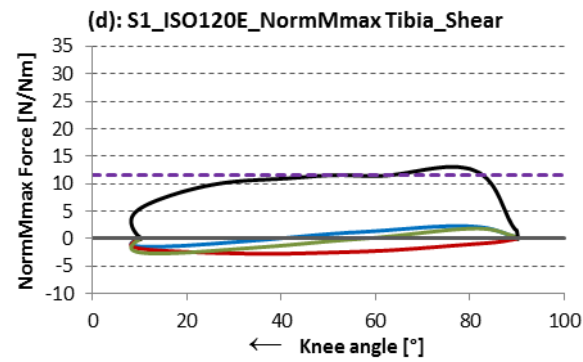
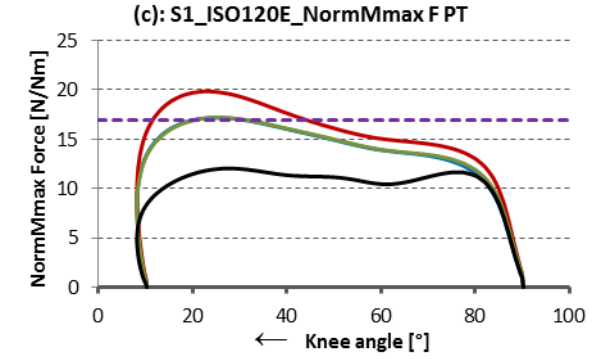
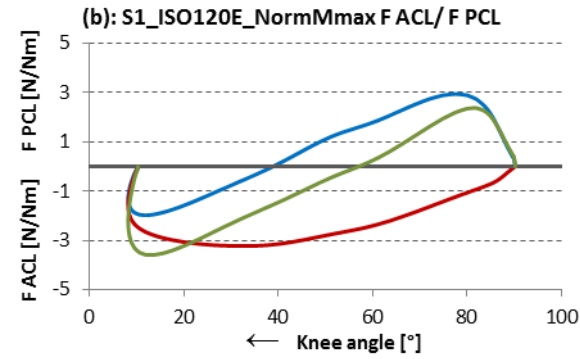
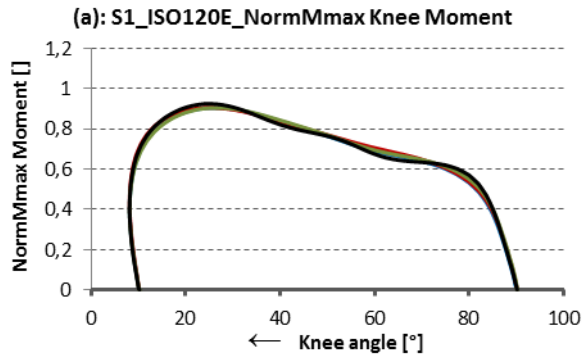


Fig.A.1.11: S1_120°/s_Flexion

— OSIM — Mod1 — Mod2 - - - limit value (- - - OSIM BFL - - - Mod1 BFL - - - Mod2 BFL)

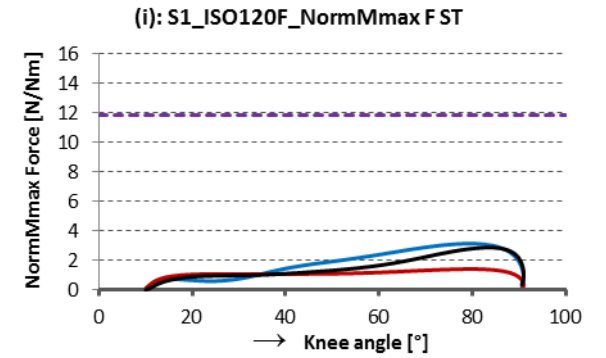
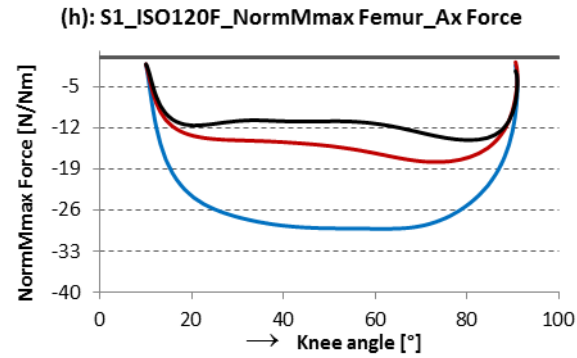
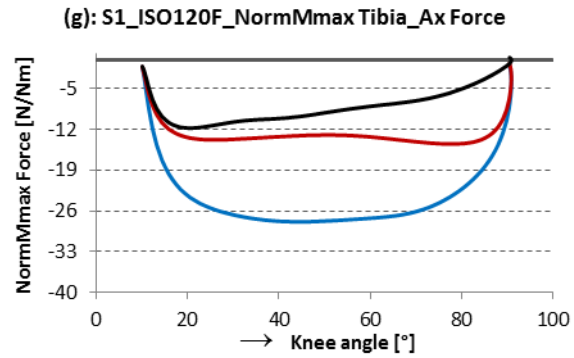
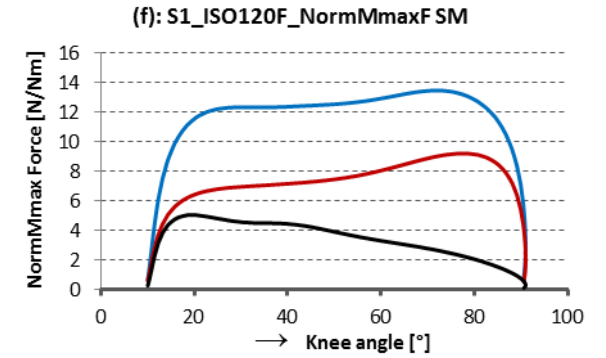
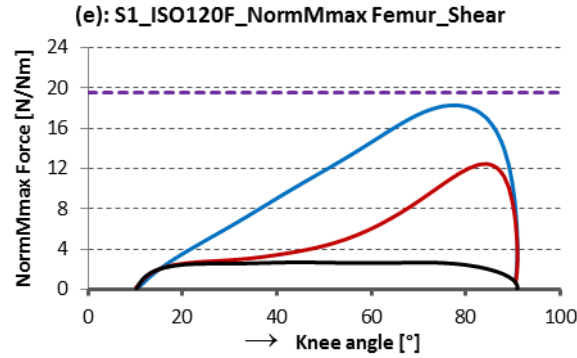
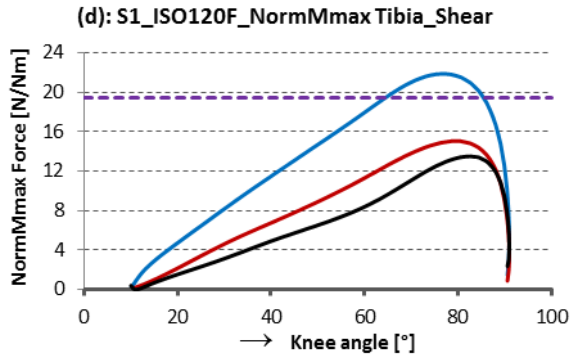
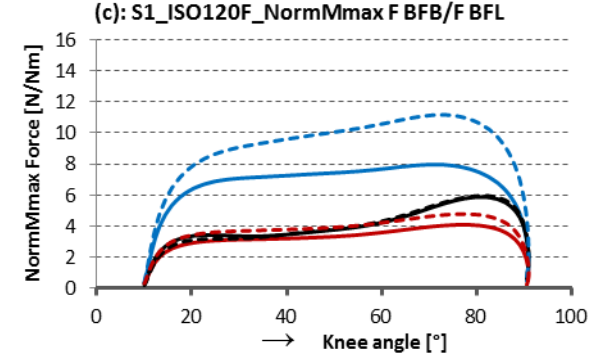
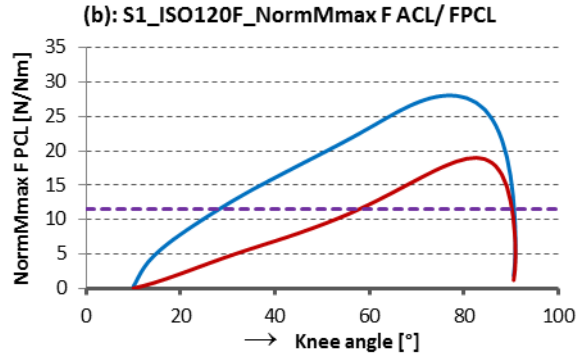
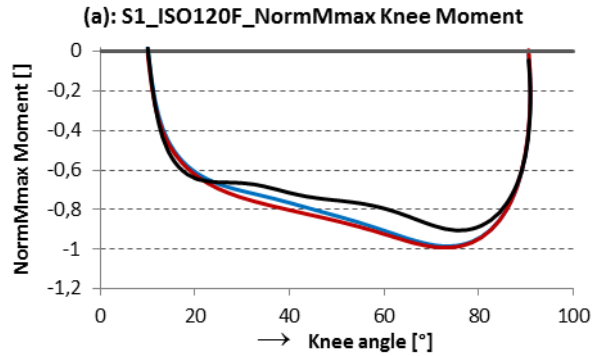


Fig.A.1.12: S1_180°/s_Extension

— OSIM — Mod1_Herzog — Mod1_Van Eijden — Mod2 - - - limit value

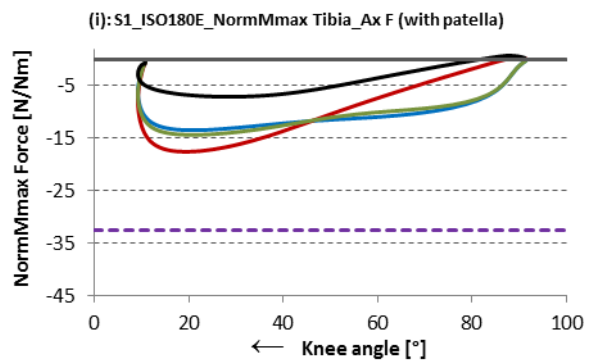
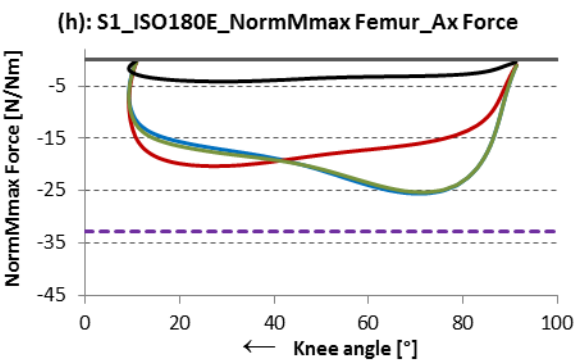
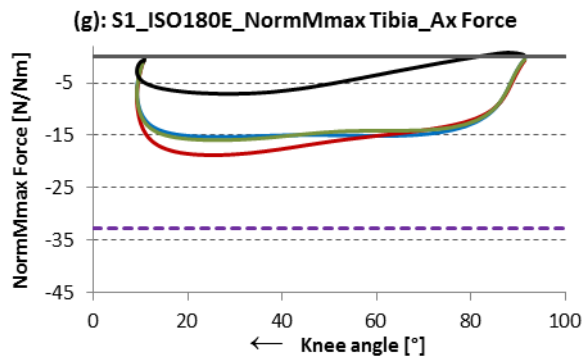
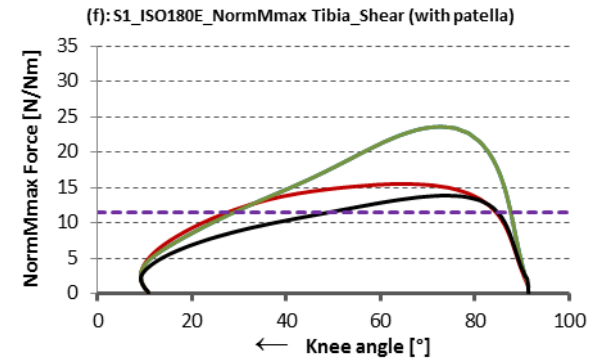
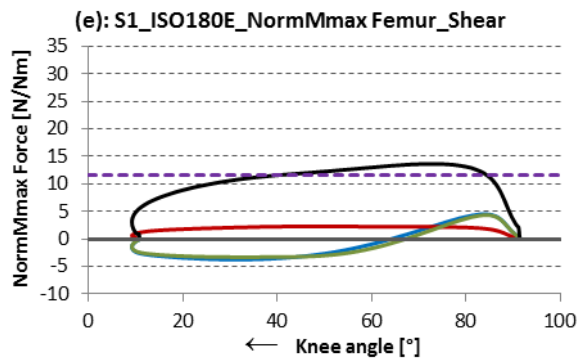
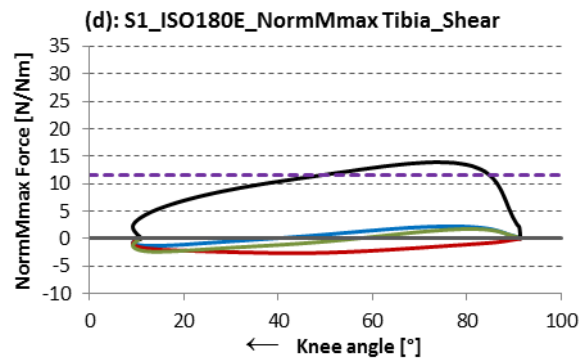
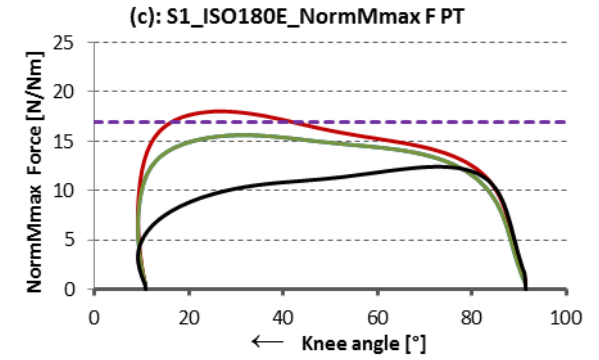
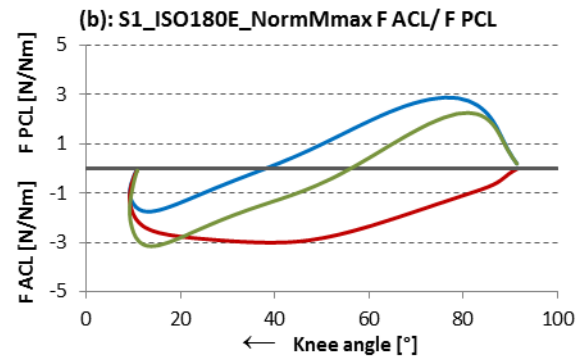
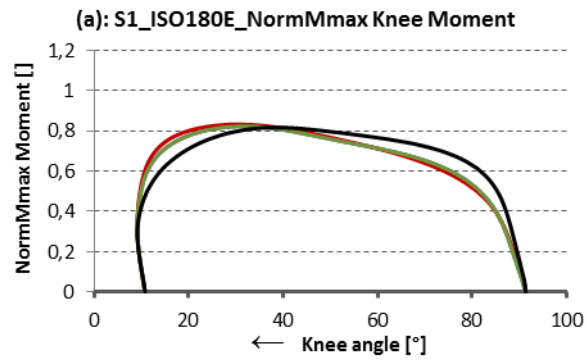


Fig.A.1.13: S1_180°/s_Flexion

— OSIM — Mod1 — Mod2 - - - limit value (•••• OSIM BFL •••• Mod1 BFL •••• Mod2 BFL)

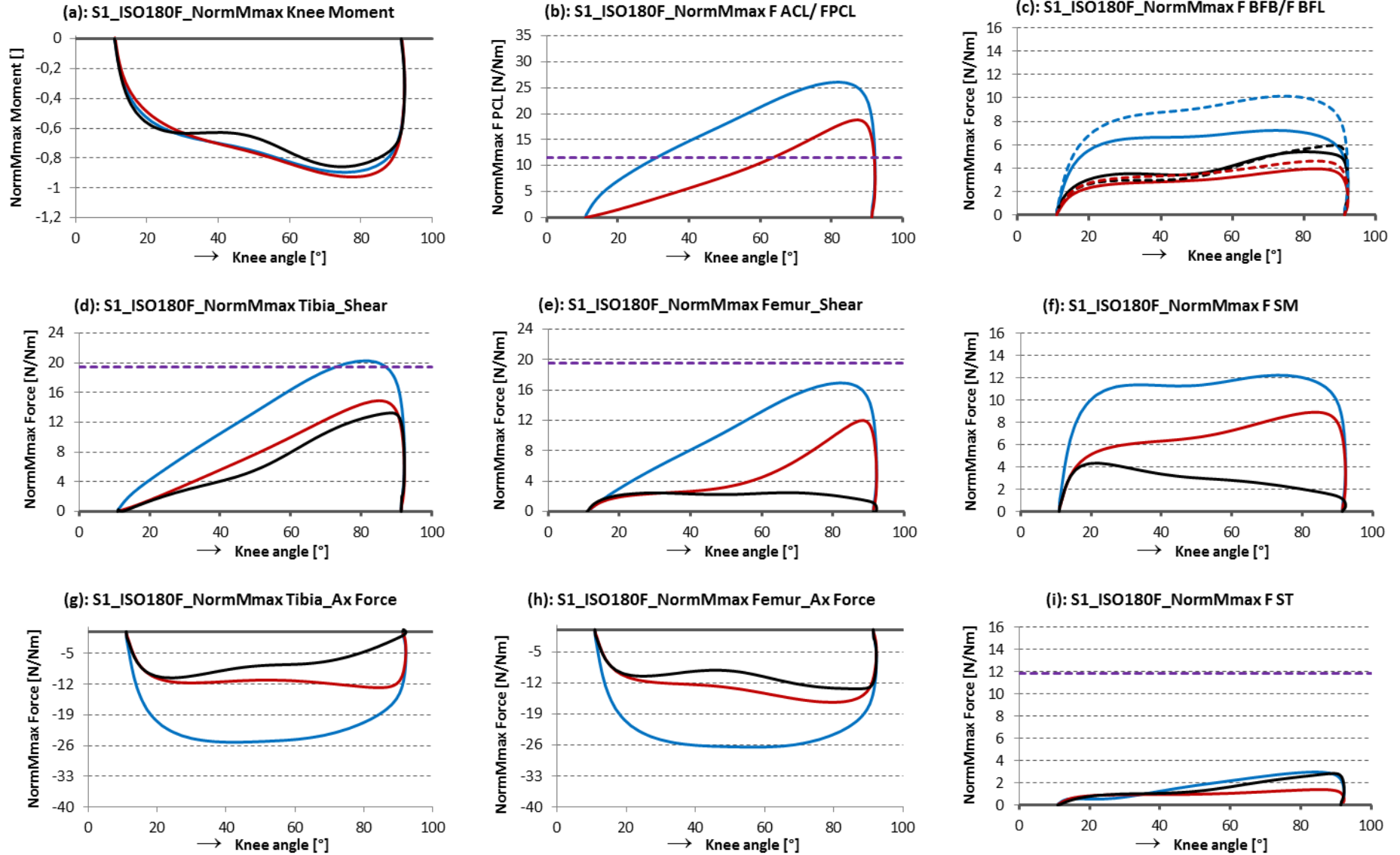


Fig.A.1.14: S1_240°/s_Extension

— OSIM — Mod1_Herzog — Mod1_Van Eijden — Mod2 - - - - limit value

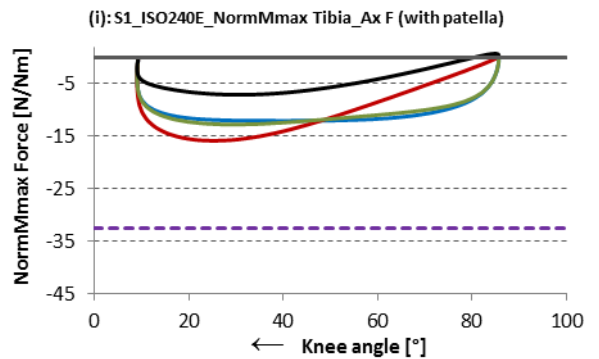
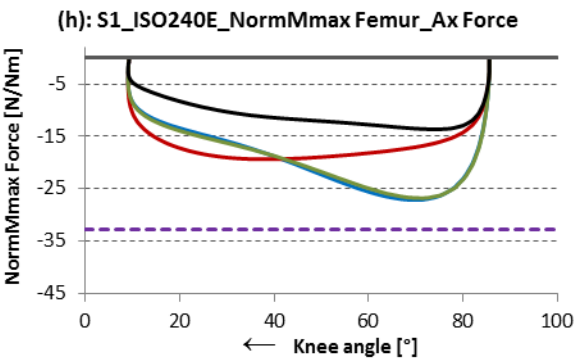
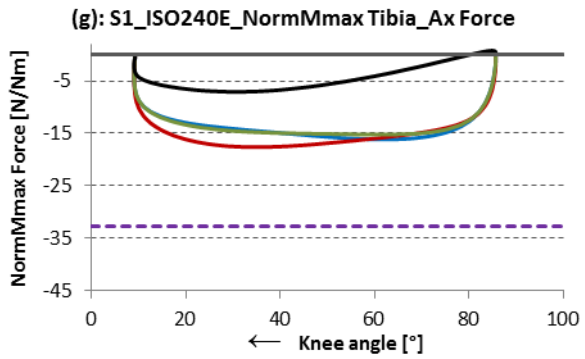
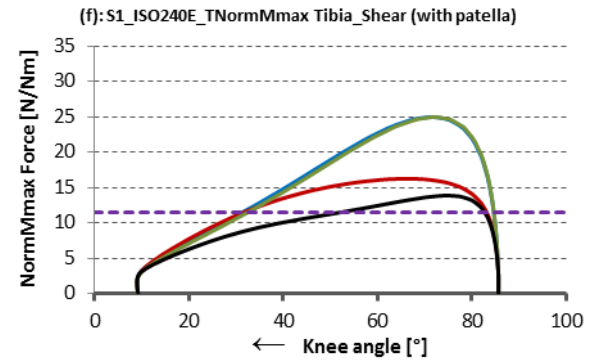
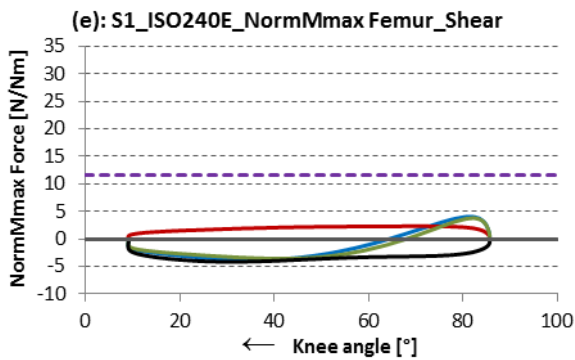
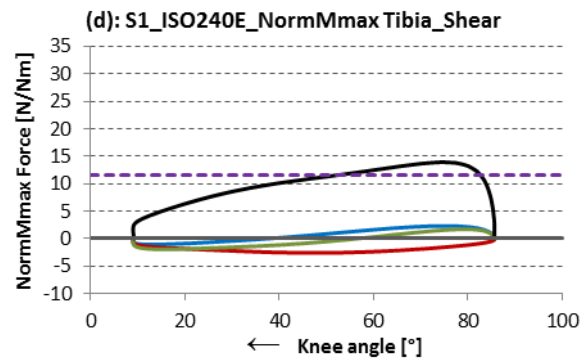
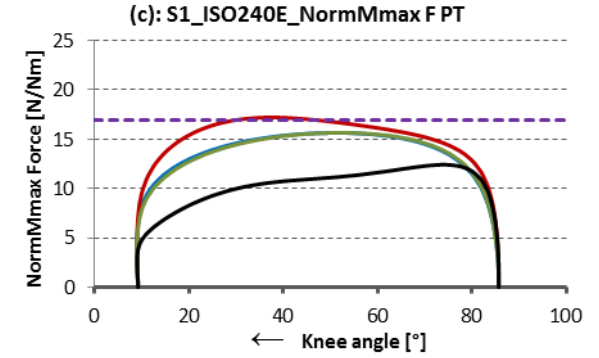
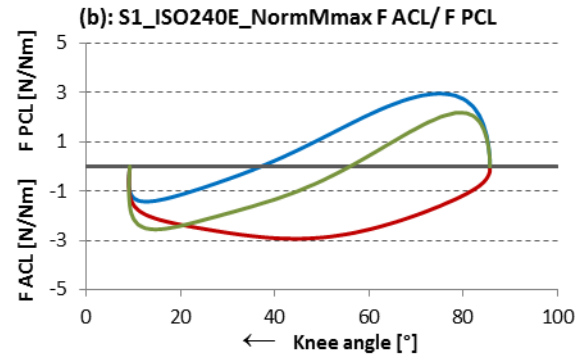
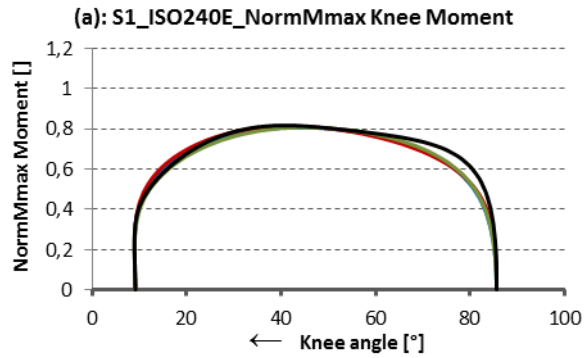
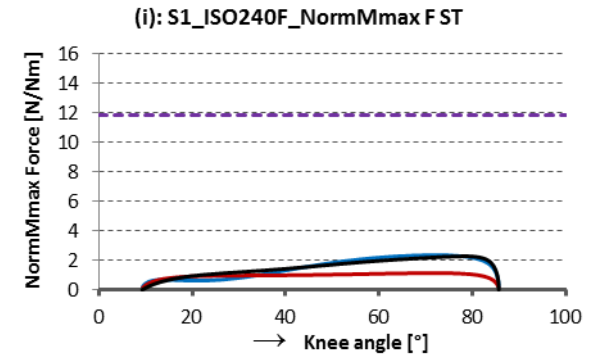
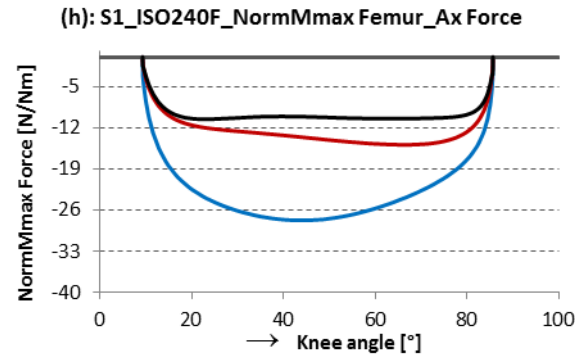
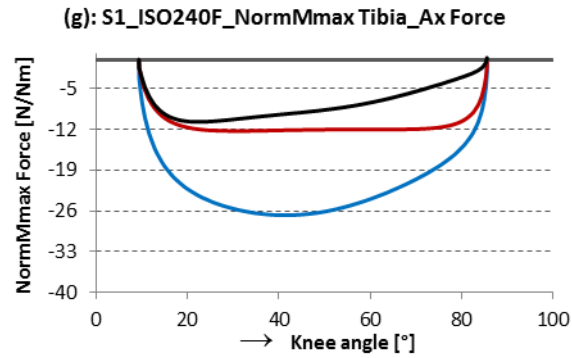
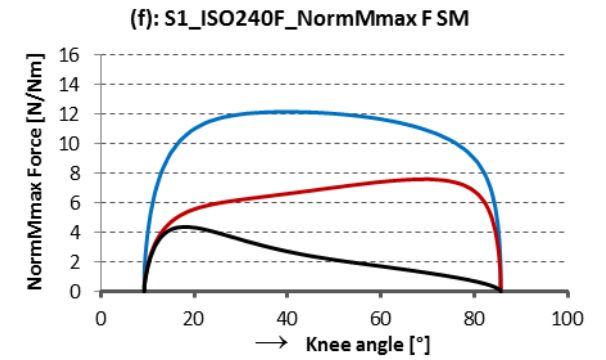
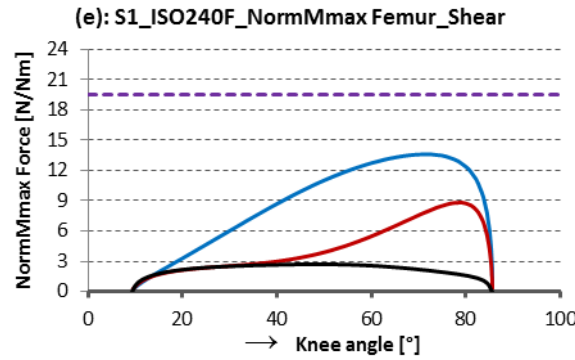
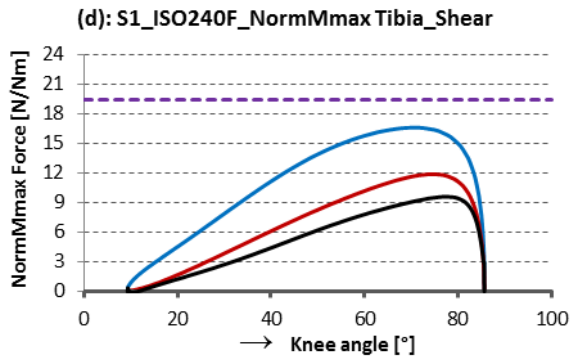
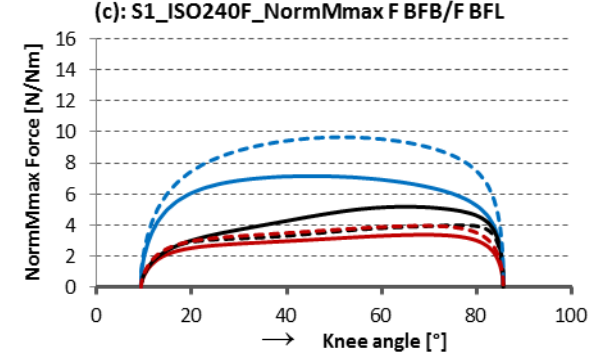
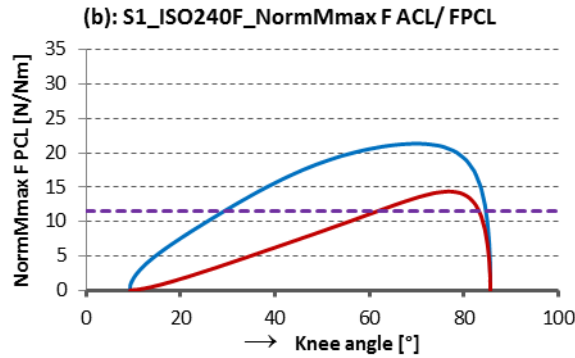
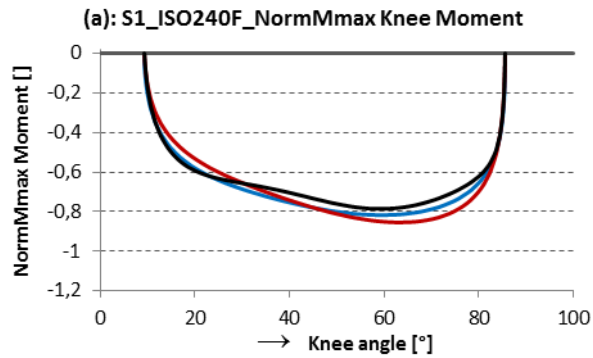


Fig.A.1.15: S1_240°/s_Flexion

— OSIM — Mod1 — Mod2 - - - limit value (•••• OSIM BFL •••• Mod1 BFL •••• Mod2 BFL)



A.2.Results of Subject 2 (S2)

Torque at the servo-motor

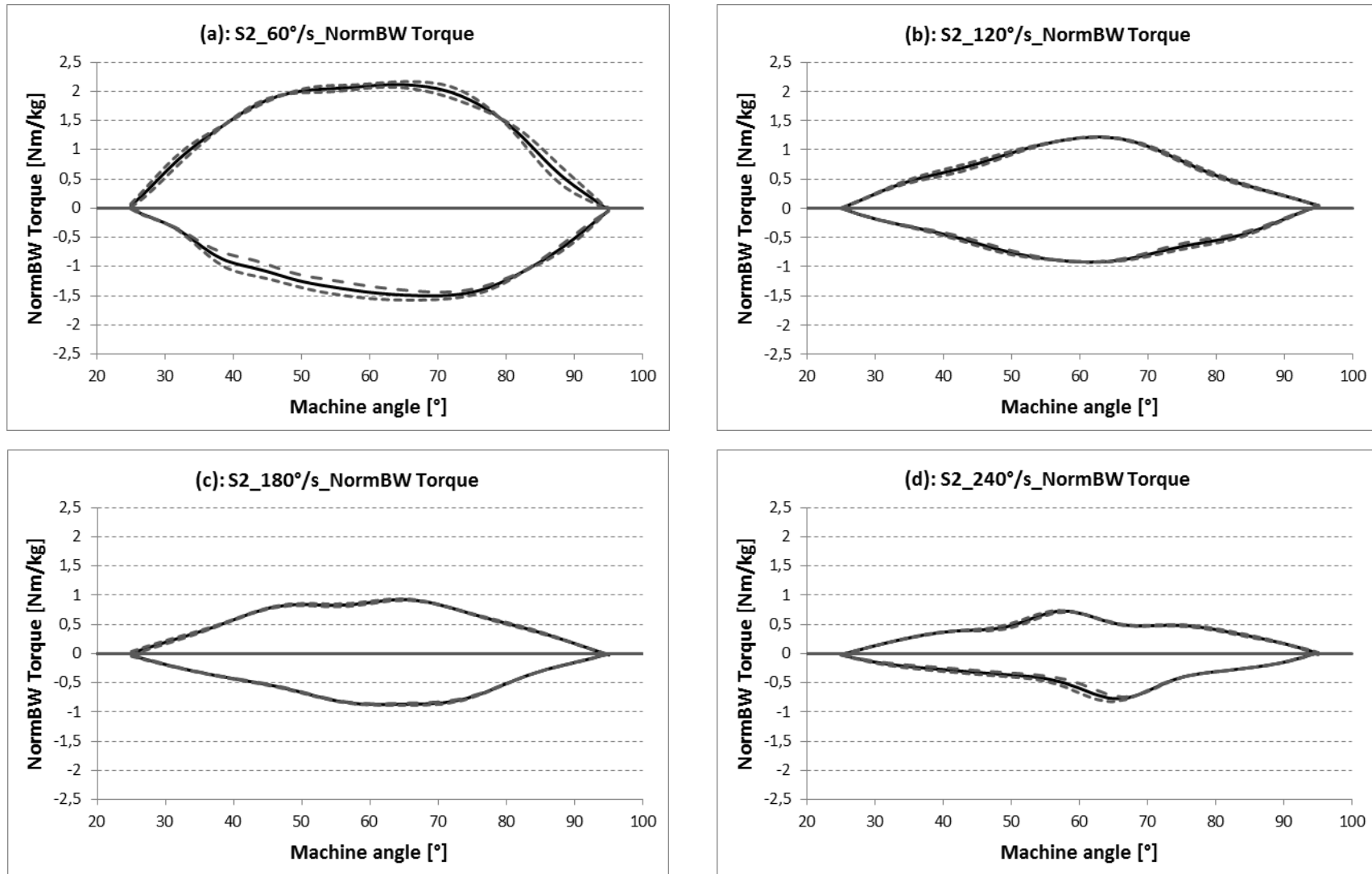


Fig.A.2.1: Normalized Torque of S2 at 60°/s (a), 120°/s (b), 180°/s (c) and 240°/s (d).

Flexors and Extensors Balance

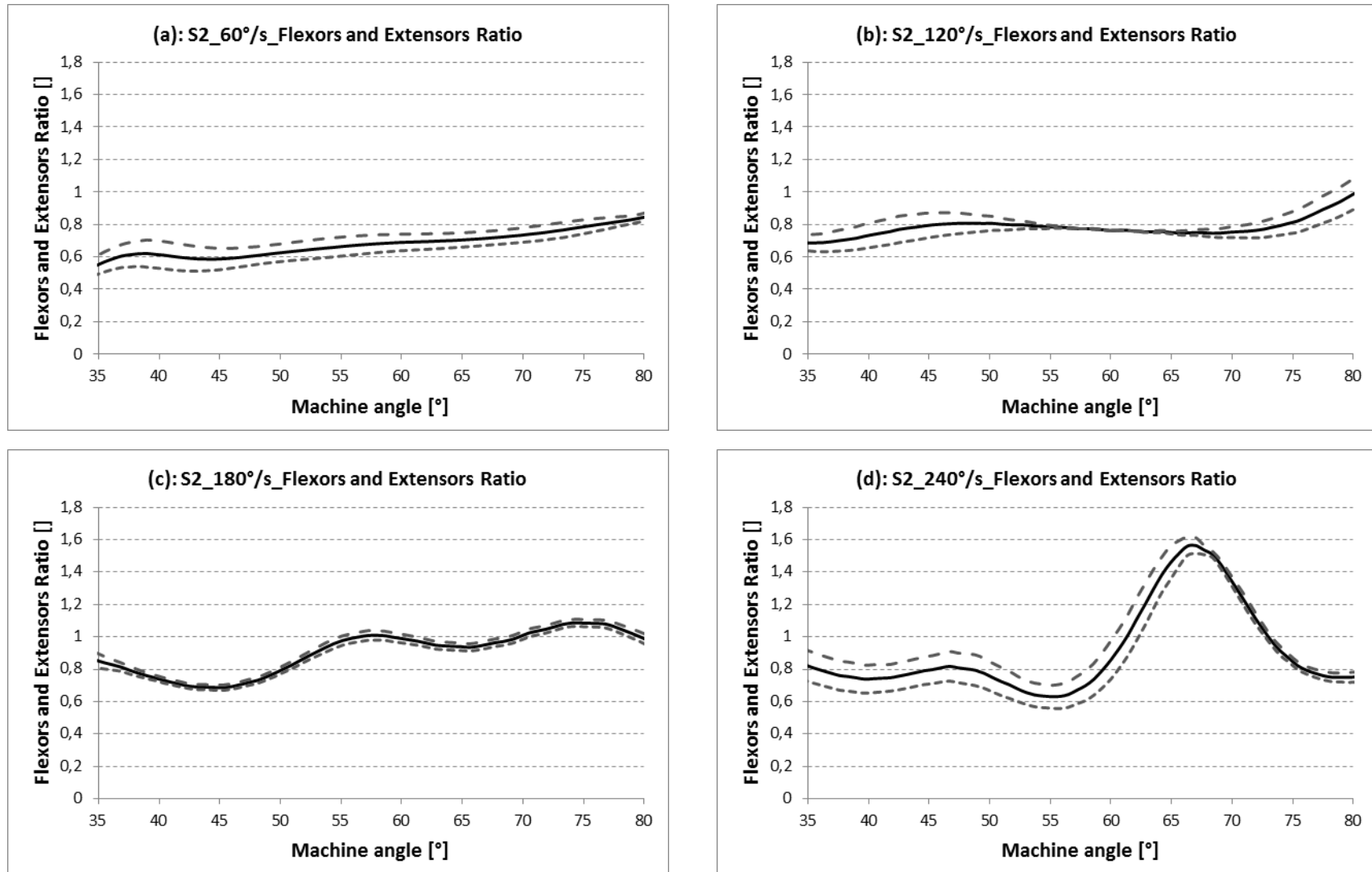


Fig.A.2.2: Flexors and extensors balance of S2 at 60°/s (a), 120°/s (b), 180°/s (c) and 240°/s (d).

Comparison of EMG signal and OpenSim muscle activation

M = 75 kg H = 1,78 m age = 27

adjust ratio for OpenSim: $\frac{SM_{S1}}{SM_{model}} = 1,315$

Maximum effort exerted in isokinetic and isometric exercises [mV]:

	Isokinetic exercise				Isometric exercise				
	60 °/s	120 °/s	180 °/s	240 °/s	ISO_25°	ISO_40°	ISO_55°	ISO_70°	ISO_95°
RF	0,354	0,204	0,187	0,181	0,205	0,171	0,236	0,206	0,103
VL	0,202	0,153	0,15	0,101	0,161	0,104	0,006	0,067	0,124
VM	0,204	0,177	0,174	0,102	0,162	0,077	0,06	0,077	0,162
BF	0,136	0,089	0,079	0,065	0,036	0,139	0,152	0,065	0,073

Tab.A.2.1: Maximum effort of S2 in [mV] during isokinetic and isometric exercises.

60 °/s

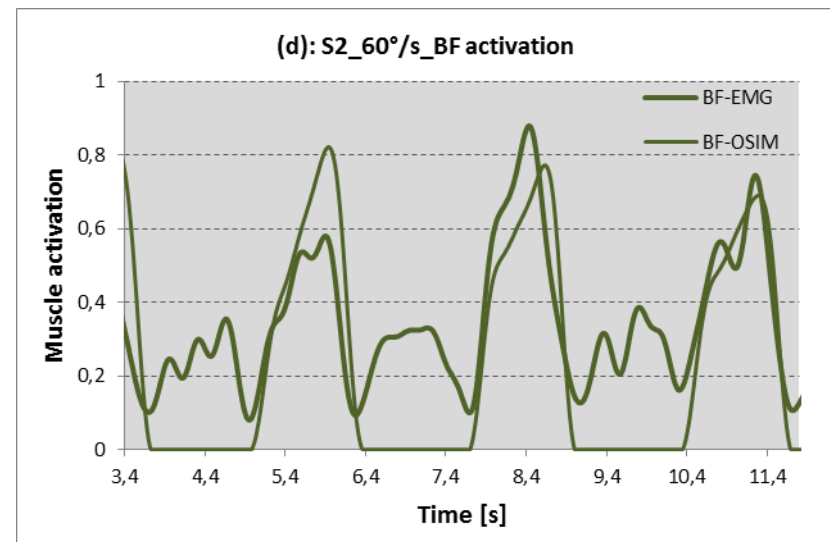
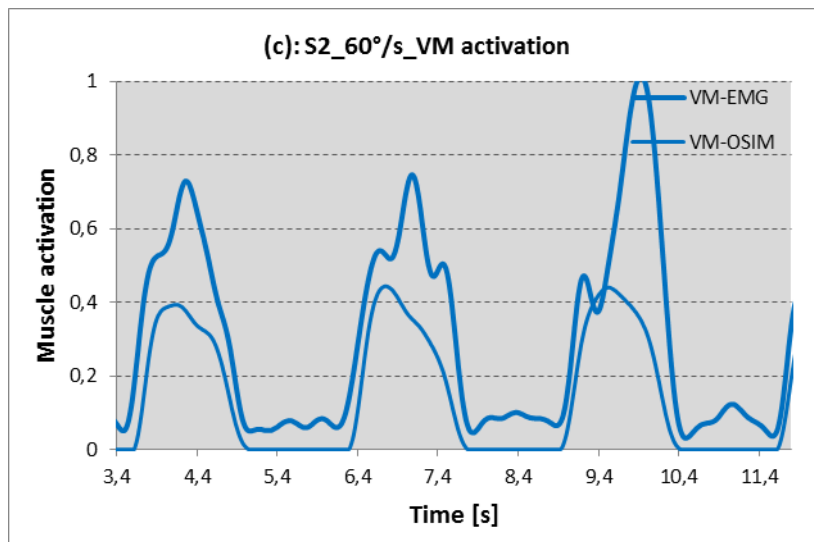
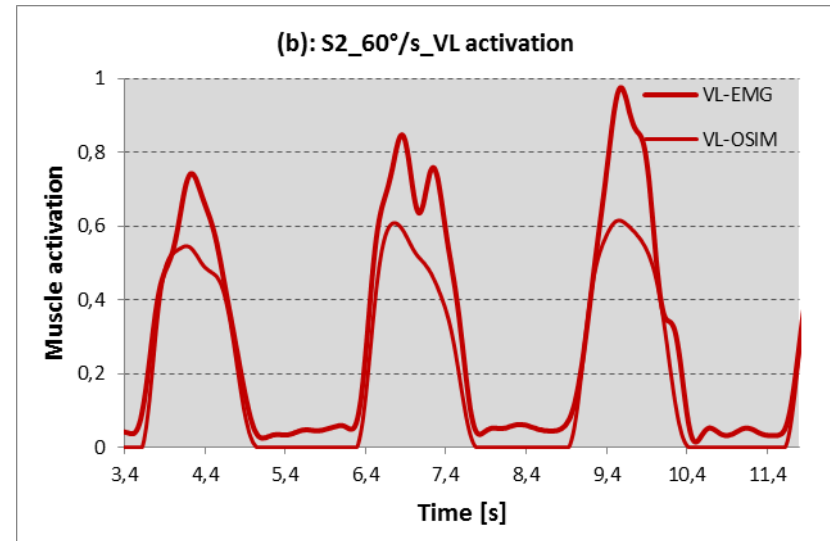
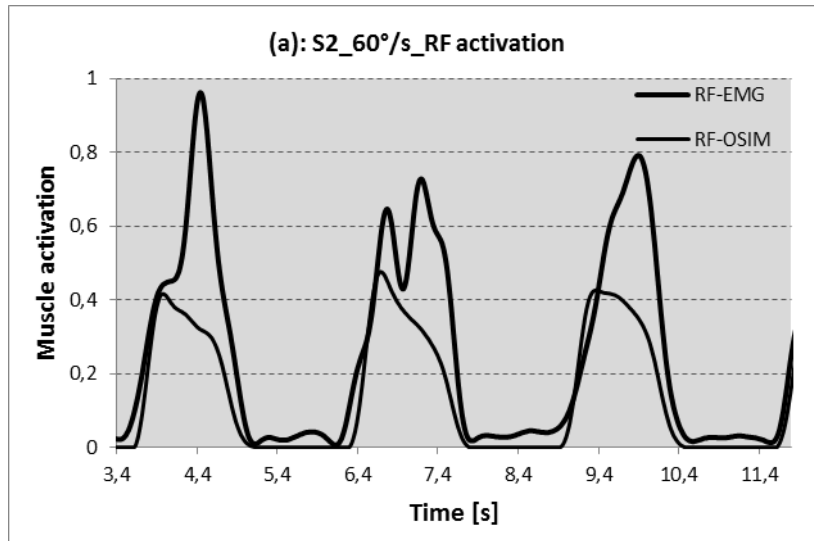


Fig.A.2.3: EMG and OpenSim muscle activation of S2 at 60°/s of RF (a), VL (b), VM (c) and BF(d).

120 °/s

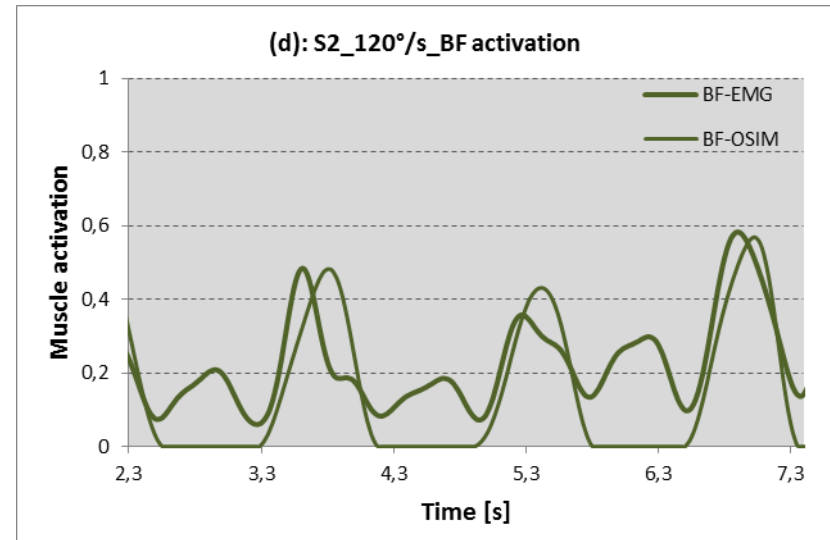
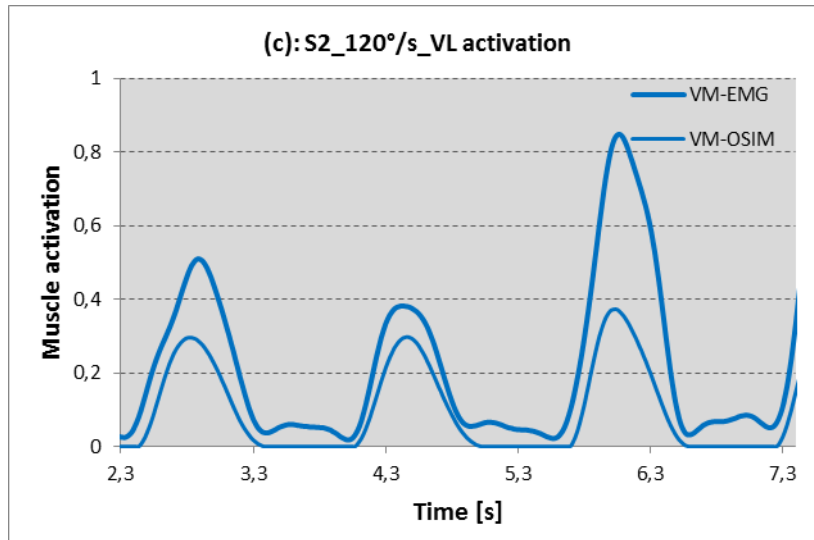
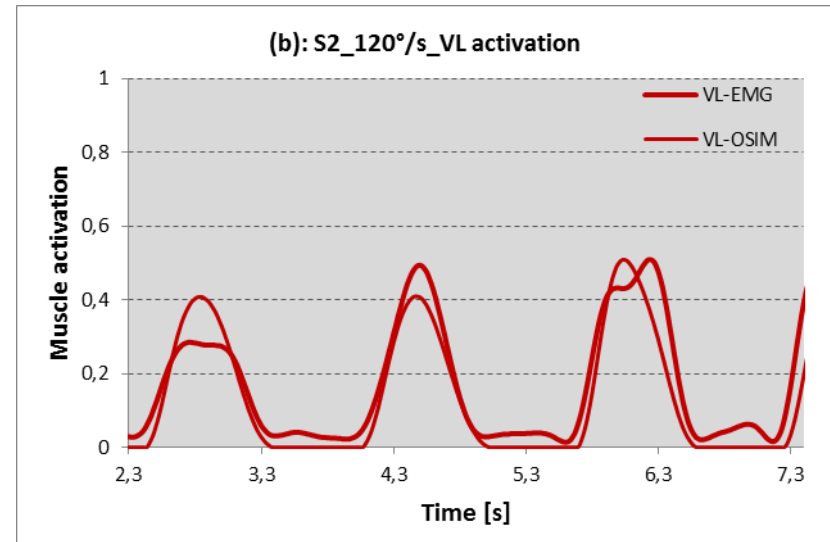
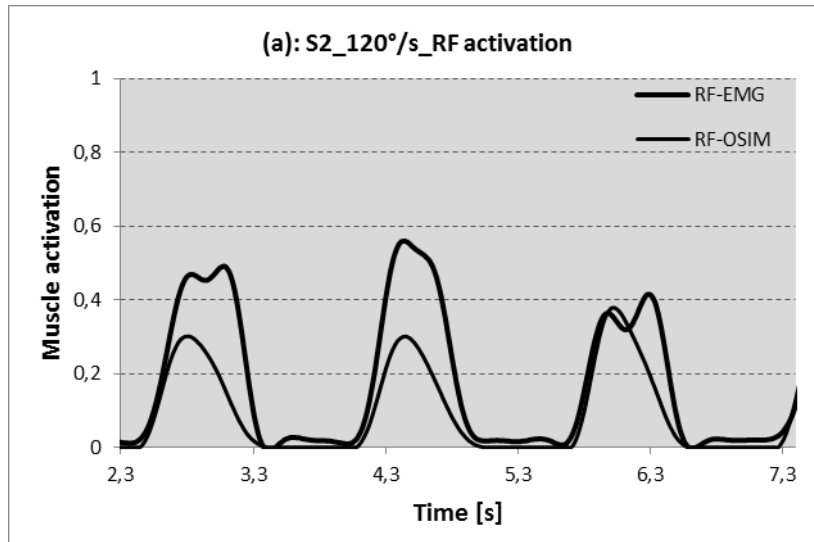


Fig.A.2.4: EMG and OpenSim muscle activation of S2 at 120°/s of RF (a), VL (b), VM (c) and BF (d).

180 °/s

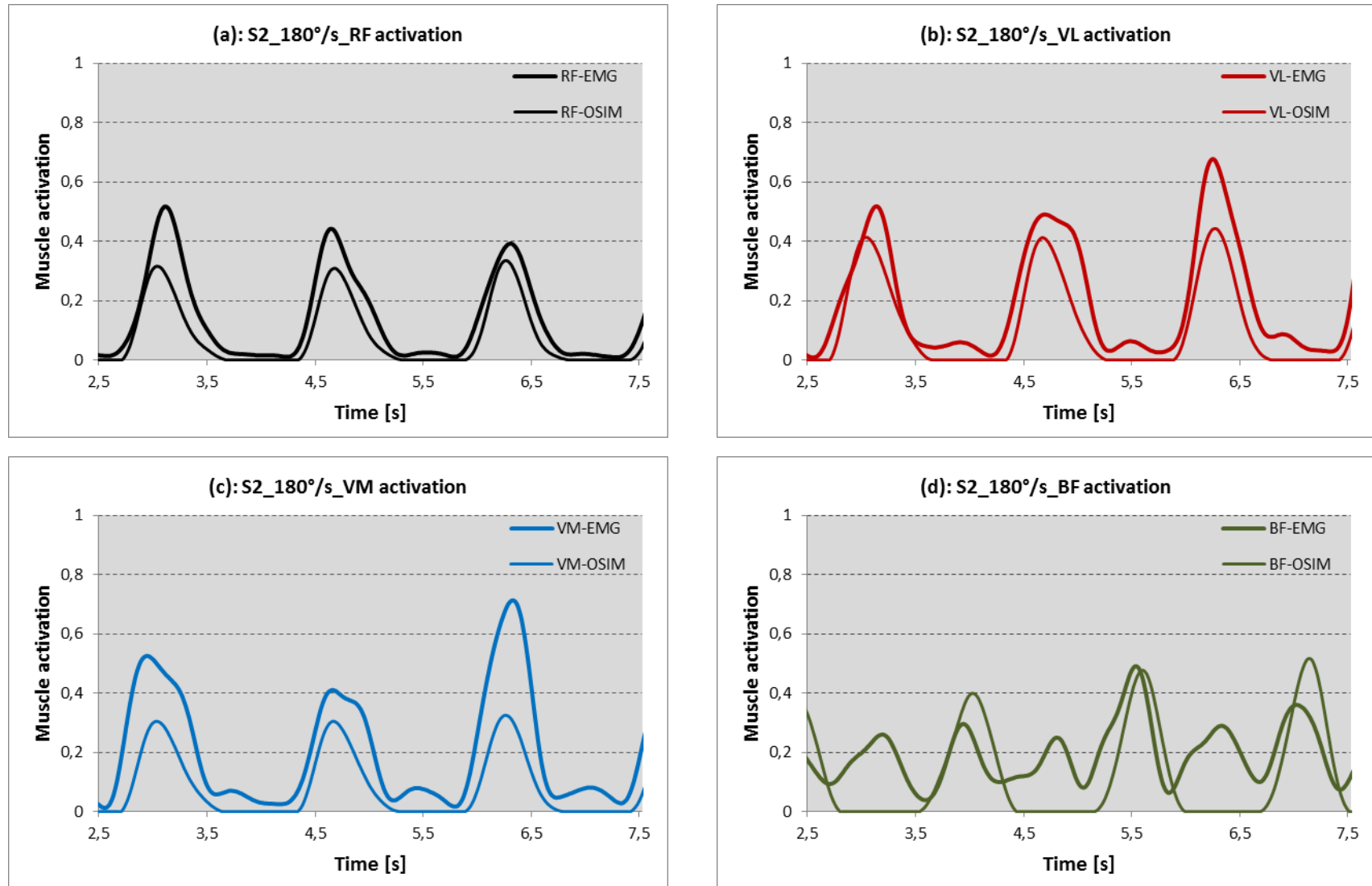


Fig.A.2.5: EMG and OpenSim muscle activation of S2 at 180°/s of RF (a), VL (b), VM (c) and BF (d).

240 °/s

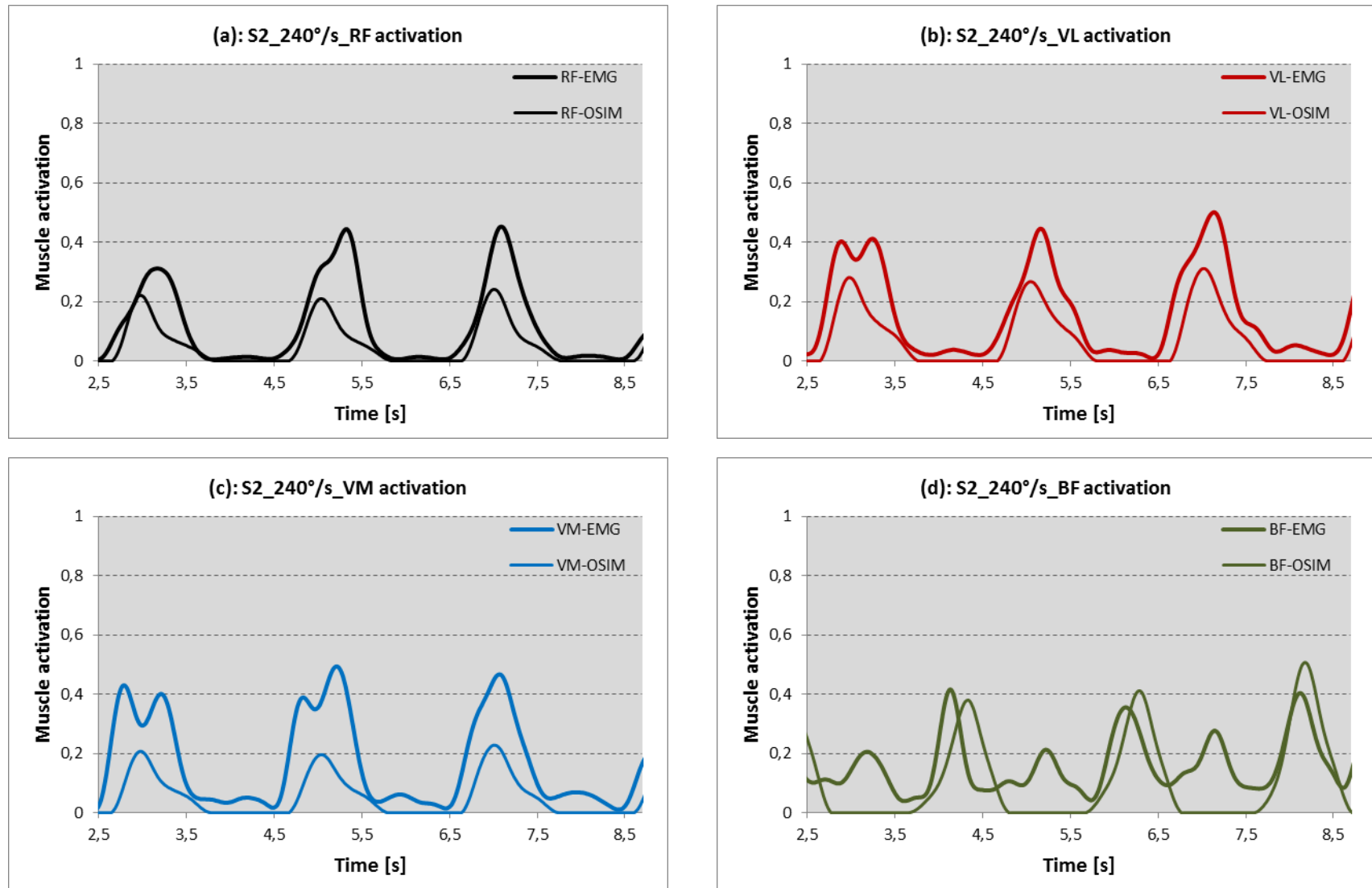


Fig.A.2.6: EMG and OpenSim muscle activation of S2 at 240°/s of RF (a), VL (b), VM (c) and BF (d).

Comparison of EMG signal and OpenSim muscle activation: quantitative results

	60 °/s	120 °/s	180 °/s	240 °/s
RF	45,79±11,10	31,18±19,84	27,84±12,32	42,77±12,35
VL	30,56±5,57	-8,72±31,01	23,58±9,75	36,52±4,36
VM	47,76±8,10	39,99±17,10	40,64±14,45	54,45±5,09
BF	-7,29±29,77	-5,80±12,68	-25,09±24,57	-10,86±17,59

Tab.A.2.2: Peak error of S2 in [%] of RF, VL, VM and BF at 60°/s, 120°/s, 180°/s and 240°/s.

	60 °/s	120 °/s	180 °/s	240 °/s
RF	17,77±2,27	9,75±9,27	41,97±9,22	8,37±5,81
VL	3,64±2,90	1,30±11,85	29,68±12,07	7,70±4,54
VM	9,27±4,67	0,33±2,96	66,33±11,90	0,74±7,44
BF	-3,87±3,63	-8,40±1,87	-20,93±9,08	-7,13±1,86

Tab.A.2.3: Time error of S2 in [%] of RF, VL, VM and BF at 60°/s, 120°/s, 180°/s and 240°/s.

	60 °/s	120 °/s	180 °/s	240 °/s
RF	40,69±3,84	42,01±13,10	41,97±9,22	45,42±7,42
VL	18,64±9,70	1,82±14,90	29,68±12,07	53,43±5,37
VM	43,36±6,76	57,04±9,05	66,33±11,90	63,23±3,24
BF	-13,83±16,80	6,23±10,46	-20,93±9,08	-6,92±4,71

Tab.A.2.4: Area error of S2 in [%] of RF, VL, VM and BF at 60°/s, 120°/s, 180°/s and 240°/s.

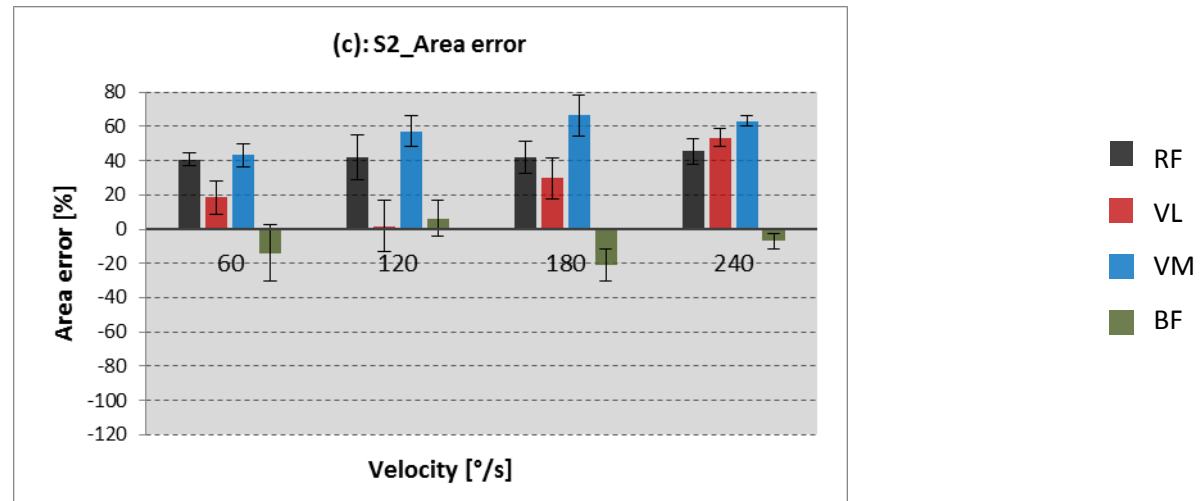
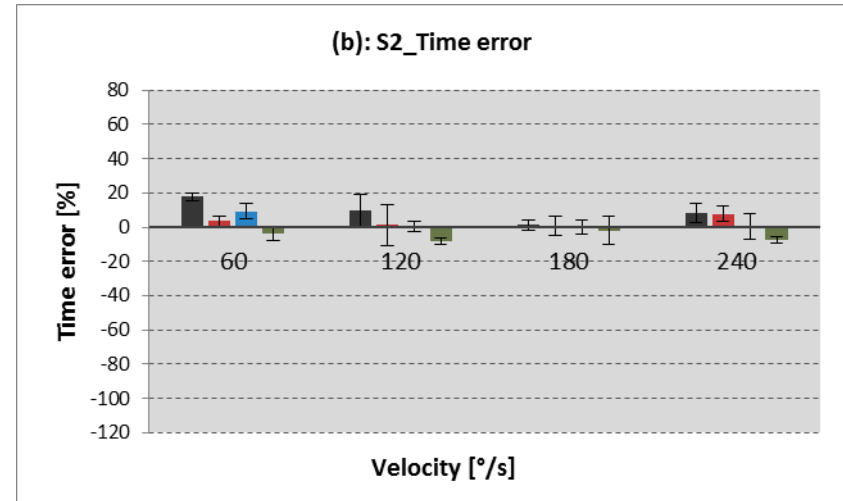
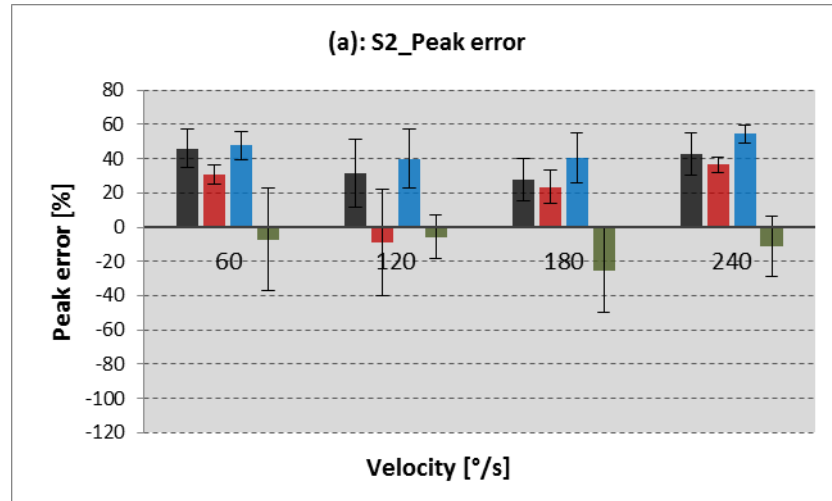


Fig.A.2.7: Quantitative results of muscle activation analysis of S2: (a): Peak error at different velocities; (b): Time error at different velocities;(c): Area error at different velocities.

Comparison of analytical models and OpenSim model

Model 1: parameters

$$\text{Tibia: } m_{\text{tibia}} = 3,7 \text{ kg} \quad I_{G \text{ tibia}} = 0,066 \text{ kg} \cdot \text{m}^2 \quad \Delta_{y \text{ tibia}} = 0,488 \text{ m} \quad \Delta_{y \text{ G tibia}} = 0,212 \text{ m}$$

$$\text{Talus: } m_{\text{talus}} = 0,1 \text{ kg} \quad I_{G \text{ talus}} = 9 \cdot 10^{-4} \text{ kg} \cdot \text{m}^2 \quad \Delta_{y \text{ talus}} = 0,488 \text{ m} \quad \Delta_{y \text{ G talus}} = 0,488 \text{ m}$$

$$\text{Calc: } m_{\text{calc}} = 1,247 \text{ kg} \quad I_{G \text{ calc}} = 0,0037 \text{ kg} \cdot \text{m}^2 \quad \Delta_{x \text{ calc}} = 0,0463 \text{ m} \quad \Delta_{y \text{ calc}} = 0,04 \text{ m}$$

$$\Delta_{x \text{ G calc}} = 0,095 \text{ m} \quad \Delta_{y \text{ G calc}} = 0,028 \text{ m}$$

$$\text{Toes: } m_{\text{toes}} = 0,216 \text{ kg} \quad I_{G \text{ toes}} = 9 \cdot 10^{-5} \text{ kg} \cdot \text{m}^2 \quad \Delta_{x \text{ toes}} = 0,17 \text{ m} \quad \Delta_{y \text{ toes}} = 0,0019 \text{ m}$$

$$\Delta_{x \text{ G toes}} = 0,033 \text{ m} \quad \Delta_{y \text{ G toes}} = 0,0057 \text{ m}$$

Model 2: parameters

$$\text{Tibia: } m_{\text{tibia}} = 3,375 \text{ kg} \quad I_{G \text{ tibia}} = 0,052 \text{ kg} \cdot \text{m}^2 \quad \Delta_{y \text{ tibia}} = 0,413 \text{ m} \quad \Delta_{y \text{ G tibia}} = 0,179 \text{ m}$$

$$\text{Foot: } m_{\text{foot}} = 1,05 \text{ kg} \quad I_{G \text{ foot}} = 0,006 \text{ kg} \cdot \text{m}^2 \quad \Delta_{x \text{ G foot}} = 0,071 \text{ m} \quad \Delta_{y \text{ G foot}} = 0,035 \text{ m}$$

$$D_{Q2} = 0,085 \text{ m} \quad H_{Q2} = 0,0276 \text{ m} \quad D_{Q1} = 0,319 \text{ m} \quad H_{Q1} = 0,032 \text{ m}$$

$$B_{PT} [\text{m}] = (0,0097 \cdot \varphi_{k+}^5 - 0,0215 \cdot \varphi_{k+}^4 - 0,0098 \cdot \varphi_{k+}^3 + 0,0366 \cdot \varphi_{k+}^2 - 0,0141 \cdot \varphi_{k+} + 0,0464) \cdot 1,06 \quad \varphi_{k+} [\text{rad}]$$

$$\text{BFB: } D_{\text{BFB1}} = 0,2125 \text{ m} \quad D_{\text{BFB2}} = 0,0425 \text{ m} \quad H_{\text{BFB1}} = 0,0425 \text{ m} \quad H_{\text{BFB2}} = 0,0319 \text{ m}$$

$$\text{BFL: } D_{\text{BFL1}} = 0,5206 \text{ m} \quad D_{\text{BFL2}} = 0,0425 \text{ m} \quad H_{\text{BFL1}} = 0,0425 \text{ m} \quad H_{\text{BFL2}} = 0,0319 \text{ m}$$

$$\text{SM: } D_{\text{SM1}} = 0,5206 \text{ m} \quad D_{\text{SM2}} = 0,0531 \text{ m} \quad H_{\text{SM1}} = 0,0425 \text{ m} \quad H_{\text{SM2}} = 0,0372 \text{ m}$$

$$\text{ST: } D_{\text{ST1}} = 0,5206 \text{ m} \quad H_{\text{ST1}} = 0,0531 \text{ m} \quad B_{\text{ST}} = 0,0425 \text{ m} \quad \alpha_{\text{ST}} = 0,52 \text{ rad}$$

Fig.A.2.8: S2_60°/s_Extension

— OSIM — Mod1_Herzog — Mod1_Van Eijden — Mod2 - - - limit value

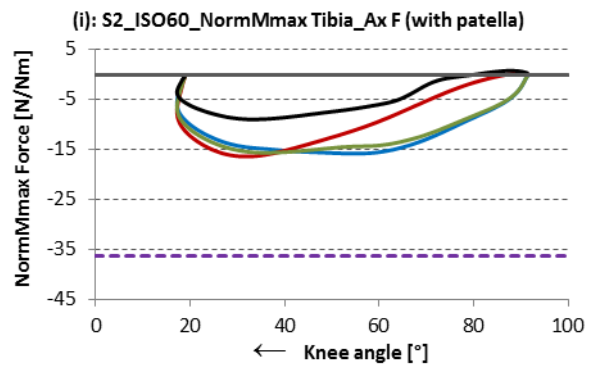
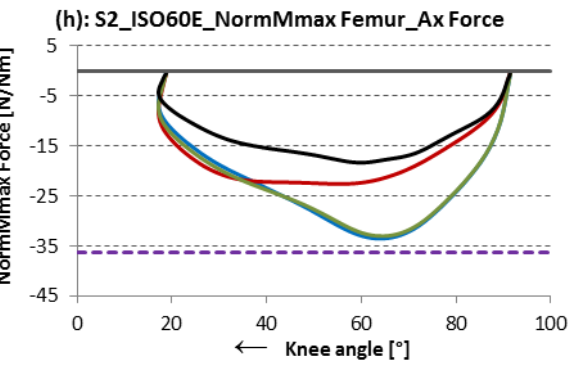
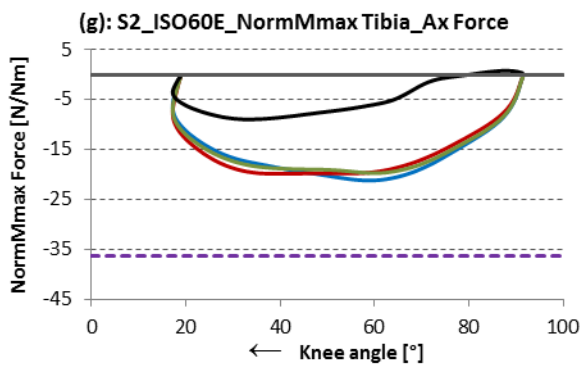
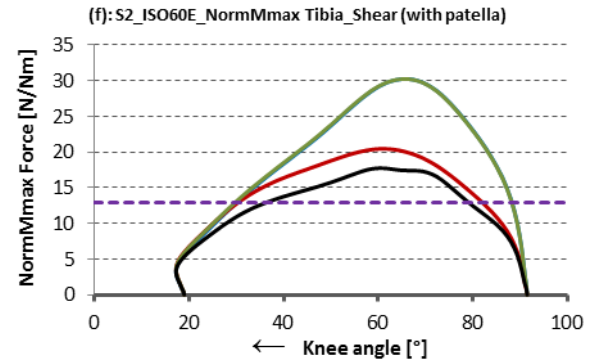
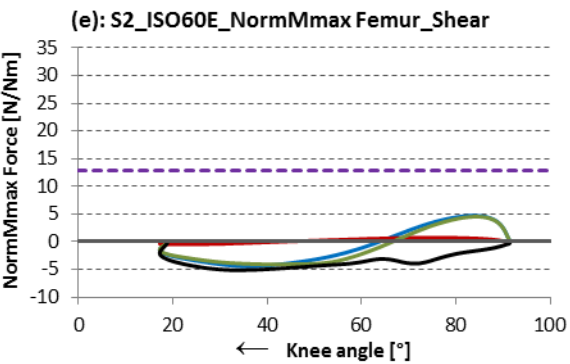
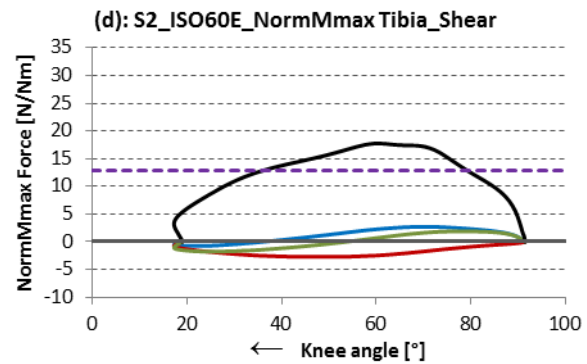
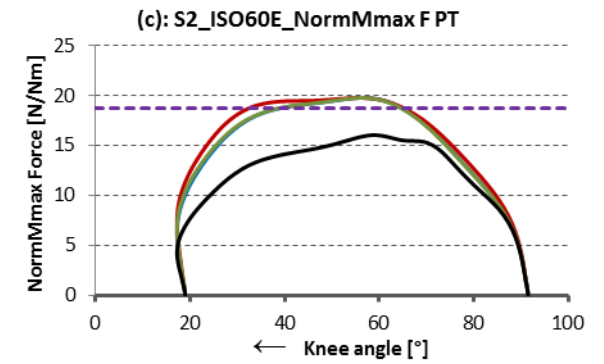
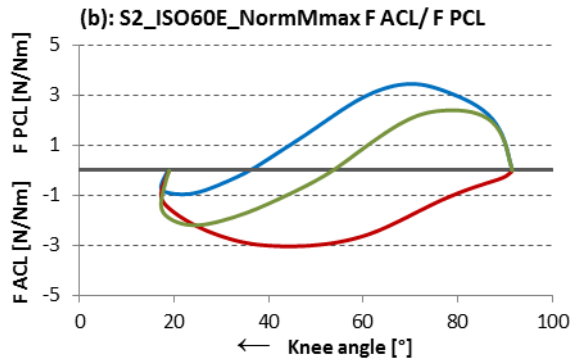
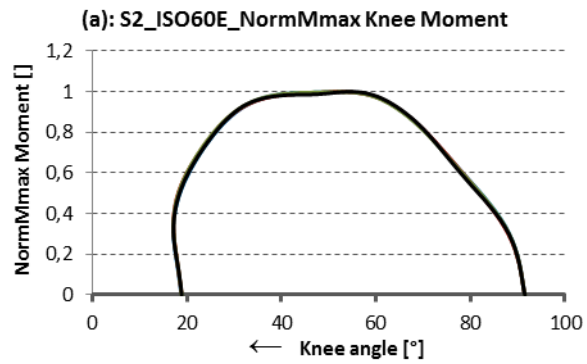


Fig.A.2.9: S2_60°/s_Flexion

— OSIM — Mod1 — Mod2 - - - limit value (•••• OSIM BFL •••• Mod1 BFL •••• Mod2 BFL)

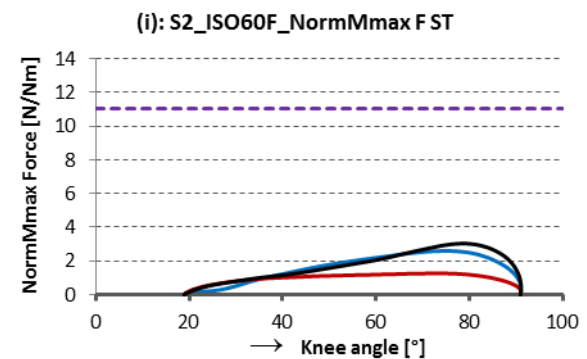
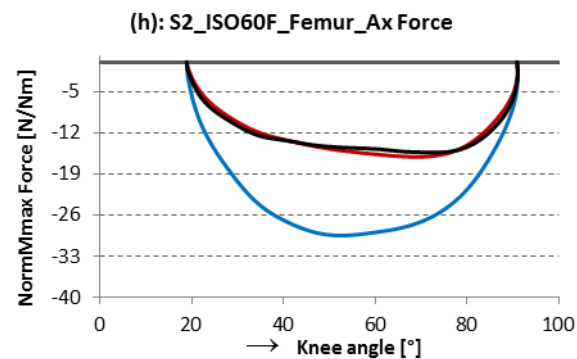
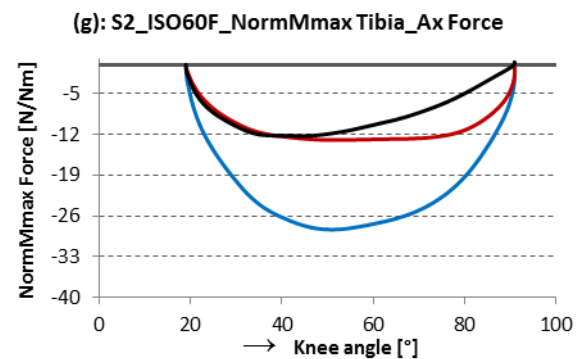
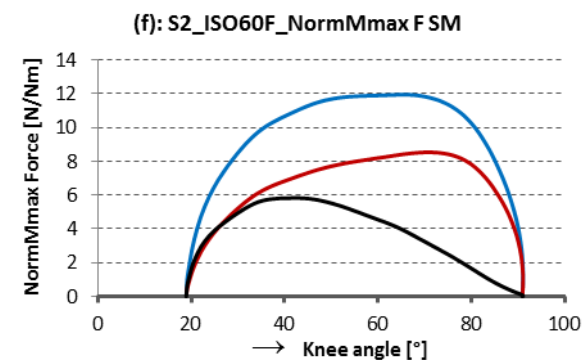
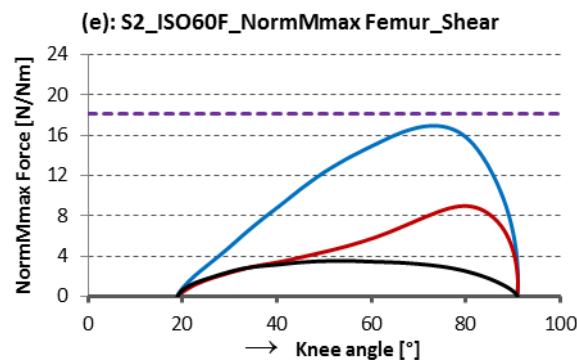
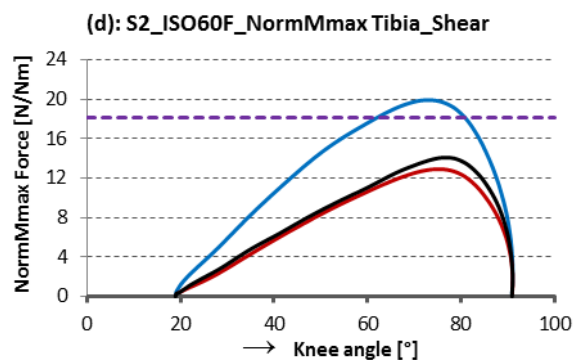
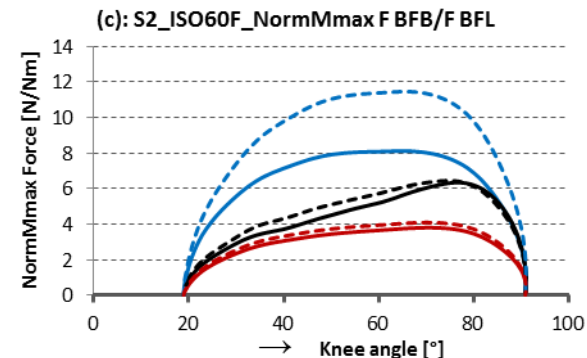
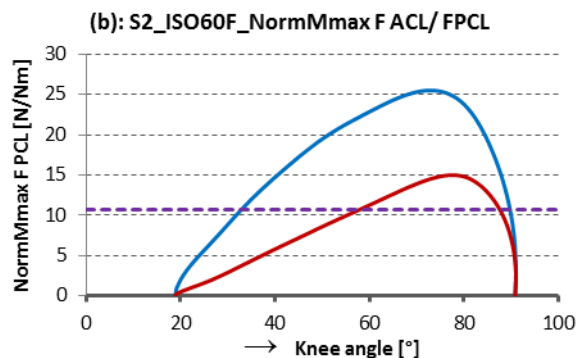
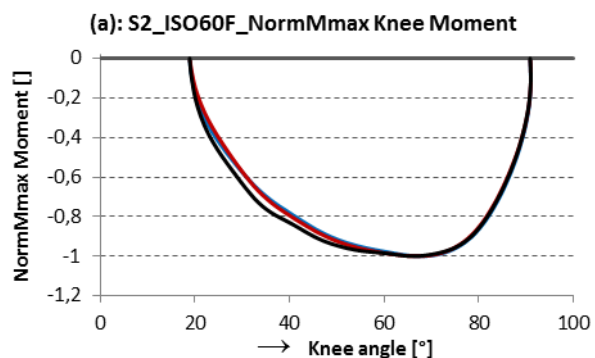


Fig.A.2.10: S2_120°/s_Extension

— OSIM — Mod1_Herzog — Mod1_Van Eijden — Mod2 - - - - limit value

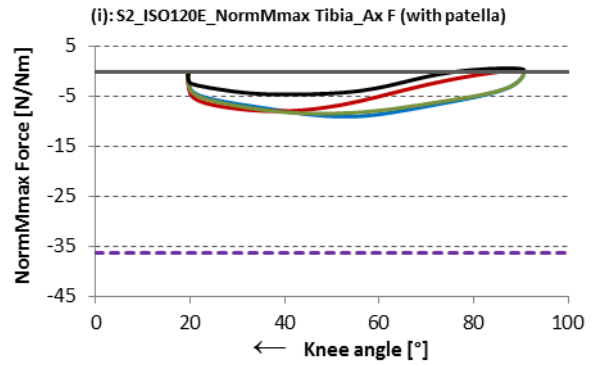
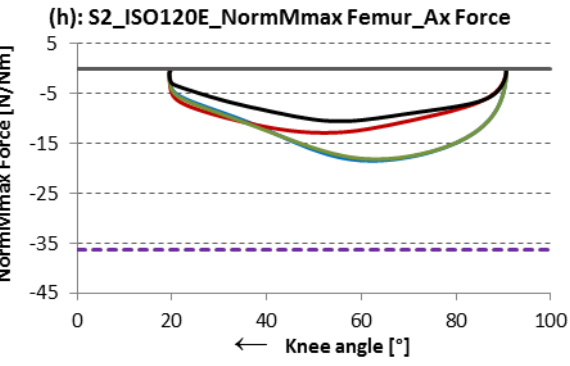
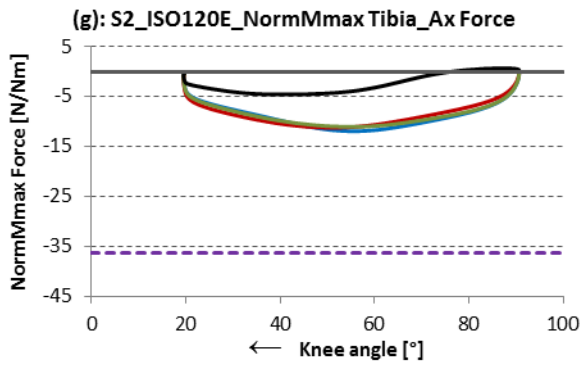
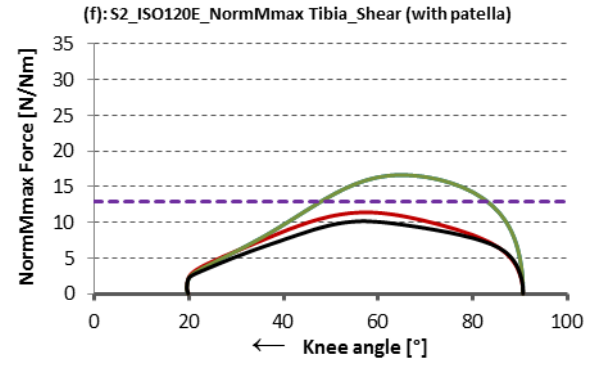
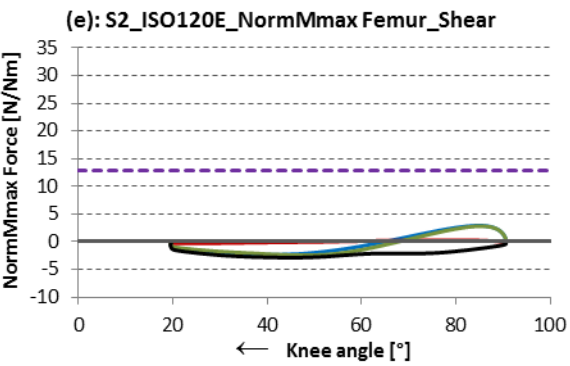
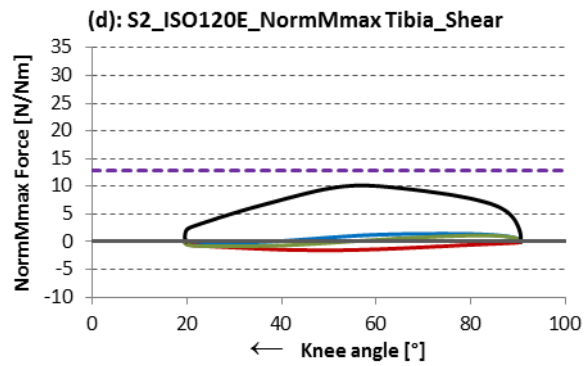
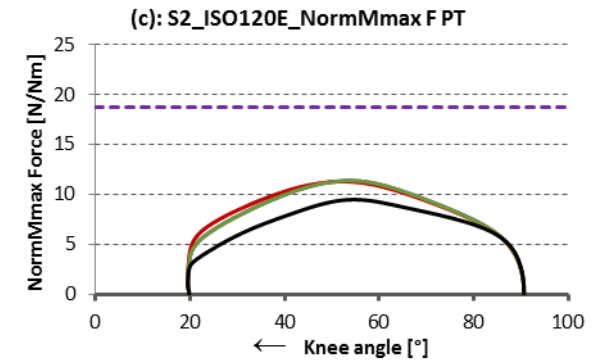
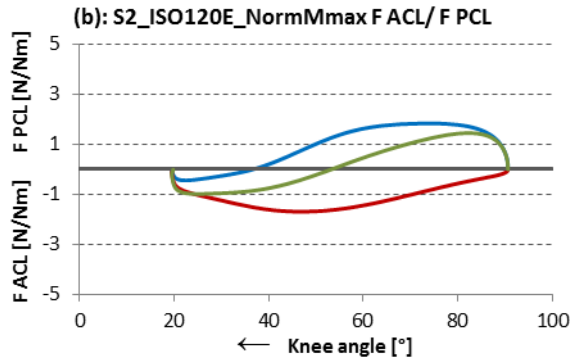
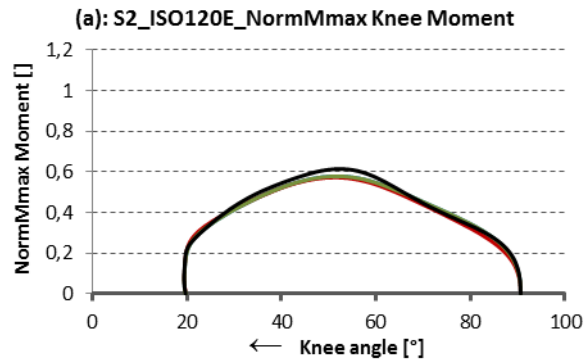


Fig.A.2.11: S2_120°/s_Flexion

— OSIM — Mod1 — Mod2 - - - - limit value (- - - - OSIM BFL - - - - Mod1 BFL - - - - Mod2 BFL)

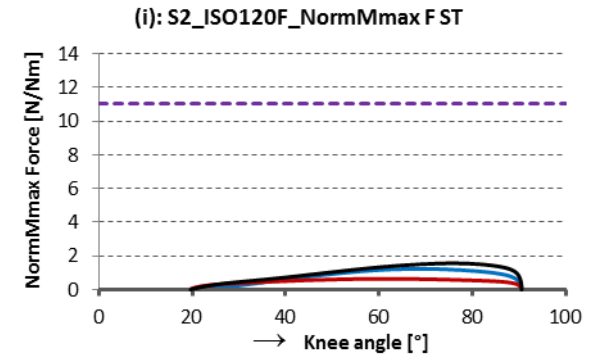
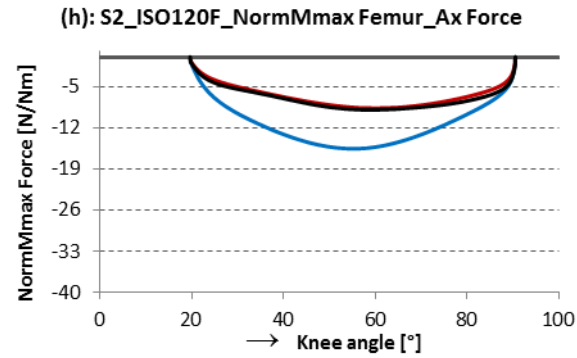
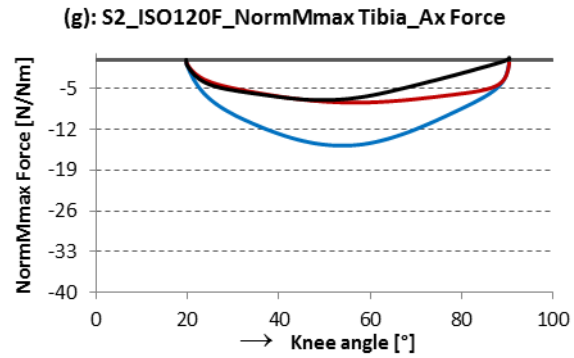
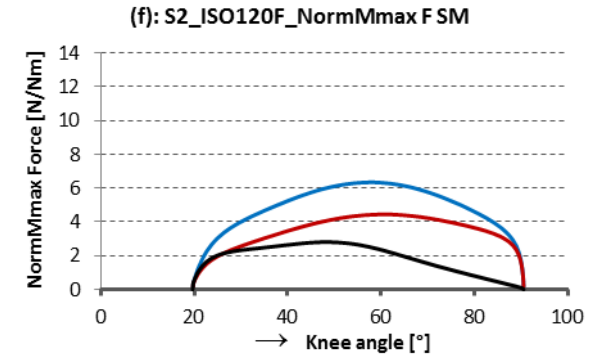
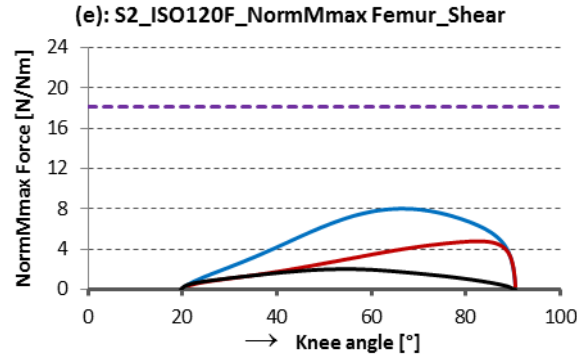
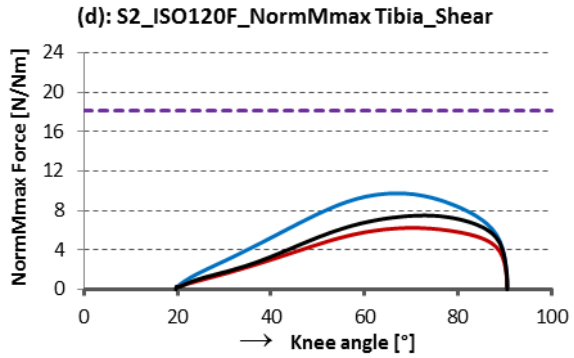
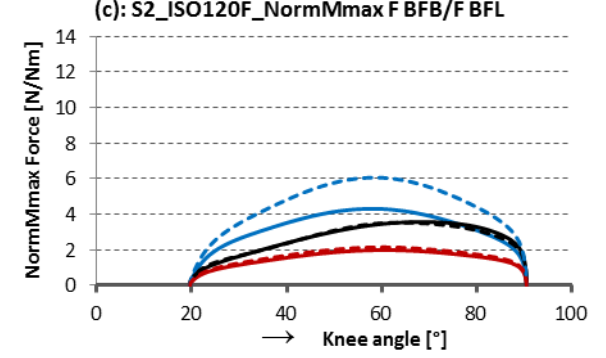
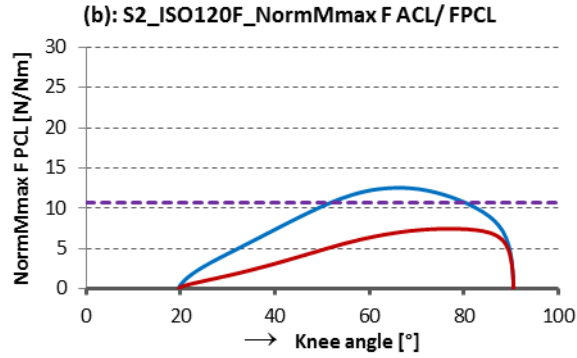
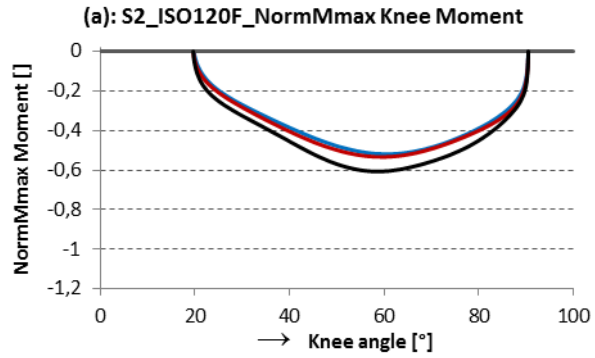


Fig.A.2.12: S2_180°/s_Extension

— OSIM — Mod1_Herzog — Mod1_Van Eijden — Mod2 - - - - limit value

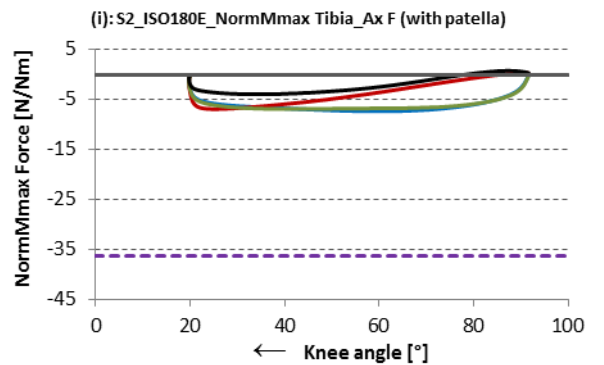
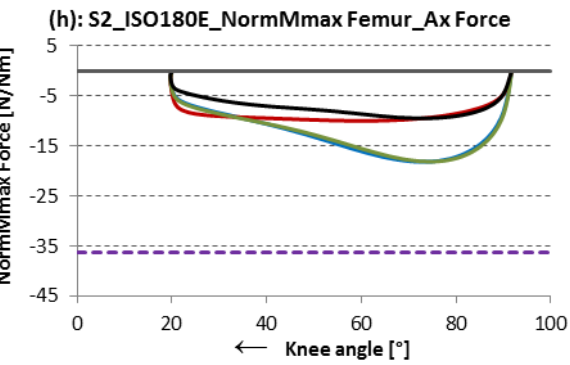
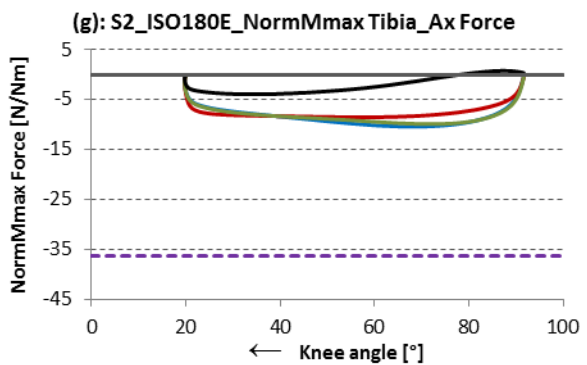
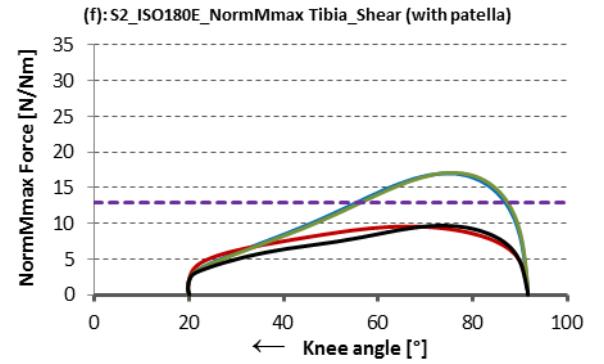
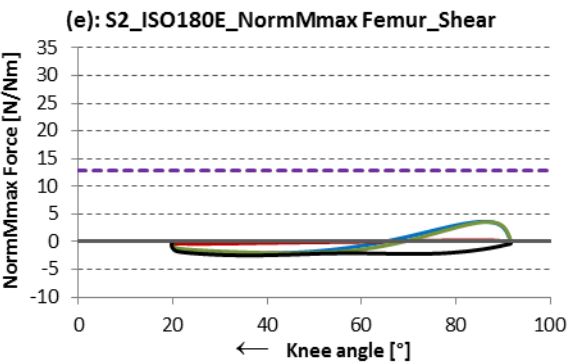
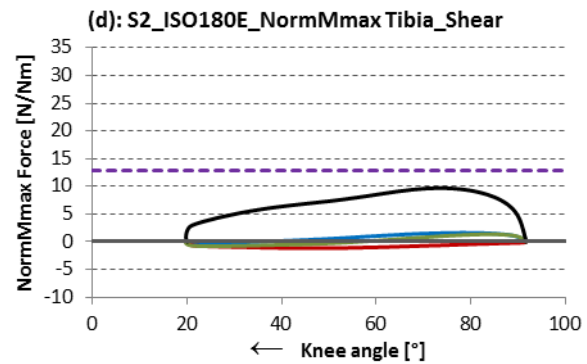
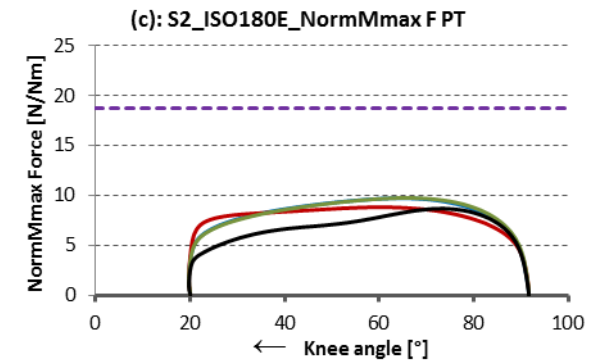
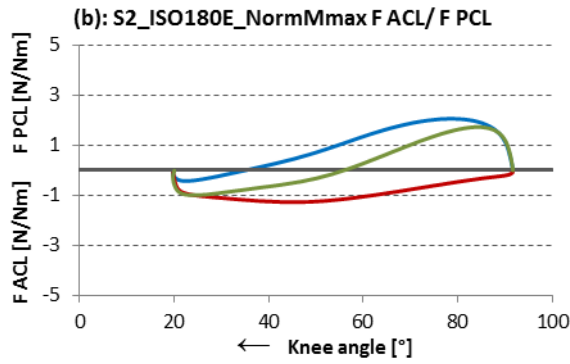
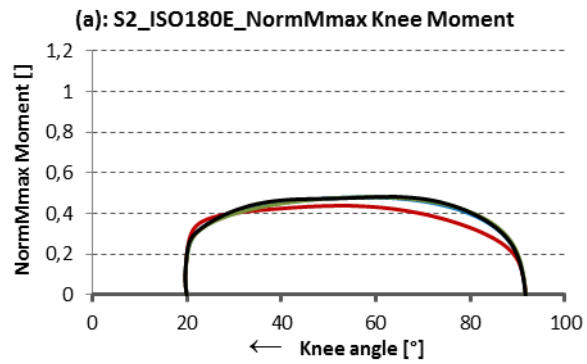


Fig.A.2.13: S2_180°/s_Flexion

— OSIM — Mod1 — Mod2 - - - limit value (- - - OSIM BFL - - - Mod1 BFL - - - Mod2 BFL)

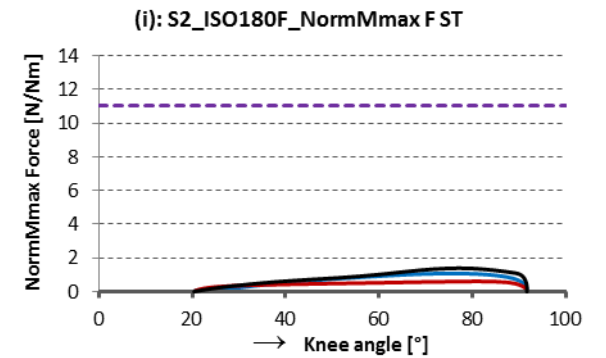
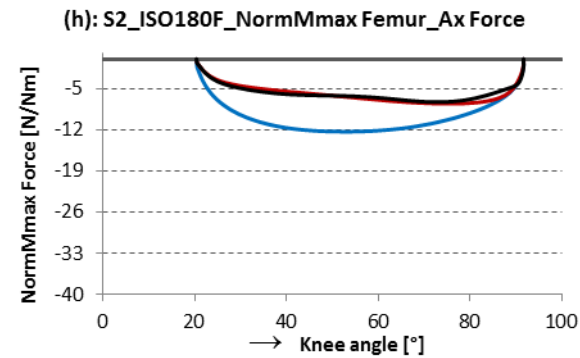
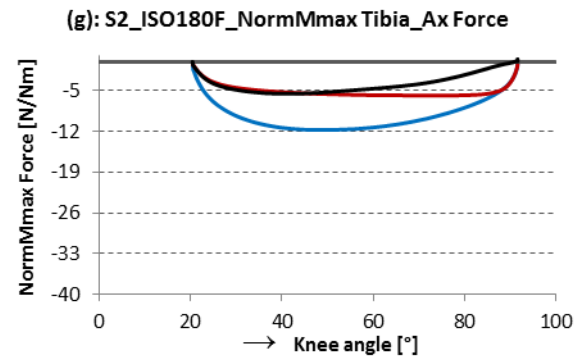
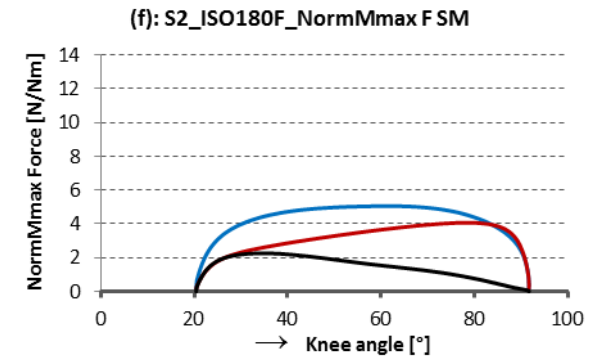
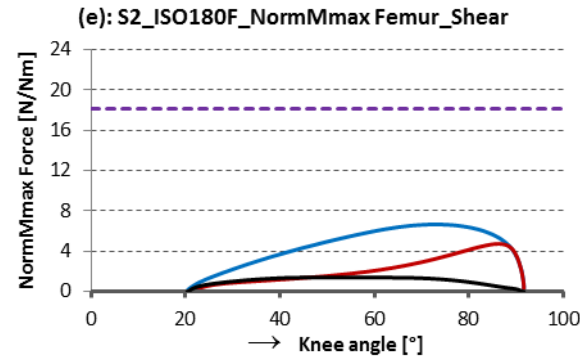
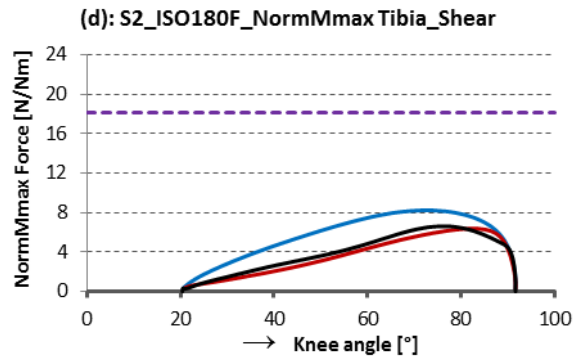
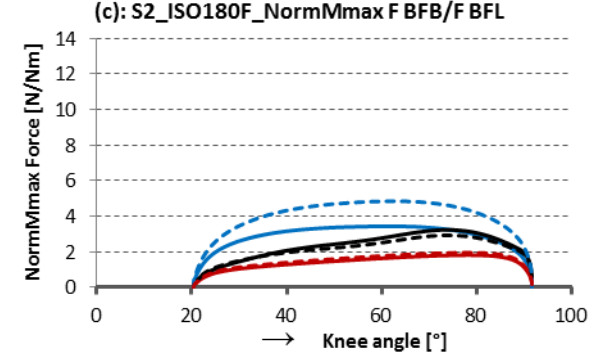
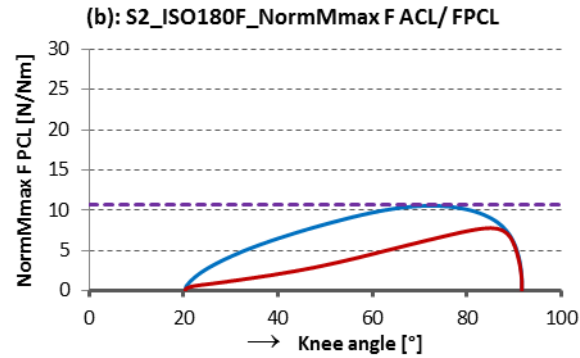
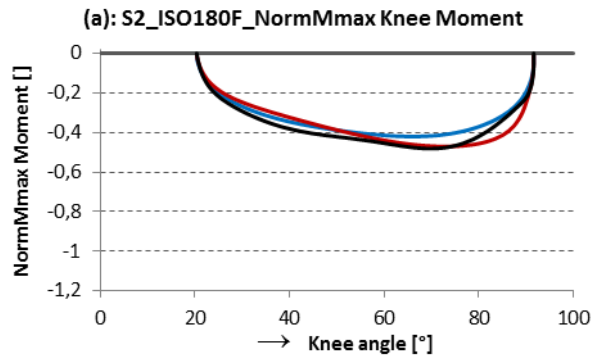


Fig.A.2.14: S2_240°/s_Extension

— OSIM — Mod1_Herzog — Mod1_Van Eijden — Mod2 - - - limit value

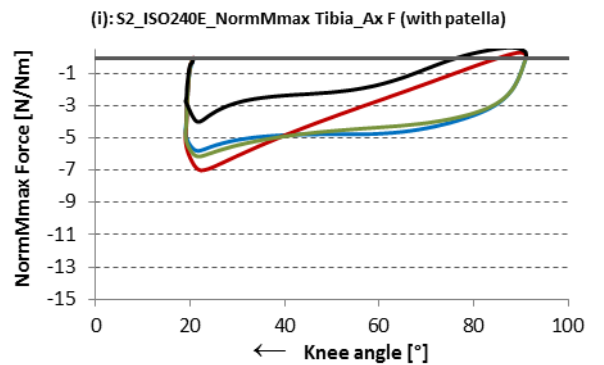
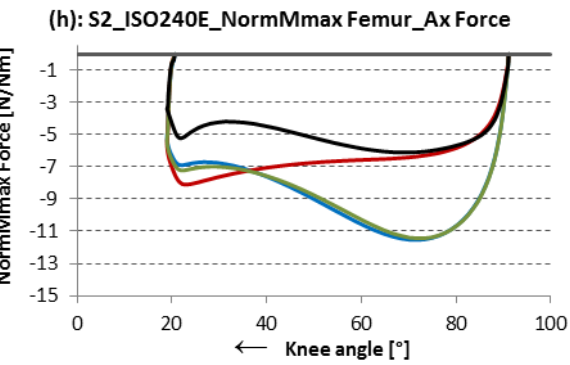
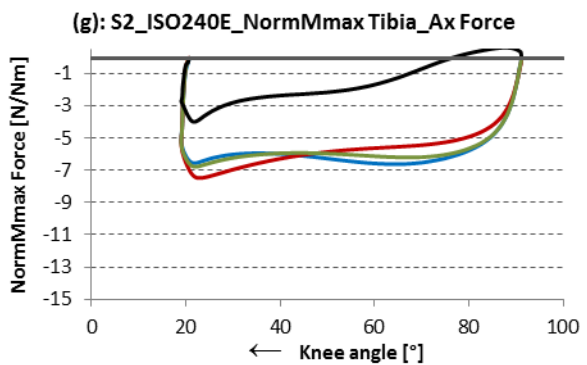
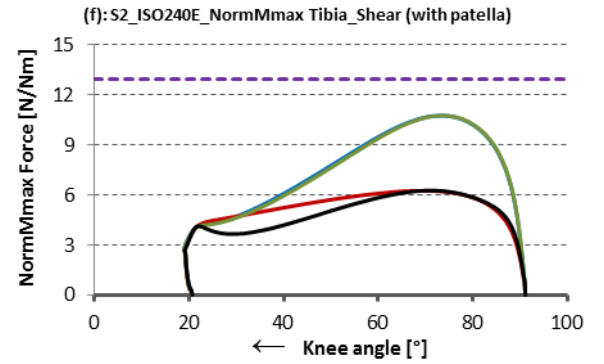
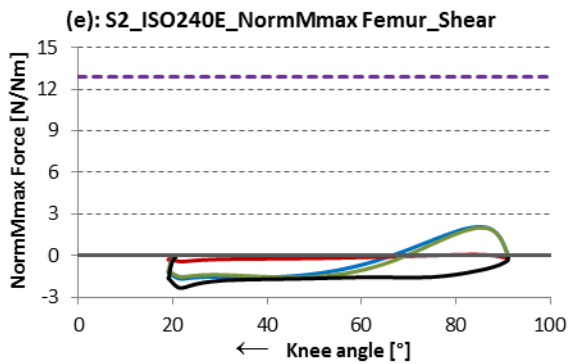
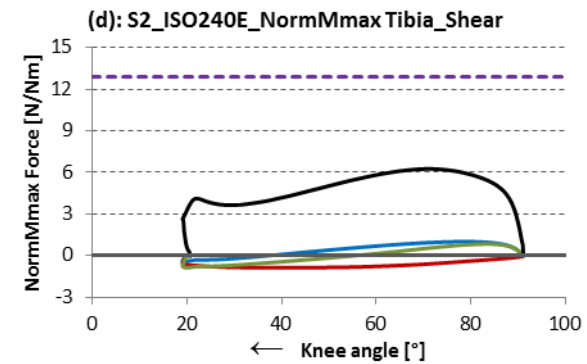
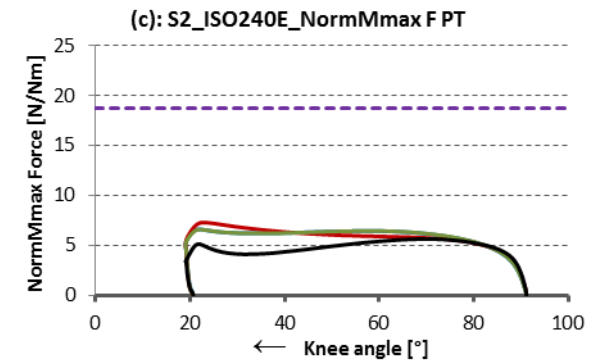
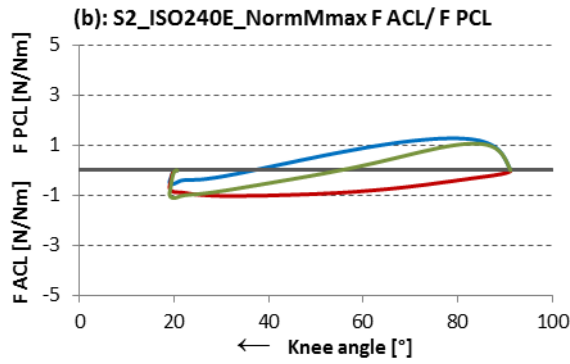
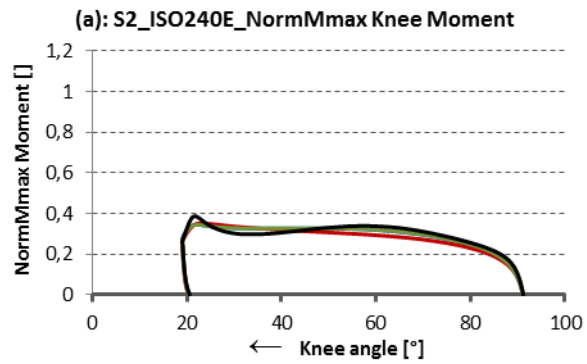
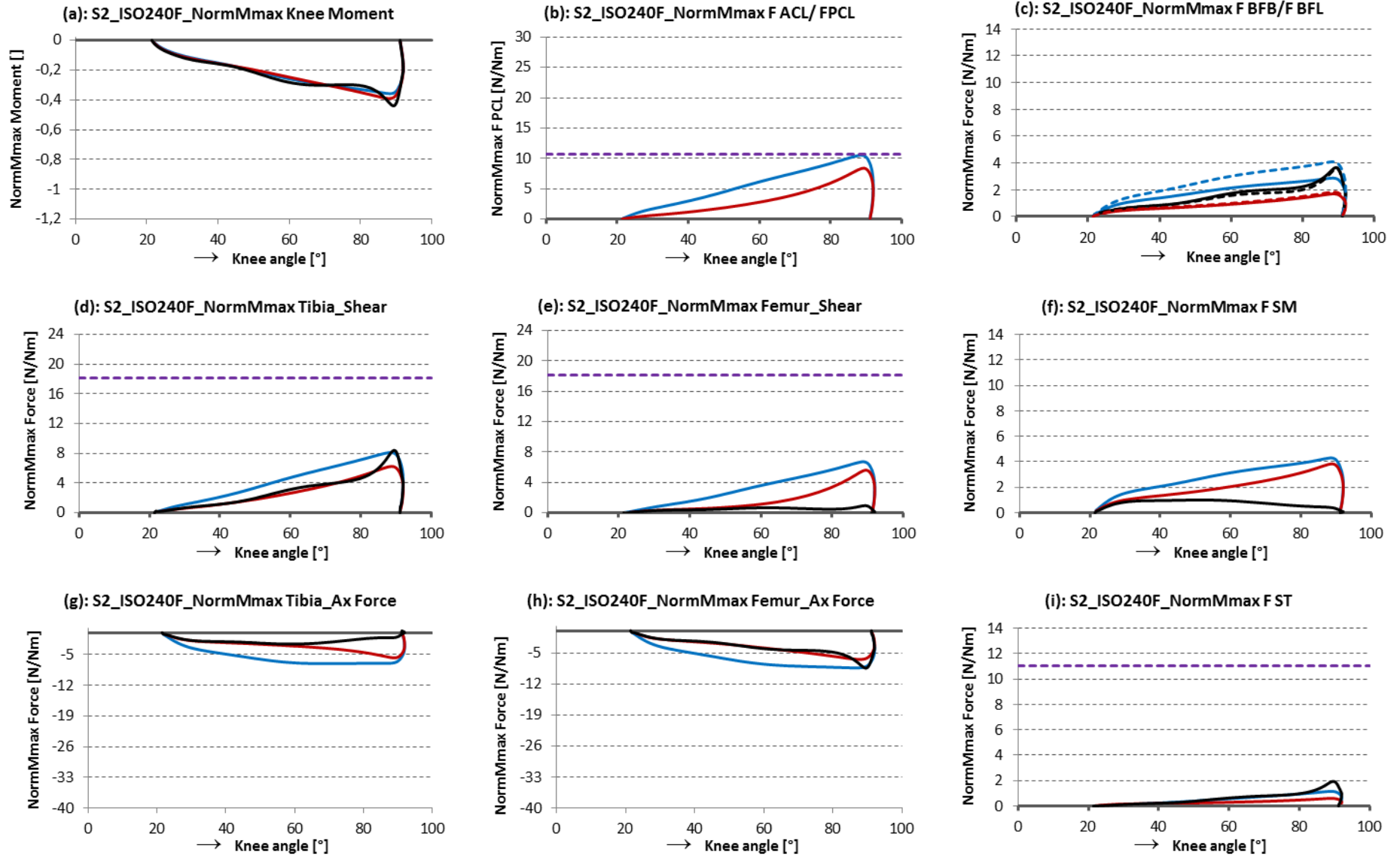


Fig.A.2.15: S2_240°/s_Flexion

— OSIM — Mod1 — Mod2 - - - - limit value (•••• OSIM BFL •••• Mod1 BFL •••• Mod2 BFL)



A.3.Results of Subject 3 (S3)

Torque at the servo-motor

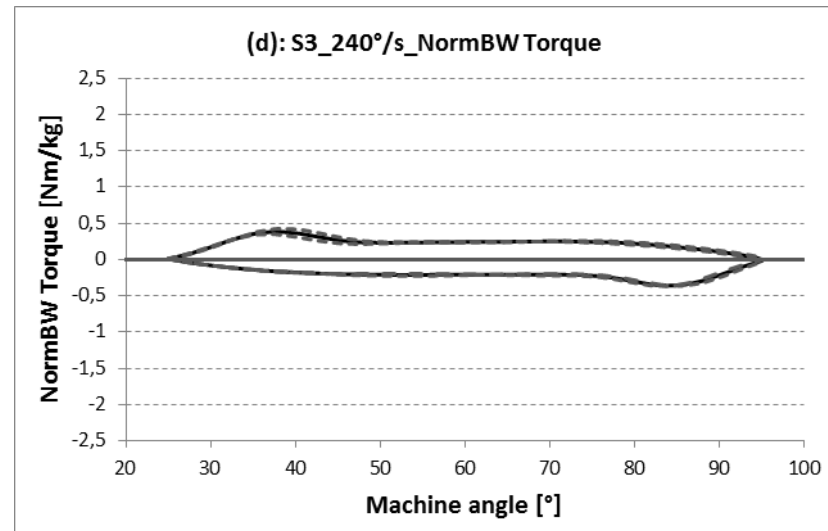
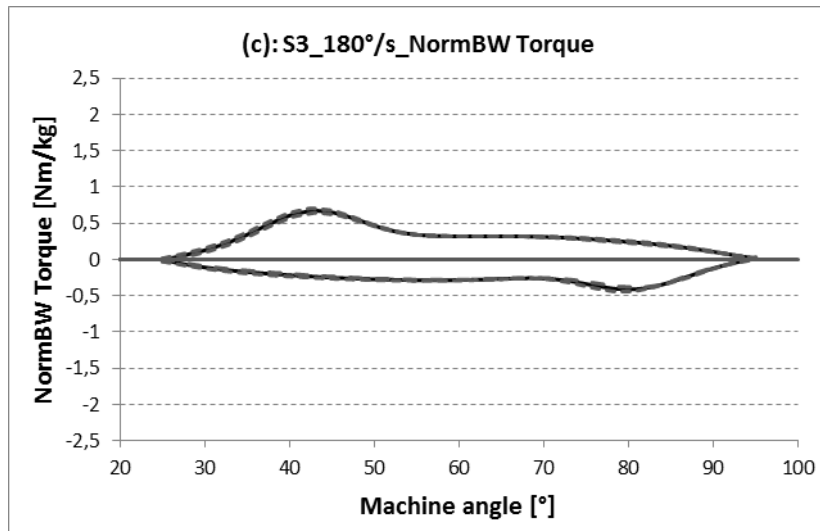
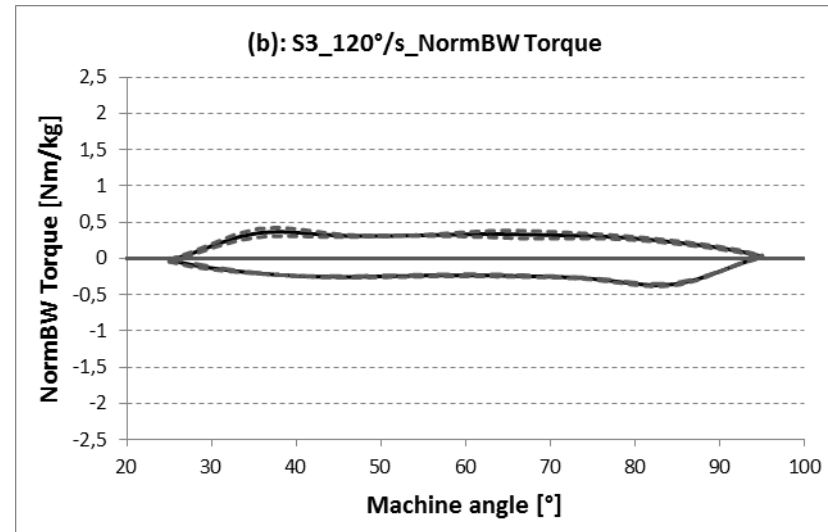
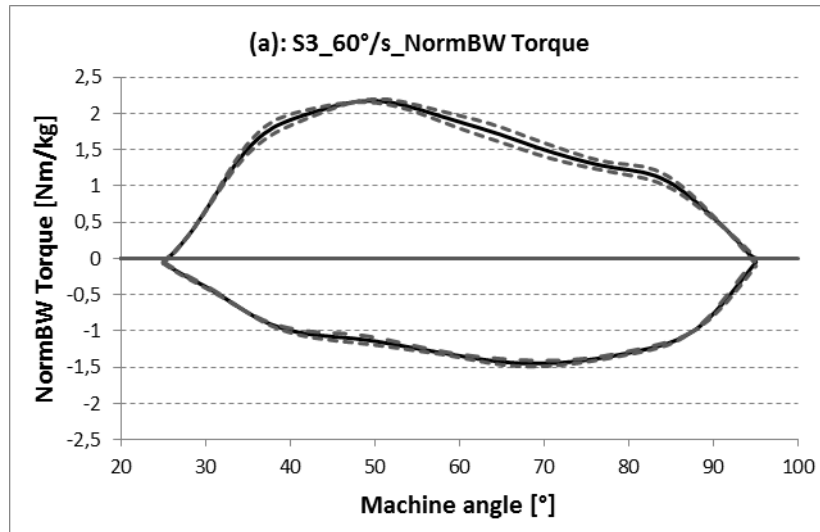


Fig.A.3.1: Normalized Torque of S3 at 60°/s (a), 120°/s (b), 180°/s (c) and 240°/s (d).

Flexors and Extensors Balance

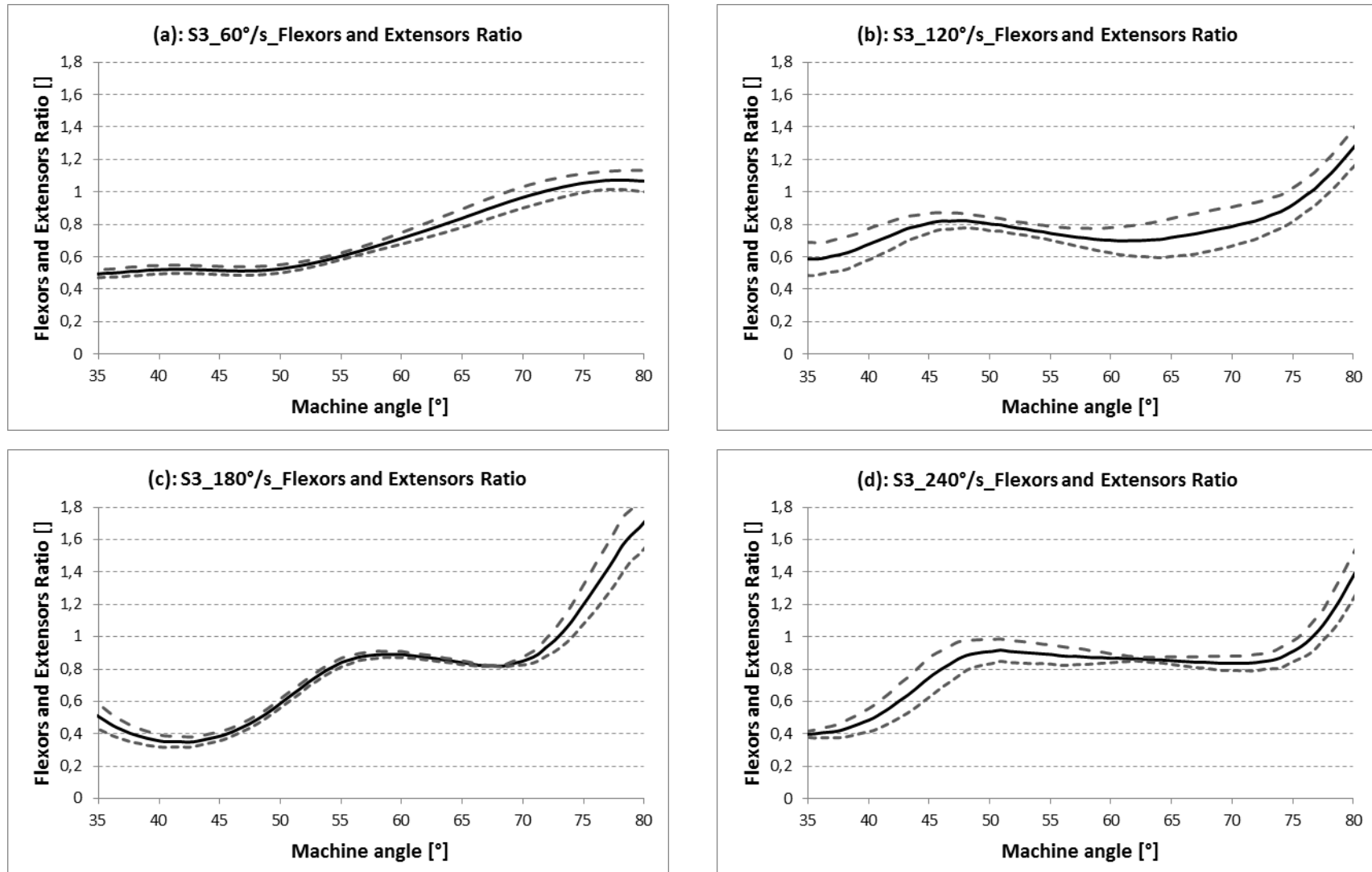


Fig.A.3.2: Flexors and extensors balance of S2 at 60°/s (a), 120°/s (b), 180°/s (c) and 240°/s (d).

Comparison of EMG signal and OpenSim muscle activation

M = 69 kg H = 1,70 m age = 25

adjust ratio for OpenSim: $\frac{SM_{S3}}{SM_{model}} = 1,23$

Maximum effort exerted in isokinetic and isometric exercises [mV]:

	Isokinetic exercise				Isometric exercise				
	60 °/s	120 °/s	180 °/s	240 °/s	ISO_25°	ISO_40°	ISO_55°	ISO_70°	ISO_95°
RF	0,643	0,304	0,32	0,174	0,363	0,507	0,427	0,471	0,601
VL	0,61	0,185	0,372	0,139	0,505	0,543	0,449	0,521	0,61
VM	0,632	0,173	0,23	0,098	0,463	0,572	0,399	0,441	0,737
BF	0,373	0,1	0,135	0,058	0,272	0,303	0,267	0,197	0,375

Tab.A.3.1: Mamimum effort of S3 in [mV] during isokinetic and isometric exercises.

60 °/s

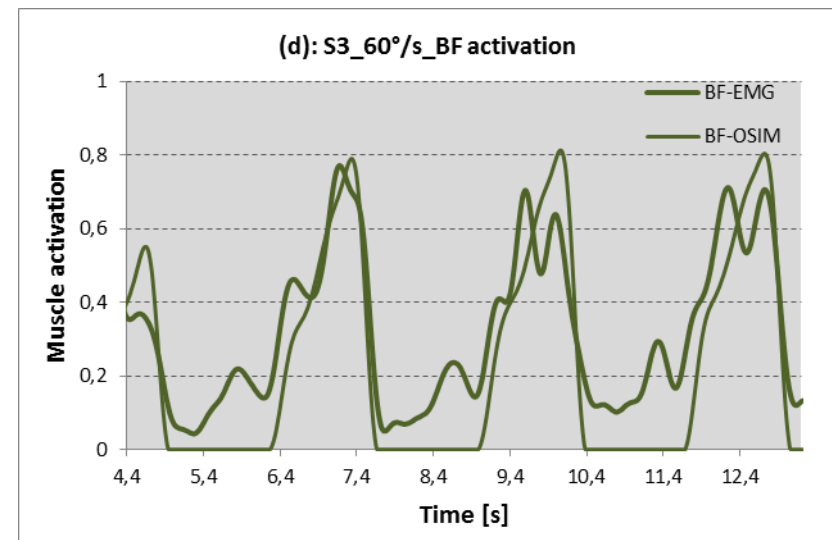
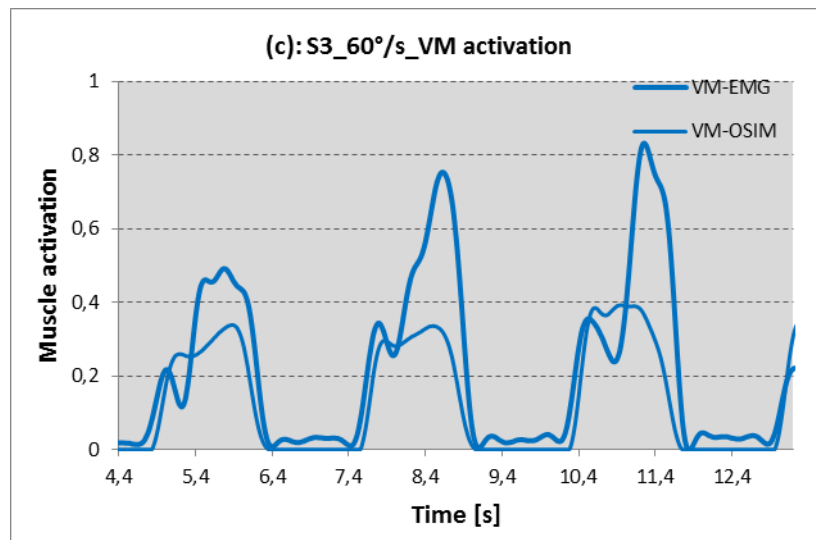
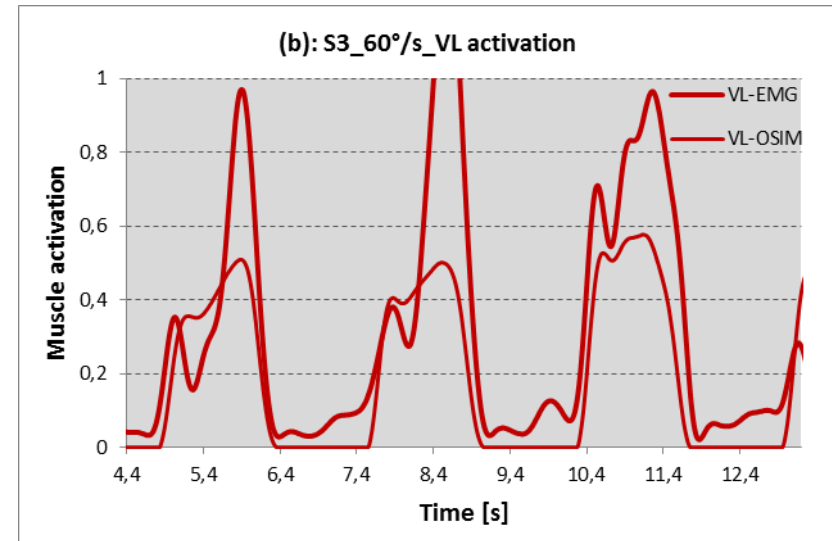
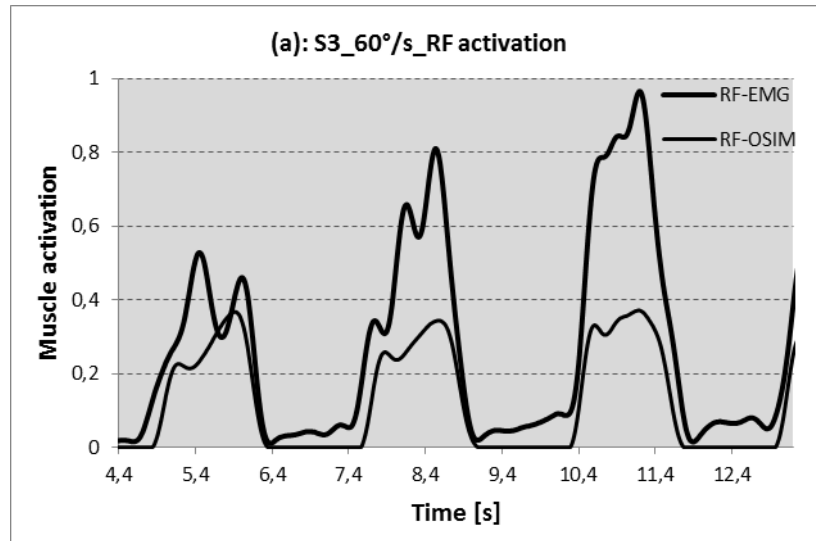


Fig.A.3.3: EMG and OpenSim muscle activation of S3 at 60°/s of RF (a), VL (b), VM (c) and BF (d).

120 °/s

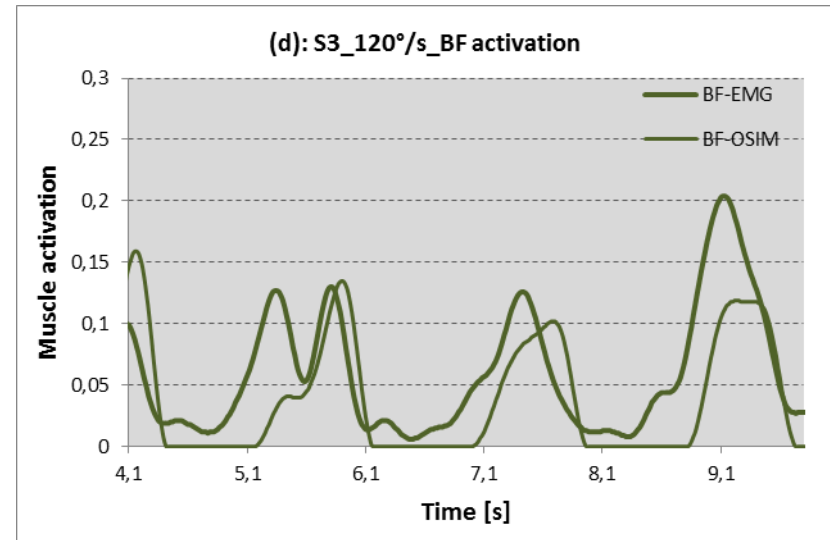
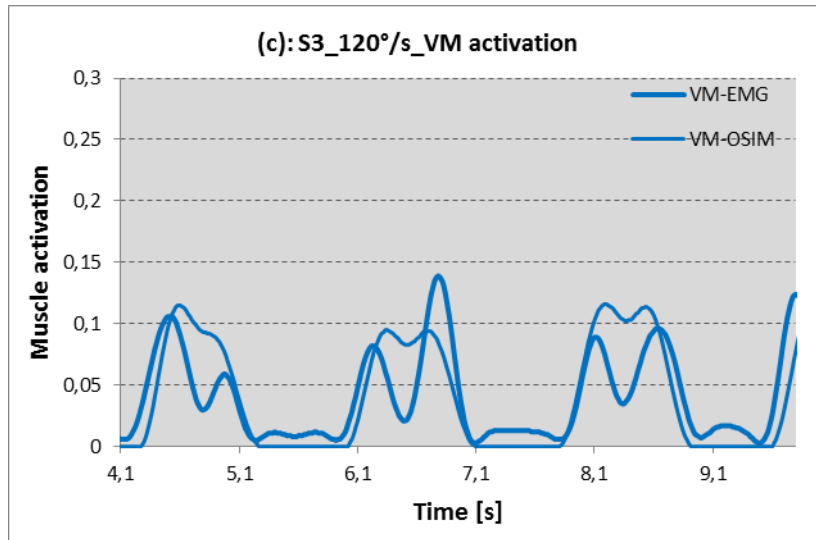
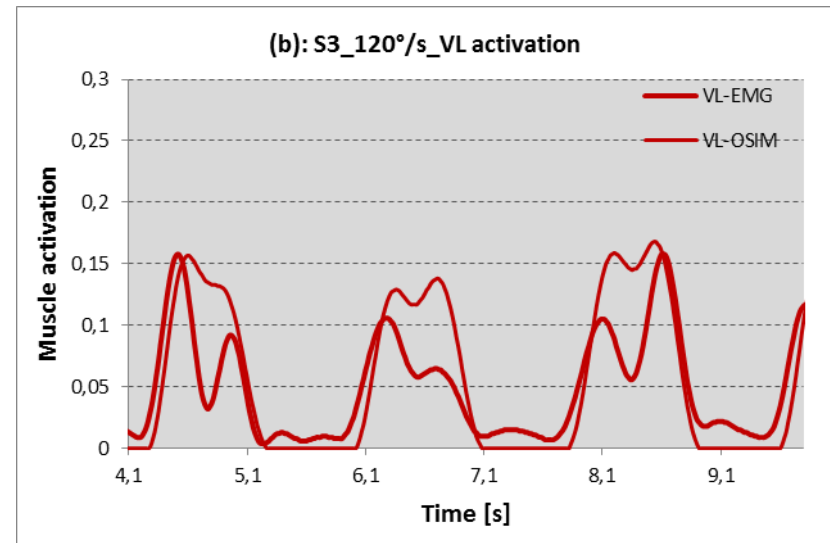
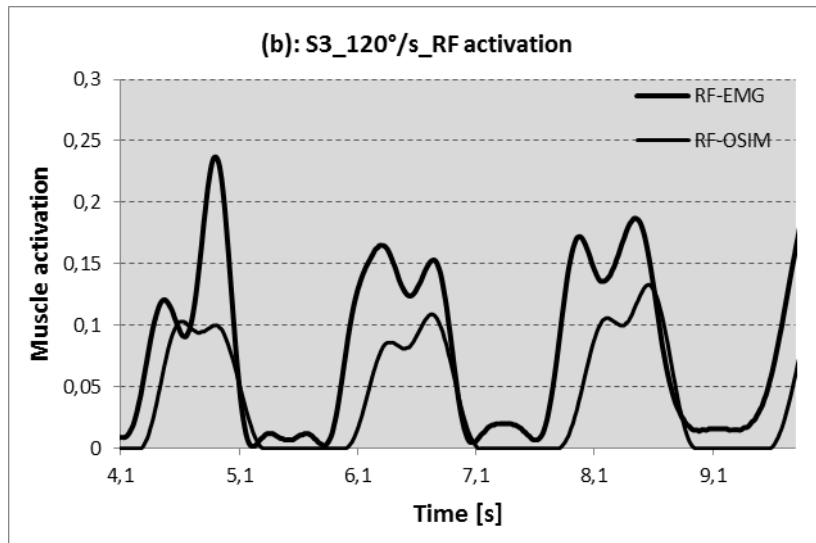


Fig.A.3.4: EMG and OpenSim muscle activation of S3 at 120°/s of RF (a), VL (b), VM (c) and BF (d).

180 °/s

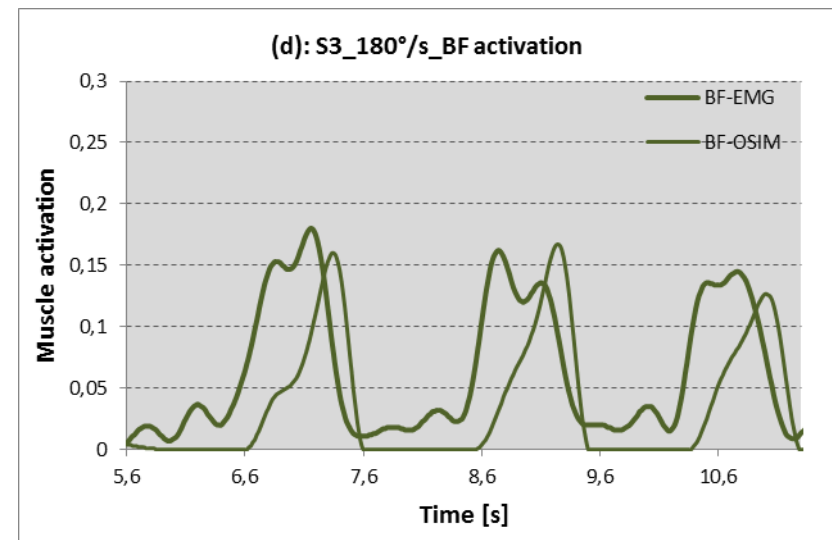
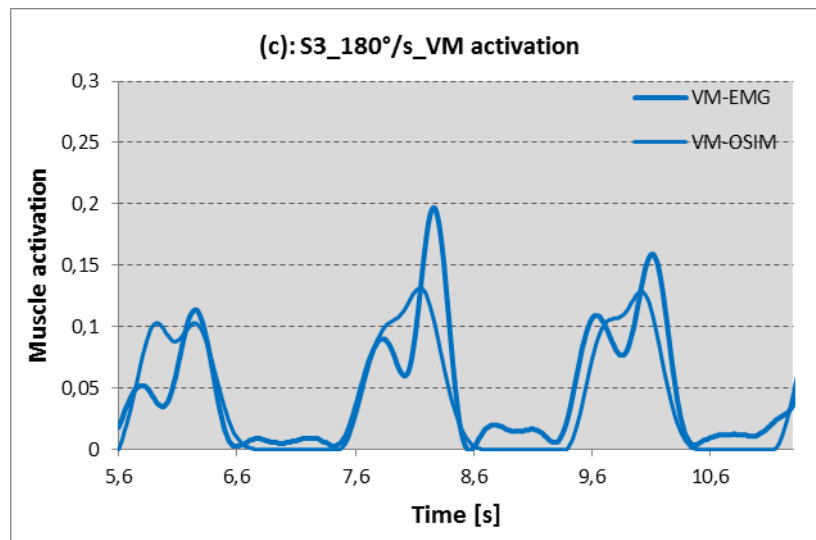
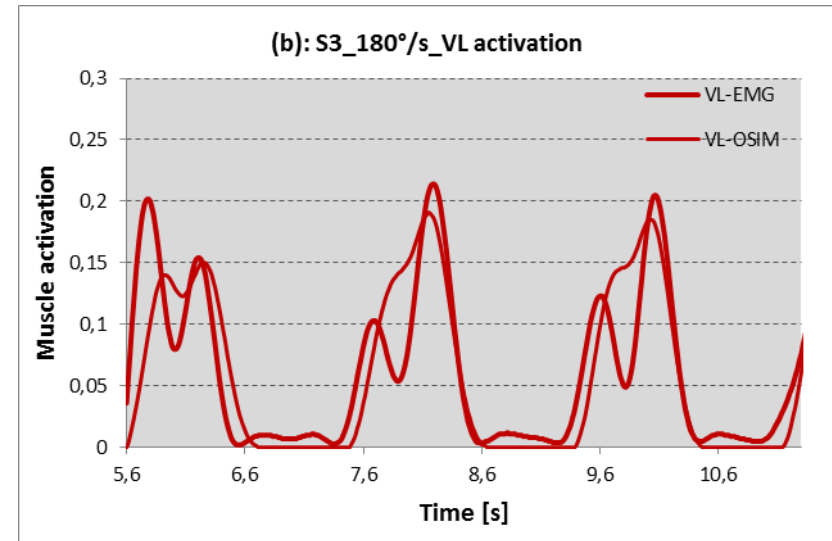
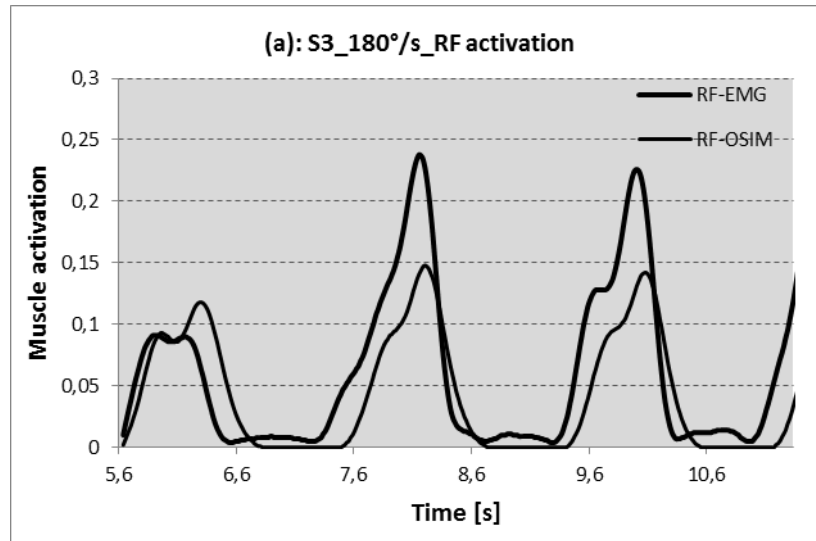


Fig.A.3.5: EMG and OpenSim muscle activation of S3 at 180°/s of RF (a), VL (b), VM (c) and BF (d).

240 °/s

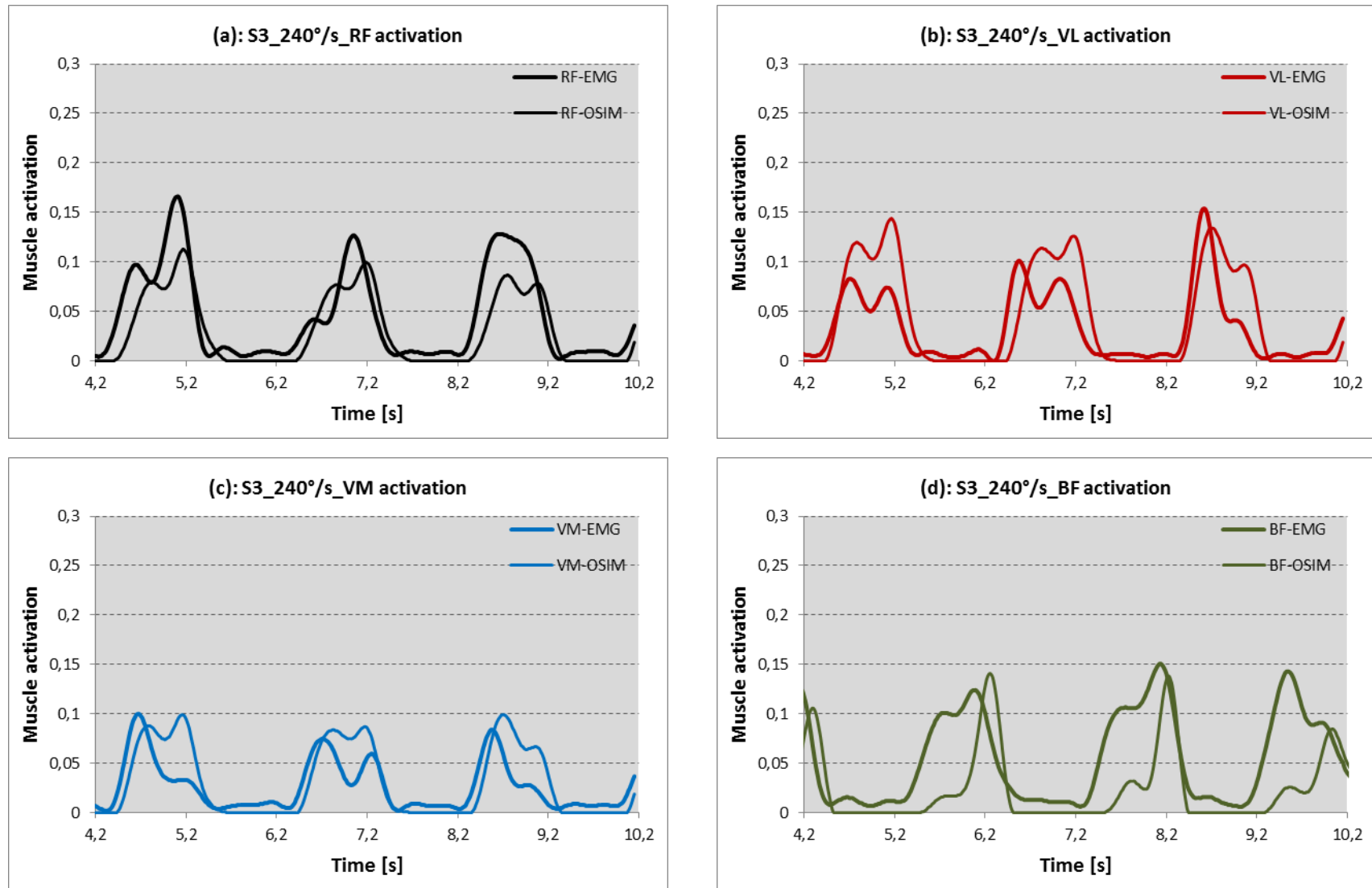


Fig.A.3.6: EMG and OpenSim muscle activation of S3 at 240°/s of RF (a), VL (b), VM (c) and BF (d).

Comparison of EMG signal and OpenSim muscle activation: quantitative results

	60 °/s	120 °/s	180 °/s	240 °/s
RF	49,86±16,89	39,79±14,73	15,10±38,78	28,41±6,19
VL	50,75±12,43	-11,96±16,16	15,42±8,96	-28,42±43,36
VM	46,47±13,32	0,78±27,44	20,50±11,76	-10,95±10,39
BF	-10,30±6,88	18,96±22,76	6,81±8,60	11,82±27,28

Tab.A.3.2: Peak error of S3 in [%] of RF, VL, VM and BF at 60°/s, 120°/s, 180°/s and 240°/s.

	60 °/s	120 °/s	180 °/s	240 °/s
RF	37,17±4,00	-5,33±19,35	-9,20±8,94	-5,00±1,80
VL	-29,39±5,75	-7,04±15,39	-6,10±14,93	-18,27±13,61
VM	-24,00±3,94	14,70±15,26	2,80±2,43	-10,27±11,05
BF	39,51±6,01	-7,70±5,71	-24,80±21,82	-11,87±8,46

Tab.A.3.3: Time error of S3 in [%] of RF, VL, VM and BF at 60°/s, 120°/s, 180°/s and 240°/s.

	240 °/s	180 °/s	120 °/s	60 °/s
RF	37,50±18,58	37,17±4,00	-5,88±33,65	41,15±13,22
VL	24,26±14,28	-29,39±5,75	-2,72±7,12	-48,29±14,38
VM	27,62±10,15	-24,00±3,94	-12,73±27,24	-33,79±15,00
BF	11,47±2,60	39,51±6,01	34,79±4,04	47,37±7,81

Tab.A.3.4: Area error of S3 in [%] of RF, VL, VM and BF at 60°/s, 120°/s, 180°/s and 240°/s.

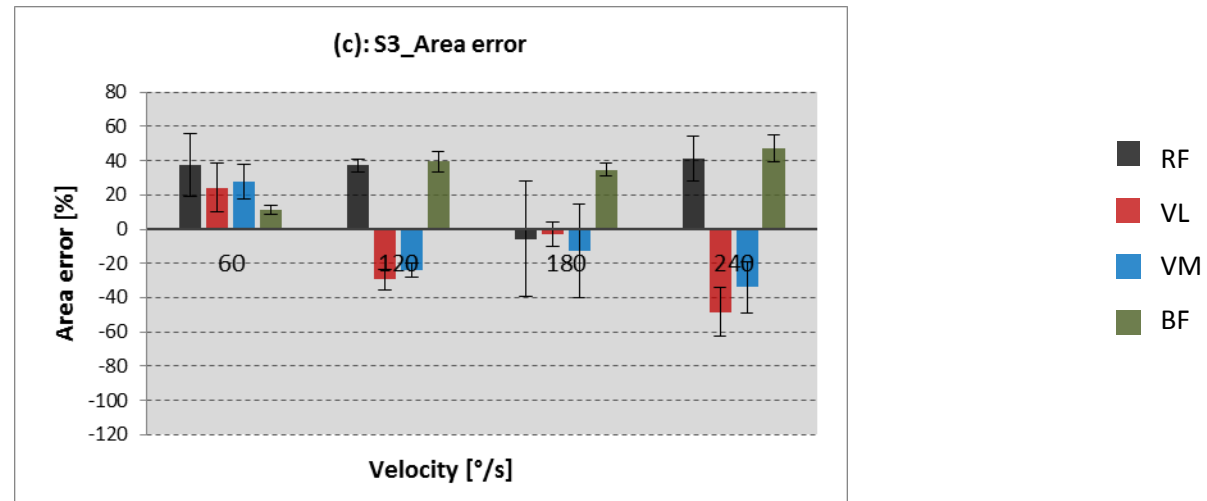
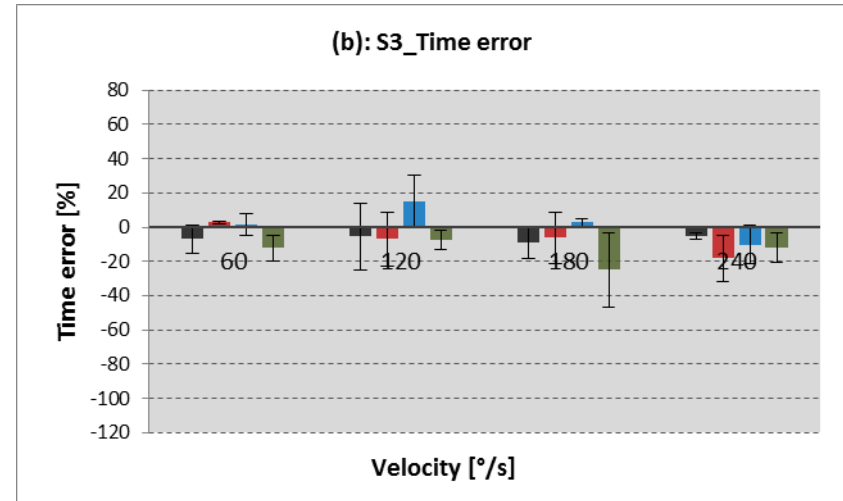
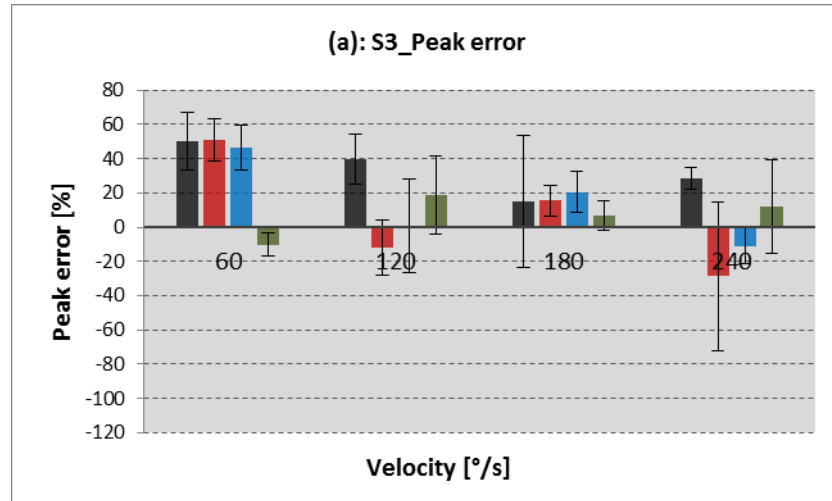


Fig.A.3.7: Quantitative results of muscle activation analysis of S3: (a): Peak error at different velocities; (b): Time error at different velocities; (c): Area error at different velocities.

Comparison of analytical models and OpenSim model

Model 1: parameters

$$\text{Tibia: } m_{\text{tibia}} = 3,354 \text{ kg} \quad I_{G \text{ tibia}} = 0,05 \text{ kg} \cdot \text{m}^2 \quad \Delta_{y \text{ tibia}} = 0,445 \text{ m} \quad \Delta_{y G \text{ tibia}} = 0,193 \text{ m}$$

$$\text{Talus: } m_{\text{talus}} = 0,09 \text{ kg} \quad I_{G \text{ talus}} = 9 \cdot 10^{-4} \text{ kg} \cdot \text{m}^2 \quad \Delta_{y \text{ talus}} = 0,445 \text{ m} \quad \Delta_{y G \text{ talus}} = 0,445 \text{ m}$$

$$\text{Calc: } m_{\text{calc}} = 1,131 \text{ kg} \quad I_{G \text{ calc}} = 0,0037 \text{ kg} \cdot \text{m}^2 \quad \Delta_{x \text{ calc}} = 0,049 \text{ m} \quad \Delta_{y \text{ calc}} = 0,0418 \text{ m}$$

$$\Delta_{x G \text{ calc}} = 0,1 \text{ m} \quad \Delta_{y G \text{ calc}} = 0,03 \text{ m}$$

$$\text{Toes: } m_{\text{toes}} = 0,196 \text{ kg} \quad I_{G \text{ toes}} = 9 \cdot 10^{-5} \text{ kg} \cdot \text{m}^2 \quad \Delta_{x \text{ toes}} = 0,178 \text{ m} \quad \Delta_{y \text{ toes}} = 0,002 \text{ m}$$

$$\Delta_{x G \text{ toes}} = 0,034 \text{ m} \quad \Delta_{y G \text{ toes}} = 0,006 \text{ m}$$

Model 2: parameters

$$\text{Tibia: } m_{\text{tibia}} = 3,06 \text{ kg} \quad I_{G \text{ tibia}} = 0,043 \text{ kg} \cdot \text{m}^2 \quad \Delta_{y \text{ tibia}} = 0,394 \text{ m} \quad \Delta_{y G \text{ tibia}} = 0,17 \text{ m}$$

$$\text{Foot: } m_{\text{foot}} = 0,952 \text{ kg} \quad I_{G \text{ foot}} = 0,005 \text{ kg} \cdot \text{m}^2 \quad \Delta_{x G \text{ foot}} = 0,068 \text{ m} \quad \Delta_{y G \text{ foot}} = 0,033 \text{ m}$$

$$D_{Q2} = 0,075 \text{ m} \quad H_{Q2} = 0,024 \text{ m} \quad D_{Q1} = 0,281 \text{ m} \quad H_{Q1} = 0,028 \text{ m}$$

$$B_{PT} [\text{m}] = (0,0097 \cdot \varphi_{k+}^5 - 0,0215 \cdot \varphi_{k+}^4 - 0,0098 \cdot \varphi_{k+}^3 + 0,0366 \cdot \varphi_{k+}^2 - 0,0141 \cdot \varphi_{k+} + 0,0464) \cdot 0,9375 \quad \varphi_{k+} [\text{rad}]$$

$$\text{BFB: } D_{\text{BFB1}} = 0,1875 \text{ m} \quad D_{\text{BFB2}} = 0,0375 \text{ m} \quad H_{\text{BFB1}} = 0,0375 \text{ m} \quad H_{\text{BFB2}} = 0,028 \text{ m}$$

$$\text{BFL: } D_{\text{BFL1}} = 0,46 \text{ m} \quad D_{\text{BFL2}} = 0,0375 \text{ m} \quad H_{\text{BFL1}} = 0,0375 \text{ m} \quad H_{\text{BFL2}} = 0,028 \text{ m}$$

$$\text{SM: } D_{\text{SM1}} = 0,46 \text{ m} \quad D_{\text{SM2}} = 0,047 \text{ m} \quad H_{\text{SM1}} = 0,0375 \text{ m} \quad H_{\text{SM2}} = 0,033 \text{ m}$$

$$\text{ST: } D_{\text{ST1}} = 0,46 \text{ m} \quad H_{\text{ST1}} = 0,047 \text{ m} \quad B_{\text{ST}} = 0,0375 \text{ m} \quad \alpha_{\text{ST}} = 0,52 \text{ rad}$$

Fig.A.3.8: S3_60°/s_Extension

— OSIM — Mod1_Herzog — Mod1_Van Eijden — Mod2 - - - limit value

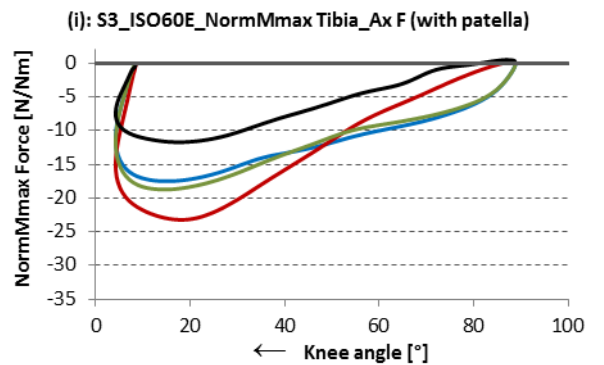
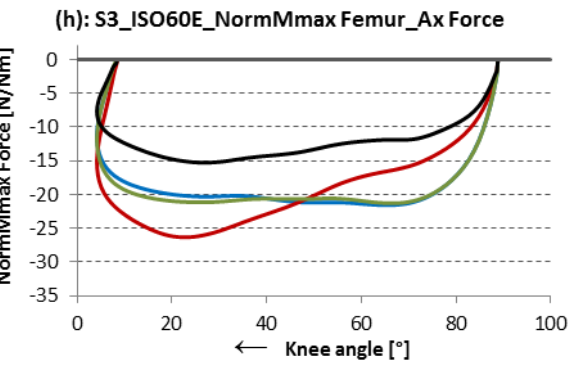
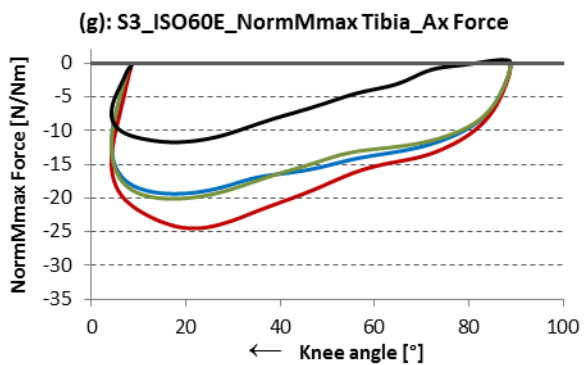
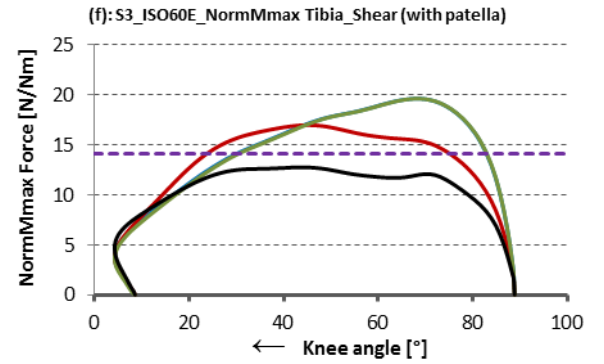
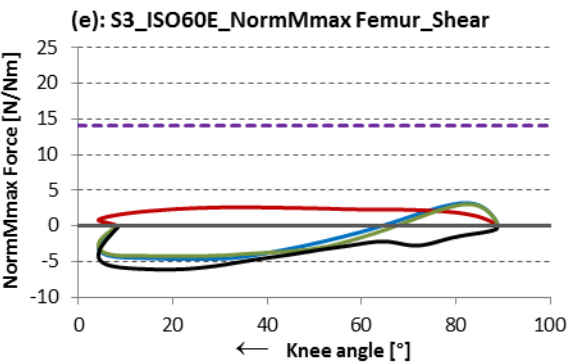
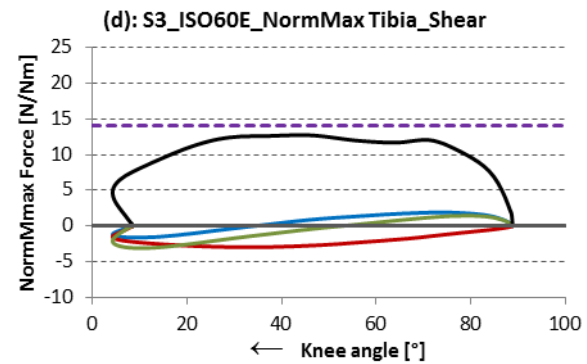
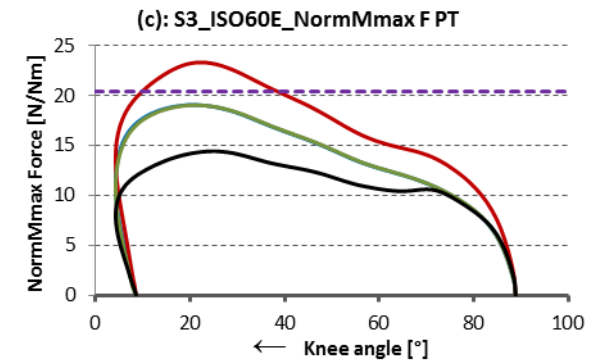
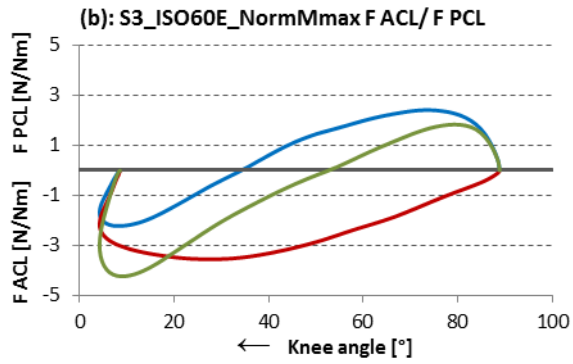
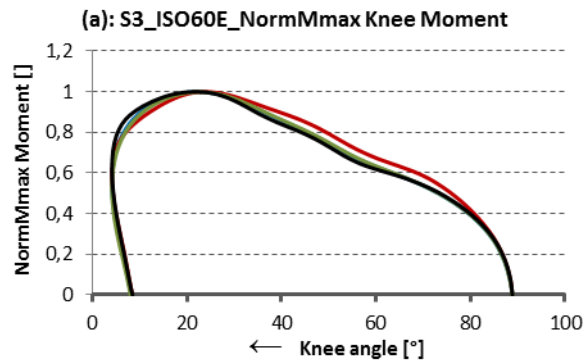


Fig.A.3.9: S3_60°/s_Flexion

— OSIM — Mod1 — Mod2 - - - limit value (•••• OSIM BFL •••• Mod1 BFL •••• Mod2 BFL)

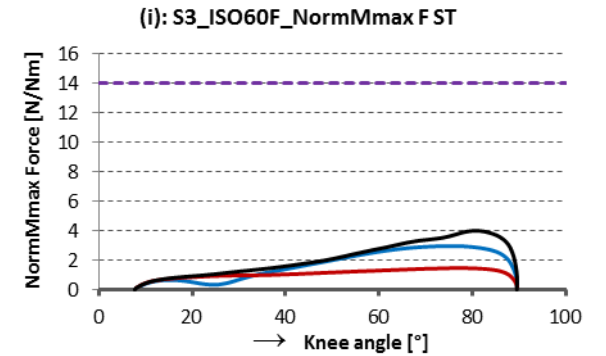
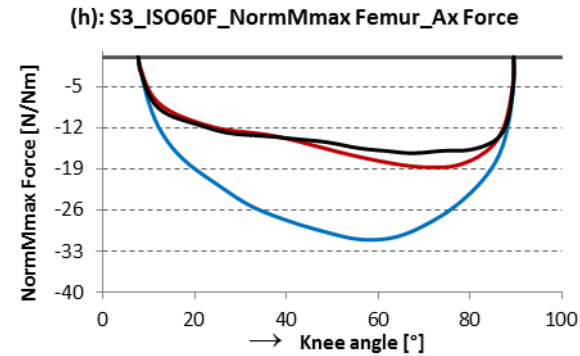
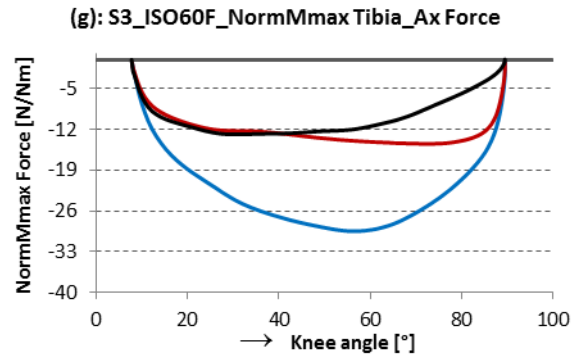
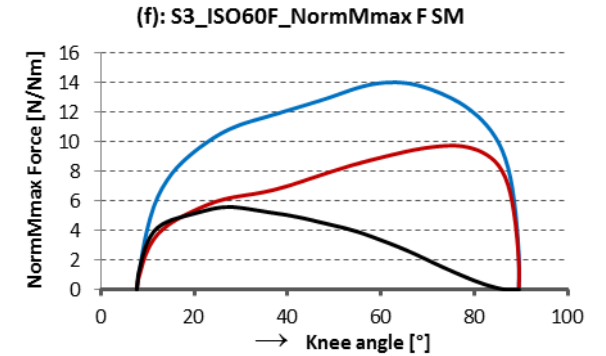
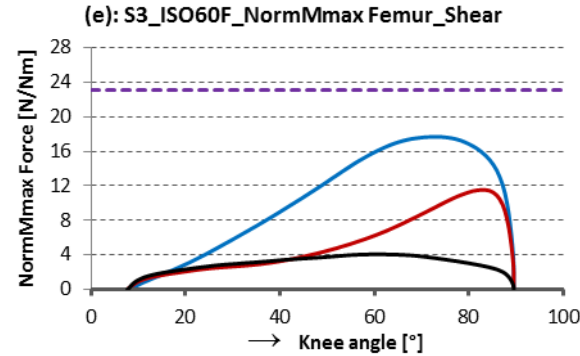
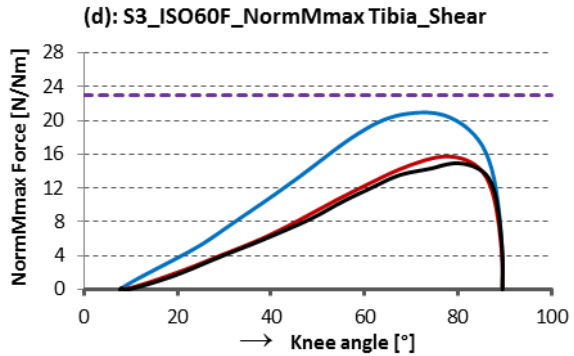
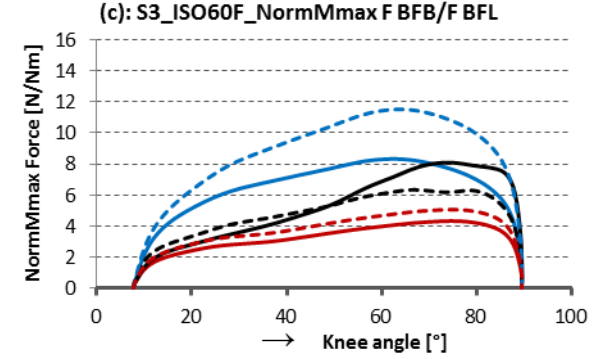
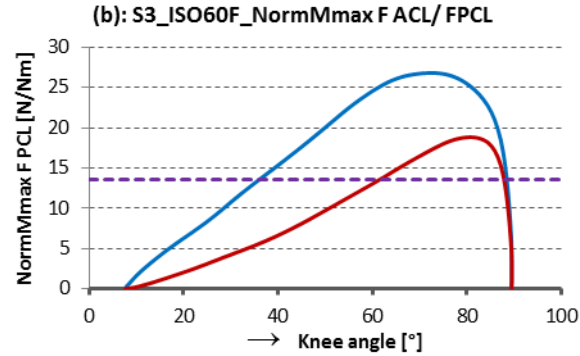
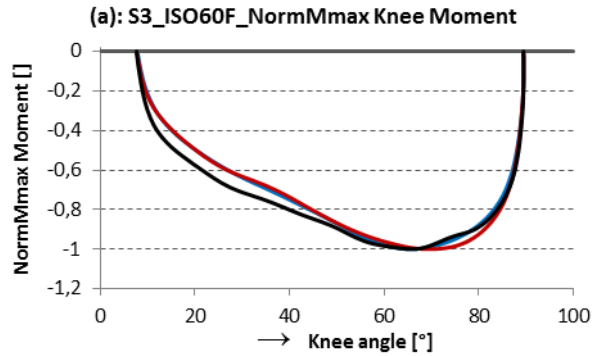


Fig.A.3.10: S3_120°/s_Extension

— OSIM — Mod1_Herzog — Mod1_Van Eijden — Mod2 ···· limit value

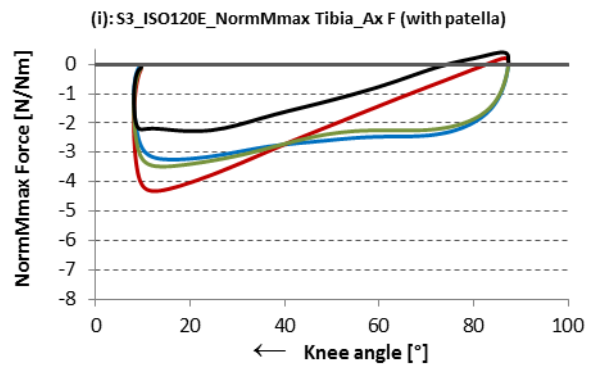
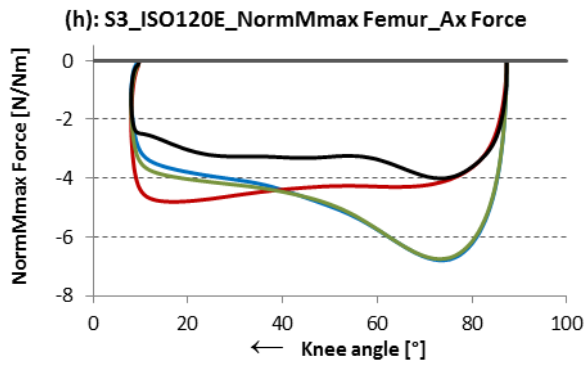
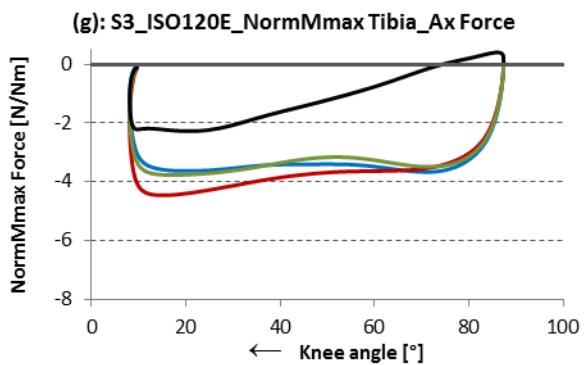
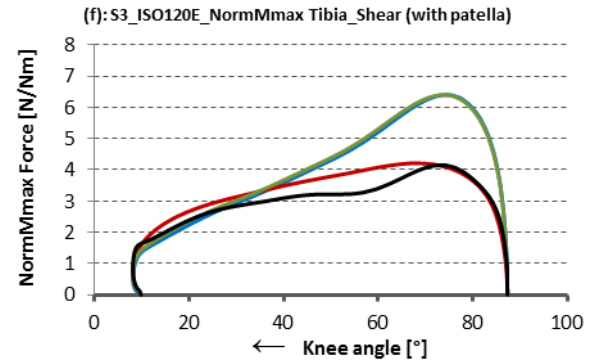
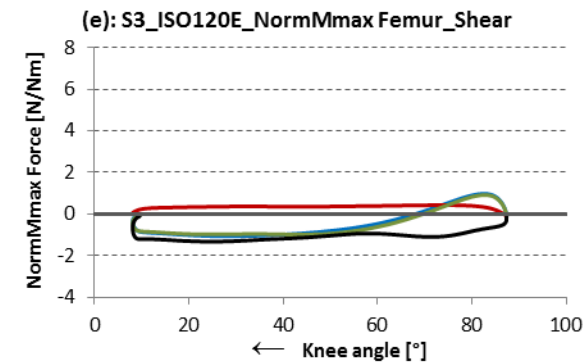
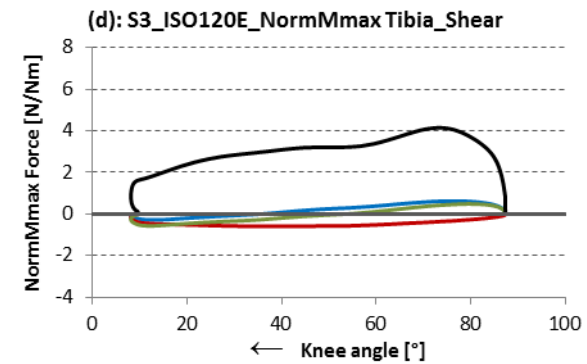
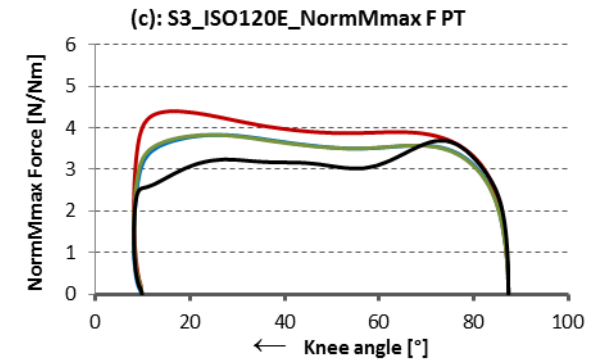
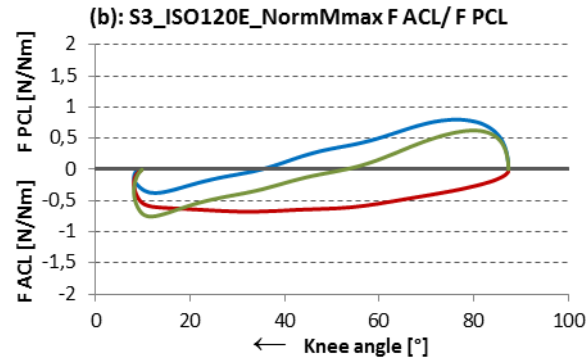
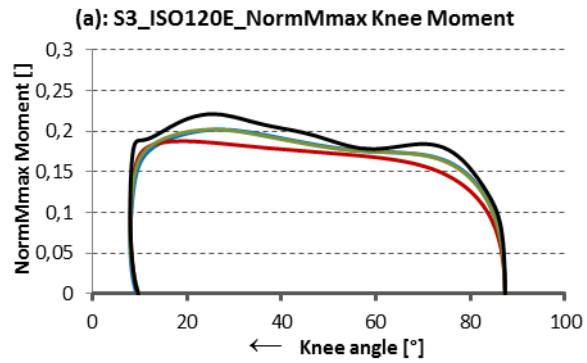


Fig.A.3.11: S3_120°/s_Flexion

— OSIM — Mod1 — Mod2 ···· limit value (····· OSIM BFL ····· Mod1 BFL ····· Mod2 BFL)

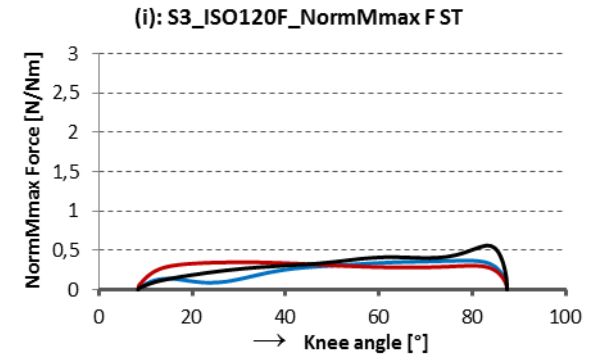
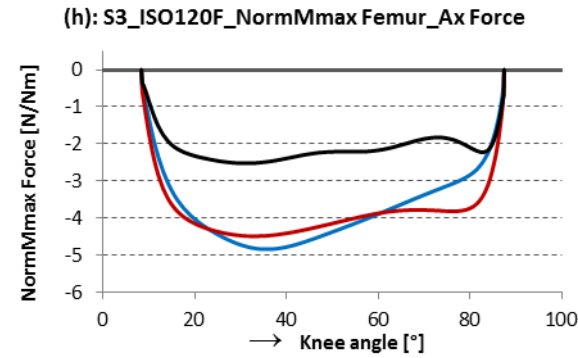
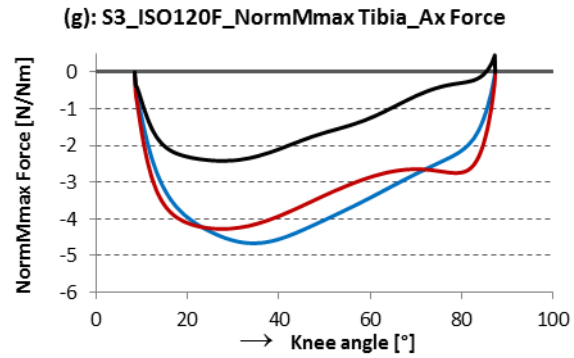
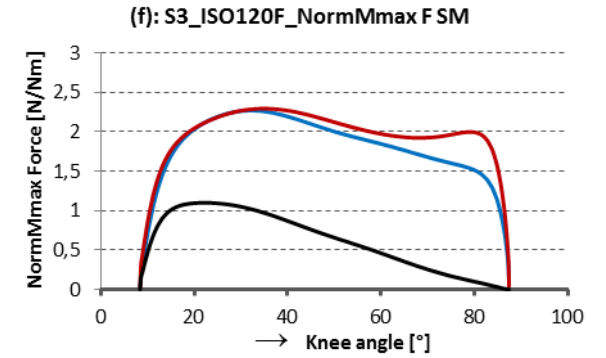
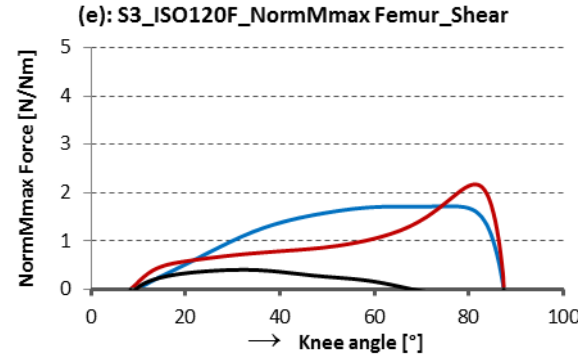
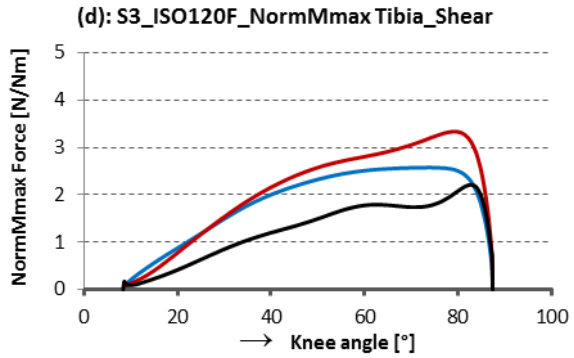
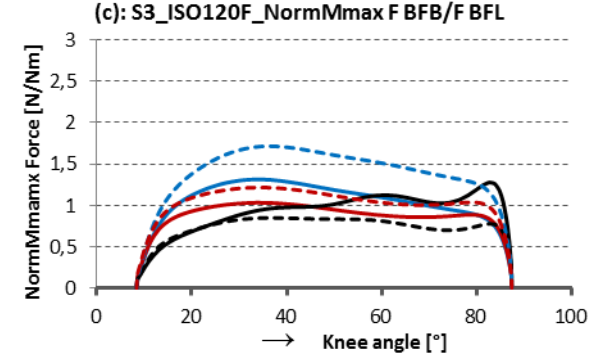
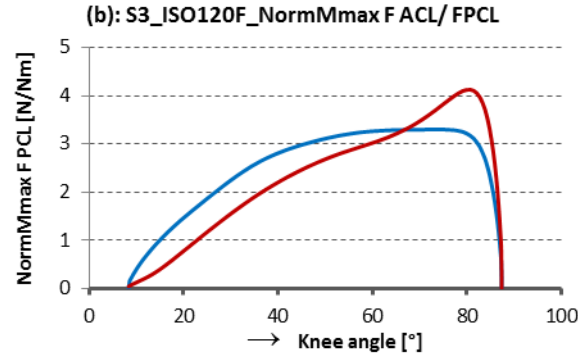
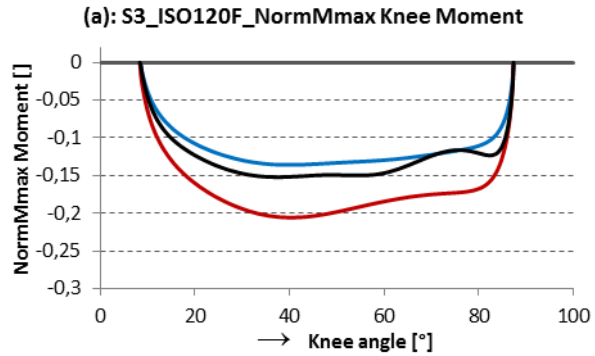


Fig.A.3.12: S2_180°/s_Extension

— OSIM — Mod1_Herzog — Mod1_Van Eijden — Mod2 - - - - - limit value

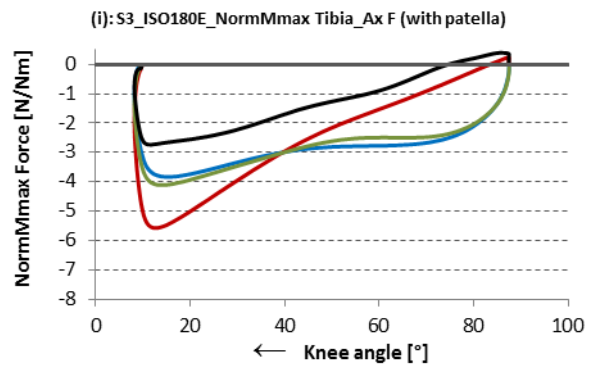
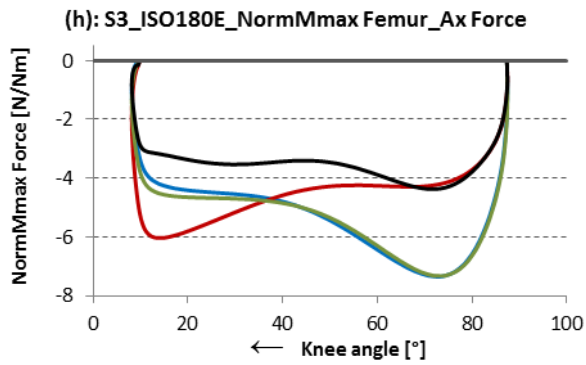
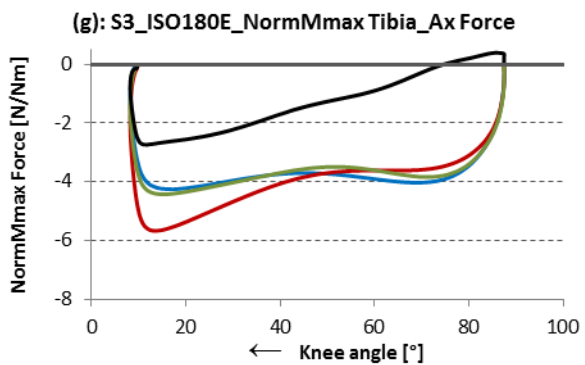
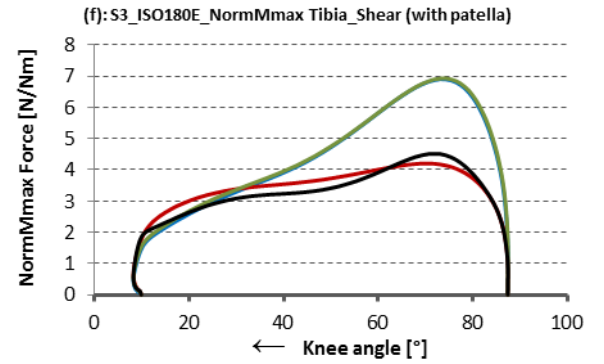
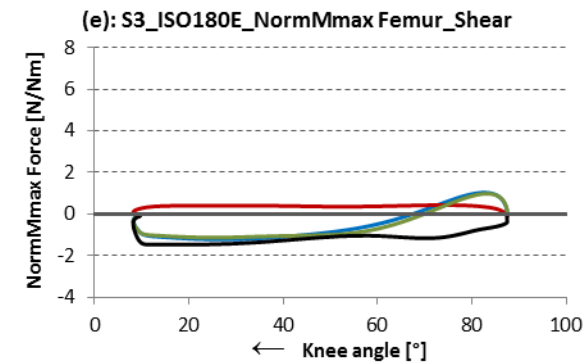
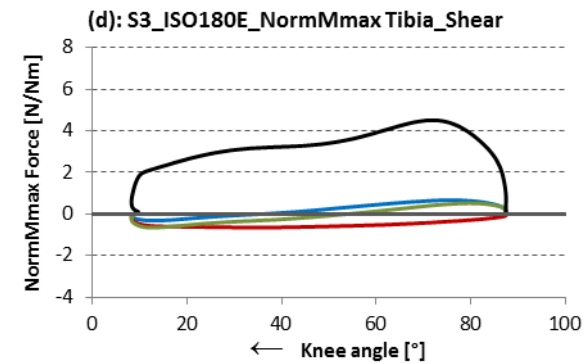
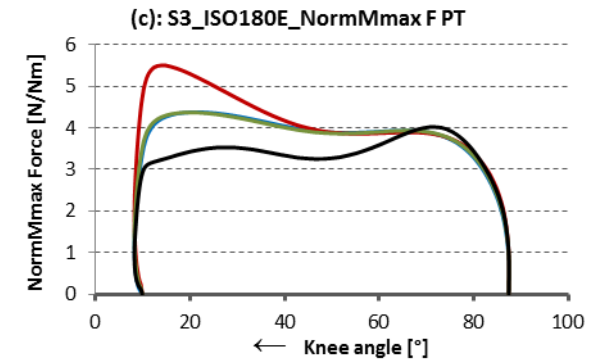
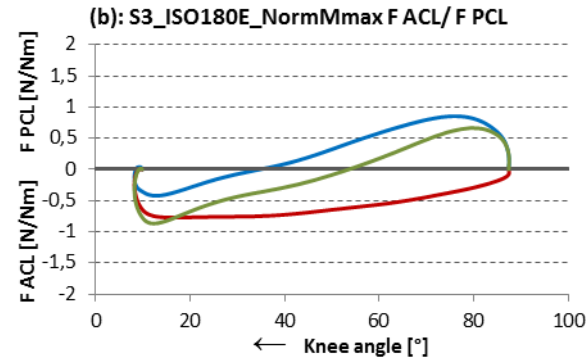
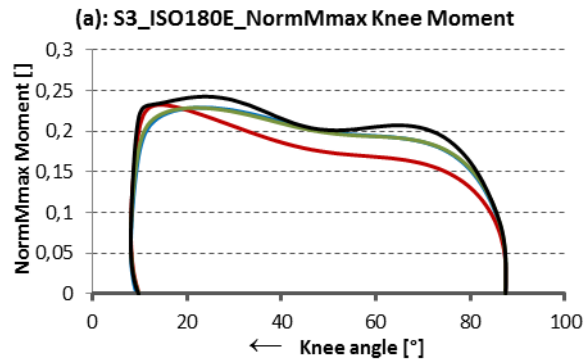


Fig.A.3.13: S3_180°/s_Flexion

— OSIM — Mod1 — Mod2 ···· limit value (···· OSIM BFL ···· Mod1 BFL ···· Mod2 BFL)

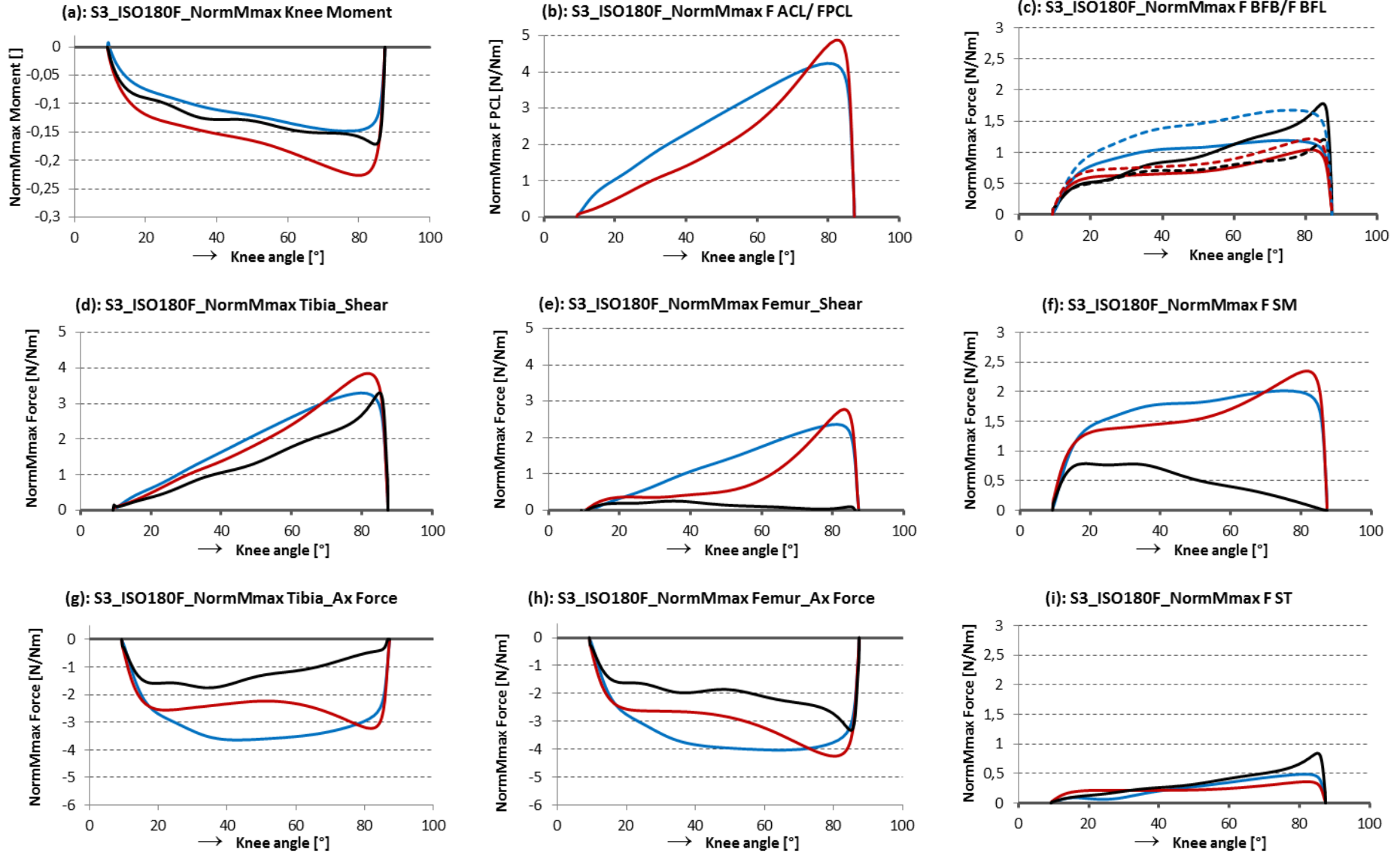


Fig.A.3.14: S3_240°/s_Extension

— OSIM — Mod1_Herzog — Mod1_Van Eijden — Mod2 ···· limit value

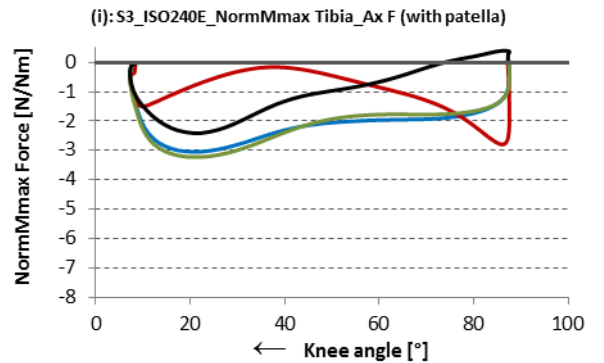
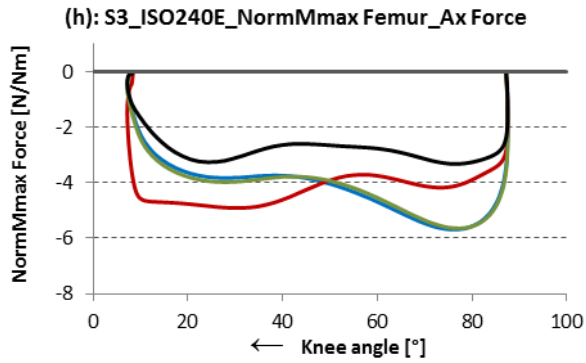
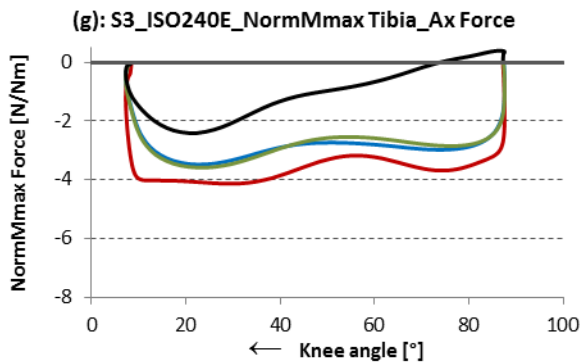
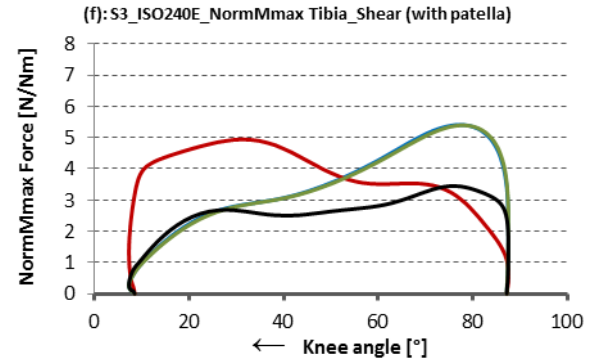
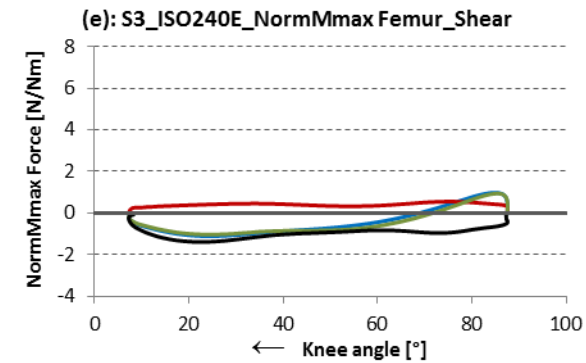
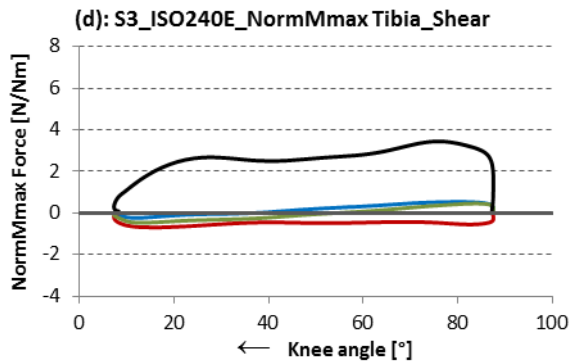
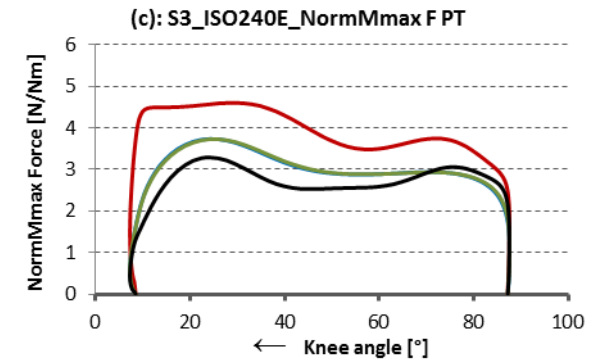
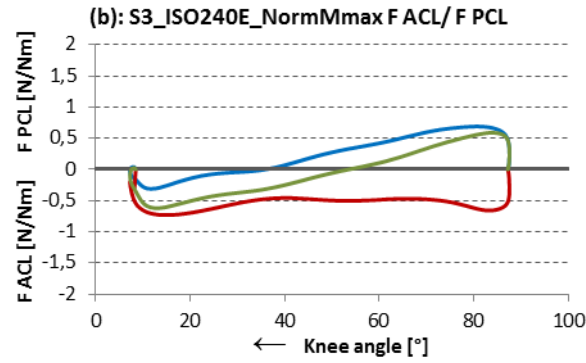
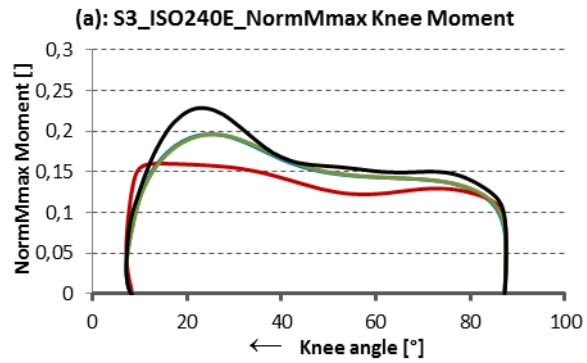
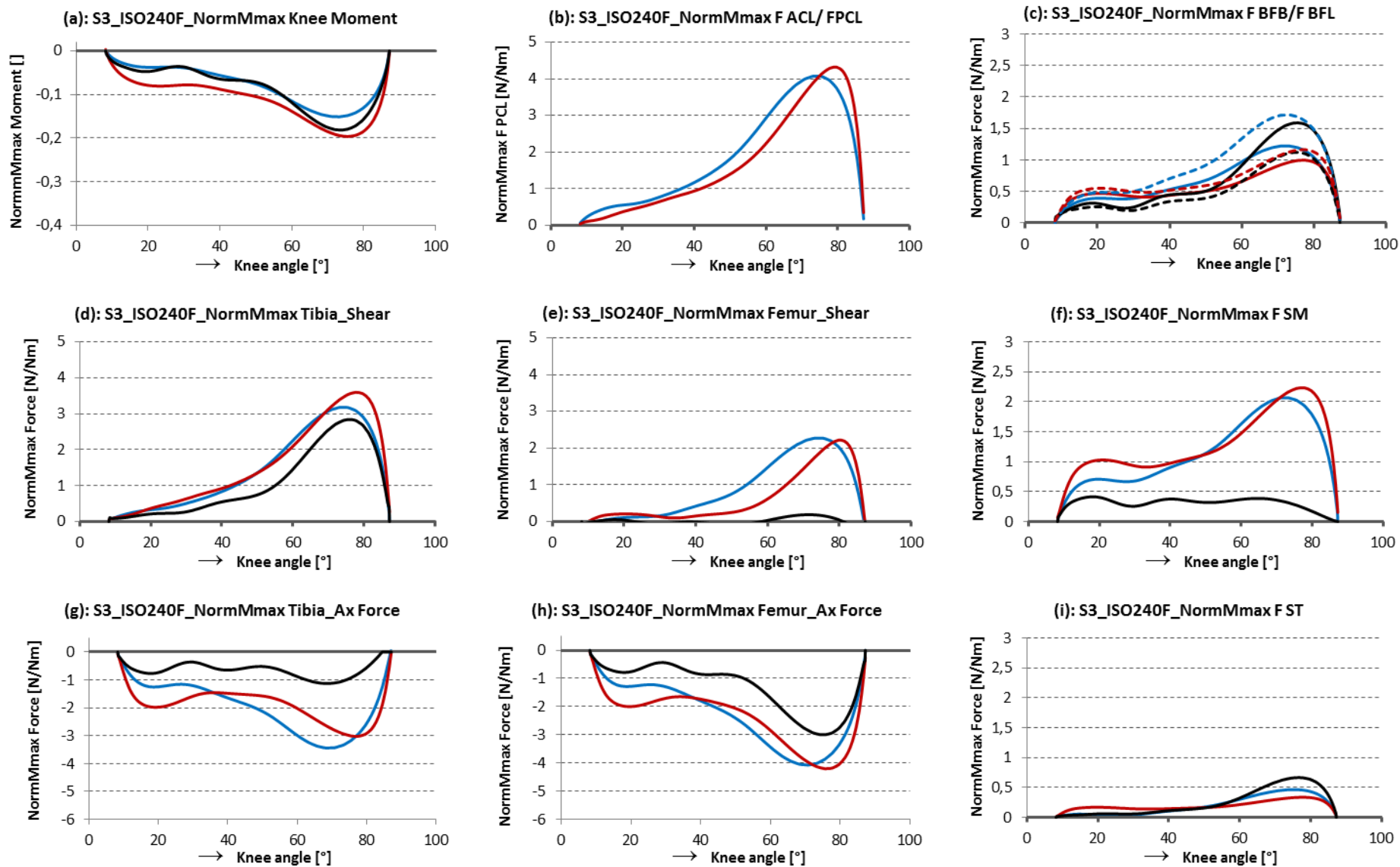


Fig.A.3.15: S3_240°/s_Flexion

— OSIM — Mod1 — Mod2 ···· limit value (···· OSIM BFL ···· Mod1 BFL ···· Mod2 BFL)



A.4.Results of Subject 4 (S4)

Torque at the servo-motor

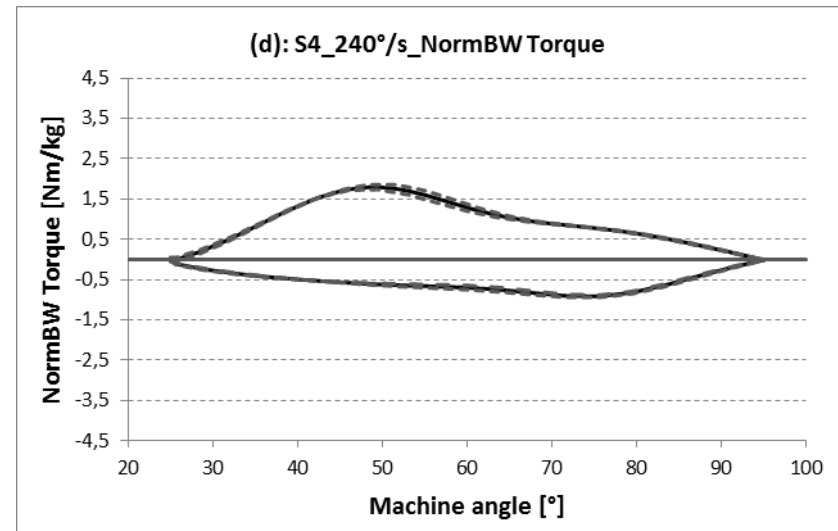
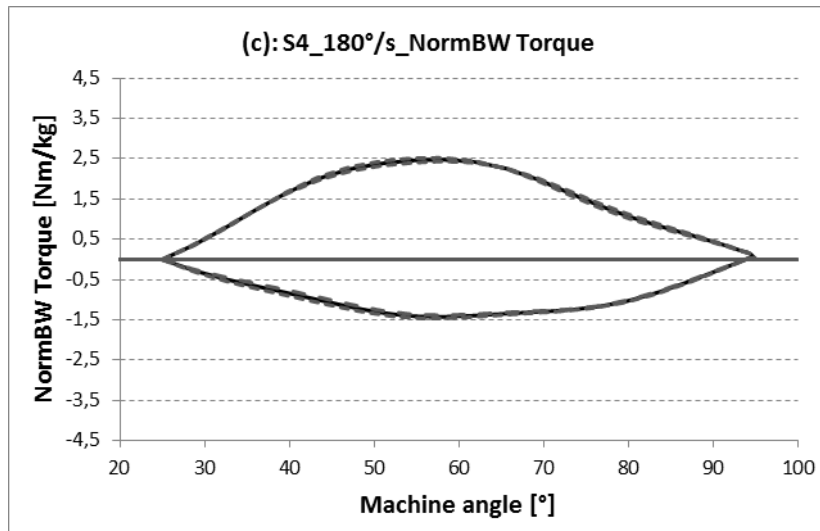
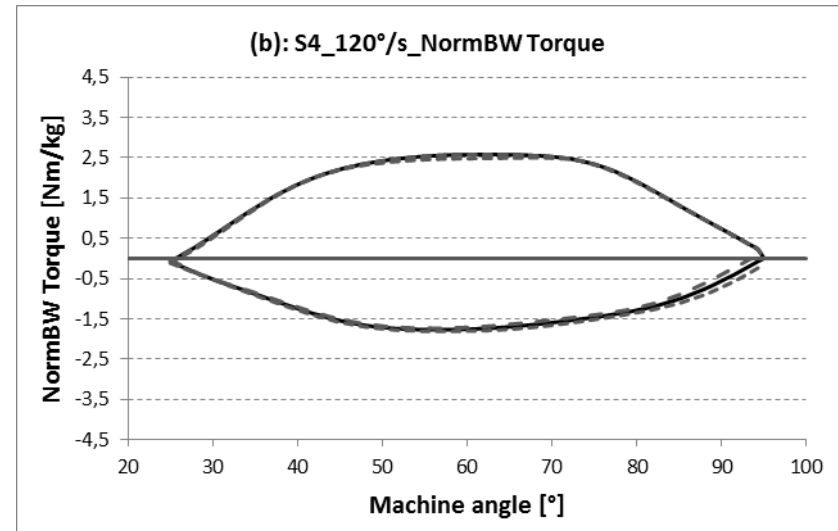
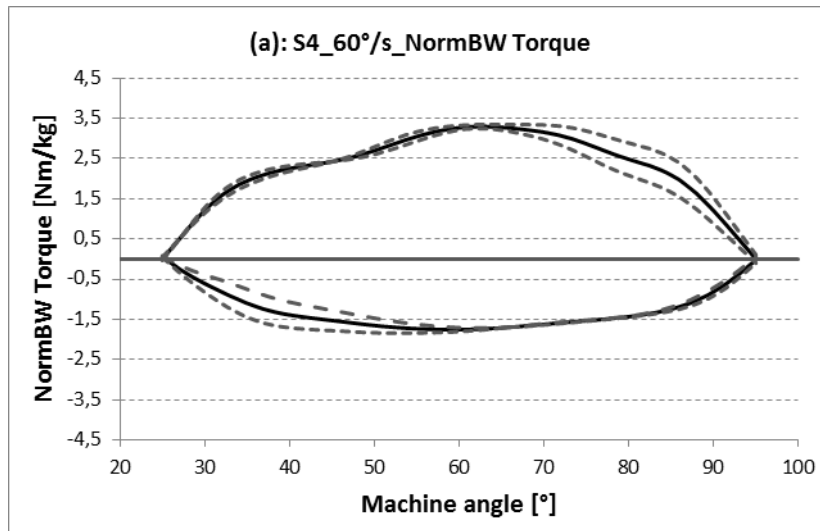


Fig.A.4.1: Normalized Torque of S4 at 60°/s (a), 120°/s (b), 180°/s (c) and 240°/s (d).

Flexors and Extensors Balance

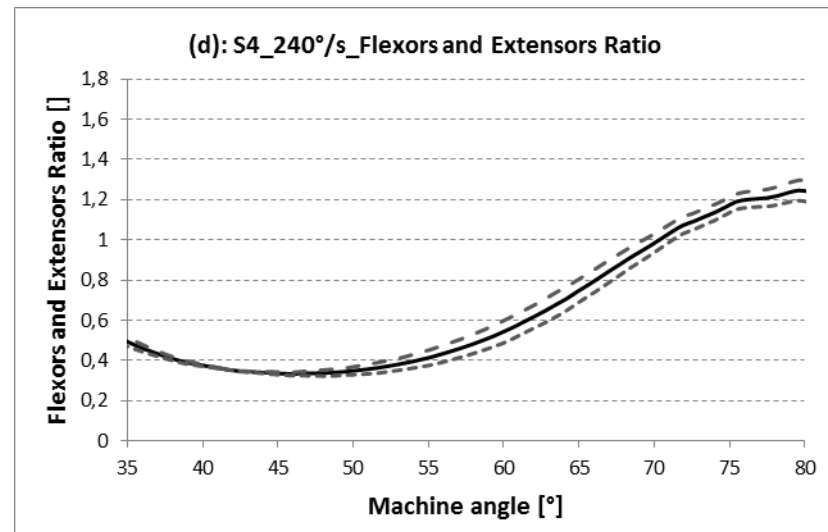
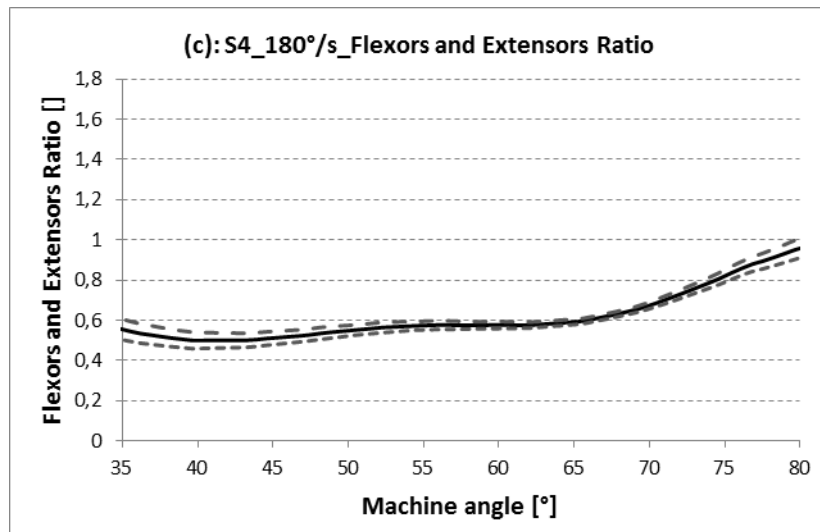
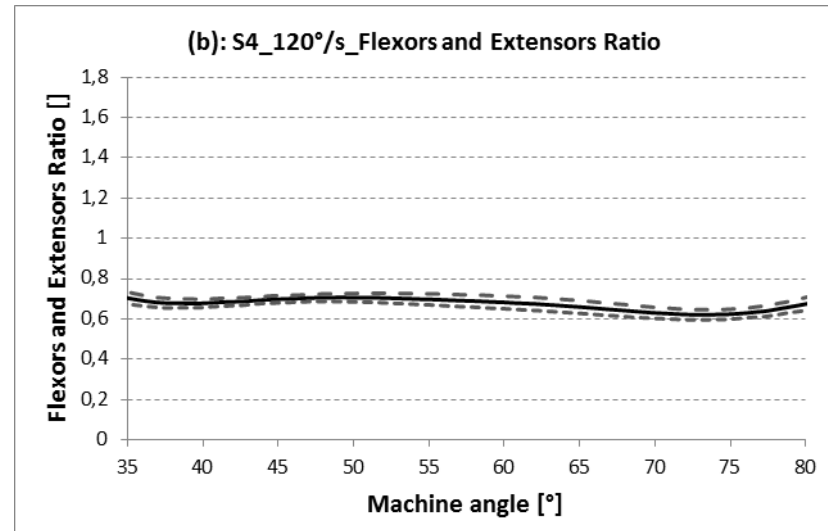
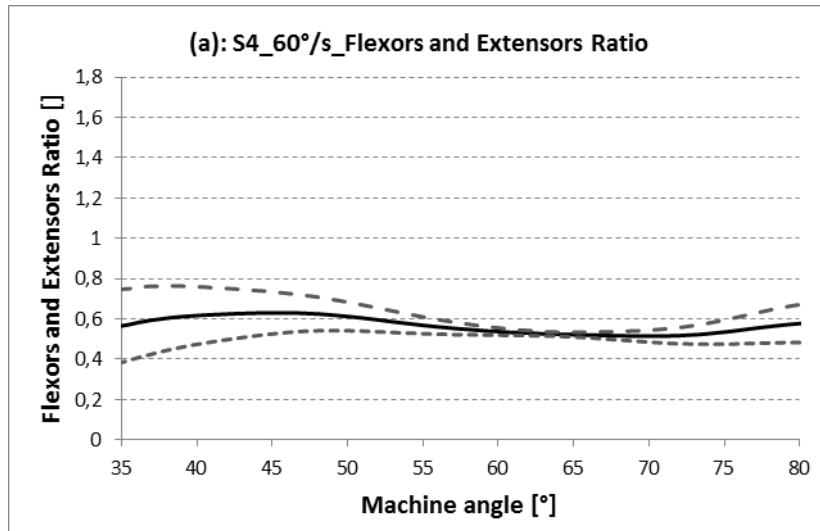


Fig.A.4.2: Flexors and extensors balance of S4 at 60°/s (a), 120°/s (b), 180°/s (c) and 240°/s (d).

Comparison of EMG signal and OpenSim muscle activation

M = 63 kg H = 1,82 m age = 25

adjust ratio for OpenSim: $\frac{SM_{S4}}{SM_{model}} = 1,218$

Maximum effort exerted in isokinetic and isometric exercises [mV]:

	Isokinetic exercise				Isometric exercise				
	60 °/s	120 °/s	180 °/s	240 °/s	ISO_25°	ISO_40°	ISO_55°	ISO_70°	ISO_95°
RF	0,58	0,559	0,894	0,361	0,189	0,138	0,208	0,201	0,434
VL	1,138	0,913	0,8	0,7	0,206	0,086	0,156	0,366	0,678
VM	0,685	0,838	0,959	0,693	0,309	0,124	0,197	0,326	0,71
BF	0,462	0,348	0,283	0,238	0,134	0,099	0,025	0,077	0,189

Tab.A.4.1: Mamimum effort of S4 in [mV] during isokinetic and isometric exercises.

60 °/s

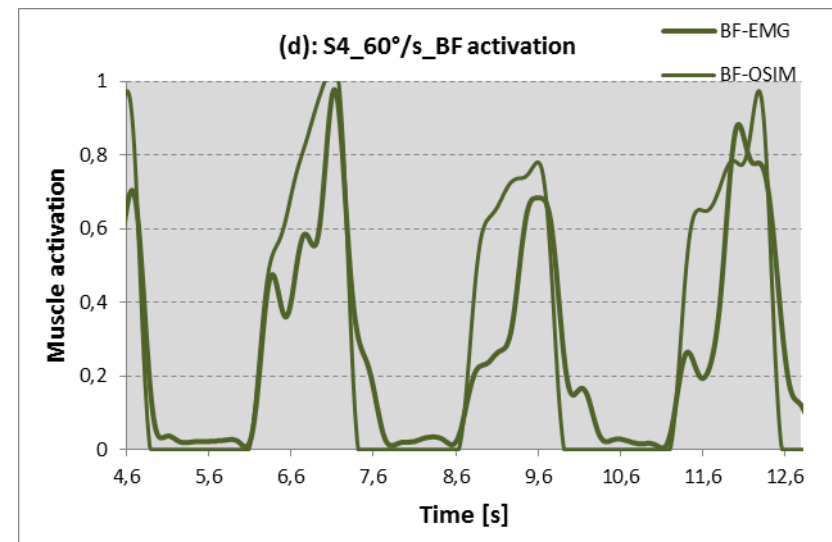
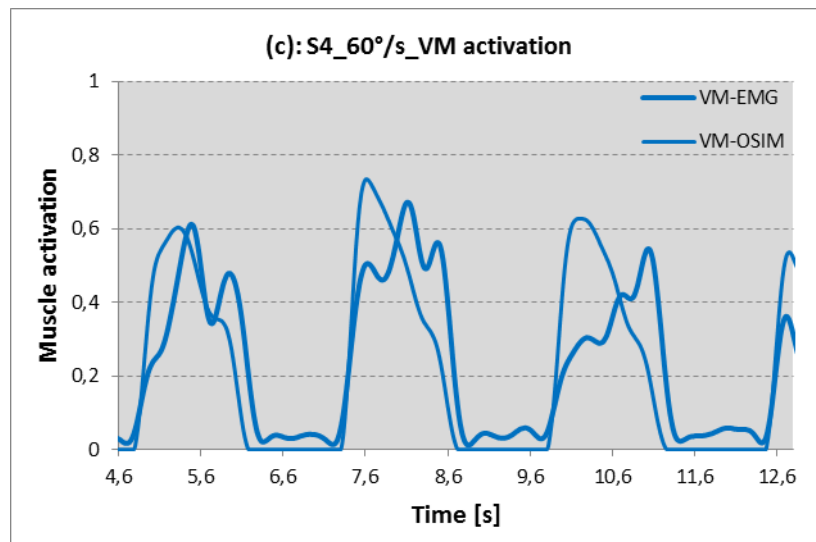
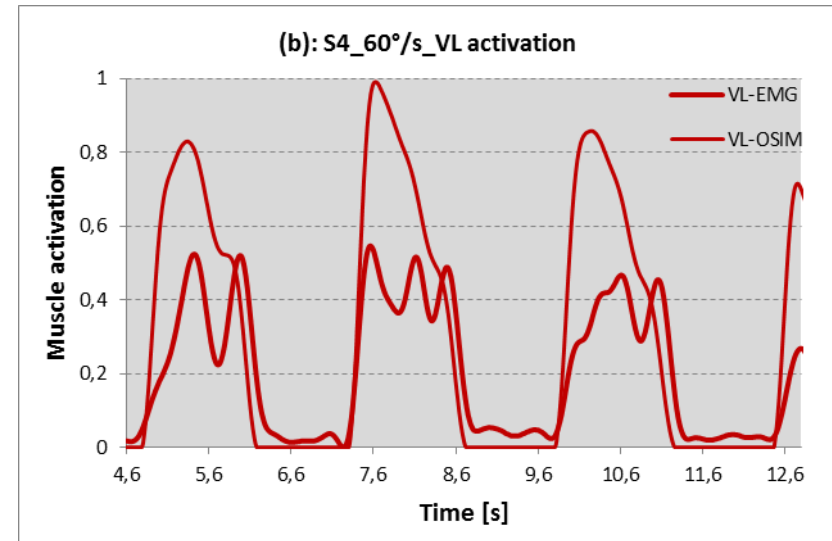
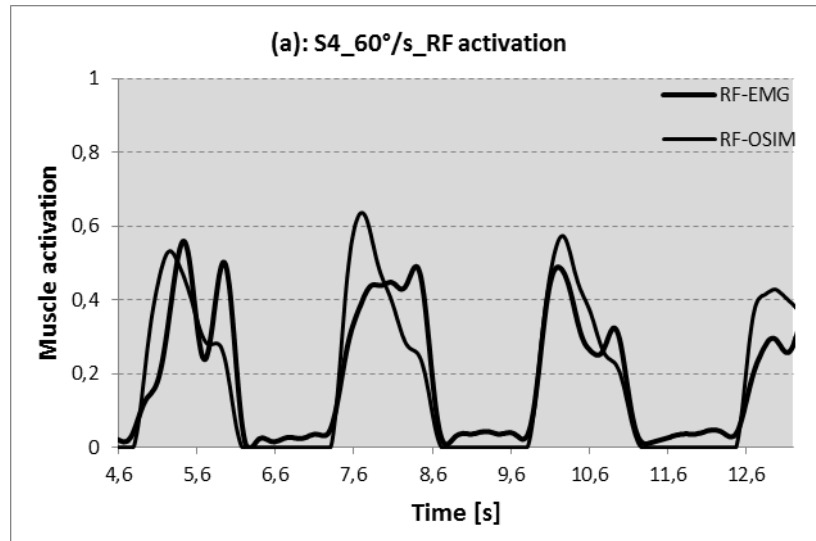


Fig.A.4.3: EMG and OpenSim muscle activation of S4 at 60°/s of RF (a), VL (b), VM (c) and BF (d).

120 °/s

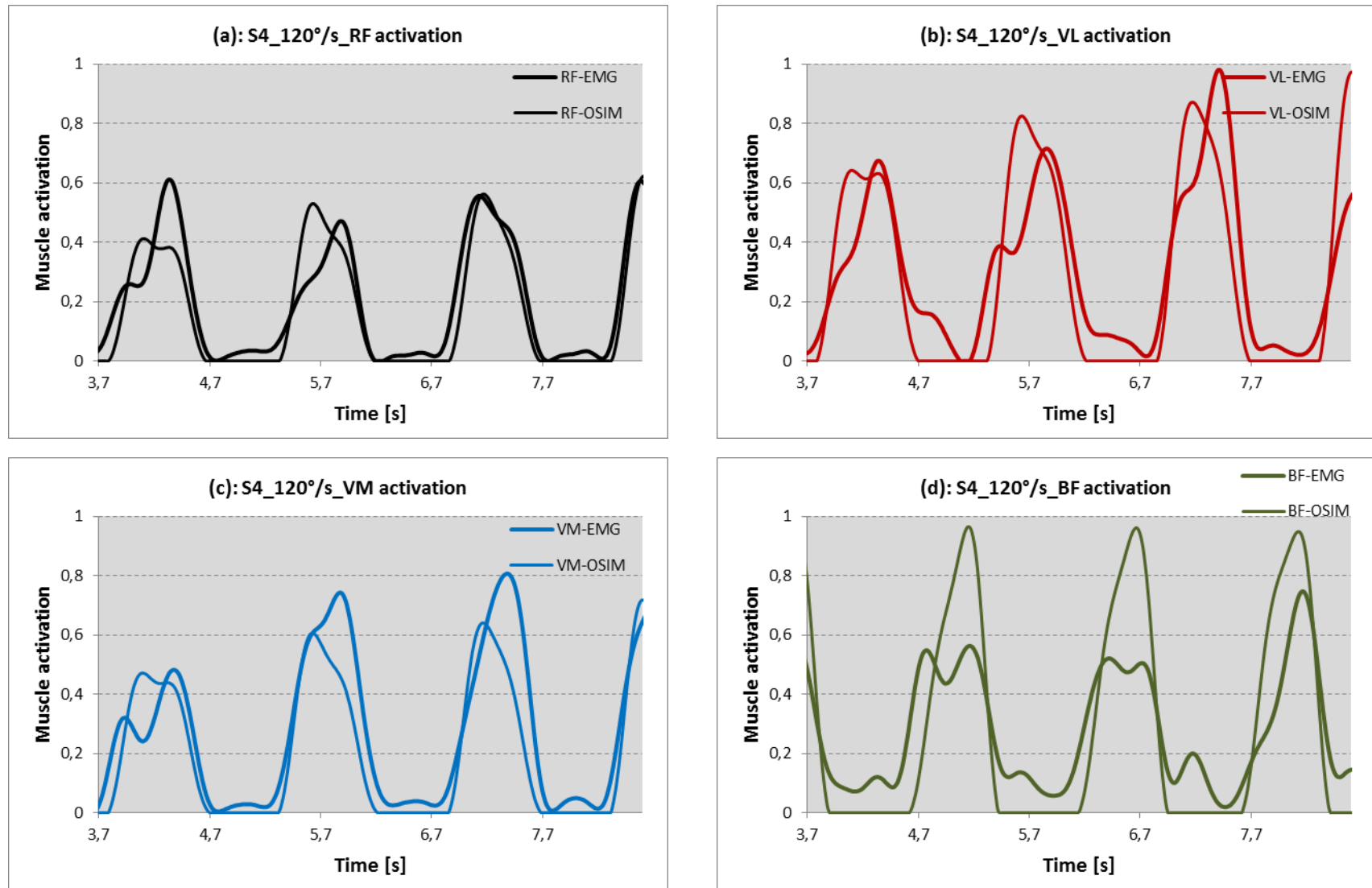


Fig.A.4.4: EMG and OpenSim muscle activation of S4 at 120°/s of RF (a), VL (b), VM (c) and BF (d).

180 °/s

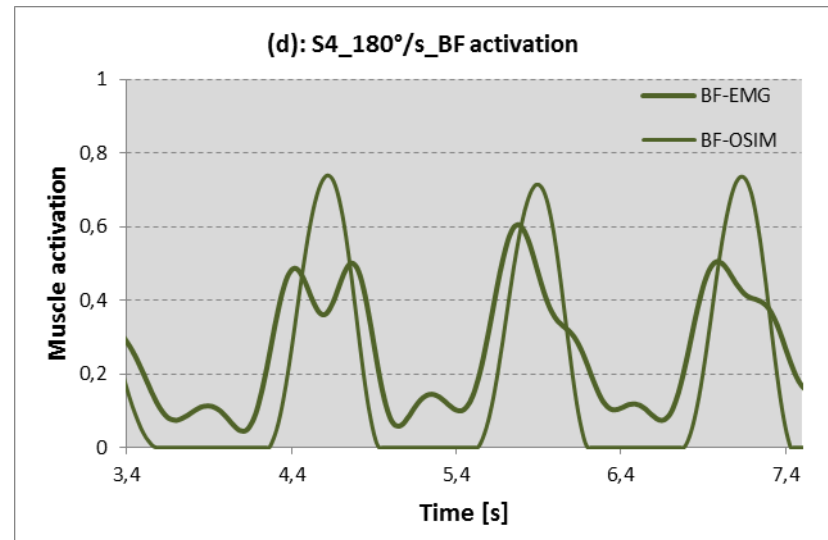
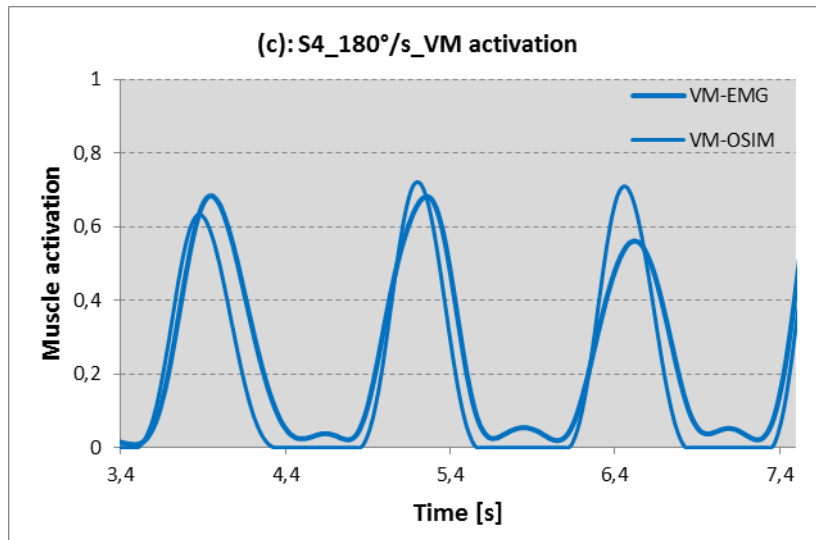
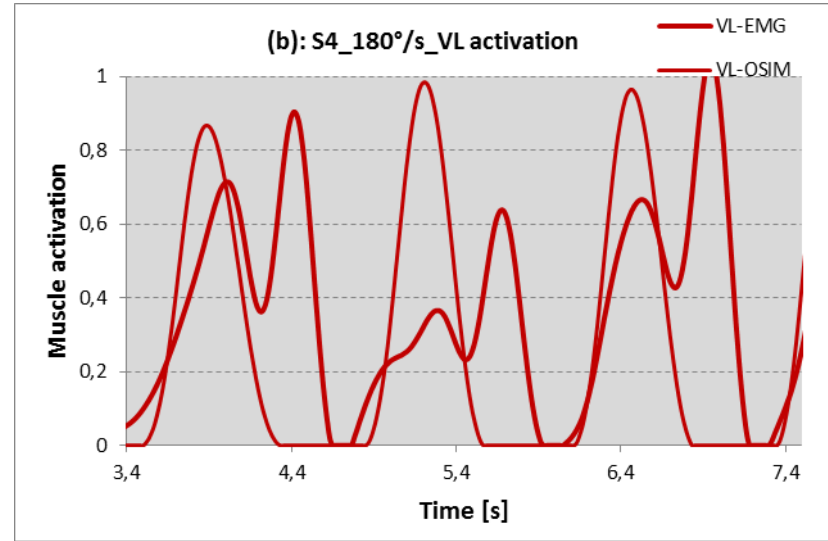
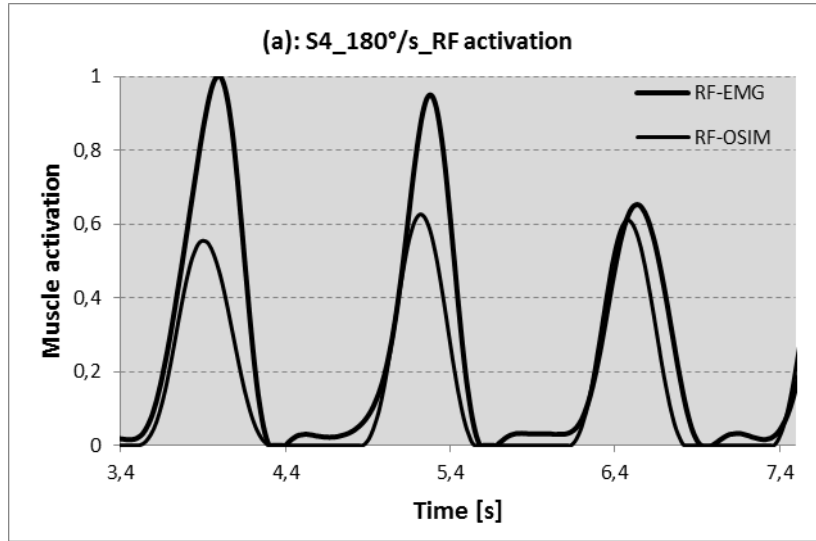


Fig.A.4.5: EMG and OpenSim muscle activation of S4 at 180°/s of RF (a), VL (b), VM (c) and BF (d).

240 °/s

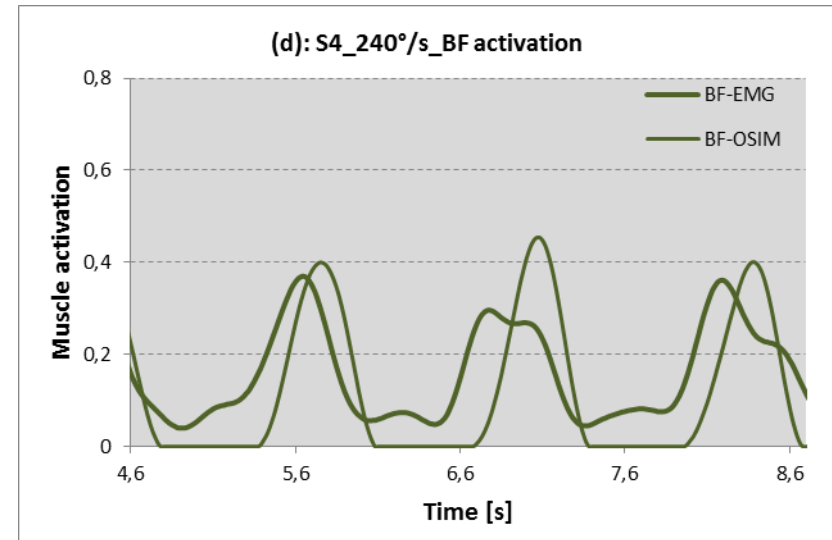
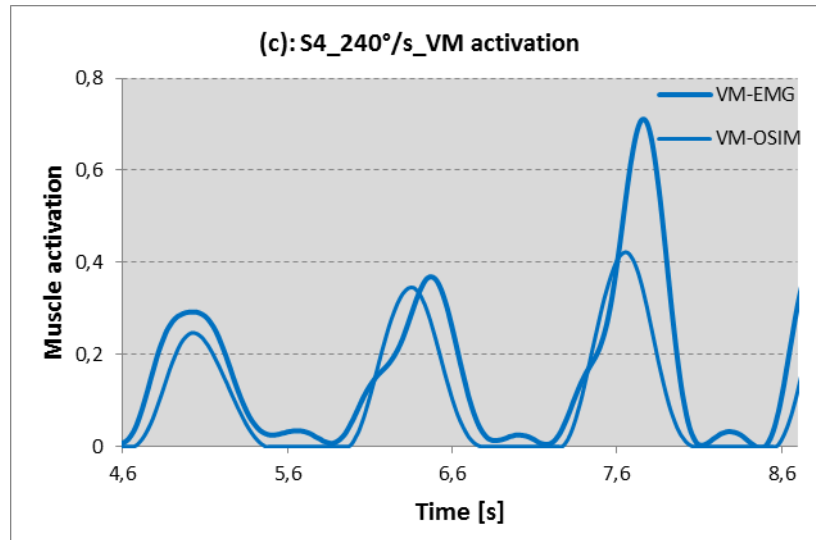
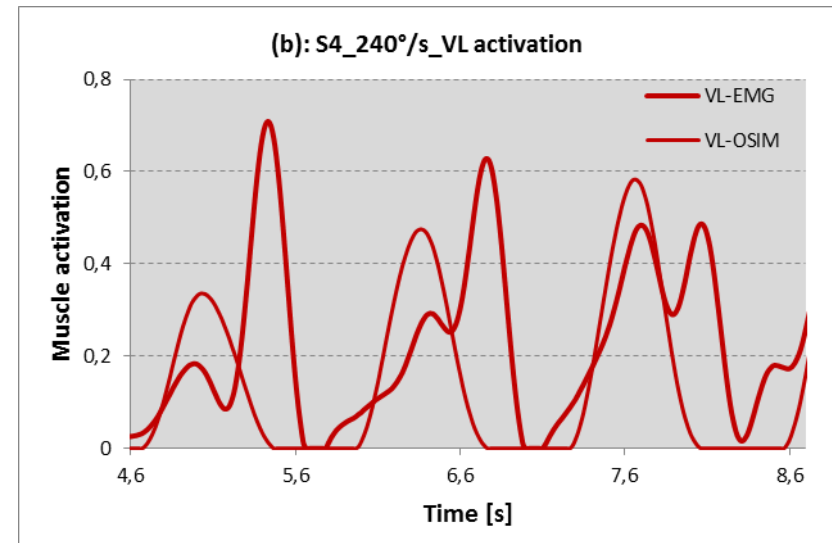
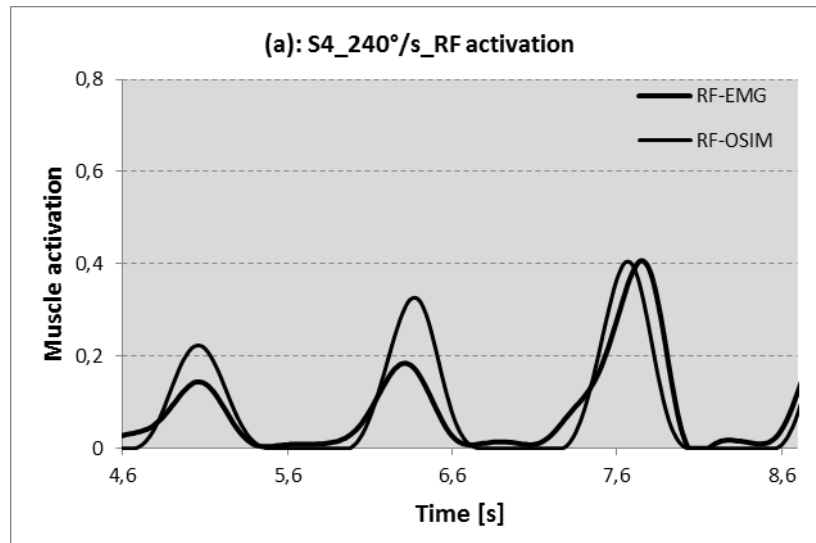


Fig.A.4.6: EMG and OpenSim muscle activation of S4 at 240°/s of RF (a), VL (b), VM (c) and BF (d).

Comparison of EMG signal and OpenSim muscle activation: quantitative results

	60 °/s	120 °/s	180 °/s	240 °/s
RF	-14,05±17,52	6,32±23,44	28,42±19,61	-43,71±39,81
VL	-74,35±14,02	0,16±13,84	-44,75±60,30	18,84±36,84
VM	-7,60±8,38	13,81±10,05	-8,22±17,11	20,76±17,82
BF	-10,84±2,96	-60,92±30,17	-37,09±16,54	-24,19±25,32

Tab.A.4.2: Peak error of S4 in [%] of RF, VL, VM and BF at 60°/s, 120°/s, 180°/s and 240°/s.

	60 °/s	120 °/s	180 °/s	240 °/s
RF	8,60±15,34	9,17±10,25	5,30±0,52	-0,40±4,75
VL	6,00±14,41	13,00±3,29	36,93±0,25	28,90±1,49
VM	22,27±6,84	15,80±2,00	5,07±2,60	-0,90±7,90
BF	-2,53±5,71	-5,07±11,90	-3,63±10,43	-13,57±7,61

Tab.A.4.3: Time error of S4 in [%] of RF, VL, VM and BF at 60°/s, 120°/s, 180°/s and 240°/s.

	240 °/s	180 °/s	120 °/s	60 °/s
RF	-5,86±6,37	17,57±3,38	40,99±17,85	-35,91±47,58
VL	-62,41±4,95	-5,10±17,23	0,40±5,99	11,50±14,03
VM	-8,87±7,96	7,71±18,33	12,17±8,42	25,45±17,34
BF	-17,55±12,01	-21,25±9,73	4,55±4,02	7,25±12,07

Tab.A.4.4: Area error of S4 in [%] of RF, VL, VM and BF at 60°/s, 120°/s, 180°/s and 240°/s.

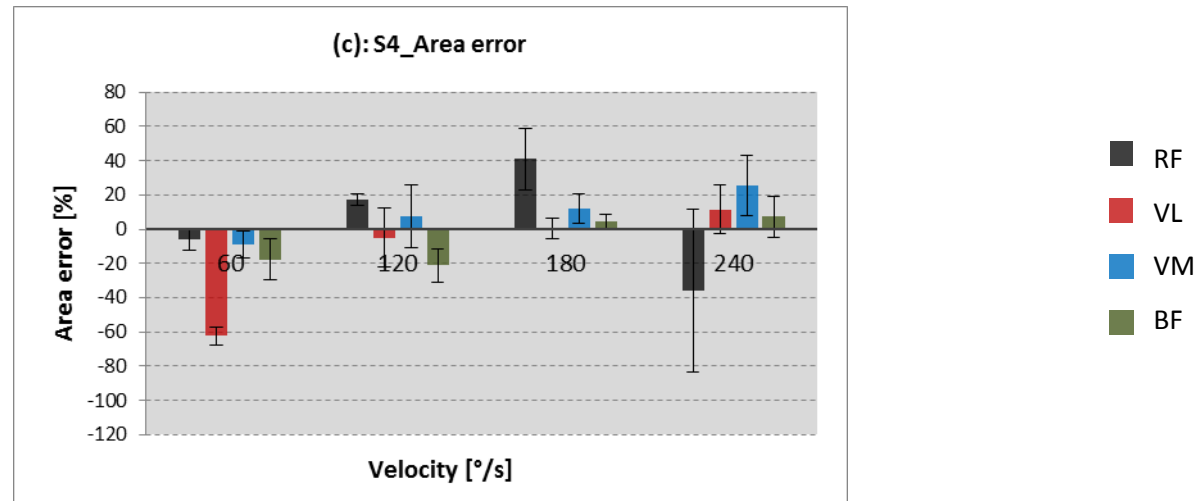
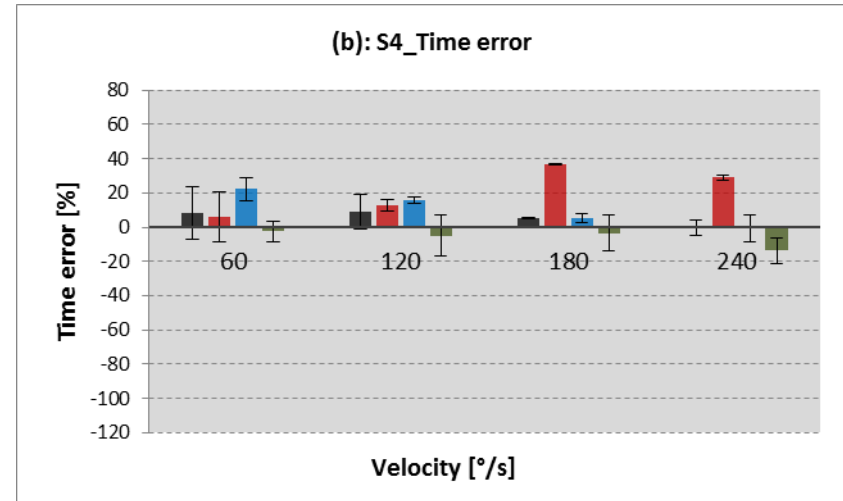
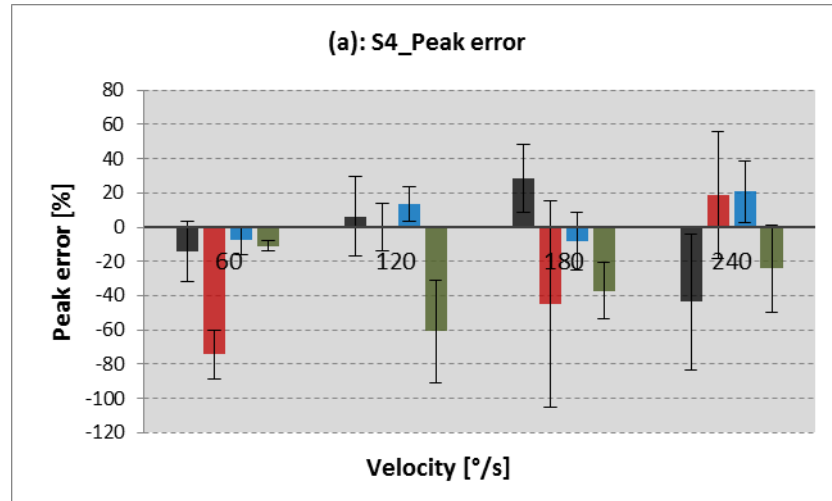


Fig.A.4.7: Quantitative results of muscle activation analysis of S4: (a): Peak error at different velocities; (b): Time error at different velocities; (c): Area error at different velocities.

Comparison of analytical models and OpenSim model

Model 1: parameters

$$\text{Tibia: } m_{\text{tibia}} = 3,107 \text{ kg} \quad I_{G \text{ tibia}} = 0,048 \text{ kg} \cdot \text{m}^2 \quad \Delta_{y \text{ tibia}} = 0,454 \text{ m} \quad \Delta_{y \text{ G tibia}} = 0,197 \text{ m}$$

$$\text{Talus: } m_{\text{talus}} = 0,08 \text{ kg} \quad I_{G \text{ talus}} = 7,3 \cdot 10^{-4} \text{ kg} \cdot \text{m}^2 \quad \Delta_{y \text{ talus}} = 0,454 \text{ m} \quad \Delta_{y \text{ G talus}} = 0,454 \text{ m}$$

$$\text{Calc: } m_{\text{calc}} = 1,048 \text{ kg} \quad I_{G \text{ calc}} = 0,003 \text{ kg} \cdot \text{m}^2 \quad \Delta_{x \text{ calc}} = 0,046 \text{ m} \quad \Delta_{y \text{ calc}} = 0,039 \text{ m}$$

$$\Delta_{x \text{ G calc}} = 0,094 \text{ m} \quad \Delta_{y \text{ G calc}} = 0,028 \text{ m}$$

$$\text{Toes: } m_{\text{toes}} = 0,182 \text{ kg} \quad I_{G \text{ toes}} = 7,3 \cdot 10^{-5} \text{ kg} \cdot \text{m}^2 \quad \Delta_{x \text{ toes}} = 0,167 \text{ m} \quad \Delta_{y \text{ toes}} = 0,0019 \text{ m}$$

$$\Delta_{x \text{ G toes}} = 0,032 \text{ m} \quad \Delta_{y \text{ G toes}} = 0,0056 \text{ m}$$

Model 2: parameters

$$\text{Tibia: } m_{\text{tibia}} = 2,835 \text{ kg} \quad I_{G \text{ tibia}} = 0,046 \text{ kg} \cdot \text{m}^2 \quad \Delta_{y \text{ tibia}} = 0,422 \text{ m} \quad \Delta_{y \text{ G tibia}} = 0,18 \text{ m}$$

$$\text{Foot: } m_{\text{foot}} = 0,882 \text{ kg} \quad I_{G \text{ foot}} = 0,005 \text{ kg} \cdot \text{m}^2 \quad \Delta_{x \text{ G foot}} = 0,073 \text{ m} \quad \Delta_{y \text{ G foot}} = 0,036 \text{ m}$$

$$D_{Q2} = 0,08 \text{ m} \quad H_{Q2} = 0,026 \text{ m} \quad D_{Q1} = 0,3 \text{ m} \quad H_{Q1} = 0,03 \text{ m}$$

$$B_{PT} [\text{m}] = 0,0097 \cdot \varphi_{k+}^5 - 0,0215 \cdot \varphi_{k+}^4 - 0,0098 \cdot \varphi_{k+}^3 + 0,0366 \cdot \varphi_{k+}^2 - 0,0141 \cdot \varphi_{k+} + 0,0464 \quad \varphi_{k+} [\text{rad}]$$

$$\text{BFB: } D_{\text{BFB1}} = 0,2 \text{ m} \quad D_{\text{BFB2}} = 0,04 \text{ m} \quad H_{\text{BFB1}} = 0,04 \text{ m} \quad H_{\text{BFB2}} = 0,03 \text{ m}$$

$$\text{BFL: } D_{\text{BFL1}} = 0,49 \text{ m} \quad D_{\text{BFL2}} = 0,04 \text{ m} \quad H_{\text{BFL1}} = 0,04 \text{ m} \quad H_{\text{BFL2}} = 0,03 \text{ m}$$

$$\text{SM: } D_{\text{SM1}} = 0,49 \text{ m} \quad D_{\text{SM2}} = 0,5 \text{ m} \quad H_{\text{SM1}} = 0,4 \text{ m} \quad H_{\text{SM2}} = 0,035 \text{ m}$$

$$\text{ST: } D_{\text{ST1}} = 0,49 \text{ m} \quad H_{\text{ST1}} = 0,5 \text{ m} \quad B_{\text{ST}} = 0,4 \text{ m} \quad \alpha_{\text{ST}} = 0,52 \text{ rad}$$

Fig.A.4.8: S4_60°/s_Extension

— OSIM — Mod1_Herzog — Mod1_Van Eijden — Mod2 - - - limit value

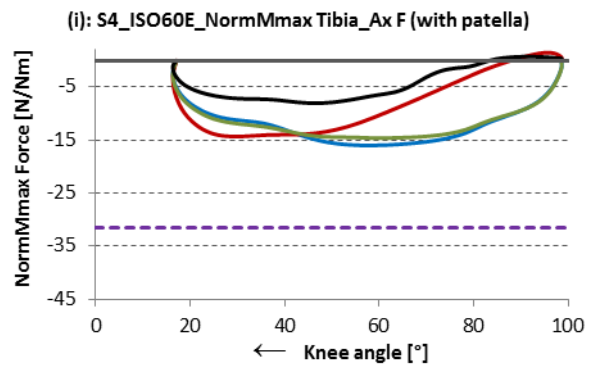
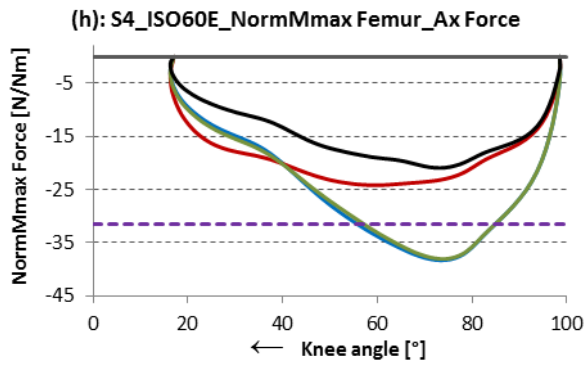
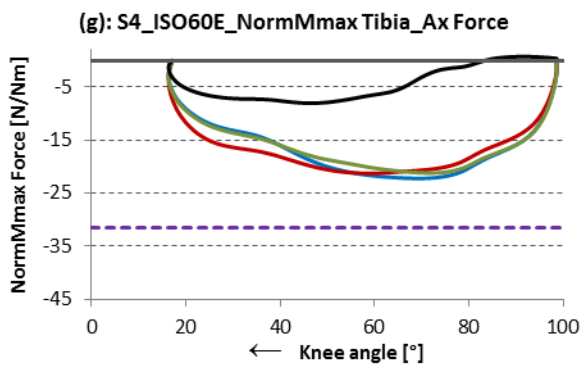
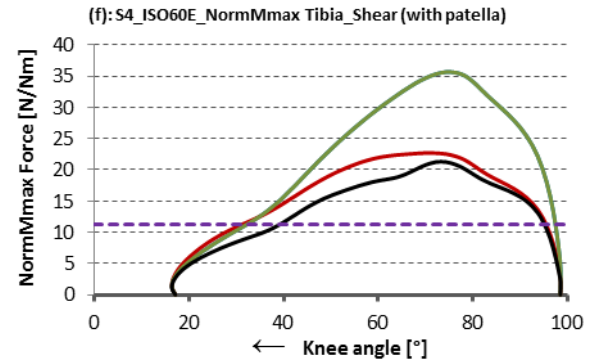
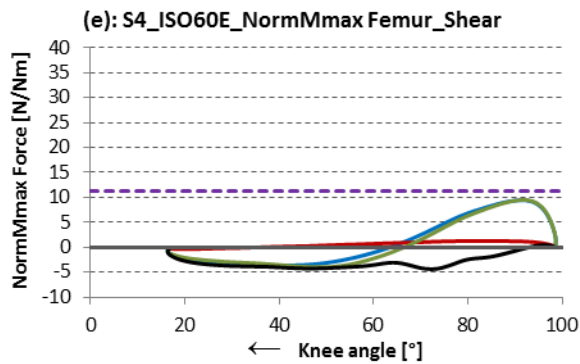
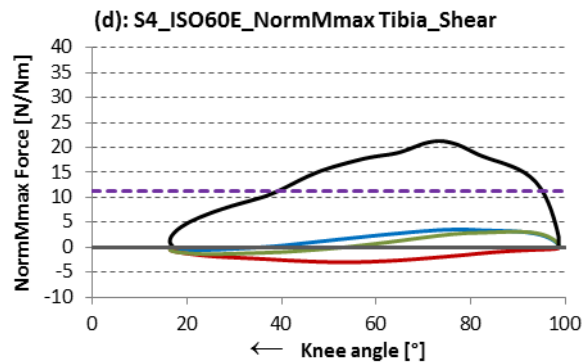
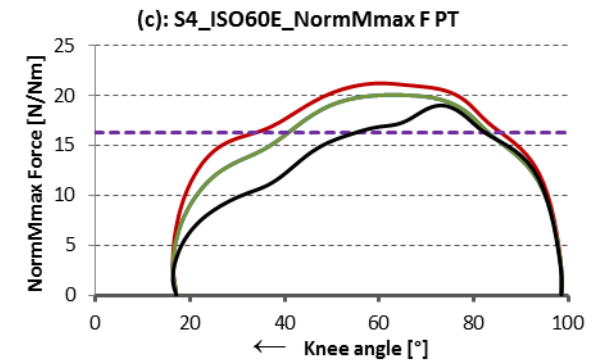
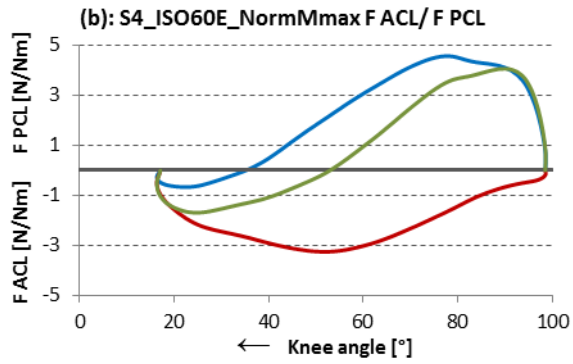
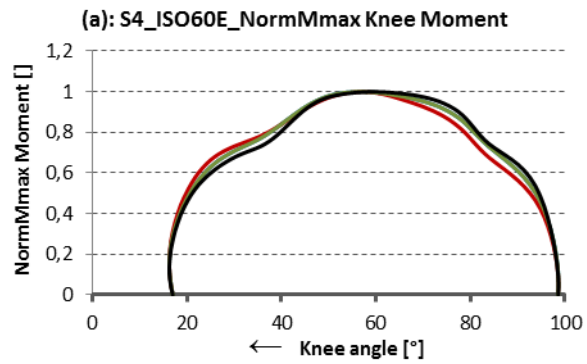


Fig.A.4.9: S4_60°/s_Flexion

— OSIM — Mod1 — Mod2 - - - limit value (•••• OSIM BFL •••• Mod1 BFL •••• Mod2 BFL)

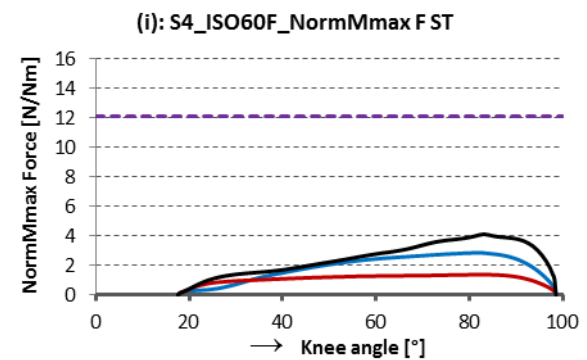
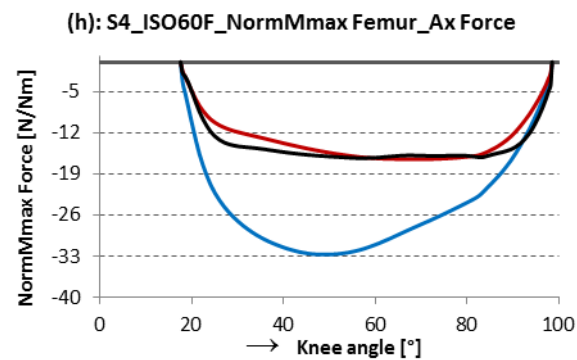
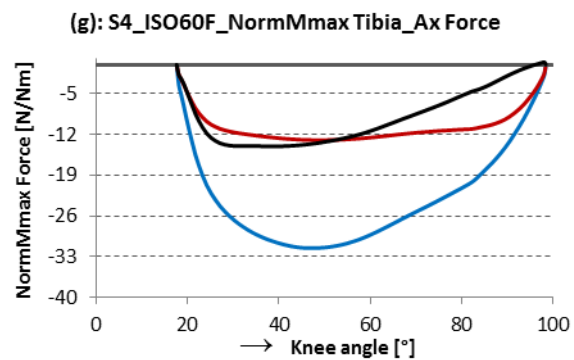
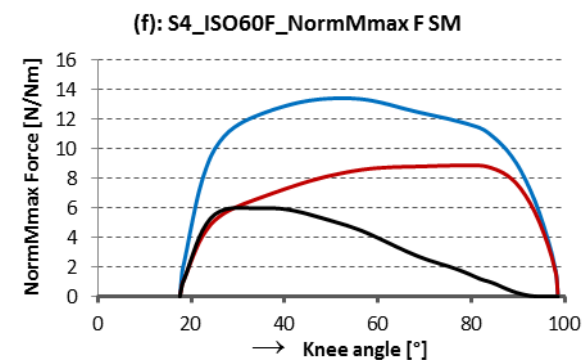
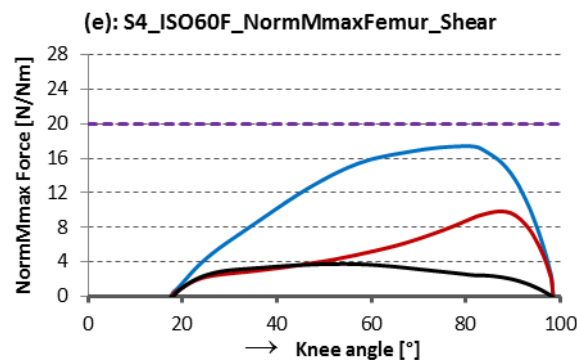
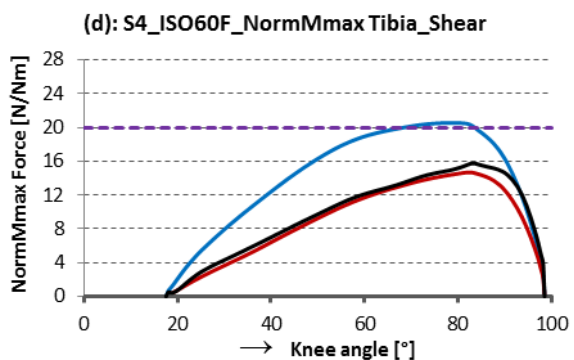
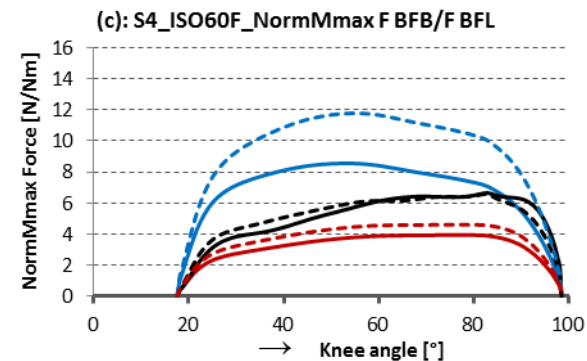
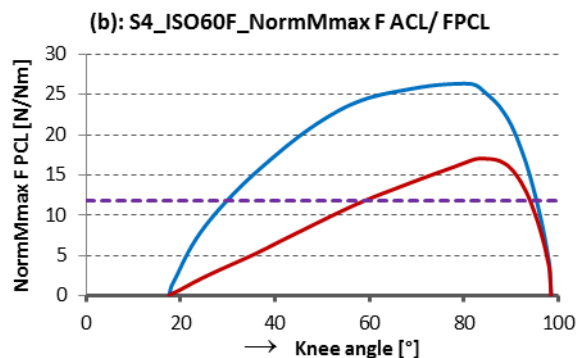
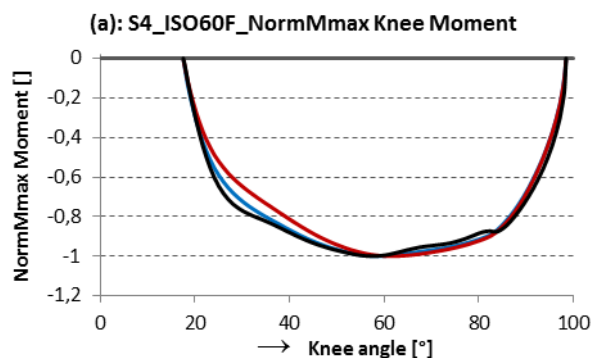


Fig.A.4.10: S4_120°/s_Extension

— OSIM — Mod1_Herzog — Mod1_Van Eijden — Mod2 - - - - - limit value

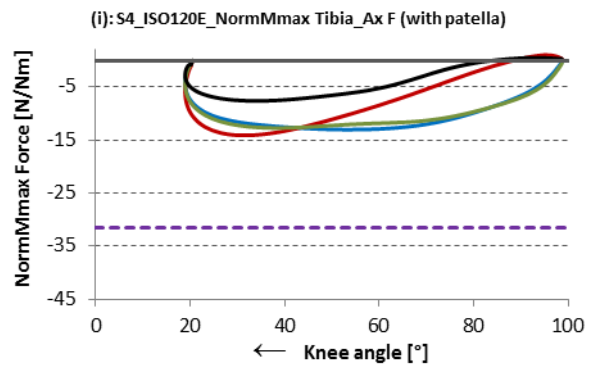
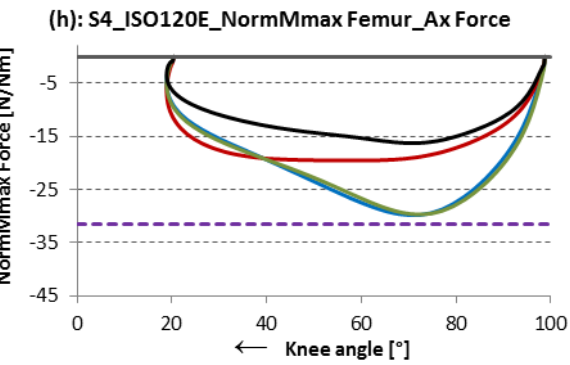
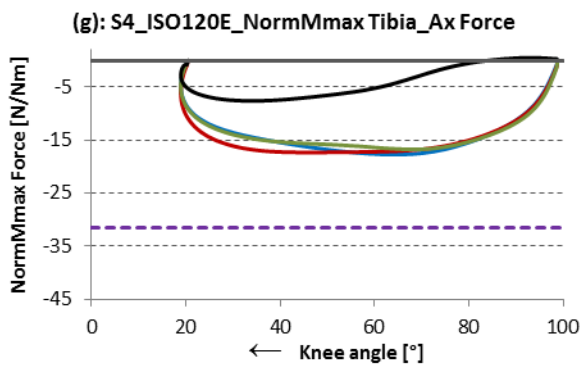
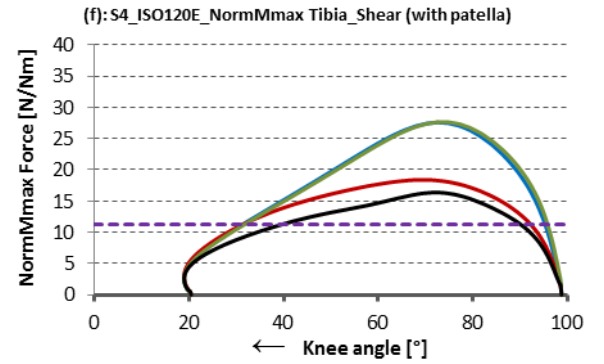
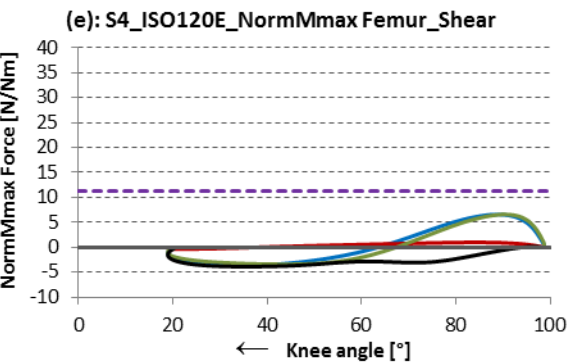
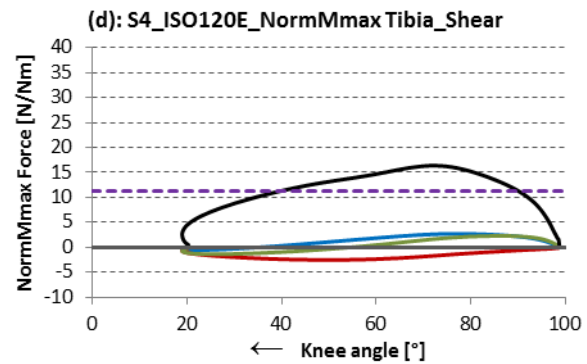
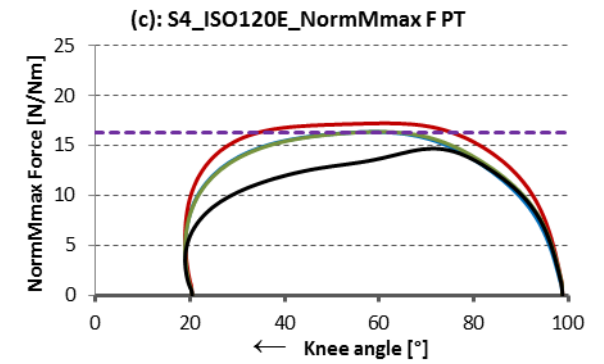
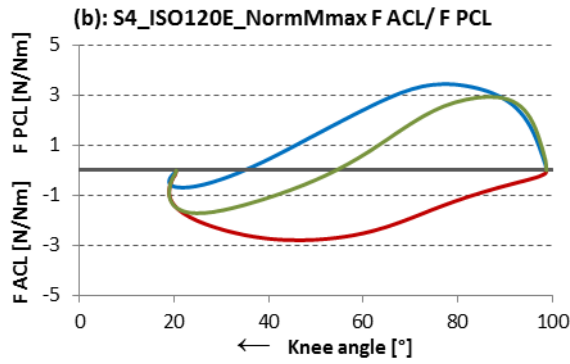
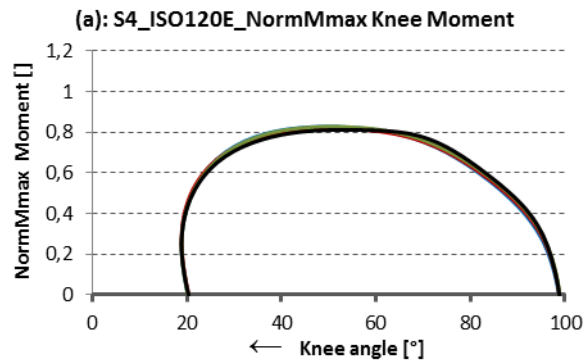


Fig.A.4.11: S4_120°/s_Flexion

— OSIM — Mod1 — Mod2 - - - - limit value (- - - - OSIM BFL - - - - Mod1 BFL - - - - Mod2 BFL)

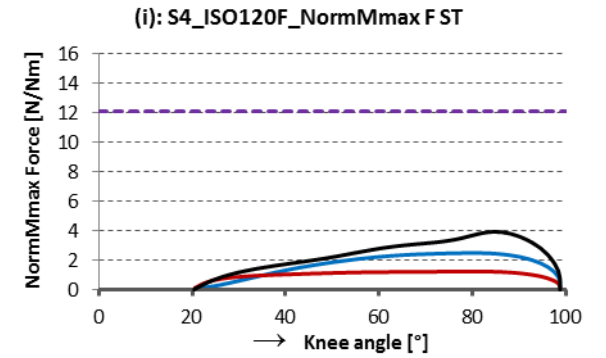
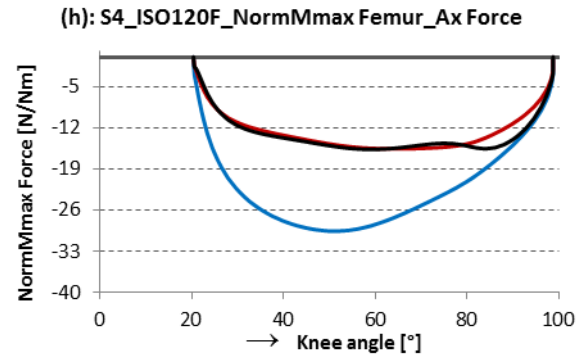
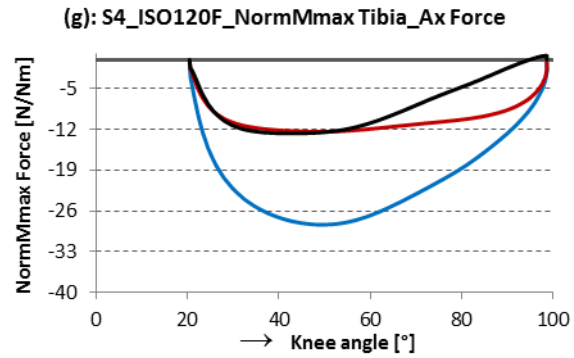
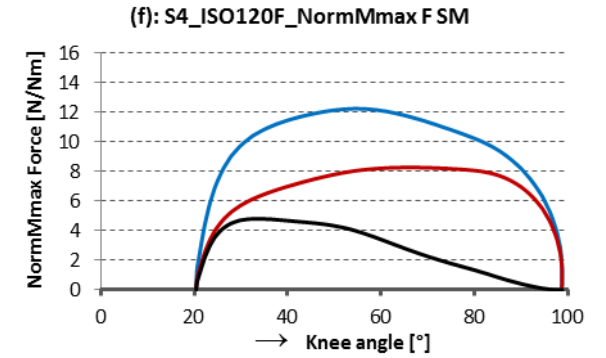
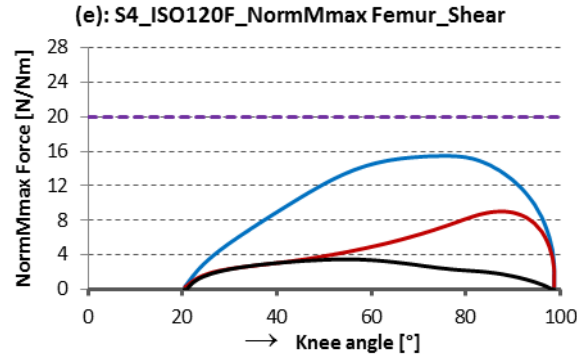
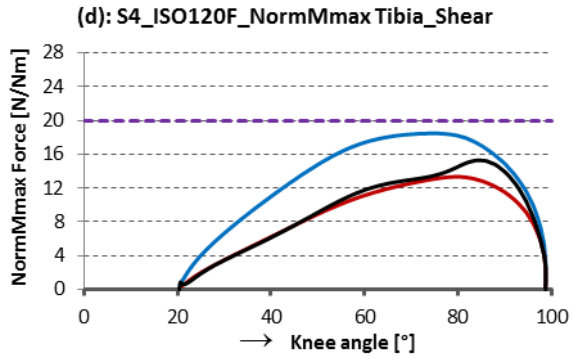
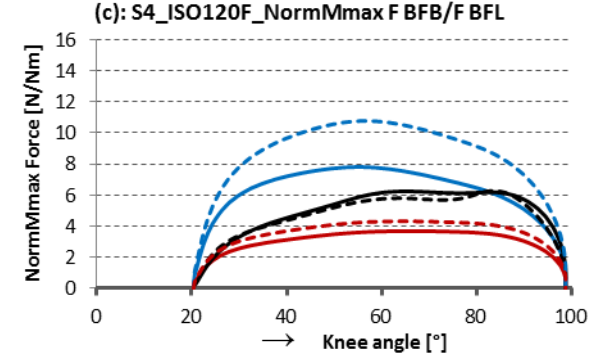
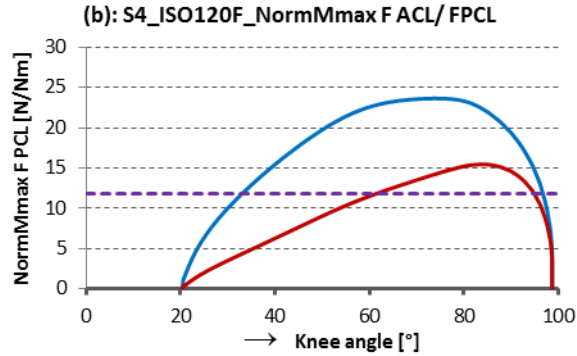
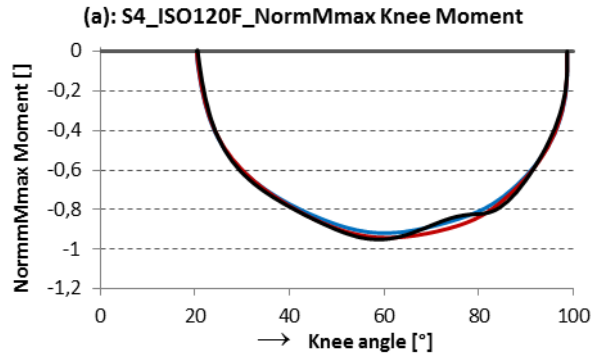


Fig.A.4.12: S4_180°/s_Extension

— OSIM — Mod1_Herzog — Mod1_Van Eijden — Mod2 - - - limit value

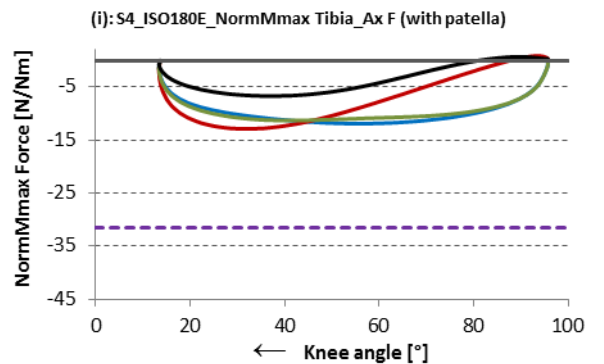
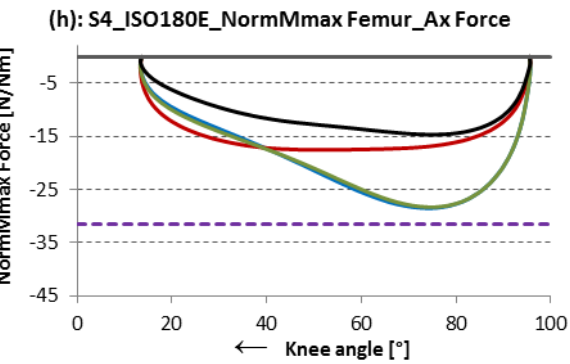
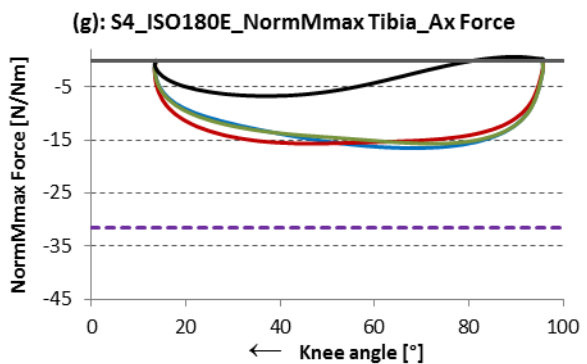
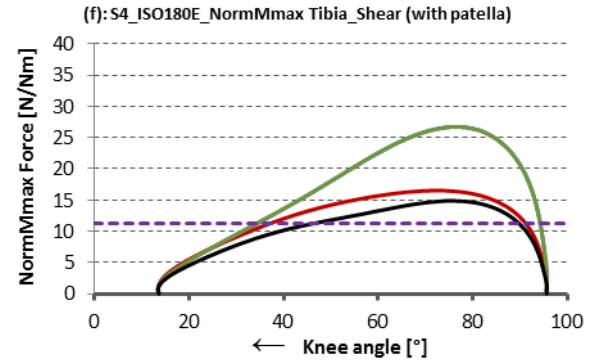
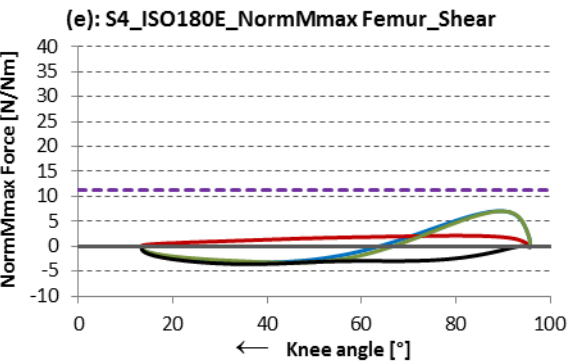
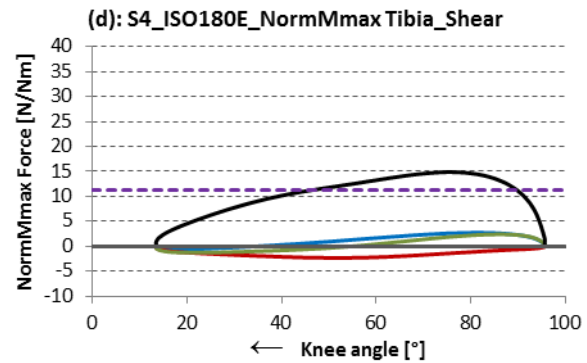
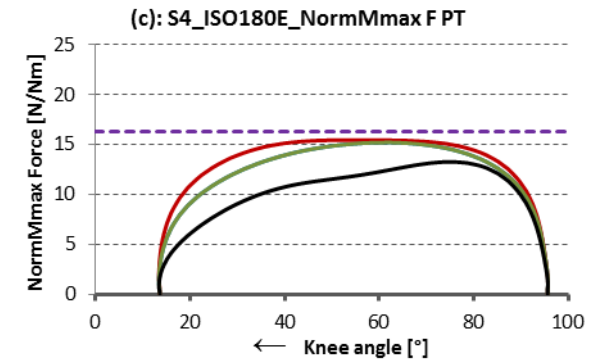
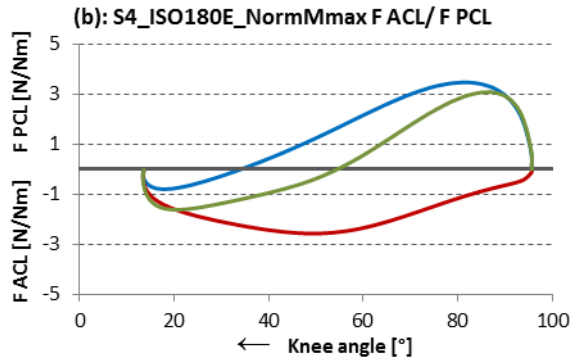
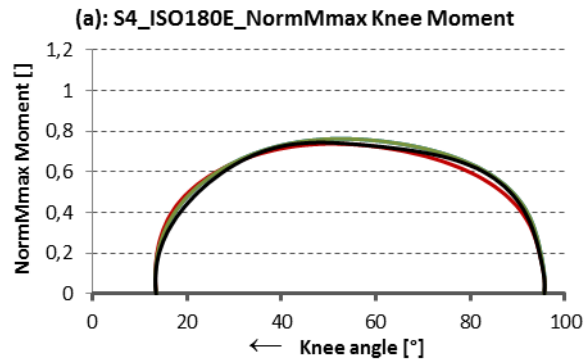


Fig.A.4.13: S4_180°/s_Flexion

— OSIM — Mod1 — Mod2 - - - limit value (•••• OSIM BFL •••• Mod1 BFL •••• Mod2 BFL)

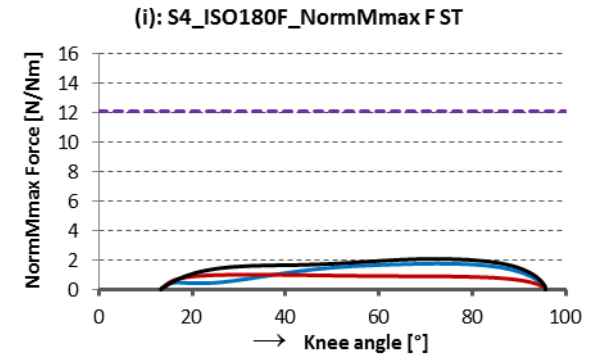
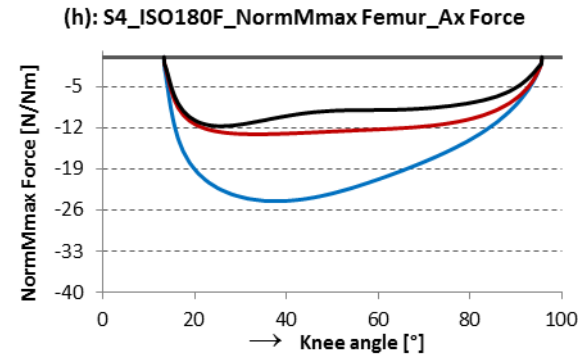
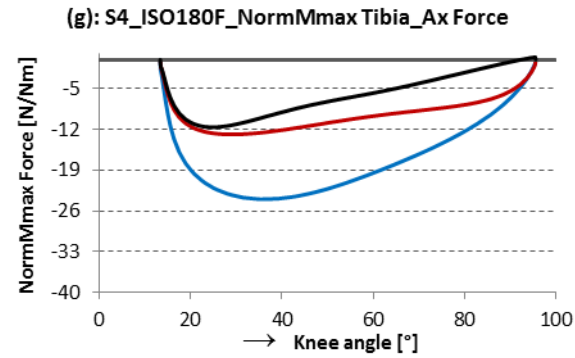
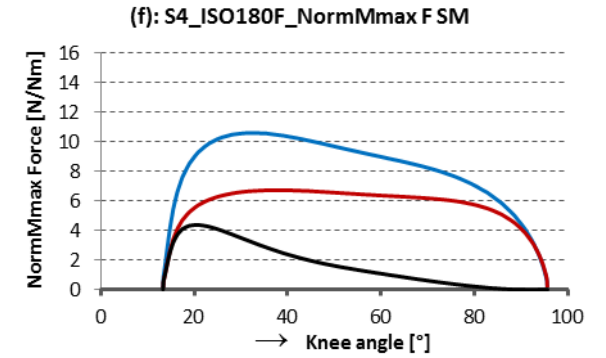
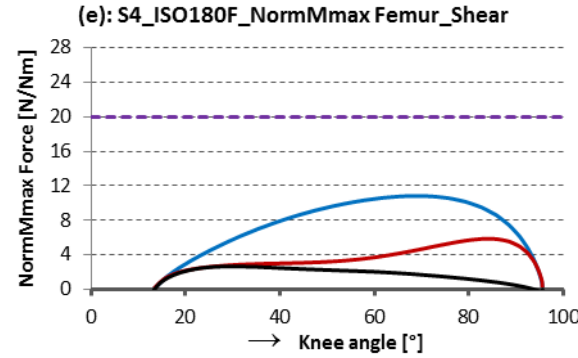
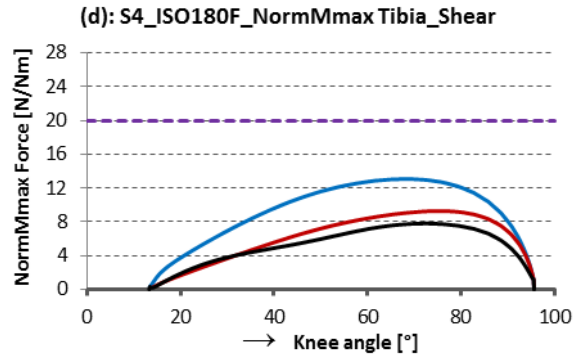
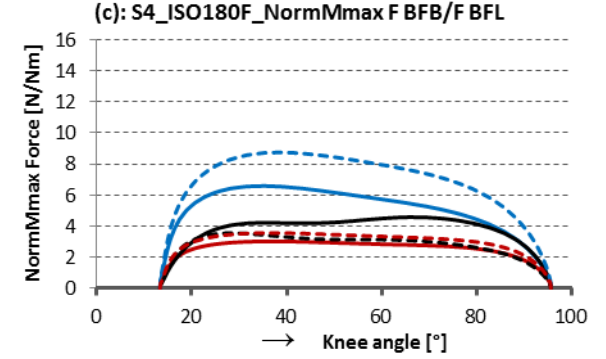
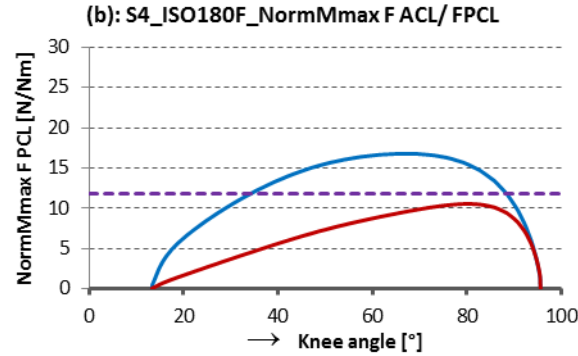
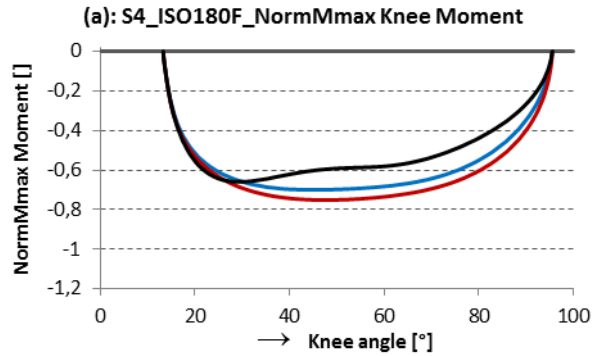


Fig.A.4.14: S4_240°/s_Extension

— OSIM — Mod1_Herzog — Mod1_Van Eijden — Mod2 - - - - limit value

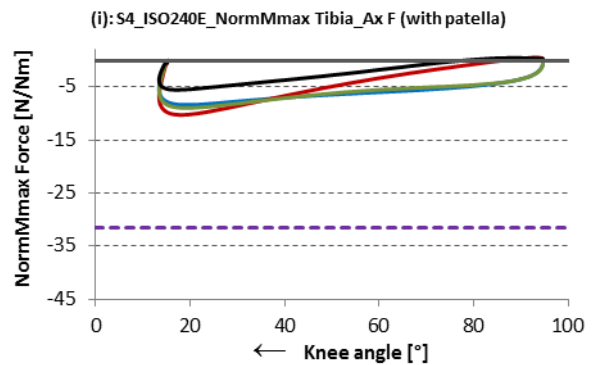
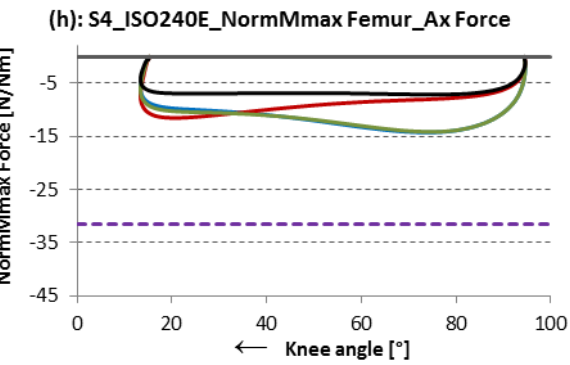
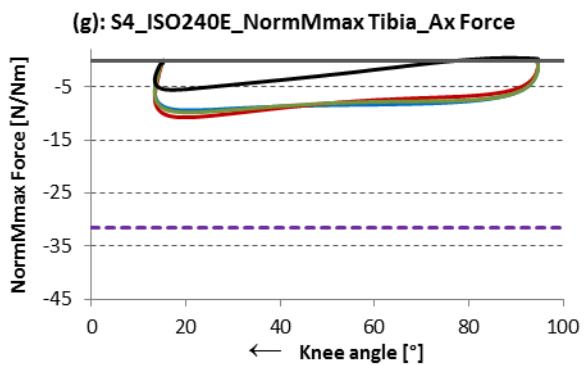
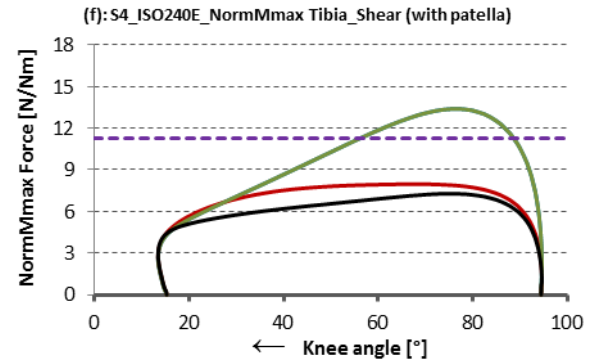
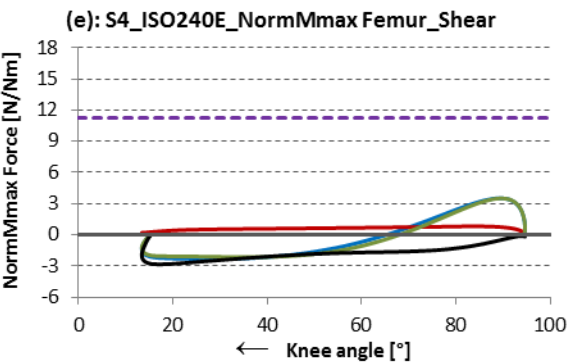
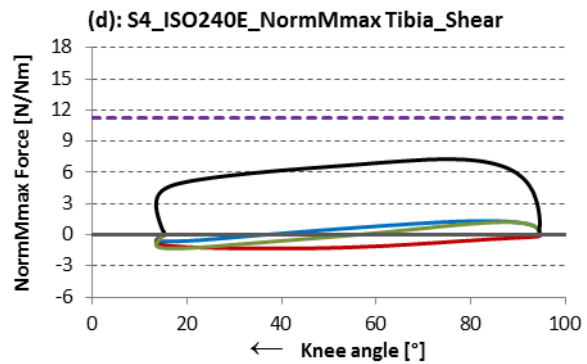
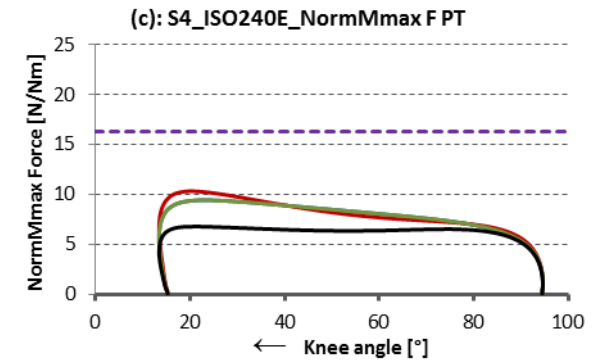
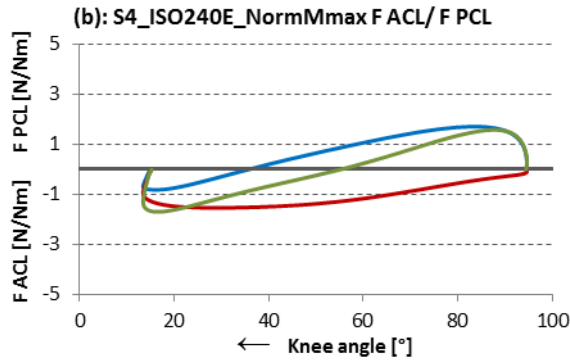
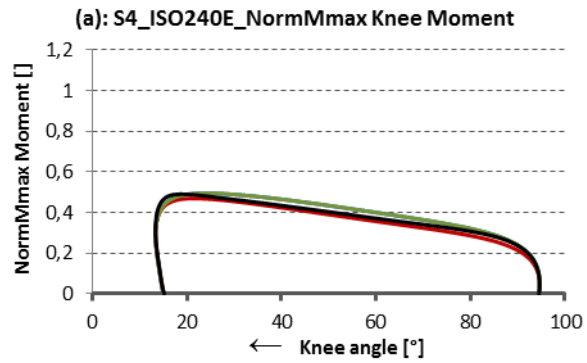
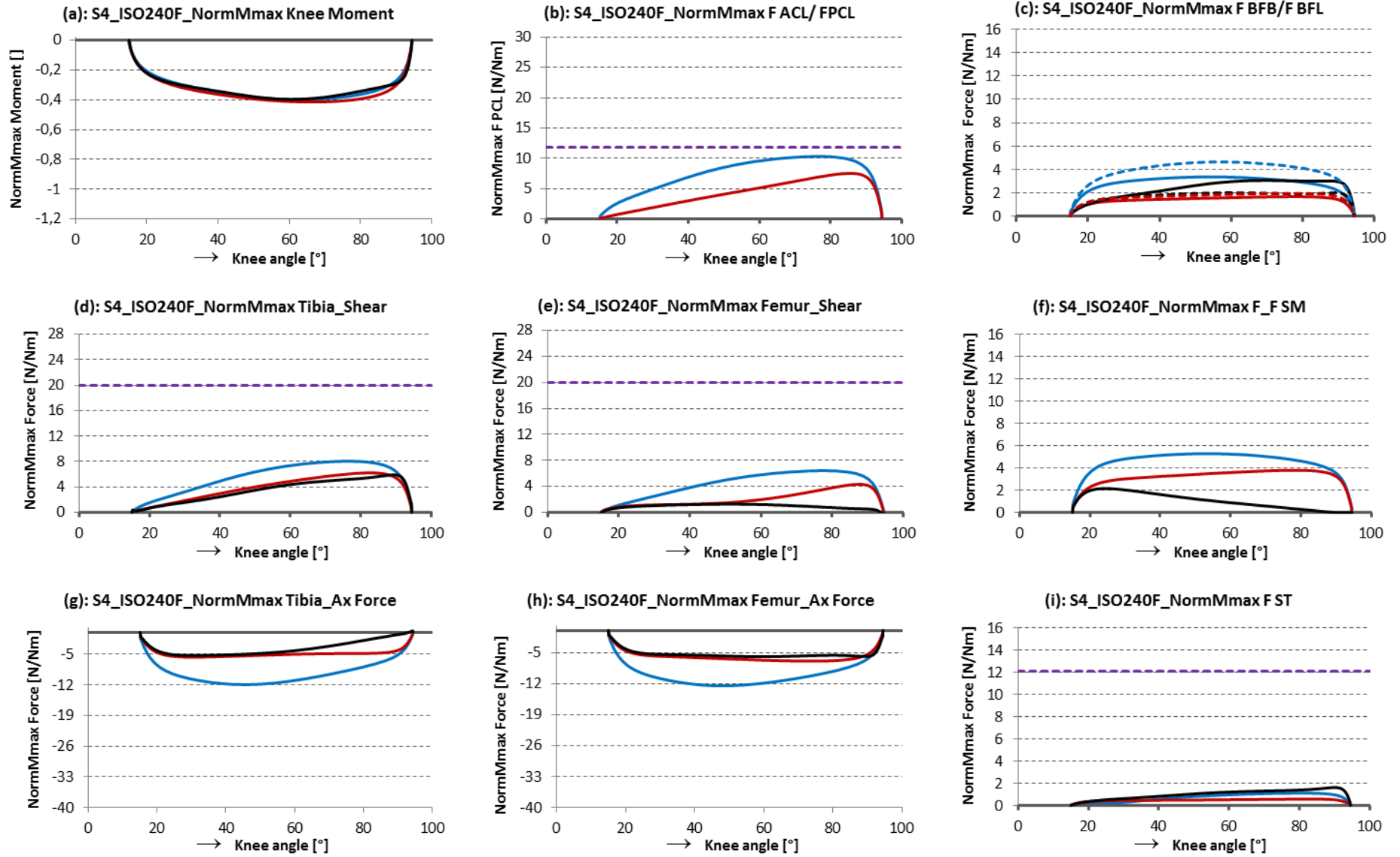


Fig.A.4.15: S4_240°/s_Flexion

— OSIM — Mod1 — Mod2 - - - - limit value (- - - - OSIM BFL - - - - Mod1 BFL - - - - Mod2 BFL)



A.5.Results of Subject 5 (S5)

Torque at the servo-motor

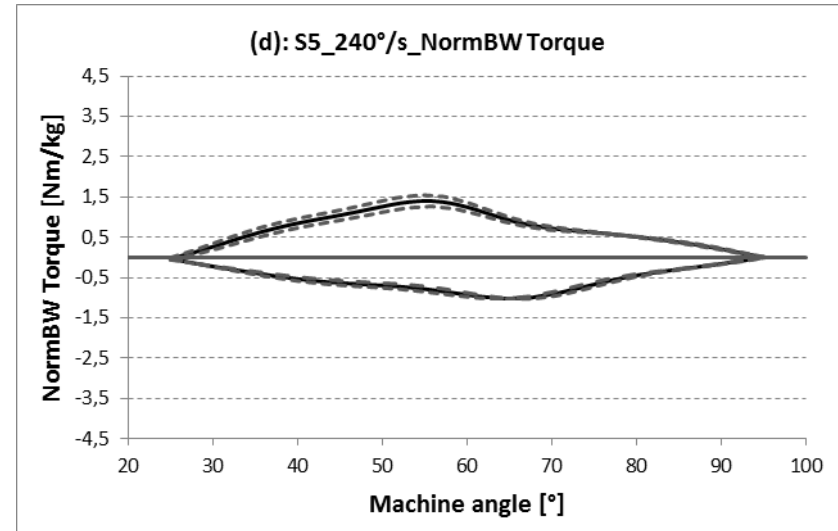
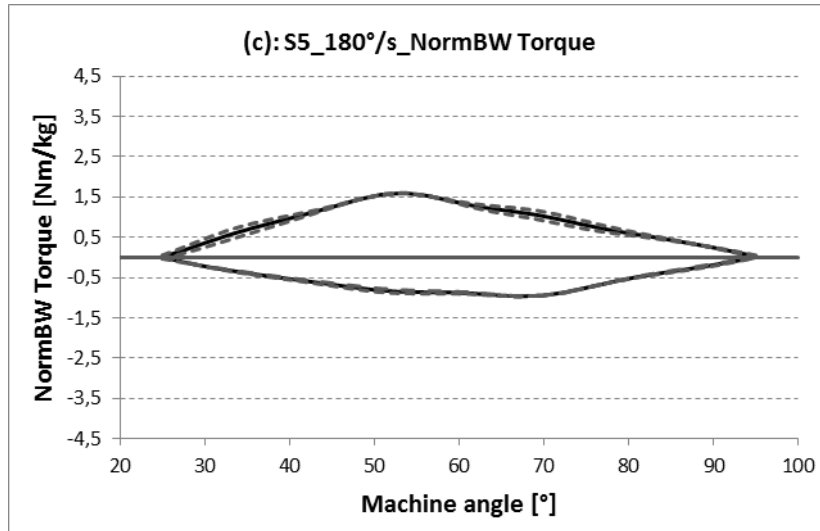
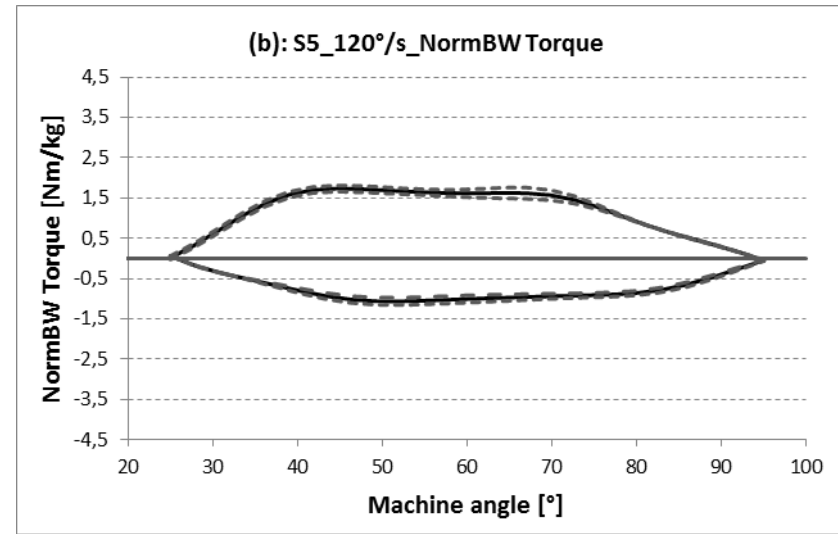
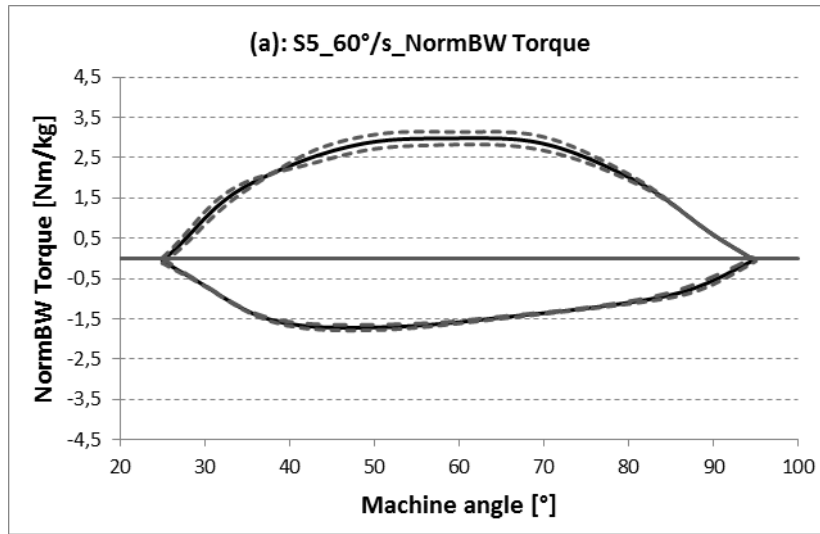


Fig.A.5.1: Normalized Torque of S5 at 60°/s (a), 120°/s (b), 180°/s (c) and 240°/s (d).

Flexors and Extensors Balance

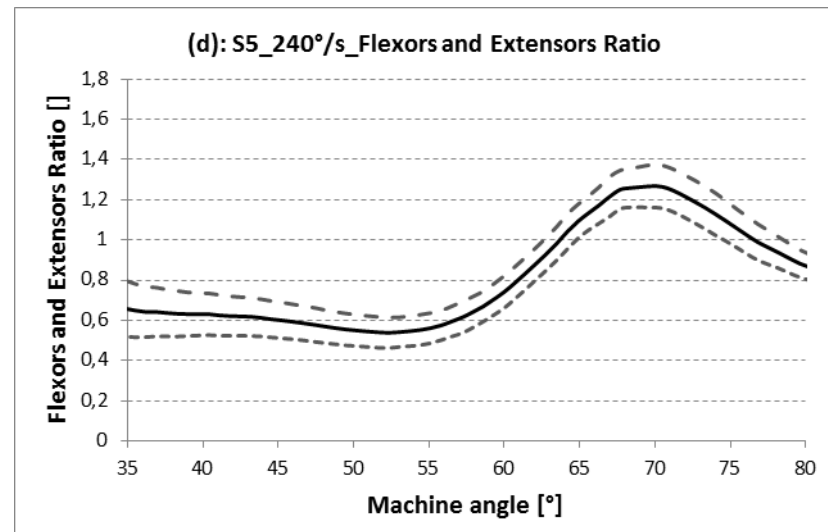
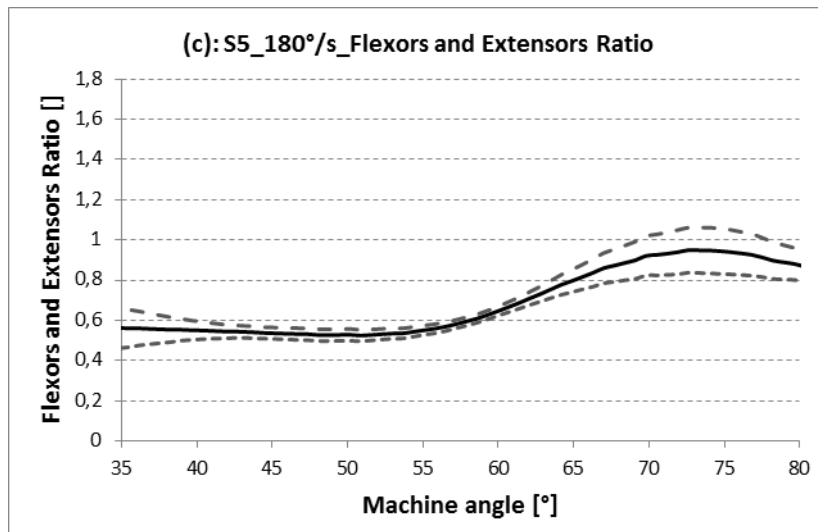
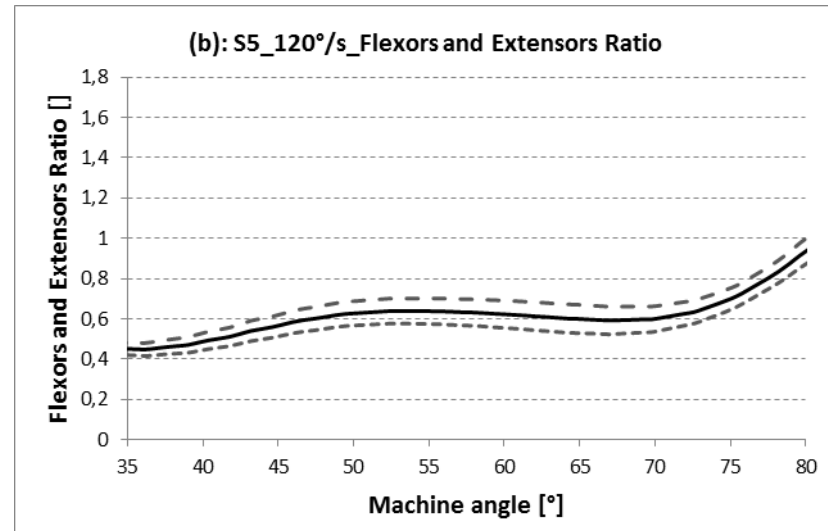
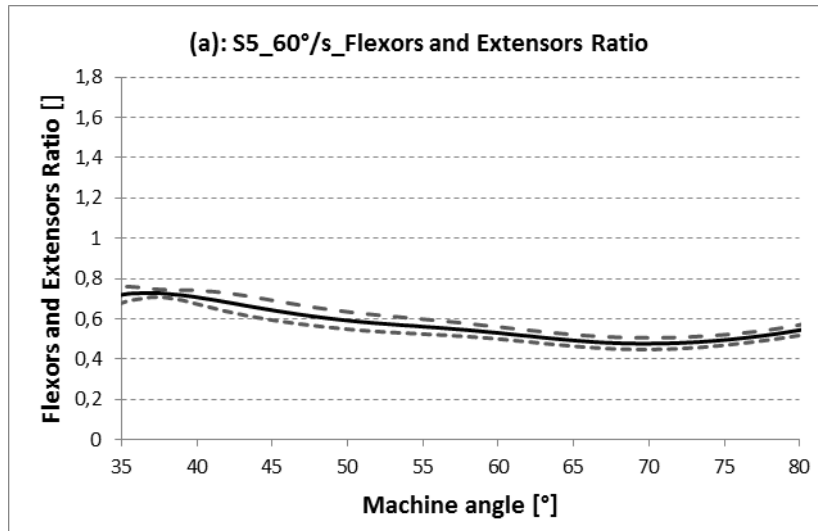


Fig.A.5.2: Flexors and extensors balance of S5 at 60°/s (a), 120°/s (b), 180°/s (c) and 240°/s (d).

Comparison of EMG signal and OpenSim muscle activation

M = 70 kg H = 1,67 m age = 24

adjust ratio for OpenSim: $\frac{SM_{S5}}{SM_{model}} = 1,244$

Maximum effort exerted in isokinetic and isometric exercises [mV]:

	Isokinetic exercise				Isometric exercise				
	60 °/s	120 °/s	180 °/s	240 °/s	ISO_25°	ISO_40°	ISO_55°	ISO_70°	ISO_95°
RF	0,401	0,37	0,317	0,446	0,309	0,256	0,356	0,339	0,4
VL	0,4	0,28	0,238	0,313	0,162	0,16	0,148	0,173	0,398
VM	0,4	0,285	0,304	0,20	0,182	0,156	0,173	0,234	0,286
BF	0,289	0,285	0,306	0,313	0,111	0,177	0,201	0,186	0,245

Tab.A.5.1: Mamimum effort of S5 in [mV] during isokinetic and isometric exercises.

60 °/s

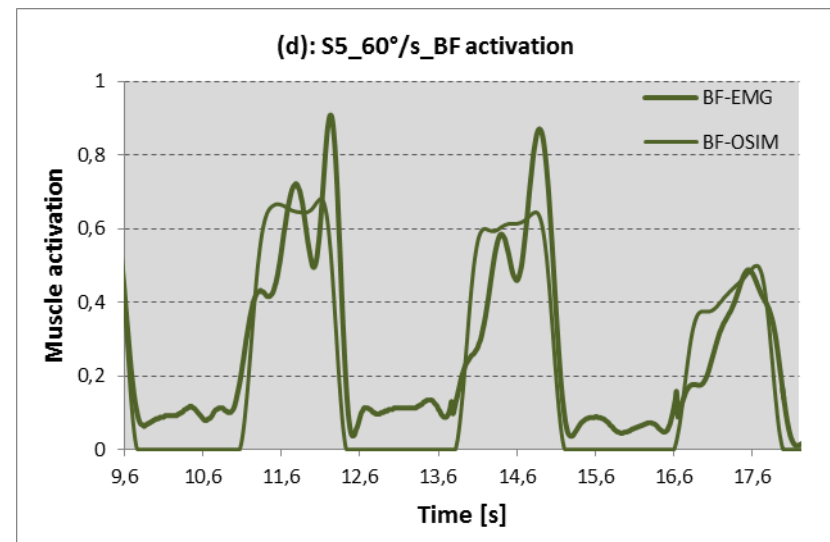
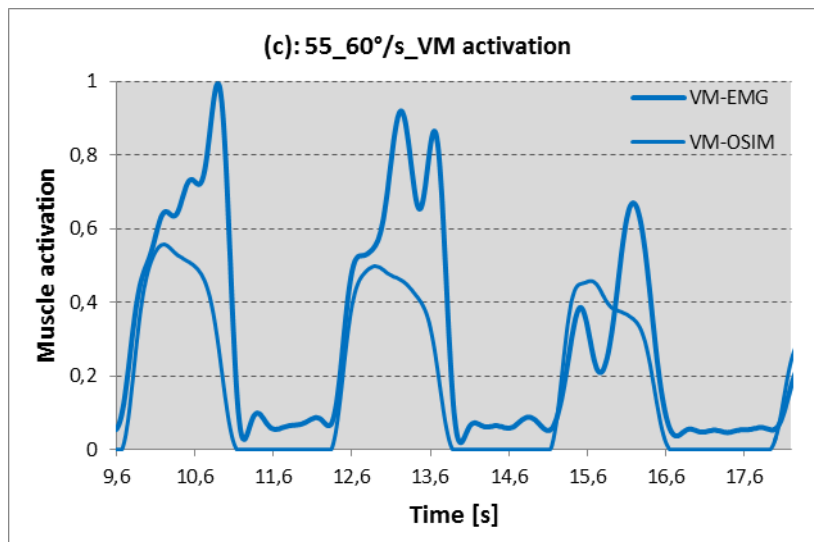
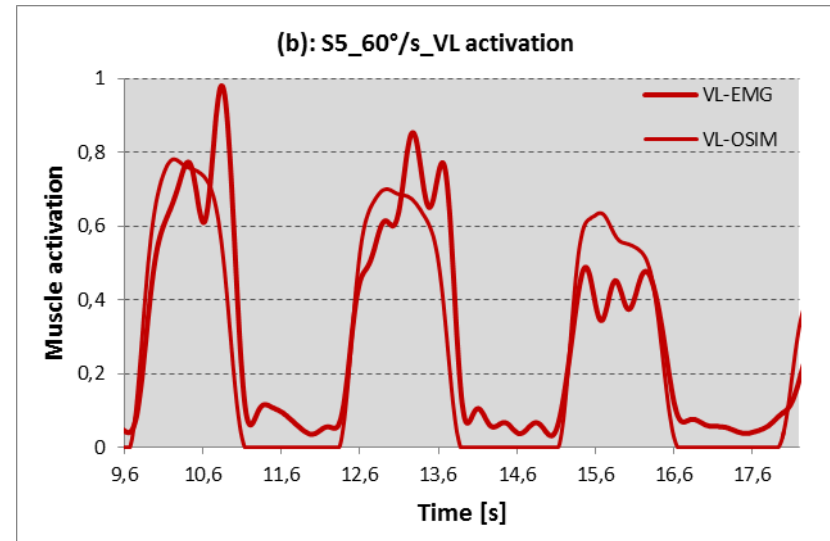
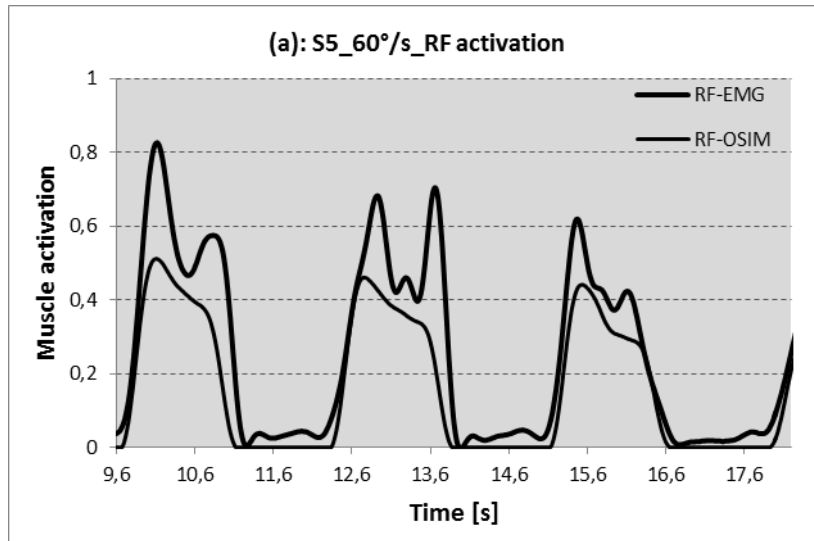


Fig.A.5.3: EMG and OpenSim muscle activation of S5 at 60°/s of RF (a), VL (b), VM (c) and BF (d).

120 °/s

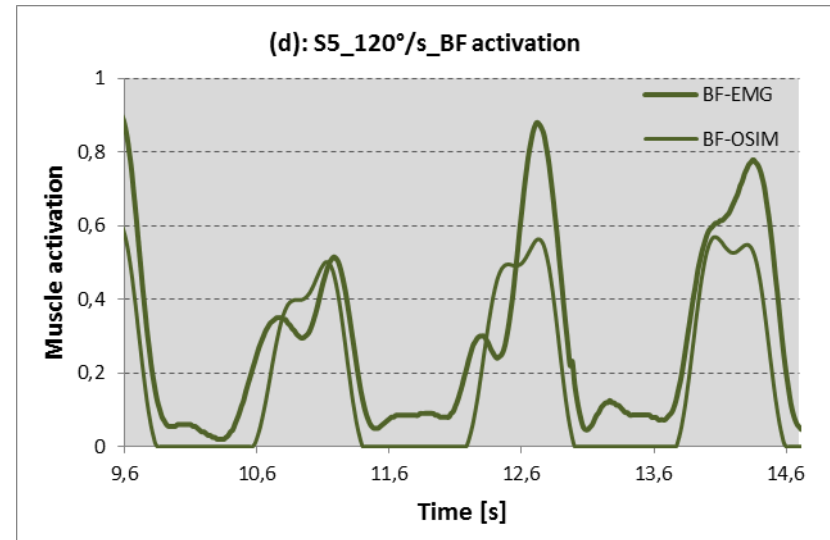
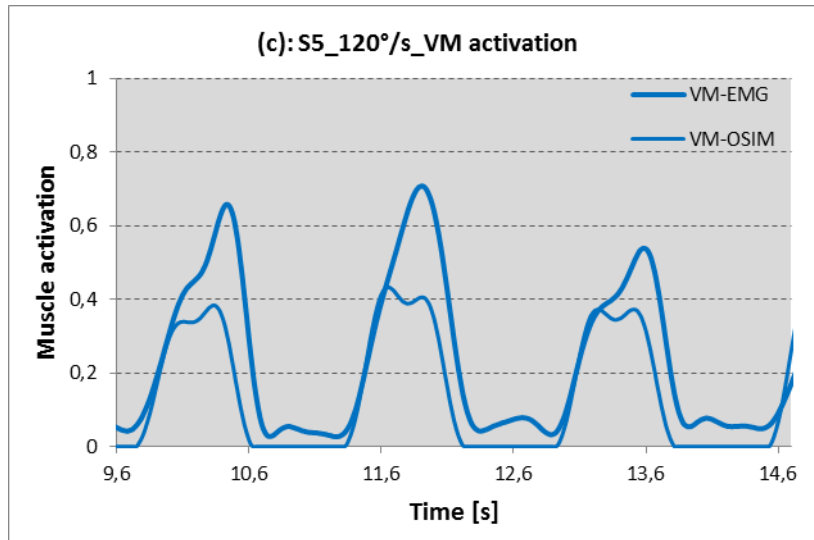
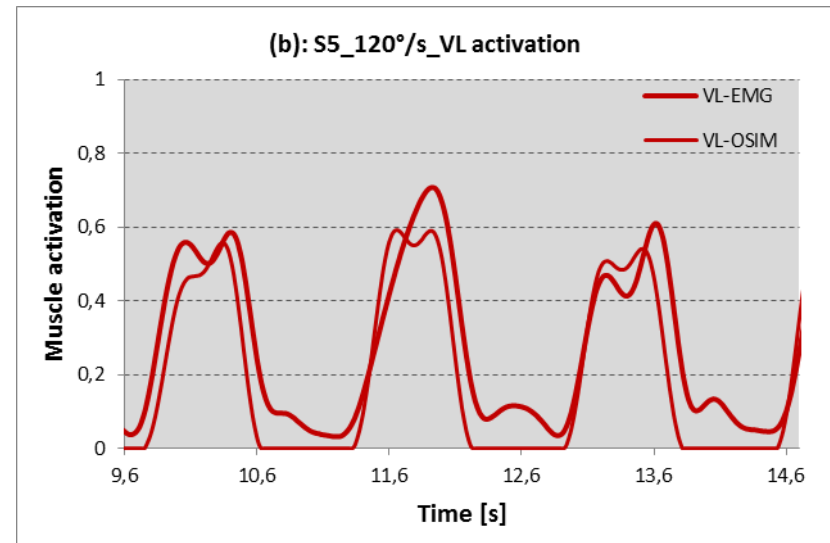
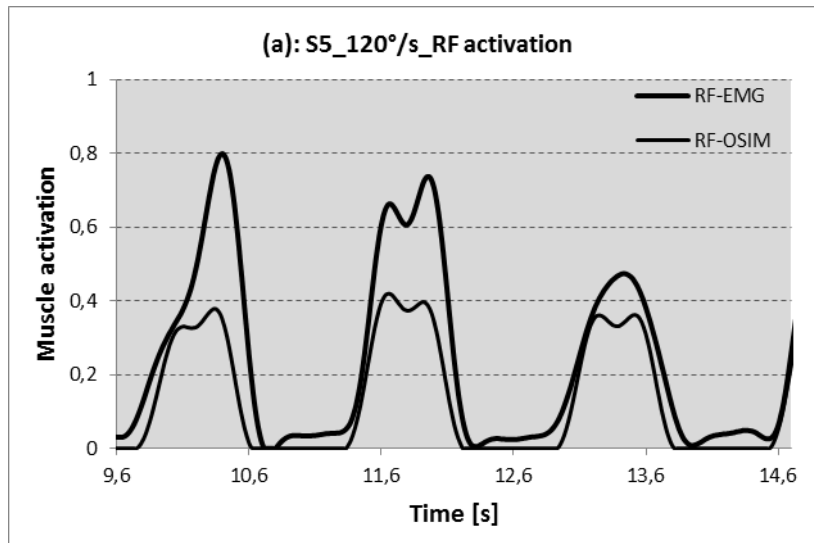


Fig.A.5.4: EMG and OpenSim muscle activation of S5 at 120°/s of RF (a), VL (b), VM (c) and BF (d).

180 °/s

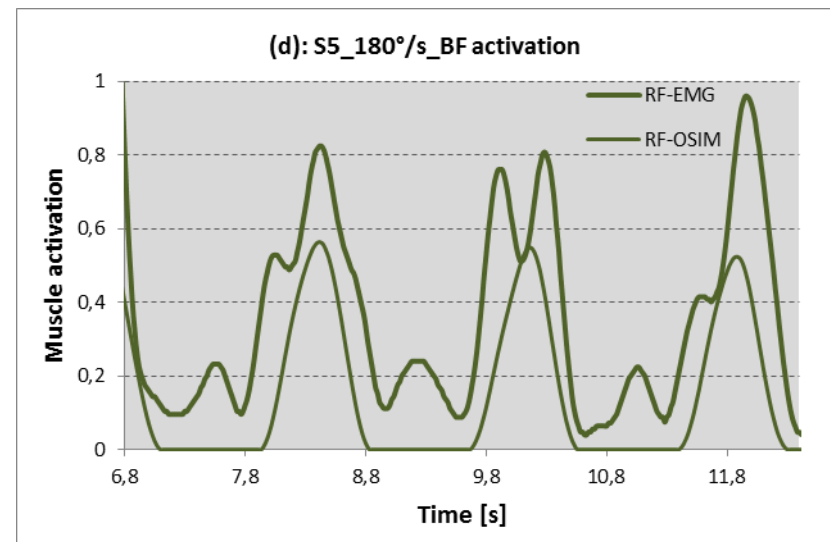
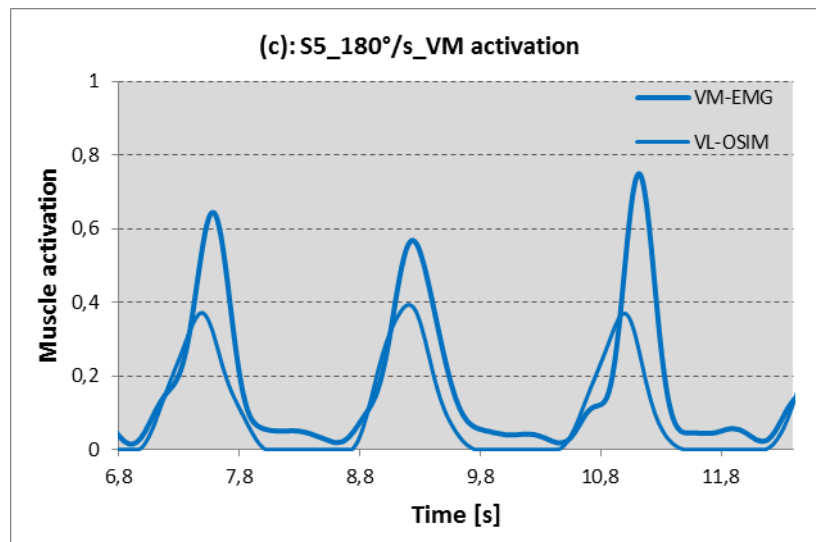
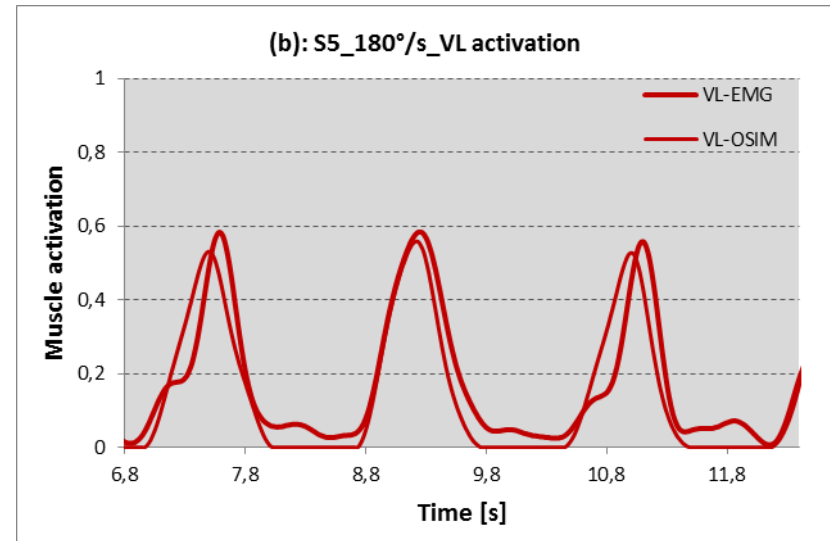
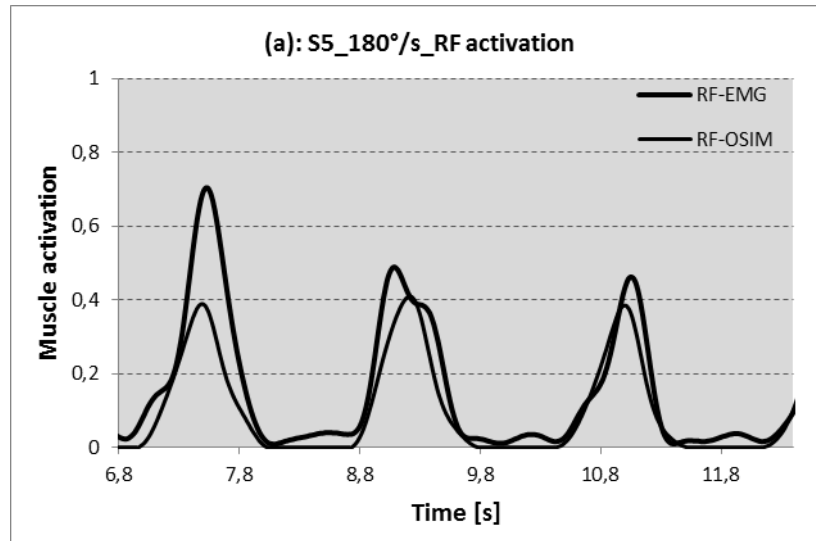


Fig.A.5.5: EMG and OpenSim muscle activation of S5 at 180°/s of RF (a), VL (b), VM (c) and BF (d).

240 °/s

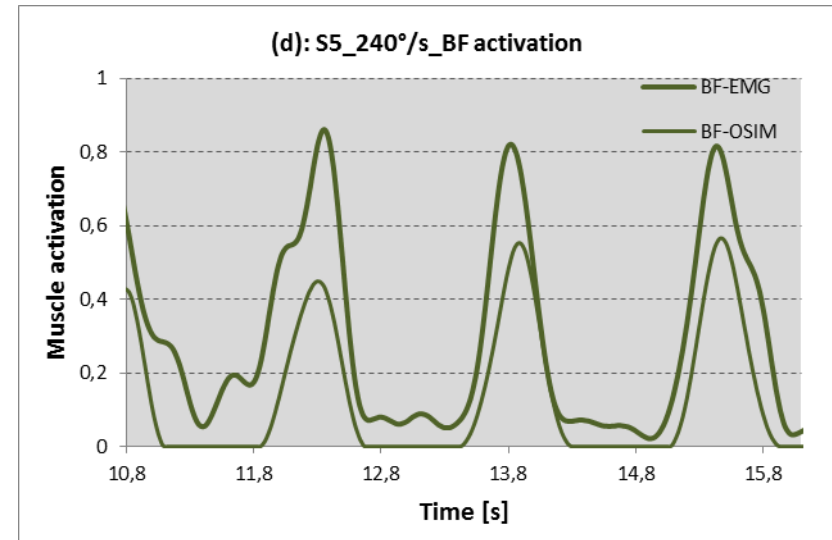
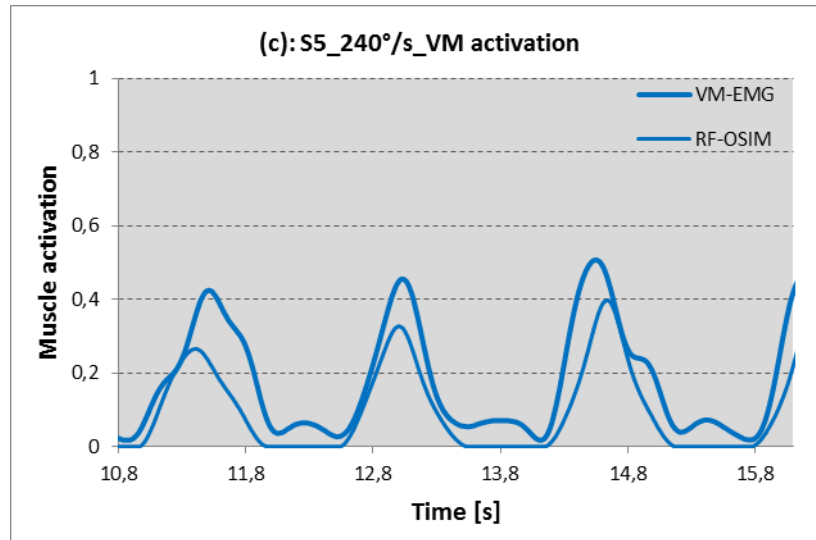
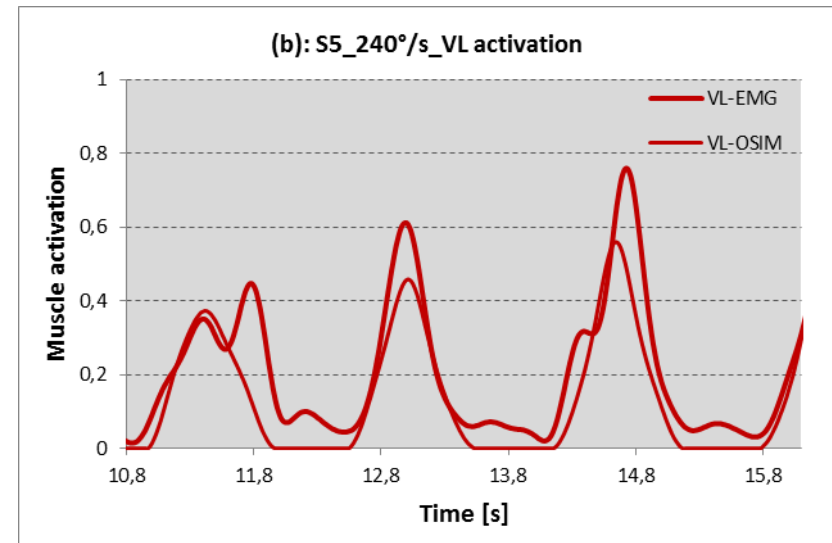
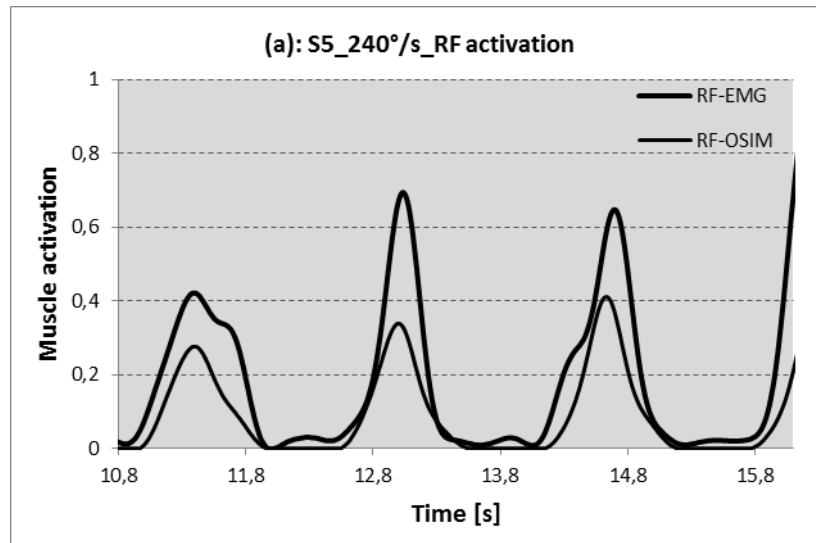


Fig.A.5.6: EMG and OpenSim muscle activation of S5 at 240°/s of RF (a), VL (b), VM (c) and BF (d).

Comparison of EMG signal and OpenSim muscle activation: quantitative results

	60 °/s	120 °/s	180 °/s	240 °/s
RF	33,77±4,72	39,82±14,81	25,92±16,30	40,69 ± 9,12
VL	2,71±28,46	10,89±5,74	6,31±2,33	22,62±5,28
VM	40,50±7,60	37,13±5,51	41,27±9,94	29,11±7,95
BF	16,32±15,98	22,28±17,40	36,32±7,82	37,04±9,41

Tab.A.5.2: Peak error of S5 in [%] of RF, VL, VM and BF at 60°/s, 120°/s, 180°/s and 240°/s.

	60 °/s	120 °/s	180 °/s	240 °/s
RF	9,74±18,84	6,65±10,86	-0,67±6,80	1,91±1,64
VL	13,73±5,41	2,97±2,86	3,87±1,96	8,43±12,65
VM	18,07±8,21	7,97±5,19	3,47±3,34	0,67±5,91
BF	0,93±4,10	7,59±8,97	3,17±3,54	-0,77±3,19

Tab.A.5.3: Time error of S5 in [%] of RF, VL, VM and BF at 60°/s, 120°/s, 180°/s and 240°/s.

	240 °/s	180 °/s	120 °/s	60 °/s
RF	34,02±8,55	38,53±10,80	35,43±20,92	47,57±4,18
VL	-0,69±15,99	20,53±7,27	-0,16±3,41	31,40±0,61
VM	29,69±16,40	33,99±7,06	35,65±2,75	46,70±7,50
BF	-1,33±16,79	15,71±20,81	52,49±4,07	56,72±9,84

Tab.A.5.4: Area error of S5 in [%] of RF, VL, VM and BF at 60°/s, 120°/s, 180°/s and 240°/s.

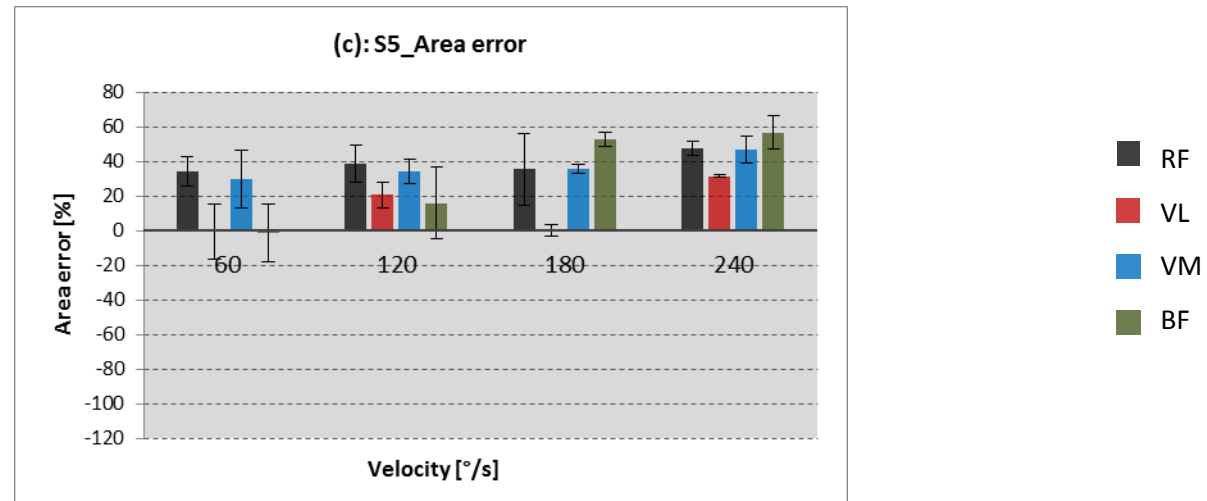
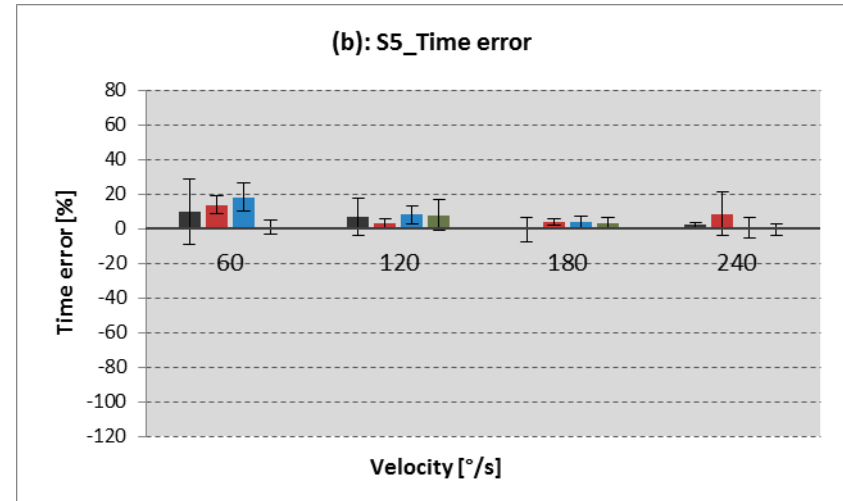
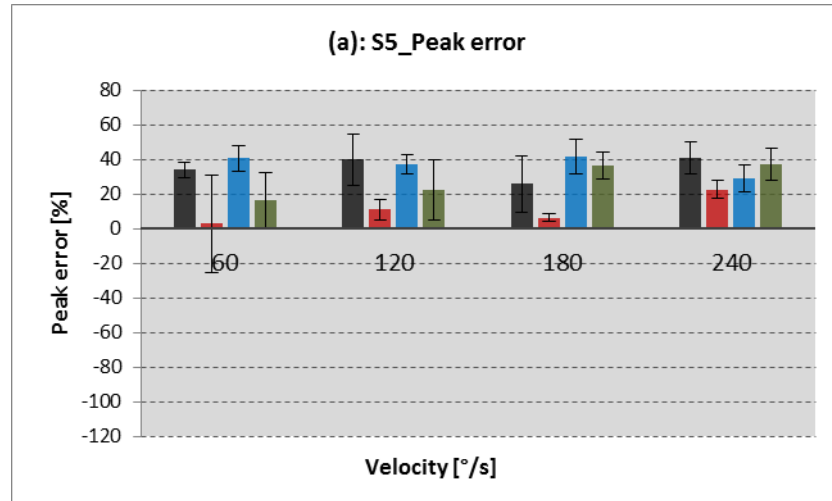


Fig.A.5.7: Quantitative results of muscle activation analysis of S5: (a): Peak error at different velocities; (b): Time error at different velocities; (c): Area error at different velocities.

Comparison of analytical models and OpenSim model

Model 1: parameters

$$\text{Tibia: } m_{\text{tibia}} = 3,453 \text{ kg} \quad I_{G \text{ tibia}} = 0,043 \text{ kg} \cdot \text{m}^2 \quad \Delta_{y \text{ tibia}} = 0,41 \text{ m} \quad \Delta_{y G \text{ tibia}} = 0,178 \text{ m}$$

$$\text{Talus: } m_{\text{talus}} = 0,093 \text{ kg} \quad I_{G \text{ talus}} = 8,7 \cdot 10^{-4} \text{ kg} \cdot \text{m}^2 \quad \Delta_{y \text{ talus}} = 0,41 \text{ m} \quad \Delta_{y G \text{ talus}} = 0,41 \text{ m}$$

$$\text{Calc: } m_{\text{calc}} = 1,164 \text{ kg} \quad I_{G \text{ calc}} = 0,0036 \text{ kg} \cdot \text{m}^2 \quad \Delta_{x \text{ calc}} = 0,047 \text{ m} \quad \Delta_{y \text{ calc}} = 0,041 \text{ m}$$

$$\Delta_{x G \text{ calc}} = 0,097 \text{ m} \quad \Delta_{y G \text{ calc}} = 0,029 \text{ m}$$

$$\text{Toes: } m_{\text{toes}} = 0,2017 \text{ kg} \quad I_{G \text{ toes}} = 8,8 \cdot 10^{-5} \text{ kg} \cdot \text{m}^2 \quad \Delta_{x \text{ toes}} = 0,174 \text{ m} \quad \Delta_{y \text{ toes}} = 0,0019 \text{ m}$$

$$\Delta_{x G \text{ toes}} = 0,034 \text{ m} \quad \Delta_{y G \text{ toes}} = 0,0058 \text{ m}$$

Model 2: parameters

$$\text{Tibia: } m_{\text{tibia}} = 3,156 \text{ kg} \quad I_{G \text{ tibia}} = 0,043 \text{ kg} \cdot \text{m}^2 \quad \Delta_{y \text{ tibia}} = 0,387 \text{ m} \quad \Delta_{y G \text{ tibia}} = 0,168 \text{ m}$$

$$\text{Foot: } m_{\text{foot}} = 0,98 \text{ kg} \quad I_{G \text{ foot}} = 0,0049 \text{ kg} \cdot \text{m}^2 \quad \Delta_{x G \text{ foot}} = 0,067 \text{ m} \quad \Delta_{y G \text{ foot}} = 0,033 \text{ m}$$

$$D_{Q2} = 0,08 \text{ m} \quad H_{Q2} = 0,026 \text{ m} \quad D_{Q1} = 0,3 \text{ m} \quad H_{Q1} = 0,03 \text{ m}$$

$$B_{PT} [\text{m}] = 0,0097 \cdot \varphi_{k+}^5 - 0,0215 \cdot \varphi_{k+}^4 - 0,0098 \cdot \varphi_{k+}^3 + 0,0366 \cdot \varphi_{k+}^2 - 0,0141 \cdot \varphi_{k+} + 0,0464 \quad \varphi_{k+} [\text{rad}]$$

$$\text{BFB: } D_{\text{BFB1}} = 0,2 \text{ m} \quad D_{\text{BFB2}} = 0,04 \text{ m} \quad H_{\text{BFB1}} = 0,04 \text{ m} \quad H_{\text{BFB2}} = 0,03 \text{ m}$$

$$\text{BFL: } D_{\text{BFL1}} = 0,49 \text{ m} \quad D_{\text{BFL2}} = 0,04 \text{ m} \quad H_{\text{BFL1}} = 0,04 \text{ m} \quad H_{\text{BFL2}} = 0,03 \text{ m}$$

$$\text{SM: } D_{\text{SM1}} = 0,49 \text{ m} \quad D_{\text{SM2}} = 0,5 \text{ m} \quad H_{\text{SM1}} = 0,4 \text{ m} \quad H_{\text{SM2}} = 0,035 \text{ m}$$

$$\text{ST: } D_{\text{ST1}} = 0,49 \text{ m} \quad H_{\text{ST1}} = 0,5 \text{ m} \quad B_{\text{ST}} = 0,4 \text{ m} \quad \alpha_{\text{ST}} = 0,52 \text{ rad}$$

Fig.A.5.8: S5_60°/s_Extension

— OSIM — Mod1_Herzog — Mod1_Van Eijden — Mod2 - - - limit value

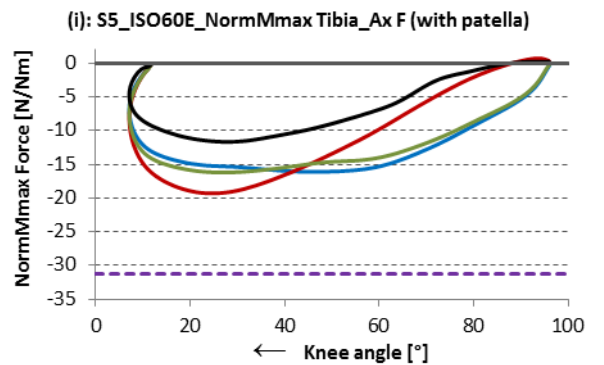
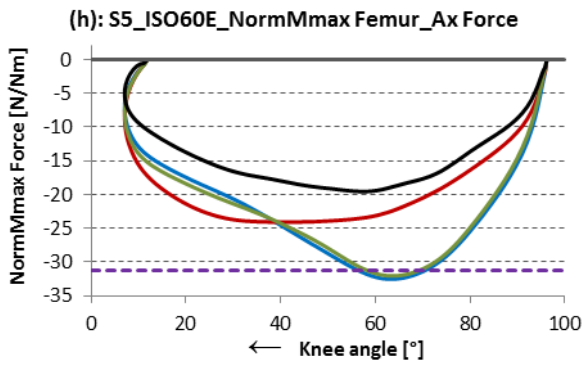
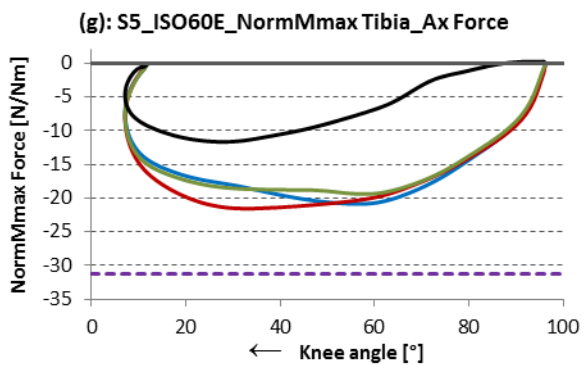
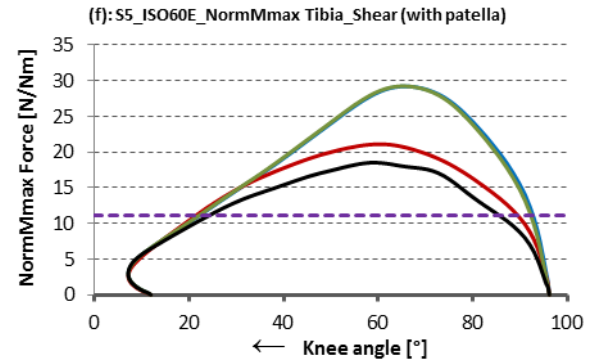
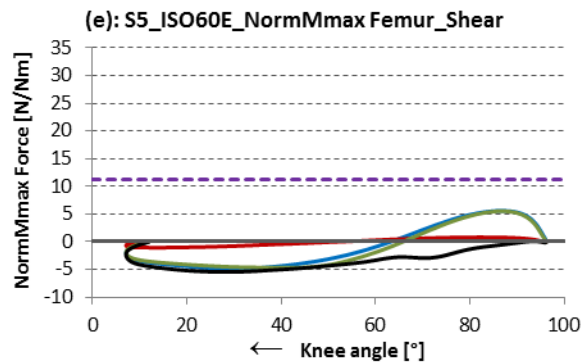
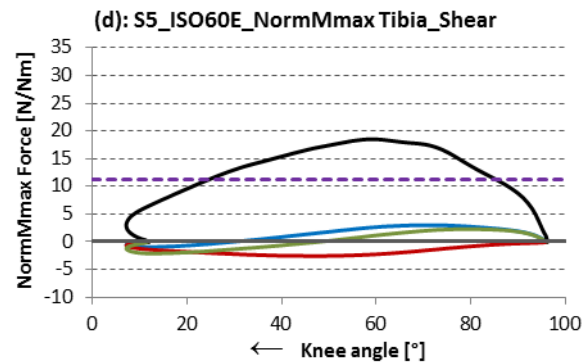
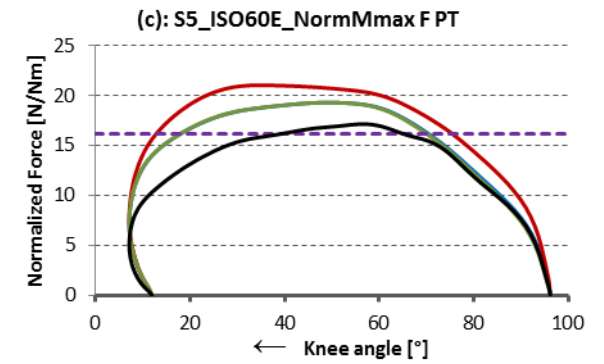
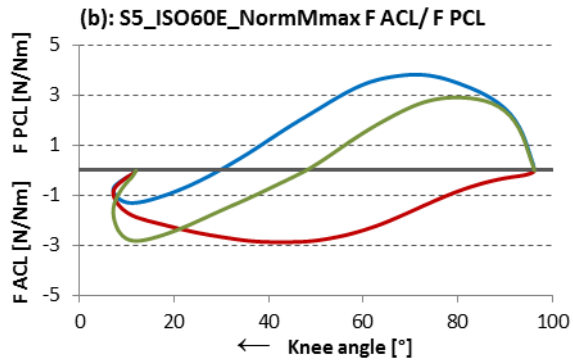
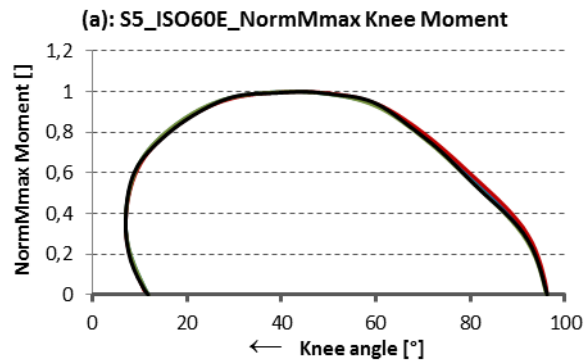


Fig.A.5.9: S9_60°/s_Flexion

— OSIM — Mod1 — Mod2 - - - limit value (•••• OSIM BFL •••• Mod1 BFL •••• Mod2 BFL)

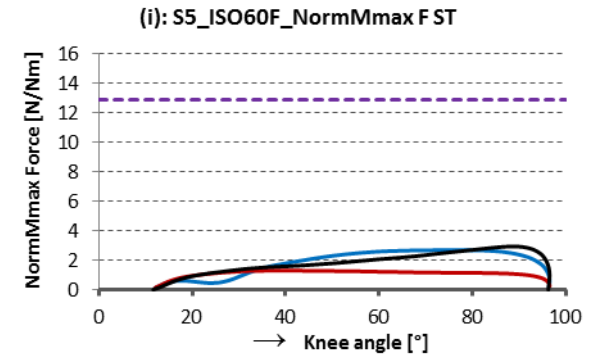
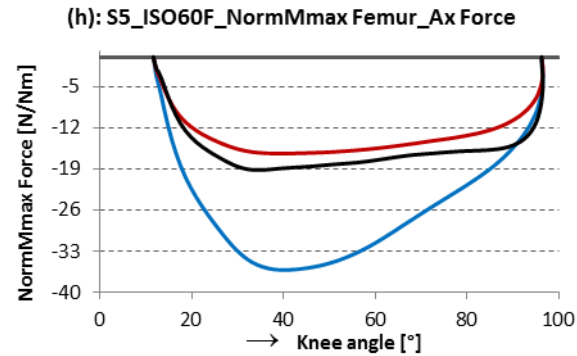
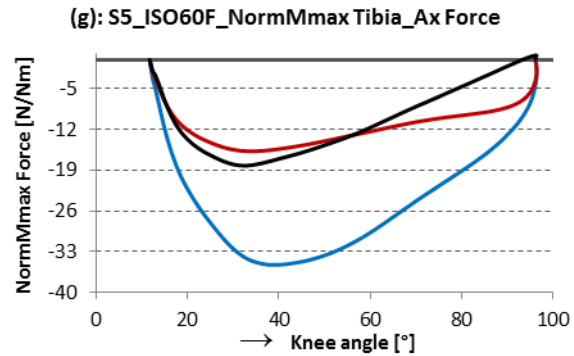
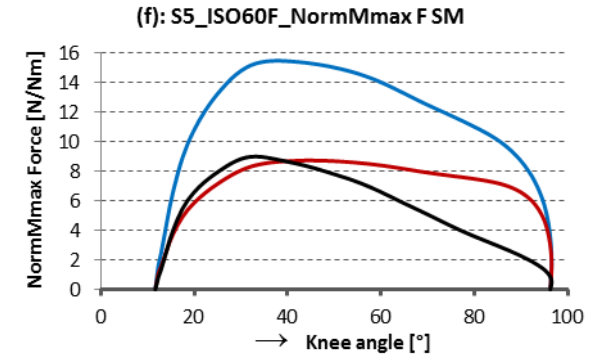
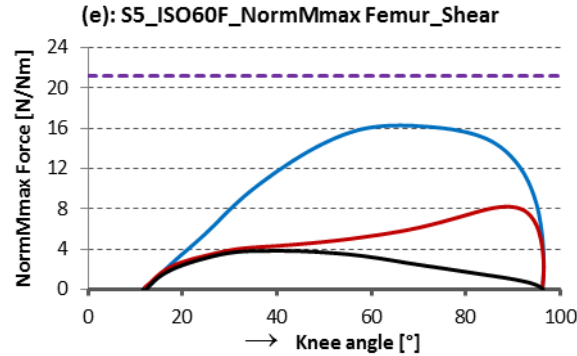
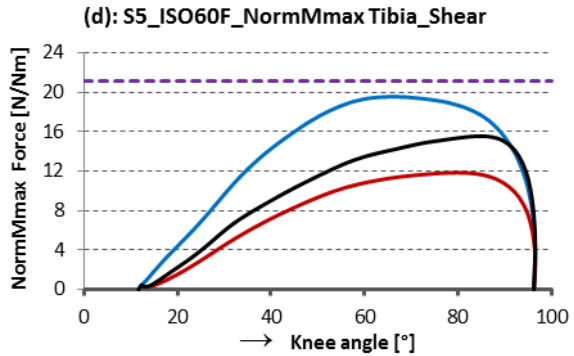
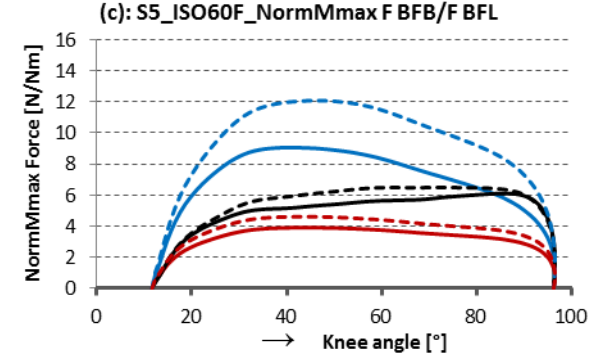
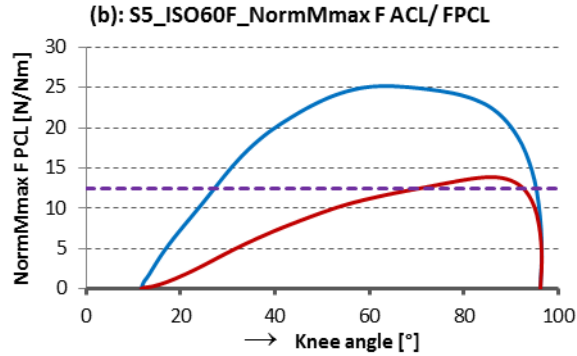
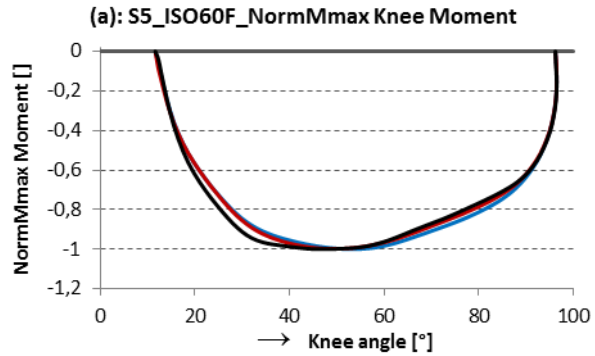


Fig.A.5.10: S5_120°/s_Extension

— OSIM — Mod1_Herzog — Mod1_Van Eijden — Mod2 - - - - limit value

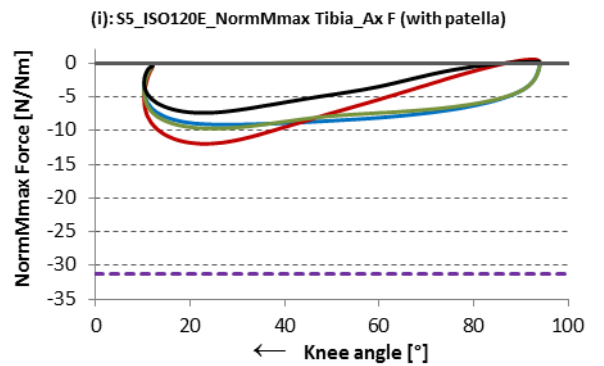
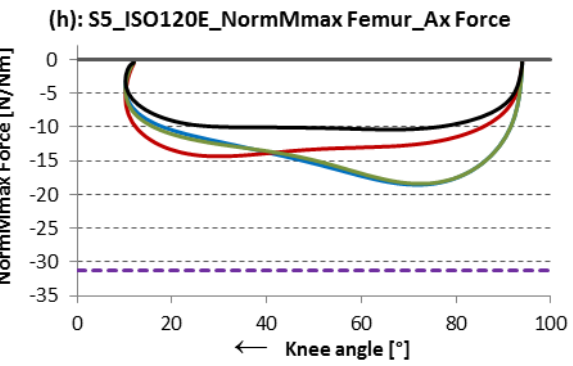
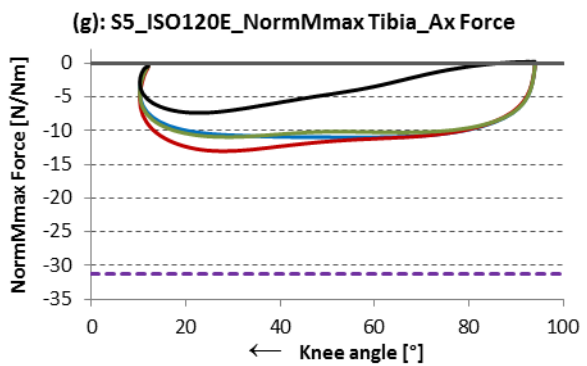
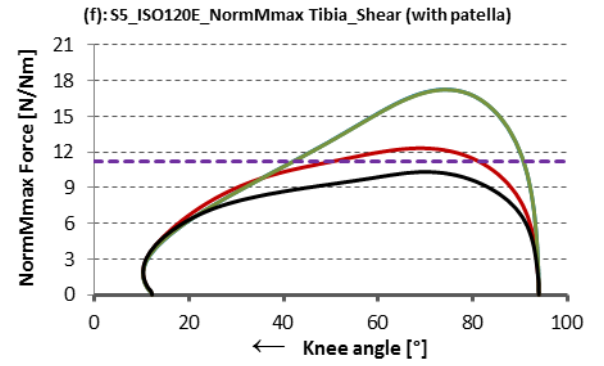
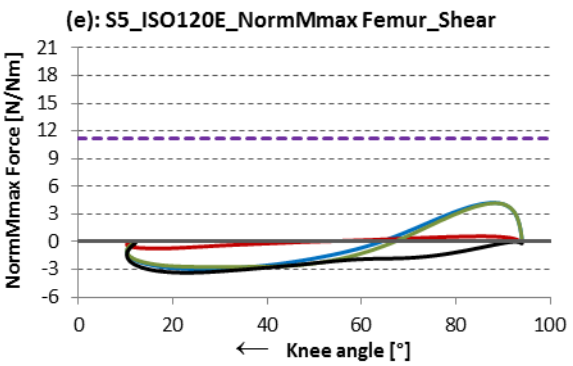
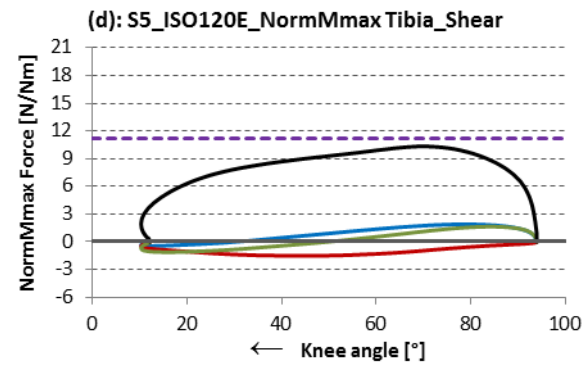
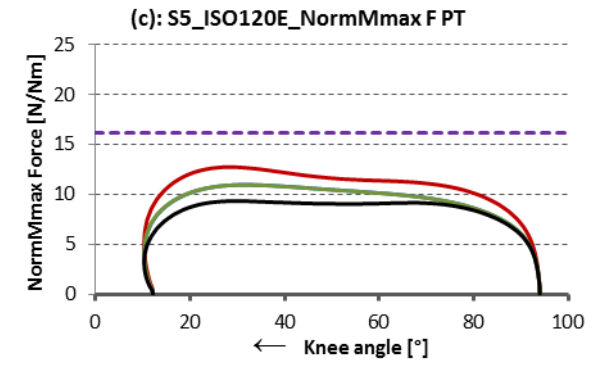
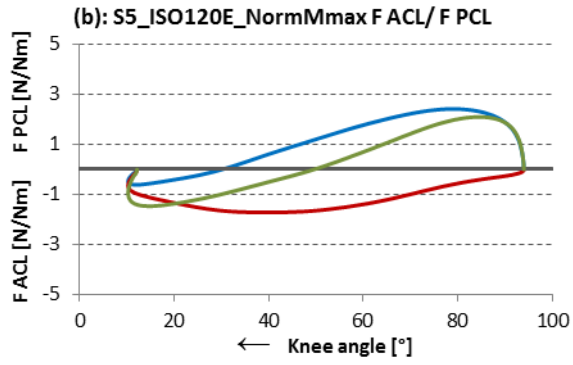
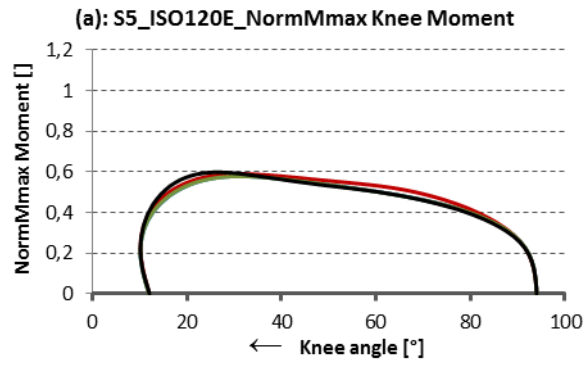


Fig.A.5.11: S5_120°/s_Flexion

— OSIM — Mod1 — Mod2 - - - limit value (- - - OSIM BFL - - - Mod1 BFL - - - Mod2 BFL)

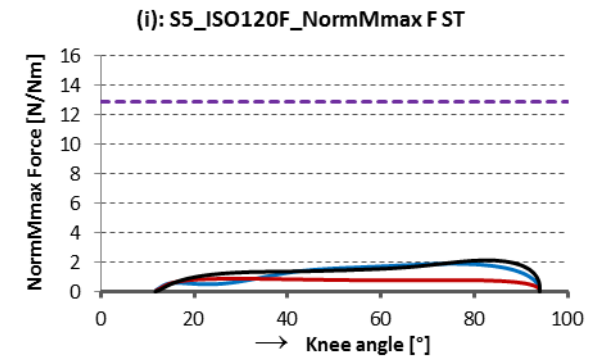
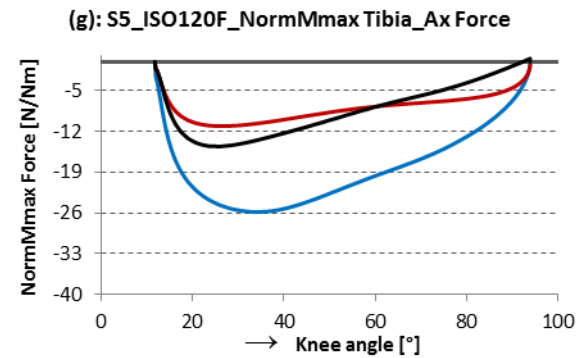
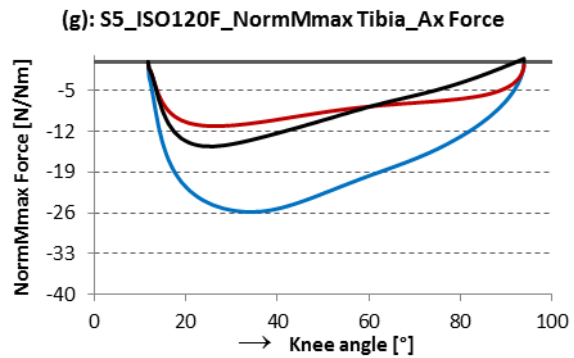
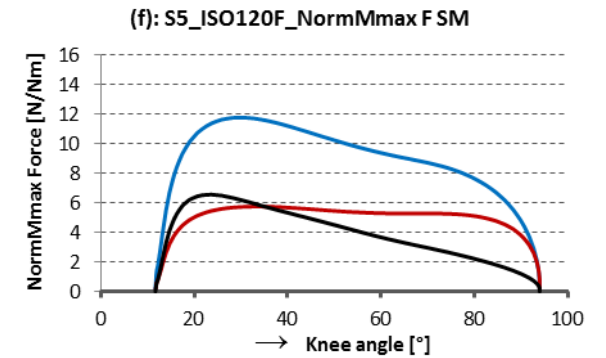
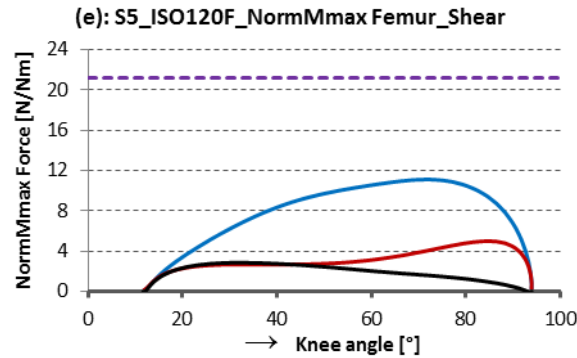
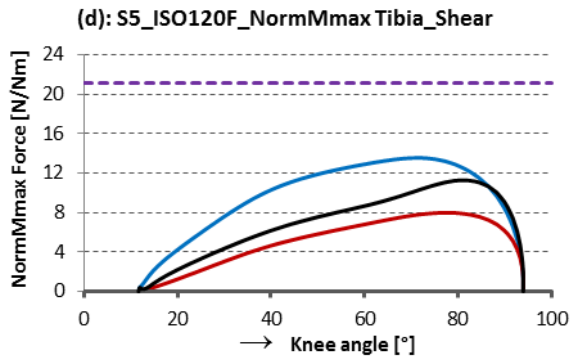
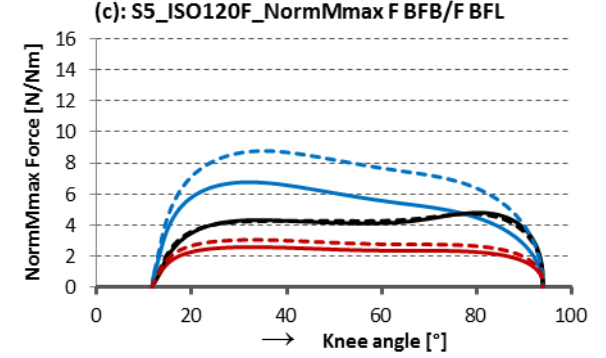
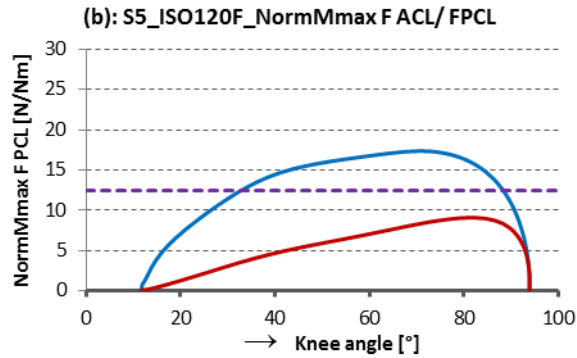
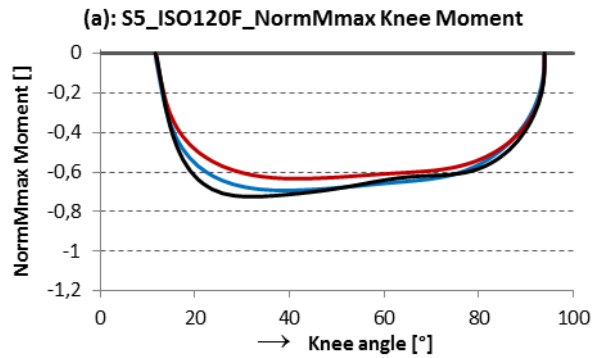


Fig.A.5.12: S5_180°/s_Extension

— OSIM — Mod1_Herzog — Mod1_Van Eijden — Mod2 - - - limit value

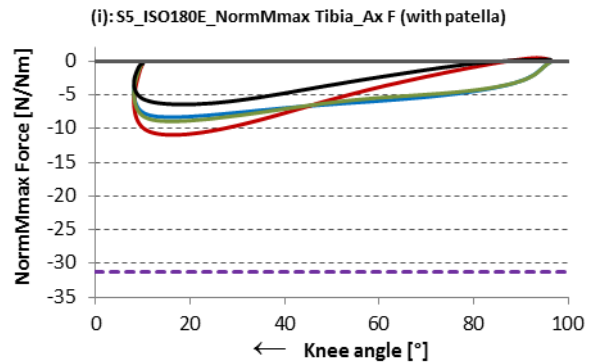
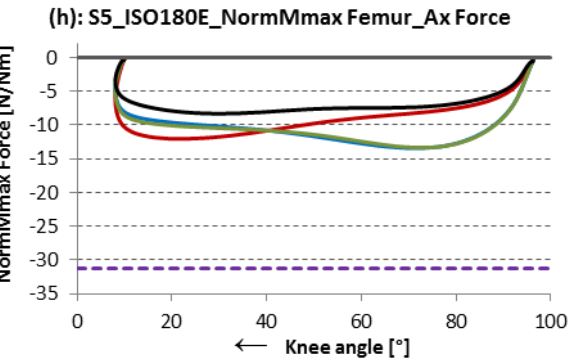
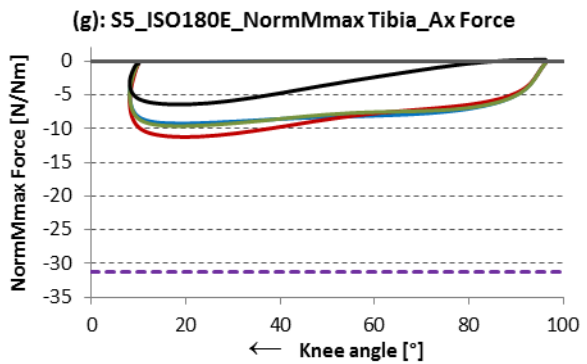
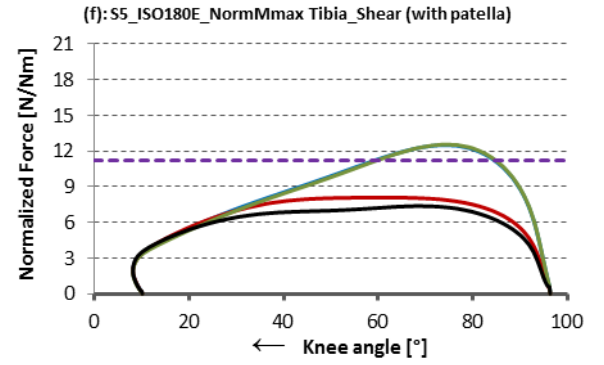
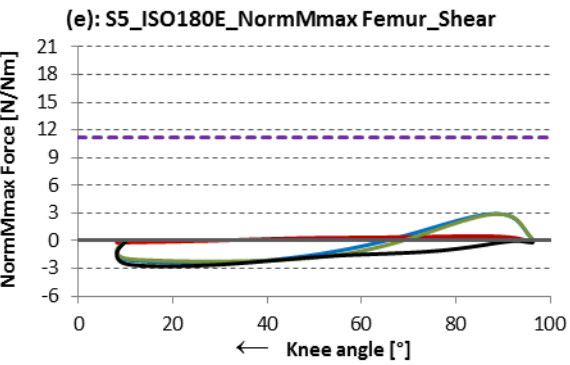
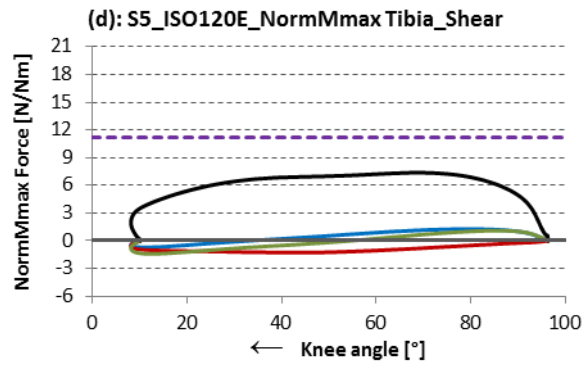
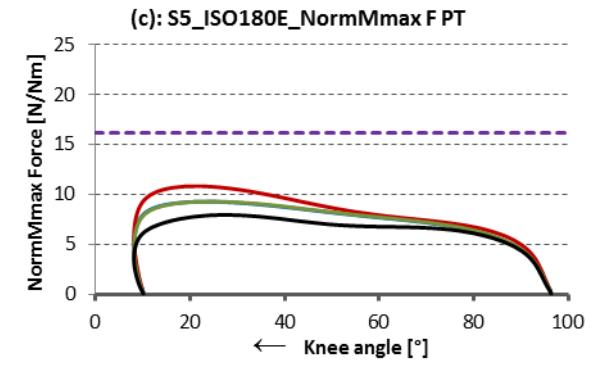
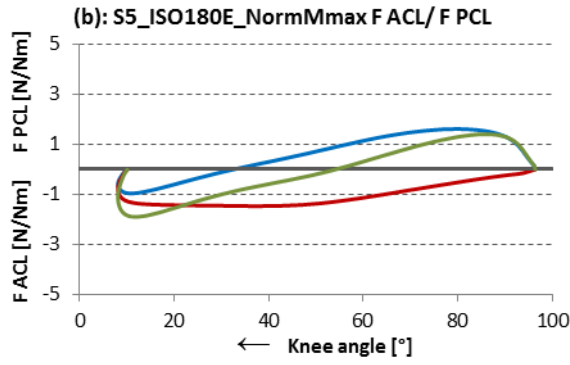
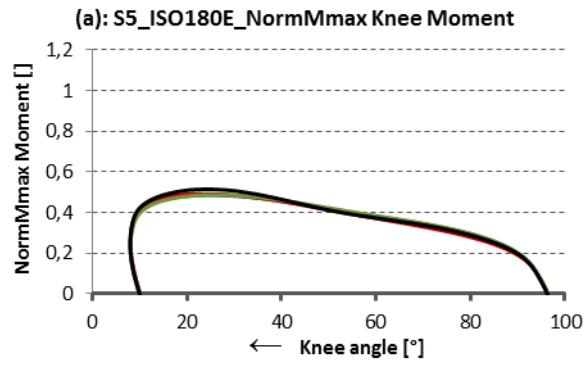


Fig.A.5.13: S5_180°/s_Flexion

— OSIM — Mod1 — Mod2 - - - - limit value (•••• OSIM BFL •••• Mod1 BFL •••• Mod2 BFL)

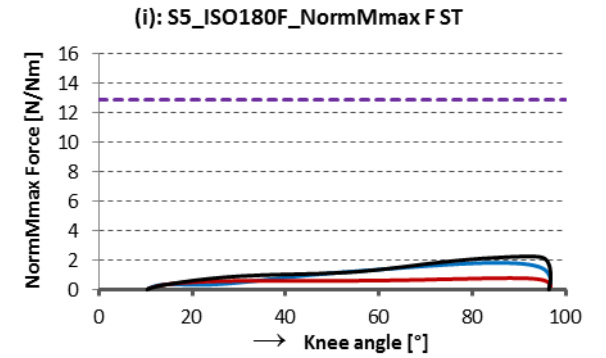
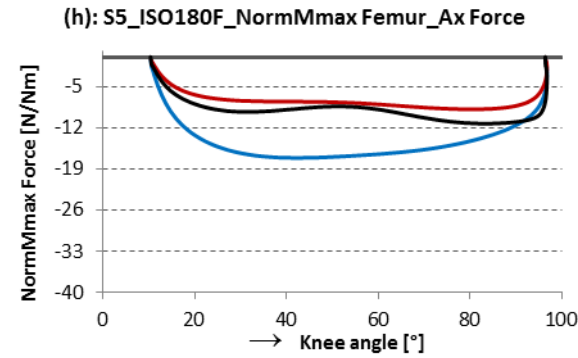
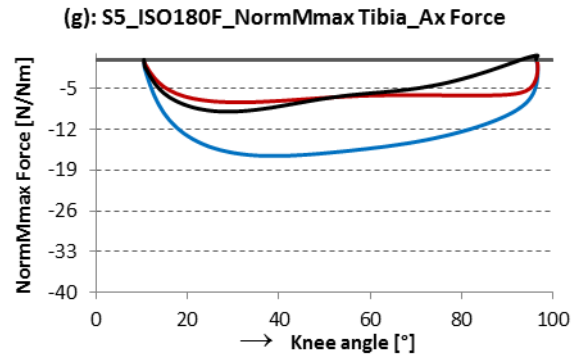
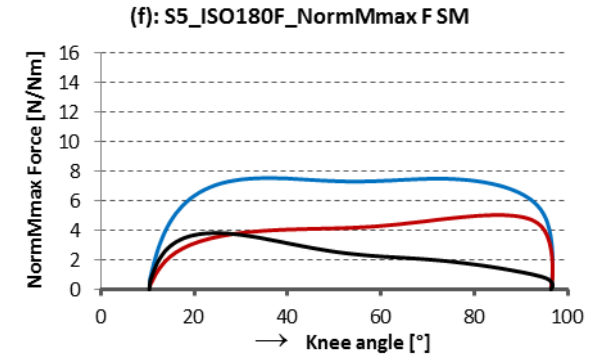
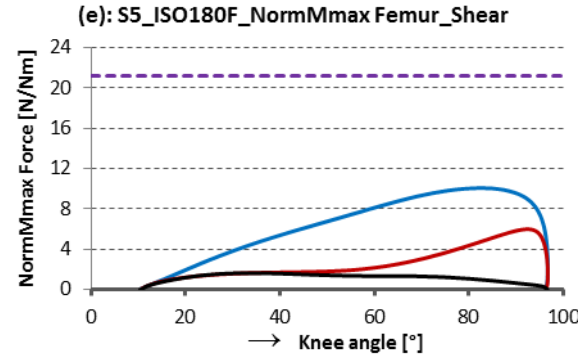
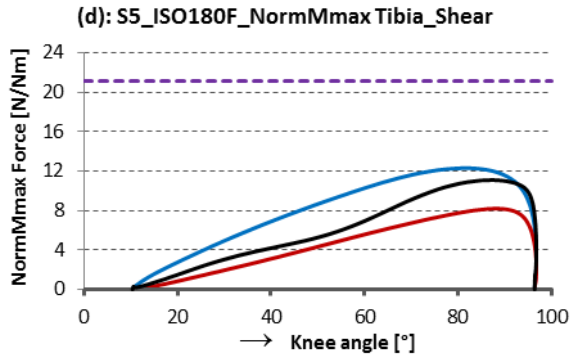
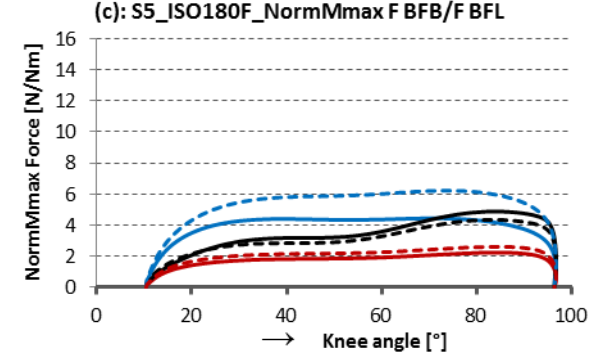
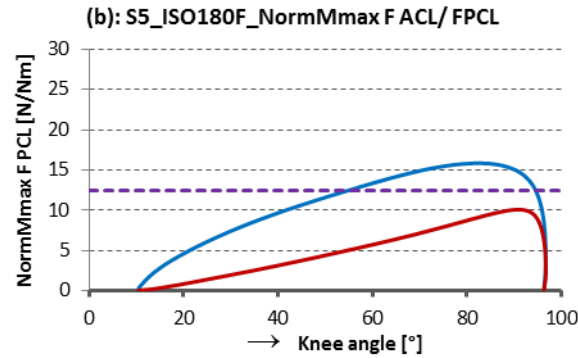
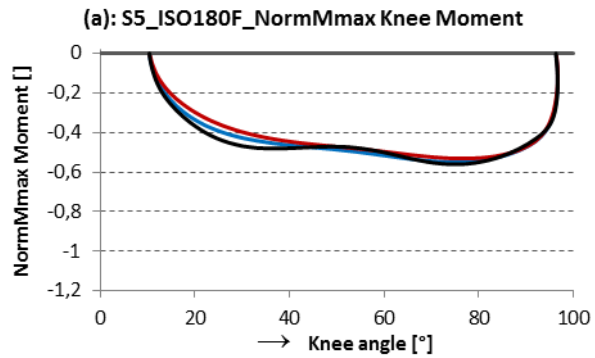


Fig.A.5.14: S5_240°/s_Extension

— OSIM — Mod1_Herzog — Mod1_Van Eijden — Mod2 - - - - - limit value

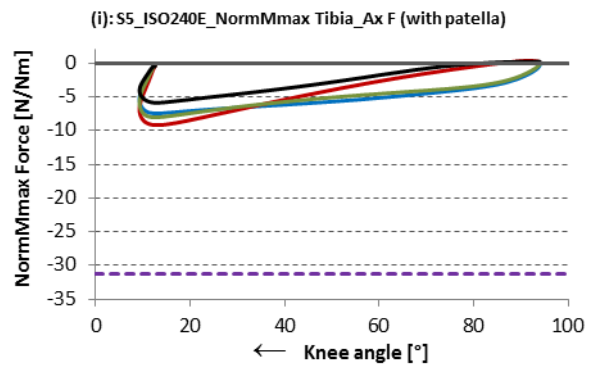
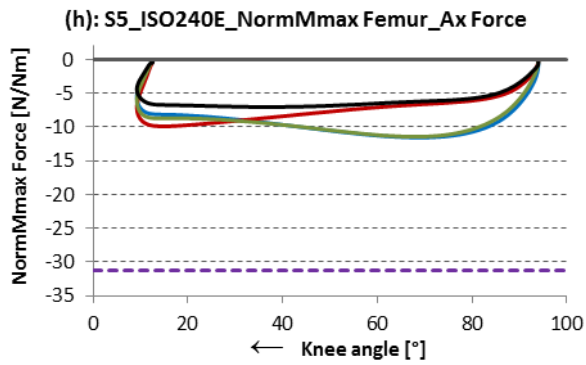
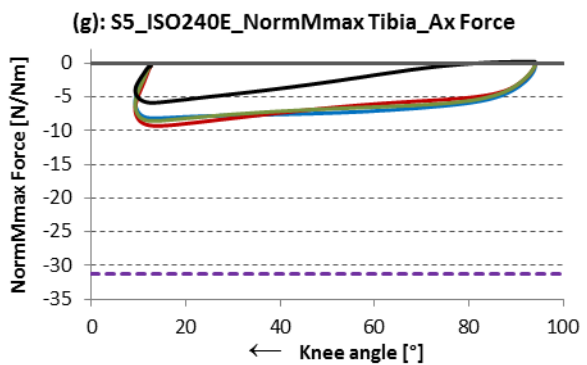
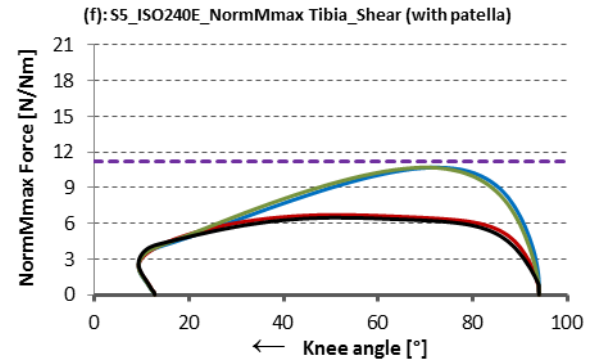
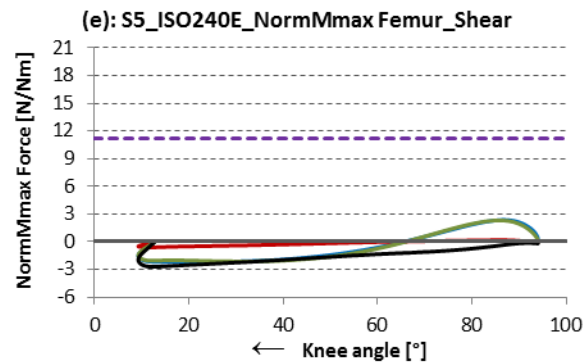
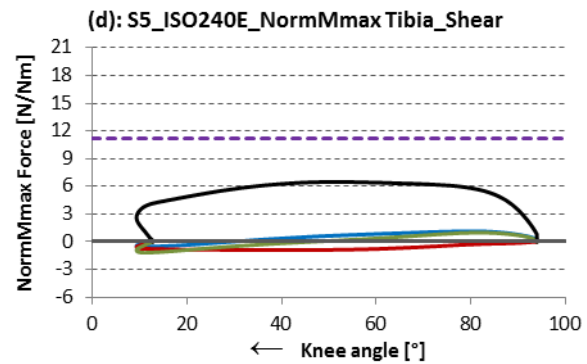
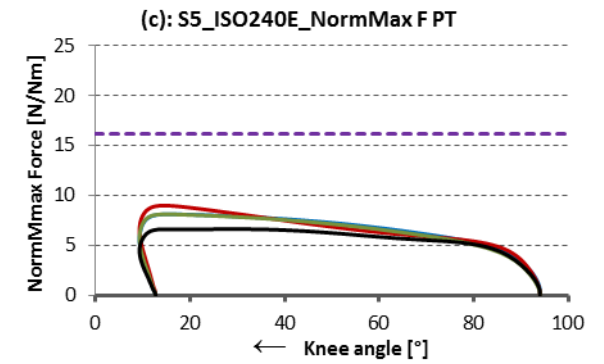
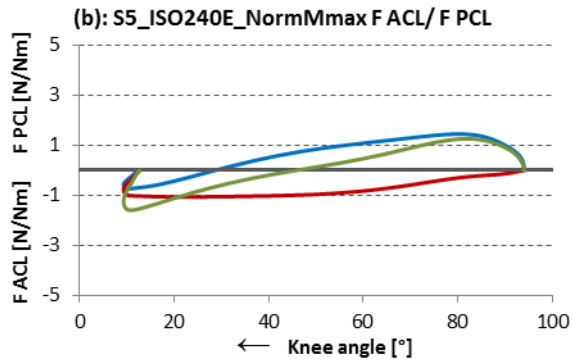
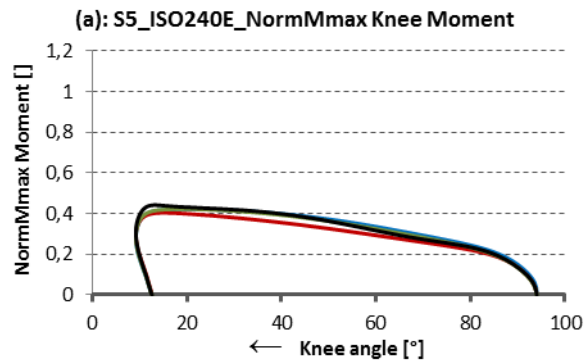
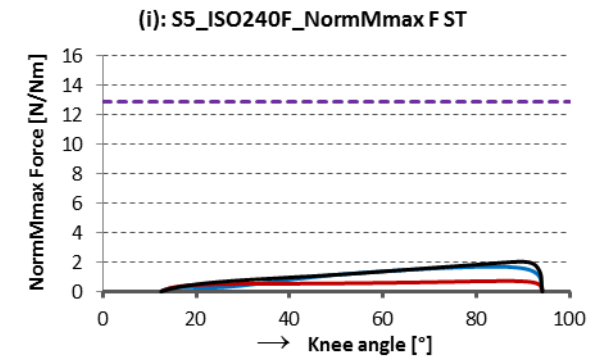
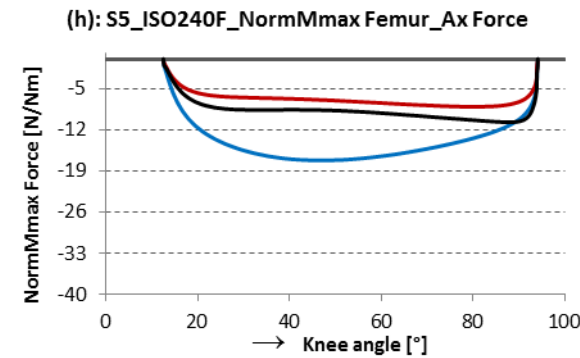
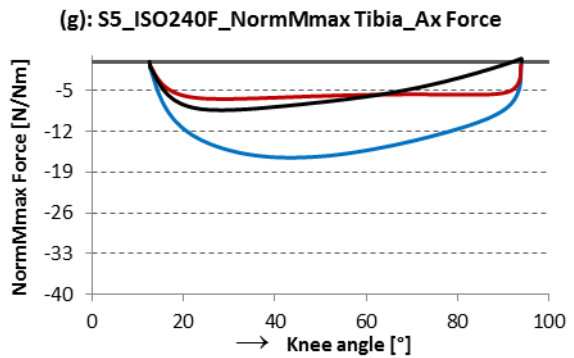
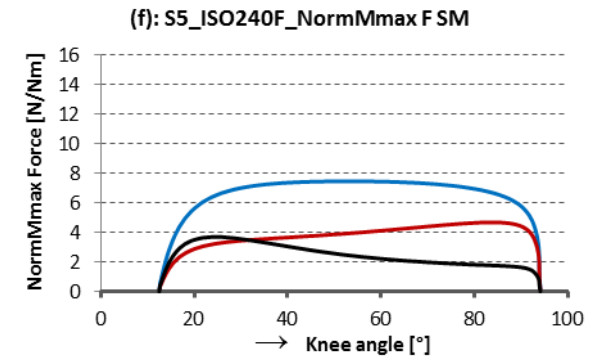
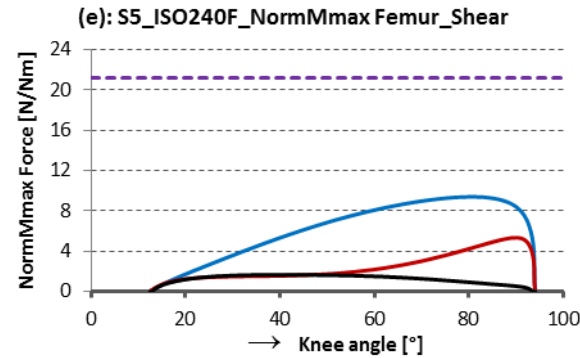
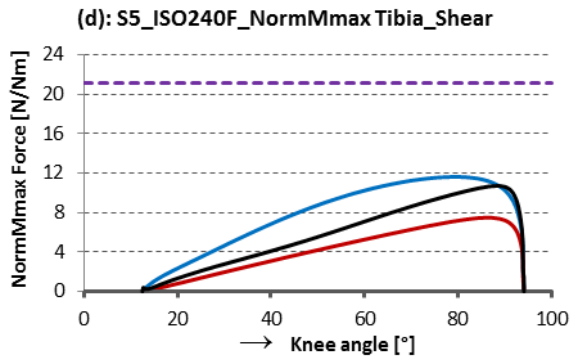
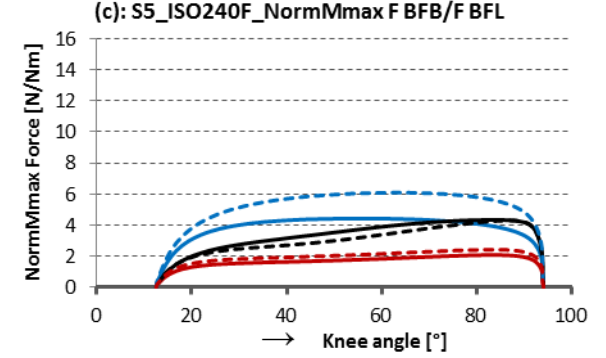
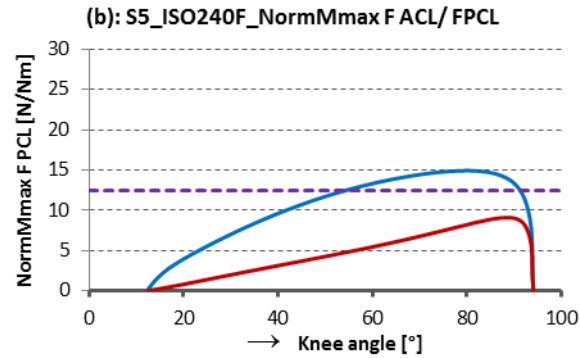
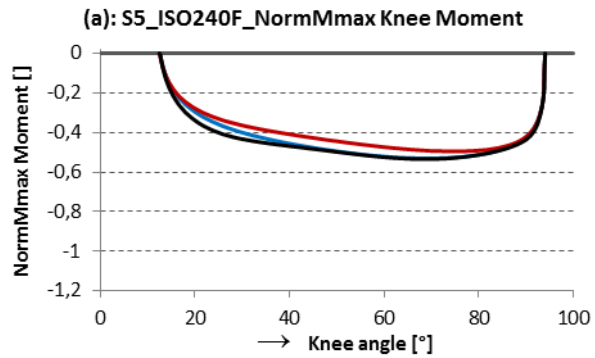


Fig.A.5.15: S5_240°/s_Flexion

— OSIM — Mod1 — Mod2 - - - - limit value (- - - - OSIM BFL - - - - Mod1 BFL - - - - Mod2 BFL)



A.6.Results of Subject 6 (S6)

Torque at the servo-motor

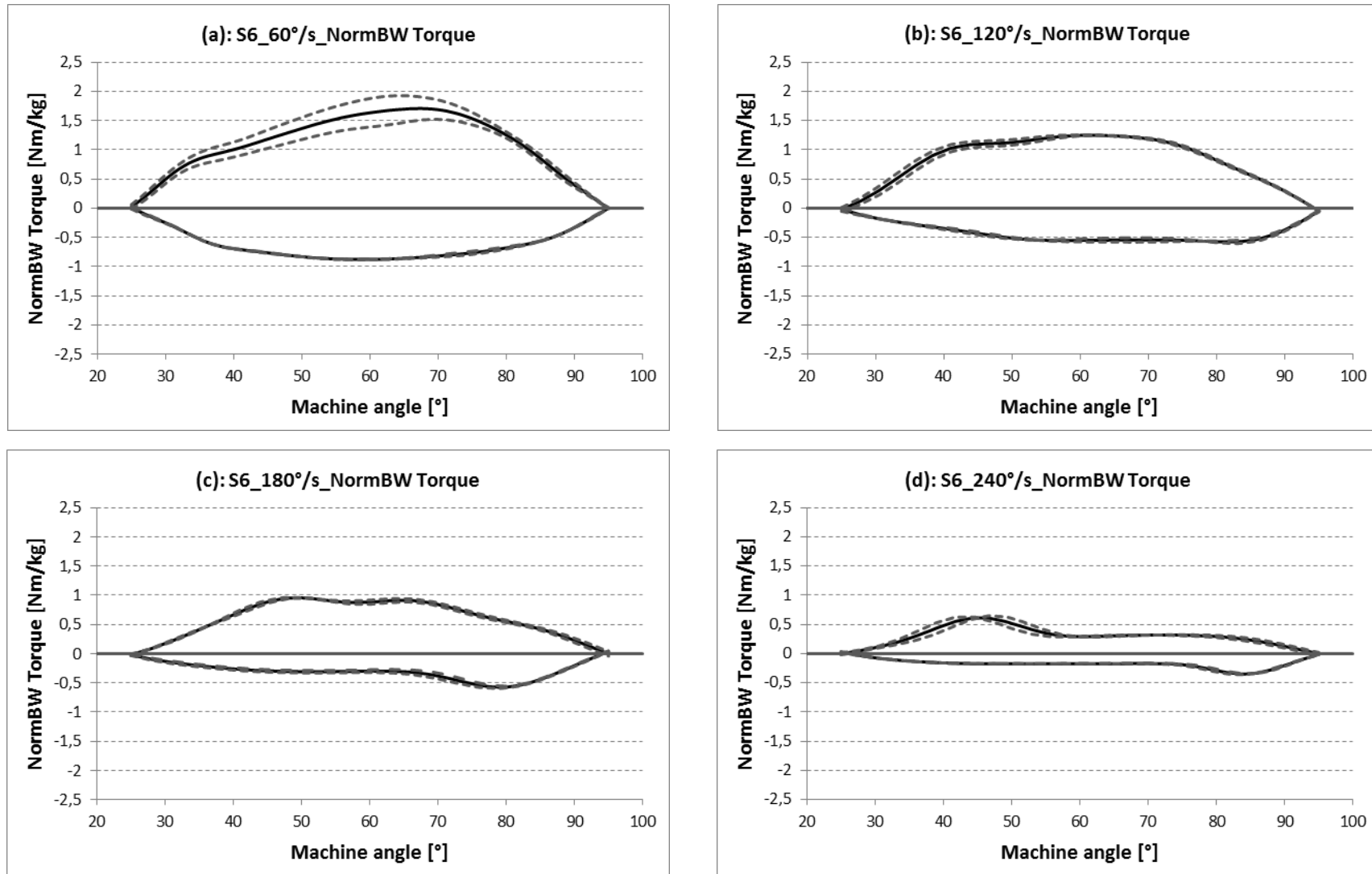


Fig.A.6.1: Normalized Torque of S6 at 60°/s (a), 120°/s (b), 180°/s (c) and 240°/s (d).

Flexors and Extensors Balance

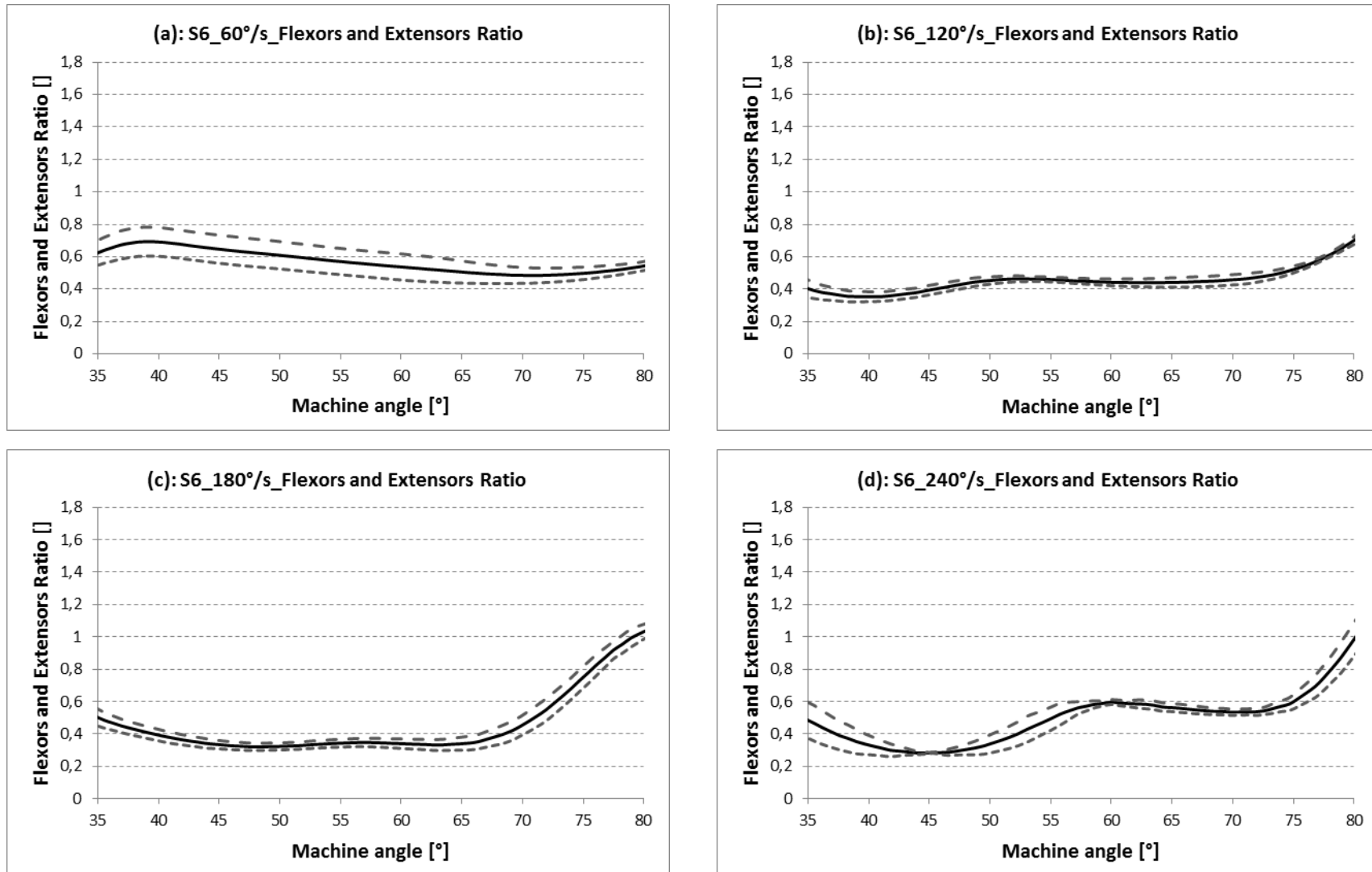


Fig.A.6.2: Flexors and extensors balance of S6 at 60°/s (a), 120°/s (b), 180°/s (c) and 240°/s (d).

Comparison of EMG signal and OpenSim muscle activation

M = 83 kg H = 1,78 m age = 37

adjust ratio for OpenSim: $\frac{SM_{S6}}{SM_{model}} = 1,37$

Maximum effort exerted in isokinetic and isometric exercises [mV]:

	Isokinetic exercise				Isometric exercise				
	60 °/s	120 °/s	180 °/s	240 °/s	ISO_25°	ISO_40°	ISO_55°	ISO_70°	ISO_95°
RF	0,119	0,11	0,097	0,061	0,066	0,039	0,044	0,049	0,035
VL	0,113	0,147	0,126	0,065	0,07	0,081	0,064	0,098	0,088
VM	0,11	0,084	0,075	0,035	0,064	0,035	0,025	0,041	0,086
BF	0,114	0,107	0,088	0,066	0,103	0,082	0,066	0,059	0,055

Tab.A.6.1: Maximum effort of S6 in [mV] during isokinetic and isometric exercises.

60 °/s

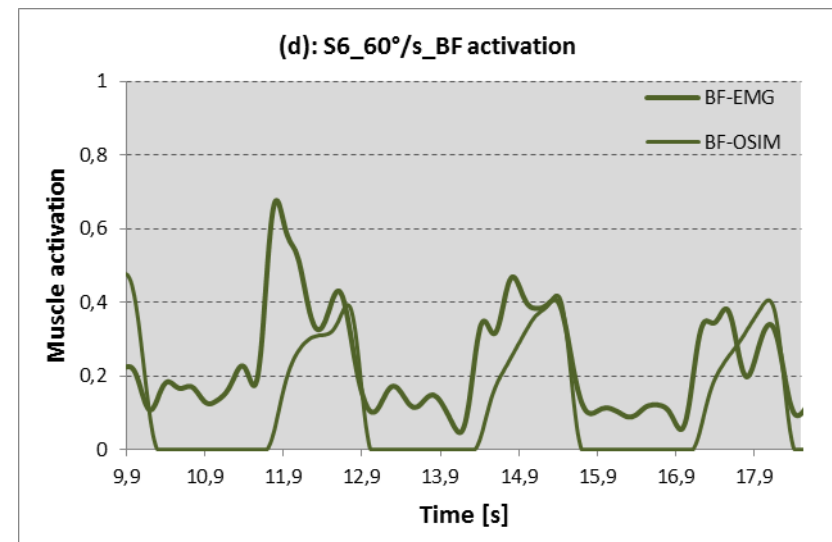
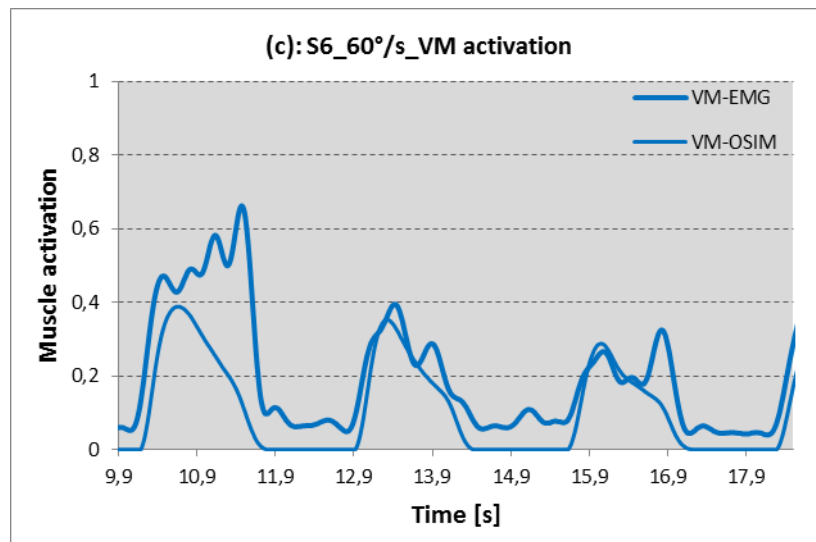
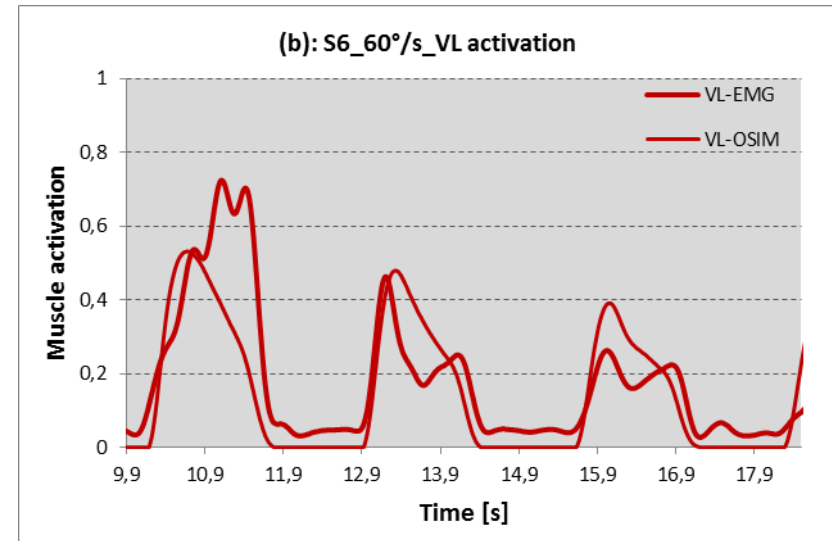
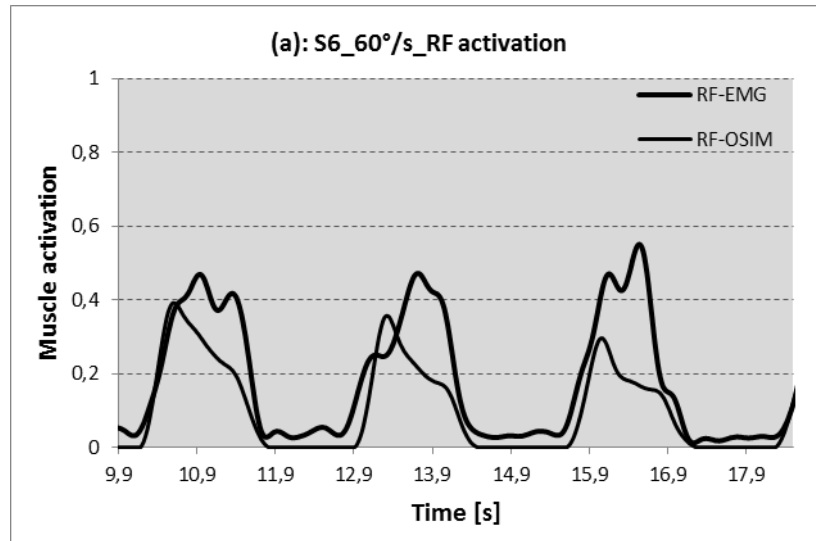


Fig.A.6.3: EMG and OpenSim muscle activation of S6 at 60°/s of RF (a), VL (b), VM (c) and BF (d).

120 °/s

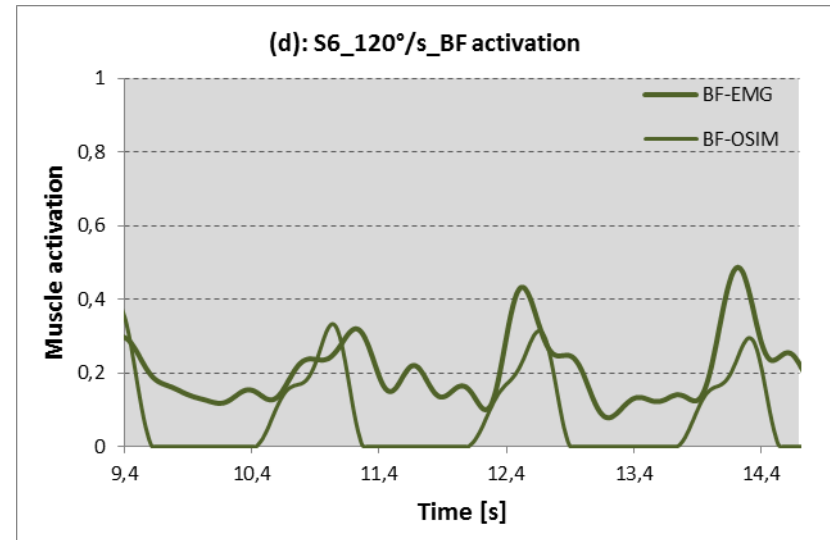
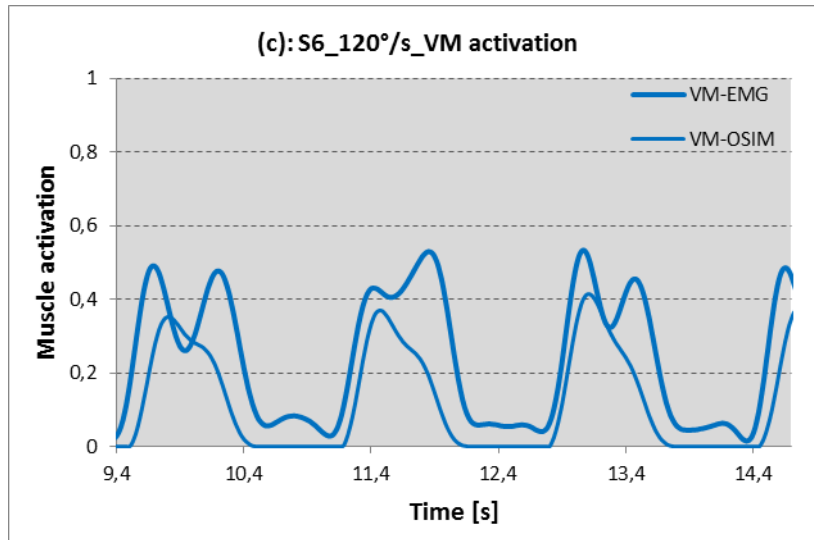
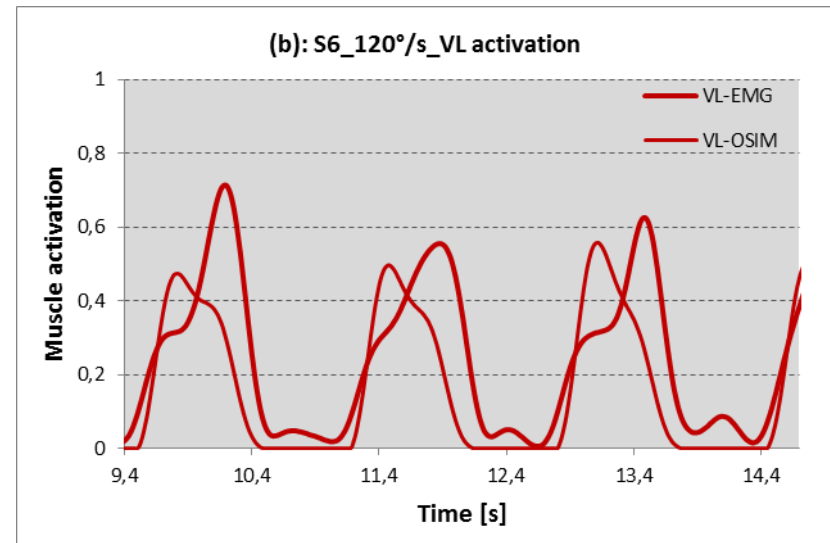
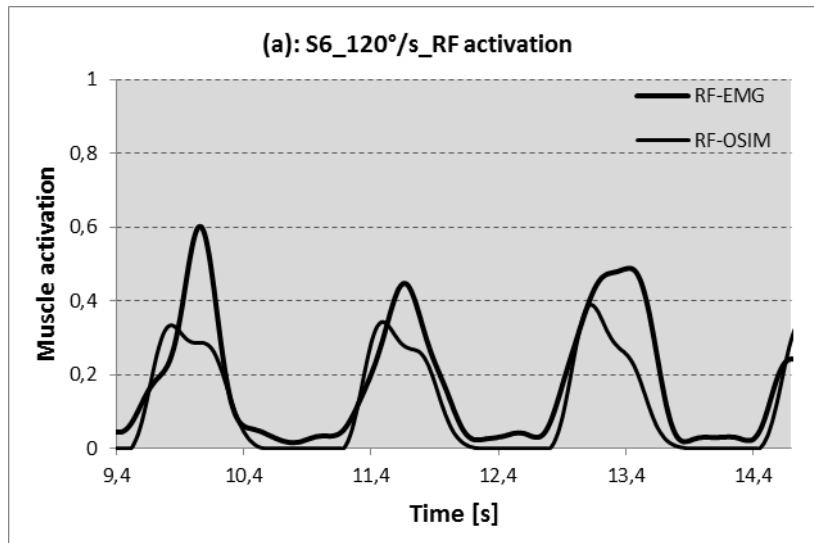


Fig.A.6.4: EMG and OpenSim muscle activation of S6 at 120°/s of RF (a), VL (b), VM (c) and BF (d).

180 °/s

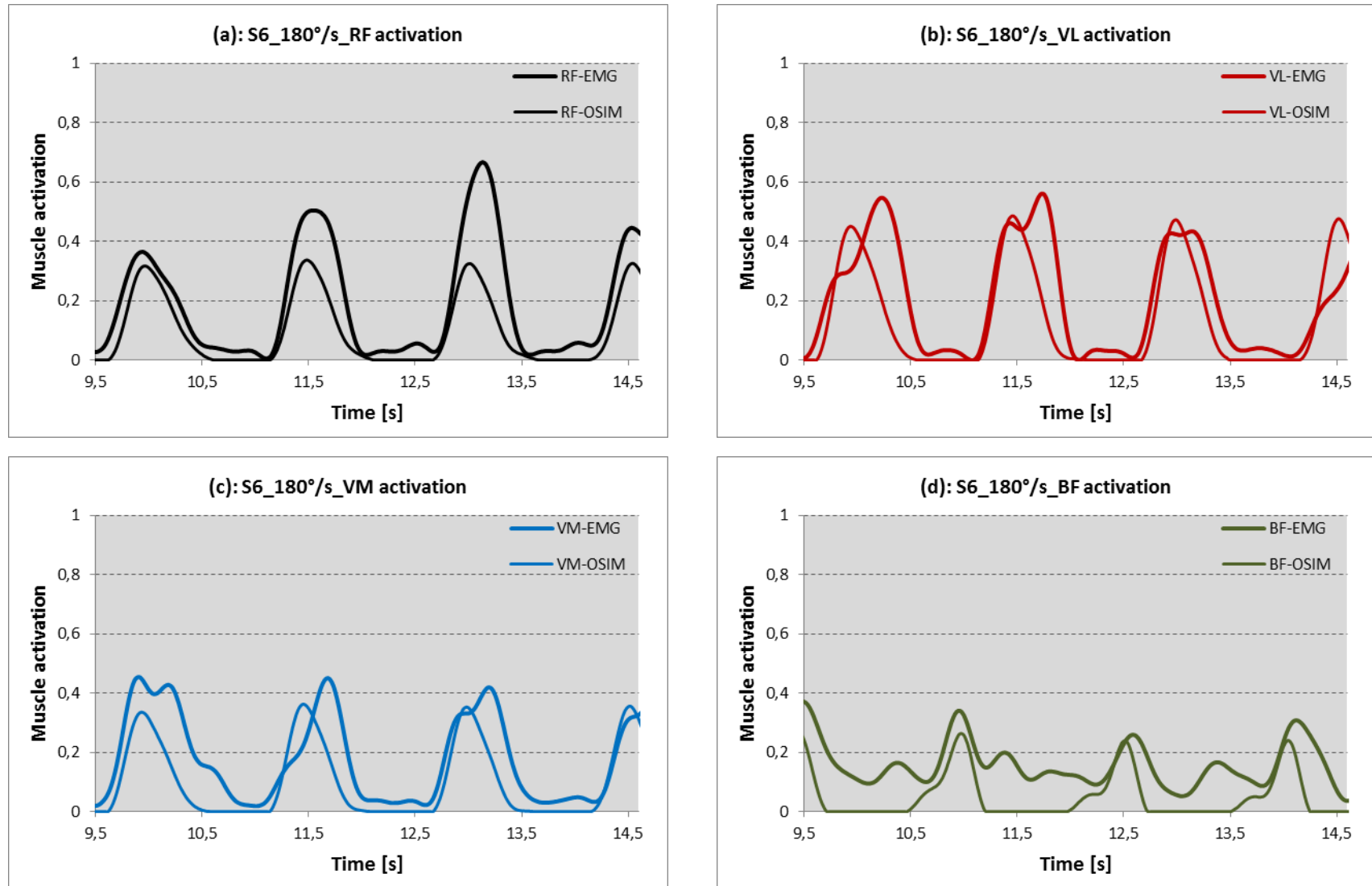


Fig.A.6.5: EMG and OpenSim muscle activation of S6 at 180°/s of RF (a), VL (b), VM (c) and BF (d).

240 °/s

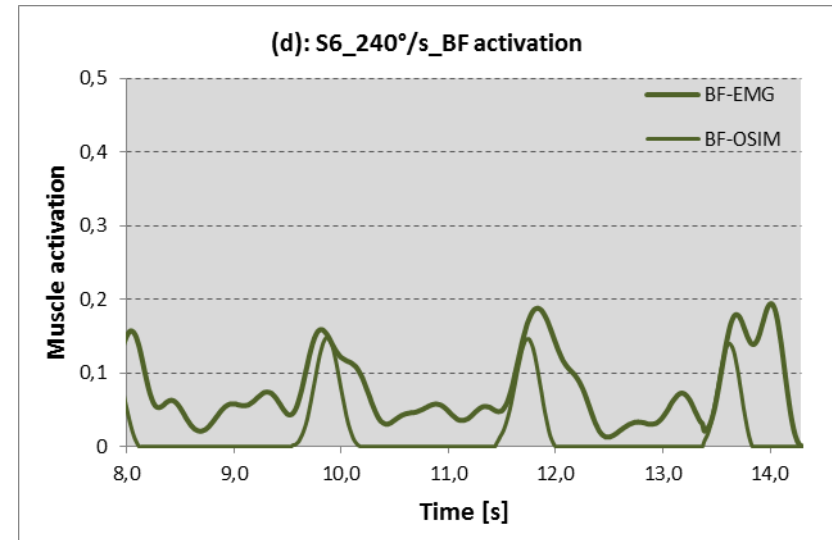
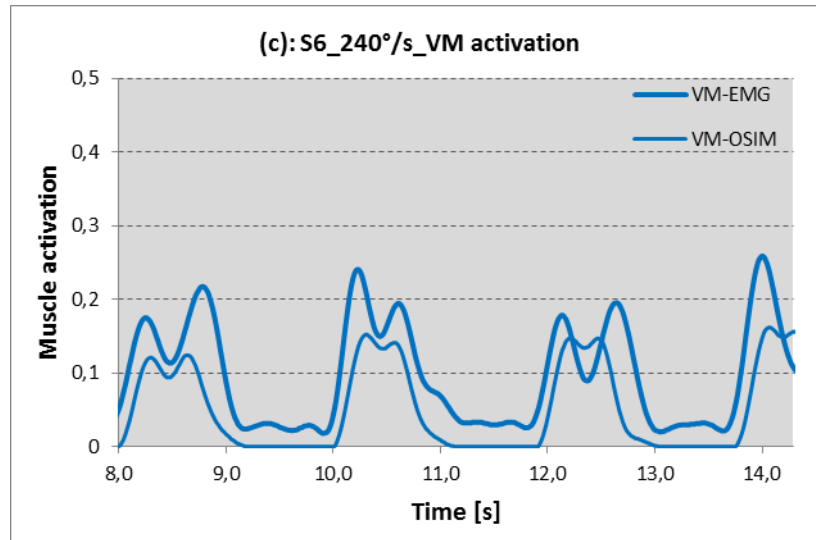
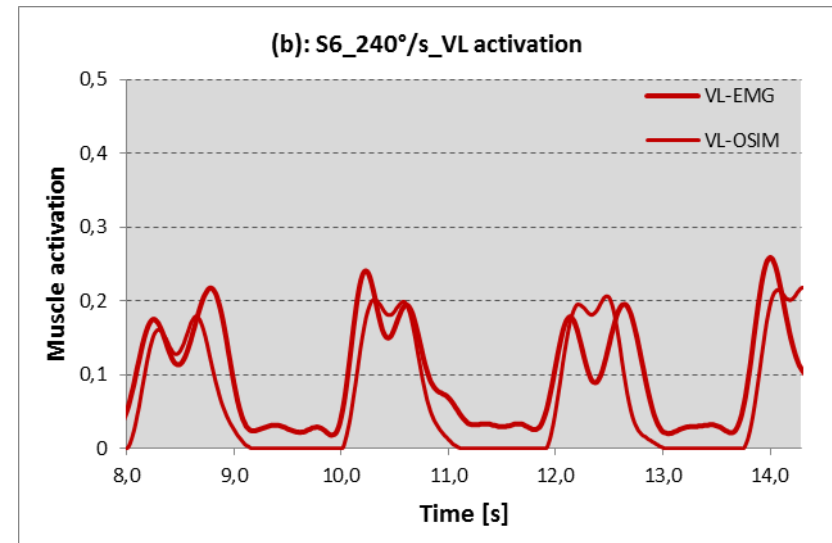
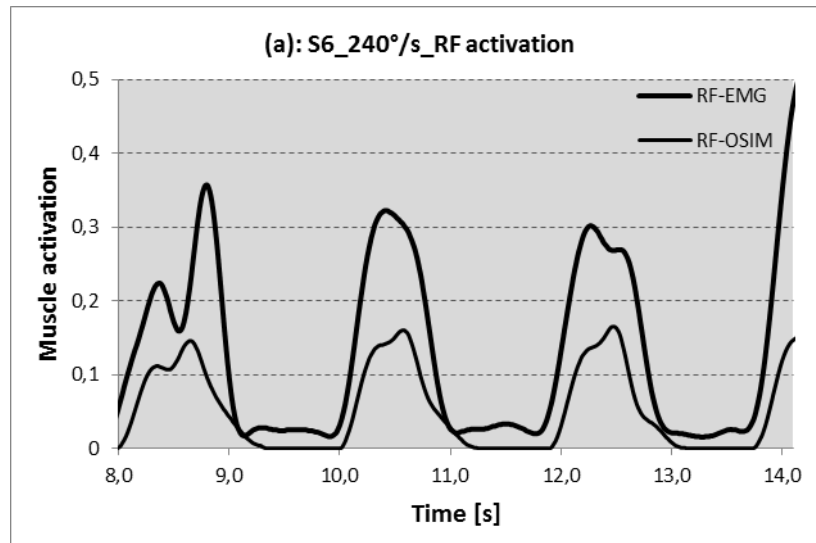


Fig.A.6.6: EMG and OpenSim muscle activation of S6 at 240°/s of RF (a), VL (b), VM (c) and BF (d).

Comparison of EMG signal and OpenSim muscle activation: quantitative results

	60 °/s	120 °/s	180 °/s	240 °/s
RF	29,01±15,44	29,36±13,17	32,41±19,16	51,59±6,96
VL	-8,49±37,91	18,34±13,17	7,39±14,35	28,41±16,26
VM	21,14±17,54	26,93±4,04	20,39±5,22	34,79±9,32
BF	15,46±24,39	20,97±22,41	17,60±8,46	17,06±8,78

Tab.A.6.2: Peak error of S6 in [%] of RF, VL, VM and BF at 60°/s, 120°/s, 180°/s and 240°/s.

	60 °/s	120 °/s	180 °/s	240 °/s
RF	14,97±3,95	13,43±4,15	3,10±4,25	4,23±10,53
VL	2,57±11,91	22,00±0,95	15,10±4,20	5,47±6,26
VM	20,93±13,19	3,37±15,05	8,23±8,95	3,97±7,88
BF	-28,70±8,31	-0,77±10,52	3,37±4,57	6,70±11,26

Tab.A.6.3: Time error of S6 in [%] of RF, VL, VM and BF at 60°/s, 120°/s, 180°/s and 240°/s.

	240 °/s	180 °/s	120 °/s	60 °/s
RF	42,54±11,75	32,96±7,00	37,02±16,36	54,86±1,12
VL	34,96±57,42	28,98±8,13	34,76±6,26	27,93±8,25
VM	64,75±48,16	43,28±2,79	55,97±16,91	43,20±5,75
BF	33,04±15,01	42,25±4,48	49,07±8,70	44,92±4,54

Tab.A.6.4: Area error of S6 in [%] of RF, VL, VM and BF at 60°/s, 120°/s, 180°/s and 240°/s.

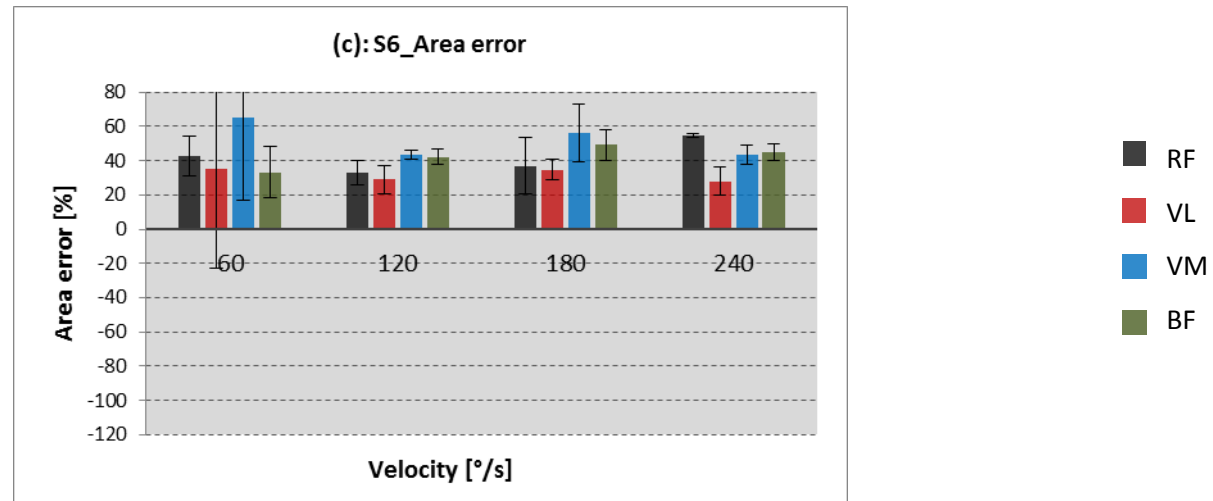
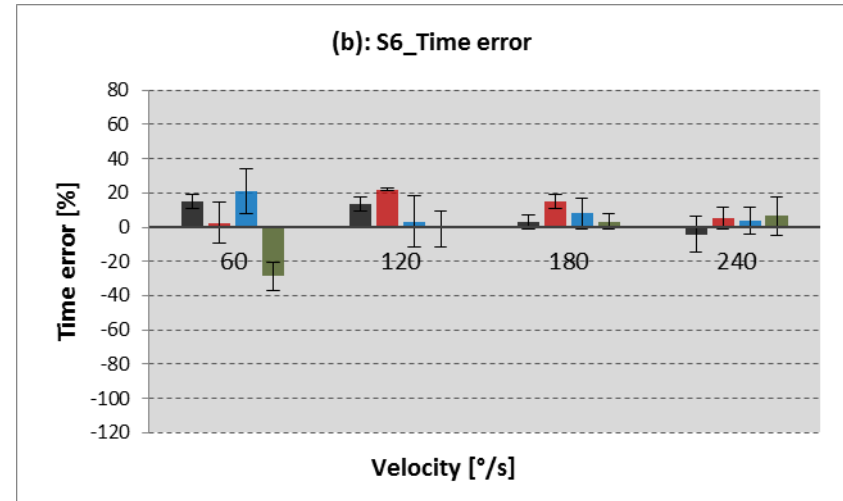
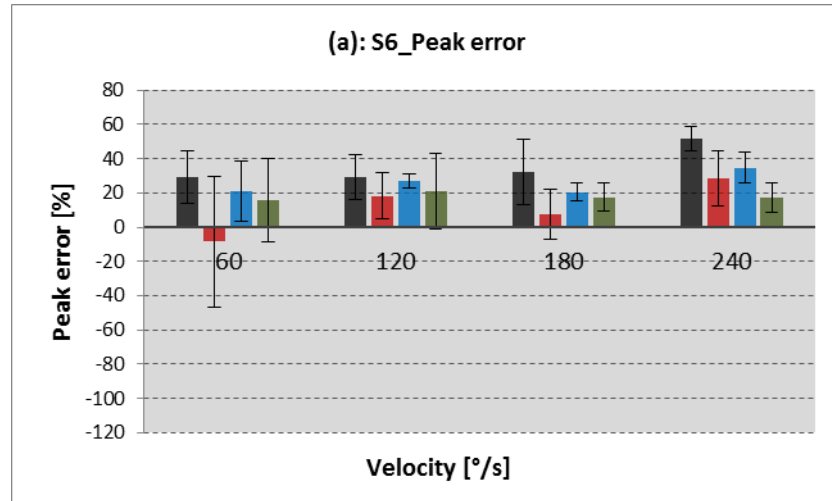


Fig.A.6.1: Quantitative results of muscle activation analysis of S6: (a): Peak error at different velocities; (b): Time error at different velocities; (c): Area error at different velocities.

Model 1: parameters

$$\text{Tibia: } m_{\text{tibia}} = 4,094 \text{ kg} \quad I_{G \text{ tibia}} = 0,077 \text{ kg} \cdot \text{m}^2 \quad \Delta_{y \text{ tibia}} = 0,5 \text{ m} \quad \Delta_{y G \text{ tibia}} = 0,218 \text{ m}$$

$$\text{Talus: } m_{\text{talus}} = 0,11 \text{ kg} \quad I_{G \text{ talus}} = 0,0012 \text{ kg} \cdot \text{m}^2 \quad \Delta_{y \text{ talus}} = 0,5 \text{ m} \quad \Delta_{y G \text{ talus}} = 0,5 \text{ m}$$

$$\text{Calc: } m_{\text{calc}} = 1,38 \text{ kg} \quad I_{G \text{ calc}} = 0,005 \text{ kg} \cdot \text{m}^2 \quad \Delta_{x \text{ calc}} = 0,051 \text{ m} \quad \Delta_{y \text{ calc}} = 0,044 \text{ m}$$

$$\Delta_{x G \text{ calc}} = 0,105 \text{ m} \quad \Delta_{y G \text{ calc}} = 0,032 \text{ m}$$

$$\text{Toes: } m_{\text{toes}} = 0,239 \text{ kg} \quad I_{G \text{ toes}} = 1,2 \cdot 10^{-4} \text{ kg} \cdot \text{m}^2 \quad \Delta_{x \text{ toes}} = 0,188 \text{ m} \quad \Delta_{y \text{ toes}} = 0,0021 \text{ m}$$

$$\Delta_{x G \text{ toes}} = 0,036 \text{ m} \quad \Delta_{y G \text{ toes}} = 0,0063 \text{ m}$$

Model 2: parameters

$$\text{Tibia: } m_{\text{tibia}} = 3,735 \text{ kg} \quad I_{G \text{ tibia}} = 0,061 \text{ kg} \cdot \text{m}^2 \quad \Delta_{y \text{ tibia}} = 0,424 \text{ m} \quad \Delta_{y G \text{ tibia}} = 0,184 \text{ m}$$

$$\text{Foot: } m_{\text{foot}} = 1,162 \text{ kg} \quad I_{G \text{ foot}} = 0,007 \text{ kg} \cdot \text{m}^2 \quad \Delta_{x G \text{ foot}} = 0,073 \text{ m} \quad \Delta_{y G \text{ foot}} = 0,036 \text{ m}$$

$$D_{PT} = 0,08 \text{ m} \quad H_{PT} = 0,026 \text{ m} \quad D_Q = 0,3 \text{ m} \quad H_Q = 0,03 \text{ m}$$

$$B_{PT} [\text{m}] = 0,0097 \cdot \varphi_{k+}^5 - 0,0215 \cdot \varphi_{k+}^4 - 0,0098 \cdot \varphi_{k+}^3 + 0,0366 \cdot \varphi_{k+}^2 - 0,0141 \cdot \varphi_{k+} + 0,0464 \quad \varphi_{k+} [\text{rad}]$$

$$\text{BFB: } D_{BFB1} = 0,2 \text{ m} \quad D_{BFB2} = 0,04 \text{ m} \quad H_{BFB1} = 0,04 \text{ m} \quad H_{BFB2} = 0,03 \text{ m}$$

$$\text{BFL: } D_{BFL1} = 0,49 \text{ m} \quad D_{BFL2} = 0,04 \text{ m} \quad H_{BFL1} = 0,04 \text{ m} \quad H_{BFL2} = 0,03 \text{ m}$$

$$\text{SM: } D_{SM1} = 0,49 \text{ m} \quad D_{SM2} = 0,05 \text{ m} \quad H_{SM1} = 0,04 \text{ m} \quad H_{SM2} = 0,035 \text{ m}$$

$$\text{ST: } D_{ST1} = 0,49 \text{ m} \quad H_{ST1} = 0,05 \text{ m} \quad B_{ST} = 0,04 \text{ m} \quad \alpha_{ST} = 0,52 \text{ rad}$$

Fig.A.6.8: S6_60°/s_Extension

— OSIM — Mod1_Herzog — Mod1_Van Eijden — Mod2 - - - limit value

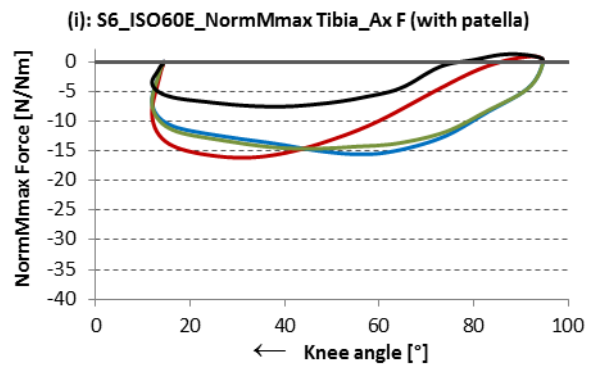
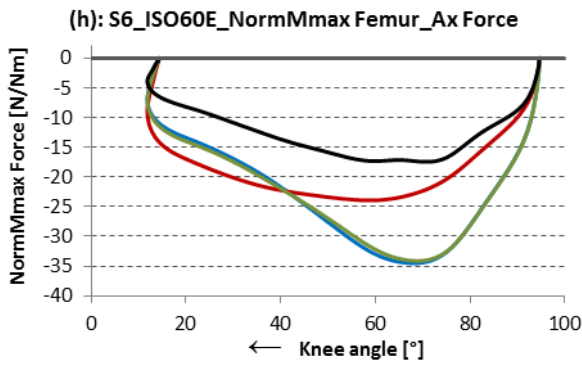
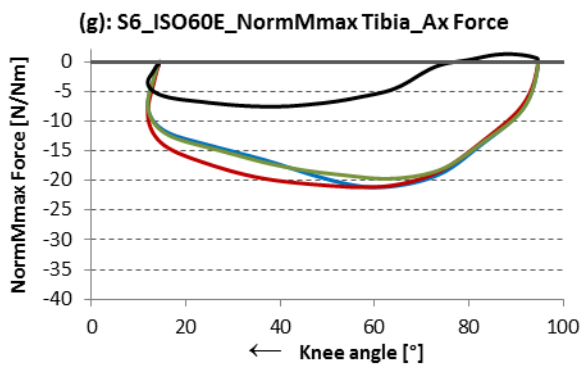
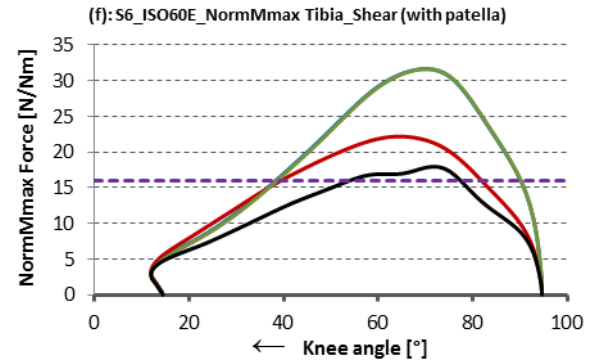
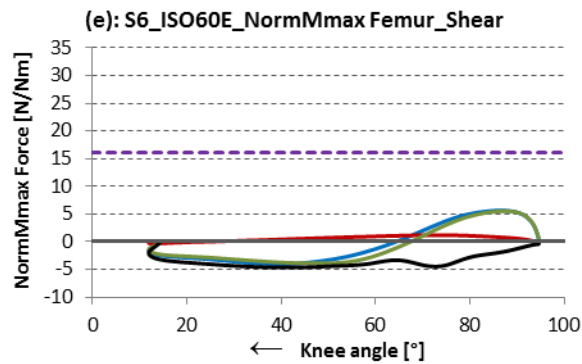
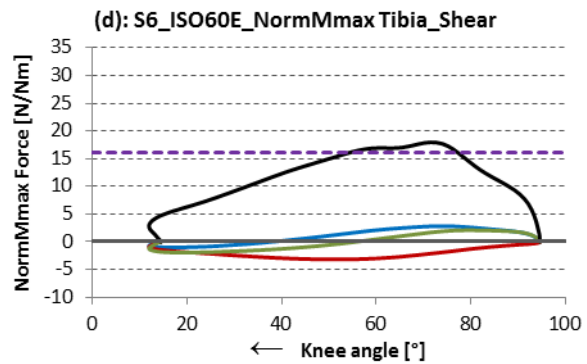
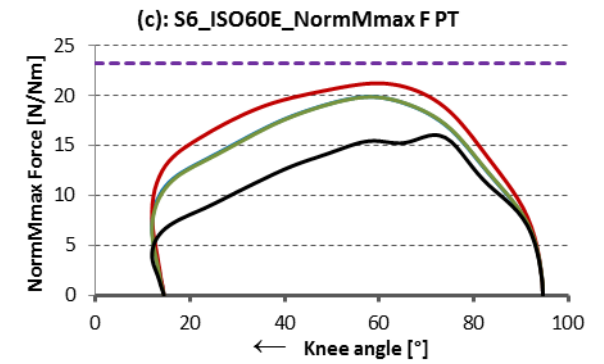
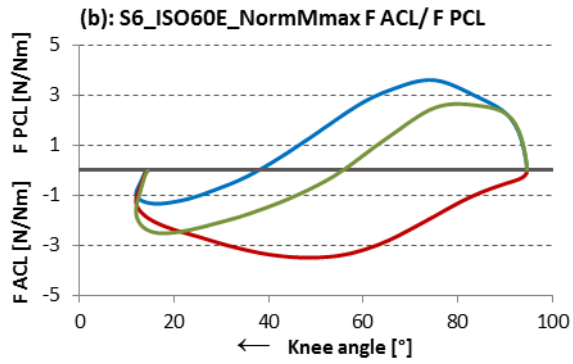
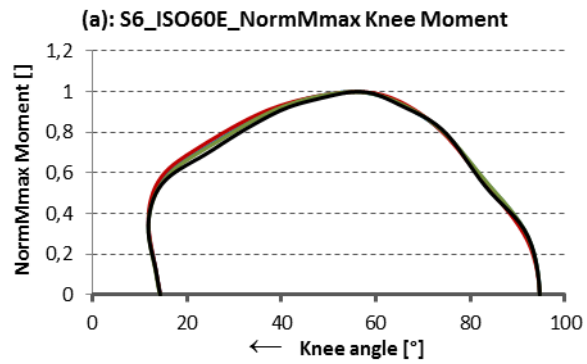


Fig.A.6.9: S6_60°/s_Flexion

— OSIM — Mod1 — Mod2 - - - limit value (•••• OSIM BFL •••• Mod1 BFL •••• Mod2 BFL

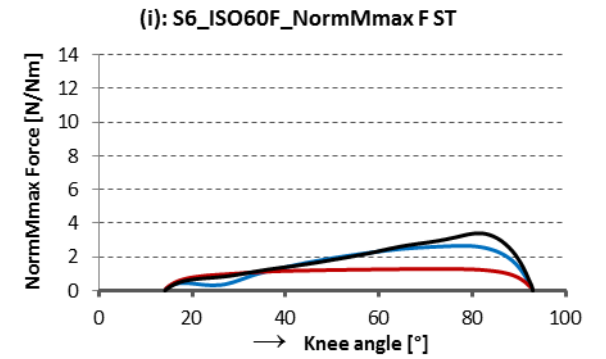
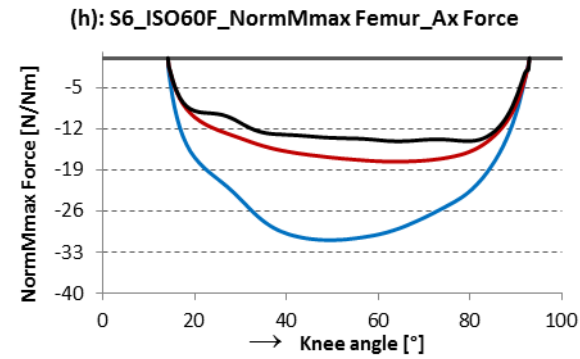
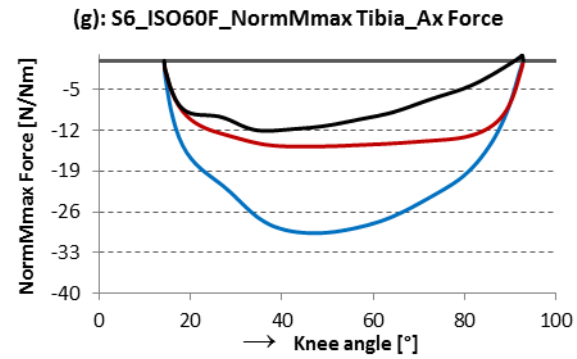
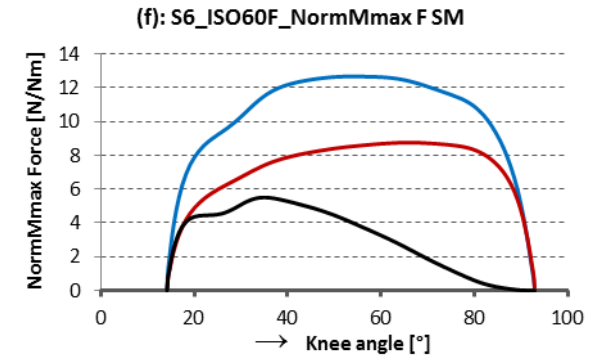
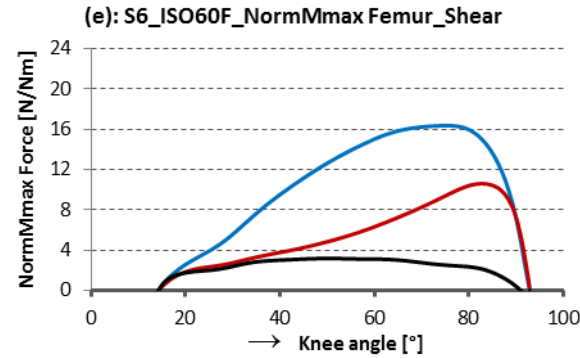
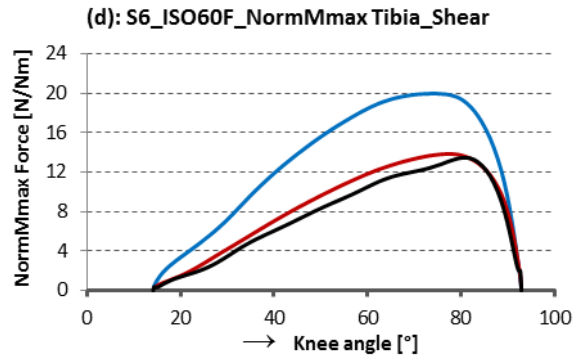
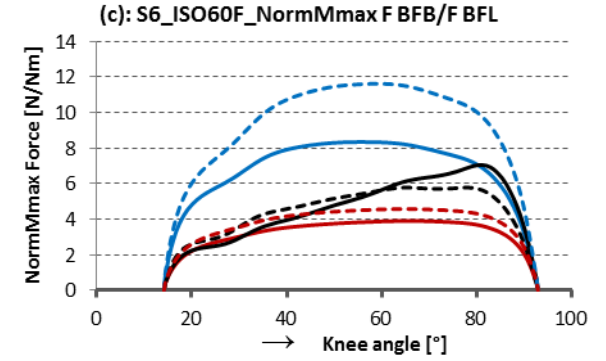
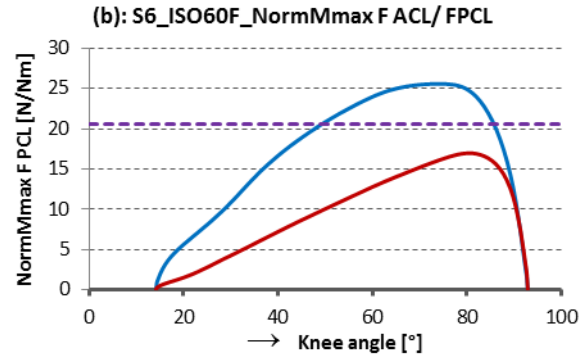
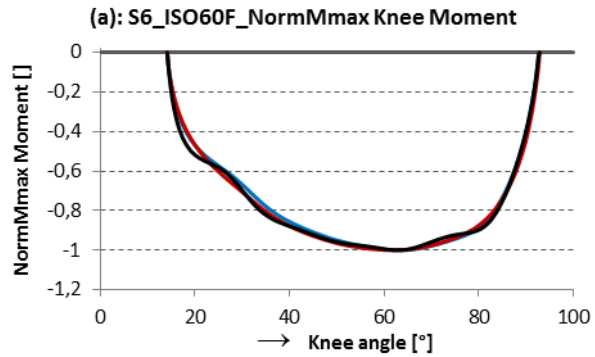


Fig.A.6.10: S6_120°/s_Extension

— OSIM — Mod1_Herzog — Mod1_Van Eijden — Mod2 - - - - limit value

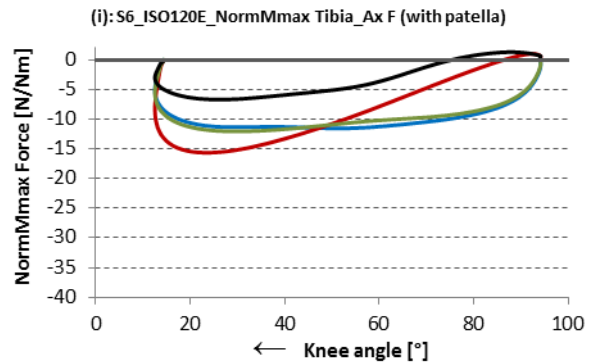
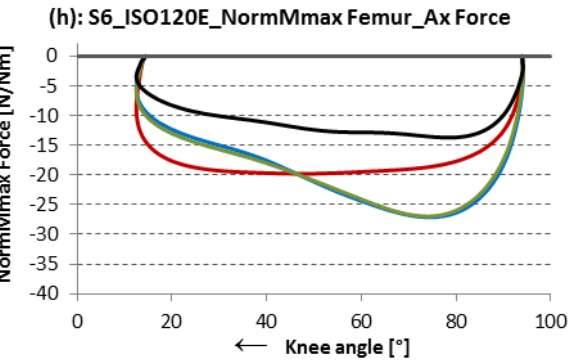
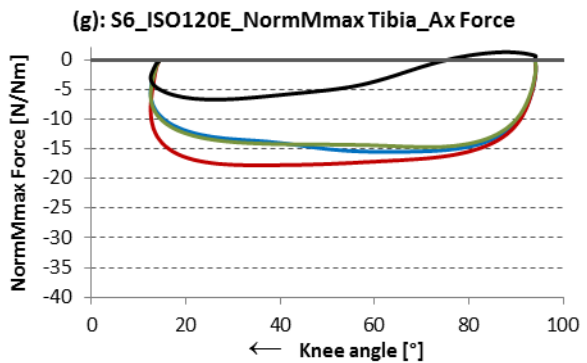
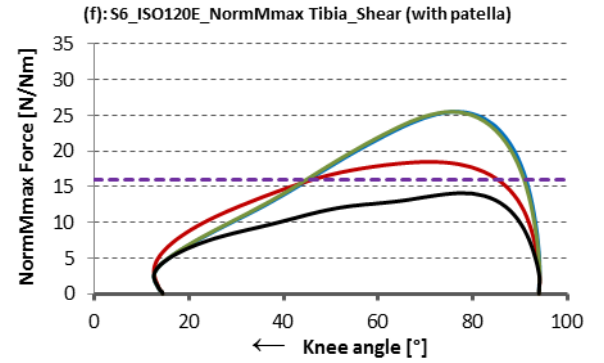
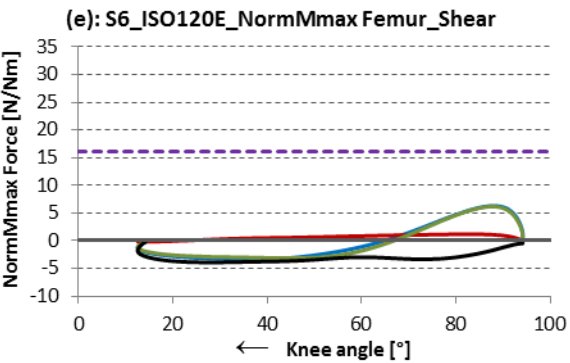
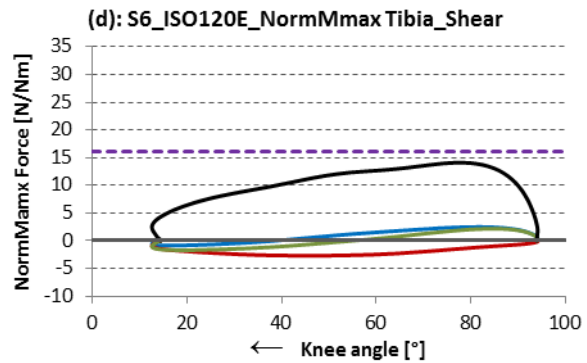
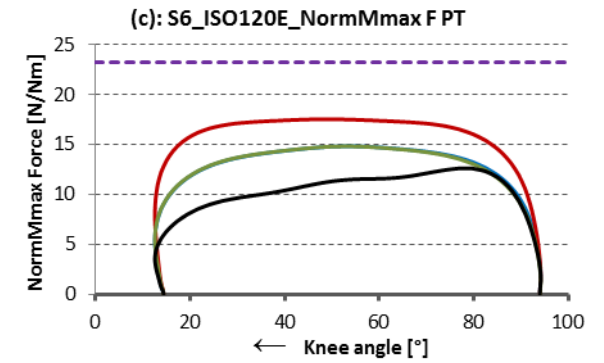
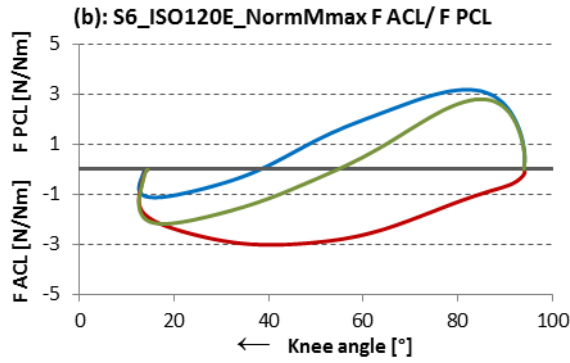
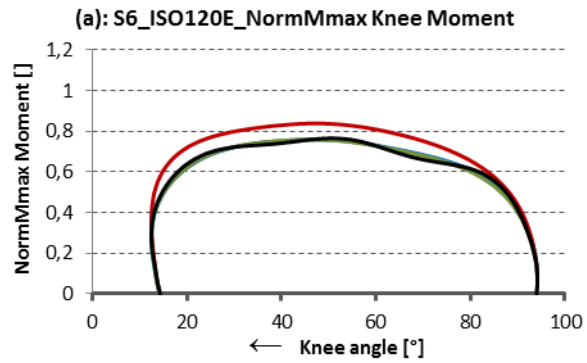


Fig.A.6.11: S6_120°/s_Flexion

— OSIM — Mod1 — Mod2 - - - - limit value (- - - - OSIM BFL - - - - Mod1 BFL - - - - Mod2 BFL)

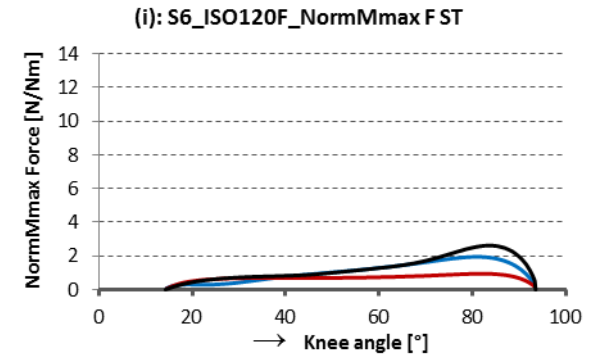
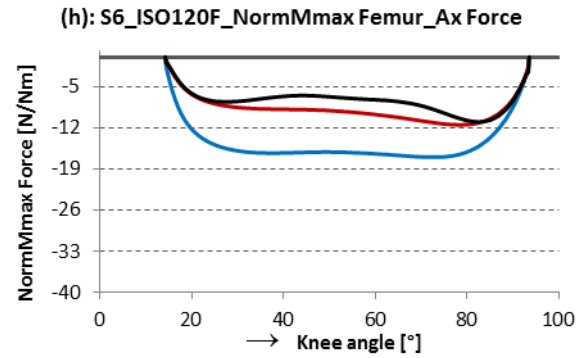
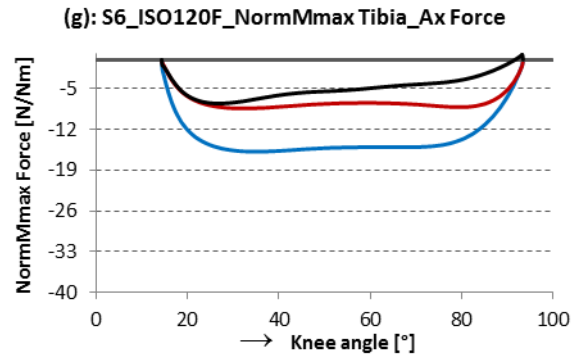
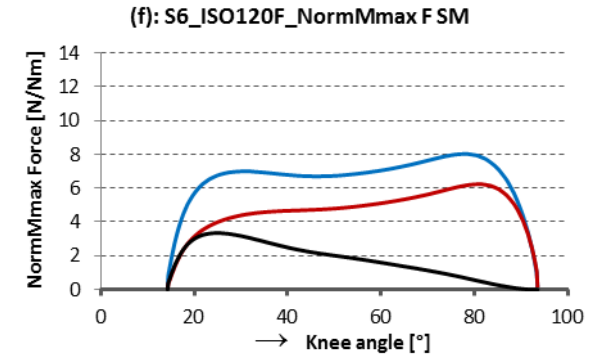
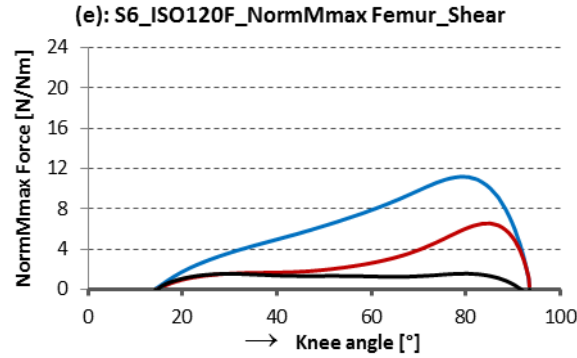
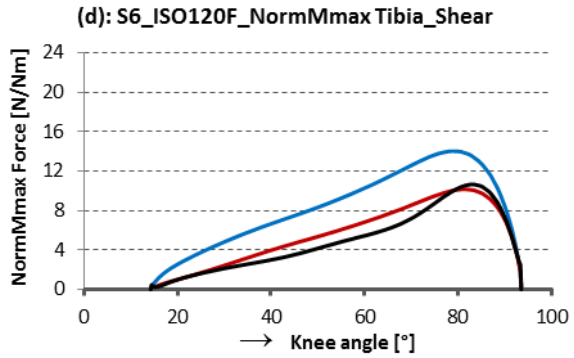
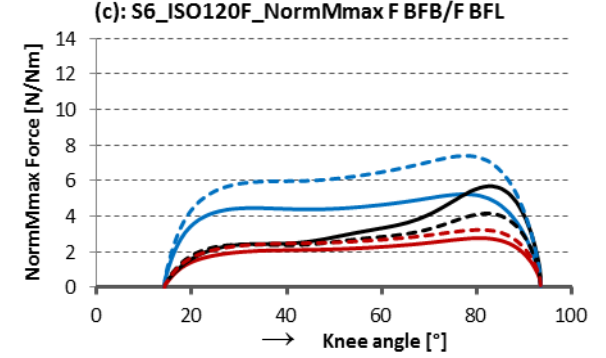
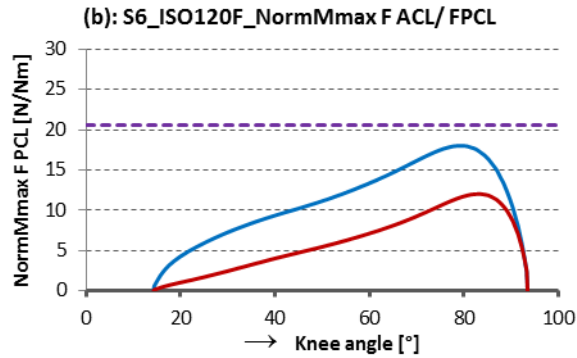
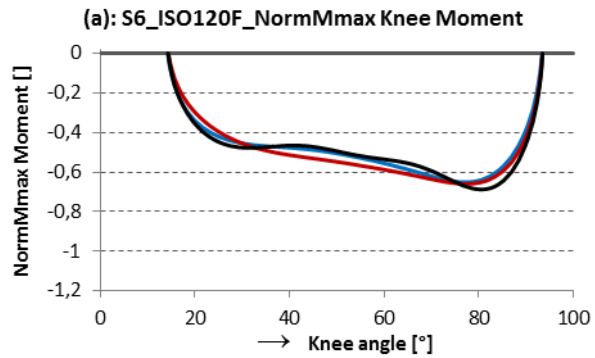


Fig.A.6.12: S6_180°/s_Extension

— OSIM — Mod1_Herzog — Mod1_Van Eijden — Mod2 - - - - - limit value

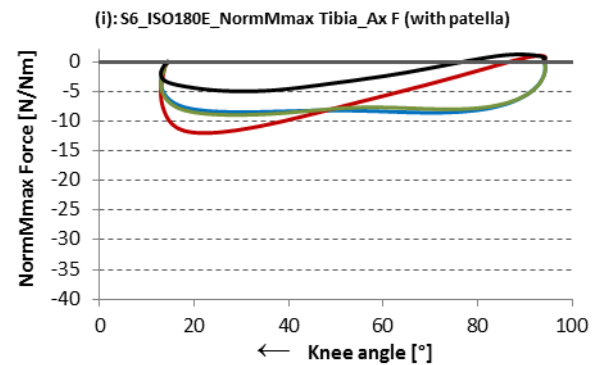
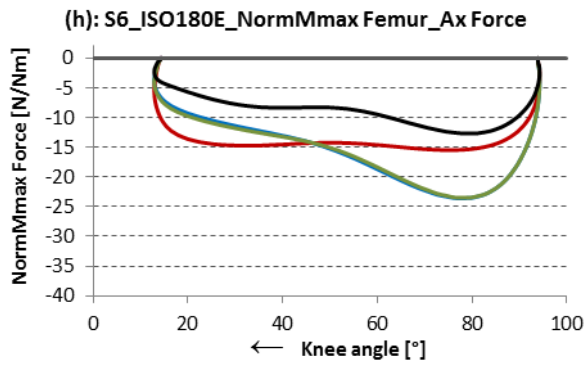
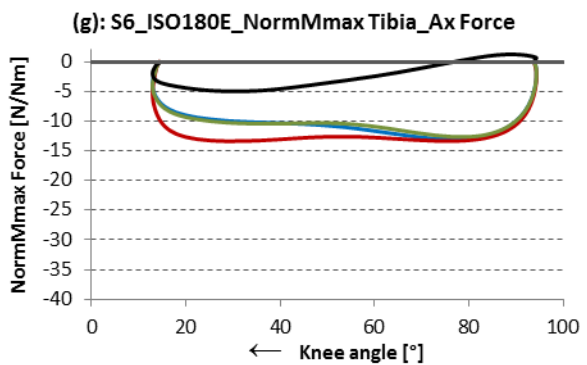
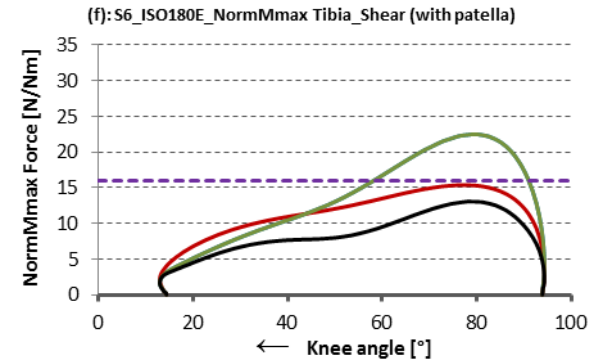
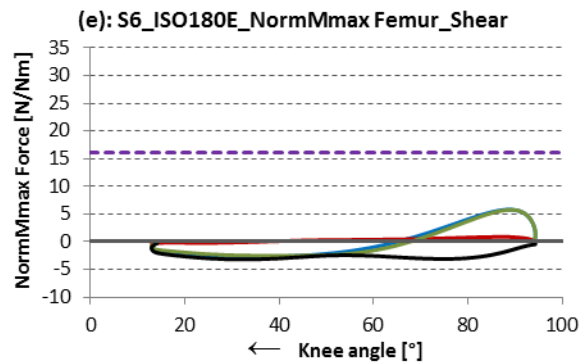
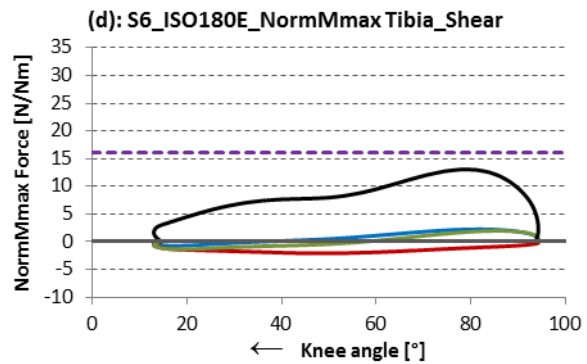
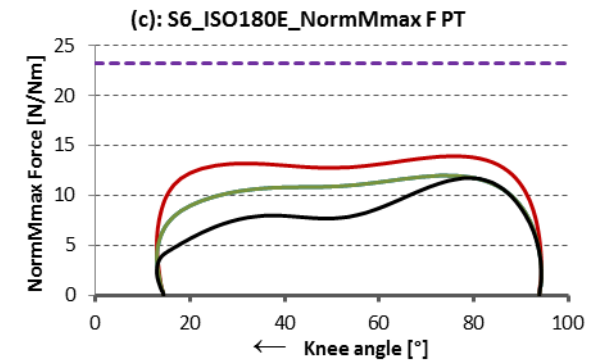
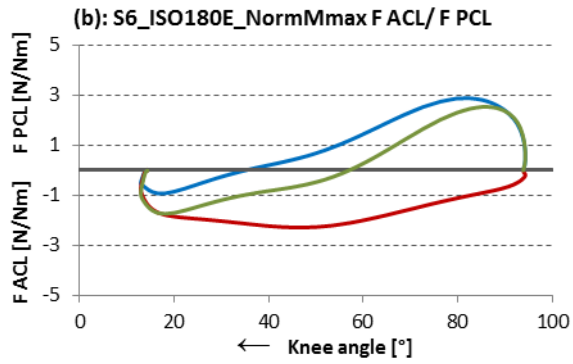
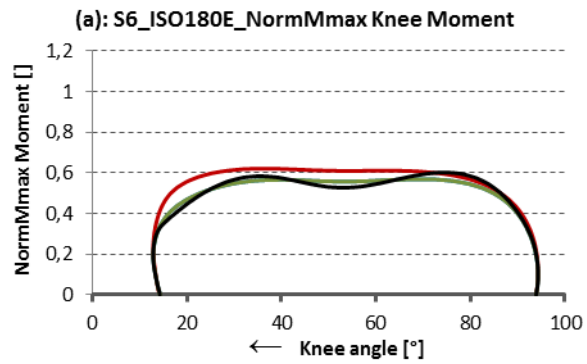


Fig.A.6.13: S6_180°/s_Flexion

— OSIM — Mod1 — Mod2 - - - - limit value (•••• OSIM BFL •••• Mod1 BFL •••• Mod2 BFL)

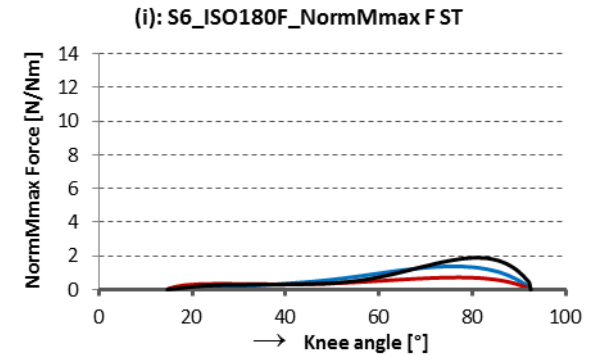
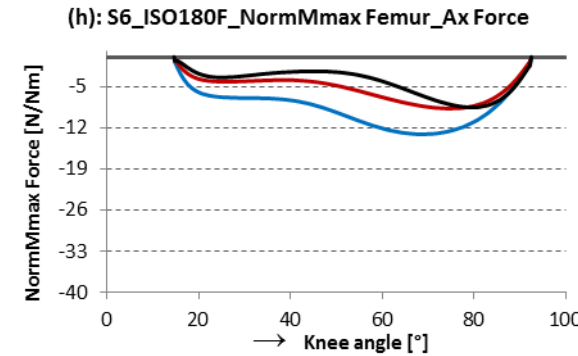
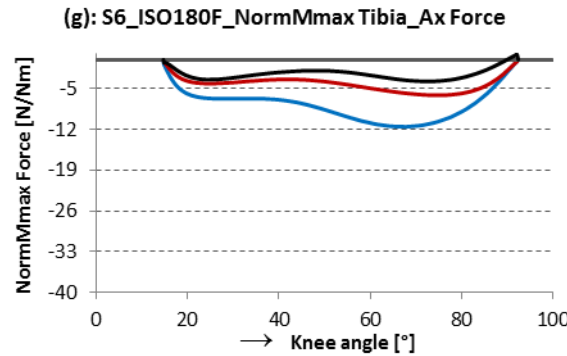
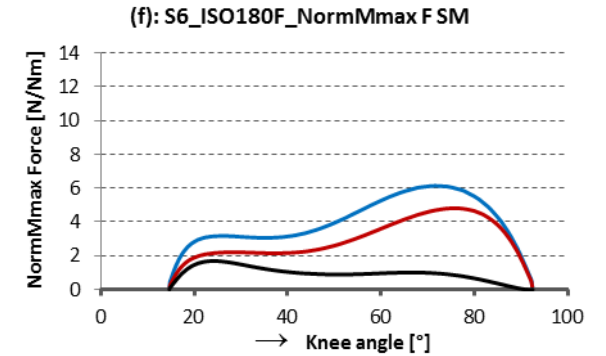
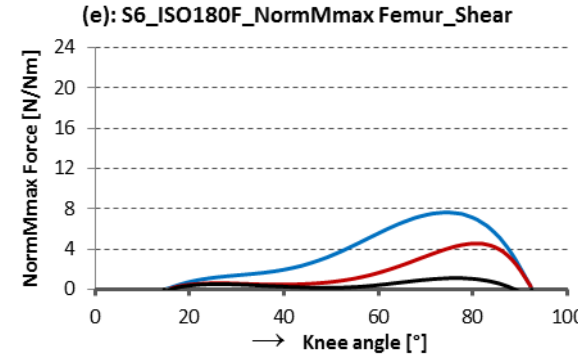
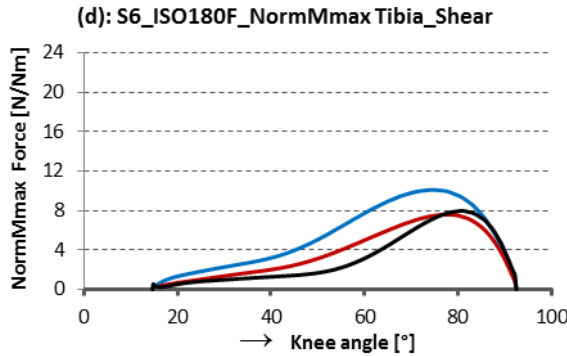
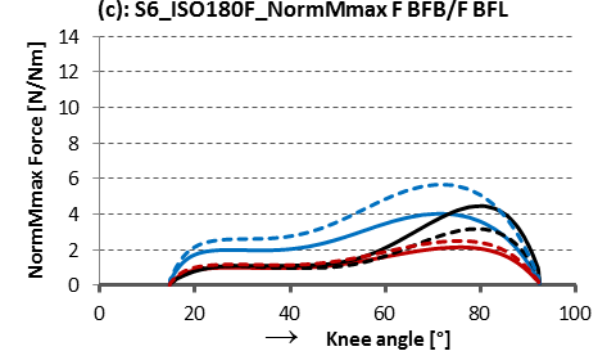
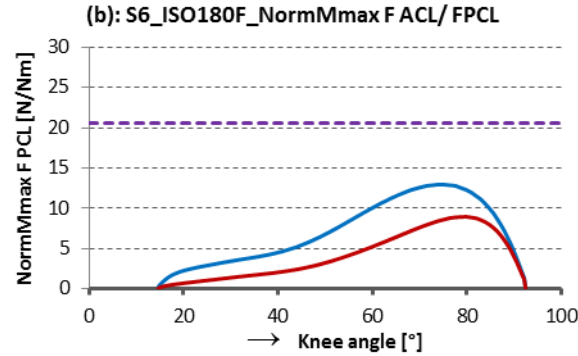
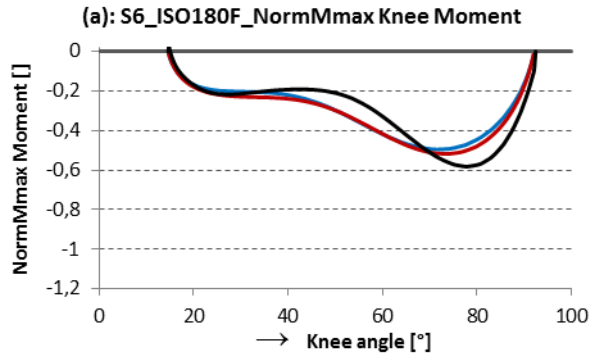


Fig.A.6.14: S6_240°/s_Extension

— OSIM — Mod1_Herzog — Mod1_Van Eijden — Mod2 - - - - limit value

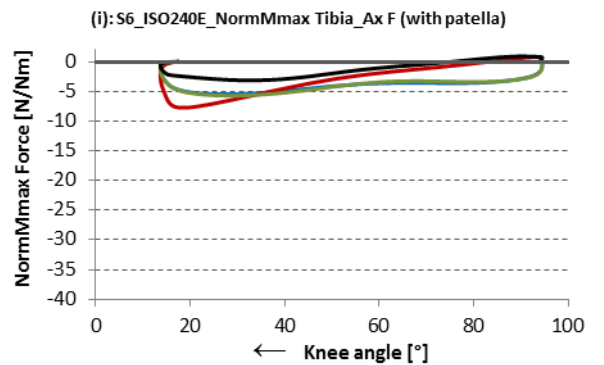
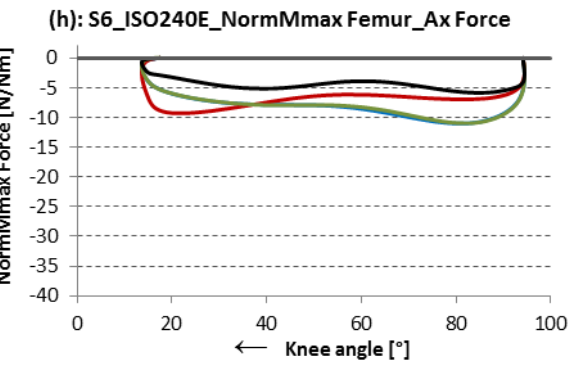
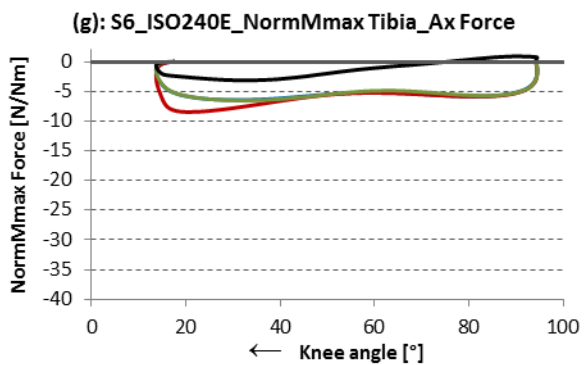
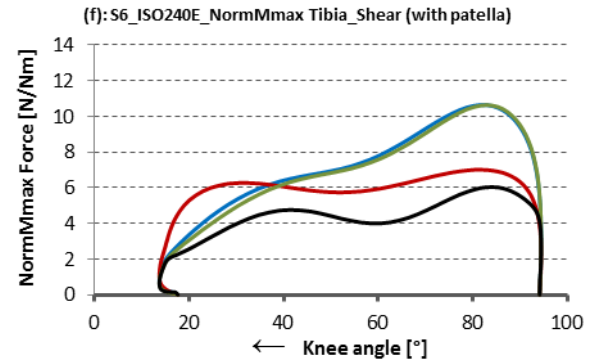
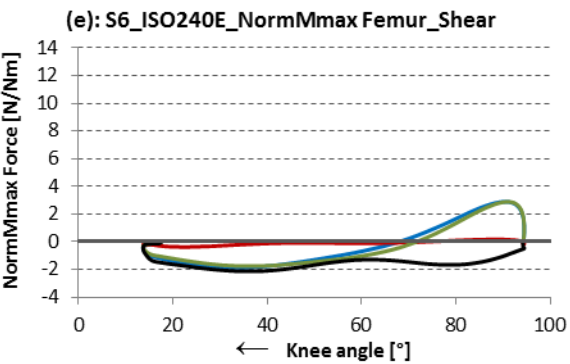
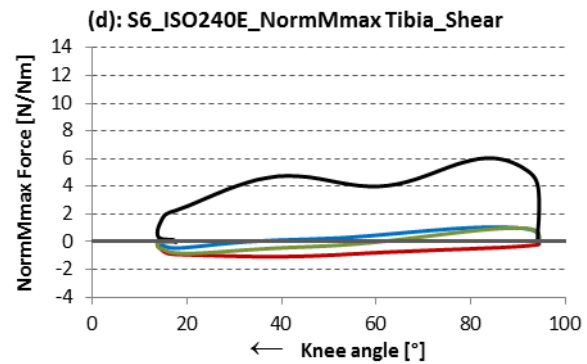
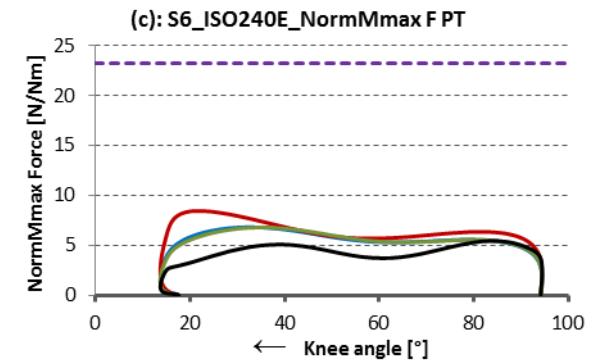
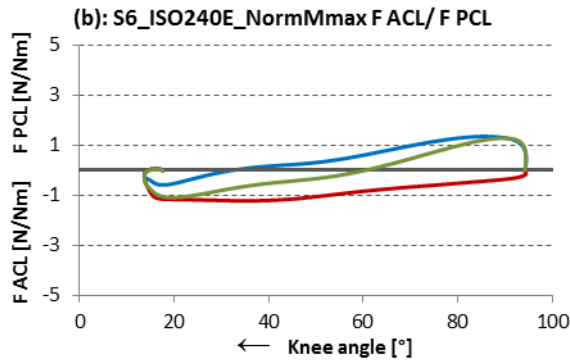
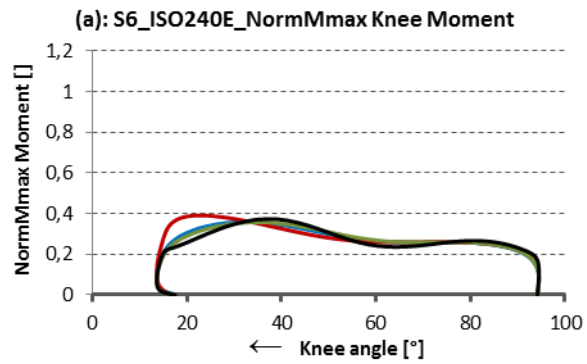
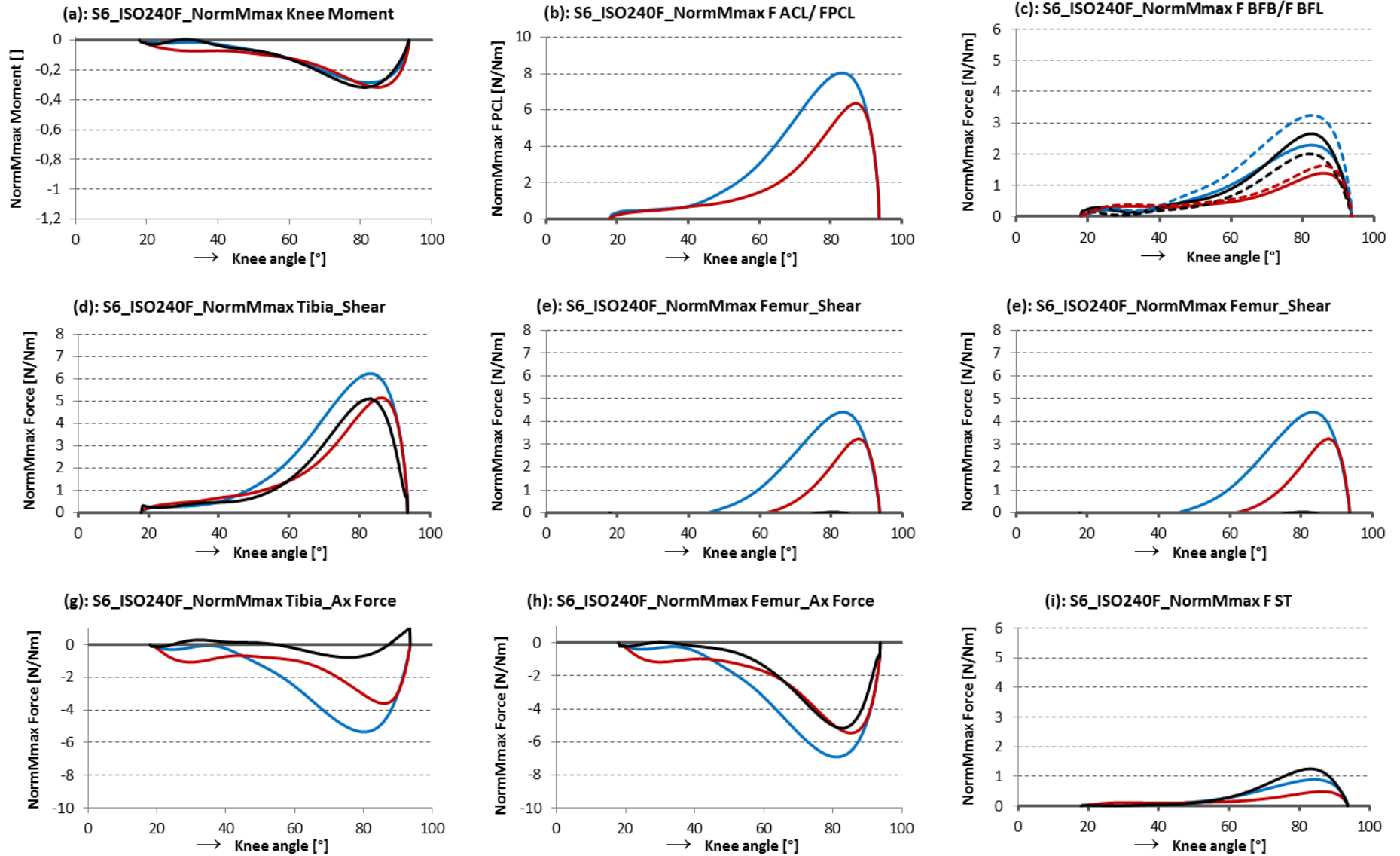


Fig.A.6.15: S6_240°/s_Flexion

— OSIM — Mod1 — Mod2 ···· limit value (···· OSIM BFL ···· Mod1 BFL ···· Mod2 BFL)



References and notes

1. Amis AA, Bull AMJ, Gupte CM, Hijazi I, Race A, Robinson JR. **Biomechanics of the PCL and related structures: Posterolateral, posteromedial and meniscofemoral ligaments.** *Knee Surg. Sports Traumatol. Arthrosc.* 2003, 11:271-281
2. Beynnon BD, Fleming BC. **Anterior cruciate ligament strain in-vivo: A review of previous work.** *J Biomech* 1998, 31(6):519-525
3. Beynnon BD, Howe JG, Pope MH, Johnson RJ, Fleming BC. **The measurement of anterior cruciate ligament strain in vivo.** *Int Orthop* 1992, 16:1-12
4. Beynnon BD, Johnson RJ et al. **The strain behavior of the anterior cruciate ligament during squatting and active flexion-extension: A comparison of open and closed kinetic chain exercise.** *Am J Sports Med* 1997, 25(6):823-829.
5. D'Lima DD, Fregly BJ, Colwell CW Jr. **Implantable sensors technology: measuring bone and joint biomechanics of daily life in vivo.** *Arthritis R&L* 2013, 15-203
6. D'Lima DD, Patil S, Steklov N, Chien S, Colwell CW Jr. **In vivo knee moments and shear after total knee arthroplasty.** *J Biomech* 2007, 40:S11-S17
7. D'Lima DD, Patil S, Steklov N, Colwell CW Jr. **The Mark Coventry Award: in vivo knee forces during recreation and exercise after knee arthroplasty.** *Clin Orthop Relat Res* 2008, 466:2605-2611
8. D'Lima DD, Patil S, Steklov N, Slamin JE, Colwell CW Jr. **The Chitranjan Ranawat Award: in vivo knee forces after total knee arthroplasty.** *Clin Orthop Relat Res* 2005 ,440:45-49
9. D'Lima DD, Patil S, Steklov N, Slamin JE, Colwell CW Jr. **Tibial forces measured in vivo after total knee arthroplasty.** *J Arthroplasty* 2006, 21:255-262
10. D'Lima DD, Townsend CP, Arms SW, Morris BA, Colwell CW Jr. **An implantable telemetry device to measure intra-articular tibial forces.** *J Biomech* 2005, 38:299-304
11. Gray H, Carter HV. **Anatomy of the Human Body.** 2008
12. Heinlein B, Kutzner I, Graichen F, Bender A, Rohlmann A, Halder AM, Beier A, Bergmann G. **ESB Clinical Biomechanics Award 2008:Complete data of total knee replacement loading for level walking and stair climbing measured in vivo with a follow-up of 6-10 months.** *Clin Biomech (Bristol, Avon)* 2009, 24:315-326
13. Herzog W, Read LJ. **Lines of action and moment arms of the major force-carrying structures crossing the human knee joint.** *J. Anat.* 1993, 183:213-230
14. Kapandji AI. **Fisiologia articolare, Vol II.** 2011
15. Kaufman KR, An Kai-Nan, Litchy WJ, Morrey BF, Chao EYES. **Dynamic joint forces during knee isokinetic exercise.** *Am J Sports Med* 1991, 19(3):305-316
16. Kawaguchi Y, Kondo E, Takeda R, Akita K, Yasuda K, Amis AA. **The Role of Fibers in the Femoral Attachment of the Anterior Cruciate Ligament in Resisting Tibial Displacement.** *J Anthroscopy* 2015, 31(3):435-444
17. Kennedy JC, Hawkins RJ, Willis RB, Danylchuck KD. **Tension studies of human knee ligaments. Yield point, ultimate failure, and disruption of the cruciate and tibial collateral ligaments.** *J Bone Joint Surg Am* 1976, 58:350-355

18. Kirking B, Krevolin J, Townsend C, Colwell CW Jr, D’Lima DD. **A multiaxial force-sensing implantable tibial prosthesis.** *J Biomech* 2006, 39:1744-1751
19. Konrad P. **The ABC of EMG.** 2005
20. Kutzner I, Kuther S, Heinlein B, Dymke J, Bender A, Halder AM, Bergmann G. **The effect of valgus braces on medial compartment load of the knee joint – in vivo load measurement in three subjects.** *J Biomech* 2011, 44:1354-1360
21. Lee RC, Wang ZM, Heo M, Ross R, Janssen I, Heymsfield SB. **Total-body skeletal muscle mass: development and cross-validation of anthropometric prediction models.** *Am J Clin Nutr* 2000, 72:796–803
22. Marinozzi G, Pappalardo S, Steindler R. **Human knee ligaments: mechanical tests and ultrastructural observations.** *Ital J Orthop Traumatol* 1983, 9:231–240
23. Nigg BM, Herzog W. **Biomechanics of the Musculo-skeletal System, Second Edition.** 2003
24. Noyes FR, Butler DL, Grood ES, Zernicke RF, Hefzy MS. **Biomechanical analysis of human ligaments grafts used in knee ligament repair and reconstruction.** *J. Bone Joint Surg. Am.* 1984, 66:344-352
25. Peterson DR, Bronzino JD. **Biomechanics, Principles and Applications.** 2008
26. Pontaga I. Hip and knee flexors and extensors balance in dependence on the velocity of movements. *Biol.Sport* 2004, 21:261:272
27. Pontin A, Petrone N. **Analisi biomeccanica dei carichi articolari durante esercizi sportivi con attrezzi.** *Padua Thesis UNIPD* 2012.
28. Prietto MP, Bain JR, Stonebrook SN, Settlage RA. **Tensile strength of the human posterior cruciate ligament (PCL).** *Trans 34th Ann ORS* 1988, 13:195
29. Reichard LB, Croisier JL, Malnati M, Katz-Leurer M, Dvir Z. **Testing knee extension and flexion strength at different ranges of motion: an isokinetic and electromyographic study.** *Eur J Appl Physiol* 2005, 95(4):371-376.
30. Tregnagi D, Petrone N. **Modellazione del movimento di flesso-estensione isocinetico del ginocchio con codice OpenSim 1.9.1 e confronto con analisi sperimentali.** *Padua Thesis UNIPD* 2010
31. Trent PS, Walker PS, Wolf B. **Ligament length patterns, strength, and rotational axes of the knee joint.** *Clin Orthop* 1976, 117:263–270
32. Van Eijden TMGJ, Kouwenhoven E., Verburg J., et al. **A mathematical model of the patellofemoral joint.** *J. Biomech* 1986, 19:219–229 (pag. 3-12 Peterson-Bronzino)
33. Worrell TW. **Factors associated with hamstring injuries: An approach to treatment and preventive measures.** *Sports Med* 1994, 17:338-345.
34. Yamaguchi GT, Zajac FE. **A planar model of the knee joint to characterize the knee extensor mechanism.** *J. Biomech* 1989, 22(1):1-10

Supporting online material

35. Delp S, Anderson F, Arnold A, Loan P, Habib A, John C, Guendelman E, Thelen D. **OpenSim: Open-source Software to Create and Analyze Dynamic Simulations of Movement.** *IEEE Transactions on Biomedical Engineering* 2007
36. Muscle Atlas. Available: www.rad.washington.edu/academics/academic-sections/msk/muscle-atlas
37. Force-length-velocity relation. Available: www.studyblue.com/notes/note/n/muscle/deck
38. OpenSim support online. Available:
<http://simtk-confluence.stanford.edu:8080/display/OpenSim/OpenSim+Support>

RINGRAZIAMENTI

Ringrazio i miei genitori, per avermi accompagnato in questi venticinque anni della mia vita lasciandomi libero nelle mie scelte e al tempo stesso consigliandomi quando ne avevo bisogno; in particolare li ringrazio per aver cercato di farmi vivere in maniera meno pesante possibile le avversità incontrate in quest'ultimo periodo. Ringrazio inoltre tutti i miei familiari, che, sebbene anche con una sola parola, mi hanno sempre fatto capire il loro affetto.

Ringrazio il mio relatore, prof. Nicola Petrone, per avermi sempre spronato a non arrendermi di fronte ai numerosi problemi incontrati e per aver cercato lui stesso di presentarmi possibili soluzioni per progredire nel lavoro; lo ringrazio inoltre per i consigli utili che mi ha dato e per il suo punto di vista accorto. Ringrazio poi il dott. Giuseppe Marcolin e Matteo Cognolato per l'aiuto datomi con la strumentazione utilizzata e per esser sempre stati disponibili quando ne avevo bisogno.

Ringrazio Martina Barzan, per il fondamentale contributo datomi con il software OpenSim, in particolare per la pazienza e premura con cui mi ha trasmesso le cose, e per il sostegno che ha sempre dimostrato nei miei confronti.

Ringrazio tutti coloro che si sono prestati ad eseguire gli esercizi delle mie prove per la pazienza che hanno dimostrato, in particolare ringrazio Alessio Schiavon ed Edoardo Gentile.